PB90-240581

Chamber and Modeling Study to Assess the Photochemistry of Formaldehyde

North Carolina Univ. at Chapel Hill

Prepared for:

Environmental Protection Agency, Research Triangle Park, NC

Jul 90

U.S. Department of Commerce
National Technical Information Service
NTIS

TECHNICAL REPORT DATA

(Please read Instructions on the reverse before completi

1. REPORT NO. EPA/600/3-90/052	**2.**	**3.** PB90-240581
4. TITLE AND SUBTITLE A CHAMBER AND MODELING STUDY TO ASSESS THE PHOTOCHEMISTRY OF FORMALDEHYDE		**5. REPORT DATE** July 1990 **6. PERFORMING ORGANIZATION CODE**
7. AUTHOR(S) H. E. Jeffries, K. G. Sexton, J. R. Arnold, Y. Bai		**8. PERFORMING ORGANIZATION REPORT NO.**
9. PERFORMING ORGANIZATION NAME AND ADDRESS University of North Carolina School of Public Health Chapel Hill, North Carolina 27514		**10. PROGRAM ELEMENT NO.** A101G/B/63/20 - Task 2/A **11. CONTRACT/GRANT NO.** CA813964
12. SPONSORING AGENCY NAME AND ADDRESS Atmospheric Research and Exposure Assessment Lab-RTP Office of Research and Development U. S. Environmental Protection Agency Research Triangle Park, North Carolina 27711		**13. TYPE OF REPORT AND PERIOD COVERED** Final (2/88 - 2/90) **14. SPONSORING AGENCY CODE** EPA/600/09
15. SUPPLEMENTARY NOTES		

16. ABSTRACT

A new analytical method for formaldehyde (HCHO) was implemented for use in the UNC outdoor smog chamber. HCHO measurements obtained with this method were compared with those obtained using other analytical techniques. Six different calibration standards for HCHO were found to agree within ±2%, and the different HCHO analytical methods had precisions of ±10%. New experiments in which HCHO was produced chemically were performed. An explicit chemical reaction mechanism for ethene and propene was formulated to explain the chamber observations. The ethene mechanism showed excellent agreement with the observed data; the propene mechanism, however, did not perform as satisfactory. A comparison of these explicit mechanisms with the Carbon Bond IV (CB4) mechanism showed excellent agreement for ozone (<10% error), nitrogen oxides, and hydrocarbon oxidation rates; the CB4, however, consistently underpredicted the HCHO maximum by about 13%. An analysis of a simulation of an urban scenario showed that chemical production of HCHO was the dominant factor governing afternoon HCHO concentrations. Ethene and other olefins were the source of 58-62% of the HCHO produced and aromatics were responsible for 10-12%. It was concluded that the CB4 mechanism can be used to predict ambient HCHO levels with an error of about 20%.

17. KEY WORDS AND DOCUMENT ANALYSIS

a. DESCRIPTORS	b. IDENTIFIERS/OPEN ENDED TERMS	c. COSATI Field/Group

18. DISTRIBUTION STATEMENT RELEASE TO PUBLIC	**19. SECURITY CLASS** *(This Report)* UNCLASSIFIED	**21. NO. OF PAGES** 311
	20 SECURITY CLASS *(This page)* UNCLASSIFIED	**22. PRICE**

EPA Form 2220-1 (9-73)

PB90-240581

EPA/600/3-90/052

July 1990

A Chamber and Modeling Study To Assess the Photochemistry of Formaldehyde

H. E. Jeffries, K. G. Sexton,
J. R. Arnold, Y. Bai, J.L. Li, and R. Crouse

Department of Environmental Sciences
and Engineering
School of Public Health
University of North Carolina
Chapel Hill, N.C. 27514

Cooperative Agreement 813964

Project Officer
Marcia Dodge

Chemical Processes and Characterization Division
Atmospheric Research and Exposure Assessment Laboratory
Research Triangle Park, N.C. 27711

ATMOSPHERIC RESEARCH AND EXPOSURE ASSESSMENT LABORATORY
OFFICE OF RESEARCH AND DEVELOPMENT
U. S. ENVIRONMENTAL PROTECTION AGENCY
RESEARCH TRIANGLE PARK, N.C. 27711

REPRODUCED BY
U.S. DEPARTMENT OF COMMERCE
NATIONAL TECHNICAL
INFORMATION SERVICE
SPRINGFIELD, VA 22161

Abstract

Because of a growing concern about the health risks of exposure to formaldehyde (HCHO), the U.S. EPA is considering regulating HCHO ambient levels. An initial exposure assessment conducted by EPA concluded that 80–90% of the ambient HCHO was produced by the photochemical oxidation of other hydrocarbons (HC). Thus photochemical reaction models would have to be used to relate emissions and emission controls to ambient levels of HCHO. Current photochemical models accepted by EPA for use in oxidant prediction were not specifically developed to predict HCHO; such predictions are coincidential to the ozone predictions. In fact, the model developers had reservations about the HCHO chamber data and had only made limited comparisons between the model predictions and the observations for HCHO. In particular, it had been suggested by model developers that the UNC HCHO chamber measurements may have suffered from positive interferences and thus could be too high by almost a factor of two. Thus the accuracy of HCHO predictions obtained with the existing EPA photochemical models was uncertain mainly because of a lack of believable measurements of HCHO in the chamber data used to develop and test the models.

The purpose of this study was to determine if existing EPA photochemical reaction mechanisms could be used to predict accurate ambient levels of HCHO. The approach taken was a) to implement and test newer and more reliable HCHO analytical methods and calibration sources for use in UNC chamber experiments; b) to conduct new chamber experiments with newer and older HCHO analytical methodology; c) to compare new results with those in the existing 12-year data base used to develop the EPA models; d) to perform modeling exercises to diagose problems in data and model formulations; and e) to examine HCHO predictions obtained with the Carbon Bond Four (CB4) mechanism in light of new information.

A new diffusion-scrubber, fluorescence detector, HCHO monitor (Dasgupta Monitor) was implimented and its performance was compared with seven different techniques for measuring HCHO. These tests included intercomparisons with the long path FTIR system at the University of California at Riverside and with EPA's DNPH/HPLC method (both of these use different standards than at UNC). The absolute accuracy of UNC's calibration system was shown to be ±2% at 155 ppb HCHO. Furthermore, the precision of calibration of the newer and older HCHO monitoring methods was shown to be better than ±10% when 4 replicate determinations of the calibration factor were used. The newer and older instruments, based upon totally different chemical principles, showed excellent agreement for a wide range of chamber HCHO levels. Thus we have strong evidence that the UNC HCHO chamber data are accurate. Therefore, the disagreement among model and chamber observations is due to inaccurate representations in the models.

An explicit photochemical reaction mechanism was formulated using existing kinetics data reviews and the literature. The mechanism includes explicit chemistry for methane, formaldehyde, ethane, acetaldehyde, organic nitrates and peroxyacetylnitrate, ethene, glycoaldehyde, glyoxal, propene, and detailed radical representations. Particular attention was paid to the state of knowledge for the fate of the Criegee biradicals as review suggested that this was the most likely area in the existing EPA mechanisms where carbon was being treated as unreactive and therefore omitted. The explicit mechanism was used to simulate: a) the kinetics of ozone-ethene experiments conducted by Su, Calvert, and Shaw and by Hatakeyama and colleagues; b) NO_x-CO experiments, HCHO-NO_x experiments, acetaldehyde-NO_x experiments, many ethene-NO_x experiments and many propene-NO_x experiments conducted in the UNC chamber. In almost all cases except propene, the agreements

between the simulations and the observations were excellent for NO_x, O_3, HCs, and HCHO. In propene, the theory and the sparse kinetics information for the two-carbon Criegee biradical are in substantial disagreement with the chamber results for NO_x-propene experiments. Some modelers have made *ad hoc* adjustments to the propene-ozone mechanism to allow better simulation of chamber data and in doing so may have compromised the HCHO predictions.

A comparison of the explicit mechanism's predictions with that of the CB4 mechanism leads to suggestions for modifying these mechanisms to predict HCHO better.

A time-resolved mass balance method was used to analyze the HCHO predictions obtained with a simple trajectory model. This analysis shows that even though the initial HC mixture contained 3% HCHO, within 300 minutes this initial HCHO is diluted and reacted away and more than 90% of the HCHO in the air parcel is caused by photochemical oxidation reactions of other VOCs.

We conclude that CB4 can be used to produce reasonably accurate HCHO predictions; there are errors in some parts of this mechanism but the errors are small, probably resulting in no more than a 20% error in the HCHO predictions.

DISCLAIMER

This report has been reviewed by the U. S. Environmental Protection Agency, and approved for publication. Approval does not signify that the contents necessarily reflect the views and policies of the U. S. Environmental Protection Agency, nor does mention of trade names or commercial products constitute endorsement or recommendation for use.

Contents

1 **Introduction** 1

Background 1

Purpose 5

Approach 5

2 **Analytical Methods** 7

Calibration Standards and Sources 7
- Injection of Paraformaldehyde into the Chambers 8
- Permeation of Paraformaldehyde (Dynamic source of HCHO) 9
- Formaldehyde Stock Solution 10
- EPA DNPH SGC Calibration Source 10

Analytical Methods and Instrumentation 12
- Chromotropic Acid Bubbler 12
- CEA Automated Modified Schiff Procedure 13
- Dasgupta Diffusion Scrubber System 17
- EPA DNPH Cartridges 24
- Belman Fluorimetric Technique 25
- Nash Colorimetric-Bubbler Technique 26

History of UNC HCHO Analytical Methods 27

Quality Assurance and Analysis 30
- Quality Assurance Procedures 30
- Calibration Databases 31
- Calibration Standards Comparison At UNC 33

Calibration Standards Comparison at UCR/EC 38

Assessment of Overall Measurement Uncertainty 42
- Accuracy of HCHO Measurements 42
- Precision 42

UNC and SAPRC Joint HCHO Experiments 45
- ITC Results 45

3 New Experiments 52

4 Explicit Mechanism: 1 76

A Species Hierarchy 76

Reaction Modules 76

Special Rate Constant Forms 77

I = Inorganic Chemistry 78
  Section a: NO_2 photolysis 80
  Section b: O_3 photolysis 83
  Section c: $NO_3^{\cdot}$ Chemistry 86
  Section d: HONO Chemistry 89
  Section e: $HO_2^{\cdot}$-NO_X Reactions 90
  Section f: $^{\cdot}OH$ Termination Reactions 92
  Section g: $HO_2^{\cdot}$ Termination Reactions 92
  Section h: CO/H_2 Reactions 93

P1 = Methane Chemistry 95

C1 = Formaldehyde Chemistry 100

P2 = Ethane Chemistry 107

C2 = Acetaldehyde Chemistry 109

PA1 = Peroxyacetyl Radical Chemistry 110

5 Chamber Modeling: 1 112

UNC Chamber Specific Reactions 112
  Adjustable Inputs for Chamber-Dependent Reactions 117
  Other Chamber-Related Model Inputs 119

Carbon Monoxide Simulations 120

Initial Formaldehyde Simulations 123

Initial Acetaldehyde Simulations 130

6 **Explicit Mechanism: 2** 142

O2 = Ethene Chemistry 142
- Section a: O(3P) attack 143
- Section b: $^{\cdot}OH$ Attack 143
- Section c: $NO_3^{\cdot}$ Attack 148
- Section d: O_3 Attack 149

BR1 = Criegee Biradical Chemistry 152

GA = Glycoaldehyde Chemistry 161
- Selection of Rate Constant for PGAN Decomposition 167

D2 = Glyoxal Chemistry 171

7 **Chamber Modeling: 2** 178
- Chamber Conditions for ITC Ethene Simulations 179

Extent of "Reasonable Agreement" 180

Carbon Balances in an Ethene System 203

8 **Explicit Mechanism: 3** 206

O3 = Propene Chemistry 206

O3.d = Ozone+Propene Chemistry 207

BR2 = Two Carbon Criegee Biradical Chemistry 208

Nighttime Propene Simulation 211

9 **Chamber Modeling: 3** 213

Extent of "Reasonable Agreement" 214

10 CB4 Comparison 231

CB4 Mechanism for Acetaldehyde, Ethene, and Propene 231
  Acetaldehyde 231
  Ethene 232
  Propene 233

Comparison of Explicit and CB4 Predictions 234

Extent of "Reasonable Agreement" 235

Mass Balance Analysis of CB4 and EXP Simulations 244

11 Urban Modeling 248

Conditions 248

Mass Balance Analysis 249

Conclusions From Analysis 267

12 Conclusions 271

Formaldehyde Measurements 271

Formaldehyde Chemistry 272

Ethene Chemistry 273

Propene Chemistry 274

Performance of CB4 275

Urban Simulations 276

Final Conclusion 277

References 278

M Mechanism Listings 282

Tables

1. Names and Abbreviations Used for HCHO Methods and Calibration Sources 9
2. Response of Various Compounds Tested For Interference to Dasgupta Monitor 26
3. Joint UNC-UCR Experiments Conducted at UCR 45
4. Initial Conditions for New Experiments 53
5. Cross Sections and Quantum Yields for NO_2 81
6. Cross Sections and Quantum Yields for O_3 84
7. Cross Sections and Quantum Yields for O_3 85
8. Cross Sections and Quantum Yields for NO_3 87
9. Cross Sections and Quantum Yields for NO_3 87
10. Cross Sections and Quantum Yields for HONO 90
11. Cross Sections and Quantum Yields for H_2O_2 93
12. Cross Sections and Quantum Yields for $H_2C{=}O$ 103
13. Cross Sections and Quantum Yields for $H_2C{=}O$ 104
14. Cross Sections and Quantum Yields for $CH_3HC{=}O$ 110
15. Chamber-Dependent Reaction Parameters Used 118
16. Initial Conditions and integrated reaction rates for selected reactions for four dual $CO{-}NO_X$ experiments 121
17. Integrated Reaction Rates for Simulation of Su, Calvert, Shaw's ozone and ethene experiments with the UNC Explicit Mechanism. 157
18. Cross Sections and Quantum Yields for $(HC{=}O)_2$ 175
19. Cross Sections and Quantum Yields for $(HC{=}O)_2$ 177
20. Mass Balance for Explicit and CB4 Mechanism 247

Figures

1. Formaldehyde Production and Loss Cycle 2
2. Examples of model predictions of UNC smog chamber data for formaldehyde. 4
3. Formaldehyde and selected HC profiles obtained in SAPRC ITC replicate chamber experiment 5
4. Schematic of Dynacalibrator Permeation Tube Conditioner 10
5. Formaldehyde Permeation Tube Mass History 11
6. Example Calibration Curve for Chromotropic Acid Method 13
7. Diagram of CEA Formaldehyde Monitor 14
8. Photocopied Example Output of CEA Monitor for Ideal Operating conditions 15
9. BAC? Photocopied Example Output of CEA Monitor for non-Ideal Operating conditions 17
10. Schematic of Dasgupta Scrubber 18
11. Diagram of Dasgupta Formaldehyde Monitor 19
12. // Example of Output of Dasgupta Monitor in Ideal Operating Condition 20
13. Response of Dasgupta Fluromonitor to HCHO standards 21
14. Step Injection of Paraformaldehyde and Response of CEA and UNC-Dasgupta Formaldehyde Monitor 22
15. // Example of Output of Dasgupta Monitor in non-Ideal Operating Condition 23
16. Example of Data from Output of Dasgupta Monitor in non-Ideal Operating Condition: July 15, 1988 24
17. Response of Dasgupta Monitor to Permeation Tube for 10 hours 25
18. Response of Carle 211 GC with methanizer to 1.2 ppm formaldehyde and zero air with 1.5 ppm methane 28
19. Calibration Factor History of CEA Monitor for 1986 32
20. Calibration Factor History of CEA Monitor for 1988 32
21. Calibration Factor History of CEA Monitor for 1989 33
22. Calibration Factor History of Dasgupta Monitor for 1988 33
23. Calibration Factor History of Dasgupta Monitor for 1989 34
24. Diagram of Comparison of Formaldehyde Methods and Standards 36
25. Calibration Factors for CEA for 1986 Intercomparison Study 37
26. Comparison of Formaldehyde Methods and Standards 38
27. Comparison of Three HCHO Methods the UCR-SAPRC EC Chamber 40
28. Results of UCR smog chamber experiments: October 3 and 4, 1989 47
29. Results of UCR smog chamber experiments: October 5 and 9 1989 48
30. Results of UCR smog chamber experiments: October 10 and 11 1989 49
31. Results of UCR smog chamber experiments: October 12 1989 50
32. Differential ethene concentrations at same NO_x: JL0688 54
33. Differential ethene concentrations at same NO_x: JL0688 55
34. Differential formaldehyde concentrations at same NO_x: JL1588 56
35. Differential formaldehyde concentrations at same NO_x: JL1588 57
36. Differential ethene concentrations at same NO_x: AU0988 58
37. Differential ethene concentrations at same NO_x: AU0988 59
38. Differential ethene concentrations at same NO_x: AU1088 60
39. Differential ethene concentrations at same NO_x: AU1088 61

40. Differential propene concentrations at same NO_X: AU1288 62
41. Differential propene concentrations at same NO_X: AU1288 63
42. Formaldehyde vs. ethene at same NO_X: AU1688 64
43. Formaldehyde vs. ethene at same NO_X: AU1688 65
44. Toluene vs. M-xylene at same NO_X: AU1788 66
45. Toluene vs. M-xylene at same NO_X: AU1788 67
46. Differential Synthetic Auto-exhaust concentrations at same NO_X: AU1888 68
47. Differential Synthetic Auto-exhaust concentrations at same NO_X: AU1888 69
48. Propene vs. 1-butene at same NO_X: ST0788 70
49. Propene vs. 1-butene at same NO_X: ST0788 71
50. Background air vs. formaldehyde at background NO_X: ST2788 72
51. Background air vs. formaldehyde at background NO_X: ST2788 73
52. Differential ethene concentrations at same NO_X: AU0389 74
53. Differential ethene concentrations at same NO_X: AU0389 75
54. A Species Hierarchy 77
55. Comparison of Bass and Moortgat Formaldehyde Absorption Cross Sections 101
56. In-chamber Formaldehyde Photolysis Rates 102
57. Formaldehyde Absorption Cross Sections and Quantum Yields. 105
58. Background VOC from a cannister sample within 15 miles of the chamber site. 114
59. Water Uptake on FEP Teflon Film as a Function of Relative Humidty 116
60. Carbon Monoxide and Nitrogen Oxides Experiment in UNC Outdoor Smog Chamber and Simulation with UNC Explicit Mechanism 123
61. Carbon Monoxide and Nitrogen Oxides Experiment in UNC Outdoor Smog Chamber and Simulation with UNC Explicit Mechanism 124
62. Carbon Monoxide and Nitrogen Oxides Experiment in UNC Outdoor Smog Chamber and Simulation with UNC Explicit Mechanism 125
63. Carbon Monoxide and Nitrogen Oxides Experiment in UNC Outdoor Smog Chamber and Simulation with UNC Explicit Mechanism 126
64. Carbon Monoxide and Nitrogen Oxides Experiment in UNC Outdoor Smog Chamber and Simulation with UNC Explicit Mechanism 127
65. Formaldehyde and Nitrogen Oxides Experiment in UNC Outdoor Smog Chamber and Simulation with UNC Explicit Mechanism 130
66. Formaldehyde and Nitrogen Oxides Experiment in UNC Outdoor Smog Chamber and Simulation with UNC Explicit Mechanism 131
67. Formaldehyde and Nitrogen Oxides Experiment in UNC Outdoor Smog Chamber and Simulation with UNC Explicit Mechanism 132
68. Formaldehyde and Nitrogen Oxides Experiment in UNC Outdoor Smog Chamber and Simulation with UNC Explicit Mechanism 133
69. Formaldehyde/Acetaldehyde and Nitrogen Oxides Experiment in UNC Outdoor Smog Chamber and Simulation with UNC Explicit Mechanism 134
70. Formaldehyde/Acetaldehyde and Nitrogen Oxides Experiment in UNC Outdoor Smog Chamber and Simulation with UNC Explicit Mechanism 135
71. Acetaldehyde and Nitrogen Oxides Experiment in UNC Outdoor Smog Chamber and Simulation with UNC Explicit Mechanism 138
72. Acetaldehyde and Nitrogen Oxides Experiment in UNC Outdoor Smog Chamber and Simulation with UNC Explicit Mechanism 139
73. Acetaldehyde and Nitrogen Oxides Experiment in UNC Outdoor Smog Chamber and Simulation with UNC Explicit Mechanism 140

74. Acetaldehyde and Nitrogen Oxides Experiment in UNC Outdoor Smog Chamber and Simulation with UNC Explicit Mechanism 141
75. Mechanism for hydroxyl radical initiated oxidation of ethene 144
76. Sensitivity of Simulation to Hydroxy-alkyl-nitrate Formation, NO_x data 146
77. Sensitivity of Simulation to Hydroxy-alkyl-nitrate Formation: HC data 147
78. Mechanism for ozone initiated oxidation of ethene 150
79. Simulation of Su, Calvert, Shaw's ozone and ethene experiments with the UNC Explicit Mechanism. 155
80. Simulation of Su, Calvert, Shaw's ozone and ethene experiments with the UNC Explicit Mechanism. 156
81. Mass Balance on HCHO in Su, Calvert, Shaw systems 158
82. Simulation of Hatakeyama's ozone and ethene experiments with the UNC Explicit Mechanism. 159
83. Yields of formic acid and formaldehyde as a function of water vapor in the photolysis of ketene 161
84. Scheme for peroxymethylene reaction with water 161
85. Temperature and dewpoint in chamber during experiment 162
86. Ozone injected into ethene in BLUE chamber; background air and injected ozone only in RED 163
87. Ozone injected into ethene in BLUE chamber; background air and injected ozone only in RED 164
88. Mechanism for oxidation of glycoaldehyde 165
89. Effect of setting PGAN decomposition rate to 20 times PAN rate in both summer and fall experiments 169
91,92?
90. Carbon Species Predicted in 3.2 ppmC Ethene Experiment 171
93. Sensitivity of Simulation to Additonal PGAN Loss Reaction, Summer and Fall 172
94. Sensitivity of Simulation to Additonal PGAN Loss Reaction at Different Ethene Concentrations 173
95. Explicit mechanism simulation: AU1688 180
96. Explicit mechanism simulation: AU1688 181
97. Explicit mechanism simulation: JL0986 182
98. Explicit mechanism simulation: JL0986 183
99. Explicit mechanism simulation: AU0988 184
100. Explicit mechanism simulation: AU0988 185
101. Explicit mechanism simulation: AU0389 186
102. Explicit mechanism simulation: AU0389 187
103. Explicit mechanism simulation: AU2378 188
104. Explicit mechanism simulation: AU2378 189
105. Explicit mechanism simulation: AU1088 190
106. Explicit mechanism simulation: AU1088 191
107. Explicit mechanism simulation: JL0688 192
108. Explicit mechanism simulation: JL0688 193
109. Explicit mechanism simulation: OC0584 194
110. Explicit mechanism simulation: OC0584 195
111. Explicit mechanism simulation: ITC 4.0 ppmC Ethene Experiment 196
112. Explicit mechanism simulation: ITC 4.0 ppmC Ethene Experiment 197
113. Explicit mechanism simulation: ITC 8.0 ppmC Ethene Experiment 198
114. Explicit mechanism simulation: ITC 8.0 ppmC Ethene Experiment 199

115. Carbon Balance Predicted in 3.2 ppmC Ethene Experiment 204
116. Relative Organic Contributions to HCHO, $HO_2^{\cdot}$, NO_2, and O_3 Predicted in 3.2 ppmC Ethene Experiment 205
117. Mechanism for Two Carbon Creigee Reaction 209
118. Ozone injected into propene in BLUE chamber; background air and injected ozone only in RED 212
119. Explicit mechanism simulation: JL1386 214
120. Explicit mechanism simulation: JL1386 215
121. Explicit mechanism simulation: OC1184 216
122. Explicit mechanism simulation: OC1184 217
123. Explicit mechanism simulation: OC1284 218
124. Explicit mechanism simulation: OC1284 219
125. Explicit mechanism simulation: JL3078 220
126. Explicit mechanism simulation: JL3078 221
127. Explicit mechanism simulation: OC0484 222
128. Explicit mechanism simulation: OC0484 223
129. Explicit mechanism simulation: OC0484 224
130. Explicit mechanism simulation: AU1288 225
131. Explicit mechanism simulation: AU1288 226
132. Explicit mechanism simulation: ST0788 227
133. Explicit mechanism simulation: ST0788 228
134. Comparison of PAN Rates Used in CB4 and EXP Mechanisms 233
135. Explicit mechanism simulation: AU1088 235
136. Explicit mechanism simulation: AU1088 236
137. Explicit mechanism simulation: JL0688 237
138. Explicit mechanism simulation: JL0688 238
139. Explicit mechanism simulation: OC0584 239
140. Explicit mechanism simulation: OC0584 240
141. Explicit mechanism simulation: OC0484 241
142. Explicit mechanism simulation: OC0484 242
143. Explicit mechanism simulation: OC0484 243
144. Relative Organic Contributions to HCHO, $HO_2^{\cdot}$, and NO_2 Predicted in 3.2 ppmC Ethene Experiment by CB4. 246
145. Ozone and Nitrogen Oxides Concentration-Time Profiles for Base Case and Zero Initial Aldehyde 251
146. Ozone Sources and Sinks As a Function of Time 253
147. Formaldehyde Sources and Sinks: Day Average 255
148. Formaldehyde: Net Sources 257
149. Formaldehyde: Sources and Sinks 259
150. Contribution of HCHO from Each HC: Day Average 261
151. Contribution of HCHO from Each HC: Time Analysis 263
152. Relative Contribution From HCs With More Than One Reaction Producing HCHO: Day Average 265
153. Relative Contribution From HCs With More Than One Reaction Producing HCHO: Time Analysis Base Case 267
154. Relative Contribution From HCs With More Than One Reaction Producing HCHO: Tiem Analysis Zero Initial Aldehyde Case 268

Acknowledgements

We are indebted to William Carter, University of California, Riverside and Mike Gery, Atmospheric Research Inc., for their time and cooperation in sharing their mechanisms and drafts of their current development work. Without this contribution, this project would not have been possible. We also thank Jim Killus for discussions and preprints of papers on wall effects.

Special thanks go to Roger Atkinson for sharing a pre-print of his latest kinetics review before publication.

We thank William Wilson, EPA, for making available the funds under the U.S. EPA/People's Republic of China Cooperative Agreement that enabled two of the authors to visit UNC for a year.

We also thank students at UNC for careful efforts in performing data processing and quality assurance activities on our data files.

1

Introduction

Background

In a memorandum written in 1986,[1] Charles Gray, Director of the Emissions Control Technology Division (ECTD) at EPA, described work undertaken by ECTD and by the Pollutant Assessment Branch (PAB) of the Office of Air Quality Planning and Standards (OAQPS) to perform a preliminary formaldehyde exposure assessment. Below is a summary from this memorandum:

- Current outdoor urban exposures to formaldehyde may be responsible for up to 2000 tumors per year.
- Direct formaldehyde emissions from point sources do not appear to contribute substantially to the total (less than one tumor per year).
- Photochemical decomposition of hydrocarbons is the largest source of ambient formaldehyde.
- Combustion processes are the second largest source.
- The analysis did not account for indoor source or workplace related exposure to formaldehyde. Both of these may be significant contributors to tumorgenesis.
- There were various uncertainties in the existing analysis which require clarification.

The analysis conducted by ECTD and PAB suggested that 80–90% of the formaldehyde ($HCHO$ or $H_2C{=}O$) originates from the photochemical creation of $HCHO$ in the reactions of other VOC emissions and the direct emission of formaldehyde from fuel combustion. This is not surprising, since in theory, formaldehyde is a photooxidation product of *all* hydrocarbon species. Its major global source is the oxidation of methane (CH_4) by hydroxyl radical ($^{\cdot}OH$). But formaldehyde is not only ***produced*** in the photooxidation of other species, it is itself a key ***reactant*** (see

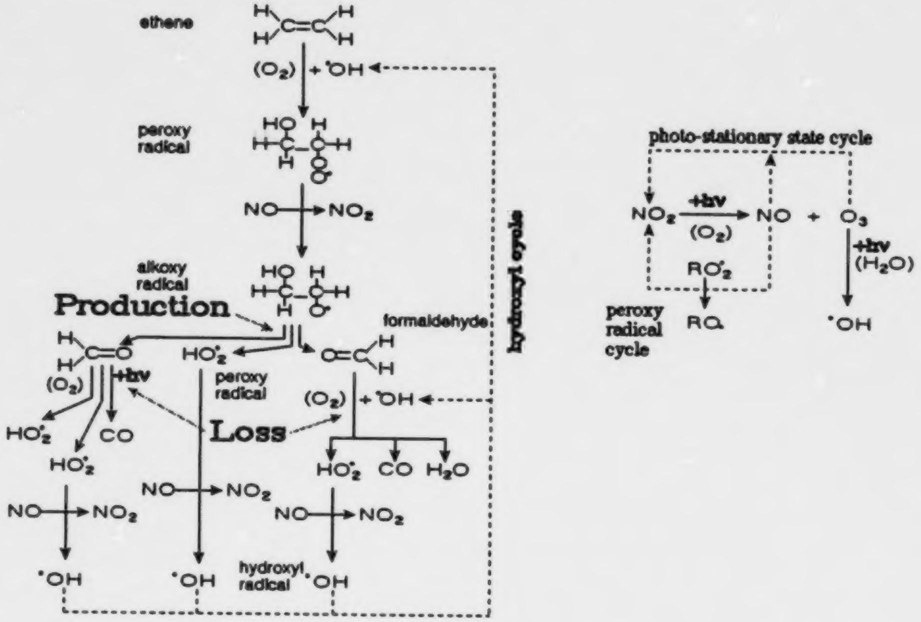
ethene
(O_2) + •OH
peroxy radical
NO → NO_2
alkoxy radical
Production
formaldehyde
$HO_2^•$
peroxy radical
+hv
(O_2)
CO
H_2O
Loss
hydroxyl radical
•OH
hydroxyl cycle
photo-stationary state cycle
NO_2 → NO + O_3
(O_2)
$RO_2^•$
RO
+hv (H_2O)
peroxy radical cycle

Figure 1. Formaldehyde Production and Loss Cycle. Nitrogen dioxide photolysis ($h\nu$) and peroxy radical oxidation cycle.

Figure 1): it is an important ingredient in producing and maintaining the photooxidation process. Photolysis of formaldehyde *is* a major source of the radicals that make photochemical smog possible. These radicals convert NO to NO_2, thereby making ozone, and produce other radicals that oxidize hydrocarbons, producing more formaldehyde. These same radicals also consume formaldehyde. Thus, one useful image of its chemistry is one in which formaldehyde is in a time-dependent, dynamic equilibrium in the sunlit atmosphere: it is created by oxidation of hydrocarbons; it is consumed by the same oxidation process; it is also consumed by photolysis which produces radicals that ultimately consume hydrocarbons to produce more formaldehyde, a process that is in part dependent upon the levels of NO_x present in the atmosphere.

Even this simple view of the system reveals some of the complex and interconnectedness of the atmospheric chemistry that produces formaldehyde. This description therefore suggests that only through the use of atmospheric simulation models containing chemical mechanisms developed with the help of reliable chamber data are we likely to produce a sound understanding of formaldehyde atmospheric concentrations.

Chemical reaction mechanisms are developed using laboratory kinetics data for those reactions that have been studied and kinetics reasoning coupled with fitting chamber data for those reactions not yet studied in the laboratory.[2,3] The current reaction mechanisms are quite good for ozone, but tend to significantly underpredict formaldehyde concentrations in many single hydrocarbon chamber experiments (see Figure 2).[4] The reaction mechanisms for these simple hydrocarbon systems are supposed to be well-understood,[5,6] so given such poor agreement between the model predictions and the observations, modellers had hypothisized that the UNC formaldehyde data were often too high—perhaps by as much as a factor of two.[2]

The quality of the SAPRC formaldehyde data has also been questioned. In 1986, Carter said:

> The reliability of the SAPRC formaldehyde data have been variable over the years, and there are a number of runs where anomalously low formaldehyde measurements (compared to yields observed in replicate runs, or amounts known to be injected into the chamber) were obtained. These anomalously low readings are attributed to problems with sample collection efficiency. ... More infrequently, anomalously high measurements (presumably due to contamination) are obtained, but usually these anomalous data points are isolated and thus can be readily identified as such. At best, the SAPRC formaldehyde data is precise to within ±20–30% and is useful only for formaldehyde concentrations above approximately 50 ppb.

An example of replicate-run variability in the SAPRC formaldehyde data is shown in Figure 3.

Because photochemical decomposition of hydrocarbons was recognized as the major source of HCHO, OAQPS asked if the photochemical oxidant models could be used to predict HCHO ambient levels for various scenarios of VOC and individual HC control. In meetings with OAQPS staff and ORD researchers, Jeffries argued that, based on his testing of models with UNC chamber data,[4] and based on the modelers' own tests,[2,3] the chemical mechanisms likely to be used in such applications (*e.g.*, CB4 or CAL) had problems predicting HCHO accurately. He stated that both mechanisms ***under-predicted*** HCHO yields in simple olefin systems (*e.g.*, ethene and propene), and ***over-predicted*** yields in single-component aromatics systems (*e.g.*, toluene and the xylenes). The models showed better agreement with HCHO observations in various synthethic urban mixtures, but he argued that this was the result of compensating errors between low predictions in the olefins portion of the HC mixture and high predictions in the aromatics portions of the mixture. Thus depending upon the mixture composition, the model fits to the experimental HCHO data would agree or disagree with experimental data. Thus, an ambient air application of the mechanisms could have variable accuracy for HCHO, depending upon the urban HC

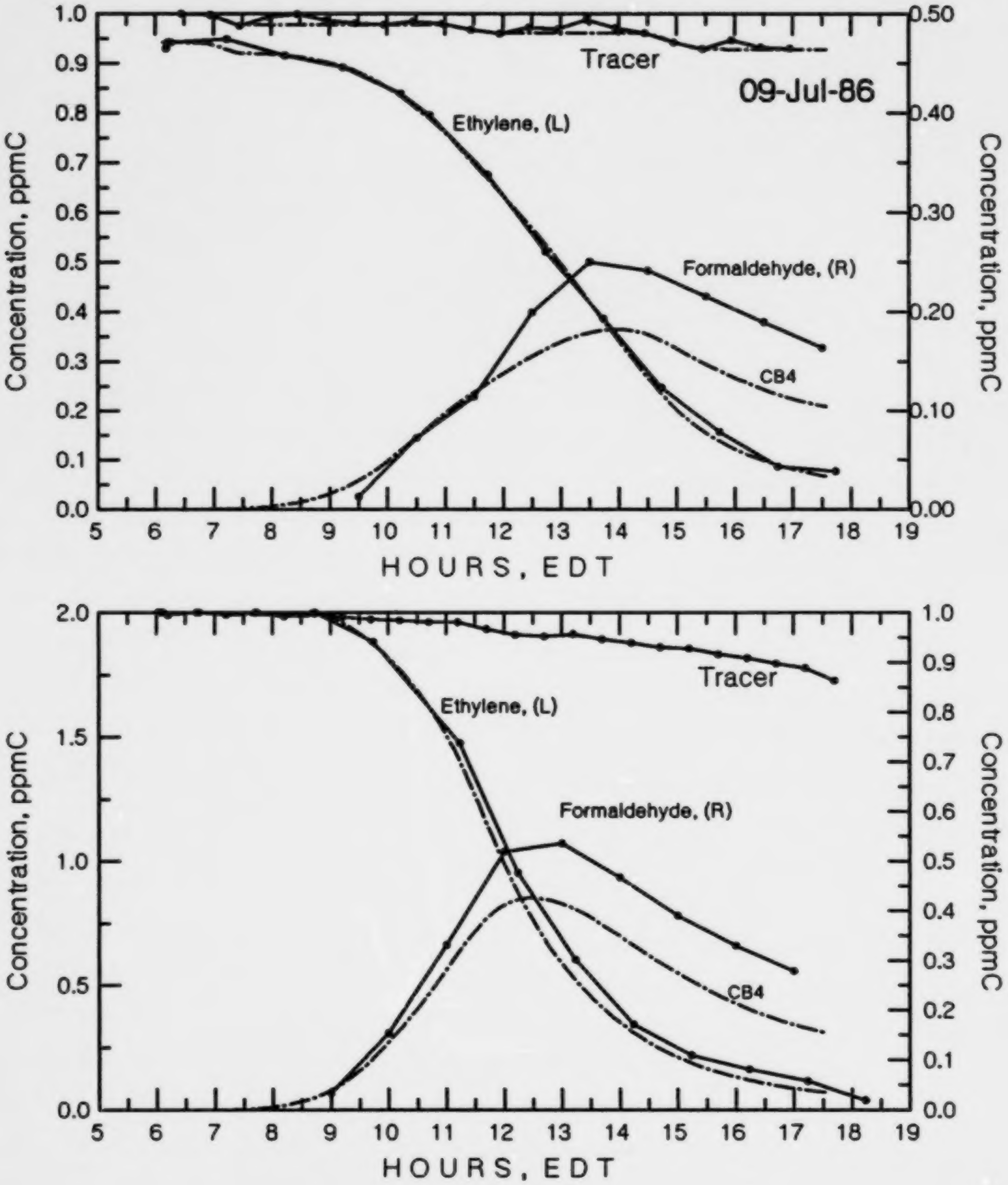

Figure 2. Examples of model predictions of UNC smog chamber data for formaldehyde. Two initial concentrations of ethene at same NO_x.

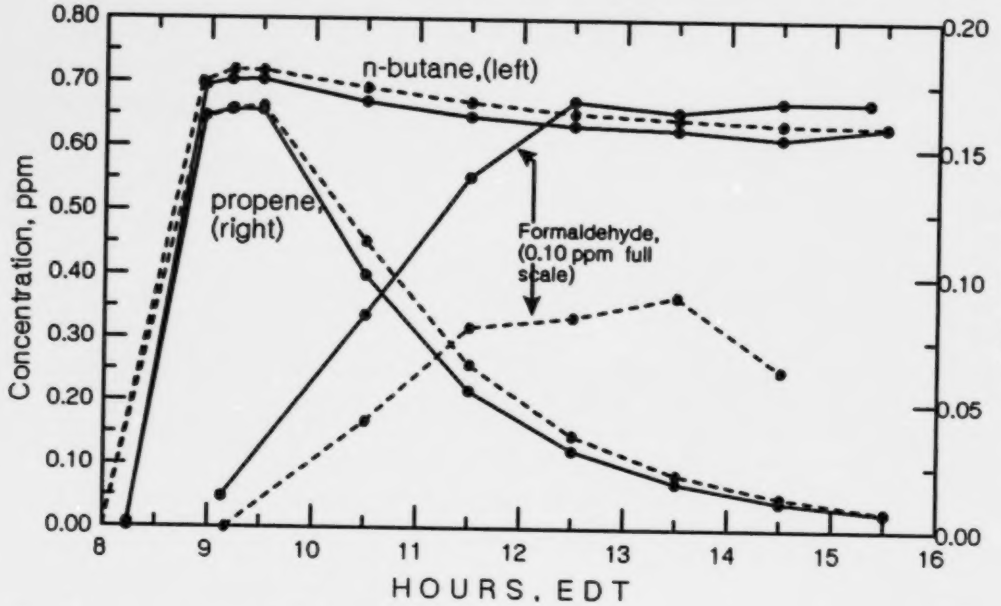

Figure 3. Formaldehyde and selected HC profiles obtained in SAPRC ITC replicate chamber experiments. Initial conditions were 4.00 ppmC synthetic urban HC mixture and 0.090 ppm NO_x; only two HC profiles shown.

composition used in the simulation.

The alternative to the models being incorrect was that the UNC HCHO data *were* too high. Although the most likely interfering compounds had been tested, there still remained the possibility that the UNC HCHO measurement method was subject to positive interferences.

Thus, it was important to assess the cause of the difference between HCHO data from smog chambers and the model predictions. The major component in this assessment had to be new, confirming data for HCHO yields in the chamber experiments.

Purpose

The purpose of this study was to determine if present photochemical reaction mechanisms could be used to predict accurate ambient levels of HCHO.

Approach

The approach for this study was to:

- implement and test an additional HCHO analytical method for use in smog chambers;
- conduct new chamber experiments to determine HCHO yields; compare new HCHO yields with those in the existing chamber data base used to develop and test existing mechanisms;
- perform modeling exercises including diagnostic tests with an explicit mechanism to demonstrate extent of agreement between model predictions and observed HCHO yields;
- compare explicit mechanism predictions with those from currently accepted EPA air quality modeling mechanisms (*i.e.*, CB4 and CAL); and
- analyze CB4 predictions of HCHO in urban scenarios.

Each of these topics will be covered in a separate chapter.

2

Analytical Methods

The purpose of this chapter is to describe the accuracy and precision of formaldehyde measurements made in this study. This chapter will also show what quality assurance (QA) procedures were performed to assure that the measurements were reliably made and that resulting data were carefully processed in both the present study and in past formaldehyde work.

This chapter is divided into six sub-sections:

1) Calibration Standards
2) Analytical Methods
3) QA Procedures
4) History of Formaldehyde Methods and QA Procedures at UNC
5) Accuracy, Precision, and Uncertainty Analysis of HCHO data
6) SAPRC/UNC Formaldehyde Intercomparison of HCHO Measurements

Table 1 lists the analytical methods, calibration sources, and abbreviations which will be used throughout this report.

Calibration Standards and Sources

Calibration sources of formaldehyde include:

- serial dilutions of standard liquid 37% formaldehyde which can be standardized by titration with sodium thiosulfate which in turn can be calibrated by titration with potassium dicromate, and

- solid paraformaldehyde which can be weighed and sublimed to yield gaseous HCHO:
  - ▹ 50-200 mg sublimed into a large known volume (smog chamber) or
  - ▹ continuous sublimation from a permeation tube into a dilution flowstream.

Paraformaldehyde can be injected into a dark chamber for a single point standard. The problem with this method is that it requires the use of the chamber, which then must be vented after the calibration and before it can be used to set-up an experiment. Therefore the calibration using the chamber is performed the day before or after the experiment, and we must assume no change in instrument sensitivity from the time of calibration to that of the experiment. A dynamic source of HCHO is needed for routine and convenient calibration of ambient HCHO monitors the same day of the experiment. A permeation tube containing paraformaldehyde was used for this purpose. Its output can be directly determined by its weight-loss history. The concentration produced by the dynamic source was also determined by other techniques and monitored to assure its stability. The output from the dynamic calibrator can be sampled for long periods of time and easily analyzed with methods which may not be sensitive enough for ambient use but have other absolute calibration standards (such as chromotropic acid). These methods require liquid formaldehyde standards which are analyzed by titration against recognized primary standards such as potassium dichromate. In this study we also had independent analyses performed by Tejada at the U.S. Environmental Protection Agency (EPA) in the Research Triangle Park (RTP), North Carolina.[7] Details about the different sources follow. Consistency among different calibration sources provides conclusive evidence about the accuracy of the measurements.

Injection of Paraformaldehyde into the Chambers

The UNC chambers are very large and accurate amounts of paraformaldehyde can be precisely weighed and sublimed into the large volume (about 200 mg gives 1 ppm). The paraformaldehyde (J.T. Baker Chemical S898-7 Lot 540717) for chamber injections was weighed on an 4-place, stabilized analytical balance located at the site. The balance is a Christian Brothers Torbal Model SEA-1, capable of measuring 200 mg mass with a precision of 0.05%. The accuracy of the balance is routinely checked with a series of standard lab scale weights (Will Corporation). The weighted mass was sublimed or injected by heated air passing over the solid in a U-tube directly under the chamber. The Teflon tubing line from the U-tube to the chamber was less than 6 inches. The chamber volume was determined previously by three independent strapping operations which agreed to within 0.5%. All injection

Table 1. Names and Abbreviations Used for Methods and Calibration Sources

Item	Abbreviation
Paraformaldehyde Permeation Tube	UNC-DynaCal
Paraformaldehyde Solid Sublimation	
Formaldehyde Stock Solution	
Dasgupta Scrubber-Nash Reagent	UNC-Dasgupta
CEA 555 Modified Shiff Procedure	UNC-CEA
UNC Chromotropic Acid Bubbler	UNC-CAB
UCR Chromotropic Acid Bubbler	UCR-CAB
Belman Bubbler	UNC-Belman
Nash Bubbler	UNC-Nash
EPA 2,4-DNPH on Silica Gel Cartridge	EPA-DNPH
UCR-FTIR	UCR-FTIR

lines and sample lines are heated (standard procedure). In these calibration operations, the HCHO monitors first sample background and then the injected amount. The initial reading before any decay occurs is reported as the calibration response. This injection procedure has been used since 1976 and our experience has shown that this is a reproducible technique yielding results highly consistent with several other methods of calibration.

Permeation of Paraformaldehyde (Dynamic source of HCHO)

Constant mass-loss in a controlled flowrate yields a continuous, dynamic, stable source of HCHO.[8] This source was used for routine calibration of the continuous HCHO monitors. A permeation tube (Type 2300, 5.0-cm, SN 81-33586 from VICI Metronics Dynacalibrator) containing paraformaldehyde (supplied by Fluka, lot no. 76240, 100% pure) was purchased and installed in a Dynacalibrator temperature-controlled, flow-controlled, permeation tube conditioner (also manufactored by VICI Metronics - Dynacalibrator Model 300-05) to produce a continuous stable source of sub-ppm concentration levels of formaldehyde in air. Zero-air from an Addco zero-air generator is passed over the permeation tube at a stable fixed rate and temperature (70°C), and diluted with additional zero air (adjustable but stable; monitored with a rotameter) to obtain the desired concentration range needed (see Figure 4). The permeation tube mass was measured throughout the study (see Figure 5). Standard operation procedures include observing the temperature and

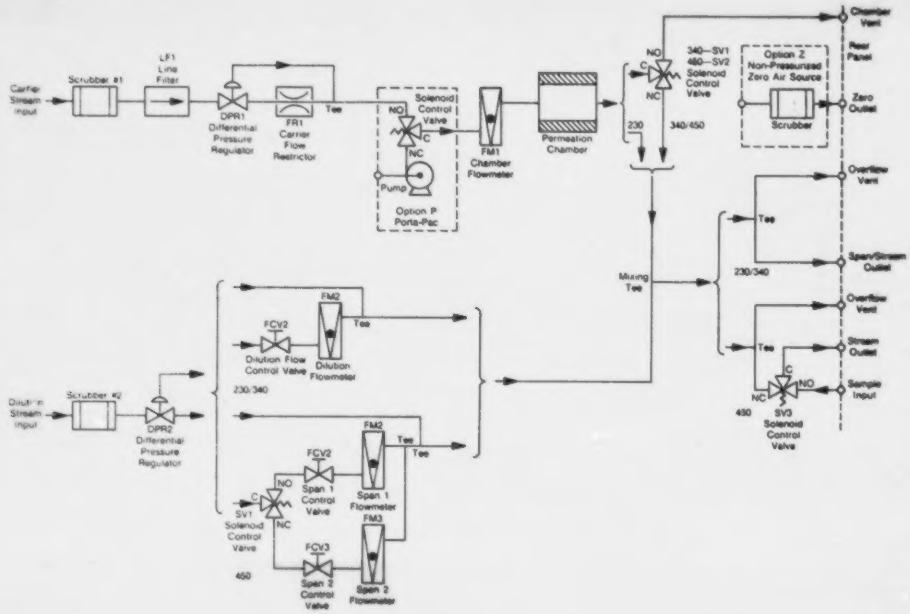
Carrier Stream Input
Scrubber #1
LF1 Line Filter
DPR1 Differential Pressure Regulator
FR1 Carrier Flow Restrictor
Tee
Solenoid Control Valve
NO
C
NC
Pump
Option P Porta-Pac
FM1 Chamber Flowmeter
Permeation Chamber
NO
C
NC
340—SV1
480—SV2
Solenoid Control Valve
230
340/450
Option Z Non-Pressurized Zero Air Source
Scrubber
Chamber Vent
Rear Panel
Zero Outlet
Overflow Vent
Tee
Span/Stream Outlet
230/340
Mixing Tee
Overflow Vent
Tee
Stream Outlet
C
NO
NC
Sample Input
450
SV3 Solenoid Control Valve
FM2
FCV2
Tee
Dilution Flow Control Valve
Dilution Flowmeter
230/340
Dilution Stream Input
Scrubber #2
DPR2 Differential Pressure Regulator
FM2
Tee
Tee
FCV2
NO
C
Span 1 Control Valve
Span 1 Flowmeter
SV1 Solenoid Control Valve
NC
FM3
FCV3
450
Span 2 Control Valve
Span 2 Flowmeter

Figure 4. Schematic of Dynacalibrator Permeation Tube Conditioner

rotameter setting on the Dynacalibrator sytems frequently and logging the check on the stripchart along the calibration response. The flowrate of the total air output is checked with a bubbletower and stopwatch.

Formaldehyde Stock Solution

A stock solution for serial dilutions for standards necessary for various wet chemical methods was prepared from 36.5% $HCHO$ (Fisher, Lot 876132) and analyzed by titrations back to I_2, with sodium thiosulfate ($Na_2S_2O_3$), which was further titrated with potassium dicromate ($K_2Cr_2O_7$). The source of the potassium dicromate was EM Science PX1445-1 Lot no. 7055 which after careful drying and weighing was treated as a primary standard. The procedure followed for standardization of formaldehyde solution is given in Standard Methods for Air Pollution.[9]

EPA DNPH SGC Calibration Source

Tejada at the EPA at the Research Triangle Park has a method for measuring ambient aldehydes including $HCHO$ using 2,4-dinitro-phenyl-hydrazine (EPA-DNPH-

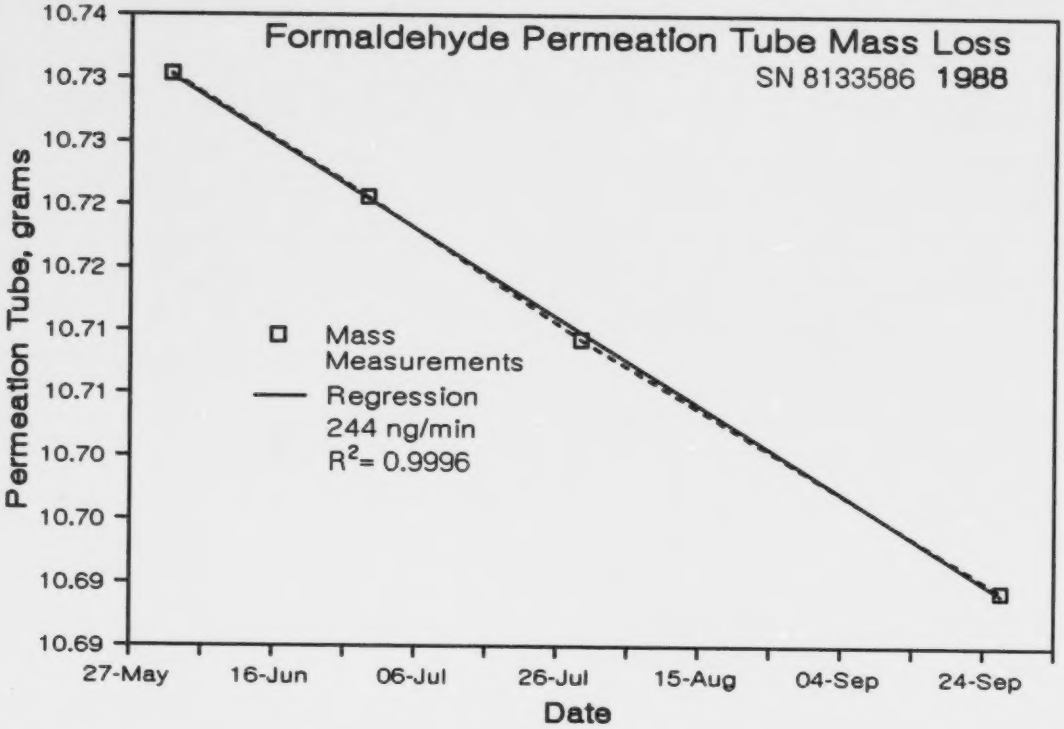

Figure 5. Formaldehyde Permeation Tube Mass History

SGC) coated on a silica gel cartridge (see full desciption below). Cartridges were used for sampling from the permeation tube source. In addition cartridges were taken to UCR to sample HCHO injections in the Riverside chambers. These cartridges were returned to EPA for analysis. The standards used in the EPA chromatography were made by dissolving weighed quantities of pure hydrazone derivatives of the aldehydes in acetonitrile (ACN). The hydrazone derivatives were prepared by reaction of individual carbonyl compounds with saturated DNPH solution in 2 N HCl. Purity was determined by melting point measurement and by HPLC analysis. These analyses provided an excellent independent cross-comparison to our own standards.

Analytical Methods and Instrumentation

Chromotropic Acid Bubbler

In this method air is sampled through a bubbler containing 0.1% chromotropic acid in concentrated sulfuric acid solution. A purple monocationic chromogen is formed when HCHO reacts with the chromotropic acid. The sample is heated and then analyzed by measuring its absorbance at 580 nm.[10] Serial dilutions of a stock HCHO solution standardized by titration are used to prepare standards. Usually two bubblers are used in series. The main limitation of this method is its low sensitivity. To obtain a sufficiently large color development for a reliable reading, a sample of at least 30 minutes is required; 60 minutes is better for lower concentrations. Because the measurement is a time-average peak concentrations may be missed, and few measurements can be made during one experiment.

The procedure is:

1. Reagents:
   i) Chromotropic acid solution: 0.1% chromotropic acid in concentrated sulfuric acid.
   ii) Dilute standard formaldehyde solution: 100 μg(HCHO)/ml.
2. Preparation of calibration curve: Transfer separately exactly 10, 8, 6, 4, and 2 ml of the dilute standard formaldehyde solution to five 100 ml volumetric flasks and dilute each to the mark with distilled water. These solutions should contain approximately 10, 8, 6, 4, and 2 μg of HCHO per ml. Transfer separately 1.0 ml of each test solution into 10 ml volumetric flasks. Add to each approximately 7 ml of 0.1% chromotropic acid solution and cool to room temperature; then dilute to the mark with additional 0.1% chromotropic acid solution. Transfer the contents of the volumetric flasks to Pyrex test tubes and heat in a boiling water bath for 15 minutes. Allow the solutions to cool to nearly 25°C and then measure the absorbance and transmission of each test solution against an acid blank at 580 nm. A Bausch & Lomb Spectronic 20 spectrophotometer was used. Calibrations were performed for every day the chromotropic acid method was used (13 different days). Figure 6 shows an example calibration curve.
3. Sampling: Assemble a sampling train in the following order: two all-glass absorbers (Mae West bubblers with filter sampling tubes) in which 15 ml and 10 ml of 0.1% reagent solution have been separately added, trap to protect the flowmeter, pressure gauge, and vacuum pump. Before and after sampling, the actual flow rate was determined by means of a soap bubble flowmeter. Additionally, a 1 m manometer was added at the outlet of the vacuum pump to

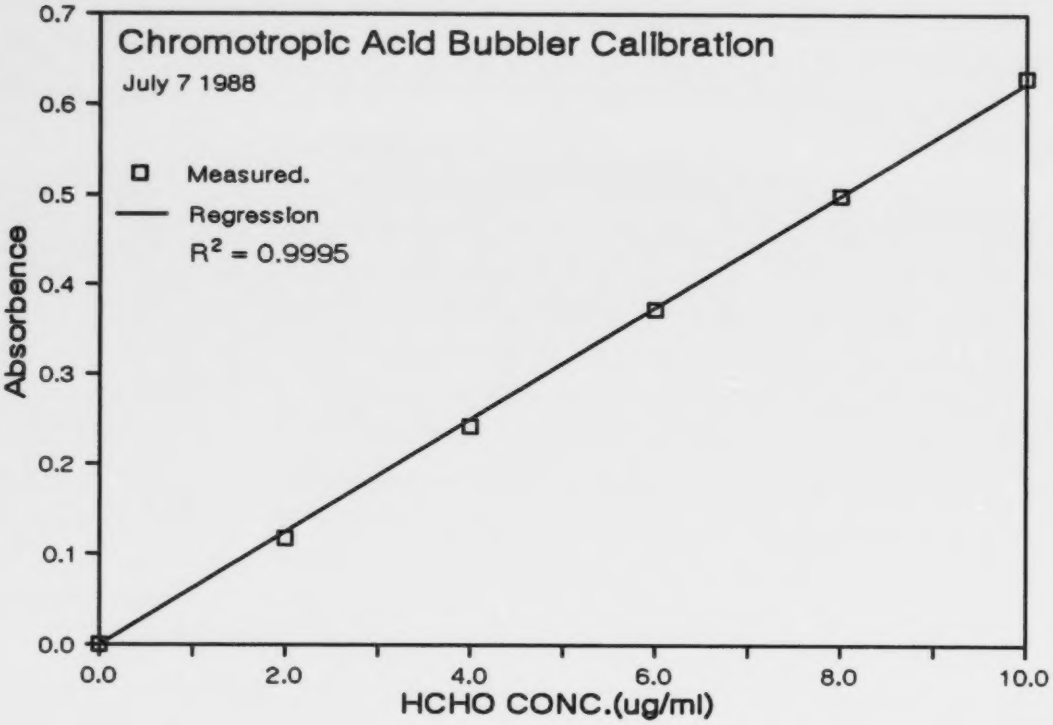

Figure 6. Example Calibration Curve for Chromotropic Acid Method

insure that the flowrate did not vary during the sample. The actual air sample was drawn through the sample train at approximately 0.5-1.0 liter/min for approximately 60 minutes. The absorbing reagent, now colored by the sample of HCHO, was transferred from the absorbers to a Pyrex test tube and heated at 100°C, allowed to cool, and then read in the spectrophotometer according to the same protocol described above for the HCHO standards curve.

CEA Automated Modified Schiff Procedure

CEA Instruments, Inc. of Westwood, NJ manufactures a HCHO monitor based on the automated modified Schiff procedure developed by Lyles, Dowling, and Blanchard[11] and hence requires a continuous supply of wet chemicals which include highly purified pararosanaline, mercuric chloride, sodium chloride, and sodium sulfite. HCHO in air is absorbed in a sodium tetrachloromercurate solution that contains a fixed quantity of sodium sulfite. Acid bleached pararosaniline is added, and the intensity of the resultant dye is measured at 550 nm. See Figure 7 for diagram.

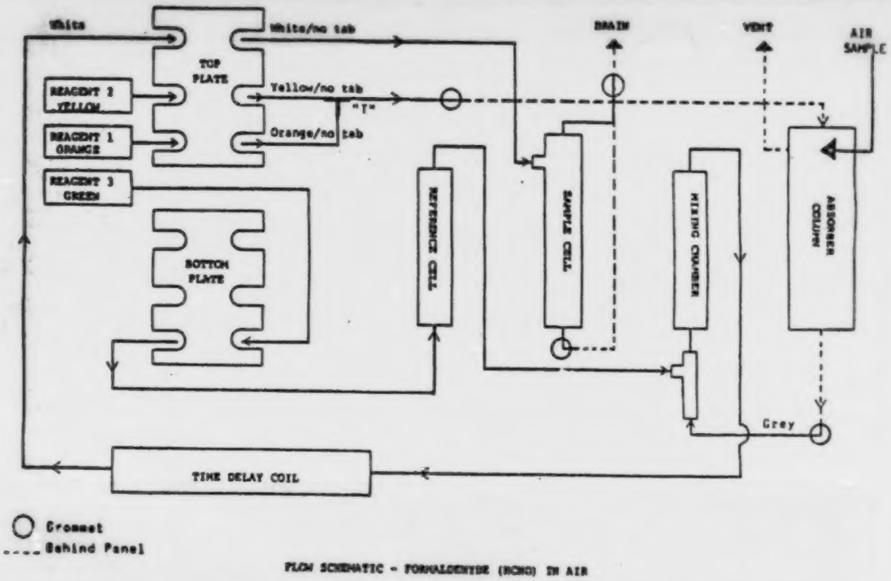
White
White/no tab
TOP PLATE
REAGENT 2 YELLOW
Yellow/no tab
"T"
REAGENT 1 ORANGE
Orange/no tab
REAGENT 3 GREEN
BOTTOM PLATE
REFERENCE CELL
SAMPLE CELL
MIXING CHAMBER
ABSORBER COLUMN
DRAIN
VENT
AIR SAMPLE
Grey
TIME DELAY COIL
Grommet
Behind Panel
FLOW SCHEMATIC - FORMALDEHYDE (HCHO) IN AIR

Figure 7. Diagram of CEA Formaldehyde Monitor

Sensitivity: When first purchased in 1979, the CEA instrument was much less noisy and hence its minimum concentration detection level was much lower than it is today. The original specifications stated by the manufacturer were 2 ppb detection limit. We originally felt confident in a minimum reading of 5 to 10 ppb. Today the detection limit is 15–20 ppb. Normal sensitivity is about 200 ppb per inch of chart deflection. It has a lag time of about 15 minutes and requires 15 to 20 minutes to achieve full change of response. An example of the instrument output is shown in Figure 8.

Calibration Procedures: For this study, the permeation tube was used as the routine calibration source, usually twice daily. The sample line of the CEA instrument is connected to the output of the Dynacalibrator. After allowing the instrument to sample through a zero filter of activated charcoal, the response is recorded. Another technique used for cross-comparison in this study and used more often historically at UNC, is the slug injection of paraformaldehyde into the chamber, typically resulting in HCHO concentrations of 500, 1000, and 2000 ppb. Stock HCHO solutions were used in the past, prepared by serial dilution of 37% formaldehyde solution to produce standards of about 1 mg/liter (equivalent to about 300 ppb in air given the instrument liquid and air flowrates).

Linearity: Injecting different concentrations of paraformaldehyde into the two

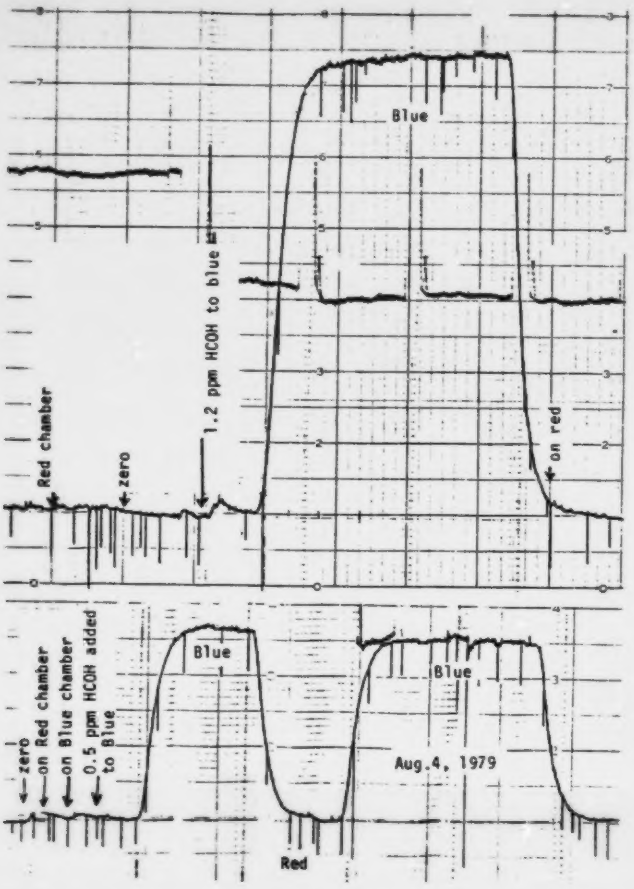

Figure 8. Photocopied Example Output of CEA Monitor for Ideal Operating conditions.

chamber halves plus cross-comparing with the response from the permeation tube calibration concentration have demonstrated that this instrument is linear in response. Several other types of tests have also been performed to test linearity. The flowrate of the dilution air for the permeation tube was altered to change the calibration concentration by more than a factor of two. As will shown later in the intercomparison of calibration sources and methods, linearity was demonstrated by agreement of the CEA's output with all other methods over this most important concentration range. Linearity has been demonstrated many times in response to the initial conditions of delta-concentration formaldehyde experiments. Further linearity tests were indirectly performed by obtaining good agreement with the Dasgupta HCHO monitor, over the full range of formaldehyde observed in smog chamber experiments. See discussion below. A night-time injection-test with paraformaldehyde was also performed to test for linearity of the CEA system (see discussion and data below under Dasgupta method below).

__Stability (and Causes of Less-Than-Ideal Performance):__ Several factors affect the stability of this instrument. The calibration is dependent on the air sampling flow rate. The flowrate is monitored with a rotameter which is checked at calibrations performed before and after the experiment and frequently during the experiment. When flowrate changes it usually drifts downward resulting in an under-reporting of the true concentration. The instrument also has a 30–50% zero drift over a 3–4 hour period, which requires that the instrument sample a zero air source every few hours to allow the baseline to be established; a clock timer is used to switch the inlet valve to a zero HCHO stream about every three hours. If a zero baseline can not be well established, then the HCHO concentrations would most likely be over-reported; this occasionally happens due to failure of the zeroing clock. In the 1986 intercomparison study conducted at UNC, the zero sample valve had to be loaned to visitors and therefore only before and after experiments zero-checks were performed for this period. Interruptions of the reagents flow from aging and crimping of the pump tubing also can suddenly effect the output of the instrument. Pieces of crystals, dye and other chemical residue occasionally dislodge from within the instrument and effect flow and light transmittance. Changes in output from reagent flow and dislodging of chemical residue are usually short term. Build-up of dye within the optical sensor slowly decrease the response. When the change is noticeable, the system is flushed with dilute nitric acid. Calibrations performed within one day (before and after an experiment) are usually very similar. Calibrations over the course of the summer can be seen to change from day to day (see later calibration discussion). An example of non-Ideal operation is shown in Figure 9.

__Interferences:__ The CEA company specifications state that there are no significant interferences citing Lyles *et al.*.[11] They also show data from a successful equivalency test with the chromotropic acid bubbler method. In our experience, acetaldehyde appears to respond approximately 5% as much as formaldehyde. A large amount of formic acid was nebulized into the smog chamber and gave no response on the CEA.

__Standard Operating Procedures:__ The instrument is started the night before an experiment to allow time for a stable baseline to be achieved and for a stable calibration response. Calibrations were performed at least before and after the experiment. The instrument is allowed to sample through a zero charcoal filter every two hours. The instrument is time- shared between the two chamber halves

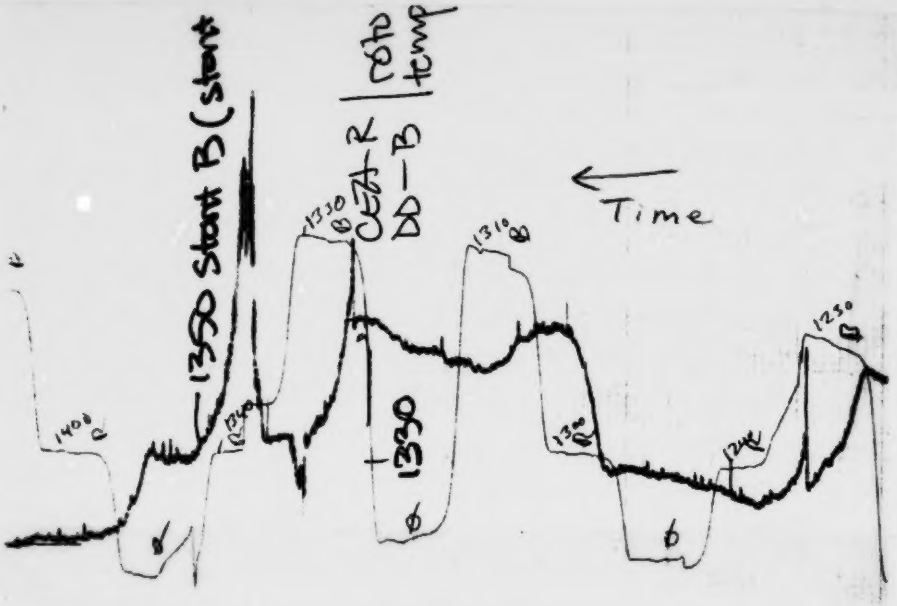

Figure 9. Photocopied Example Output of CEA Monitor for non-Ideal Operating conditions

every 30 minutes to allow full response to change in concentrations.

Dasgupta Diffusion Scrubber System

Water is pumped continuously through a filament-filled, narrow-bore microporous hydrophobic membrane tube while sample air flows around it, providing a high gas sampling rate to liquid flow rate (see Figure 10). According to studies conducted by Dasguta,[12] a constant fraction of HCHO gas is collected in the liquid. The effluent is mixed with a modified Nash reagent (154 g ammonium acetate, 0.6 ml 2,4-pentanedione, 3 ml glacial acetic acid, diluted to 1 liter with water,[13] incubated at 95°C for 25 seconds, and then analyzed with a fluorescence detector,[14] (see Figure 11). The light source is a 406 nm phosphor coated mercury pen lamp. The excitation filter is 410 nm and the emission filter is 480 nm and above.

The 2,4-pentanedione procedure is based on the Hantzsch reaction, the cyclization of a β-diketone, an amine and an aldehyde to form a dihydropyridine derivative, in this case, 3,5-diacetyl-1,4-dihydrolutidine (DDL), selected for selectivity for formaldehyde by Nash.[13] The mechanism of the Hantzsch reaction involves the following sequential steps: a) condensation of one molecule of formaldehyde

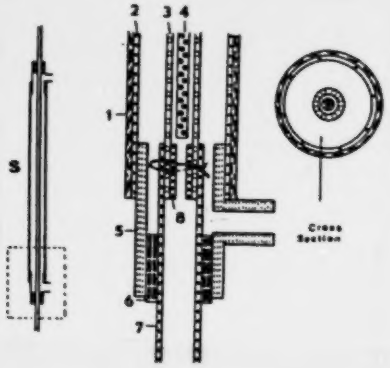

Figure 10. Schematic of Dasgupta Scrubber. The whole scrubber is given in diagram S. Center drawing shows the dotted portion in detail; a cross section is shown on right. The membrane tube, 3, (Celgard X-20, 400 μm i.d., 25 μm wall, 40% surface porosity, 0.02 μm mean pore size) is about 40 cm in length. A length of Nylon fishing line, 4, is inserted inside the membrane tube. Tube 2 is a 6.5 mm i.d. Teflon tube to form the outer air channel.

with one molecule of 2,4-pentanedione, b) condensation of a second molecule of 2,4-pentanedione with the product from a, c) condensation of ammonia with the product from b and cyclization. All three steps involved in the reaction require elimination of water and therefore temperature has a very large effect on the reaction rate. Dasgupta found that the reaction is 80% complete when the residence time of a sample in the bath (H in Figure 11) is 25 sec and the temperature of the bath is maintained at 95°C. While raising the bath temperature provides an adequate product yield in a short time, bubble formation in the flowstream exiting the bath causes severe problems. Flow restriction (L) at the detector outlet to increase system backpressure greatly reduces bubble formation and the porous membrane tube (T) de-bubbler placed before the detector provides a simple and effective solution.

Sensitivity: Dasgupta reports a detection limit of 360 ppt at a signal-to-noise ratio of 3, with a 40 cm long scrubber and an air sample rate of 1.5 L/min. The fluorescence detector has several selectable sensitivity ranges. Normal operating procedures are to calibrate and operate the instrument on only one range, selected to keep the output signal within range of the recorder during the entire experiment. Fortunately the output is not very noisy for experiments that produce as much as 1 ppm HCHO, and the minimal detectable concentration under these conditions is

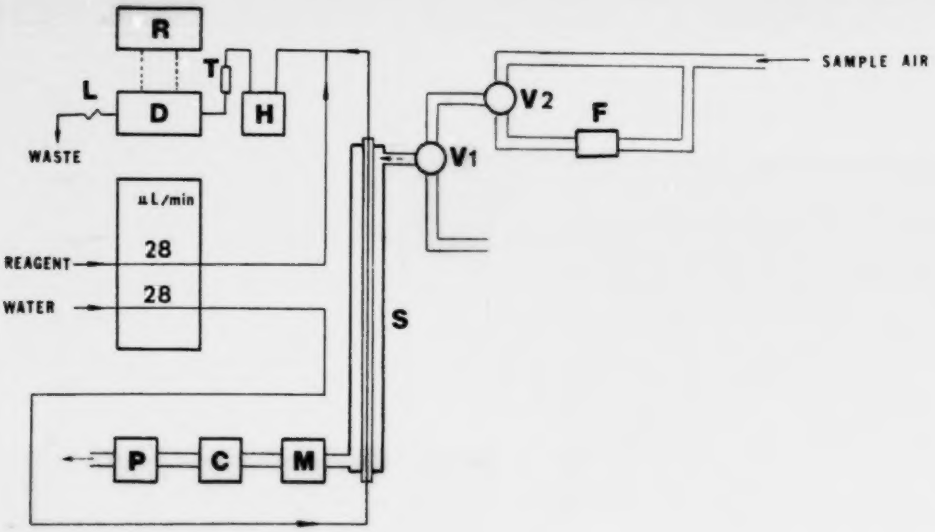

Figure 11. Diagram of Dasgupta Formaldehyde Monitor. Air flow: F–HCHO zero filter; V1, V2–valves; S–scrubber; P–pump; C–mass flow controller; M–mass flow monitor. Liquid Flow: pump; S–scrubber; H– heated bath; T–porous tube de-bubbler; D–detector; L–restriction tube; R–recorder.

about 2 to 3 ppb. For experiments producing concentrations less than 100 ppb, the signal is noisier but is still allows for concentrations less than 1 ppb to be detected. An example is shown in Figure 12. It has a lag time of about 6 minutes and requires 3 minutes to achieve full change of response. Dasgupta's original purpose for this method was to use it for ambient-level concentrations which are much less than those observed in chambers. For maximum analyses per unit time, Dasgupta adjusted the timers used to switch between zero, cal and sample to short time periods. Therefore his calibrations are for the short sampling periods which only reach about 90% of full response. In our work, we realized that it took longer to reach the widest full range of response from the larger range of concentrations observed in the chamber, hence the longer sample and zero times used.

Linearity: Belman[14] reported a slight non-linearity in response in the higher concentration ranges of formaldehyde absorbed in solution. Dasgupta demonstrated linearity for better than three-orders-of-magnitude range in formaldehyde concentration with the scrubber. As part of implementing this method, a wide range of liquid standards (0.01 to 3 μg/ml) were prepared from the stock formaldehyde solution discussed above. The standards were pumped into the system where normally

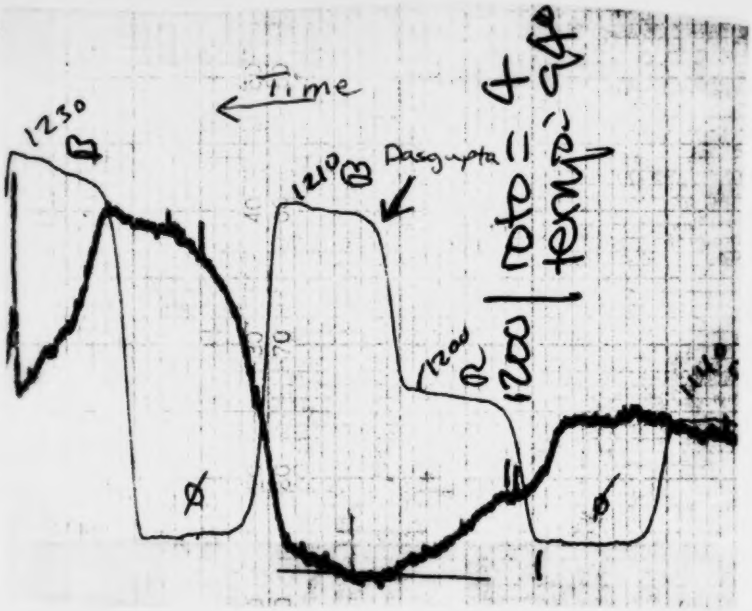

Figure 12. Photocopy of Recorder Output for Dasgupta Monitor in Ideal Operating Condition

the scrubber water from the diffusion tube would be pumped. The response is linear for the range used here for the Dasgupta method. This test was performed on seven different days (see Figure 13; note there are many low concentration points in this figure). Several types of tests were also performed to test linearity with the scrubber included. The flowrate of the dilution air for the permeation tube was altered to change the calibration concentration by more than a factor of two and linearity of the Dasgupta method was demonstrated over this most important concentration range. Linearity has been demonstrated many times in response to the initial conditions of delta-concentration formaldehyde experiments. Further linearity tests were indirectly performed by obtaining good agreement with the CEA over the full range of formaldehyde observed in smog chamber experiments. See discussion below.

A night-time injection of paraformaldehyde was also performed to test for linearity for the whole Dasgupta system including scrubber (see Figure 14). Paraformaldehyde was injected in approximately 40 mg increments starting at 2030 EDT. The first three injections were separated by 50 minutes. The next two each occured 100 minutes apart. The injected formaldehyde is corrected for chamber temperature and dilution. After the last injection, a decay rate was observed of approximately

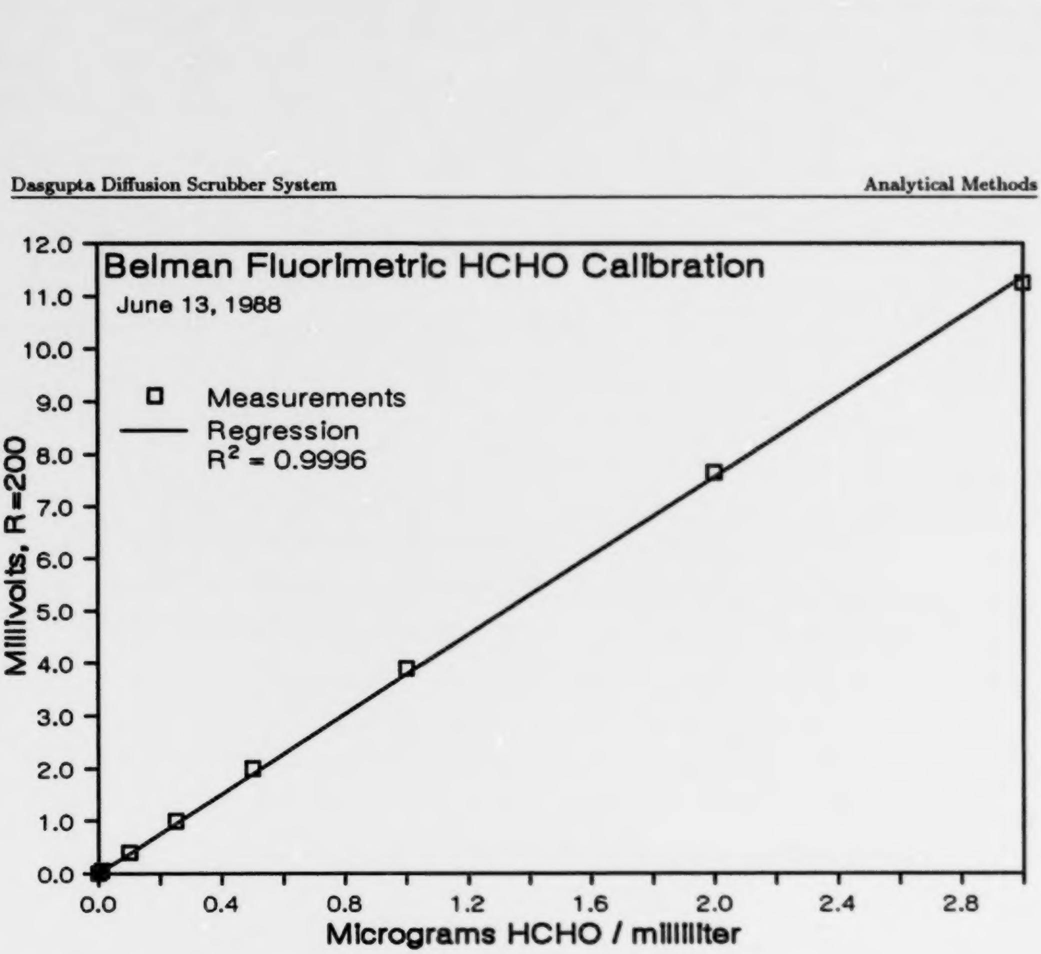

Figure 13. Response of Dasgupta Fluromonitor to HCHO standards

0.2 ppm/300 minutes (not used to correct the calculated injection concentrations). This explains the apparent curve in the response from the two instruments. There is more curvature in the last two points because of more time between the injections allowing for more decay, and being later in the night, the chamber walls were much cooler with a higher relative humidity resulting in a faster decay rate. The Dasgupta monitor is essentially linear in the earlier hours of the night when the injections were more frequent (minimal wall absorption) and both instruments track each other well. The difference between the two instruments demonstrates the possible disagreement when calibrated with a source of 0.155 ppm and then used to sample higher concentrations. The range or attenuation was not changed during the experiment, so the calibration was performed on the range used to measure the expected high response from the 1 ppm concentration. Therefore the response for the permeation tube at this range and for most smog chamber experiments is about 10% of the stripchart or instrument output. The slight difference shown in the data is accounted for by slight differences in precision in reading the response from the calibration standard accurately, less than 1% of the stripchart recorder or

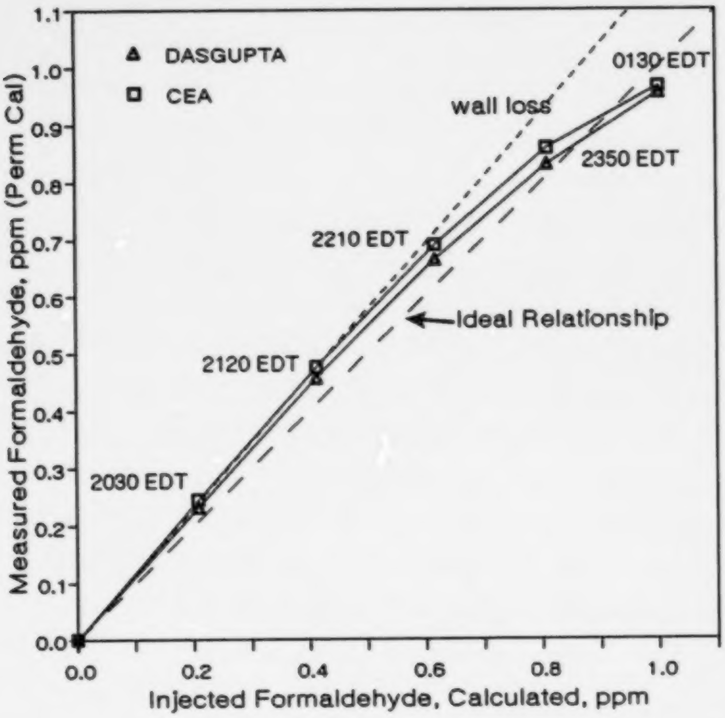

Figure 14. Step injection of paraformaldehyde into chamber on night of August 1-2, 1988 and response of UNC-CEA and UNC-Dasgupta Formaldehyde monitors

instrument output. This explains or accounts for the results which will be shown later, that the precision is about ± 10% (although the accuracy is much better).

Stability (and Causes of Less-Than-Ideal Performance): The stability of the monitor is dependent on several factors. Aging and crimping of the reagent pump tubing causes irregularities in flowrates and ultimate instrument ouput. The peristaltic pump tubing is clamped between rollers and an adjustable arm. The distance between the arm and rollers must be close enough to close off portions of the tubing but not too close to prematurely wear-out the tubing. As the tubing ages this space must be tightened to continue to assure reliable pump rates. Gas bubbles mentioned above cause sudden short-term changes in reagent flowrate and output. Occasional cleaning of the detector cell with methanol seems to help reduce output noise. An example of non-ideal operation is shown in Figure 15. It explains how the data obtained for July 6 or 15, 1988 appears as it does (Figure 16). The temperature must be maintained between 92 and 97°C to maintain the calibration. When

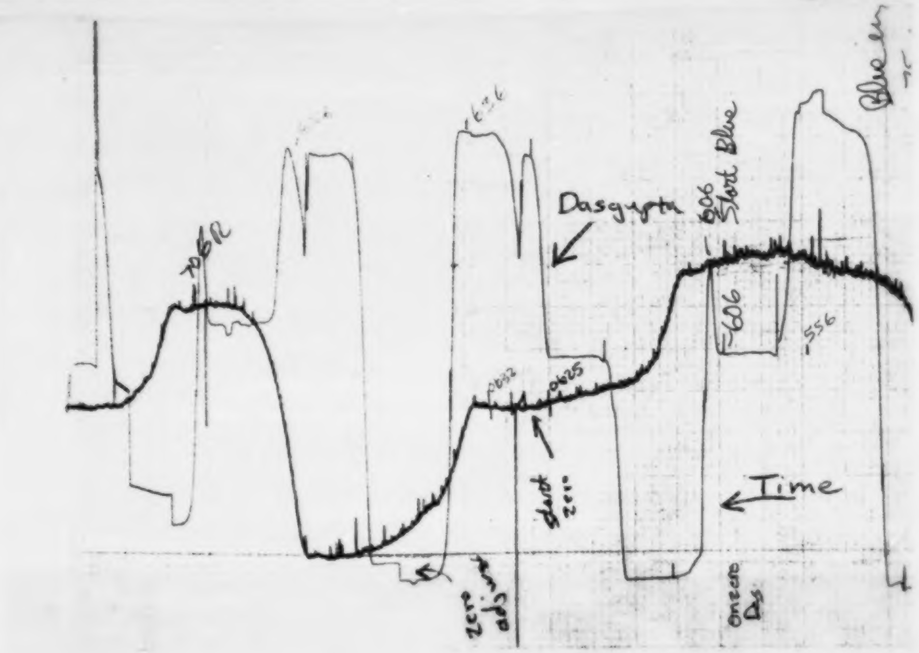

Figure 15. Photocopy of Recorder Output for Dasgupta Monitor in non-Ideal Operating Condition

the temperature drops below 85 the reaction output is noticably less. Figure 17 shows the output from the monitor from sampling from the permeation tube source continuously for 8 hours while concurrently sampling from a smog chamber experiment (July 25-26, 1988) and the zero filter. This is a better test than sampling from the permeation source alone. It shows the ability to read between zero and higher concentration levels of formaldehyde with no memory effect. The standard deviation of all the readings is 6 ppb; the relative standard deviation is 3.9%.

Interferences: The system does not show any marked interferences except to SO_2 at levels much higher than ambient concentrations.[12] Dong and Dasgupta[15] tested the response of 9 other carbonyl compounds and methanol (see Table 2). Glyoxal had the greatest response of the compounds tested giving a response of 0.81 percent as much as formaldehyde on a per molar basis. No zero nor span error was observed for the instrument for a relative humidity change of 15-85 percent. A possible 3 percent increase in the response from 15 ppb of HCHO was observed with the addition of 245 ppb of O_3.

Standard Operating Procedures: The instrument is started operating several

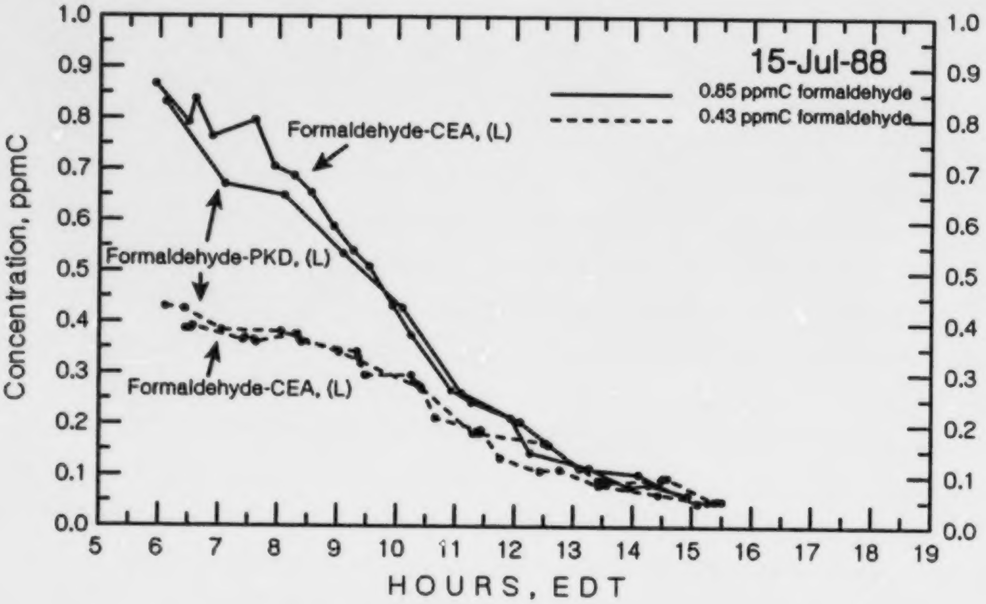

Figure 16. Example of Data from Output of Dasgupta Monitor in non-Ideal Operating Condition: July 15, 1988

hours before the start of the experiment to allow time for a stable operating temperature to be achieved and for a stable calibration response. Calibrations were performed at least before and after the experiment. On some experiments where only one side was being sampled, the permeation source was sampled throughout the day. Normal operation utilizes timers and electrically actuated valves to switch between chambers every 10 minutes with a 10 minute zeroing through activated charcoal every 30 minutes.

EPA DNPH Cartridges

This system uses commercial prepacked silica gel (100 mesh) cartridges (Sep-PAK, Waters Associates, Milford, MA) coated in situ with HCl acidified 2,4-dinitrophenylhydrazine.[7] It has been shown to be equivalent to the DNPH impinger method for sampling organic carbonyl compounds (aldehydes and ketones) including formaldehyde. The method is based on the reaction of carbonyls and DNPH to form hydrazone derivatives which are analyzed by high pressure liquid chromatography. HPLC separation was accomplished on two DuPont Zorbax ODS columns (4.6 mm by 25 cm) connected in series, using a gradient program from 60% to 100% ACN in water at 1 mL/min; in a Varian model 5000 gradient liquid chromatograph, with detec-

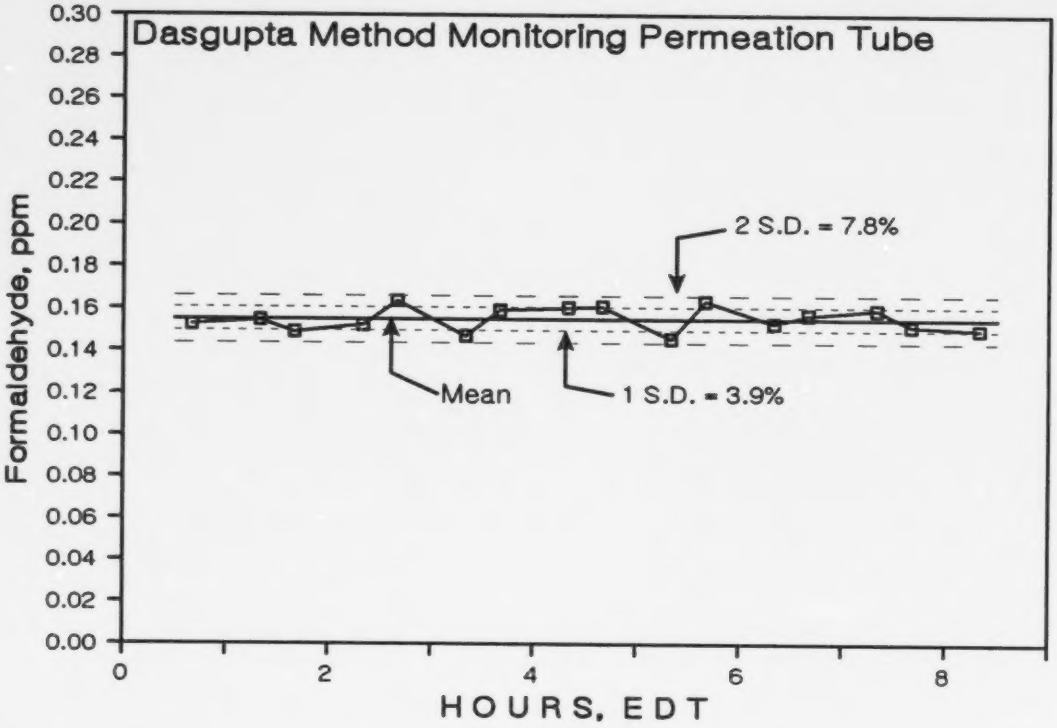

Figure 17. Response of Dasgupta Monitor to Permeation Tube for 10 hours

tion at 360 nm with an ISCO model 1840 variable wavelength detector. Peak area integration was obtained with a Spectra Physics computing integrator. Gravimetric standards were prepared with purified hydrazone derivatives checked by melting point. Air was drawn through the cartridge at a flowrate of 1 liter/min for 15 minutes. The cartridges were returned to EPA for extraction with acetonitrile and analysis by gradient liquid chromatography.

Belman Fluorimetric Technique

The Dasgupta monitor is actually an automation of the Belman fluorimetric deteremination technique (rather than colorimetric) of the Nash reagent, with the Dasgupta scrubber being utilized for sampling and absorbing HCHO in air into water very efficiently. Water samples containing HCHO can therefore be analyzed by comparing the fluorescense from the sample with the fluorescense from a series of aqueous HCHO standards. Bubblers were filled with 10 or 15 ml of water. Air samples were pulled through the bubblers at 1 liter/minute. HCHO standards covering more than two decades of concentration were prepared from the titration standard-

Table 2. Response of Various Compounds Tested For Interference to Dasgupta Monitor

Compound	Concentration Injected	Relative Fluorescence Intensity	Selectivity Factor for HCHO
formaldehyde	0.003	100.0	1
acetaldehyde	4.0	4.0	33,000
propionaldehyde	1.0	< 1.4	$> 24,000$
n-butanal	11.0	6.2	59,000
2-methylpropanal	2.0	< 1.4	$> 48,000$
3-methylbutanal	2.0	< 1.4	$> 48,000$
acrolein	2.0	5.7	11,700
glyoxal	0.10	27.0	123
glyoxalic acid	10.0	28.0	11,900
acetone	68.0	< 1.4	$> 1.6 \times 10^6$
methanol	25.0	9.5	87,000

ized HCHO stock solution discussed above. The resulting water samples were read with the same fluorescense monitor used for the Dasgupta monitor (see Figure 13).

Nash Colorimetric-Bubbler Technique

As mentioned above, Dasgupta uses the Belman Fluorescence detection technique for the Nash reagent, which was originally detected by colorimetry. This is a classic technique still used today mostly in industrial hygiene practices. A few bubblers were taken and determined by colorimetry (Spectronic 20). However, the sensitivity is much lower than with the Belman detection technique (fluroescence). The absorbance readings ranged from only 0.05 to 0.08. The same stock formaldehyde solution used to calibrate the chromotropic and Belman bubbler standards was used to calibrate the colorimetry standard curve.

History of UNC HCHO Analytical Methods

In 1976 an automated gas chromatographic system to measure formaldehyde and acetaldehyde was built by Carle Instruments for UNC. This instrument automatically injected a 2 cc air sample into a 11 ft x 1/8 inch S.S. Porapak Q precolumn (isotheremal oven at 73°F). Light hydrocarbons passed directly through to the flame detector, while formaldehyde, propylene, methanol and acetaldehyde were retained. As soon as the light hydrocarbons were passed, the precolumn was placed in series with a 2 ft x 1/8 in S.S. Porapak Q analytical column leading directly into a 400°F Ni-catalyst methanizer before the detector. In the methanizer, formaldehyde was converted to methane and measured as methane in the flame detector. Thirty minutes were required for an analysis. Background interference from water limited the sensitivity of the method. In 1977, after long periods of purging at high temperatures, we were able to maintain a column which did exhibit reasonable separation between the water ghost and formaldehyde peaks (Figure 18). The instrument was operated in this fashion from May-December 1977 with almost no maintenance. Paraformaldehyde injections into the smog chamber were used as standards for calibration. In 1978, impurities from a He tank caused deterioration of the pre-column. We were never able to recreate the column conditioning.

The Chromotropic acid bubbler method was used during the years of 1978-1979 for direct measurement of HCHO in various smog chamber experiments.

The CEA automated method was first used in 1979.

Liquid standards of formaldehyde were used for the chromotropic acid method, and for the CEA. Paraformaldehyde was used to inject formaldehyde into the smog chambers. The accuracy of this method was established by repeated determinations using the chromotropic acid bubbler method. Thus, this method was established as method for preparing reliable calibration standards in the chamber. (This also showed that we had no detectable sample line losses.) Injections of paraformaldehyde were made directly under the chamber floor as well as from the heated return manifold to verify that these were equivalent methods. A permeation tube in a temperature-controlled conditioner was purchased in 1982. This provided a quick, reliable, calibration source which could be used before and after an experiment on the same day. The permeation tubes are commercially available with a certification of output in mass/minutes. The certified value was used for calibration and compared with paraformaldehyde injections into the chamber. Before the purchase and use of the permeation tube calibration source, calibrations were done the day before and/or after a smog chamber run, because the chamber was required for

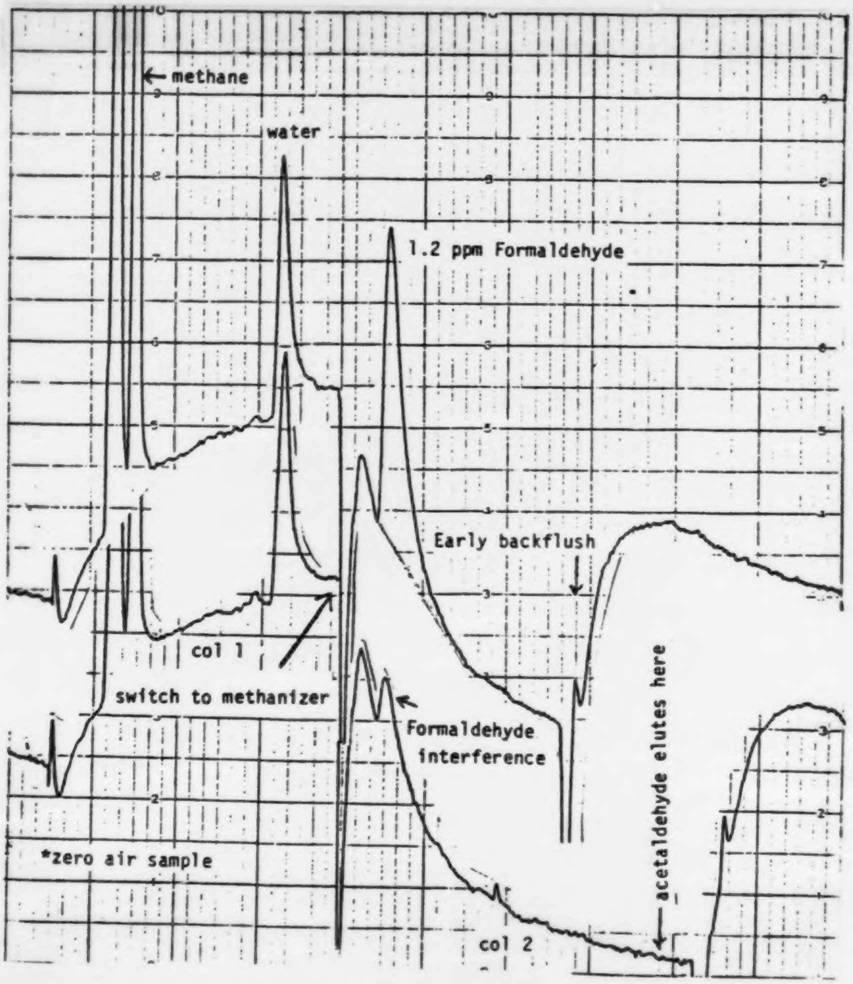

Figure 18. Response of Carle 211 GC with methanizer to 1.2 ppm formaldehyde and zero air with 1.5 ppm methane. (Two chromatograms).

injection of a paraformaldehyde calibration standard. Because experiments were performed almost everyday, several days might pass before a paraformaldehyde chamber-injection standard could be prepared. Therefore the assumption that the instrument reponse was constant between the experiment was necessary in determining the calibration factor for each experiment.

Standard operation procedure has always been that calibration of all analytical instruments is part of the experiment. Calibrations would be performed before or after an experiment, preferably both, the day of the experiment, if the techniques permitted, or the day before or after if not. Calibration data and results have always been recorded first on stripcharts, the method of recording the data for the experiment. In addition, the fact that a calibration was performed and that data is available is recorded on at least one form (Instrument Inventory), unique to the specific experiment which stays with the other data from the experiment permanently. The stripcharts and all documentation are placed in a permanent records filefolder, one per experiment. In earlier years, the calibration might also be recorded in a record book kept near the instrument, and of course, in record books maintained by the dataprocessor.

Quality Assurance and Analysis

Quality Assurance Procedures

The UNC QA procedures have always included:

- attention to maintenance,
- frequent calibrations,
- detailed record-keeping,
- comparison of results against previous experience, checking for sudden changes or trends,
- training of all workers involved in actually using the machine and processing of the data,
- frequent checking of the instrument sample rates and reagent flow rates and consumption during experiments
- use of fresh reagents,
- drying of the chamber,
- inspection of chamber for leaks, holes, open doors, condensation
- attention to sampling manifold flowrates and temperature,
- the use of checklists to assure consistent procedures are carried-out regularly and consistent results are obtained,
- allowing plenty of time for start-up and stablization before use and shut-down after use.
- repeating experiments

Improvements in QA procedures have included changing the keeping of run records and calibration records from notes in runfolders, calendars, and lists on paper in notebooks, to the use of standard forms, checklists, and computer databases, which have allowed for easier, more complete, and more frequent analysis and retrieval. Also the use of checklists in addition to training, have resulted in more consistent operation, less loss of data, and more reliable data. The analysis and refinement in QA procedures and resulting data have shown the importance of calibration frequency, which has increased over the years to the point that almost all methods now are calibrated twice daily. Concurrent development in QA procedures in other phases of the chamber and lab operation have also resulted in more time avaliable to give attention to measuring formaldehyde.

Intercomparisons of standards have been performed as a primary QA procedure, linking past data with the present. More discussion on this subject follows.

Finally, not every experiment is used. We conduct many more smog chamber experiments than we process fully. We process the best experiments, with the best quality data, including the most reliable calibration data and history.

Calibration Databases

Calibration databases contain all calibrations for an instrument and attenuation or range setting, by date. This includes calibrations that are obtained when the instrument is not in optimum condition but was used for collection of data. They are used first for QA procedures to monitor the performance and stability of the instrument. Then they are used for QA of the calibration factor processing. Odd calibration values are investigated for errors in:

1) recording of attenuation or calibration source used,
2) response measurement and recording, or calculation and recording, or
3) assumptions concerning calibration source and instrument performance such as the decay rate of a low concentration calibration source, concentration, or drift of instrument response through an experimental season.

The databases are used for determination of the calibration factor(s) to use for processing of the response data into final form. Finally, statistics from the databases can aid in determining the probable uncertainty in the resulting data.

Plots of the recent calibration databases for HCHO monitors follow.

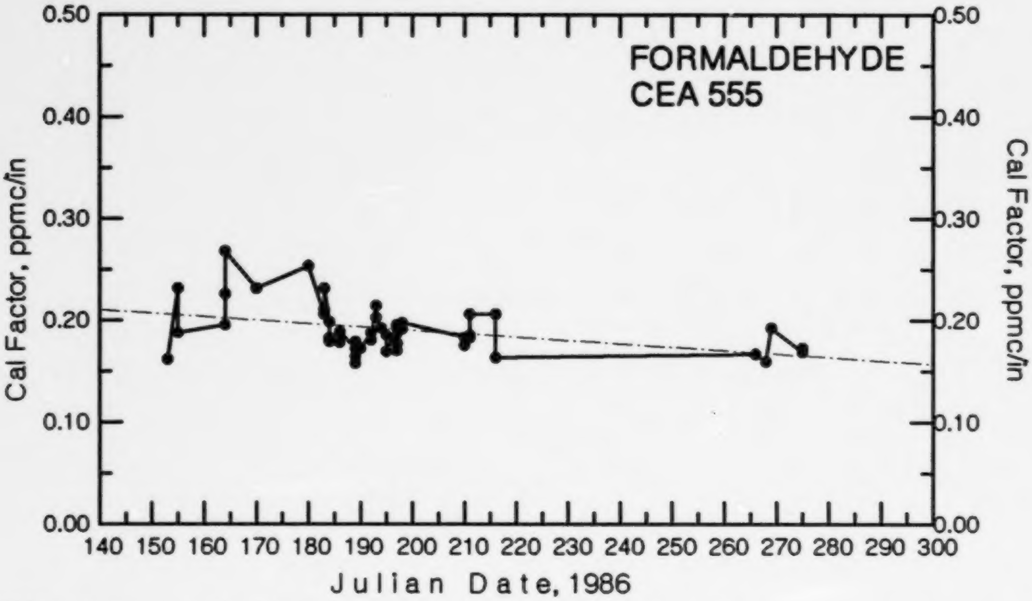

Figure 19. Calibration Factor History of CEA Monitor for 1986

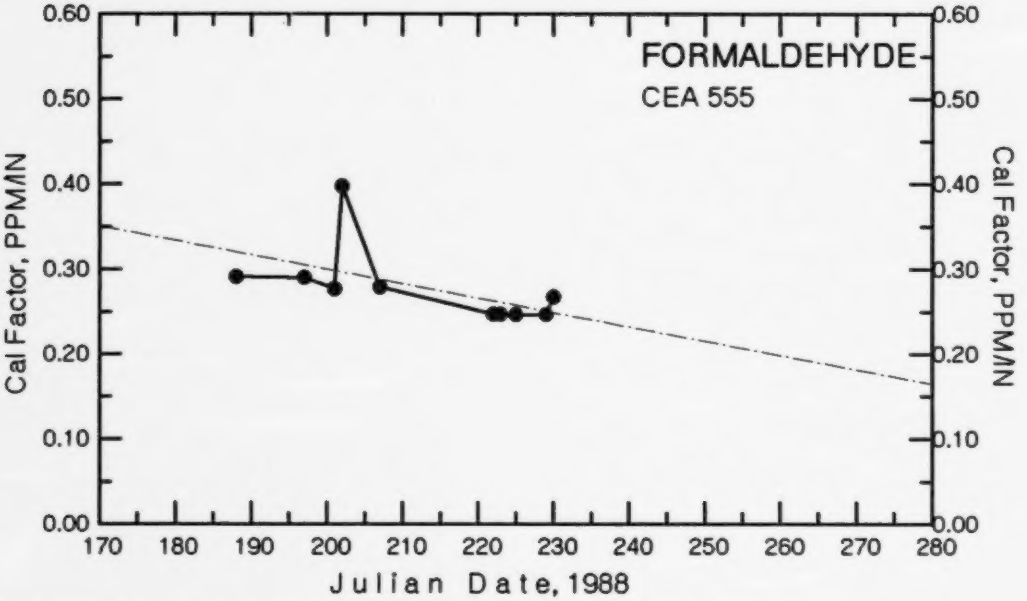

Figure 20. Calibration Factor History of CEA Monitor for 1988

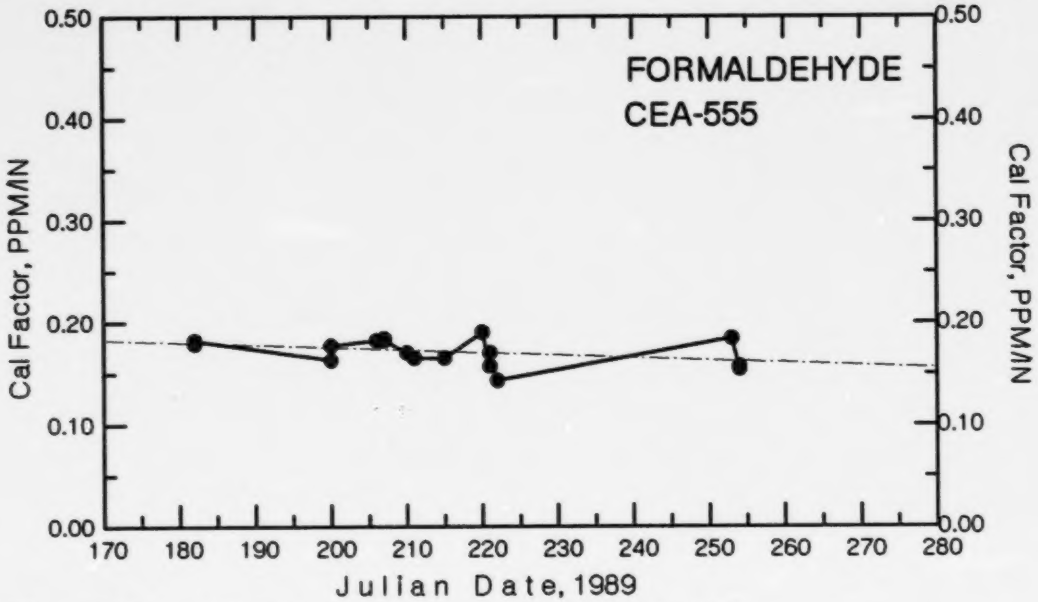

Figure 21. Calibration Factor History of CEA Monitor for 1989

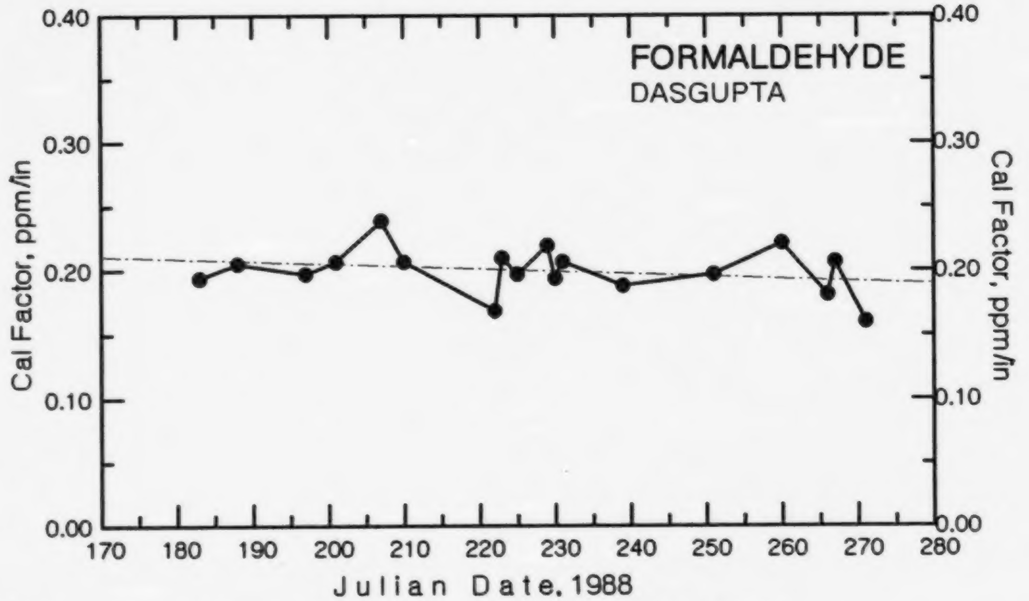

Figure 22. Calibration Factor History of Dasgupta Monitor for 1988

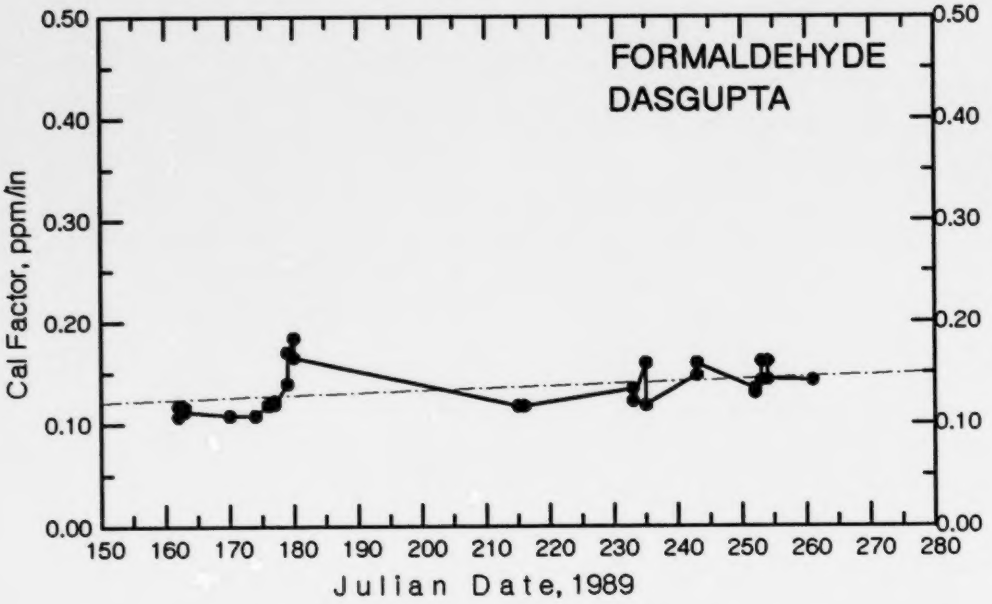

Figure 23. Calibration Factor History of Dasgupta Monitor for 1989

Calibration Standards Comparison At UNC

The intercomparisons of the different calibration sources are diagramed in Figure 24.

Figure 25 shows calibration factors, from all three sources, used in the 1986 HCHO intercomparison study at UNC along with various statistics. The plot shows, with separate symbols, the permeation tube calibration points, the chamber calibration points, that is, those based upon injection of weight samples of paraformaldehyde into the chamber, and the liquid standards calibration points. The regression equation shows extremely small negative slope and an intercept of 0.189 ppm HCHO per inch chart deflection. The standard deviation for the intercept was 8.6% and the probable error was 0.010 ppm HCHO per inch or about 5%.

Figure 26 shows the results of the intercomparison of the different methods and calibration sources used in 1988 to dctermine the output of the permeation tube, including the means and ± 1 standard deviation. The permeation tube conditioner was operated at two different air flowrates during the period. Each of the different analytical methods had at least one calibration standard other than the permeation tube. The results show that all of the calibration standards (other than permtube: liquid standards, paraformaldehyde injected to smog chamber, EPA DNPH standard) used to calibrate the analytical methods usually (80%) agreed within ± 1 standard deviation (n=42, s.d. = 0.014 ppm (rel std = 5.3%) at the high concentration level (0.261 ppm), s.d. = 0.015 ppm (rel std = 9.7%) at the lower concentration level 0.155 ppm), to the permeation tube standard, determined in turn by its mass-loss history, and measured dilution-carrier flowrate. However, the mean of all the determinations was in much better agreement with the gravimetric determination. For the 15 determinations performed at the gravimetric determined concentration of 0.261 ppm, the mean was 0.262 ppm (0.4% difference). For the remaining 27 determinations at the gravimetric determined 0.155 ppm HCHO concentration, the mean was 0.152 ppm HCHO (1.9% difference).

One should consider the sources of error which can account for disagreement. The preparation of each standard involves human error of some measurement (e.g weighing and spillage, pipeting and dilution, measurement of air flowrate and air leakage), in addition to undetectable changes in instrument operation. Perhaps more importantly, as was discussed earlier, the permeation tube response was usually compared on the same range or attenuation as used for the chamber injections which were 3 to 6 times greater in magnitude. The response from the permeation tube would usually be 10 percent of the full range. Only 1 percent imprecision would easily account for the results discussed above but still allow high accuracy agreement. Actually, one can process much better than 1% precision from a stripchart recording, and the calibration source stability measured with the Dasgupta monitor the night of July 25, 1988 shows that the variation is less than 5% for 75% of the measurements. However if one considers this imprecision with the imprecision of the preparation of the other standards and measurement errors discussed above, then the 10 % total imprecision is easily explained.

The different HCHO standards were found to be consistent with the reliable permeation tube source found to be stable through independent analysis. Accurate data were obtained with both the CEA and Dasgupta analytical methods from test mixtures of hydrocarbons and nitrogen oxides. The methods usually agreed in all types of smog chamber experiments including synthetic automobile exhaust. There is no indication of serious interferences. This suggests that more confidence can be applied to the HCHO data obtained from the UNC smog chamber programs conducted in the last 12 years.

The intercomparison of HCHO calibration standards for this study has shown that the calibration techniques used in the past are reliable, including the paraformaldehyde injections into the smog chamber as calibrations standards, and for individual initial injections for HCHO smog chamber runs. We now know that the HCHO permeation tubes output decreases about 10% per year. These tubes were

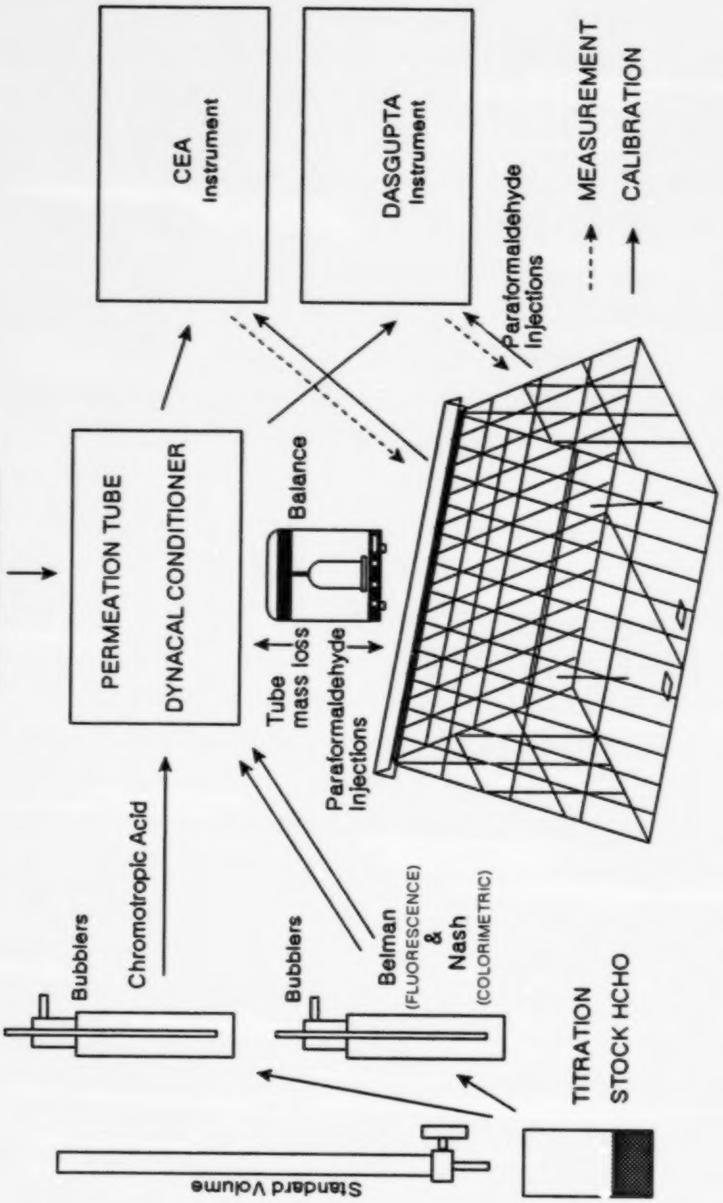
CEA Instrument
DASGUPTA Instrument
MEASUREMENT
CALIBRATION
External Standard
EPA - DNPH-SGC
PERMEATION TUBE
DYNACAL CONDITIONER
Balance
Tube mass loss
Paraformaldehyde Injections
Paraformaldehyde Injections
Bubblers
Chromotropic Acid
Bubblers
Belman (FLUORESCENCE)
&
Nash (COLORIMETRIC)
TITRATION
STOCK HCHO
Standard Volume

Figure 24. Diagram of Comparison of Formaldehyde Methods and Standards

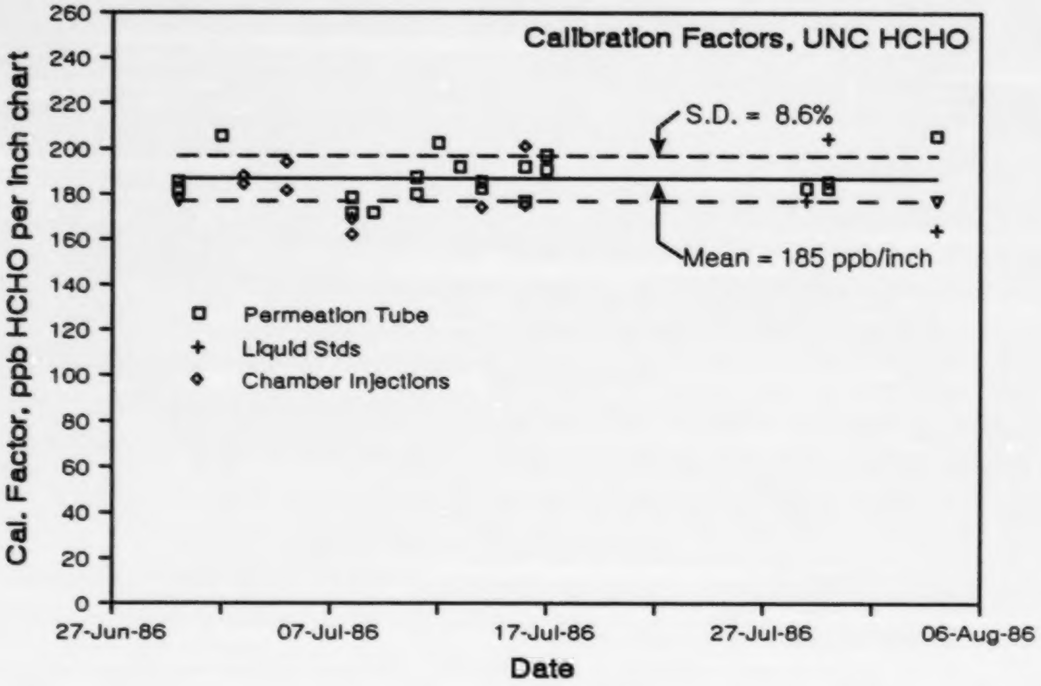

Figure 25. Calibration Factors for CEA Comparing Three Types of Calibration Sources for 1986 Intercomparison Study

replaced about every two years. The calibrations from the tubes were always compared to the calibrations from chamber injections. Actually, the chamber injections were regarded as more reliably useful for several years because of the larger response and absolute nature of the technique. Weighing of the permeation tube did not begin until 1988. Now that this method appears to be more reliable (paraformaldehyde injections can be suspect because of the human error possible in the technique), the permeation tube is regarded much more highly as a calibration source.

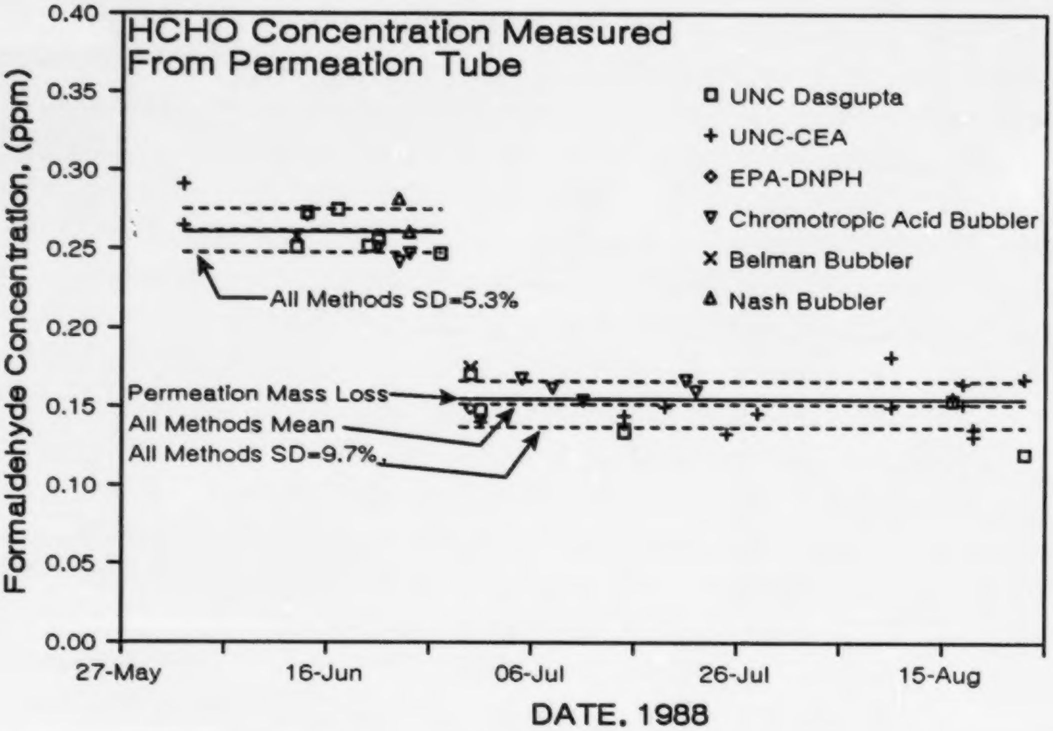

Figure 26. Comparison of Formaldehyde Methods and Standards

Calibration Standards Comparison at UCR/EC

In the fall of 1989, Ken Sexton traveled to the State Air Pollution Resource Center (SAPRC) at Riverside, California for two weeks. He took the UNC HCHO permeation system, the UNC-Dasgupta HCHO monitor, and several EPA-DNPH-SGCs. The UNC permeation tube/Dynacalibrator HCHO standard system was also utilized as a calibration source.

Formaldehyde standards were prepared in UCR's evacuable chamber (EC) from paraformaldehyde by UCR's Tuazon using a pressure bulb and vacuum system and the bulb was flushed into the chamber. In the EC four methods—the UCR-FTIR, the UCR chromotropic acid bubbler procedure, the UNC-Dasgupta method, and the EPA-DNPH-SGC method—were compared at several concentration levels. Also the UCR-CAB and EPA-DNPH tubes were used to sample the permeation tube source.

Operation of Evacuable Chamber (EC): The chamber was filled with air prepared with blended nitrogen and oxygen from gas cylinders resulting in very dry air. Injection of the HCHO standards through valve-controlled ports was followed with the use of mixing fans. A digital pressure gauge was used to monitor the chamber pressure. Sample ports and lines (unheated) were used to sample from the chamber.

UCR Chromotropic Acid Bubbler Method and Procedures: The standard Chromotropic Acid Bubbler (CAB) method is used as the routine analytical method for monitoring HCHO in UCR smog chamber runs. Mae West bubblers are used for sampling air at 1 liter per minute. A bubble tower and stopwatch are used to measure the sample rate. A needle valve is used to control the sample rate and a rotameter in-line is used to monitor the sample rate. A short unheated teflon sample-line and probe through the chamber wall are used. Two Graylab timers are used: one to start the sampling and one to control sampling time. Usually 20 liters are sampled, usually one per hour. Samples are transferred to another flask and read the next morning. Sample recovery volumes are recorded and used to correct for evaporation losses, which lowers the reported value. A Beckman 35 spectrophotometer is used to read the absorption of the color development. Calibration curves are prepared with HCHO solutions. We do not know with what frequency calibration are regularly prepared. For this study the calibration was performed a few days before the study.

Standards Preparation Procedure: Standards were prepared with paraformaldehyde on a vacuum-rack system. A calibrated-volume vessel is connected to a vacuum system which is connected to a vacuum gauge and another flask of paraformaldehyde. The paraformaldehyde is heated until a desired pressure is reached. Then clean air is allowed in for dilution. The mm Hg of HCHO over the total pressure is the concentration of the standard before injection into the EC. The known volume of the flask divided by the volume of EC times the standard flask is the final concentration.

Comparison Procedure: Samples were prepared by Tuazon and injected into the chamber. The calculations for the final concentration were also made by Tuazon. The Dasgupta monitor was allowed to sample continuously from the chamber. The FTIR recorded the spectra and the bubbler was started after allowing time for mixing. Several standards at different concentrations were prepared. Each standard was injected as an addition to the amount already in the EC.

Results: The results are shown in Figure 27. In general the agreement was good. The low UCR bubbler value was a little higher than the calculated value for the first standard, but approx 30% lower for the second standard. This comparison was

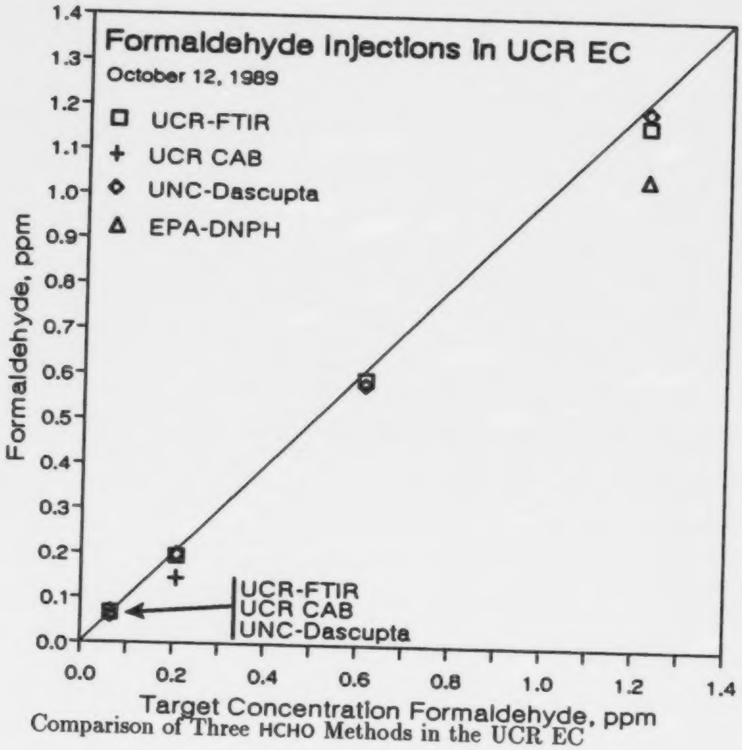

Figure 27. Comparison of Three HCHO Methods in the UCR EC

done after a normal full day of work (after regular hours) in the evening. Additional UCR chromotropic bubblers were not taken because of prior commitments of key personel normally responsible for collecting the chromotropic bubbler samples. The DNPH sample was about 14% low. Only one EPA-DNPH-SGC sample was taken, to minimize the change in pressure in the EC. The Dasgupta and FTIR methods were consistently in good agreement. However, no measurements were ever obtained which were larger than the calculated concentrations from the injected masses. The average deviation of measured response to the calculated injection concentration for the FTIR was -4.9% (not including the lowest reading which was near the detection limit) and for the Dasgupta method, -4.7%. It may be that some small fraction of HCHO was absorbed on the walls. It may also be that the assay purity of the formaldehyde is 95% rather than 100%.

Permeation Tube Measurement: UCR Chromotropic Bubblers and EPA-DNPH tubes were used to sample the permeation tube source at Riverside. The output flowrate from the Dynacalibrator was measured with a bubbletower and stopwatch. Atmospheric pressure was measured with a mercury barometer. Room temperature was measured with a mercury thermometer. The mass of the tube was last measured on September 19, 1989 and this was used to estimate the tubes output. The permeation tube output was determined to be 0.129 ppm. Two chromotropic bubblers determinations ranged from 0.127 to 0.134 averaging 0.130 ppm, only 1.4% higher than the gravimetrically determined value. The EPA-DNPH determinations ranged from 0.127 to 0.140 ppm with an average of 0.133 ppm, only 3.7% more than the gravimetrically determined value.

Assessment of Overall Measurement Uncertainty

Accuracy of HCHO Measurements

No serious interferences or other biases have appeared in any test for either the Dasgupta or CEA instruments. All formaldehyde calibration sources compared, including those used at EPA and UCR, agreed within ±2%. We therefore believe that the sources used to routinely calibrate the UNC HCHO monitors are also accurate to within ±2%. Further we believe that because there are no biases in either instrument and the various calibration sources agree to within ±2%, then the accuracy of both the Dasgupta and CEA instruments is probably ±2%.

Precision

There are several factors to consider in determining the precision of the the HCHO monitors. The precision of the intercomparison of the calibration sources, with different methods discussed above, resulted in a precision of about ±5 to 10% at a 95% confidence level depending on the concentration level investigated. However, this involves the compounded imprecision of two methods, not one.

For the Dasgupta monitor, one should look at the imprecision of monitoring the response of the permeation tube calibration standard, since this results in the imprecison of the calibration factor. Because the DynaCalibrator have very precise temperature regulation and air flow regulation, and because the tube weight loss over a season is linear, we assume that there is essentially zero variance in the permeation tube output. Thus all imprecision will be assigned to the instrument. The standard deviation of the response from the permeation tube for 16 points over 8.5 hours was 0.006 ppm when the output concentration was 0.155 ppm, a 3.8allowed to sample the tube response several times before and after the experiment if not during the experiment. The precision of determining the mean of any measurement, $P_{\bar{X}}$ is:

$$P_{\bar{X}} = \frac{t\,S_X}{\sqrt{N}}$$

where, S_X is the standard deviation, N is the number of measurements and t is from the t-distribution for $N-1$ degrees of freedom.[16]

If only 4 samples of the permeation tube were allowed for a calibration, precision would be 3.18×6 ppb/2 = 9.5 ppb or a precision of 6.2% relative to a 0.155 ppm calibration source (at a 95% confidence interval), and therefore an imprecision of 6.2% in the calculated calibration factor. Thus, if there were no other sources of imprecision, the resulting chamber measurements would also have an imprecision of 6.2%. Of course, there are other sources of imprecision—the variance in the instrument zero and sample responses. For the Dasgupta monitor, the zero is performed every 30 minutes and a zero is never taken more that 10 minutes away from a measurement. Zero drift therefore contributes a neglible amount to response imprecision. If the zero is questionable or bad then the surrounding data are not processed. The remaining imprecision in the measurement is due to the variance in the sample responses. These are caused by two factors:

1) the inherent instrument variation, which we will represent by the imprecision or variation of calibraton on the permeation tube, and
2) the mechanical conversion of the response from the stripchart record to a number for use in computer databases.

Training of dataprocessors includes testing and comparing their abilities to measure peakheights using both the electronic digitizer and rulers. Their performance is compared with experienced and skilled dataprocessing coordinators. Data processing QA procedures include plotting of the raw response data and spot measurement checks by the dataprocessing coordinators. Irregularities in the concentration-time profiles are especially investigated. Experience shows that after these QA procedures, the average error in response measurement is less than 0.02 to 0.03 inches for an average response measurement of 3 inches, resulting in a conservative imprecision value of less than 1% (0.8%). If one adds this to the 6.2% arrived at above we have an overall imprecision value of 7%.

The root-sum-square method of evaluating overall uncertainty is:

$$U_{\bar{X}} = [A^2 + (P_{\bar{X}})^2]^{1/2}$$

where A is the accuracy. If 2% is the bias (or accuracy) and 7%, the precision, then the overall uncertainty is ±7.3% at a 95% confidence interval.

The calibration database for the Dasgupta monitor can also be used to estimate the imprecision of determining the response. In 1989 the average imprecision of measuring the permeation tube during a single day calibration was 2.7% (average standard deviation). Therefore, combining the stripchart reading imprecision, the combined relative standard deviations is 3.5%. Using the above formula for calculating the imprecision value for $N = 4$ determinations, $t = 3.18$, yields 5.6% for overall precision of the method. Combining the accuracy of 2% and this precision results in an overall uncertainty of ± 5.9% for a 95% confidence interval for the 1988-89 season.

The zero check for the CEA is only performed every two hours and drift uncertainty must be estimated. For this purpose the absolute value of the zero reponse was tabulated for each run performed in 1988 and 1989 with the CEA monitor. Linear regressions were calculated (assuming linear drift) and the error of estimating or predicting the zero was also tabulated. The imprecision of predicting the zero throughout a whole day was 1.8% (relative standard deviation). We do, however, measure zeros every two hours. These are used to process the sample measurements nearest the zeros. Therefore a conservative estimate of the imprecision of the zero portion of estimating the response is half of the imprecision of predicting the zero throughout the day or 0.9%. The average imprecision of measuring the permeation tube before and after the run for the CEA is 1.7% (average standard deviation calculated for the calibration database). Therefore the combined relative standard deviations is 2.6%. Using the above formula for calculating the imprecision value for $N = 4$ determinations, $t = 3.18$, yields 4.1% for overall precision of the method. Combining the accuracy of 2% with this precision, an overall uncertainty for the CEA for the 1988-89 season is ±4.6% at a 95% confidence interval.

For earlier seasons, although the accuracy would be the same, the uncertainty increases for the data from the instrument calibrated without the permeation tube (1979-1981, and some portions of later years), depending on the drift recorded in the calibration history surrounding each experiment. If instrument stability is shown, then calibration with paraformaldehyde chamber injections is still reasonably precise.

Table 3. Joint UNC-UCR Experiments Conducted at SAPRC in 1989.

Date	UCR No.	Experiment Description
10/3	ITC1548	4 ppm Ethene/NOx, 0.3 NO, 0.2 NO2 Duplicate of ITC926
10/4	ITC1549	0.3 ppm NO, 0.2 ppm NO2 initial; 0.5 ppm \hcho\ added after 2 hrs irradiation Duplicate of ITC864
10/5	ITC1550	1 Propene, 0.3 NO, 0.2 NO2 Duplicate of ITC925
10/9	ITC1553	0.5 ppm \hcho\, no NOx; decay
10/10	ITC1554	1 ppm \hcho\, 0.3 ppm NO, 0.2 ppm NO2
10/11	ITC1555	2 ppm Ethene, 0.3 ppm NO, 0.2 ppm NO2 Duplicate of ITC936
10/12	ITC1556	1 ppm Propene, 0.3 ppm NO, 0.2 NO2 Duplicate of ITC925

UNC and SAPRC Joint HCHO Experiments

Several smog chamber experiments were conducted in the indoor Teflon chamber (ITC) (see Table 3). Formaldehyde was monitored with the SAPRC chromotropic acid bubbler procedures (UCR-CAB), the UNC Dasgupta method, and the EPA-DNPH method.

ITC Results

Figures 28 to 31 show the formaldehyde data obtained from the three methods during several experiments. On most days the agreement was good to very good. There were, however, some discrepancies.

For the October 3 ethene/NO_x irradiation (ITC1548), the UNC and UCR data agree initially, then diverge with UCR data being less than the UNC, and finally agree again at the higher concentrations. The UNC Dasgupta methods detector saturated at about 1.3 ppm. See Figure 28.

For the October 4 $HCHO/NO_x$ irradiation (ITC1549), the two methods agreed very well except for one point after injection of the formaldehyde, and the first UCR background reading (Figure 28). The first UCR background reading was much higher than UNC's value, but the first UCR reading after injection was almost 20% lower than UNC. One EPA DNPH-SGC sample was taken 180 minutes into the experiment. Figure 28 shows that the value is exactly on the line of the UNC Dasgupta data.

A propene/NO_x irradiation was conducted on October 5 (ITC1550) and it resulted in excellent agreement for the first half of the experiment, about 12-14% disagreement for the next two hours and then excellent agreement at the last UCR reading (Figure 29).

On October 9, an HCHO-only decay experiment was conducted (ITC1553) resulting in excellent agreement for most readings. The UNC Dasgupta method was a little noisy initially (Figure 29). However the instrument was well stabilized before the lights were turned-on. UCR's first reading was about 6% lower than the UNC data. Very good agreement was obtained for the remainder of the experiment. The DNPH-SGC determination at 180 minutes into the experiment was in excellent agreement with the closely agreeing UNC and UCR data.

Unfortuately, HCHO data between UCR and UNC showed more disagreement during the remainder of the experiments, even though the UNC data from a repeated experiment showed excellent reproducibility.

The October 10 HCHO/NO_x experiment (ITC1554) resulted in the UNC data initially being 0.2 ppm higher than the UCR data, and being approximately 0.1 ppm less then the DNPH sample (Figure 30). Later, and for the remainder of the experiment, the UNC data were consistently about 0.1 ppm higher than the UCR data. Another DNPH sample, taken 140 minutes into the experiment, agreed with the UCR data point.

The worse agreement bewteen the UCR and UNC methods occurred for the October 11 ethene/NO_x experiment (ITC1555) (Figure 30). The two sets of measurements agreed rather well for most of the first two hours and then began to diverge with the UCR data approximately 30 percent lower than the UNC data.

Closer agreement was initially obtained for the October 12 propene/NOx experiment (ITC1556), that was a repeat of the October 5 experiment (see Figure 31). The only difference in this experiment and the October 5 experiment was a higher NO_2/NO_x ratio. The UNC and UCR data agreed rather well initially but differed by about 0.1 ppm (UCR less) starting at about 160 minutes. The bottom of Figure 31 compares the October 5 and October 12 data. This demonstrates that the UNC-Dasgupta method was highly repeatable.

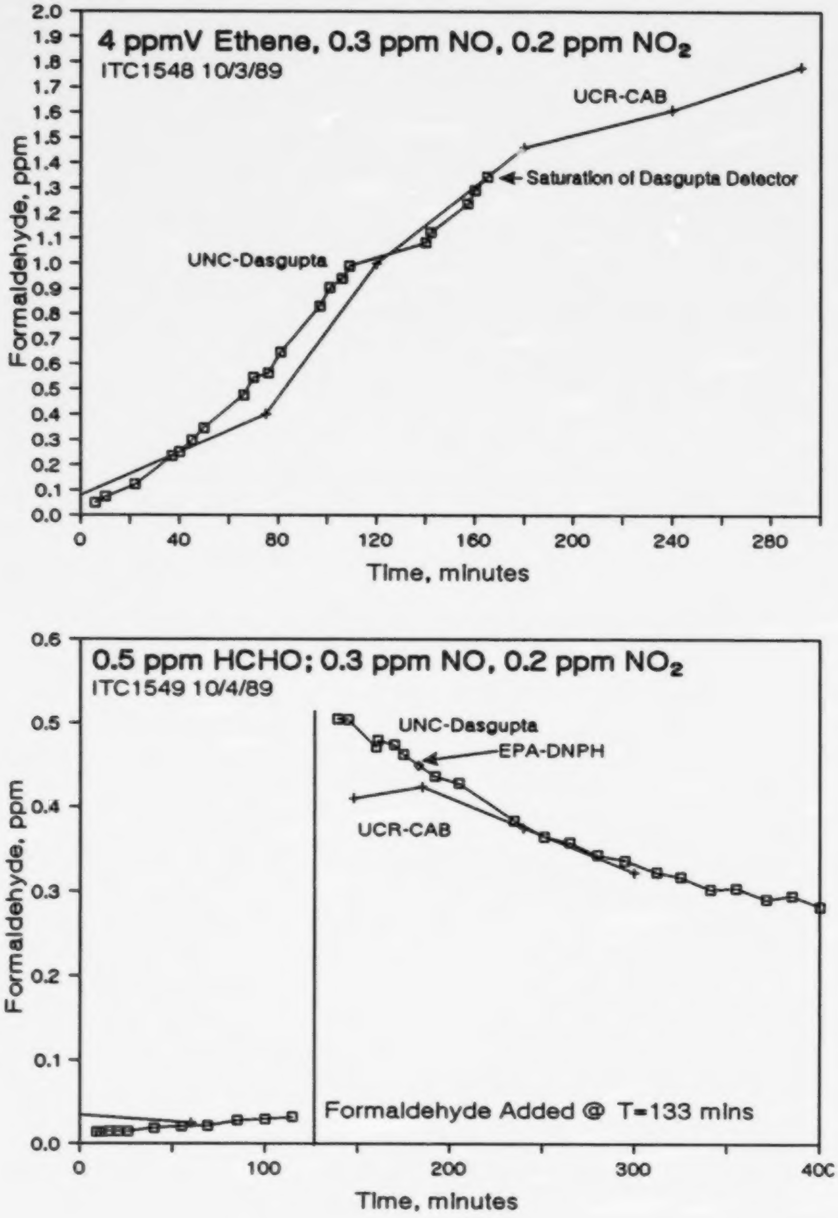

Figure 28. Results of UCR smog chamber experiments: October 3 and 4, 1989

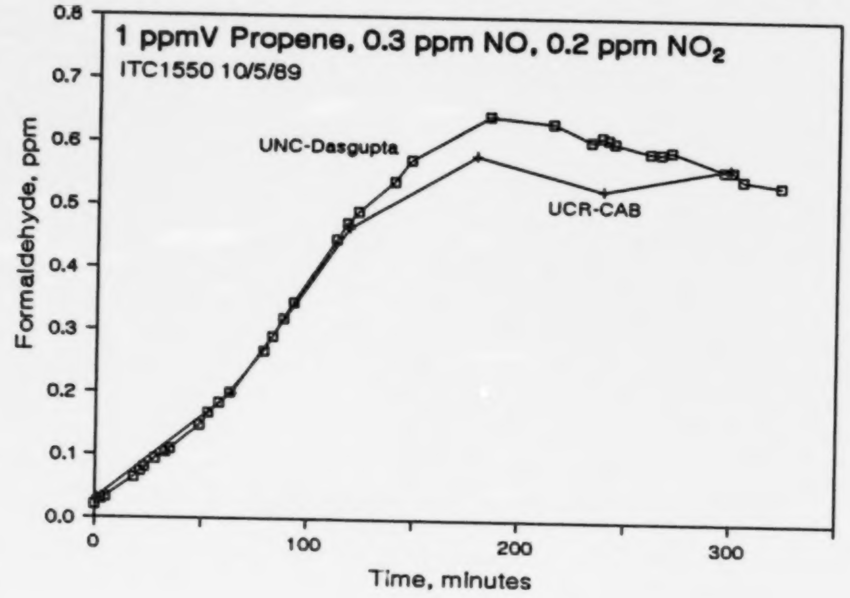

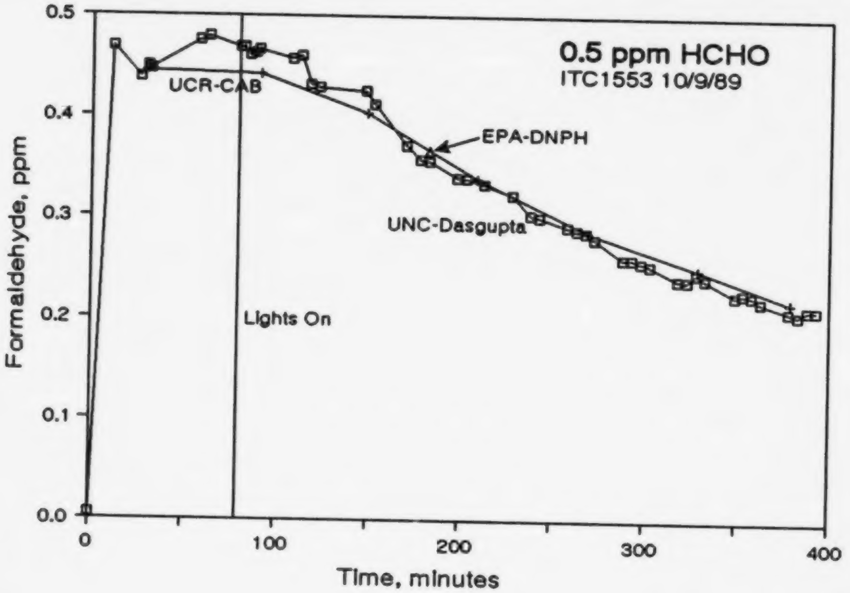

Figure 29. Results of UCR smog chamber experiments: October 5 and 9, 1989

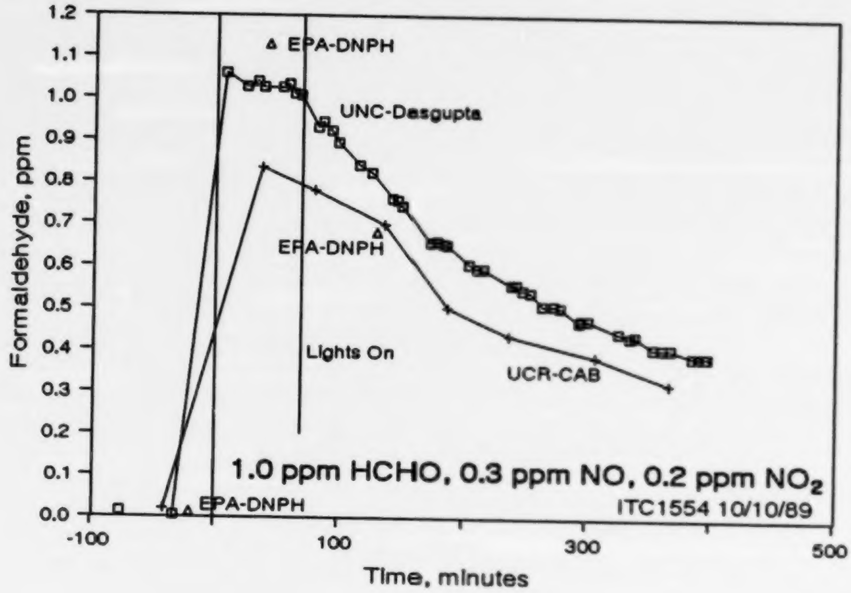

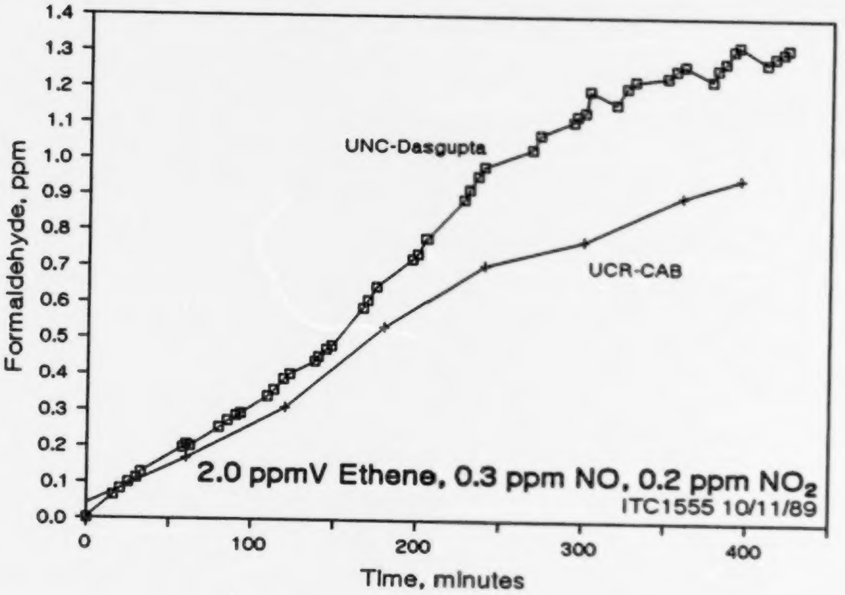

Figure 30. Results of UCR smog chamber experiments: October 10 and 11, 1989

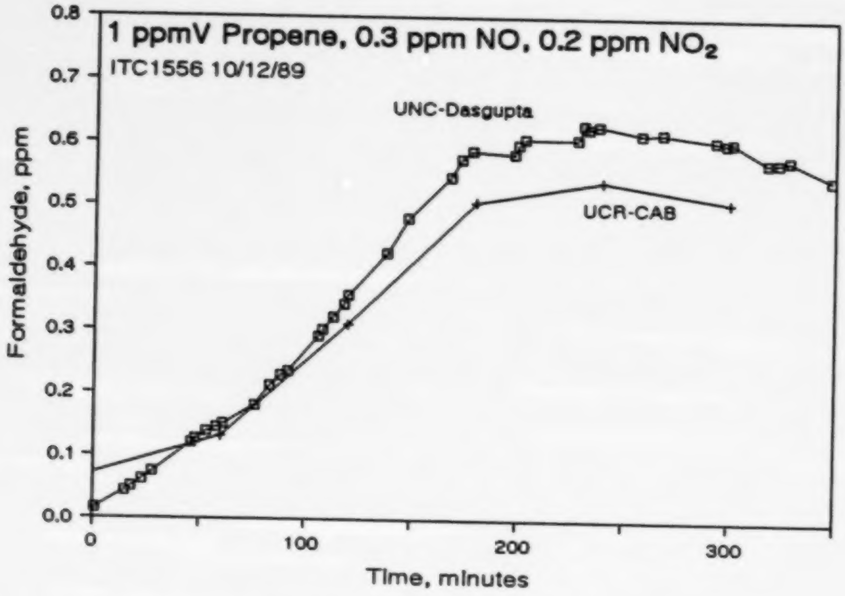

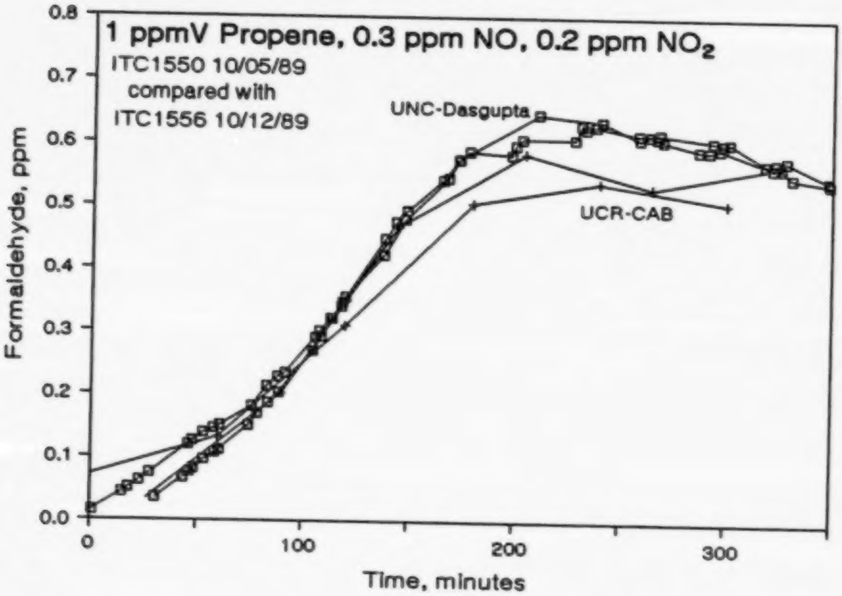

Figure 31. Results of UCR smog chamber experiments: October 12, 1989. Bottom: Comparison of October 5 and October 12, 1989.

In summary, for most of the experiments, the agreement between the three methods was generally good. The disagreement on October 12 is the most noticable and disturbing because of the implication that there is something as yet unknown which can cause significant low UCR-Chrom HCHO data randomly within a set of otherwise generally good data and that there always exist the possibility that one selected smog chamber experiment might have low formaldehyde data. This suggests that a modeler should select several experiments, and before modeling, look at the HCHO data from the set and look for low data, especially from replicate runs. The replicate runs performed showed that the UCR-CAB data were about 10% lower on the second run of the replicate set than in the first run. It should be noted that the data obtained from these experiments were from a conscious comparison of formaldehyde measurements: special attention was given to these measurements, (but not special techniques). More typical data may or may not be as carefully obtained. If these results and comparisons are typical, then a selection of smog chamber experiments should provide a set of fairly accurate and precise data for modeling: outliers should be fairly obvious; these should be investigated carefully or at least flagged as being suspicious. The UCR-CAB data were rarely above the UNC-Dasgupta data and were frequently lower than the UNC-Dasgupta HCHO data.

3

New Experiments

The purpose of this chapter is to describe the new experiments that were performed using the new analytical methods described in chapter 2. A total of 34 new dual experiments were performed as part of this project. The initial conditions for these experiments are given in Table 4.

Plots of selected experiments are presented in the rest of this chapter. These plots are labeled and thus are reasonably self-explanatory. The plots show that under a variety of situations, there was good to excellent agreement between the two HCHO methods. Unfortuately, our CO analyzer malfunctioned and was shipped to the factory for repair twice during the 1988 experimental season. A new analyzer was purchased in 1989 and was used for 10 experiments. The August 3, 1989 experimental plot with CO data is shown here. A newly purchased hydrogen chromatograph was used in many of the experiments, providing for the measurement of a species produced primarily by HCHO photolysis to stable products.

Table 4. Initial Conditions for New Experiments.

Date	NOx	ppm	HC	ppm	HC	Comment
JL0688*	0.35	3.16	ethene	0.57	ethene	
JL1588*	0.35	0.85	HCHO	0.43	HCHO	
JL1988		1.80	ozone	2.00	ethene	Night
JL2588		1.80	ozone	2.00	propene	Night
JL2888		1.80	ozone	2.00	1-butene	Night
AU0188		varying	HCHO			Night
AU0988*	0.30	1.75	ethene	0.89	ethene	
AU1088*	0.30	3.35	ethene	1.70	ethene	
AU1288*	0.50	1.59	propene	0.78	propene	
AU1688*	0.30	1.94	ethene	0.80	HCHO	
AU1788*	0.30	5.00	toluene	1.72	m-xylene	
AU1888*	0.35	3.31	SynAuto	1.92	SynAuto	
AU2388		2.00	HCHO			
AU2688		1.50	HCHO			
ST0788*	0.35	1.35	propene	1.35	1-butene	
ST1288	0.35	5.00	n-butane	5.00	n-butane	
ST1588	0.35	10.00	n-butane	10.00	n-butane	
ST1688	0.40	4.00	propene	4.00	propene	
ST2288	0.40		bckgnd	50.00	CO	
ST2388	0.90		bckgnd	50.00	CO	
ST2788*		1.00	HCHO			36-hr decay
ST2888	0.30		bckgnd		bckgnd	
JN1289			bckgnd		bckgnd	NOx-test
JN1389			'cont			
JN1489			'cont			
JN2889	0.25	2.00	n-butane	2.00	n-butane	
JL1189	0.30	1.50	ethene	4.00	n-butane	
JL1289	0.30	4.00	n-butane	1.50	ethene	
JL2589	0.30	0.50	ethene	1.00	ethene	
JL2689	0.30	0.50	ethene	1.00	ethene	
JL2989	0.30	1.00	ethene	2.00	ethene	
AU0389*	0.30	1.06	ethene	1.91	ethene	
AU0489		2.00	biacetyl	2.00	biacetyl	
AU2189	0.50	2.00	propene	2.00	propene	50 ppm CO
AU2389	0.30	1.00	ethene	1.00	ethene	

* plot included here

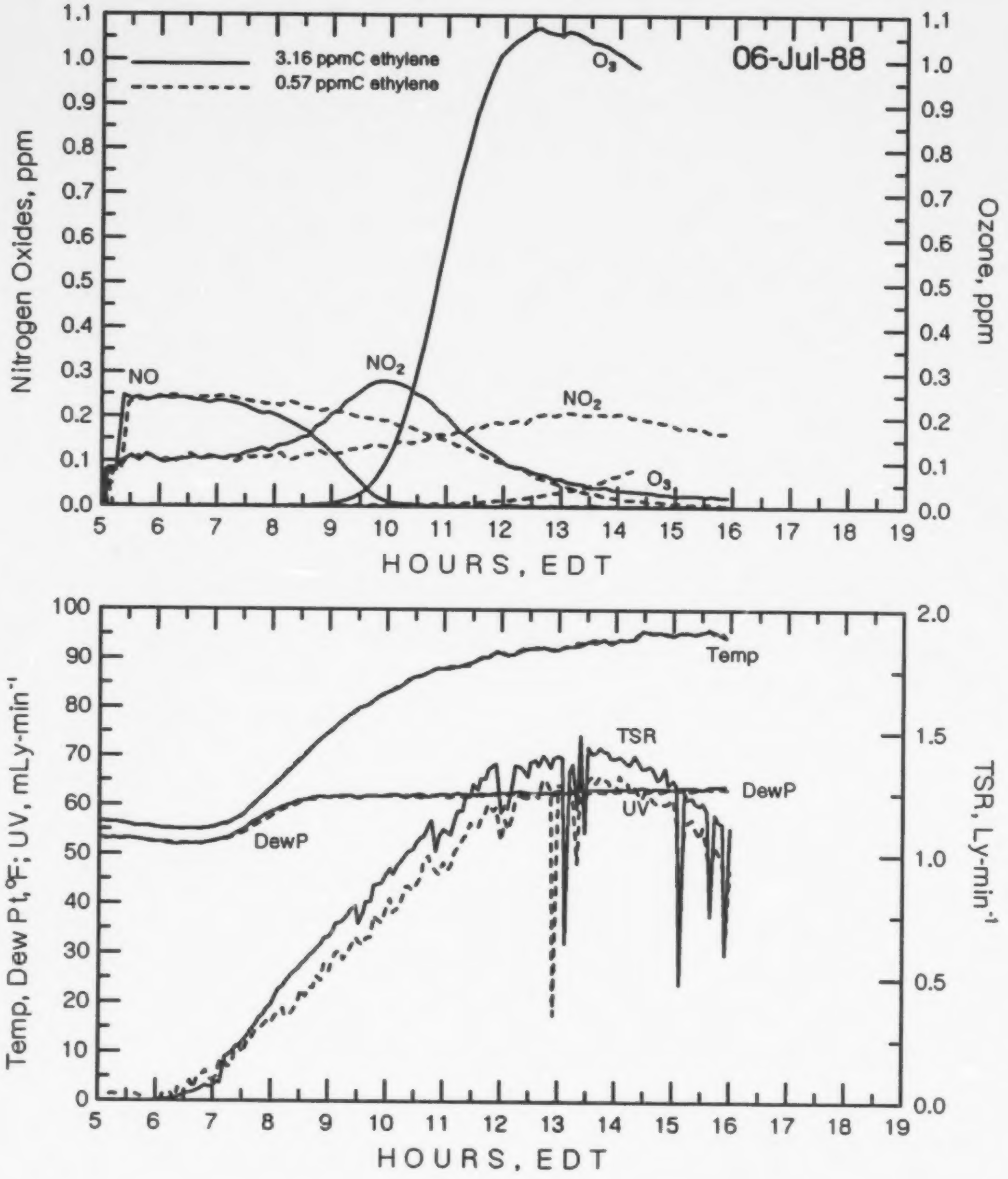

Figure 32. Differential ethene concentrations at same NO$_x$.

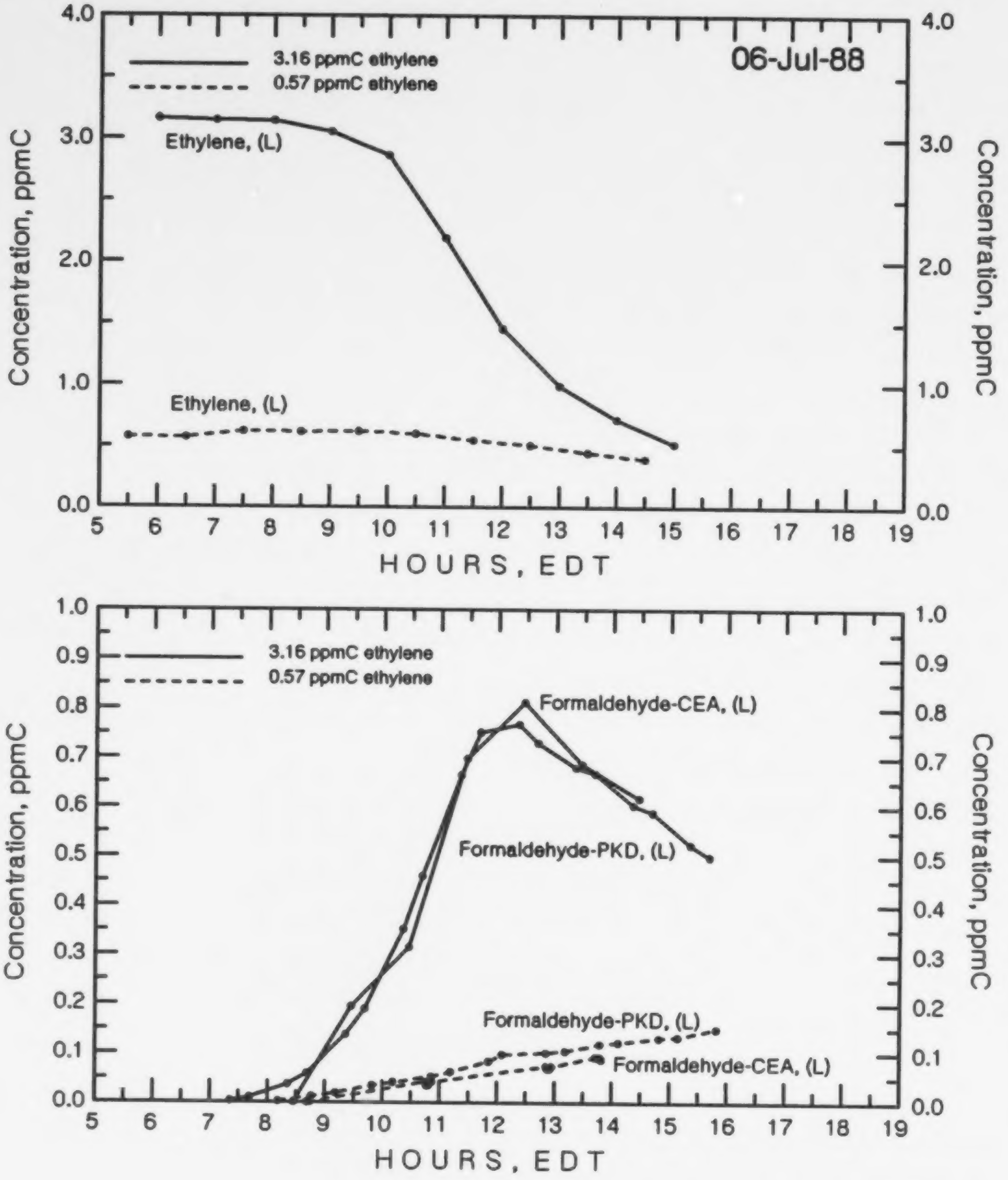

Figure 33. Differential ethene concentrations at same NO_x.

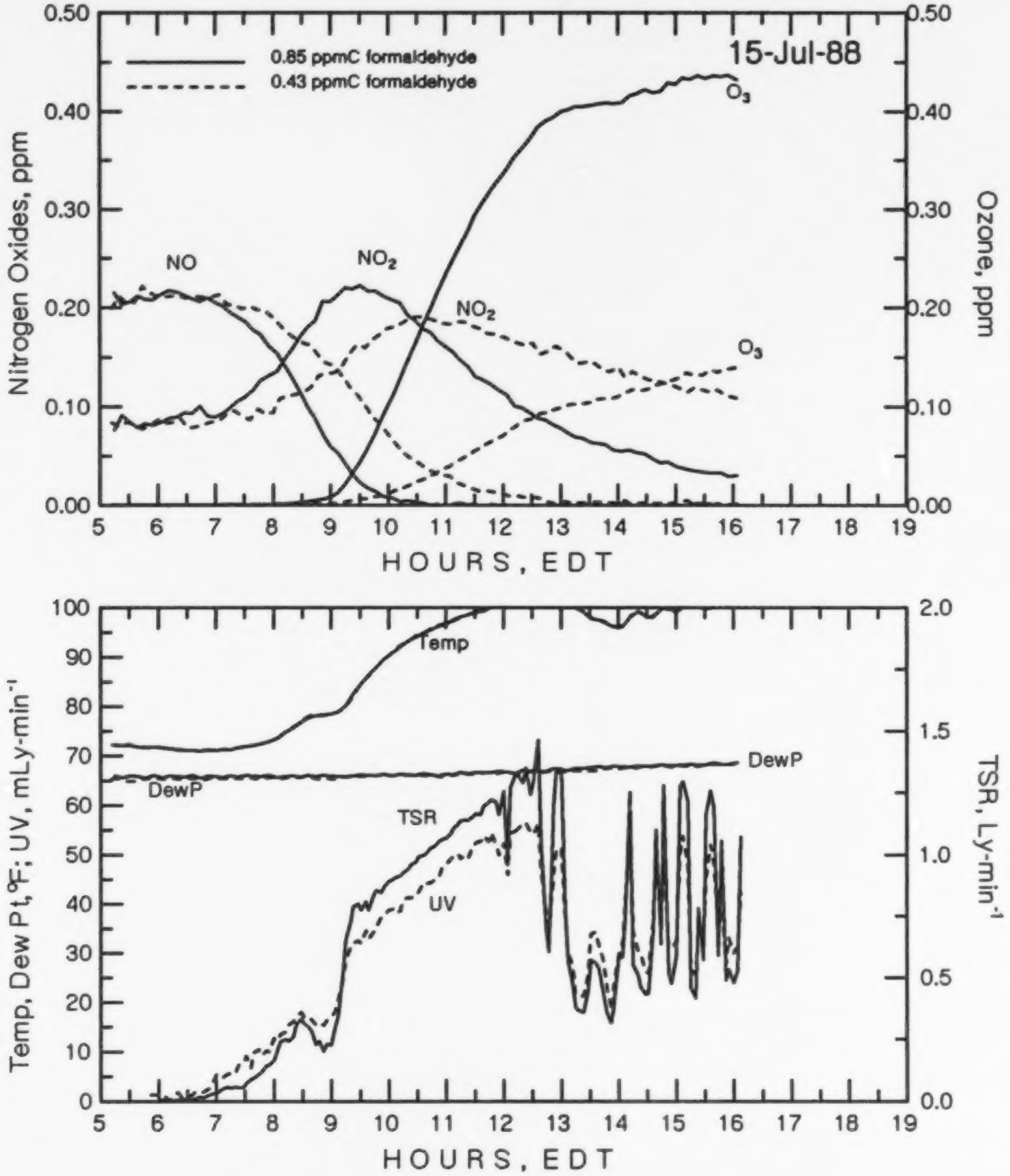

Figure 34. Differential formaldehyde concentrations at same NO_x.

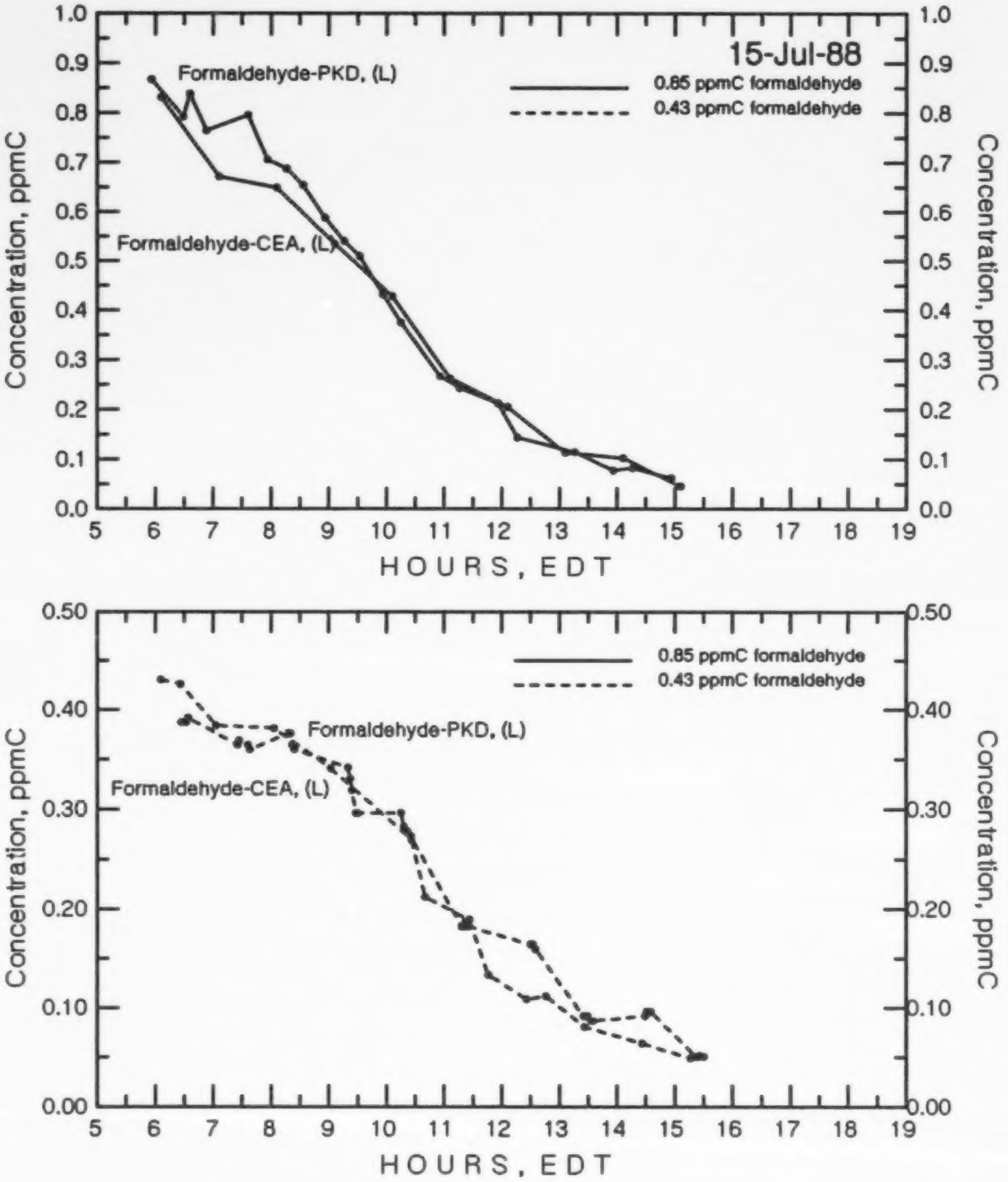

Figure 35. Differential formaldehyde concentrations at same NO_x.

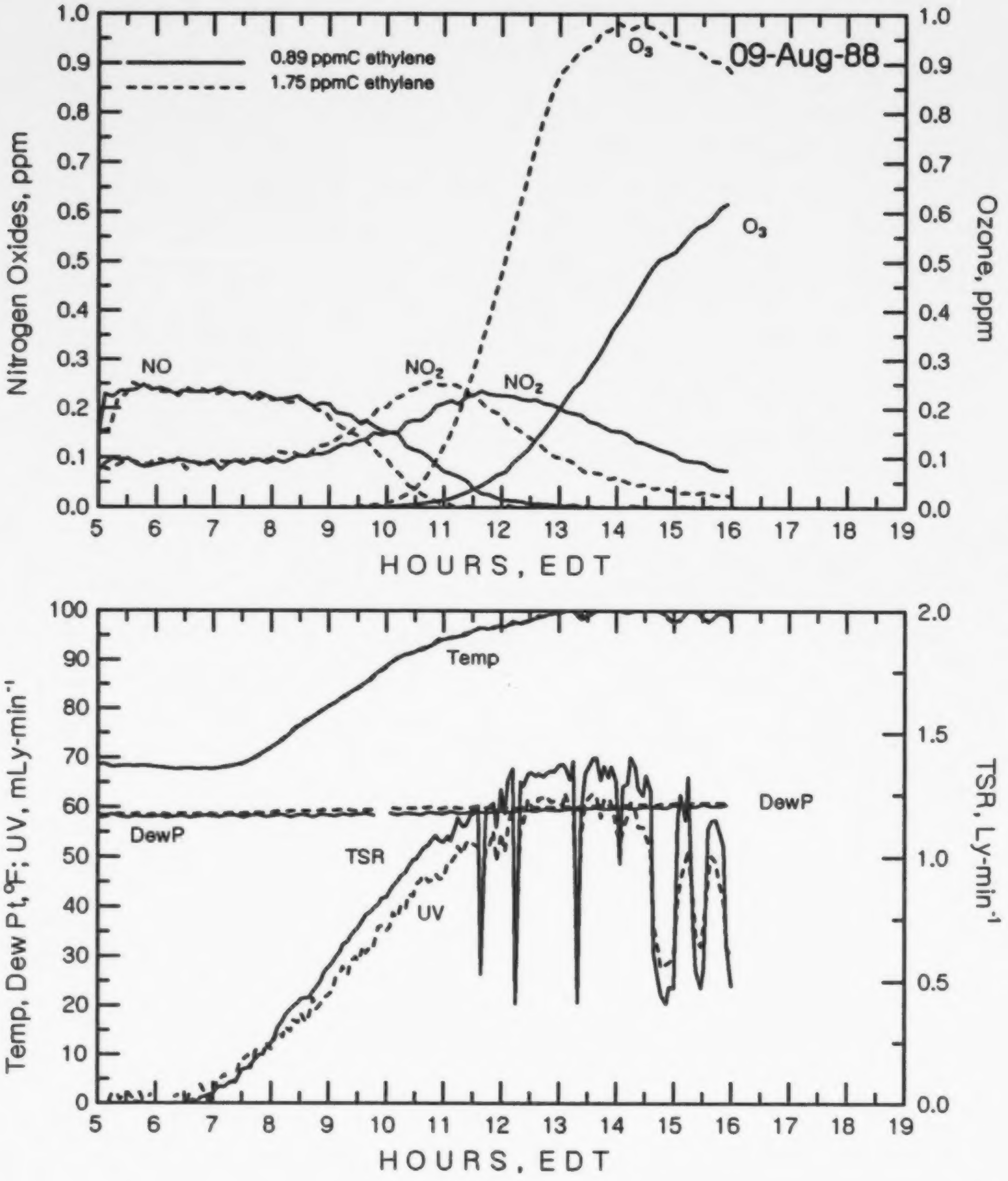

Figure 36. Differential ethene concentrations at same NO_x.

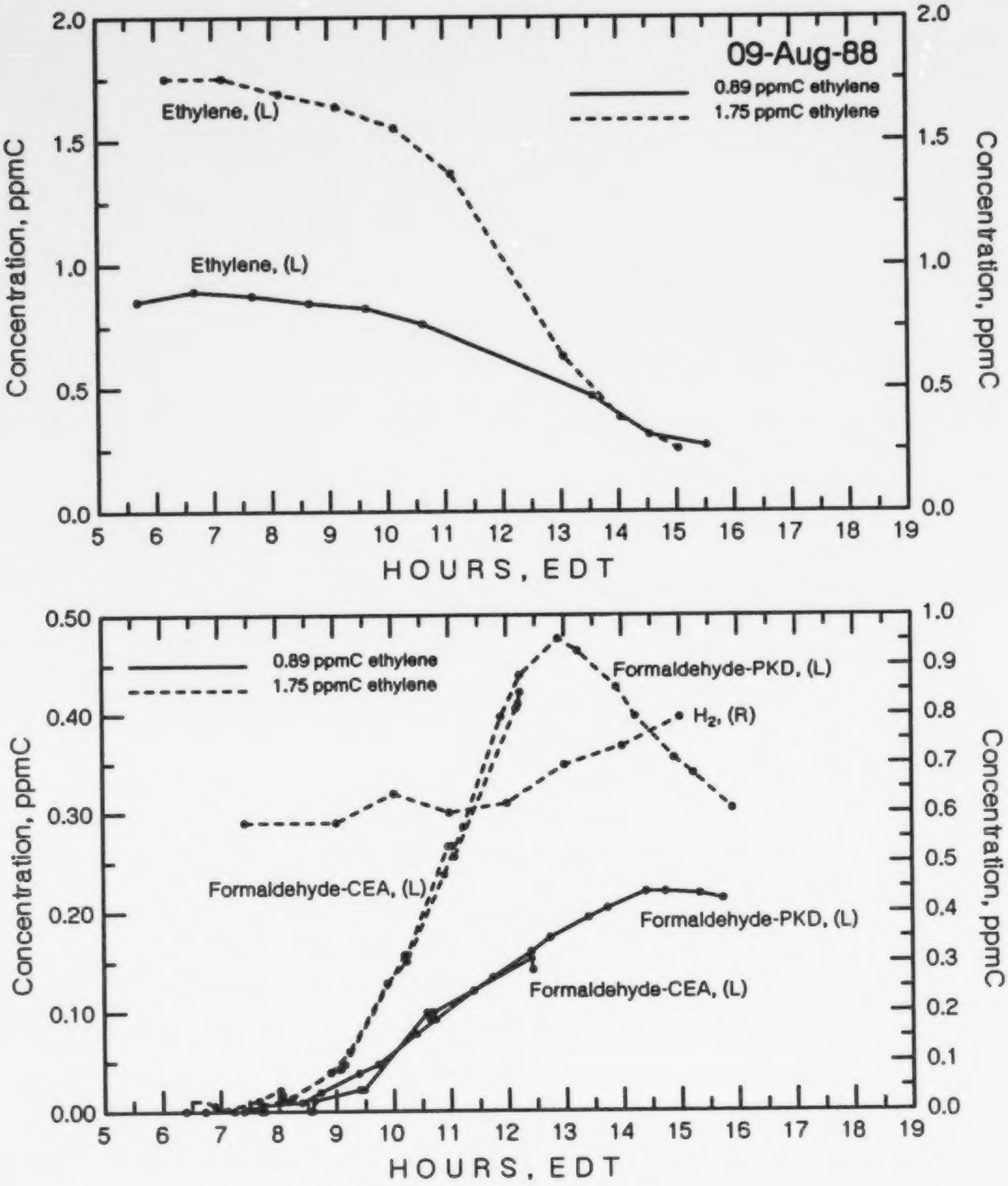

Figure 37. Differential ethene concentrations at same NO_x.

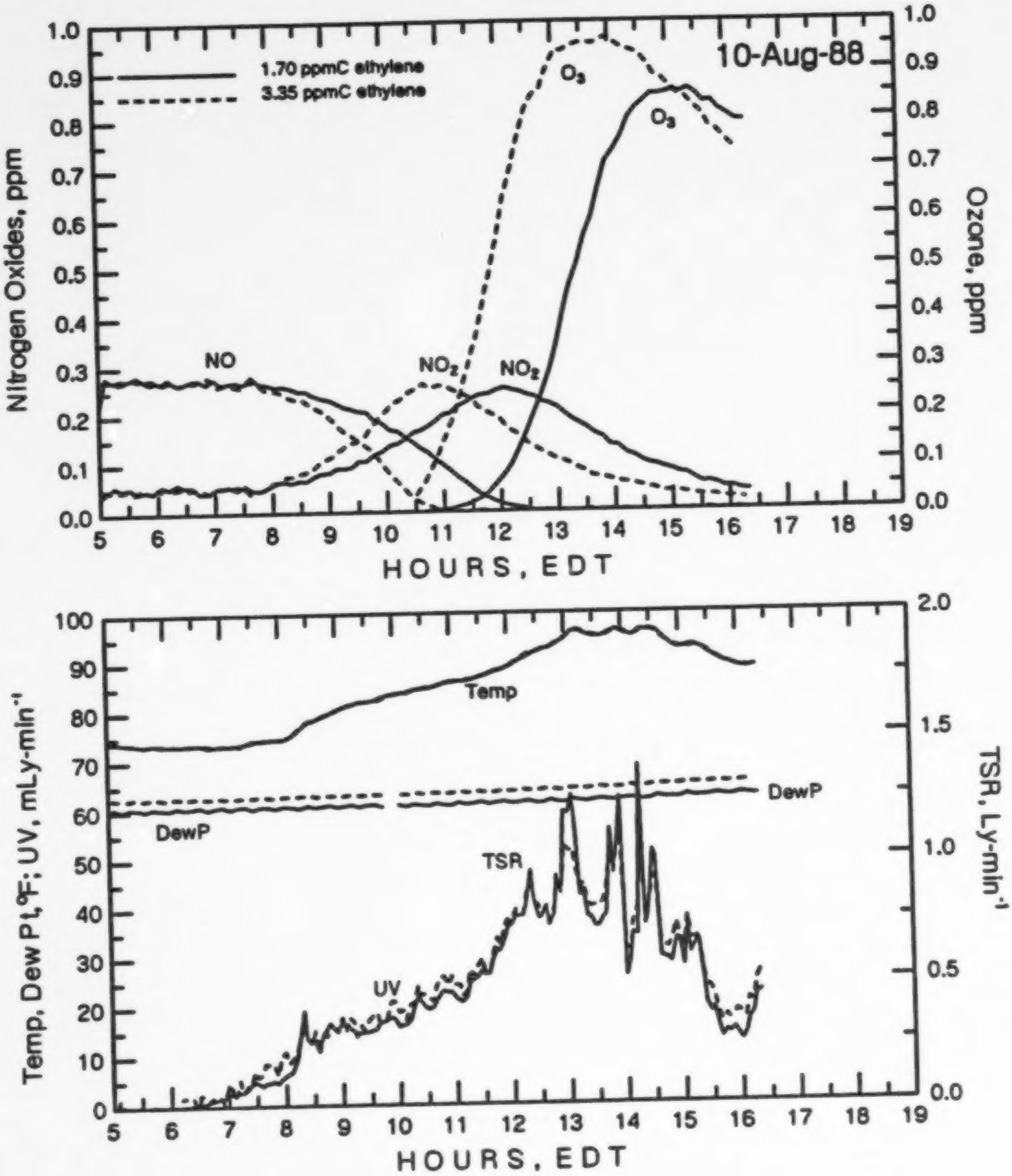

Figure 38. Differential ethene concentrations at same NO_x.

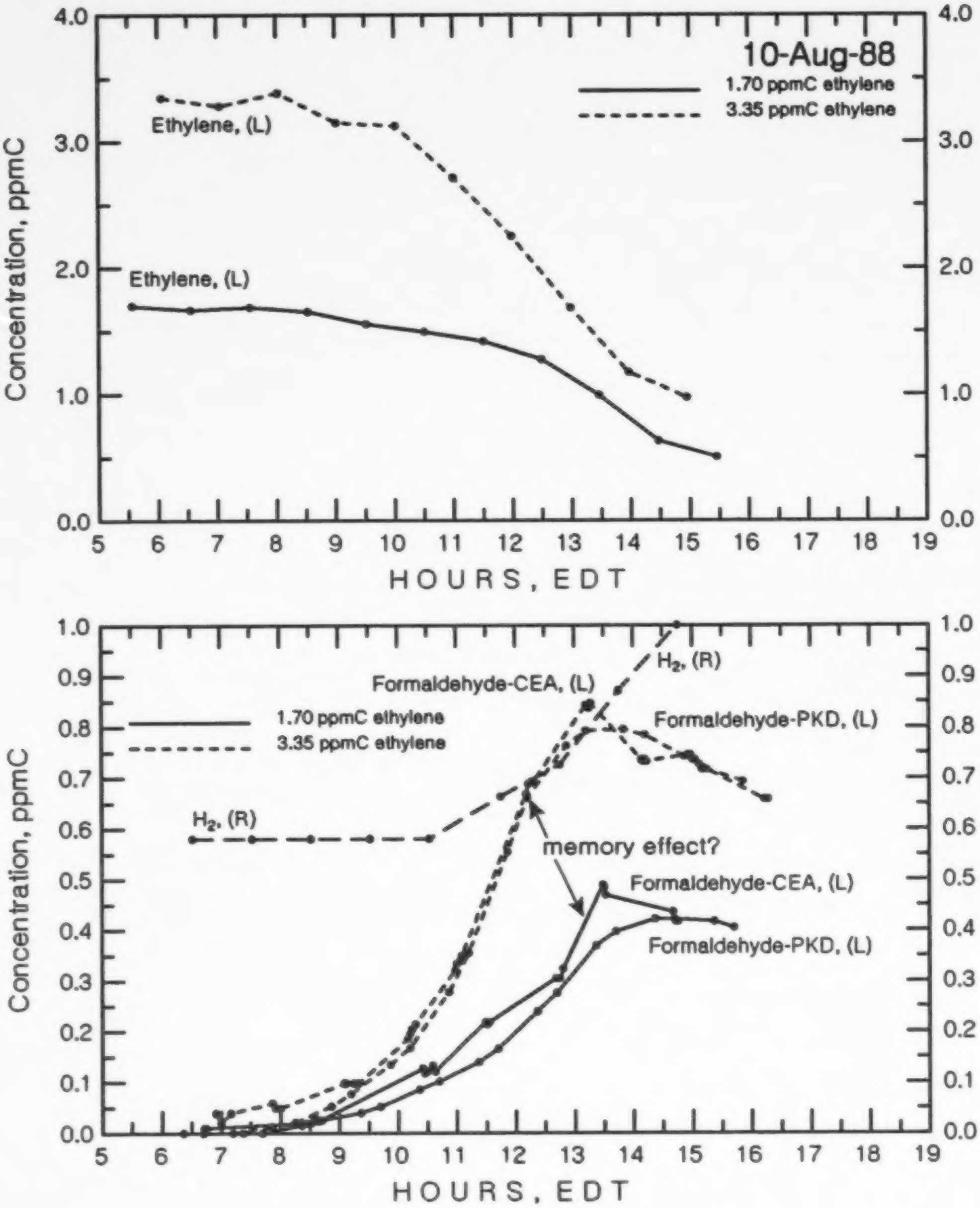

Figure 39. Differential ethene concentrations at same NO_x.

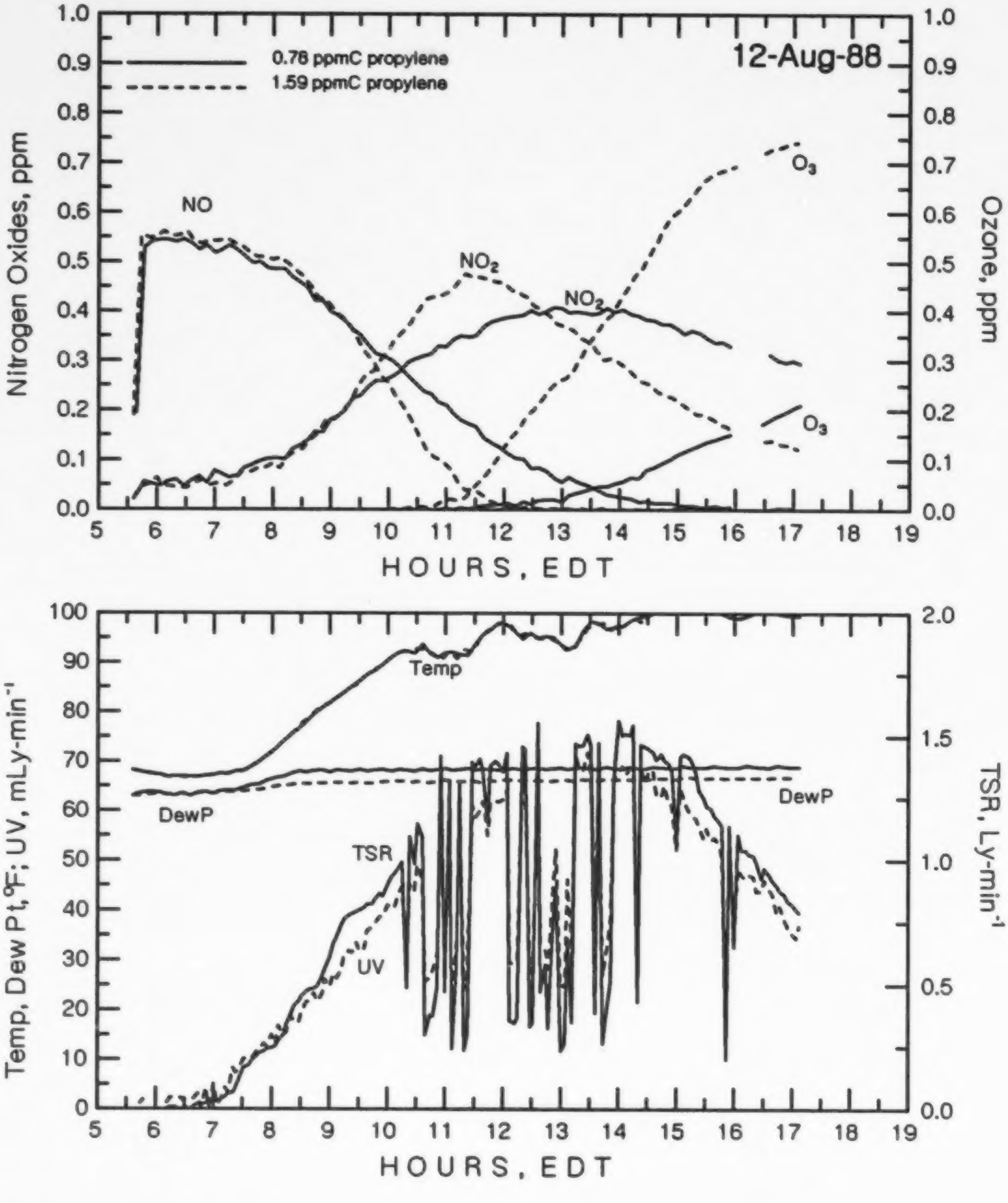

Figure 40. Differential propene concentrations at same NO_x.

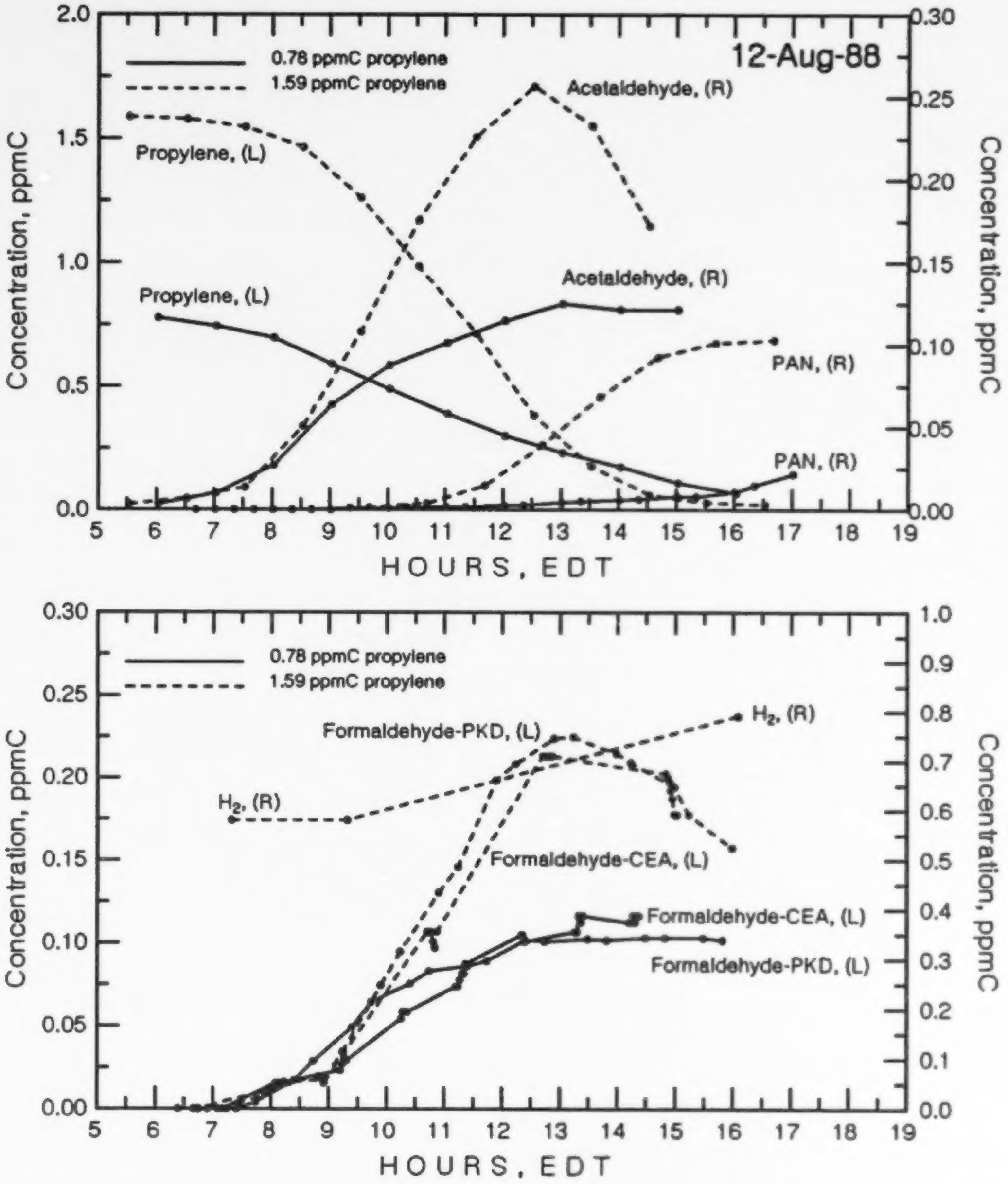

Figure 41. Differential propene concentrations at same NO_x.

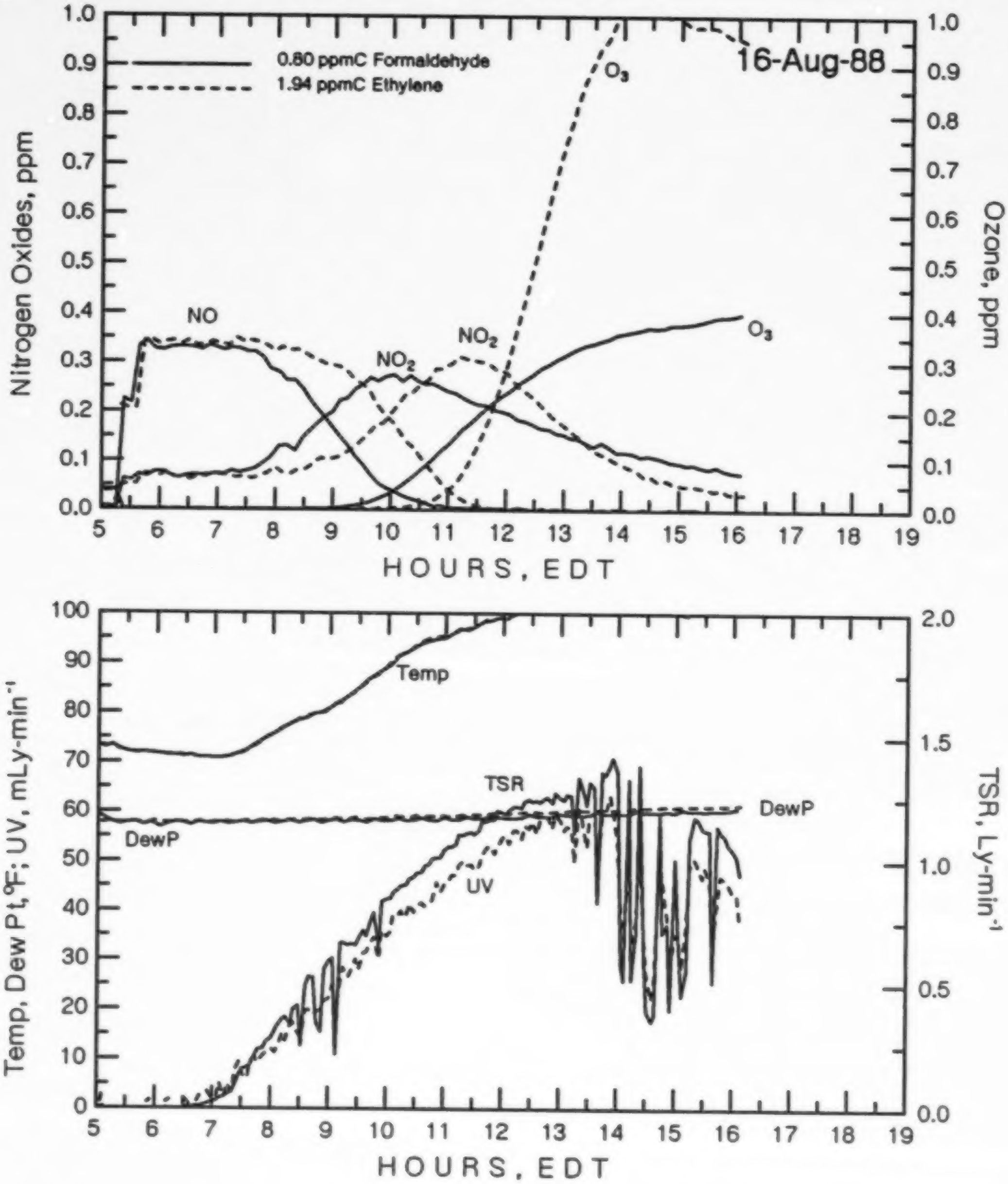

Figure 42. Formaldehyde vs. ethene at same NO_x.

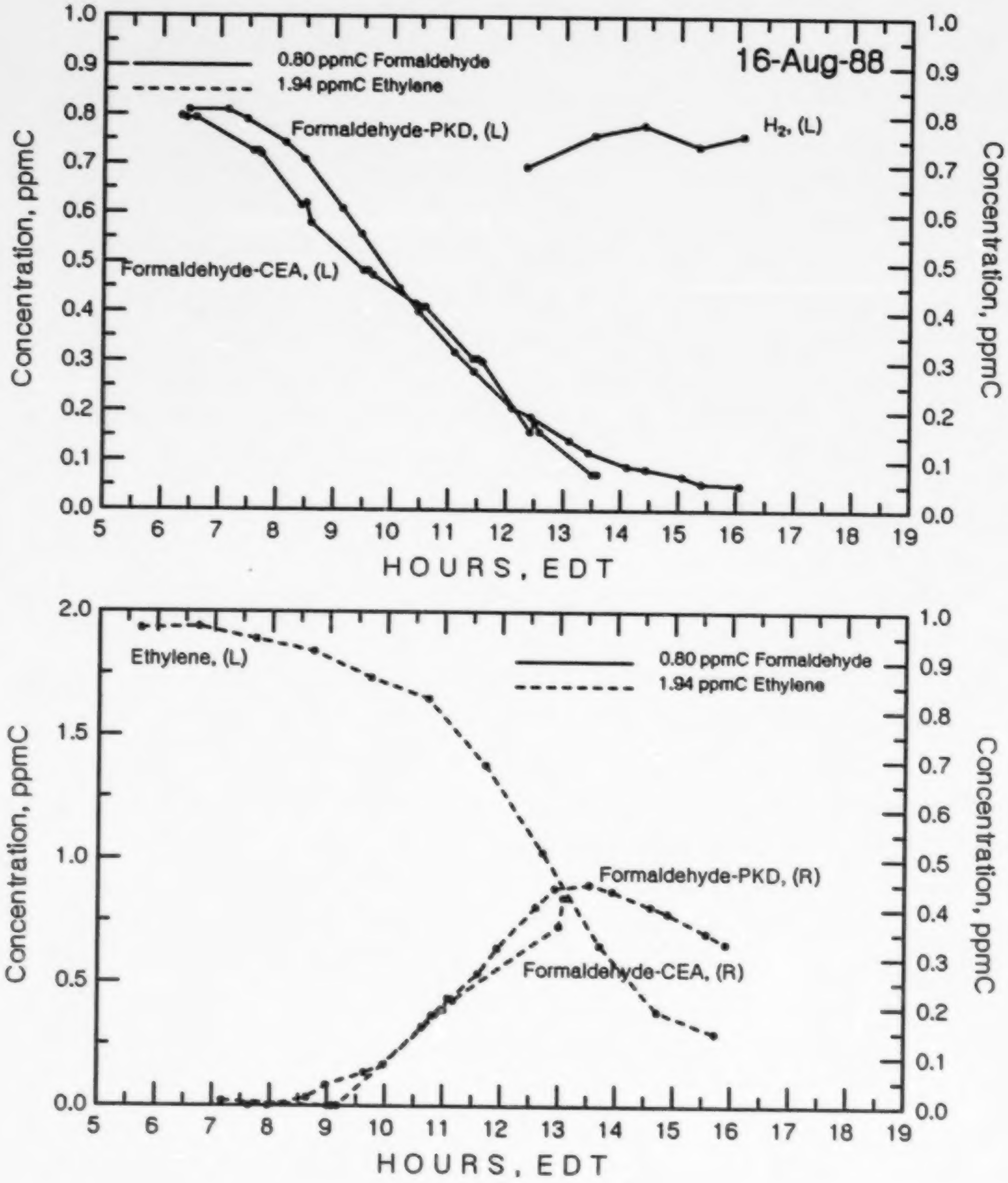

Figure 43. Formaldehyde vs. ethene at same NO_x.

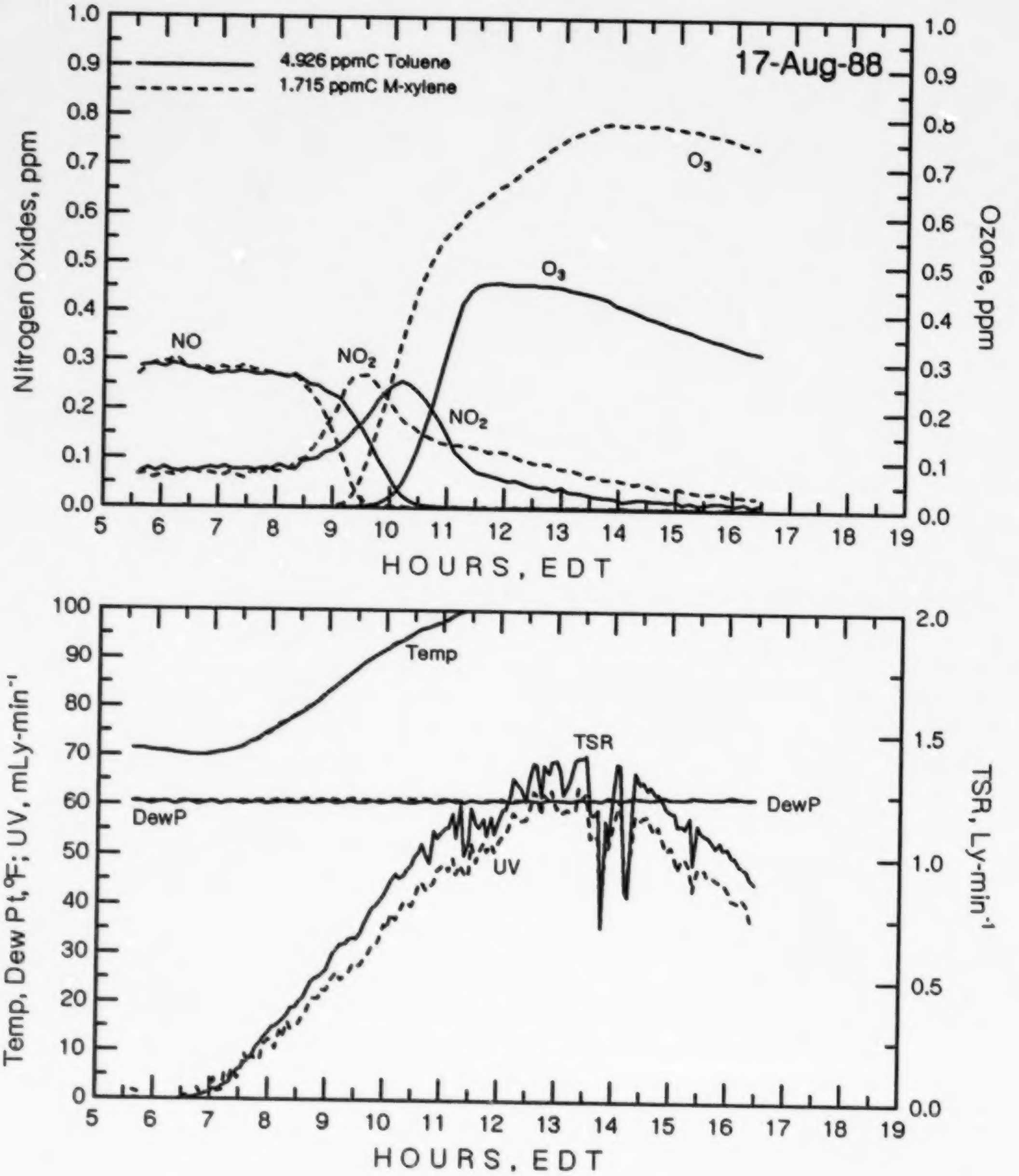

Figure 44. Toluene vs. M-xylene at same NO_x.

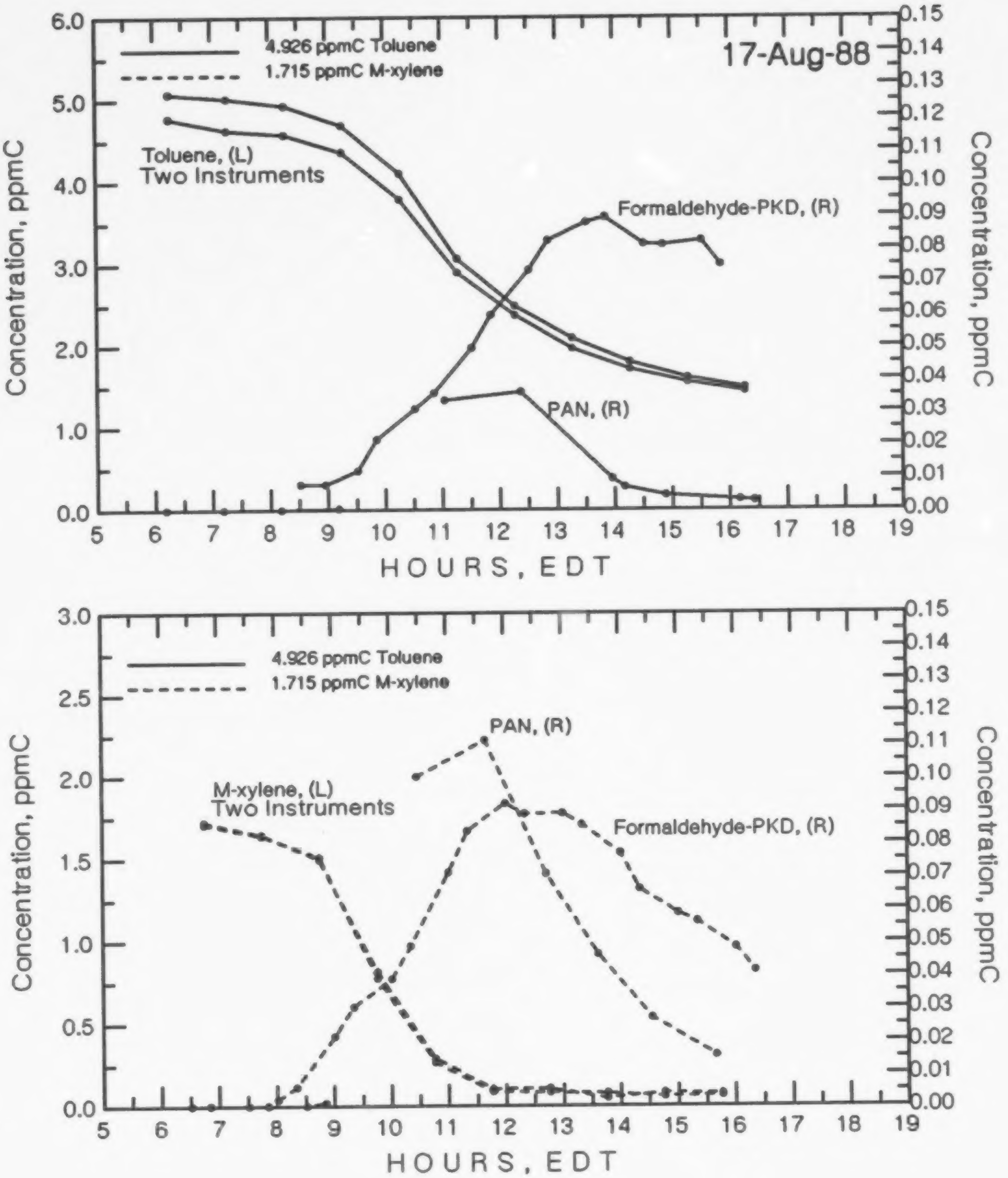

Figure 45. Toluene vs. M-xylene at same NO_x.

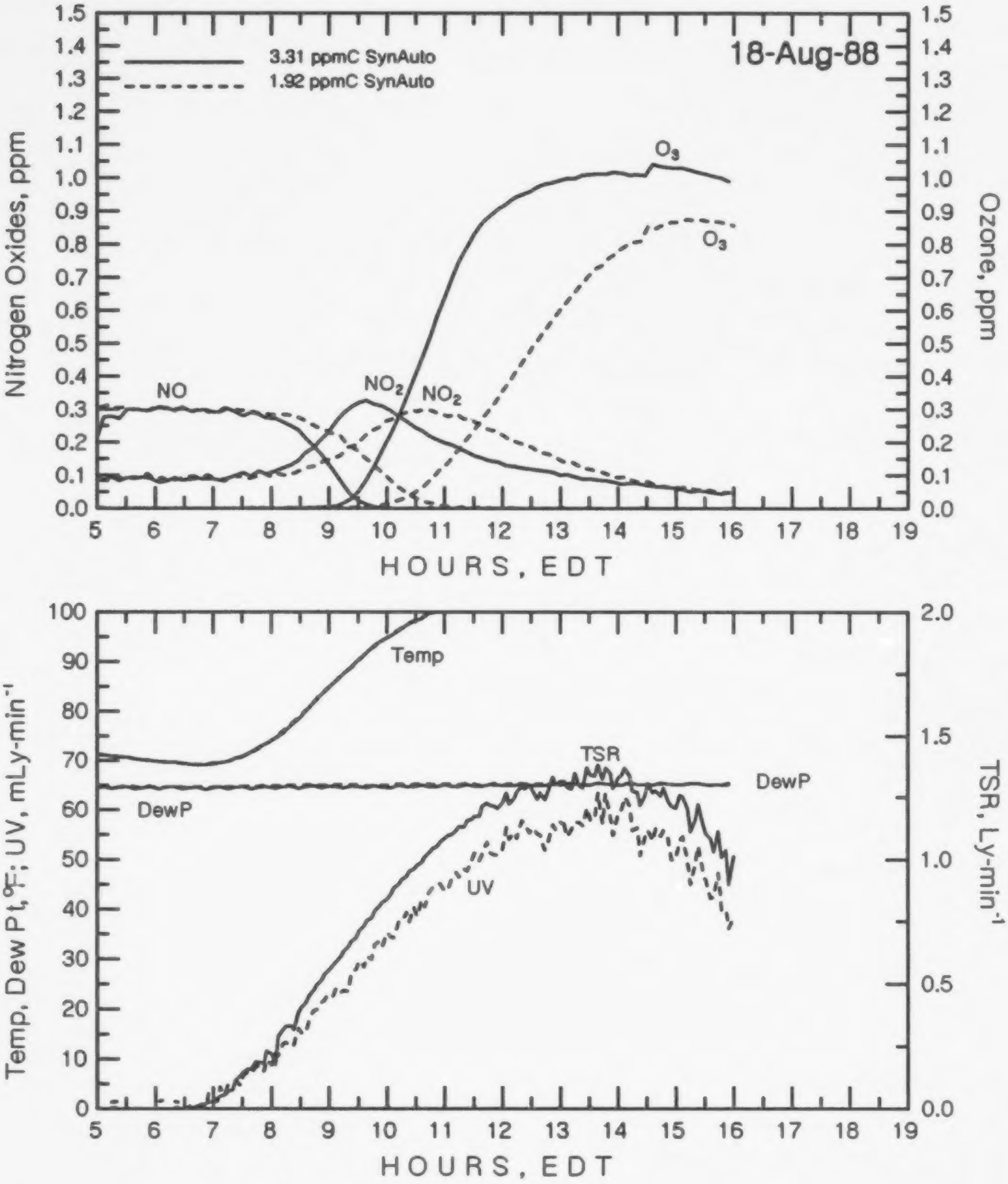

Figure 46. Differential Synthetic Auto-exhaust concentrations at same NO_x.

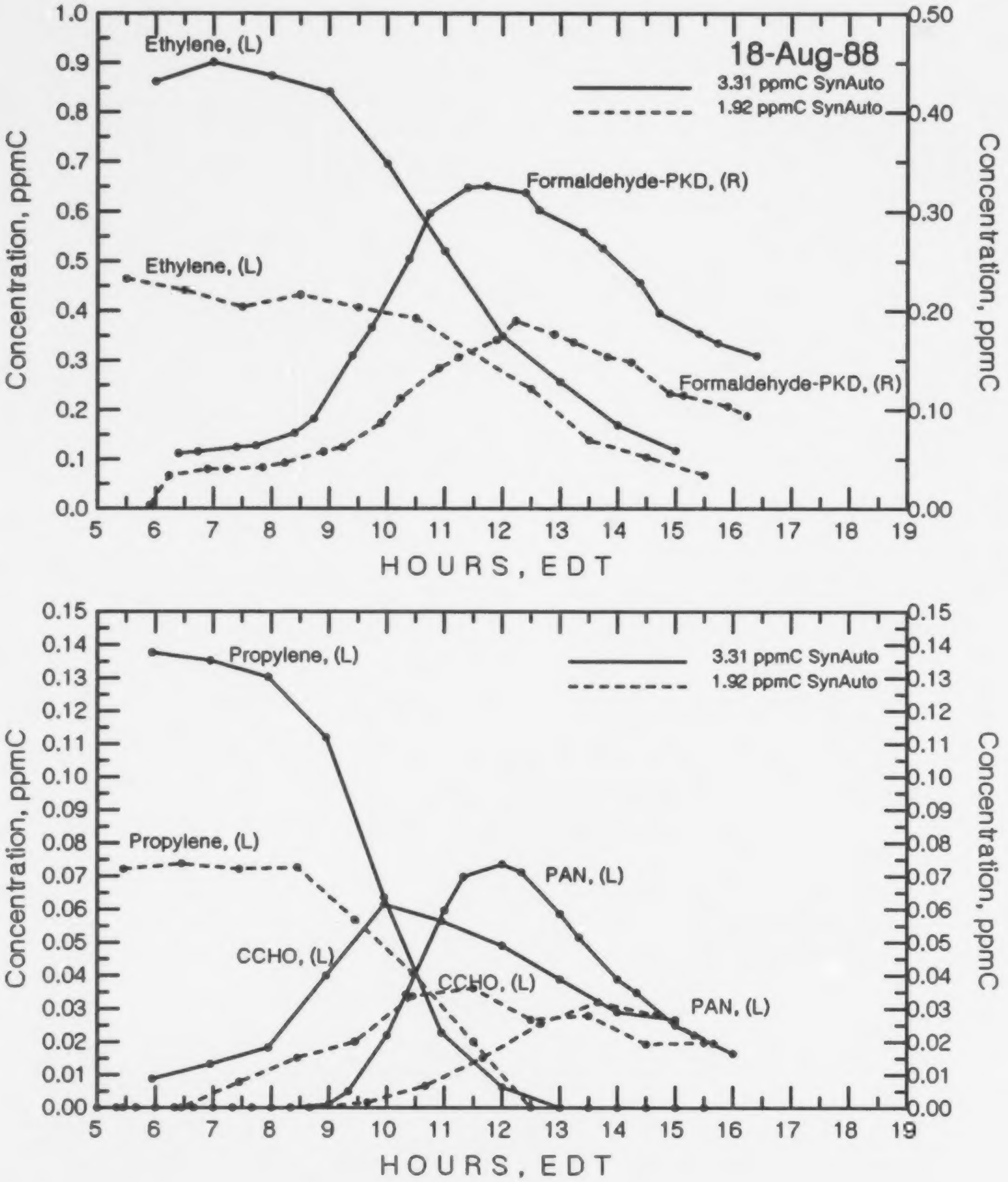

Figure 47. Differential Synthetic Auto-exhaust concentrations at same NO_x.

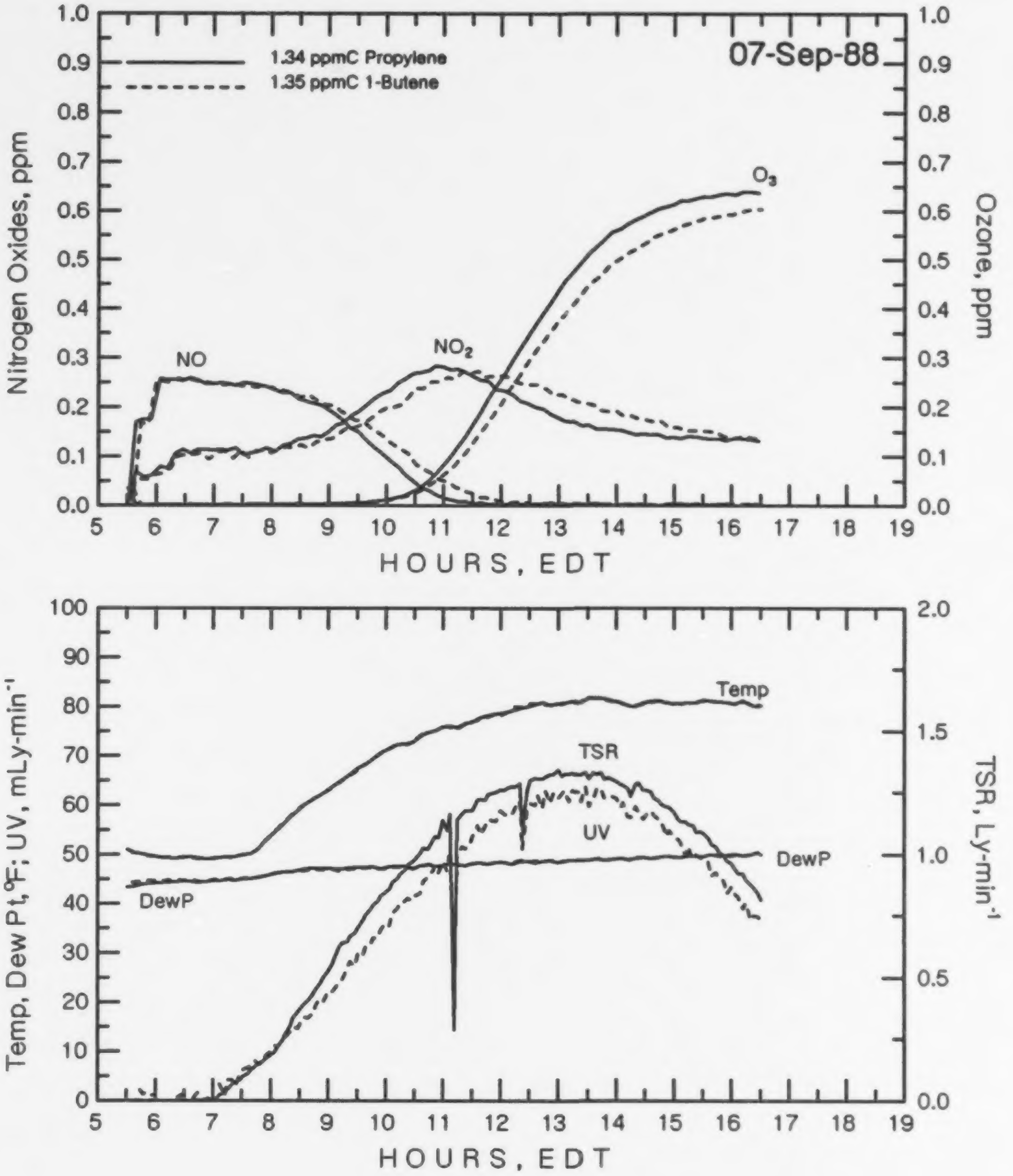

Figure 48. Propene vs. 1-butene at same NO$_x$.

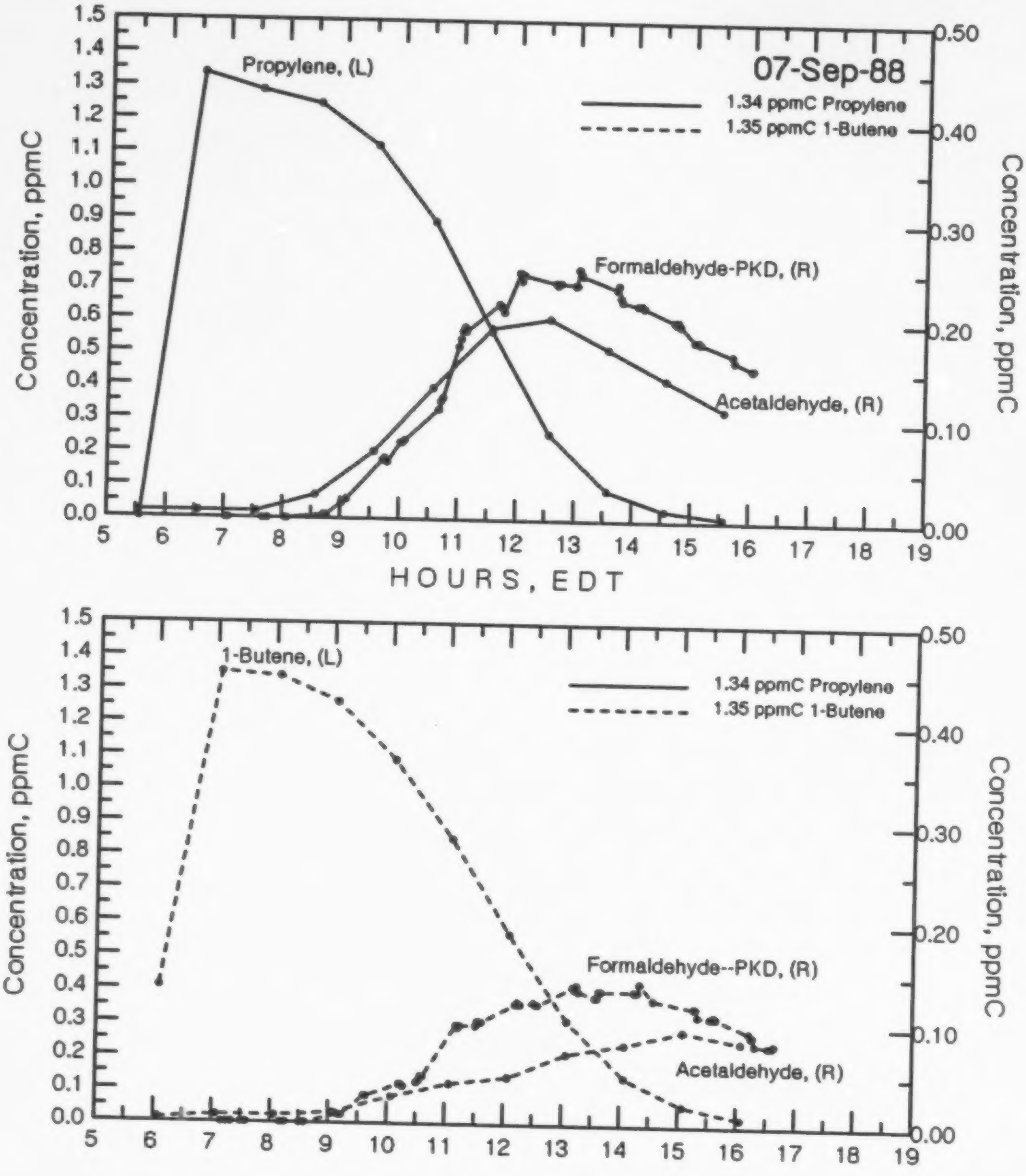

Figure 49. Propene vs. 1-butene at same NO_x.

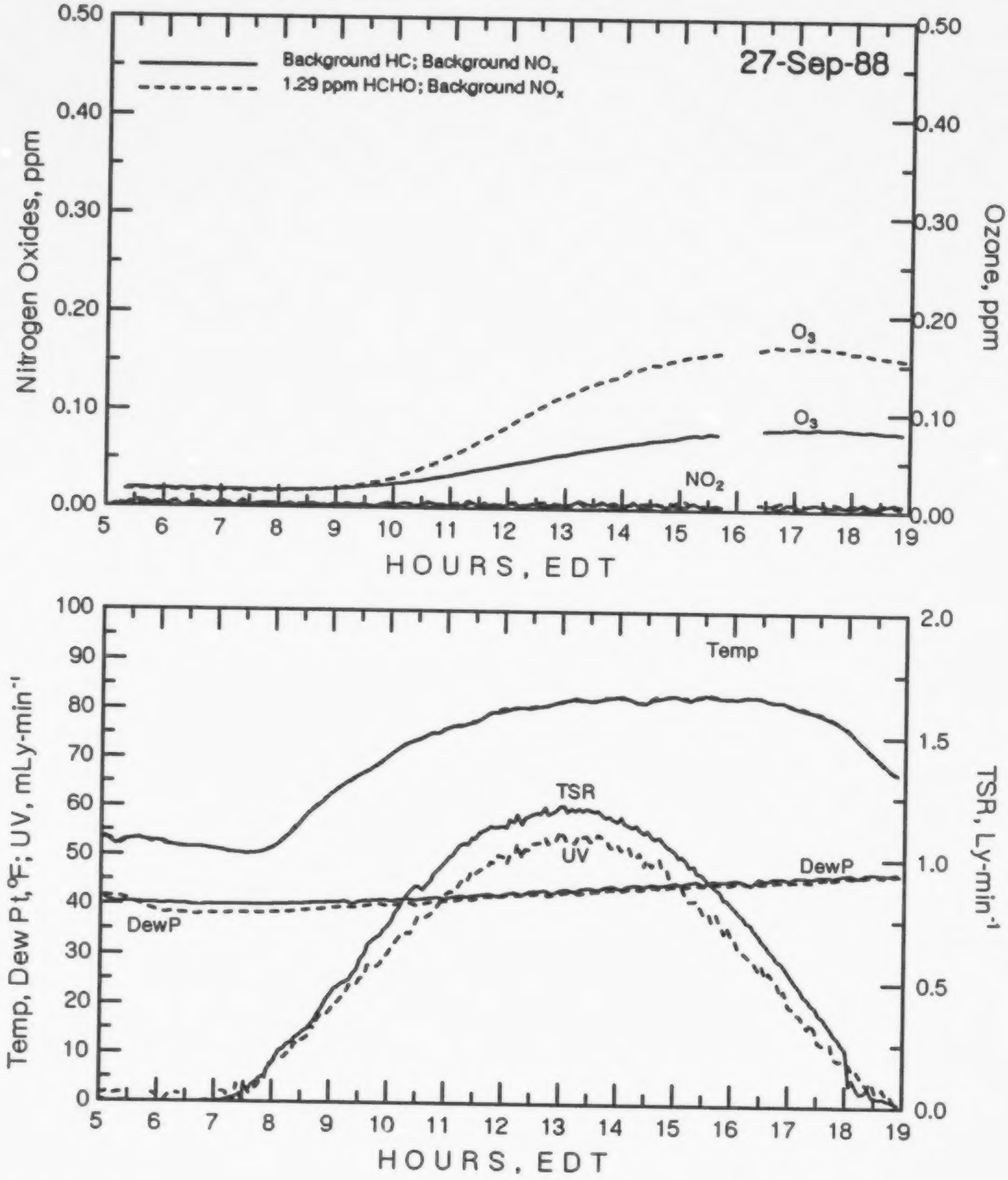

Figure 50. Background air vs. formaldehyde at background NO_x.

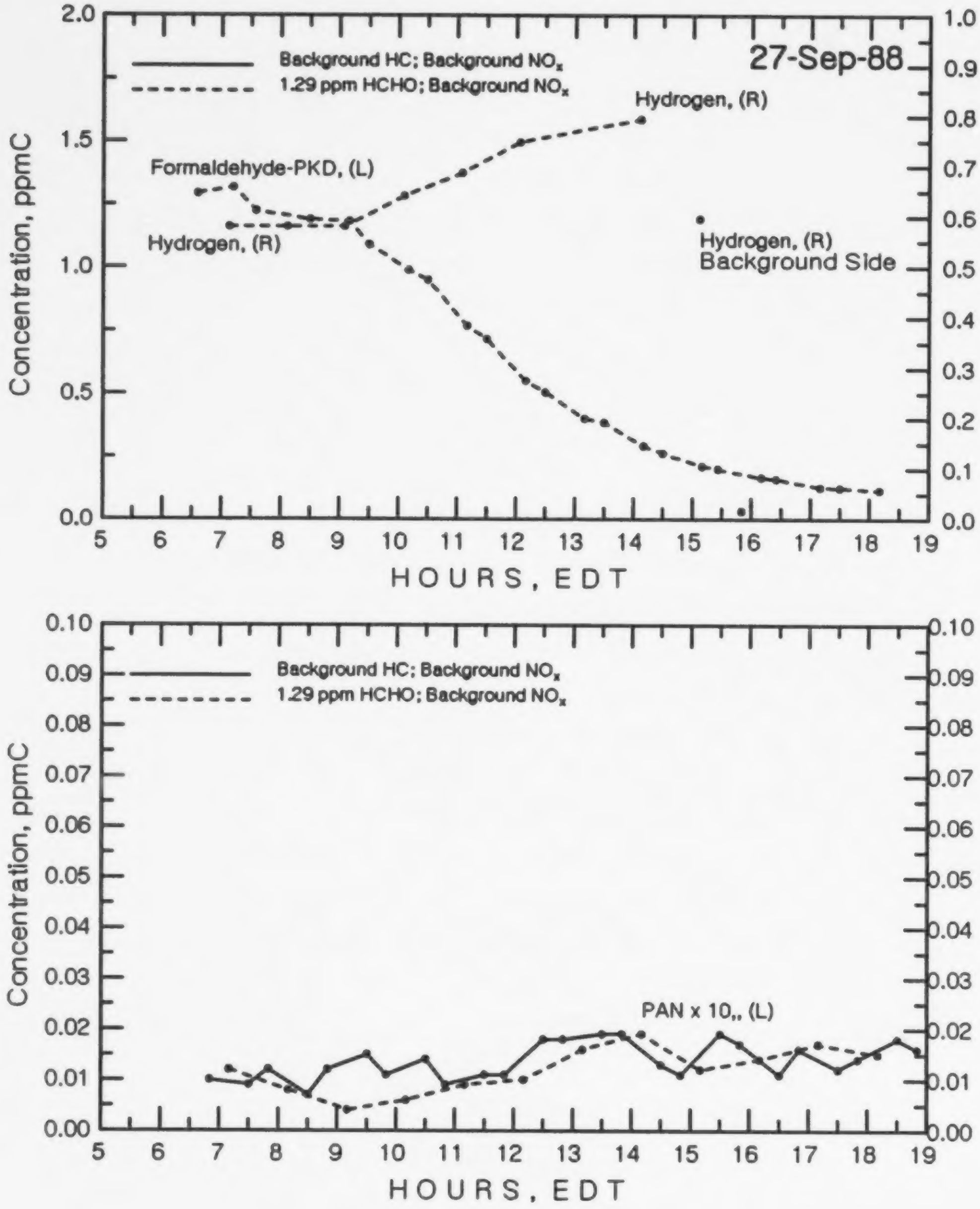

Figure 51. Background air vs. formaldehyde at background NO$_x$.

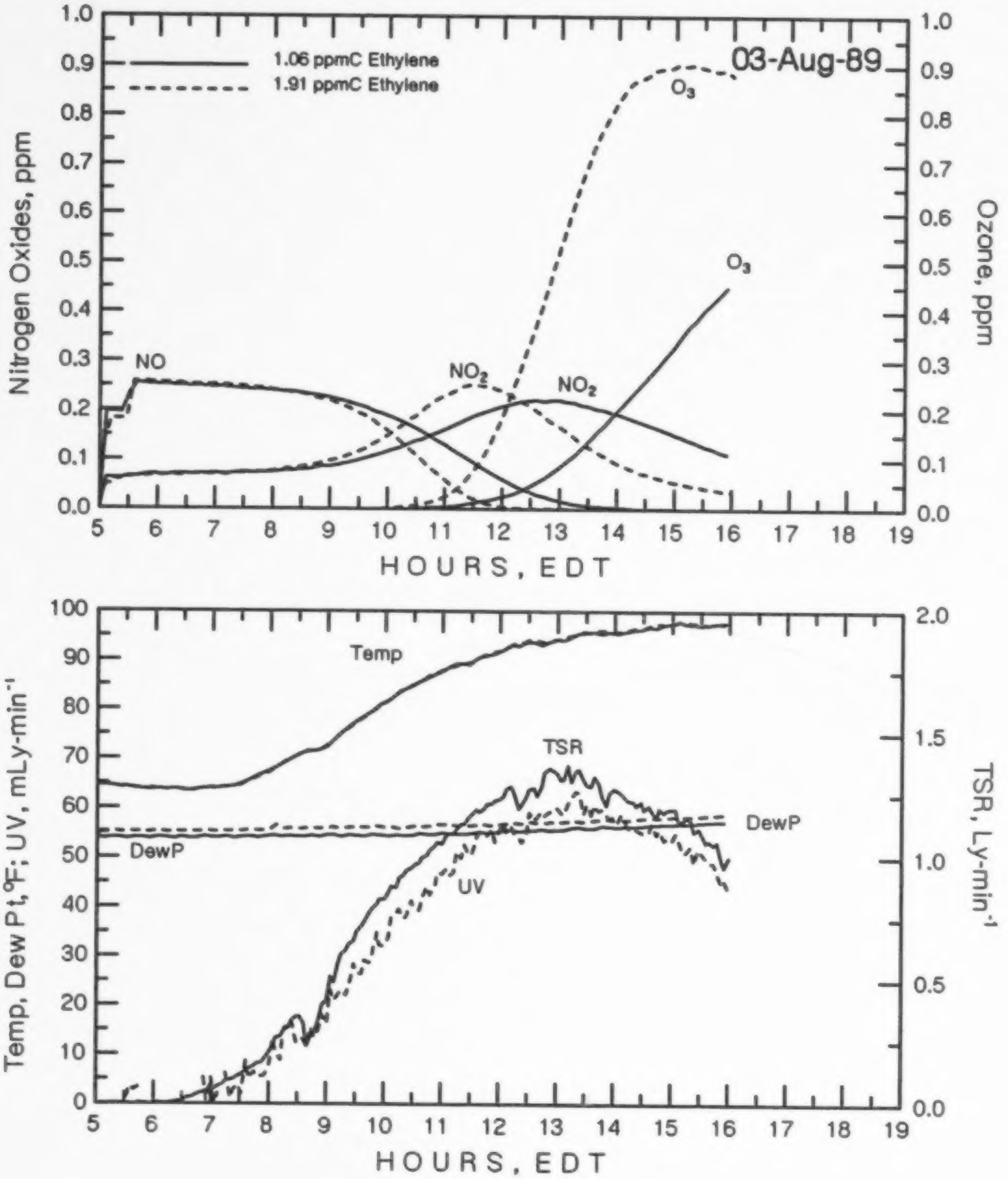

Figure 52. Differential ethene concentrations at same NO_x.

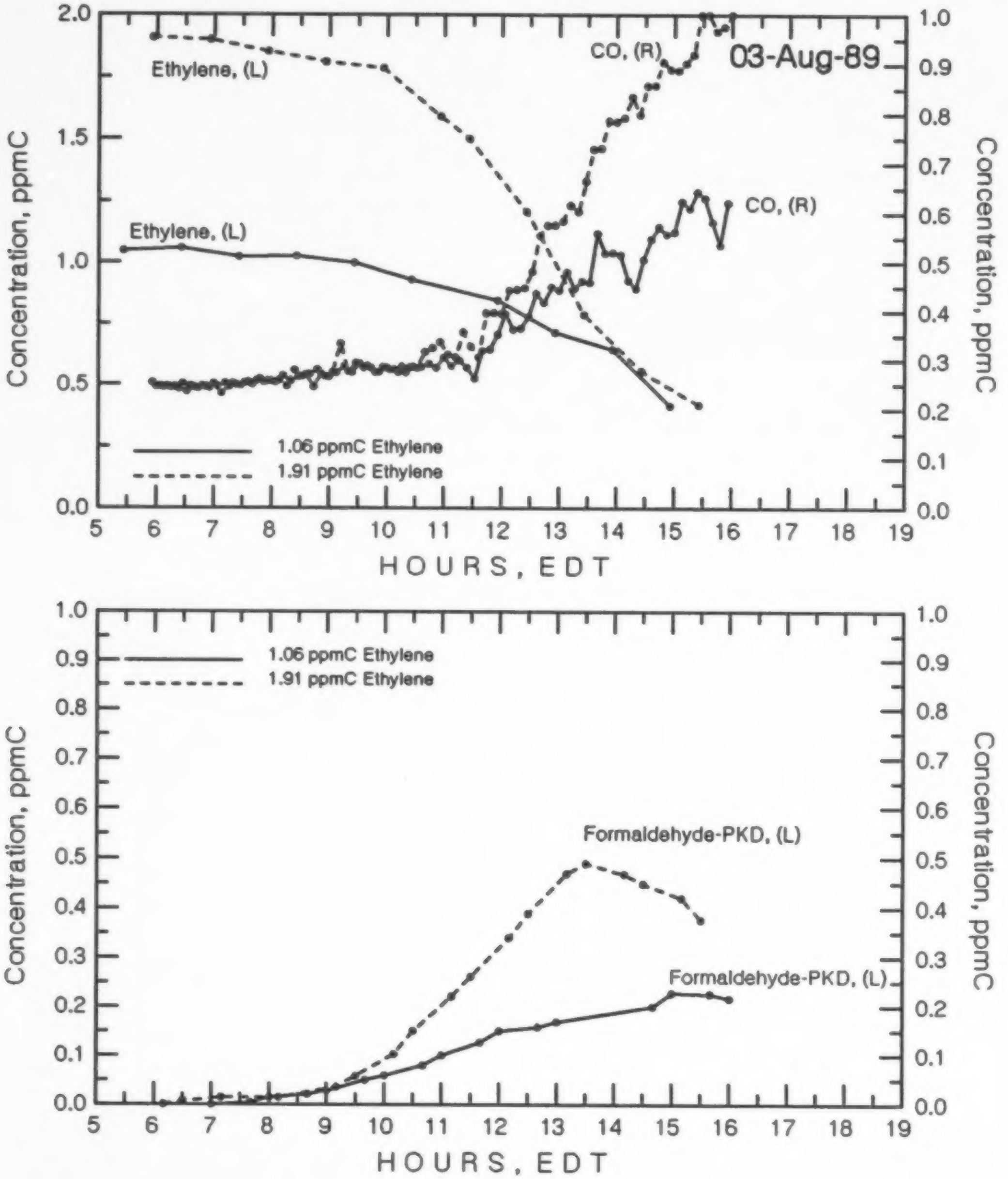

Figure 53. Differential ethene concentrations at same NO_x.

4

Explicit Mechanism: 1

To investigate the discrepancies between HCHO predictions obtained with the CB4 and CAL mechanisms and the UNC chamber data, it is necessary to use a reaction mechanism that does not have the species and reaction limitations of the air quality simulation model mechanisms. That is, a mechanism is needed that includes details on many processes that are omitted or compressed in the CB4 and CAL mechanisms. In addition, we wished to investigate the impact that the various omissions and compressions made in producing these mechanisms might have had on HCHO predictions. Note that these mechanisms were specifically designed to predict ozone and therefore the predictions of formaldehyde were coincidential to the ozone predictions. We will show that ozone can be predicted fairly accurately in a chamber while at the same time ***formaldehyde concentrations and time profiles may not be accurately predicted.***

A Species Hierarchy

In 1982, Gary Whitten introduced the concept of a hierarchy of chemical species; a slightly different version of Whitten's hierarchy is shown in Figure 54. In this concept, each species in oxidant formation can be assigned to a hierarchical level on the basis of the number of HC/NO_x systems in which it occurs, with the most ubiquitous species occupying the lowest levels. Thus CO is lower than HCHO, which is lower than $CH_3HC{=}O$. In the discussion here, this concept forms both the basis of presenting the reactions that make up the mechanism and the order in which the mechanism will be tested in later chapters. The mechanism will be described and demonstrated in parts. Each major part is further divided into reaction modules.

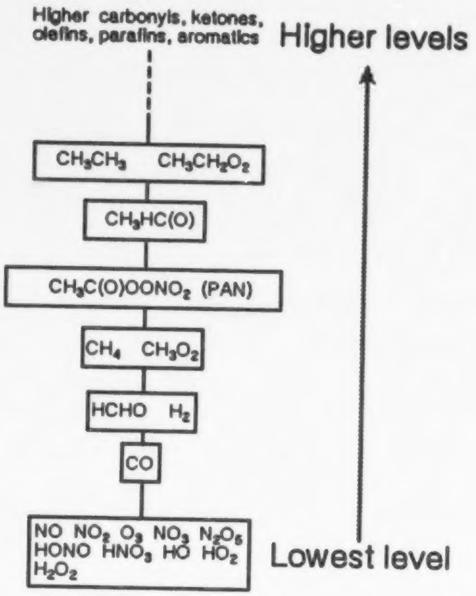
Higher carbonyls, ketones, olefins, parafins, aromatics
Higher levels
CH_3CH_3 $CH_3CH_2O_2$
$CH_3HC(O)$
$CH_3C(O)OONO_2$ (PAN)
CH_4 CH_3O_2
HCHO H_2
CO
NO NO_2 O_3 NO_3 N_2O_5 HONO HNO_3 HO HO_2 H_2O_2
Lowest level

Figure 54. A Species Hierarchy.

Reaction Modules

The first part includes the inorganic, methane, formaldehyde, ethane, acetaldehyde, and peroxyacetyl nitrate modules. Other reaction sequences will be described in later chapters after we have tested the mechanism for these simple VOC species. The mechanism is listed in full in Appendix M.

All reactions have labels which are shown here in bold letters. Reaction labels are assigned leading letters that identify the various reaction modules, for example:

- ▹ **I** – inorganic reactions
- ▹ **P1** – methane reactions
- ▹ **C1** – formaldehyde reactions
- ▹ **P2** – ethane reactions
- ▹ **C2** – acetaldehyde reactions
- ▹ **PA2** – PAN reactions

The modules are further divided into related reaction clusters which are described in each section below.

Special Rate Constant Forms

There are two special forms of pressure-dependent rate constants used in the mechanism, the Troe "fall off" expression and the Lindemann-Hinshelwood expression.

In the "fall off" expression, the rate constant is given by

$$k = \left(\frac{k_o[\mathsf{M}]}{1+r}\right) F^g$$

where

$$r = \frac{k_o[\mathsf{M}]}{k_\infty}$$

$$g = \frac{1}{1+\left(\frac{1}{N} log_{10}(r)\right)^2}$$

and $[\mathsf{M}]$ is the total molecular concentration (*i.e.*, molecules/cm^3). The need to use this expression for the rate constant of a reaction will be indicated by

$$k = \mathsf{FallOff}$$

followed by the expressions for k_∞, k_o, F, and N. Since k_∞ and k_o usually have two parameters each, as many as six parameters may be needed to specify a rate constant for a fall off reaction.

In the Lindemann-Hinshelwood expression, the rate constant is given by

$$k = k_o + \frac{k_3[\mathsf{M}]}{1+\frac{k_3[\mathsf{M}]}{k_2}}$$

The need to use this expression will be indicated by

$$k = \mathsf{Lindemann\text{-}Hinshelwood}$$

followed by expressions for k_o, k_2, and k_3. Again six parameters may be needed to specify a rate constant.

Photolytic rate constants are indicated by

$$k = \mathsf{HVtablename}$$

where **HVtablename** names a externally supplied table that contains the rate as a function of time. The absorption cross sections and quantum yields used to compute these rates for a given set of actinic fluxes are listed in tables in each module description near the photolysis reaction itself.

I = Inorganic Chemistry

The explict mechanism contains 42 inorganic reactions divided into eight sections:

a) nitrogen dioxide (NO_2) photolysis,
b) ozone (O_3) photolysis,
c) nitrogen trioxide radical ($NO_3^{\cdot}$) chemistry,
d) nitrous acid (HONO) chemistry,
e) hydroperoxy radical ($HO_2^{\cdot}$)-nitrogen oxides (NO_x) reactions,
f) hydroxyl radical ($^{\cdot}OH$) termination reactions,
g) $HO_2^{\cdot}$ termination reactions, and
h) carbon monoxide (CO)-hydrogen (H_2) chemistry.

All of these inorganic reactions have been studied in the laboratory and appear in several reviews of kinetic data. The source used for most of these reactions is the review produced by the NASA Panel for Data Evaluation (DeMore, *et al.*, "Chemical Kinetics and Photochemical Data for Use in Stratospheric Modeling, Evaluation Number 8", 1987)[17] referred to here as NASA87. Because of this extensive review, little needs to be said about these reactions. Occasionally an inorganic reaction that may be important in the smog chamber does not appear in NASA87. Other reviews such as CODATA (Baulch *et al.*, "Evaluated Kinetic and Photochemical Data for Atmospheric Chemistry," 1984)[18] or Atkinson and Lloyd, 1984[19] are used as the source for these—see the individual reaction comments.

Section a: NO_2 photolysis

Ia1 $NO_2 \xrightarrow{h\nu} NO + O(3P)$

$$k = \mathrm{HVNO2} \quad s^{-1}$$

The absorption cross-sections used for NO_2 were those of Bass, Ledford, and Laufer.[20] The quantum yields were from Garnder *et al.*[21] The absorption cross-sections were given as 1/8-nanometer point values. The quantum yields were given as 5-nm values from 290 to 380 nm and 1-nm values from 380 to 424 nm. These data were integral averaged to 1-nm ending intervals using the UNC `CsQyAvg` program; the resulting values appear in Table 5. The method used to compute in-chamber actinic flux and the in-chamber photolysis rates is a minor revision of the method described in Jeffries, *et al.* 1989.[4]

Ia2 $O(3P) + O_2 + M \longrightarrow O_3 + M$

This reaction and rate constant are from NASA87, Table 2:

$$k = 6.0 \times 10^{-34}(T/300)^{-2.3} \quad \text{cm}^6\text{-molecules}^{-2}\text{-s}^{-1}$$

Ia3 $O_3 + NO \longrightarrow NO_2 + O_2$

This reaction and rate constant are from NASA87, Table 1:

$$k = 2.0 \times 10^{-12} e^{-1400/T} \quad \text{cm}^3\text{-molecules}^{-1}\text{-s}^{-1}$$

Ia4 $NO + NO + O_2 \longrightarrow 2NO_2$

This reaction and rate constant are from Atkinson and Lloyd, 1984:

$$k = 3.3 \times 10^{-39} e^{530/T} \quad \text{cm}^6\text{-molecules}^{-2}\text{-s}^{-1}$$

Table 5. Cross Sections and Quantum Yields for NO_2

$(NO_2 \xrightarrow{h\nu} NO + O(3P))$

(units are nanometers, $\times 10^{20}$ cm^2-$molecule^{-1}$, base *e*)

λ	σ_λ	Φ_λ	λ	σ_λ	Φ_λ	λ	σ_λ	Φ_λ
298	13.0762	0.9975	341	38.7887	0.9889	384	55.7454	0.9715
299	11.8406	0.9973	342	41.6575	0.9887	385	59.9087	0.9700
300	12.3244	0.9971	343	36.4994	0.9885	386	58.8442	0.9680
301	12.0737	0.9969	344	38.1173	0.9883	387	55.1511	0.9665
302	13.0038	0.9967	345	39.8107	0.9881	388	59.2727	0.9650
303	14.6137	0.9965	346	41.0781	0.9879	389	57.9805	0.9630
304	15.4912	0.9963	347	44.0630	0.9877	390	60.0955	0.9610
305	15.3719	0.9961	348	43.2169	0.9875	391	59.6780	0.9595
306	15.4137	0.9959	349	50.1038	0.9873	392	62.2339	0.9580
307	15.4850	0.9957	350	41.1461	0.9871	393	59.9294	0.9550
308	16.7306	0.9955	351	43.4794	0.9869	394	54.3645	0.9515
309	17.0212	0.9953	352	44.3613	0.9867	395	54.4453	0.9460
310	18.5213	0.9951	353	43.3586	0.9865	396	62.2927	0.9320
311	18.4694	0.9949	354	43.9583	0.9863	397	56.7043	0.8960
312	19.5206	0.9947	355	53.9105	0.9862	398	57.5889	0.8450
313	20.6831	0.9945	356	47.4056	0.9858	399	63.9028	0.7900
314	19.6344	0.9943	357	49.4844	0.9855	400	59.9580	0.7275
315	21.1694	0.9941	358	54.1505	0.9851	401	65.4565	0.6650
316	21.7706	0.9939	359	48.4862	0.9848	402	61.4414	0.5975
317	21.7594	0.9937	360	45.5769	0.9844	403	53.1899	0.5225
318	23.6799	0.9935	361	49.9193	0.9841	404	55.4019	0.4550
319	23.4193	0.9933	362	51.2462	0.9837	405	58.9150	0.3875
320	24.3282	0.9931	363	50.8627	0.9834	406	59.0605	0.3200
321	26.0206	0.9929	364	49.2869	0.9830	407	50.9722	0.2575
322	25.7632	0.9927	365	53.8564	0.9827	408	53.1895	0.2050
323	27.0232	0.9925	366	58.1191	0.9823	409	64.9121	0.1690
324	26.1693	0.9923	367	50.3062	0.9820	410	59.4600	0.1415
325	27.2432	0.9921	368	54.5300	0.9816	411	59.0000	0.1200
326	29.3356	0.9919	369	52.6089	0.9813	412	59.8200	0.1020
327	29.3450	0.9917	370	52.8513	0.9809	413	60.8800	0.0885
328	29.6781	0.9915	371	51.6187	0.9806	414	61.9400	0.0765
329	29.0938	0.9913	372	55.6838	0.9802	415	63.0000	0.0645
330	30.5056	0.9911	373	58.6765	0.9799	416	62.8600	0.0535
331	30.0505	0.9909	374	53.8809	0.9795	417	62.7200	0.0435
332	31.1738	0.9907	375	52.0286	0.9794	418	62.5800	0.0345
333	34.6706	0.9905	376	58.2527	0.9786	419	62.4400	0.0265
334	33.9006	0.9903	377	62.1152	0.9778	420	62.3000	0.0205
335	31.8175	0.9901	378	52.9526	0.9770	421	61.8400	0.0150
336	33.8964	0.9899	379	52.2119	0.9762	422	61.3800	0.0100
337	34.8694	0.9897	380	59.8696	0.9754	423	60.9200	0.0060
338	33.9031	0.9895	381	58.6157	0.9745	424	60.4600	0.0020
339	37.7600	0.9893	382	56.2312	0.9735	425	60.0000	0.0000
340	38.4726	0.9891	383	54.0598	0.9725			

Ia5a $O(3P) + NO_2 \longrightarrow NO + O_2$

This reaction and rate constant are from NASA87, Table 1:

$$k = 6.5 \times 10^{-12} e^{120/T} \quad \text{cm}^3\text{-molecules}^{-1}\text{-s}^{-1}$$

Ia5b $O(3P) + NO_2 \xrightarrow{M} NO_3^{\cdot}$

This reaction and rate constant are from NASA87, Table 2:

$$k = \mathsf{FallOff} \quad \text{cm}^3\text{-molecules}^{-1}\text{-s}^{-1}$$
$$k_\infty = 2.2 \times 10^{-11} \quad k_o = 9.0 \times 10^{-32}(T/300)^{-2} \quad F = 0.6 \quad N = 1$$

Ia6 $O(3P) + NO \xrightarrow{M} NO_2$

This reaction and rate constant are from NASA87, Table 2:

$$k = \mathsf{FallOff} \quad \text{cm}^3\text{-molecules}^{-1}\text{-s}^{-1}$$
$$k_\infty = 3.0 \times 10^{-11} \quad k_o = 9.0 \times 10^{-32}(T/300)^{-1.5} F = 0.6 \quad N = 1$$

This reaction is not included in Carter's 1989 mechanism.

Section b: O_3 photolysis

Ib1 $O_3 \xrightarrow{h\nu} O(3P) + O_2$

$$k = \mathrm{HVO3O3P} \quad s^{-1}$$

The absorption coefficients for 280–320 nm are from Bass and Paur, 1985,[22] and those for > 320 nm were reported in Carter *et al.*, 1986.[23] These data were treated as point spectra for rate calculations. The quantum yields are calculated by difference between 1.0 and the quantum yields used for reaction Ib2. These values are reported in Table 6.

Ib2 $O_3 \xrightarrow{h\nu} O(1D) + O_2$

$$k = \mathrm{HVO3O1D} \quad s^{-1}$$

The absorption coefficients are from Bass and Paur, 1985, and the quantum yields are from NASA87 for $T = 300$ K. See Table 7.

Ib3 $O(1D) + M \longrightarrow O(3P) + M$

This reaction is from CODATA84, Table 2. The rate constant used here is:

$$k = 2.09 \times 10^{-11} e^{95.3/T} \mathrm{cm}^3\text{-molecules}^{-1}\text{-s}^{-1}$$

This rate constant is based on a weighted regression with $M = N_2$, which occurs 79.05% and $M = O_2$, which occurs 20.95% of the time. The rate constants given in CODATA84 were

$$O(1D) + N_2 \longrightarrow O(3P) + N_2 \quad 1.8 \times 10^{-11} e^{107/T}$$
$$O(1D) + O_2 \longrightarrow O(3P) + O_2 \quad 3.2 \times 10^{-11} e^{67/T}$$

These were evaluated over the temperature range 273-315 K, weighted by the factors above and a new rate constant was fitted by regression to the weighted rate constant values.

Table 6. Cross Sections and Quantum Yields for O_3
($O_3 \xrightarrow{h\nu} O(3P)+O_2$)

(units are nanometers, $\times 10^{20}$ cm^2-molecule^{-1}, base e)

λ	σ_λ	Φ_λ	λ	σ_λ	Φ_λ	λ	σ_λ	Φ_λ
280	397.00	0.100	299	45.190	0.100	318	3.720	0.976
281	360.00	0.100	300	39.240	0.100	319	2.690	0.997
282	324.00	0.100	301	34.240	0.100	320	3.232	1.000
283	301.00	0.100	302	30.550	0.100	330	0.670	1.000
284	273.00	0.100	303	26.010	0.100	340	0.170	1.000
285	244.00	0.100	304	23.740	0.100	350	0.040	1.000
286	221.00	0.100	305	20.110	0.112	355	0.000	1.000
287	201.00	0.100	306	17.870	0.149	400	0.000	1.000
288	176.00	0.100	307	15.600	0.197	450	0.016	1.000
289	158.00	0.100	308	13.760	0.259	500	0.134	1.000
290	141.00	0.100	309	12.520	0.339	550	0.332	1.000
291	126.00	0.100	310	10.200	0.437	600	0.506	1.000
292	110.00	0.100	311	9.170	0.546	650	0.245	1.000
293	98.90	0.100	312	7.880	0.652	700	0.087	1.000
294	85.94	0.100	313	6.770	0.743	750	0.032	1.000
295	76.97	0.100	314	6.350	0.816	800	0.016	1.000
296	66.68	0.100	315	5.099	0.872	900	0.000	1.000
297	58.41	0.100	316	4.610	0.916			
298	50.65	0.100	317	4.170	0.949			

Ib4 $O(1D) + H_2O \longrightarrow 2\,{}^{\cdot}OH$

This reaction and rate constant are from NASA87, Table 2:

$$k = 2.2 \times 10^{-10} \quad cm^3\text{-molecules}^{-1}\text{-s}^{-1}$$

Ib5 $O_3 + {}^{\cdot}OH \longrightarrow HO_2^{\cdot} + O_2$

This reaction and rate constant are from NASA87, Table 1:

$$k = 1.6 \times 10^{-12} e^{-940/T} \quad cm^3\text{-molecules}^{-1}\text{-s}^{-1}$$

Ib6 $O_3 + HO_2^{\cdot} \longrightarrow {}^{\cdot}OH + 2\,O_2$

Table 7. Cross Sections and Quantum Yields for O_3
$(O_3 \xrightarrow{h\nu} O(1D)+O_2)$

(units are nanometers, $\times 10^{20}$ cm^2-molecule^{-1}, base e)

λ	σ_λ	Φ_λ	λ	σ_λ	Φ_λ	λ	σ_λ	Φ_λ
280	397.0	0.900	294	85.942	0.900	308	13.760	0.738
281	360.0	0.900	295	76.968	0.900	309	12.520	0.657
282	324.0	0.900	296	66.677	0.900	310	10.200	0.558
283	301.0	0.900	297	58.414	0.900	311	9.170	0.448
284	273.0	0.900	298	50.654	0.900	312	7.880	0.344
285	244.0	0.900	299	45.187	0.900	313	6.770	0.250
286	221.0	0.900	300	39.245	0.900	314	6.350	0.178
287	201.0	0.900	301	34.245	0.900	315	5.099	0.123
288	176.0	0.900	302	30.547	0.900	316	4.610	0.081
289	158.0	0.900	303	26.011	0.900	317	4.170	0.048
290	141.0	0.900	304	23.741	0.900	318	3.720	0.022
291	126.0	0.900	305	20.112	0.884	319	2.690	0.002
292	110.0	0.900	306	17.870	0.848	320	3.232	0.000
293	98.9	0.900	307	15.600	0.800			

This reaction and rate constant are from NASA87, Table 1:

$$k = 1.1 \times 10^{-14} e^{-500/T} \quad \text{cm}^3\text{-molecules}^{-1}\text{-s}^{-1}$$

Section c: $NO_3^{\cdot}$ Chemistry

Ic1 $O_3 + NO_2 \longrightarrow NO_3^{\cdot} + O_2$

This reaction and rate constant are from NASA87, Table 1:

$$k = 1.4 \times 10^{-13} e^{-2450/T} \quad \text{cm}^3\text{-molecules}^{-1}\text{-s}^{-1}$$

Ic2a $NO_3^{\cdot} \xrightarrow{h\nu} NO + O_2$

$$k = \text{HVNO3NO} \quad \text{s}^{-1}$$

The $NO_3^{\cdot}$ absorption coefficients and quantum yields are those used in the Carter 1989 mechanism. These were based on the evaluation of Atkinson and Lloyd, 1984.[19] These appear to be centered intervals and were used in this way to compute rates. The quantum yields used were those of Magnotta and Johnston, 1980,[24] divided by 1.5 to yield unit quantum yields at 580–590 nm. These values are given in Table 8.

Ic2b $NO_3^{\cdot} \xrightarrow{h\nu} NO_2 + O(3P)$

$$k = \text{HVNO3NO2} \quad \text{s}^{-1}$$

See reaction above and Table 9.

Ic3 $NO_3^{\cdot} + NO \longrightarrow 2\, NO_2$

This reaction and rate constant are from NASA87, Table 1:

$$k = 1.7 \times 10^{-11} e^{150/T} \quad \text{cm}^3\text{-molecules}^{-1}\text{-s}^{-1}$$

IC4a $NO_3^{\cdot} + HO_2^{\cdot} \longrightarrow HNO_3 + O_2$

This reaction and rate constant are from Carter's 1989 mechanism:

$$k = 2.2 \times 10^{-13} e^{1230/T} \quad \text{cm}^3\text{-molecules}^{-1}\text{-s}^{-1}$$

Table 8. Cross Sections and Quantum Yields for $NO_3^{\cdot}$
$(NO_3^{\cdot} \xrightarrow{h\nu} NO+O_2)$

(units are nanometers, $\times 10^{20}$ cm^2-molecule^{-1}, base *e*)

λ	σ_λ	Φ_λ	λ	σ_λ	Φ_λ	λ	σ_λ	Φ_λ
580	0.0	0.000	605	345.0	0.200	630	566.0	0.050
585	277.0	0.000	610	148.0	0.200	635	145.0	0.030
590	514.0	0.250	615	196.0	0.100	640	111.0	0.000
595	408.0	0.400	620	358.0	0.100			
600	283.0	0.250	625	925.0	0.050			

Table 9. Cross Sections and Quantum Yields for $NO_3^{\cdot}$
$(NO_3^{\cdot} \xrightarrow{h\nu} NO_2+O_2)$

(units are nanometers, $\times 10^{20}$ cm^2-molecule^{-1}, base *e*)

λ	σ_λ	Φ_λ	λ	σ_λ	Φ_λ	λ	σ_λ	Φ_λ
400	0	1.00	485	69	1.00	570	254	1.00
405	3	1.00	490	88	1.00	575	274	1.00
410	4	1.00	495	95	1.00	580	305	1.00
415	5	1.00	500	101	1.00	585	277	1.00
420	8	1.00	505	110	1.00	590	514	0.75
425	10	1.00	510	132	1.00	595	408	0.60
430	13	1.00	515	140	1.00	600	283	0.55
435	18	1.00	520	145	1.00	605	345	0.40
440	19	1.00	525	148	1.00	610	145	0.30
445	22	1.00	530	194	1.00	615	196	0.25
450	28	1.00	535	204	1.00	620	358	0.20
455	33	1.00	540	181	1.00	625	925	0.15
460	37	1.00	545	181	1.00	630	566	0.05
465	43	1.00	550	236	1.00	635	145	0.00
470	51	1.00	555	268	1.00			
475	60	1.00	560	307	1.00			
480	64	1.00	565	253	1.00			

The CB4 mechanism does not contain this reaction.

Ic4b $NO_3^{\cdot} + NO_2 \longrightarrow NO + NO_2 + O_2$

This reaction and rate constant are from Atkinson and Lloyd, 1984:

$$k = 2.5 \times 10^{-14} e^{-1230/T} \quad \text{cm}^3\text{-molecules}^{-1}\text{-s}^{-1}$$

Ic5b $NO_3^{\cdot} + NO_2 \xrightarrow{M} N_2O_5$

This reaction and rate constant are from NASA87, Table 2:

$$k = \text{FallOff} \qquad \text{cm}^3\text{-molecules}^{-1}\text{-s}^{-1}$$

$$k_\infty = 1.5 \times 10^{-12}(T/300)^{-0.5} \quad k_o = 2.2 \times 10^{-30}(T/300)^{-4.3} \quad F = 0.6 \quad N = 1$$

Ic6 $N_2O_5 \xrightarrow{M} NO_3^{\cdot} + NO_2$

This reaction is in equilibrium with Ic5b and the rate constant is given by the rate constant of reaction Ic5b times $1/K_{eq}$. K_{eq} is from NASA87, Table 3:

$$k = k[\text{Ic5b}] \times 9.09 \times 10^{26} e^{-11200/T} \text{s}^{-1}$$

Ic7 $N_2O_5 + H_2O \longrightarrow 2\,HNO_3$

This reaction and rate constant are from NASA87, Table 2:

$$k = 2.0 \times 10^{-21} \quad \text{cm}^3\text{-molecules}^{-1}\text{-s}^{-1}$$

This reaction only represents the homogeneous rate. The similar heterogeneous reaction is described in the **Wall** reaction section later.

Section d: HONO Chemistry

Id1 $NO + NO_2 + H_2O \longrightarrow 2\,HONO$
Id2 $HONO + HONO \longrightarrow NO + NO_2 + H_2O$

These reactions and rate constants are from Kaiser and Wu, 1977:

$$k_{\mathrm{Id1}} = 4.4 \times 10^{-40} \quad \mathrm{cm^6\text{-}molecules^{-2}\text{-}s^{-1}}$$
$$k_{\mathrm{Id2}} = 1.01 \times 10^{-20} \quad \mathrm{cm^3\text{-}molecules^{-1}\text{-}s^{-1}}$$

These reactions do not appear in Carter's 1989 mechanism. They are included here for their potential impact on initiation in the chamber in the morning.

Id3 $^{\cdot}OH + NO \xrightarrow{M} HONO$

This reaction and rate constant are from NASA87, Table 2:

$$k = \mathsf{FallOff} \quad \mathrm{cm^3\text{-}molecules^{-1}\text{-}s^{-1}}$$
$$k_\infty = 1.5 \times 10^{-11}(T/300)^{-0.5} \quad k_o = 7.0 \times 10^{-31}(T/300)^{-2.6} \quad F = 0.6 \quad N = 1$$

Id4 $HONO \xrightarrow{h\nu} {}^{\cdot}OH + NO$

This reaction is from CODATA84:

$$k = \mathsf{HVNO2} \times \mathsf{HONOtoNO2R} \quad \mathrm{s^{-1}}$$

The absorption cross sections used for this reaction are from Stockwell and Calvert, 1978;[25] unit quantum yields are assumed (see Table 10). Because the wavelength dependance of the rate of this reaction is so similar to that of NO_2, we use a ratio of the HONO-to-NO_2 and the NO_2 photolysis rate to compute the rate of this reaction. The value of HONOtoNO2R is 0.171 which was computed by averaging ratios of computed rates throughout the day for July 13 1986 at the UNC Site.

Id5 $^{\cdot}OH + HONO \longrightarrow NO_2 + H_2O$

This reaction and rate constant are from Atkinson and Lloyd, 1984:

$$k = 6.6 \times 10^{-12} \quad \mathrm{cm^3\text{-}molecules^{-1}\text{-}s^{-1}}$$

Table 10. Cross Sections and Quantum Yields for HONO
($HONO \xrightarrow{h\nu} {}^{\cdot}OH + NO$)

(units are nanometers, $\times 10^{20}$ cm^2-molecule^{-1}, base *e*)

λ	σ_λ	Φ_λ	λ	σ_λ	Φ_λ	λ	σ_λ	Φ_λ
311	0.00	1.0	339	16.30	1.0	367	35.20	1.0
312	0.20	1.0	340	10.50	1.0	368	45.00	1.0
313	0.42	1.0	341	8.70	1.0	369	29.30	1.0
314	0.46	1.0	342	33.50	1.0	370	11.90	1.0
315	0.42	1.0	343	20.10	1.0	371	9.46	1.0
316	0.30	1.0	344	10.20	1.0	372	8.85	1.0
317	0.46	1.0	345	8.54	1.0	373	7.44	1.0
318	3.60	1.0	346	8.32	1.0	374	4.77	1.0
319	6.10	1.0	347	8.20	1.0	375	2.70	1.0
320	2.10	1.0	348	7.49	1.0	376	1.90	1.0
321	4.27	1.0	349	7.13	1.0	377	1.50	1.0
322	4.01	1.0	350	6.83	1.0	378	1.90	1.0
323	3.93	1.0	351	17.40	1.0	379	5.80	1.0
324	4.01	1.0	352	11.40	1.0	380	7.78	1.0
325	4.04	1.0	353	37.10	1.0	381	11.40	1.0
326	3.13	1.0	354	49.60	1.0	382	14.00	1.0
327	4.12	1.0	355	24.60	1.0	383	17.20	1.0
328	7.55	1.0	356	11.90	1.0	384	19.90	1.0
329	6.64	1.0	357	9.35	1.0	385	19.00	1.0
330	7.29	1.0	358	7.78	1.0	386	11.90	1.0
331	8.70	1.0	359	7.29	1.0	387	5.65	1.0
332	13.80	1.0	360	6.83	1.0	388	3.20	1.0
333	5.91	1.0	361	6.90	1.0	389	1.90	1.0
334	5.91	1.0	362	7.32	1.0	390	1.20	1.0
335	6.45	1.0	363	9.00	1.0	391	0.50	1.0
336	5.91	1.0	364	12.10	1.0	392	0.00	0.0
337	4.58	1.0	365	13.30	1.0			
338	19.10	1.0	366	21.30	1.0			

This reaction does not appear in Carter's 1989 mechanism, but does appear in the CB4 mechanism.

Section e: $HO_2^{\cdot}$-NO_x Reactions

Ie1 $HO_2^{\cdot} + NO \longrightarrow {}^{\cdot}OH + NO_2$

This reaction and rate constant are from NASA87, Table 1:

$$k = 3.7 \times 10^{-12} e^{242./T} \quad \text{cm}^3\text{-molecules}^{-1}\text{-s}^{-1}$$

Ie2 $HO_2^{\cdot} + NO_2 \xrightarrow{M} HO_2NO_2$

This reaction and rate constant are from NASA87, Table 2:

$$k = \text{FallOff} \quad \text{cm}^3\text{-molecules}^{-1}\text{-s}^{-1}$$
$$k_\infty = 4.7 \times 10^{-12} (T/300)^{-1.4} \quad k_o = 1.8 \times 10^{-31} (T/300)^{-3.2} \quad F = 0.6 \quad N = 1$$

Ie3 $HO_2NO_2 \xrightarrow{M} HO_2^{\cdot} + NO_2$

This reaction and rate constant are from NASA87, Table 3:

$$k = k[\text{Ie2}] \times 4.76 \times 10^{26} e^{-10900/T} \quad \text{s}^{-1}$$

This reaction is in equilibrium with reaction Ie2. The numerical value here is $1/K_{eq}$.

Ie4 $^{\cdot}OH + HO_2NO_2 \longrightarrow NO_2 + H_2O + O2$

This reaction and rate constant are from NASA87, Table 1:

$$k = 1.3 \times 10^{-12} e^{380/T} \quad \text{cm}^3\text{-molecules}^{-1}\text{-s}^{-1}$$

Section f: $^{\cdot}OH$ Termination Reactions

If1 $^{\cdot}OH + NO_2 \xrightarrow{M} HNO_3$

This reaction and rate constant are from NASA87, Table 2:

$$k = \text{FallOff} \quad \text{cm}^3\text{-molecules}^{-1}\text{-s}^{-1}$$
$$k_\infty = 2.4 \times 10^{-11}(T/300)^{-1.3} \quad k_o = 2.6 \times 10^{-30}(T/300)^{-3.2} \quad F = 0.6 \quad N = 1$$

If2 $^{\cdot}OH + HNO_3 \longrightarrow NO_3^{\cdot} + H_2O$

This reaction and rate constant are from NASA87, Table 1:

$$k = \text{Lindemann-Hinshelwood} \quad \text{cm}^3\text{-molecules}^{-1}\text{-s}^{-1}$$
$$k_o = 7.2 \times 10^{-15}e^{785/T} \quad k_2 = 4.1 \times 10^{-16}e^{1440/T} \quad k_3 = 1.9 \times 10^{-33}e^{725/T}$$

If3 $^{\cdot}OH + HO_2^{\cdot} \longrightarrow H_2O + O_2$

This reaction and rate constant are from NASA87, Table 1:

$$k = 4.6 \times 10^{-11}e^{230/T} \quad \text{cm}^3\text{-molecules}^{-1}\text{-s}^{-1}$$

Section g: $HO_2^{\cdot}$ Termination Reactions

Ig1a $HO_2^{\cdot} + HO_2^{\cdot} \longrightarrow H_2O_2 + O_2$
Ig1b $HO_2^{\cdot} + HO_2^{\cdot} + M \longrightarrow H_2O_2 + O_2 + M$
Ig1c $HO_2^{\cdot} + HO_2^{\cdot} + H_2O \longrightarrow H_2O_2 + O_2 + H_2O$

These reactions and rate constants are from Carter *et al.*, 1986:[23]

$$k_{\text{Ig1a}} = 2.2 \times 10^{-13}e^{621/T} \quad \text{cm}^3\text{-molecules}^{-1}\text{-s}^{-1}$$
$$k_{\text{Ig1b}} = 1.9 \times 10^{-33}e^{985/T} \quad \text{cm}^6\text{-molecules}^{-2}\text{-s}^{-1}$$
$$k_{\text{Ig1c}} = 3.1 \times 10^{-34}e^{2828/T} \quad \text{cm}^6\text{-molecules}^{-2}\text{-s}^{-1}$$

Table 11. Cross Sections and Quantum Yields for H_2O_2
($H_2O_2 \xrightarrow{h\nu} 2\,{}^{\cdot}OH$)

(units are nanometers, $\times 10^{20}$ cm^2-molecule^{-1}, base e)

λ	σ_λ	Φ_λ	λ	σ_λ	Φ_λ	λ	σ_λ	Φ_λ
250	8.30	1.0	290	1.13	1.0	330	0.12	1.0
255	6.70	1.0	295	0.87	1.0	335	0.09	1.0
260	5.20	1.0	300	0.66	1.0	340	0.07	1.0
265	4.20	1.0	305	0.49	1.0	345	0.05	1.0
270	3.20	1.0	310	0.37	1.0	350	0.03	1.0
275	2.50	1.0	315	0.28	1.0	355	0.00	1.0
280	2.00	1.0	320	0.20	1.0			
285	1.50	1.0	325	0.15	1.0			

Ig2 $H_2O_2 \xrightarrow{h\nu} 2\,{}^{\cdot}OH$

This reaction is from NASA87.

$$k = \mathrm{HVH2O2} \quad s^{-1}$$

The absorption cross sections are from NASA87 (see Table 11); unit quantum yields were assumed based upon discussion in Atkinson and Lloyd, 1984.

Ig3 ${}^{\cdot}OH + H_2O_2 \longrightarrow HO_2^{\cdot} + H_2O$

This reaction and rate constant are from NASA87, Table 1:

$$k = 3.1 \times 10^{-12} e^{-187/T} \quad cm^3\text{-molecules}^{-1}\text{-s}^{-1}$$

Section h: CO/H_2 Reactions

Ih1 ${}^{\cdot}OH + CO \longrightarrow HO_2^{\cdot} + CO_2$

This reaction and rate constant are from NASA87, Table 1:

$$k = 1.5 \times 10^{-13}(1 + 0.6)\mathrm{Pressure} \quad cm^3\text{-molecules}^{-1}\text{-s}^{-1}$$

Ih2 $\cdot OH + H_2 \longrightarrow HO_2^{\cdot} + H_2O$

This reaction and rate constant are from NASA87, Table 1:

$$k = 7.7 \times 10^{-12} e^{-2100/T} \quad \text{cm}^3\text{-molecules}^{-1}\text{-s}^{-1}$$

This reaction does not appear in either Carter's 1989 or the CB4 mechanism. Because H_2 was measured in several UNC experiments, it is included in the UNC mechanism. The background H_2 concentration is ca. 0.55 ppm and this reaction makes a contribution to background reactivity.

P1 = Methane Chemistry

Much of the methane atmospheric chemistry has been extensively studied and it too appears in the kinetics reviews described in the introduction to the inorganic reactions section. Subsequent reactions involve entities that are common to organic atmospheric photochemistry and these reactions appear in a series of kinetic reviews including the CODATA84 mentioned above and those by Atkinson and his coauthors, including Atkinson and Lloyd, 1984,[19] and Atkinson, "Gas Phase Tropospheric Chemistry of Organic Compounds: A Review," in Atmospheric Environment, 1990.[26] Because of the relative simplicity of these organic free radical entities there is a reasonable amount of laboratory data to support their reaction mechanism. This is not as true for more complex organic free radicals and it is often necessary to assume that the more complex radicals act similarly to the simpler ones derived from methane.

In our mechanism, as in Carter's 1989 mechanism, and consistent with Atkinson's recommendation, the methyl-peroxy ($CH_3O_2^{\cdot}$) + NO reaction will be treated as the prototype reaction for higher peroxy reactions. Its rate constant will be given a symbolic name, RO2NORATE, which will be used as the rate of all higher peroxy + NO reactions.

Likewise, the $CH_3O_2^{\cdot} + HO_2^{\cdot}$ reaction will be the prototype peroxy-hydroperoxy reaction with the rate constant named RO2HO2RATE. This rate will be used for all subsequent peroxy-hydroperoxy reaction rate constants. See the discussion for reaction P1.9 for an explanation of the stoichiometric factors used in these peroxy-hydroperoxy reactions.

Finally, the $CH_3O_2^{\cdot} + CH_3O_2^{\cdot}$ reaction will be the prototype peroxy-peroxy reaction with the rate constant named RO2RO2RATE. This rate will be used for all subsequent peroxy-peroxy reaction rate constants. See the discussion for reaction P1.10 for an explanation of the stoichiometric factors used in these peroxy-peroxy reactions.

P1.1 $^{\cdot}\mathrm{OH} + \mathrm{CH_4} \longrightarrow \mathrm{CH_3O_2^{\cdot}} + \mathrm{H_2O}$

This reaction and rate constant are from NASA87, Table 1:

$$k = 2.4 \times 10^{-12} e^{-1710/T} \quad \mathrm{cm^3\text{-}molecules^{-1}\text{-}s^{-1}}$$

This reaction does not appear in Carter's 1989 mechanism. An approximation for this reaction and subsequent $\mathrm{CH_3O_2^{\cdot}}$ reactions is included in the CB4 mechanism as a pseudo-first order reaction.

P1.2 $\mathrm{CH_3O_2^{\cdot}} + \mathrm{NO} \longrightarrow \mathrm{NO_2} + \mathrm{CH_3O^{\cdot}}$

This reaction and rate constant are from NASA87, Table 1:

$$k = 4.2 \times 10^{-12} e^{180/T} \quad \mathrm{cm^3\text{-}molecules^{-1}\text{-}s^{-1}}$$

This reaction is a prototype reaction for other $\mathrm{RO_2} + \mathrm{NO}$ reactions and its rate constant is given a symbolic name

$$\mathrm{RO2NORATE} = k[\mathrm{P1.2}].$$

P1.3 $\mathrm{CH_3O_2^{\cdot}} + \mathrm{NO_2} \longrightarrow \mathrm{CH_3O_2NO_2}$
P1.4 $\mathrm{CH_3O_2NO_2} \longrightarrow \mathrm{CH_3O_2^{\cdot}} + \mathrm{NO_2}$

These reactions and rate constants are from NASA87, Tables 2 and 3. Because reaction P1.4 is so fast at surface temperatures, these reactions are ignored in the current mechanism.

P1.5a $\mathrm{CH_3O^{\cdot}} + \mathrm{O_2} \longrightarrow \mathrm{H_2C{=}O} + \mathrm{HO_2^{\cdot}}$
P1.5b $\mathrm{CH_3O^{\cdot}} + \mathrm{NO} \longrightarrow \mathrm{CH_3ONO}$
P1.5c $\mathrm{CH_3O^{\cdot}} + \mathrm{NO_2} \xrightarrow{M} \mathrm{CH_3ONO_2}$
P1.5d $\mathrm{CH_3O^{\cdot}} + \mathrm{NO_2} \longrightarrow \mathrm{H_2C{=}O} + \mathrm{HONO}$

These reactions are from Atkinson, 1990 and CODATA84:

$$k_a = 5.5 \times 10^{-14} e^{-1000/T} \quad \mathrm{cm^3\text{-}molecules^{-1}\text{-}s^{-1}}$$

$$k_b = 1.3 \times 10^{-11} e^{300/T} \mathrm{cm^3\text{-}molecules^{-1}\text{-}s^{-1}}$$

$$k_c = 1.2 \times 10^{-11} \mathrm{cm^3\text{-}molecules^{-1}\text{-}s^{-1}}$$

$$k_d = k[\mathrm{P1.5c}] \times 0.1$$

Carter's 1989 mechanism ignores these reactions. These reactions also do not appear in the CB4 mechanism because the mechanism developers assumed that P1.5a occurs exclusively and thus $CH_3O^{\cdot}$ was replaced with $H_2C{=}O$ and $HO_2^{\cdot}$ everywhere in CB4 mechanism.

P1.6 $CH_3ONO \xrightarrow{h\nu} CH_3O^{\cdot} + NO$

This reaction is from Atkinson and Lloyd, 1984. Using absorption cross sections and quantum yields recommended by them, this reaction is treated in a manner similar to reaction Id4 (HONO) and is modeled with a rate proportional to HVNO2. The value computed for MNITtoNO2R is 0.3.

$$k = \mathrm{HVNO2} \times \mathrm{MNITtoNO2R} \quad s^{-1}$$

This reaction does not appear in Carter's 1989 mechanism or in the CB4 mechanism.

P1.7 $CH_3ONO + {}^{\cdot}OH \longrightarrow H_2C{=}O + NO + H_2O$

This reaction and rate constant are from Atkinson and Lloyd, 1984:

$$k = 2.0 \times 10^{-13} \quad \mathrm{cm^3\text{-}molecules^{-1}\text{-}s^{-1}}$$

P1.8 $CH_3ONO_2 + {}^{\cdot}OH \longrightarrow H_2C{=}O + NO_2 + H_2O$

This reaction and rate constant are from Atkinson and Lloyd, 1984:

$$k = 3.0 \times 10^{-13} \quad \mathrm{cm^3\text{-}molecules^{-1}\text{-}s^{-1}}$$

P1.9 $CH_3O_2^{\cdot} + HO_2^{\cdot} \longrightarrow f_{ald}(H_2C{=}O + H_2O + O_2) + f_{per}(CH_3OOH + O_2)$

This reaction and rate constant are from Atkinson, 1990.

$$k = 1.75 \times 10^{-13} e^{1000/T} \quad \mathrm{cm^3\text{-}molecules^{-1}\text{-}s^{-1}}$$

This reaction is a prototype reaction for other $RO_2 + HO_2^{\cdot}$ reactions and its rate constant is given a symbolic name

$$\mathsf{RO2HO2RATE} = k[\mathrm{P1.9}].$$

This rate ($k(298\mathrm{K}) = 4.9 \times 10^{-12}$ cm^3-molecules^{-1}-s^{-1}) differs slightly from the NASA87 recommendation ($k(298\mathrm{K}) = 6.0 \times 10^{-12}$ cm^3-molecules^{-1}-s^{-1}). Neither review discussed the work of Cattell, Cavanagh, Cox and Jenkins, 1986[27] or that of McAdam, Veyret and Lesclaux, 1987[28]. When measuring the loss of $CH_3O_2^{\cdot}$, both of these groups obtained rate constants in good agreement with the NASA87 recommendations, ca. 6×10^{-12} cm^3-molecules^{-1}-s^{-1}. McAdam *et al.*, however, contrasted their results with those groups (Moortgat and Kan) measuring the rate by the appearance of the peroxide product, CH_3OOH; the rate based on reactant loss was 2 to 6 times higher than the rate of appearance of peroxide product. McAdam explained the difference by suggesting the reaction

$$CH_3O_2^{\cdot} + HO_2^{\cdot} \longrightarrow H_2C{=}O + H_2O + O_2$$

might react two to six times faster than the one forming the peroxide.

Cattell *et al.* also cited Niki *et al.*'s rate determination based on the appearance of the peroxide product which was 1.5×10^{-12} cm^3-molecules^{-1}-s^{-1}. They listed four possible alternative reactions:

$$\begin{array}{lll} & & \text{kCal/mol} \\ CH_3O_2^{\cdot} + HO_2^{\cdot} & \longrightarrow H_2C{=}O + H_2O + O_2 & \Delta H = -90 \text{ (a)} \\ & \longrightarrow CH_3OOH + O_2 & \Delta H = -37 \text{ (b)} \\ & \longrightarrow CH_3OH + O_2 & \Delta H = -20 \text{ (c)} \\ & \longrightarrow CH_3O^{\cdot} + {}^{\cdot}OH + O_2 & \Delta H = 6 \text{ (d)} \end{array}$$

Reaction (d), which is the reaction included in the CB4 mechanism, was described as "unlikely" because of its endotherminity. Reactions (a) and (b) are most likely and these are the only two paths used in the UNC mechanism. The values of the relative splits were derived from the Atkinson 1990 total rate and the Niki and Kan peroxide formation rate:

$$f_{ald} = 0.75$$
$$f_{per} = 0.25$$

These coefficients also become prototype cofficients for higher peroxy radicals.

P1.10 $$CH_3O_2^{\cdot} + CH_3O_2^{\cdot} \longrightarrow f^2_{sta1}(CH_3OH + H_2C{=}O + O_2) + f^2_{rad}(CH_3O^{\cdot} + CH_3O^{\cdot} + O_2) + f^2_{sta2}(CH_3OOCH_3 + O_2)$$

These reactions and their rates appear in both CODATA84 and NASA87:

$$k = 1.6 \times 10^{-13} e^{220/T} \quad \text{cm}^3\text{-molecules}^{-1}\text{-s}^{-1}$$

This reaction is a prototype reaction for other $RO_2 + CH_3O_2^{\cdot}$ reactions and its rate constant is given a symbolic name

$$\text{RO2RO2RATE} = k[\text{P1.10}].$$

Note that the NASA87 and NASA85 reports have a typographical error in that the first and last reaction relative rate ratios are switched. The relative factors used here are from CODATA84 and are:

$$f^2_{sta1} = 0.575$$
$$f^2_{rad} = 0.350$$
$$f^2_{sta2} = 0.075$$

These coefficients also become prototype coefficients for higher peroxy radicals.

The Atkinson 1990 recommendation is to ignore f^2_{sta2} and to assume a 0.50 to 0.50 distribution. This recommendation was followed by Carter in his 1989 mechanism. The CB4 mechanism also ignores the formation of CH_3OOCH_3, but uses a ratio of 0.64 to 0.35 for stable to radical yields.

P1.11 $$CH_3OH + {}^{\cdot}OH \longrightarrow CH_3O^{\cdot} + H_2O$$

This reaction and rate constant are from Atkinson, 1990:

$$k = 1.0 \times 10^{-12} \quad \text{cm}^3\text{-molecules}^{-1}\text{-s}^{-1}$$

C1 = Formaldehyde Chemistry

Formaldehyde ($H_2C{=}O$) chemistry is believed to be well understood with one exception: the magnitude of the absorption cross-sections are uncertain, a problem described in reaction C1.2 below.

C1.1 $H_2C{=}O \xrightarrow{h\nu} 2\,HO_2^{\cdot} + CO$

This reaction is from NASA87:

$$k = \mathrm{HVHCHOR} \quad s^{-1}$$

C1.2 $H_2C{=}O \xrightarrow{h\nu} CO + H_2$

This reaction is from NASA87:

$$k = \mathrm{HVHCHOS} \quad s^{-1}$$

These reactions have received extensive study and the quantum yields are well established. The absorption cross sections determined by two highly respected groups, however, differ by as much as 30% in some spectral regions. Bass[29] and Moortgat[30] have both determined the absorption cross sections. Bass used the NBS system and reported his data with 1/40-nm resolution. Moortgat used a Cary system with 0.5-nm resolution. Both data sets have been obtained from these researchers by Mike Gery and we have received copies from Gery. Figure 55 shows these data. These differences lead to significant differences in in-chamber photolysis rates as a function of time. Rates as a function of time and the spectra differences in the two sets of photolysis rates are shown in Figure 56.

Recent unpublished data by Biermann, University of California, Riverside, and by Ford and NCAR researchers suggest that the data of Moortgat are more accurate. Both sets of data have been used to simulate a wide range of UNC chamber experiments (including $H_2C{=}O\text{-}NO_x$ systems) and we find better agreement between model predictions and all species data when using the Moortgat cross-sections. *The Moortgat cross-sections have been used in the remainder of this report.* The 0.5-nm cross-section were integral averaged to 1-nm ending intervals to match the actinic flux spectral interval using the UNC **CsQyAvg** program. These data are listed in Tables 12 and 13 and are plotted in Figure 57.

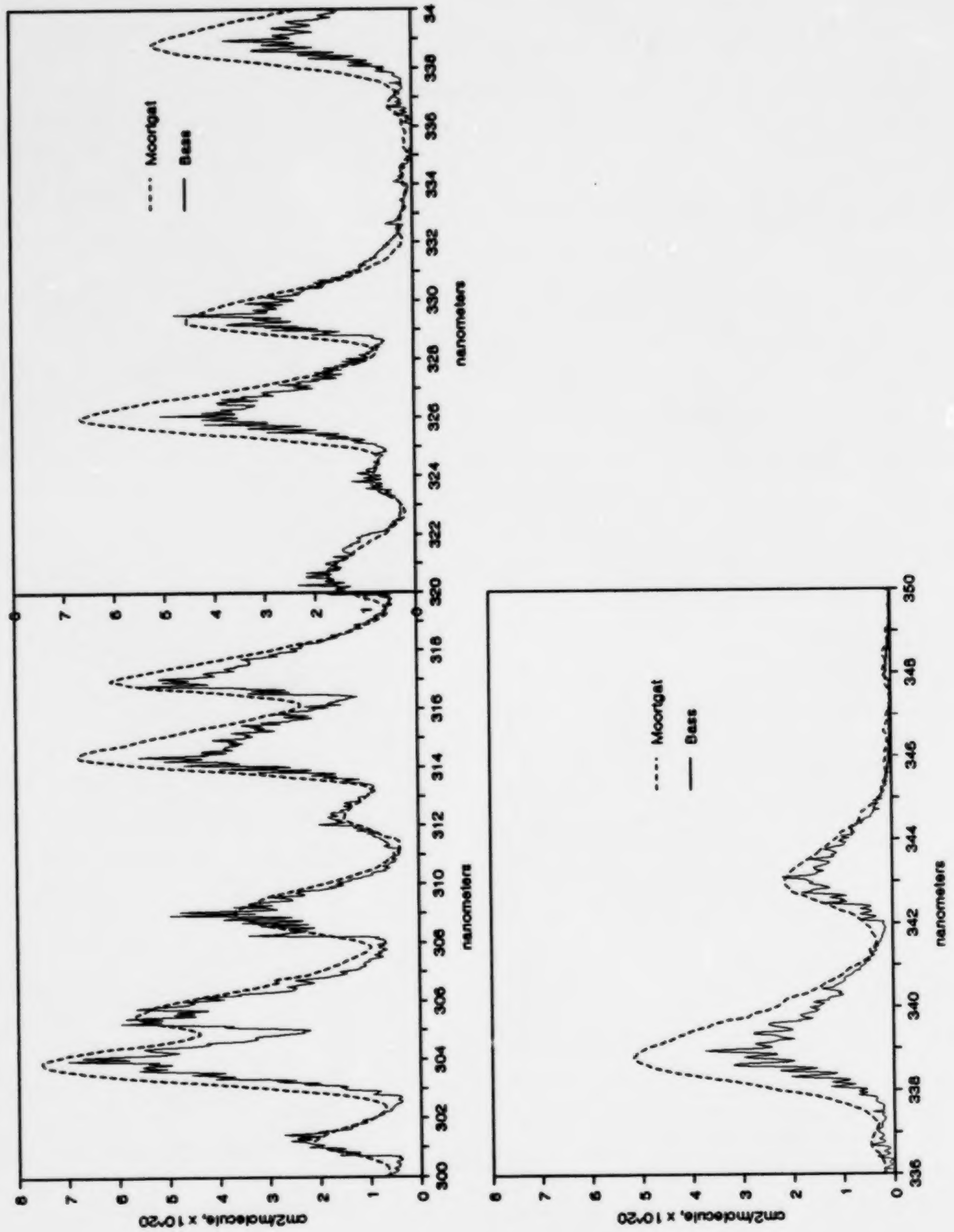

Figure 55. Comparison of Bass and Moortgat Formaldehyde Absorption Cross Sections

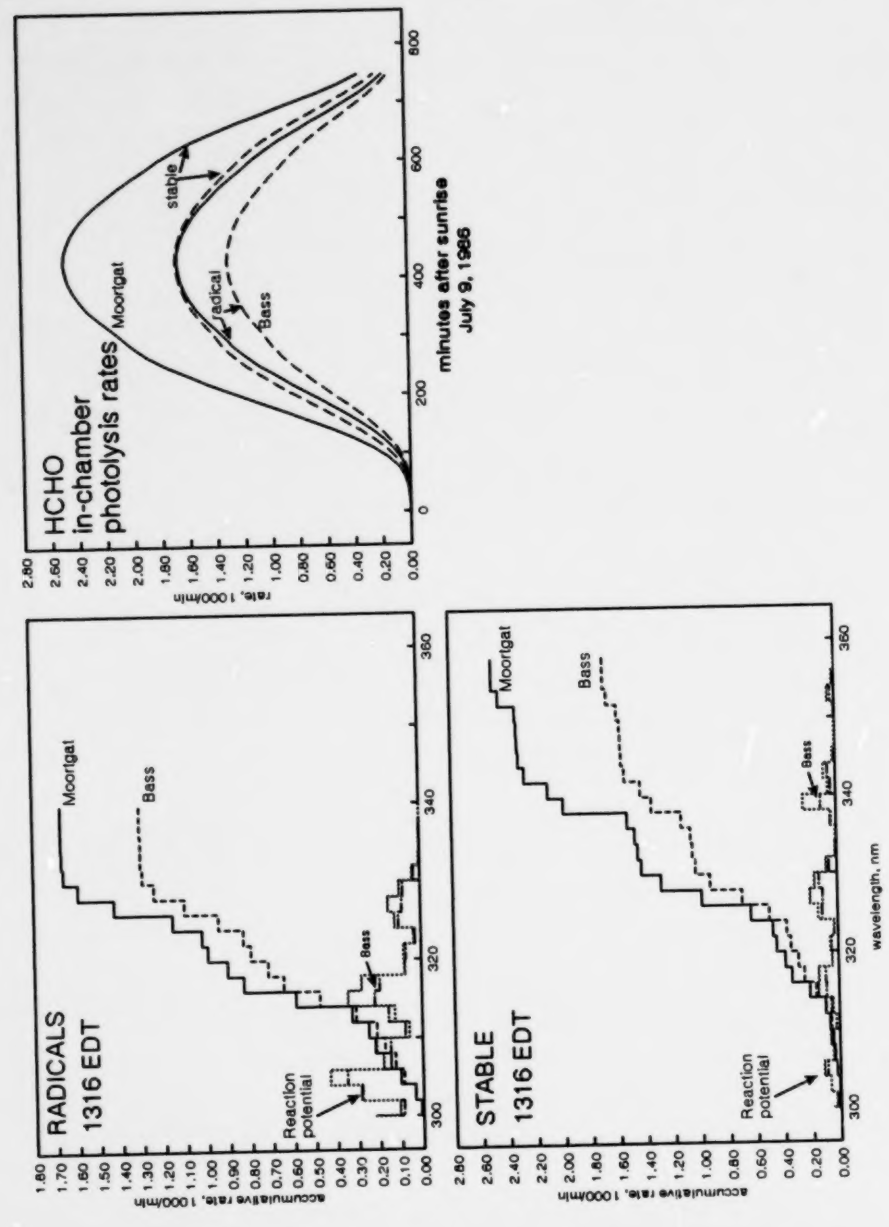

Figure 56. In-chamber Formaldehyde Photolysis Rates Computed with Bass and Moortgat Cross-sections For July 9, 1986. The plots on the left give the spectral accumulative rate for 1316 EDT. Reaction potential is the product of the absorption cross section and the quantum yield.

Table 12. Cross Sections and Quantum Yields for $H_2C{=}O$

$(H_2C{=}O \xrightarrow[O_2]{h\nu} 2\ HO_2^{\cdot} + CO)$

(units are nanometers, $\times 10^{20}$ cm^2-molecule^{-1}, base e)

λ	σ_λ	Φ_λ	λ	σ_λ	Φ_λ	λ	σ_λ	Φ_λ
280	0.000	0.00	301	1.0298	0.80	322	1.1100	0.57
281	1.581	0.56	302	1.6848	0.80	323	0.3326	0.54
282	1.194	0.58	303	1.2104	0.80	324	0.6726	0.51
283	0.733	0.60	304	6.0172	0.80	325	0.8374	0.49
284	2.689	0.62	305	5.6610	0.79	326	4.3582	0.46
285	4.726	0.63	306	5.2490	0.79	327	5.2426	0.43
286	2.519	0.65	307	3.2936	0.79	328	1.9604	0.39
287	1.495	0.67	308	1.3496	0.78	329	1.5648	0.36
288	2.066	0.68	309	2.6084	0.77	330	4.1360	0.33
289	3.785	0.70	310	2.9724	0.76	331	2.0768	0.29
290	1.642	0.71	311	1.0192	0.75	332	0.5248	0.25
291	1.658	0.72	312	0.6166	0.74	333	0.2528	0.21
292	1.257	0.73	313	1.3146	0.73	334	0.1628	0.17
293	1.227	0.75	314	2.1542	0.72	335	0.1736	0.13
294	6.607	0.76	315	6.1248	0.70	336	0.1432	0.08
295	4.920	0.76	316	3.7844	0.69	337	0.3340	0.03
296	3.236	0.77	317	3.9520	0.67	338	0.8384	0.00
297	1.609	0.78	318	4.5480	0.65	339	4.2140	0.00
298	2.667	0.79	319	1.7138	0.63	340	3.7020	0.00
299	4.081	0.79	320	0.8022	0.61			
300	1.571	0.80	321	1.6452	0.59			

C1.3 $^{\cdot}OH + H_2C{=}O \longrightarrow HO_2^{\cdot} + CO + H_2O$

This reaction and rate constant are from Atkinson, 1990:

$$k = 1.13 \times 10^{-12}(T/300)^2 e^{648/T} \quad \text{cm}^3\text{-molecules}^{-1}\text{-s}^{-1}$$

C1.4 $O(3P) + H_2C{=}O \longrightarrow {^{\cdot}OH} + HO_2^{\cdot} + CO$

This reaction and rate constant are from NASA87, Table 1:

$$k = 3.4 \times 10^{-11} e^{-1600/T} \quad \text{cm}^3\text{-molecules}^{-1}\text{-s}^{-1}$$

This reaction does not appear in Carter's 1989 mechanism.

Table 13. Cross Sections and Quantum Yields for $H_2C{=}O$

$$(H_2C{=}O \xrightarrow[O_2]{h\nu} H_2 + CO)$$

(units are nanometers, ×10^{20} cm^2-molecule^{-1}, base e)

λ	σ_λ	Φ_λ	λ	σ_λ	Φ_λ	λ	σ_λ	Φ_λ
280	0.000	0.00	308	1.3496	0.22	336	0.1432	0.62
281	1.581	0.44	309	2.6084	0.23	337	0.3340	0.62
282	1.194	0.42	310	2.9724	0.24	338	0.8384	0.61
283	0.733	0.40	311	1.0192	0.25	339	4.2140	0.61
284	2.689	0.38	312	0.6166	0.26	340	3.7020	0.60
285	4.726	0.37	313	1.3146	0.27	341	1.4722	0.59
286	2.519	0.35	314	2.1542	0.28	342	0.4430	0.57
287	1.495	0.33	315	6.1248	0.30	343	1.4226	0.56
288	2.066	0.32	316	3.7844	0.31	344	1.6846	0.54
289	3.785	0.30	317	3.9520	0.33	345	0.6678	0.52
290	1.642	0.29	318	4.5480	0.35	346	0.1586	0.50
291	1.658	0.28	319	1.7138	0.37	347	0.1036	0.47
292	1.257	0.27	320	0.8022	0.39	348	0.0640	0.45
293	1.227	0.25	321	1.6452	0.41	349	0.1142	0.42
294	6.607	0.24	322	1.1100	0.43	350	0.0074	0.39
295	4.920	0.24	323	0.3326	0.46	351	0.0814	0.36
296	3.236	0.23	324	0.6726	0.49	352	0.1926	0.33
297	1.609	0.22	325	0.8374	0.51	353	1.6064	0.30
298	2.667	0.21	326	4.3582	0.54	354	2.0490	0.26
299	4.081	0.21	327	5.2426	0.55	355	1.0684	0.23
300	1.571	0.20	328	1.9604	0.57	356	0.3436	0.20
301	1.030	0.20	329	1.5648	0.58	357	0.0554	0.16
302	1.685	0.20	330	4.1360	0.59	358	0.0244	0.13
303	1.210	0.20	331	2.0768	0.60	359	0.0214	0.10
304	6.017	0.20	332	0.5248	0.61	360	0.0746	0.00
305	5.661	0.21	333	0.2528	0.62			
306	5.249	0.21	334	0.1628	0.62			
307	3.294	0.21	335	0.1736	0.62			

C1.5 $NO_3^{\cdot} + H_2C{=}O \longrightarrow HNO_3 + HO_2^{\cdot} + CO$

This reaction and rate constant are from Carter's 1989 mechanism:

$$k = 2.8 \times 10^{-12} e^{-2522/T} \quad \text{cm}^3\text{-molecules}^{-1}\text{-s}^{-1}$$

Carter notes that the rate parameters were derived from NASA87 and Atkinson, 1990 recommendation of $k(298\text{K}) = 6.0 \times 10^{-16}$ cm^3-molecules^{-1}-s^{-1} and an esti-

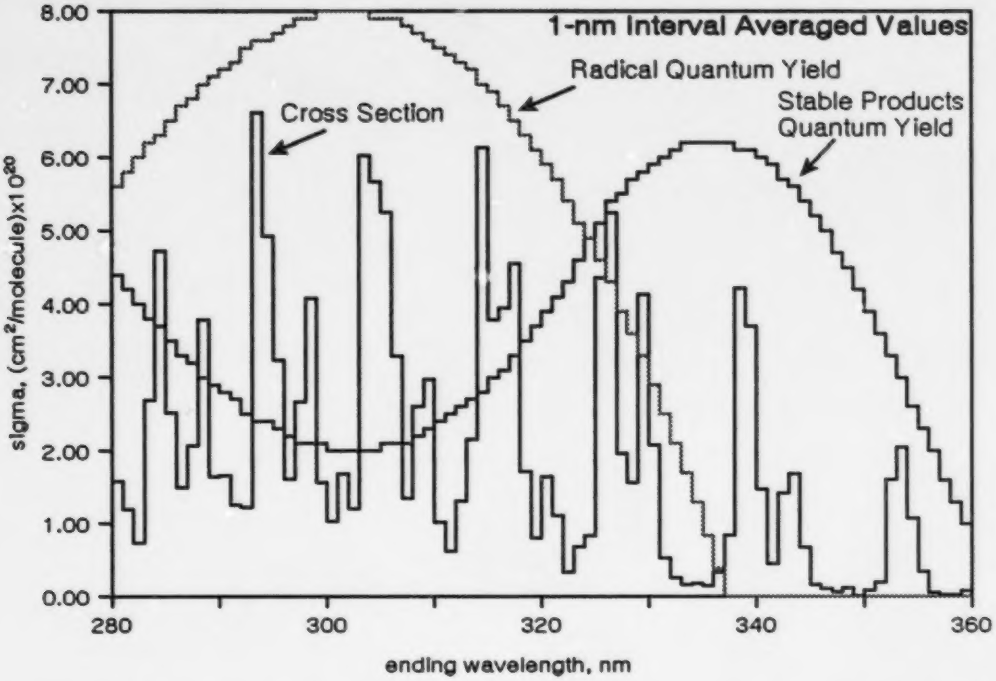

Figure 57. Formaldehyde absorption cross sections and quantum yields averaged to 1-nm ending intervals.

mated A-factor of 2.8×10^{-12} cm^3-molecules^{-1}-s^{-1} which is twice the A-factor for NO_2 + acetaldehyde that was recommended by Atkinson, *et al.*, 1989.

C1.6 $HO_2^{\cdot} + H_2C{=}O \longrightarrow HOCH_2O_2^{\cdot}$

This reaction and rate constant are from Atkinson, 1990:

$$k = 9.7 \times 10^{-15} e^{625/T} \quad \text{cm}^3\text{-molecules}^{-1}\text{-s}^{-1}$$

C1.7 $HOCH_2O_2^{\cdot} \longrightarrow HO_2^{\cdot} + H_2C{=}O$

This reaction and rate constant are from Atkinson, 1990:

$$k = 2.4 \times 10^{12} e^{-7000/T} \quad \text{s}^{-1}$$

C1.8 $HOCH_2O_2^{\cdot} + NO \longrightarrow NO_2 + HO_2^{\cdot} + H(HO)C{=}O$

This reaction and rate constant are from Atkinson, 1990:

$$k = \mathrm{RO2NORATE}$$

C1.9 $HOCH_2O_2^{\cdot} + HO_2^{\cdot} \longrightarrow f_{ald}(H(HO)C{=}O + H_2O + O_2) + f_{per}(HOCH_2OOH + O_2)$

This reaction is based reactions in the Su, *et al.* study.[31] Also see reaction P1.9:

$$k = \mathrm{RO2HO2RATE}$$

C1.10 $^{\cdot}OH + CH_3OOH \longrightarrow 0.6CH_3O_2^{\cdot} + 0.6H_2O + 0.4H_2C{=}O + 0.4\,^{\cdot}OH$

This reaction, rate constant, and coefficients are from NASA85:

$$k = 1.0 \times 10^{-12} \quad \text{cm}^3\text{-molecules}^{-1}\text{-s}^{-1}$$

C1.11 $^{\cdot}OH + H(HO)C{=}O \longrightarrow HO_2^{\cdot} + CO_2 + H_2O$

This reaction and rate constant are from Atkinson, 1990:

$$k = 4.6 \times 10^{-13} \quad \text{cm}^3\text{-molecules}^{-1}\text{-s}^{-1}$$

P2 = Ethane Chemistry

Ethane chemistry is included for the important reactions of ethyl-peroxy radical and the formation of acetaldehyde. The chemistry of acetaldehyde and its reaction product, PAN, follows this section.

The reactions of ethane are also reviewed in CODATA85, NASA87, and by Atkinson, 1990.

P2.1 $^{\cdot}OH + CH_3CH_3 \longrightarrow CH_3CH_2O_2^{\cdot} + H_2O$

This reaction and rate constant are from Atkinson, 1990:

$$k = 1.23 \times 10^{-12}(T/300)^2 e^{-445/T} \quad \text{cm}^3\text{-molecules}^{-1}\text{-s}^{-1}$$

This reaction does not appear in Carter's 1989 mechanism or in the CB4 mechanism.

P2.2 $CH_3CH_2O_2^{\cdot} + NO \longrightarrow NO_2 + CH_3HC{=}O + HO_2^{\cdot}$

This reaction is from NASA87 and the rate is recommended by Atkinson, 1990:

$$k = \text{RO2NORATE}$$

P2.3 $CH_3CH_2O_2^{\cdot} + HO_2^{\cdot} \longrightarrow f_{ald}(CH_3HC{=}O + H_2O + O_2) + f_{per}(CH_3CH_2OOH + O_2)$

This reaction and rate constant are from Atkinson, 1990:

$$k = \text{RO2HO2RATE}$$

See Reaction P1.9.

P2.4 $CH_3CH_2O_2^{\cdot} + CH_3O_2^{\cdot} \longrightarrow f^2_{sta1}(CH_3CH_2OH + H_2C{=}O + O_2) + f^2_{rad}(CH_3HC{=}O + HO_2^{\cdot} + CH_3O^{\cdot} + O_2) + f^2_{sta2}(CH_3CH_2OOCH_3 + O_2)$

$$k = \text{RO2RO2RATE}$$

See Reaction P1.10.

P2.5 $CH_3CH_2OH + {}^{\cdot}OH \longrightarrow CH_3HC{=}O + HO_2^{\cdot} + H_2O$

This reaction and rate constant are from NASA87:

$$k = 2.0 \times 10^{-12} \quad \text{cm}^3\text{-molecules}^{-1}\text{-s}^{-1}$$

P2.6 ${}^{\cdot}OH + CH_3CH_2OOH \longrightarrow 0.6CH_3CH_2O_2^{\cdot} + 0.6H_2O + 0.4CH_3HC{=}O + 0.4{}^{\cdot}OH$

This reaction and rate constant are from Atkinson, 1990; the stiochiometery is by analogy with reaction C1.10.

$$k = 1.0 \times 10^{-12} \quad \text{cm}^3\text{-molecules}^{-1}\text{-s}^{-1}$$

C2 = Acetaldehyde Chemistry

Acetaldehyde is formed in reaction **P2.2**.

C2.1 $\mathrm{CH_3HC{=}O \xrightarrow[M]{h\nu} CH_3O_2^{\cdot} + CO + HO_2^{\cdot}}$

$$k = \mathrm{HVCCHOR} \quad \mathrm{s^{-1}}$$

The absorption cross sections and quantum yields are from CODATA85. See Table 14.

C2.2 $\mathrm{O(3P) + CH_3HC{=}O \longrightarrow CH_3C({=}O)O_2^{\cdot} + {}^{\cdot}OH}$

This reaction and rate constant are from Atkinson and Lloyd, 1984:

$$k = 1.2 \times 10^{-11} e^{-986/T} \quad \mathrm{cm^3\text{-}molecules^{-1}\text{-}s^{-1}}$$

C2.3 $\mathrm{{}^{\cdot}OH + CH_3HC{=}O \longrightarrow CH_3C({=}O)O_2^{\cdot} + H_2O}$

This reaction and rate constant are from Atkinson, 1990, Table 8::

$$k = 5.55 \times 10^{-12} e^{311/T} \quad \mathrm{cm^3\text{-}molecules^{-1}\text{-}s^{-1}}$$

C2.4 $\mathrm{NO_3^{\cdot} + CH_3HC{=}O \longrightarrow CH_3C({=}O)O_2^{\cdot} + HNO_3}$

This reaction and rate constant are from NASA87:

$$k = 1.4 \times 10^{-12} e^{-1900/T} \quad \mathrm{cm^3\text{-}molecules^{-1}\text{-}s^{-1}}$$

Table 14. Cross Sections and Quantum Yields for $CH_3HC{=}O$

$$(CH_3HC{=}O \xrightarrow[M]{h\nu} CH_3O_2^{\cdot} + CO + HO_2^{\cdot})$$

(units are nanometers, $\times 10^{20}$ cm^2-molecule^{-1}, base e)

λ	σ_λ	Φ_λ	λ	σ_λ	Φ_λ	λ	σ_λ	Φ_λ
260	2.00	0.310	300	4.30	0.430	325	1.10	0.040
270	3.40	0.390	305	3.40	0.370	330	0.69	0.000
280	4.50	0.580	310	2.72	0.235			
290	4.90	0.530	315	2.10	0.170			
295	4.50	0.480	320	1.80	0.100			

PA1 = Peroxyacetyl Radical Chemistry

The peroxyacetyl radical ($CH_3C({=}O)O_2^{\cdot}$) is formed in the oxidation of acetaldehyde.

PA1.1 $CH_3C({=}O)O_2^{\cdot} + NO \longrightarrow NO_2 + CH_3O_2^{\cdot} + CO_2$

This reaction and rate constant are from Atkinson, 1990:

$$k = 5.1 \times 10^{-12} e^{200/T} \quad \text{cm}^3\text{-molecules}^{-1}\text{-s}^{-1}$$

PA1.2 $CH_3C({=}O)O_2^{\cdot} + NO_2 \longrightarrow CH_3C({=}O)O_2NO_2$

This reaction is from Atkinson, 1990; the rate constant is based on Carter's personal communication about new SAPRC kinetic measurements in which the E_a was determined to be 2200°K. This is combined with an A-factor based on fitting chamber results to give:

$$k = 6.05 \times 10^{-15} e^{2200/T} \quad \text{cm}^3\text{-molecules}^{-1}\text{-s}^{-1}$$

This results in a rate at 298°K of 9.7×10^{-12} which is 1.35 times faster than the IUPAC recommendation. Excellent fits for chamber data are obtained with this value (see later discussion and figures).

PA1.3 $CH_3C({=}O)O_2NO_2 \longrightarrow NO_2 + CH_3C({=}O)O_2^{\cdot}$

This reaction and rate constant are from Atkinson, 1990:

$$k = \mathsf{FallOff} \quad \text{cm}^3\text{-molecules}^{-1}\text{-s}^{-1}$$

$$k_\infty = 2.2 \times 10^{16} e^{-13435/T} \quad k_o = 6.3 \times 10^{-2} e^{-12784/T} \quad F = 0.27 \quad N = 1$$

PA1.4 $CH_3C(=O)O_2^{\cdot} + HO_2^{\cdot} \longrightarrow f^3_{acid}(CH_3C(=O)OH + O_3 + O_2) + f^3_{per}(CH_3C(=O)OOH + O_2)$

This reaction is from Niki, 1985.[32] The rate is from Atkinson, 1990.

$$k = 3.40 \times 10^{-13} e^{800/T} \quad \text{cm}^3\text{-molecules}^{-1}\text{-s}^{-1}$$

This is a prototype reaction and its rate is given a symbolic name:

$$\mathsf{RCO3HO2RATE} = k[\mathsf{PA1.4}] = \mathsf{RO2HO2RATE}$$

Atkinson assumes that RCO_3 radicals have the same rate with $HO_2^{\cdot}$ that RO_2 does.

The coefficients are derived from rates given in Niki's paper and are:

$$f^3_{acid} = 0.25$$
$$f^3_{per} = 0.75$$

PA1.5 $CH_3C(=O)O_2^{\cdot} + CH_3O_2^{\cdot} \longrightarrow f^3_{rad}(CH_3O^{\cdot} + CH_3O_2^{\cdot} + CO_2 + O_2) + f^3_{stab}(CH_3C(=O)OH + H_2C{=}O + O_2)$

This reaction is from Atkinson, 1990:

$$k = 1.86 \times 10^{-12} e^{529/T} \quad \text{cm}^3\text{-molecules}^{-1}\text{-s}^{-1}$$

The coefficients are also from Atkinson and are:

$$f^3_{rad} = 0.50$$
$$f^3_{stab} = 0.50$$

This reaction is a prototype reaction and its rate constant is named:

$$\mathsf{RCO3RO2RATE} = k[\mathsf{PA1.5}]$$

PA1.6 $CH_3C(=O)O_2^{\cdot} + CH_3C(=O)O_2^{\cdot} \longrightarrow 2CH_3O_2^{\cdot} + 2CO_2 + O_2$

This reaction and rate constant is from Niki, 1985:

$$k = 3.00 \times 10^{-12} e^{500/T} \quad \text{cm}^3\text{-molecules}^{-1}\text{-s}^{-1}$$

This reaction is a prototype reaction and its rate constant is named:

$$\mathsf{RCO3RCO3RATE} = k[\mathsf{PA1.5}]$$

5

Chamber Modeling: 1

In this chapter the inorganic, methane, ethane, and carbonyl mechanism is used—along with a chamber-specific reaction model—to simulate several CO–, $H_2C{=}O$– and $CH_3HC{=}O$–NO_x experiments as a demonstration that the explicit mechanism can explain the observations in these simple experiments. First, we must discuss the form of the chamber-specific reactions that must be added to the inorganic-carbonyl mechanism to account for the chamber characteristics.

UNC Chamber Specific Reactions

These reactions fall into four classes:

- entrainment of ambient background reactants with dilution air,
- organic reactants in the background chamber air used to fill the chamber,
- wall–mediated reactions of nitrogen oxides,
- wall deposition or loss reactions.

These are discussed below followed by a discussion of the selection of input parameters for this part of the model.

$$\textbf{ENTRAIN} \longrightarrow 0.50\,\mathrm{CO} + 0.07\,\mathrm{O_3} + 0.55\,\mathrm{H_2} + 1.79\,\mathrm{CH_4} + 0.002\,\mathrm{H_2C{=}O} + 0.045\,\mathrm{BVOC}$$

This reaction accounts for material introduced by the dilution air that enters the chamber to replace that drawn out by sampling. The rate of this reaction is therefore:

$$k = \mathrm{DilutionRate} \quad \text{ppm-min}^{-1}$$

Air that enters the chamber during dilution is background ambient air from a rural environment and it contains low levels of CO, O_3, and other reactants. The zeroth-order reaction, **ENTRAIN**, uses stoichiometry to represent the ppm concentrations of six important reactants in the dilution air. Background levels of CO, O_3, H_2, CH_4, and $H_2C{=}O$ are monitored in the ambient air several times each year. For maximum accuracy, adjustments in CO and CH_4 should be made for experiments conducted in the mid-1970s when background values were lower (*e.g.*, CO=0.30 ppm and CH_4=1.56 ppm). See the next reaction for a discussion of BVOC. The dilution rate is determined by measuring the concentration of carbon tetrachloride tracers injected into both chamber halves. Since the total dilution is about 10– 12%, the total amount of, for example, O_3 introduced by this reaction would only be 7 ppb for the whole day.

Because the chamber is flushed and filled with the same background air, the initial conditions for a simulation should include:

$$\begin{aligned} \mathrm{CO} &= 0.50 \text{ ppm,} \\ \mathrm{CH_4} &= 1.79 \text{ ppm,} \\ \mathrm{H_2} &= 0.55 \text{ ppm, and} \\ \mathrm{BVOC} &= 0.045 \text{ ppm,} \end{aligned}$$

Figures 50 and 51, page 72–3, show a background air experiment which produced 0.09 ppm O_3.

BCKGND $^{\cdot}\mathrm{OH} + \mathrm{BVOC} \longrightarrow 0.666\,\mathrm{CH_3O_2^{\cdot}} + 0.167\,\mathrm{CH_3C({=}O)O_2^{\cdot}}$

$$\begin{aligned} k &= 3.0 \times 10^{-12} \quad \text{cm}^3\text{-molecules}^{-1}\text{-s}^{-1} \\ &= 4444.4 \quad \text{ppm}^{-1}\text{-min}^{-1} \end{aligned}$$

As shown by Carter,[2] a slow conversion of $^{\cdot}$OH to $HO_2^{\cdot}$ is needed to sucessfully model low reactivity experiments in the UNC chamber. This is not surprising because the background air at the rural site contains low concentrations of organic material.[33] In addition, low levels of PAN appear late in experiments in which no acetaldehyde was injected (*e.g.*, HCHO–NO_x only). The $CH_3C(=O)O_2^{\cdot}$ radical must have originated from reactions of background organic material in the chamber. Bill Lonneman at the EPA AREAL laboratory is analyzing VOCs collected in cannisters at several rural sites, one of which is within 15-miles of the UNC chamber site. He has provided us with preliminary data from two cannisters taken at this site. Neither of these cannisters were during the times when the chambers are usually filled, but

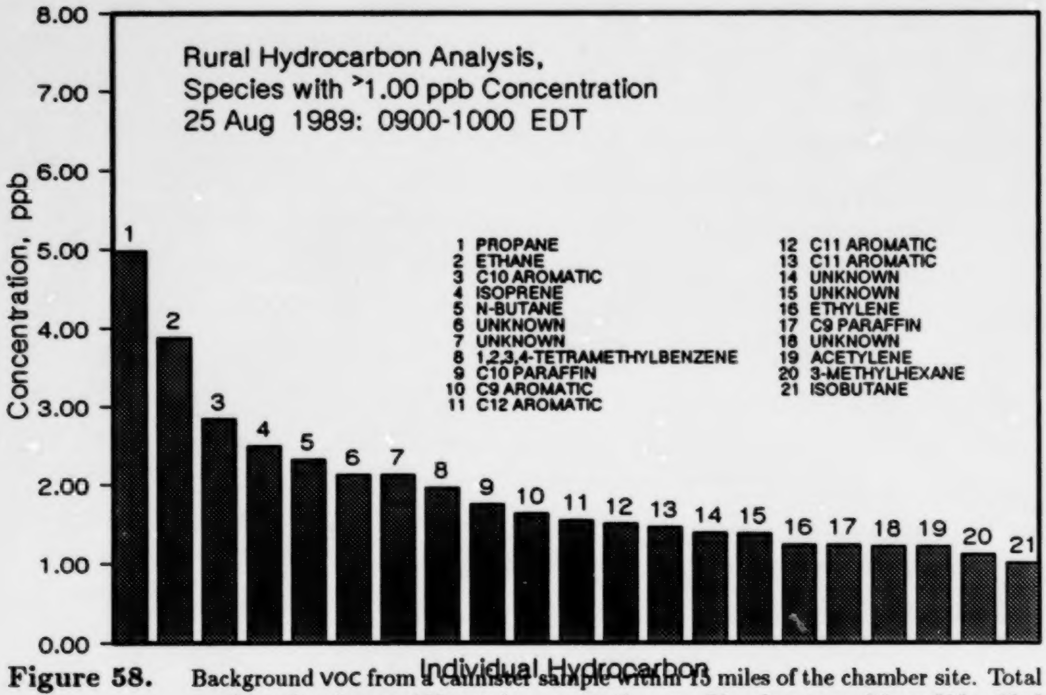

Figure 58. Background VOC from a cannister sample within 13 miles of the chamber site. Total number of peaks was 155; total concentration was 71 ppb; composition of identified peaks: ≈ 55% paraffins, 12% olefins, 18% aromatics.

the cannister analysis that is the earliest in time is shown in Figure 58. These data show that paraffins dominate the background HC distribution, but a few quite reactive HCs are also present.

We have elected to represent the reactivity of this background VOC mixture in a simple manner, yet we wish to be more complex (and representative) than Carter's simple constant conversion of $^{\cdot}OH \longrightarrow HO_2^{\cdot}$ at a constant rate (only two species produce $HO_2^{\cdot}$ directly from $^{\cdot}OH$: CO and $H_2C{=}O$, both of which are explicitly accounted for in the input conditions for our experiments). Thus, we have two-thirds of the product carbon in this reaction appear as $CH_3O_2^{\cdot}$. Producing $CH_3O_2^{\cdot}$ for each ppbC of background VOC is simpler than including explicit chemistry for propane in the mechanism. To account for the appearance of PAN when NO_2 is irradiated with background VOC, we have the other one-third of the product carbon appear as the $CH_3C({=}O)O_2^{\cdot}$ radical. For each ppbC of BVOC, k[BCKGND] is equivalent to

1.72 ppbC propane, and
0.06 ppbC acetaldehyde

Typical background levels used as initial conditions in the model are 45^{+15}_{-35} ppbC BVOC depending upon the season. This results in an average conversion of $^{\cdot}OH$ to $HO_2^{\cdot}$ approximately equal to the constant value used by Carter.[2]

WallNO2a $NO_2 \longrightarrow HONO$

WallNO2b $NO_2 \longrightarrow 0.50\,HONO + 0.50\,wall.HNO_3$

These reactions are based upon studies of wall-mediated processes for NO_2 loss.[34,35,36,37,38] Reaction *a* incorporates the so-called "photo-enhancement" factor by being proportional to the NO_2 photolysis rate, HVNO2:

$$k_a = \mathrm{HVNO2} \times \mathrm{WALLOH} \quad \text{cm}^3\text{-molecules}^{-1}\text{-s}^{-1}$$

The proportionality factor is called WALLOH which is typically 2.5×10^{-3} and can vary down to 0.0 depending upon previous chamber history, especially how long the chamber was vented between experiments and whether the previous experiments produced HNO_3 concentrations above 150 ppb. The rate for reaction *b* is from the Pitts *et al.*,[34] study of NO_2-wall reactions in the SAPRC ITC all-Teflon chamber:

$$\begin{aligned} k_b &= 2.7 \times 10^{-6} \quad \text{s}^{-1} \\ &= 1.6 \times 10^{-4} \quad \text{min}^{-1} \end{aligned}$$

WallN2O5a $N_2O_5 \longrightarrow 2.0\,wall.HNO_3$

This reaction partially accounts for the observed heterogeneous loss of N_2O_5 in the UNC chamber. This reaction is basically a wall deposition reaction for Teflon film. The rate is from Tuazon[39]

$$\begin{aligned} k_a &= 4.0 \times 10^{-5} \quad \text{s}^{-1} \\ &= 2.5 \times 10^{-3} \quad \text{min}^{-1} \end{aligned}$$

WallN2O5b $N_2O_5 + wall.H_2O \longrightarrow 2\,wall.HNO_3$

This reaction accounts for the humidity-dependent portion of the observed heterogeneous loss of N_2O_5 in the UNC chamber. This reaction, which accounts for most of the N_2O_5 loss, is presumed to be a reaction between N_2O_5 and water absorped on the Teflon walls. Svensson *et al.*[38] determined experimentally the water uptake

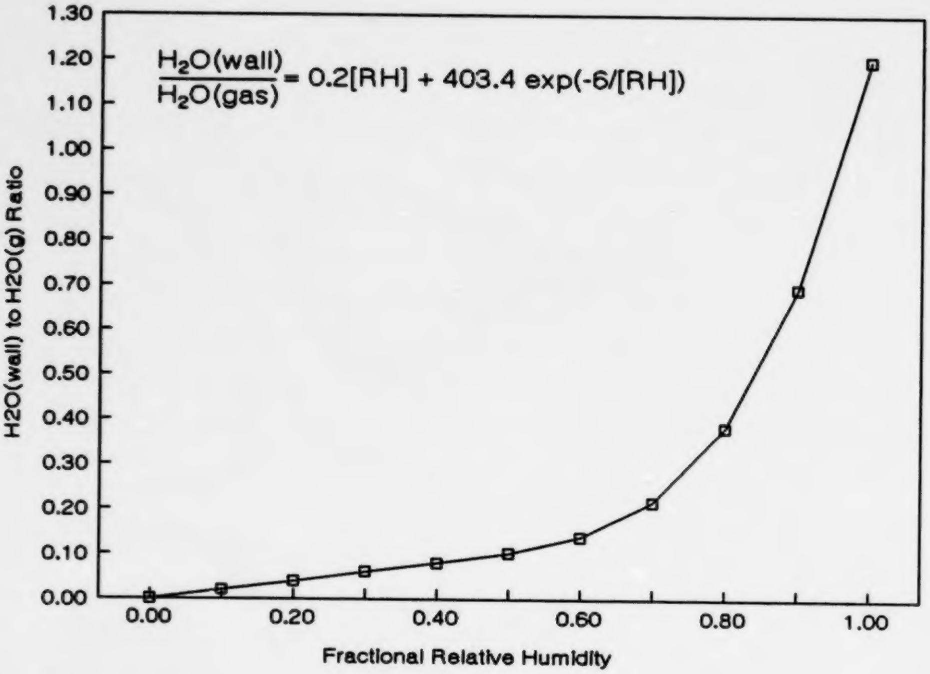

Figure 59. Water Uptake on FEP Teflon Film as a Function of Relative Humidty

on FEP Teflon film as a function of relative humidity. We derived a parameterized equation to approximate this water uptake in the form of a ratio of wall water to gas-phase water as a function of relative humidity. This function is shown in Figure 59. The simulation program (PKSS, Version 3) has built-in functions that convert the water vapor concentration and temperature to relative humidity and then calculate the wall.H_2O from the equation shown in Figure 59 and the current water vapor concentration. The rate constant was adjusted to optimize the match between the observed end-experiment O_3 production and the simulation predictions for O_3. This value was:

$$k_b = 1.3 \times 10^{-19} \quad \text{cm}^3\text{-molecules}^{-1}\text{-s}^{-1}$$
$$= 1.9 \times 10^{-4} \quad \text{ppm}^{-1}\text{-min}^{-1}$$

WallH2O2 $H_2O_2 \longrightarrow \text{wall}$

This reaction and rate are from measured loss rates in UNC chamber.

$$k = 6.7 \times 10^{-4} \quad \text{s}^{-1}$$
$$= 4.0 \times 10^{-2} \quad \text{min}^{-1}$$

WallO3 $O_3 \longrightarrow wall$

This reaction and rate are from measured loss rates in UNC chamber.

$$k = 2.3 \times 10^{-6} \quad s^{-1}$$
$$= 1.4 \times 10^{-4} \quad min^{-1}$$

Adjustable Inputs for Chamber-Dependent Reactions

The application of this chamber-dependent model requires the specification of four parameters that apparently change somewhat annually and seasonally. These are:

- the initial concentration of HONO that arises from injection of NO and NO_2 into the chamber;
- the concentraion of BVOC in background air at the site;
- the magnitude of the rate for reaction **WallNO2a**;
- the magnitude of the rate for reaction **WallN2O5b**.

Our choices for these values for experiments simulated as part of this study are presented in Table 15. The processes used to arrive at these un-measured parameters are described below.

We believe that HONO is formed during the NO_2 injection process in the UNC chamber. Tanks of 6,000 ppm NO_2 are injected into a flowing steam of chamber air in a glass manifold and must travel about 3–4 meters to be futher diluted into the whole chamber volume. Carter has suggested a "rule-of-thumb" for the SAPRC EC chamber that initial HONO concentrations can be approximated by 0.07× initial NO_2. For the UNC chamber, we generally follow this rule, but, for our injection system, the rule appears to only work for initial NO_x concentrations of 0.3–0.5 ppm and $NO_2/NO_x < 0.3$. That is, if the initial NO_2 is a significant fraction the NO_x, then less initial HONO than the 7%-rule is needed to simulate the experiment; or if the initial NO_x concentration is > 0.5 ppm, then less than the 7%-rule is needed. In practice, we begin with the 7%-rule and adjust the initial HONO up or down as needed to simulate the NO-to-NO_2 cross-over time correctly. We are planning to measure initial HONO in future experiments.

The concentration of BVOC needed to correctly simulate a large number of experiments at the UNC site appears to vary seasonally. The typical value is 45 ppbC for early summer, rising to 60 ppbC in hot, hazy August and declining to 10 ppbC

Table 15. Chamber-Dependent Reaction Parameters Used in Simulations For this Report. The actual values used are the second HONO column. Blank values of WallOH and WallN2O5 are 2.5 /ppb-min and 0.19 /ppb-min.

Date	Initial NO	Initial NO_2	7%-rule HONO	ppb HONO	ppbC BVOC	/ppb-min WallOH	/ppb-min WallN2O5
MY1877	0.286	0.075	5	5	60		
JL1877	0.378	0.141	10	40	60		
JL3078	0.395	0.080	6	20	45		0.04
AU1778	0.618	0.086	6	16	40	1.5	
AU2378	0.412	0.095	7	2	45	1.5	0.04
OC0484	0.270	0.090	6	3	10	0.5	0.4
OC0584	0.269	0.100	7	3	25	0.0	0.4
OC1184	0.243	0.108	8	7	20	0.0	0.4
OC1284	0.508	0.210	15 0	6	20	0.4	0.4
JL0886	0.120	0.040	3	3	45		0.4
JL0986	0.291	0.023	2	3	45		0.4
JL1386	0.246	0.045	3	3	45	0.5	0.4
JL0688	0.241	0.100	7	3	45		
JL1588	0.215	0.096	7	6	45		
AU0988	0.240	0.090	6	4	60		
AU1088	0.266	0.055	4	4	60		
AU1288	0.500	0.056	4	20	55		
AU1688	0.331	0.064	4	3	55		
ST0788	0.247	0.113	8	2	55		

in cool October. These values, needed for good fits of the simulations, appear to be correlated with the seasonal pattern in aerosol optical density as described in Jeffries *et al.*[40]

The choice of the rate constant for reaction **WallNO2a** is discussed in the next section.

The heterogeneous loss of N_2O_5 to the chamber walls is the controlling factor for maximum O_3 production in experiments in which high concentrations of O_3 are produced. High concentrations of O_3 lead to high concentrations of N_2O_5 via the $NO_3^{\cdot}$ radical. The loss of part of this N_2O_5 removes nitrogen from the reacting system, limiting the amount of NO_2 that can photolyze and thus limiting the O_3 production. For the vast majority of the simulations, we use the rate constant listed earlier (1.9×10^{-4} ppm^{-1}-min^{-1}) for reaction **WallN2O5b**. It is clear from the fit of the simulation to observations for some runs that this value is too low and more nitrogen was lost in the experiment than in the simulation, causing the final O_3 peak value tp be over-predicted. This was especially true for the 1986 experiments. During 1986, we experienced a major drought and the character of the chamber film surface must have been effected. All of these experiments require that reaction **WallN2O5b** have a rate of 4×10^{-4} ppm^{-1}-min^{-1}, two times higher than normal. On the other hand, 1978 experiments appear to require a lower value (4×10^{-5} ppm^{-1}-min^{-1}). Chamber drying was not commonly practiced in 1978. The 1984 experiments listed in Table 15 had much lower temperatures than all other experiments in the table. We speculate that these cooler temperatures apparently enhance the retension of N_2O_5 on the walls.

Other Chamber-Related Model Inputs

A computer program, MakeTWD, is used to read the UNC data file for each day, to extract the temperature, dew-point and tracer data, and to convert these into input tables needed by PKSS, the simulation program. Air temperature is measured in the sample manifold just under the chamber floor. Dew point is measured by a "cooled-mirror" sensor. Dilution is measured by CCl_4 concentration decreases in each side of the chamber. These are measured by electron capture/gas chromatograph. All of these data are included in each data file for each experiment.

The final sets of data needed for each experiment simulation are the photolytic rates as a function of time. These are computed from the absorption cross-sections and quantum yields given in Chapter 4 and sets of in-chamber actinic fluxes computed by the radiation transfer model and chamber transmission model described by Jeffries *et al.*[41] Parameters for the radiation transfer model such as total ozone column, ambient relative humidity, and aerosol characteristics are included in each SegFile for each experiment. The model also uses measurements from broadband sensors for total solar radiation and ultraviolet radiation as input to the model to compute cloud transmissions. These data are also included in each data file.

Carbon Monoxide Simulations

In Figure 54, the species hierarchy, the first species that should have a significant chain-propagation role is CO. Carbon monoxide, however, is not capable of generating a continuous source of "new" radicals because its oxidation product CO_2 does not photolyze. Therefore, irradiation experiments containing only CO and NO_x will be driven by the "wall-mediated" processes and the chamber background contamination. Thus these types of experiments are tools for investigating these wall-mediated processes.

The major source of ${}^{\cdot}OH$ in these CO–NO_x experiments is

$$NO_2 \xrightarrow{wall} HONO \tag{\textbf{WallNO2a}}$$

$$HONO \xrightarrow{h\nu} {}^{\cdot}OH + NO \tag{\textbf{Id4}}$$

CO can "amplify" these ${}^{\cdot}OH$ radicals by the chain

$${}^{\cdot}OH + CO \xrightarrow{O_2} HO_2^{\cdot} + CO_2 \tag{\textbf{Ih1}}$$

$$HO_2^{\cdot} + NO \longrightarrow {}^{\cdot}OH + NO_2 \tag{\textbf{Ie1}}$$

and finally, ${}^{\cdot}OH$ and $HO_2^{\cdot}$ are lost by

$${}^{\cdot}OH + NO_2 \longrightarrow HNO_3 \tag{\textbf{If1}}$$

$$HO_2^{\cdot} + HO_2^{\cdot} \longrightarrow H_2O_2 \tag{\textbf{Ig1}}$$

If sufficient CO is added, each ${}^{\cdot}OH$ will react with CO many times before reacting with NO_2. The NO to NO_2 conversion rate, therefore, is a measure of this cycling activity.

Two questions arise here about the reaction **WallNO2a**:

- Does the first-order form of the reaction provide a satisfactory fit within each experiment as the NO_2 concentration increases and decreases? and
- Are other factors important in determing the rate across experiments? *i.e.*, Does chamber history (*e.g.*, the previous loading of the walls with nitrate) influence the rate?

A good test series for this situation would be to vary initial NO_2 from low to high concentrations with and without CO.

Table 16 gives the initial conditions and integrated reaction rates for selected reactions for four dual CO–NO_x experiments. Plots of the data and simulation profiles are given in Figures 60 to 63.

Table 16. Initial Conditions and integrated reaction rates for selected reactions for four dual $CO-NO_x$ experiments

	Sept. 23, 1988		June. 27, 1982		Aug. 20, 1982		Aug. 23, 1982	
Item	Red	Blue	Red	Blue	Red	Blue	Red	Blue
Inputs:								
NO_x, ppm	0.867	0.860	0.446	0.447	0.411	0.413	0.437	0.433
NO, ppm	0.667	0.660	0.411	0.409	0.221	0.221	0.095	0.093
NO_2, ppm	0.200	0.195	0.035	0.038	0.190	0.192	0.345	0.340
CO, ppm	0.500	50.000	54.800	0.350	0.350	50.000	0.350	46.500
HONO, ppb	8	8	3	3	8	8	4	4
BVOC, ppbC	45	45	45	45	45	45	45	45
WallOH × 10^{-3}	2.5	2.5	1.5	1.5	0.75	0.75	0.4	0.4
Integrated Rates:								
$NO_2 \longrightarrow HONO$, ppb	50.0	89.0	58.9	14.5	17.1	27.1	20.1	27.3
$^{\cdot}OH+CO$, ppb	2.7	368.8	438.1	3.2	1.6	212.0	1.1	140.1
$HO_2^{\cdot}+NO$, ppb	8.0	374.2	445.2	10.3	4.8	215.3	3.9	142.9
$^{\cdot}OH+NO_2$, ppb	55.0	97.3	69.9	17.5	24.5	43.6	31.9	37.2

As shown in Table 16, the initial conditions include about a factor of two in initial NO_x, and a range of ten for initial NO_2 (0.035 ppm to 0.34 ppm). In addition the Sept. 23 and August 20 experiments contained the same initial NO_2, but with a factor of two difference in total NO_x. All simulations assumed the same level of BVOC and the results are not very sensitive to this assumption.

To answer the two questions above:

- As shown by the model's relative tracking of the observed NO_2, the first order assumption in reaction **WallNO2a** is reasonable. As will be shown later, more reactive $VOC-NO_x$ experiments are also well-fitted when using this form of the reaction. Carter's constant $^{\cdot}OH$ source shows too much reactivity late in experiments when NO_2 is low.
- Chamber history—especially the possibility of HNO_3 retension on the walls from previous experiments—appears to be very important in establishing the magnitude of the rate of reaction **WallNO2a**.

In the 1982 experiments, 24 hours of venting after a high concentration automobile exhaust experiment occurred before the June 27 experiment; 48 hours of venting occurred after a propylene/NO_x experiement before the August 20 experiment and 72 hours of venting occurred before the August 23 experiment and a total of 120 hours had elapsed since any significant quanties of HNO_3 had been produced in the chamber. As will be shown later, all 1988 experiments use a single rate factor for reaction **WallNO2a** and a standard chamber drying and filling protocol was followed in 1988. Thus it seems clear to us that the conditions of the chamber walls influence the apparent first-order rate of reaction **WallNO2a**. We speculate that absorbed nitrate on the wall is an important component in the loss of "new" NO_2 from the gas-phase to release HONO from the wall-absorbed material back into the gas-phase. Measurements of absorbed material on the UNC chamber walls, which are being conducted in another on-going project, do show fluctucting levels of nitrate, nitrite, as well as other species on the walls.

We believe that the cause of the deviation of measured NO from predicted NO in the Sept. 23, 1988 experiment is that no drying of the chamber was performed overnight for this experiment and liquid water was visible on the walls at dawn. As this water evaporated, it is possible that, as first suggested by Mike Gery for other experiments, a "burst" of HONO was released; this process was not included in the simulation model. Nevertheless, the simulation still gave a reasonable fit to the observations.

In Table 16 the processes outlined in the reaction sequence shown at the beginning of this section are quantified. The total mass of material in ppm units that passed through each major reaction path are given for each experiment. These values also support the first order nature of reaction **WallNO2a** in that they show that significantly different amounts of NO_2 reacted with the walls on the two sides of the chamber in each experiment, yet the NO-NO_2 profiles were well simulated. It should be noted that the magnitudes of the wall-mediated $^{\cdot}OH$ production is about 1 to 6% of the total $^{\cdot}OH$ reacted (1500 ppb) in many of the 1988 chamber experiments.

As a final example of the importance of reaction **WallNO2a**, Figure 64 compares a simulation without this reaction to one with the reaction. So even though the magnitude of this radical source is small compared to the total radical throughput, it is absolutely necessary to simulate UNC chamber experiments that lack significant homogeneous radical sources. But, simulations of initial $H_2C{=}O$ experiments are basically insensitive to reaction **WallNO2a** because photolysis of $H_2C{=}O$ provides an overwhelming radical source.

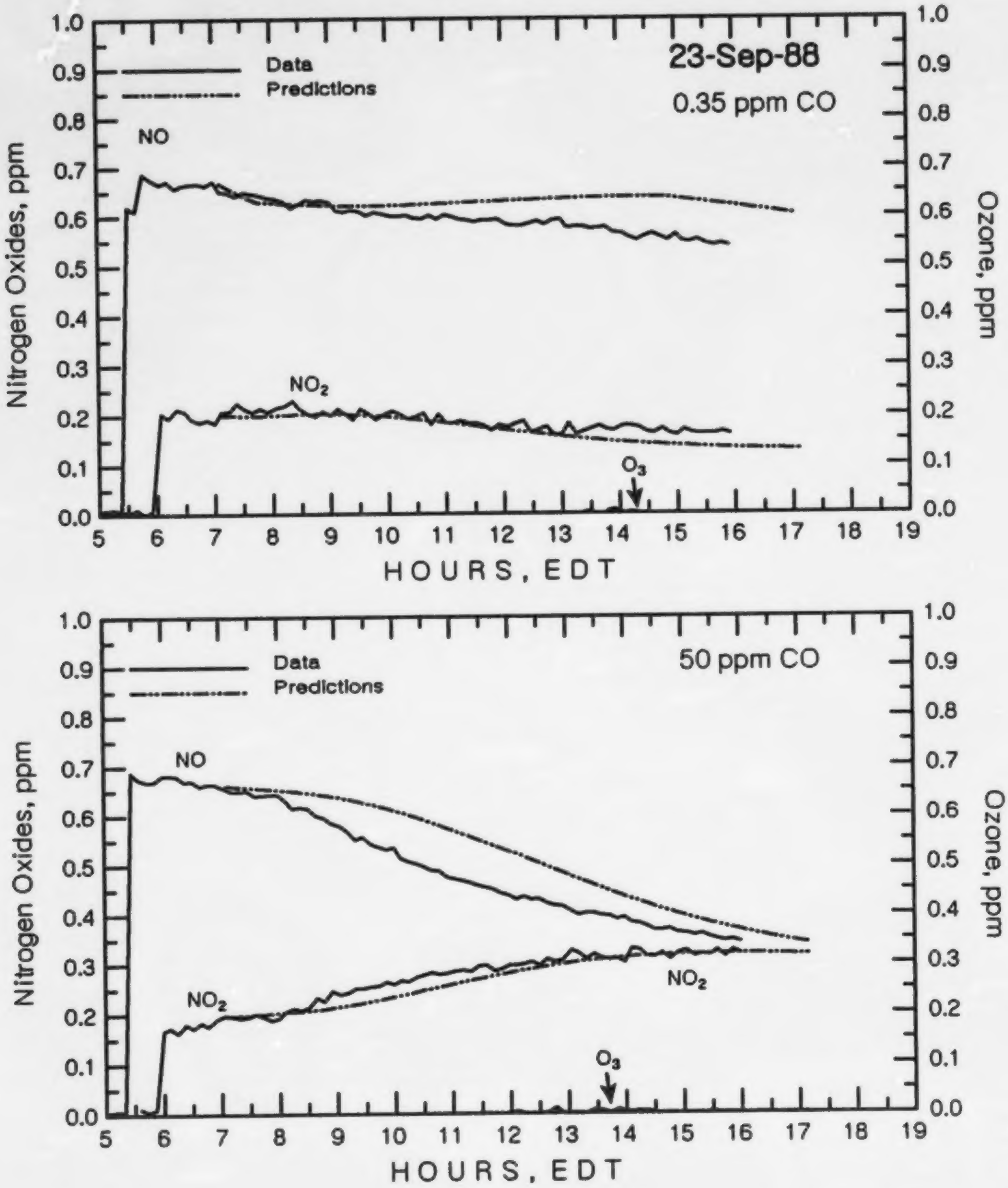

Figure 60. Carbon Monoxide and Nitrogen Oxides Experiment in UNC Outdoor Smog Chamber and Simulation with UNC Explicit Mechanism. Solid lines are chamber data.

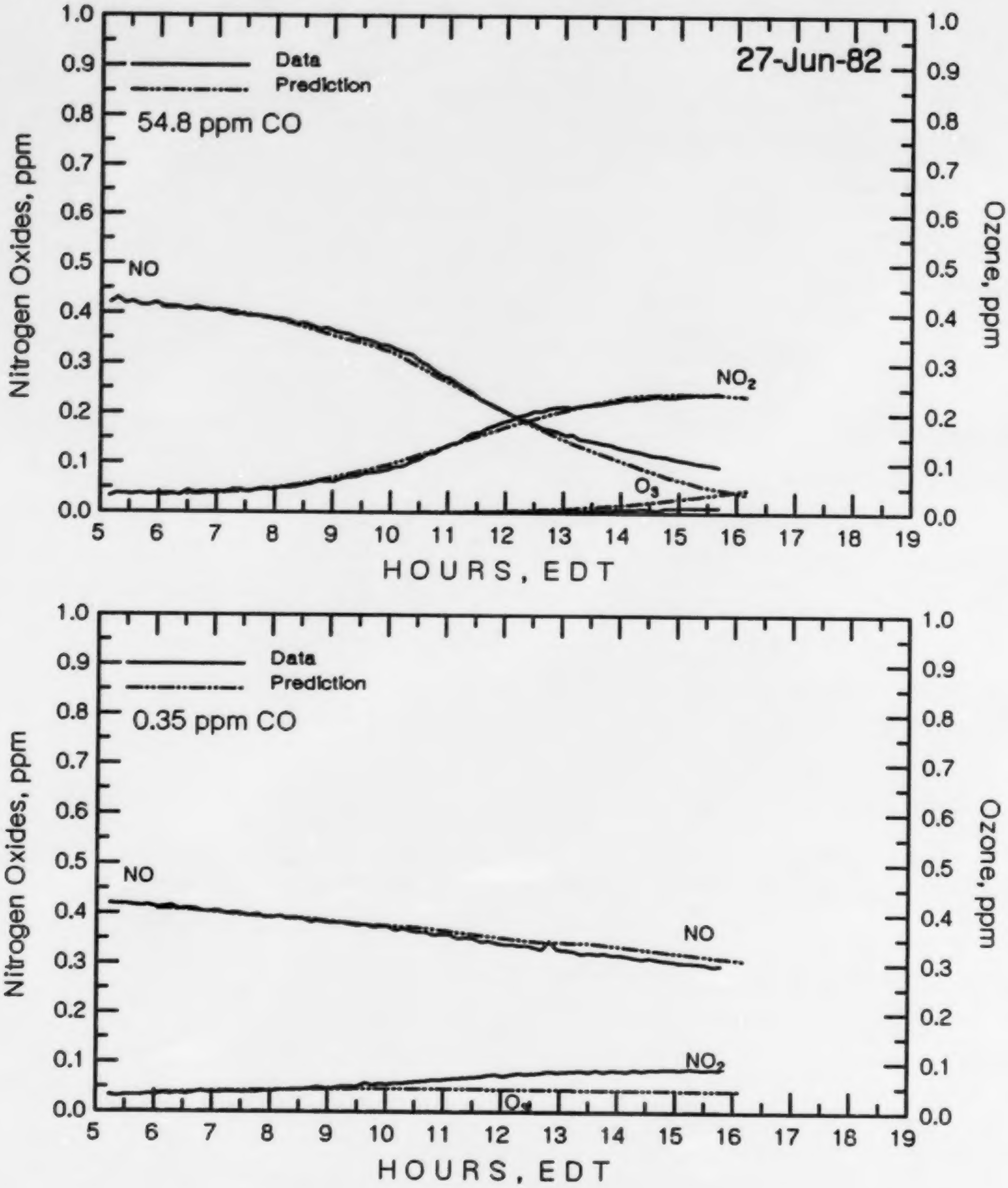

Figure 61. Carbon Monoxide and Nitrogen Oxides Experiment in UNC Outdoor Smog Chamber and Simulation with UNC Explicit Mechanism. Solid lines are chamber data.

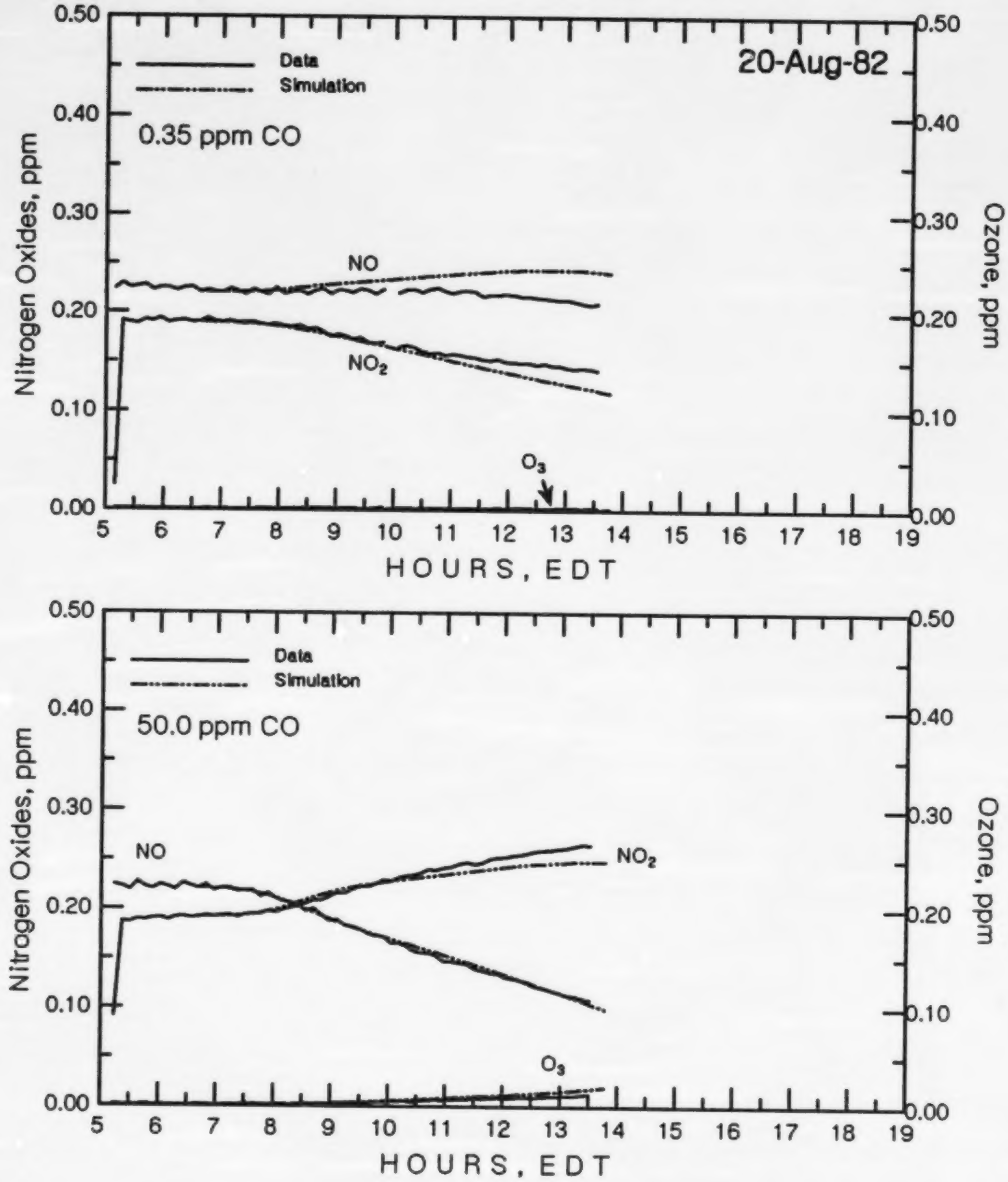

Figure 62. Carbon Monoxide and Nitrogen Oxides Experiment in UNC Outdoor Smog Chamber and Simulation with UNC Explicit Mechanism. Solid lines are chamber data.

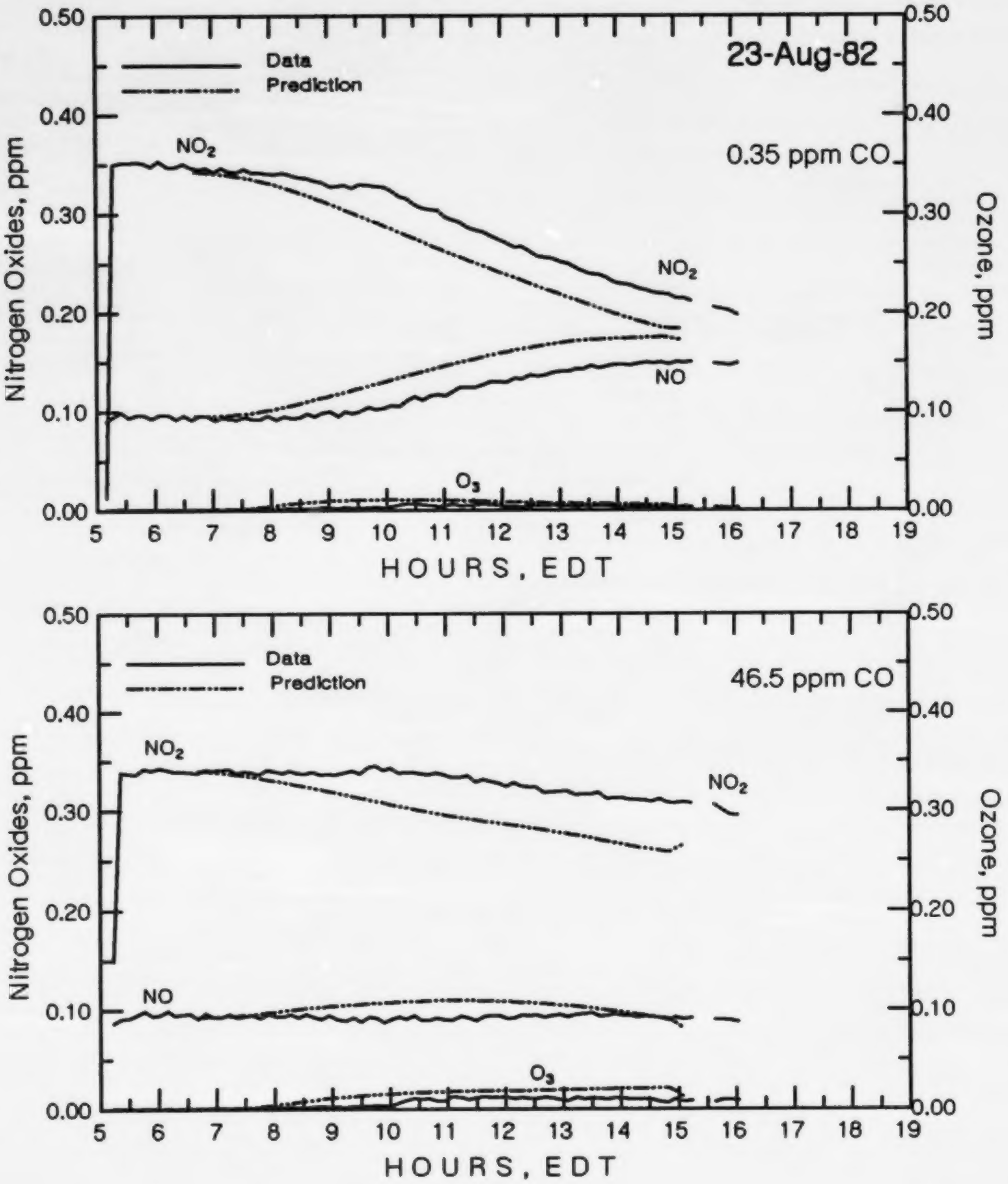

Figure 63. Carbon Monoxide and Nitrogen Oxides Experiment in UNC Outdoor Smog Chamber and Simulation with UNC Explicit Mechanism. Solid lines are chamber data.

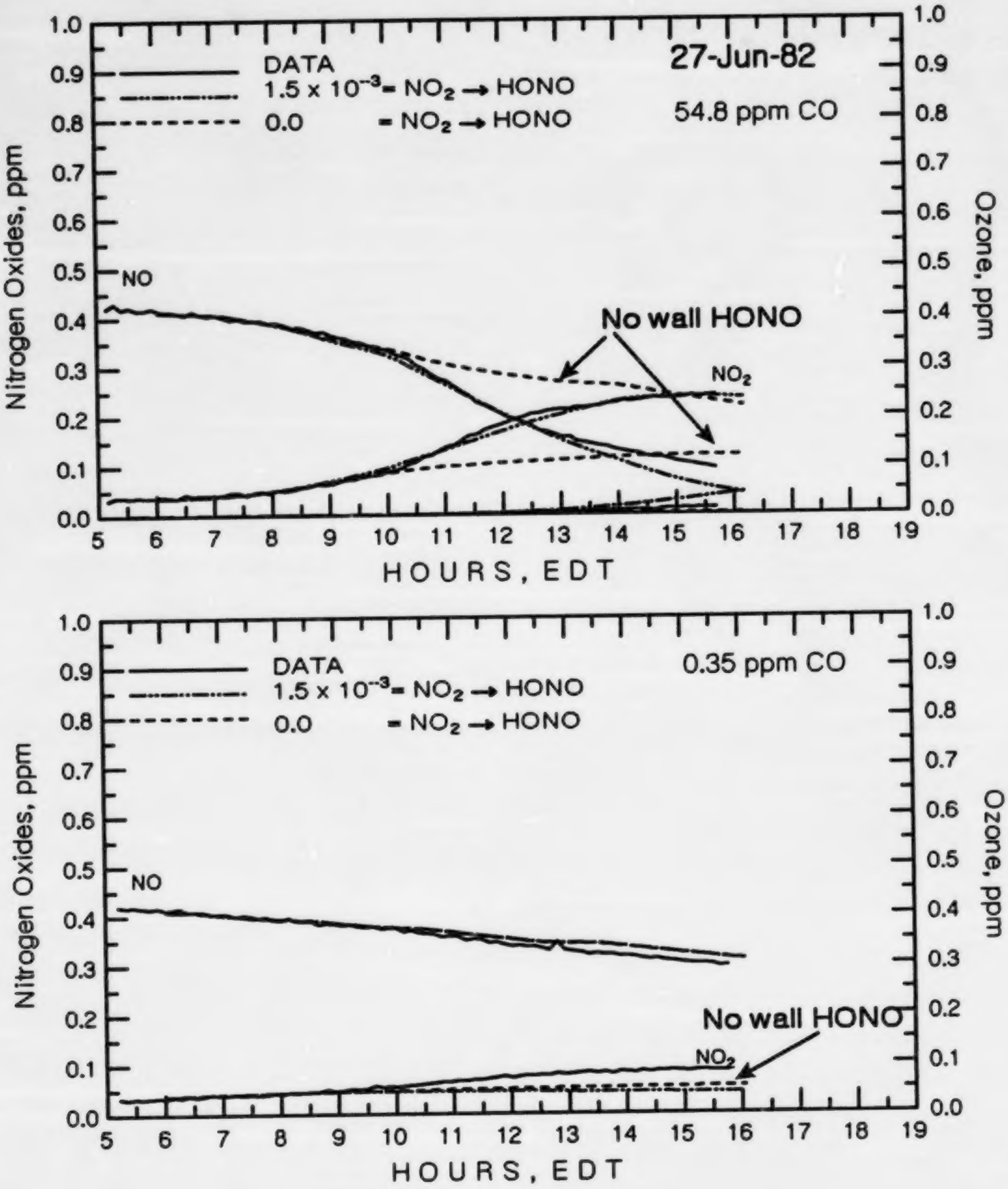

Figure 64. Carbon Monoxide and Nitrogen Oxides Experiment in UNC Outdoor Smog Chamber and Simulation with and without wall production of HONO. Solid lines are chamber data.

Initial Formaldehyde Simulations

Formaldehyde is the first hierarchial species capable of providing a source of "new" radicals to a reacting system. In this case, formaldehyde itself photolyzes:

$$H_2C{=}O \xrightarrow{O_2} 2\,HO_2^{\cdot} + CO \qquad \textbf{C1.1}$$

then, *for each* $HO_2^{\cdot}$,

$$HO_2^{\cdot} + NO \longrightarrow {}^{\cdot}OH + NO_2 \qquad \textbf{Ie1}$$

followed by,

$$\begin{aligned} {}^{\cdot}OH + H_2C{=}O &\xrightarrow{O_2} HO_2^{\cdot} + CO + H_2O && \textbf{C1.3} \\ HO_2^{\cdot} + NO &\longrightarrow {}^{\cdot}OH + NO_2 && \textbf{Ie1} \end{aligned}$$

and finally, ${}^{\cdot}OH$ and $HO_2^{\cdot}$ are lost by

$$\begin{aligned} {}^{\cdot}OH + NO_2 &\longrightarrow HNO_3 && \textbf{If1} \\ HO_2^{\cdot} + HO_2^{\cdot} &\longrightarrow H_2O_2 && \textbf{Ig1} \end{aligned}$$

Here we see that for every molecule of $H_2C{=}O$ that photolyzes in reaction **C1.1**, ***potentially*** four molecules of NO could be converted to NO_2 and two additional molecules of $H_2C{=}O$ could be lost.

Chamber experiments containing only $H_2C{=}O$ and NO_x are useful for demonstrating that

a) the photolysis rate of $H_2C{=}O$ and the relative ratio of photolysis to radicals (reaction **C1.1**) and to stable products (reaction **C1.2**) are correctly represented in the model;

b) the temporal dependence of ${}^{\cdot}OH$ attack on $H_2C{=}O$ is correct; and

c) the chamber-dependent processes are reasonablly well-represented in the simulation.

Figures 65 to 70 show three $H_2C{=}O{-}NO_x$ experiments spanning 11 years in the UNC chamber and using three different HCHO analytical techniques (JL0886: CEA analyzer; JL1588: CEA analyzer and Dasgupta analyzer; and JL1877: Gas chromatograph with photoionizaton detector). The initial HCHO concentrations range from 0.43 ppm to 1.2 ppm. The acetaldehyde data in the Blue chamber on July 18, 1977 will be discussed later.

In these Figures the **solid lines** are always chamber observations and the **dashed lines** are always model predictions. The symbol EXP stands for EXPLICIT model.

We consider these $H_2C{=}O$ simulations to be extremelly good. The worst fit is peak O_3 at the end of July 18, 1977 and this lack of fit is probably due to insufficient reactivity of BVOC for this day after all initial $H_2C{=}O$ had reacted (note the appearance of PAN in the top of Figure 70 which must have come from reacting organic species other than HCHO; the composition of BVOC used to simulate this day may not have accurately reflected the actual conditions). While the HCHO data in Figure 68 exhibit a lot of noise, the simulation profiles are clearly simulatenously in agreement with the measurements of both instruments at two different concentration levels.

Such consistent agreement between the model and the observations with different instruments and over such a long time span strongly supports our belief that the augmented model, which includes the chamber characteristics sub-models (*e.g.*, in-chamber actinic flux, dilution processes, water vapor concentrations, and wall character)—as well as the explicit mechanism—must provide a reasonably accurate description of the chamber system. Further, because the chamber conditions are different for different days, yet the model still predicts accurately, we infer that the explicit mechanism for the *reaction* of HCHO is a well-formed and accurate representation of HCHO chemistry and, therefore, it can be used for conditions other than the UNC chamber.

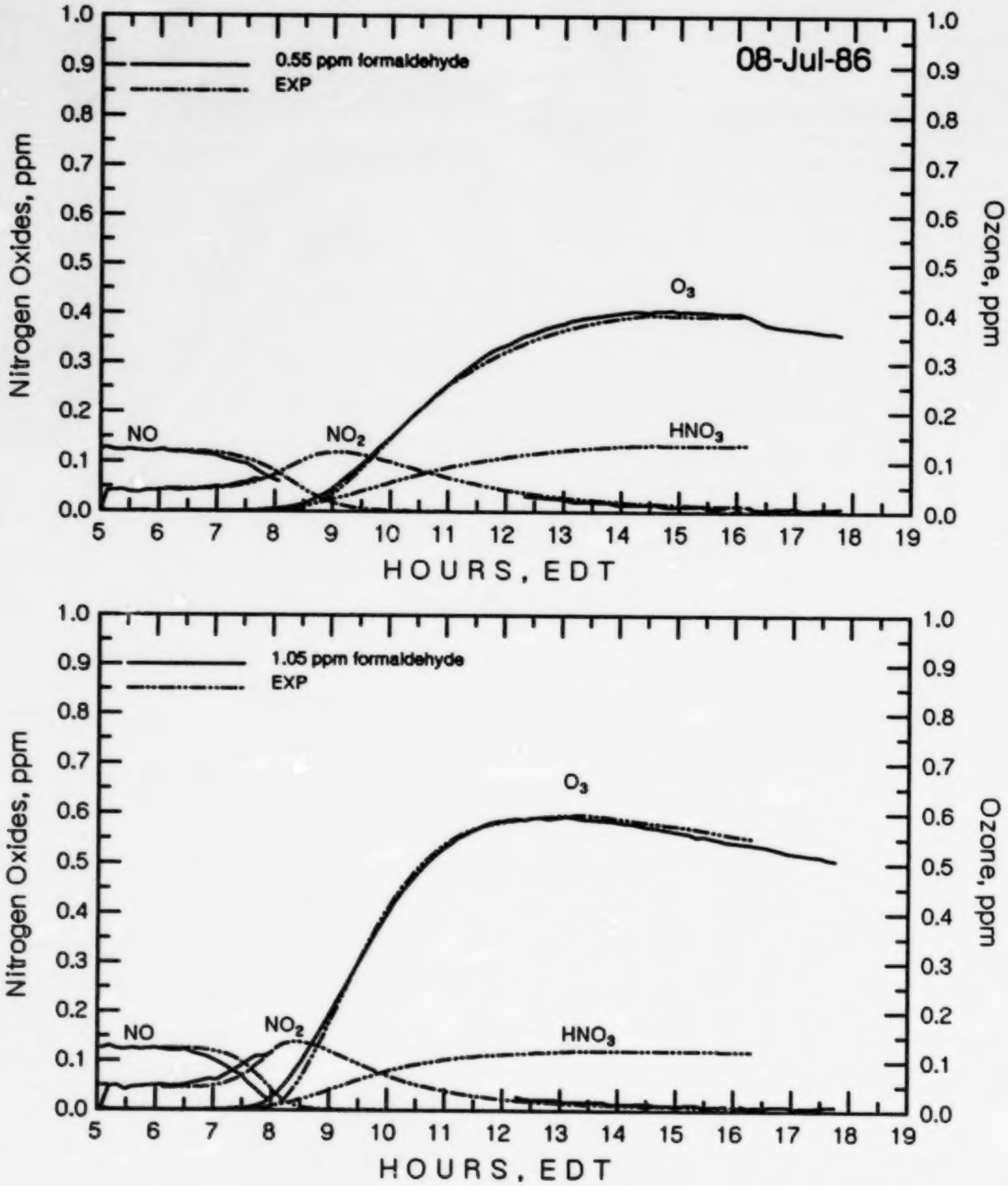

Figure 65. Formaldehyde and Nitrogen Oxides Experiment in UNC Outdoor Smog Chamber and Simulation with UNC Explicit Mechanism. Solid lines are chamber data.

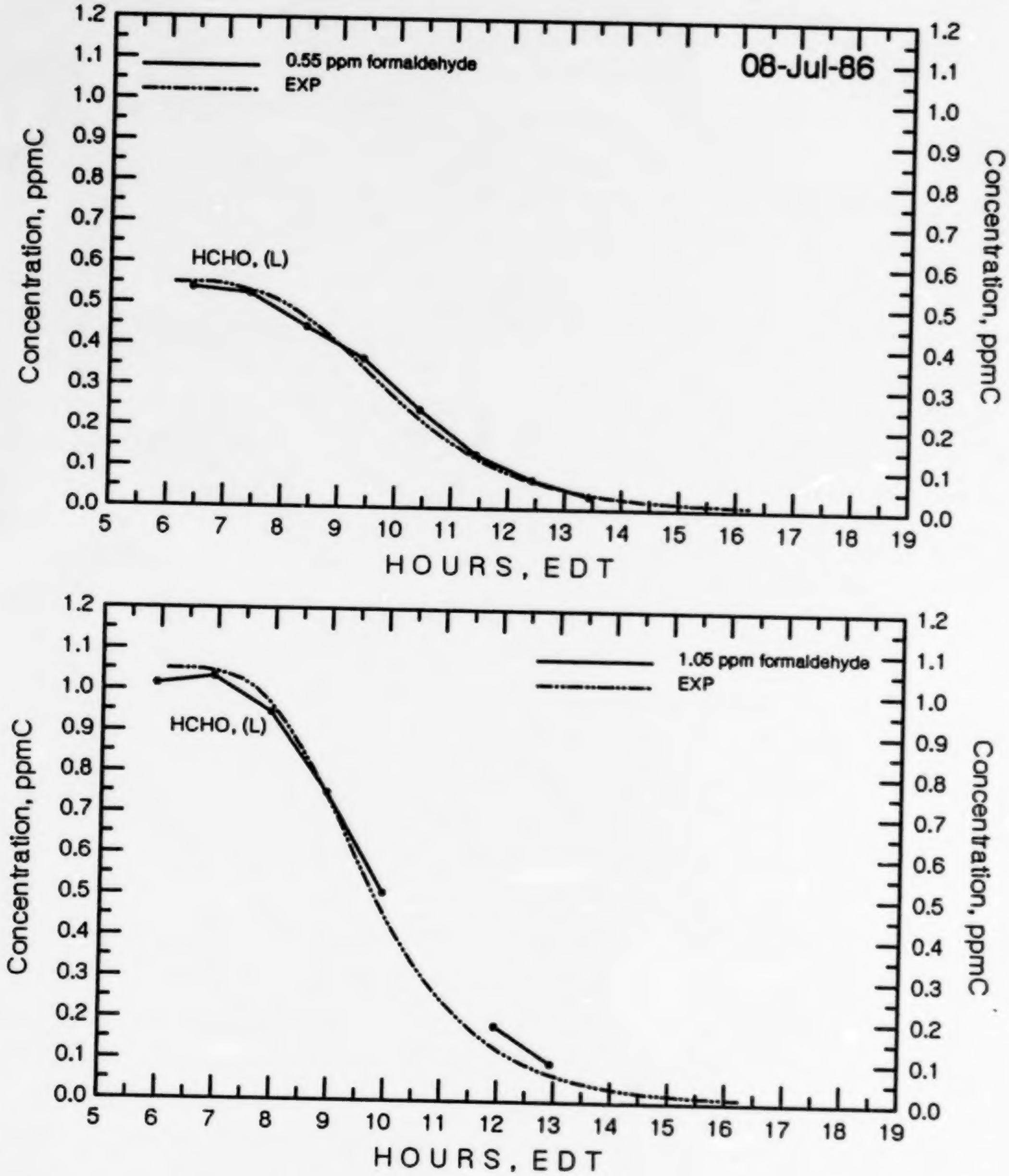

Figure 66. Formaldehyde and Nitrogen Oxides Experiment in UNC Outdoor Smog Chamber and Simulation with UNC Explicit Mechanism. Solid lines are chamber data.

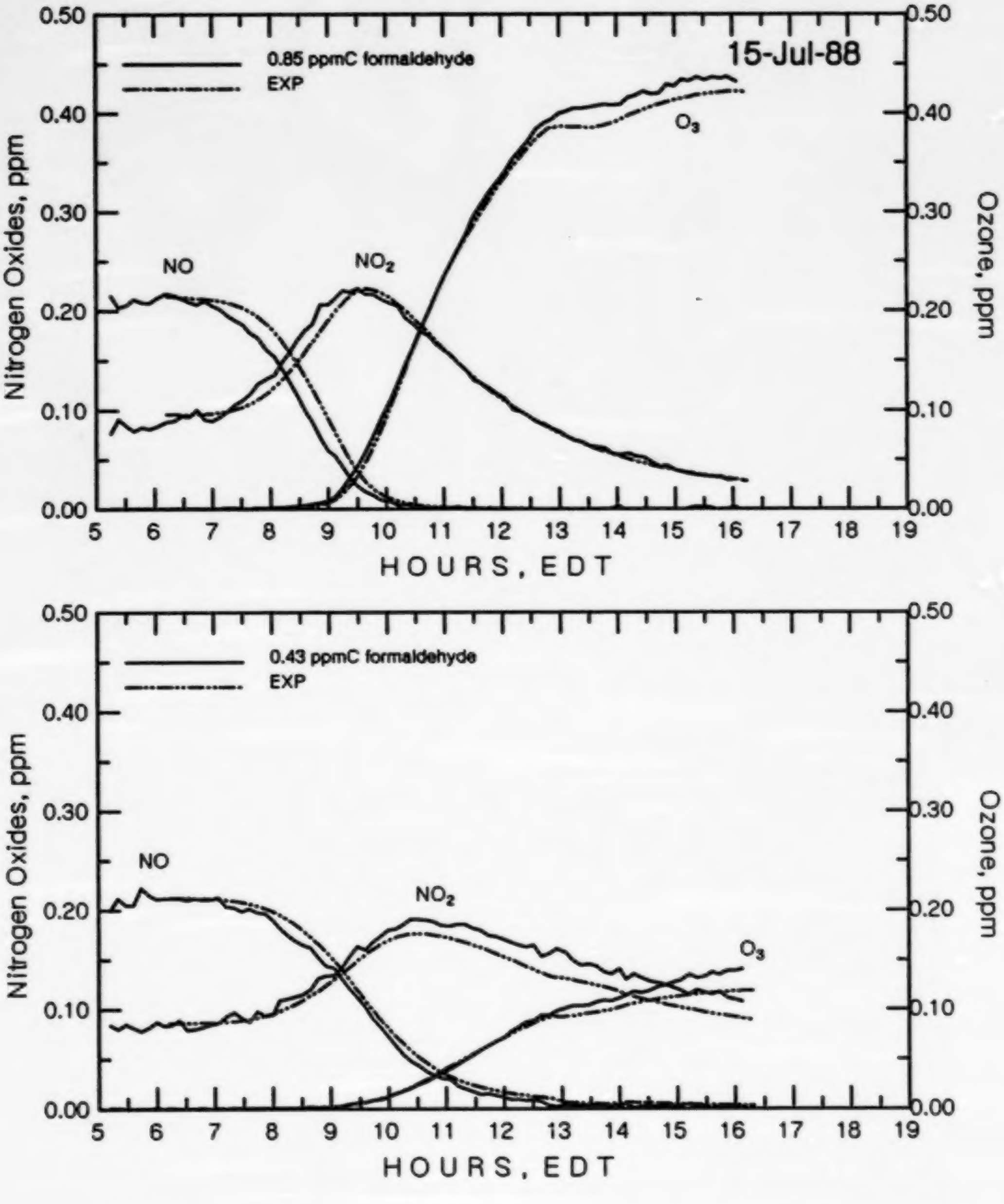

Figure 67. Formaldehyde and Nitrogen Oxides Experiment in UNC Outdoor Smog Chamber and Simulation with UNC Explicit Mechanism. Solid lines are chamber data.

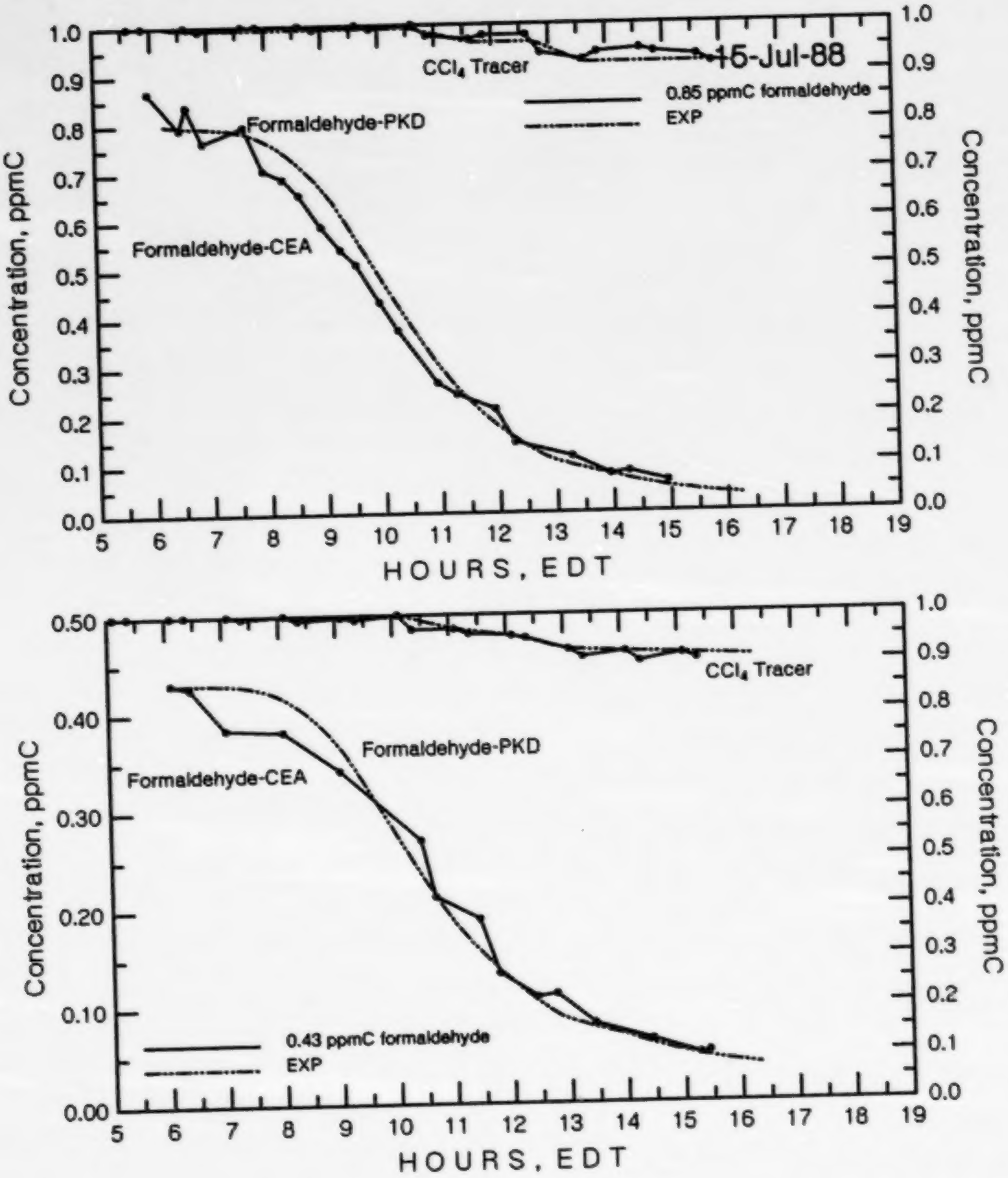

Figure 68. Formaldehyde and Nitrogen Oxides Experiment in UNC Outdoor Smog Chamber and Simulation with UNC Explicit Mechanism. Solid lines are chamber data.

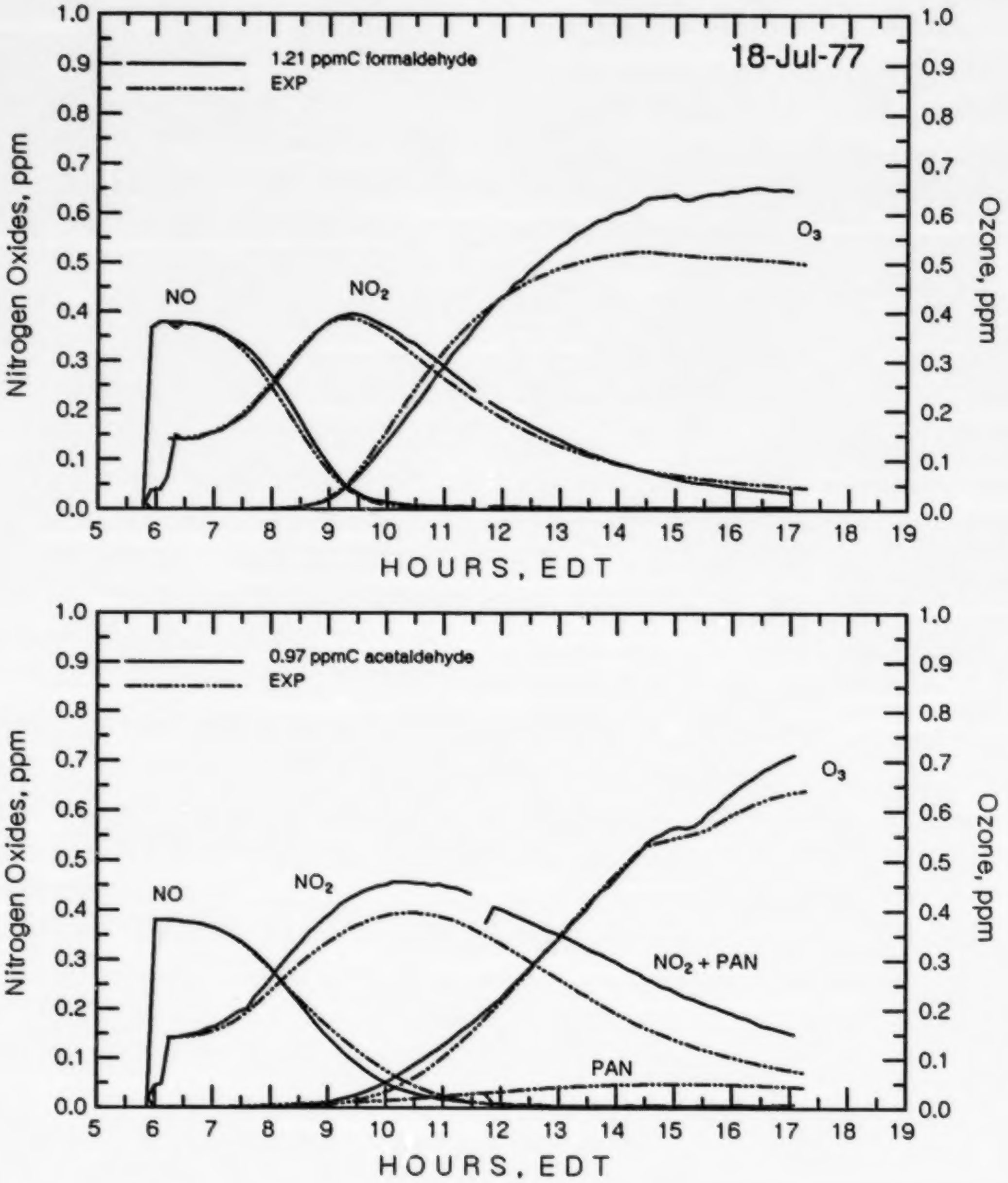

Figure 69. Formaldehyde and Nitrogen Oxides Experiment in UNC Outdoor Smog Chamber and Simulation with UNC Explicit Mechanism. Solid lines are chamber data.

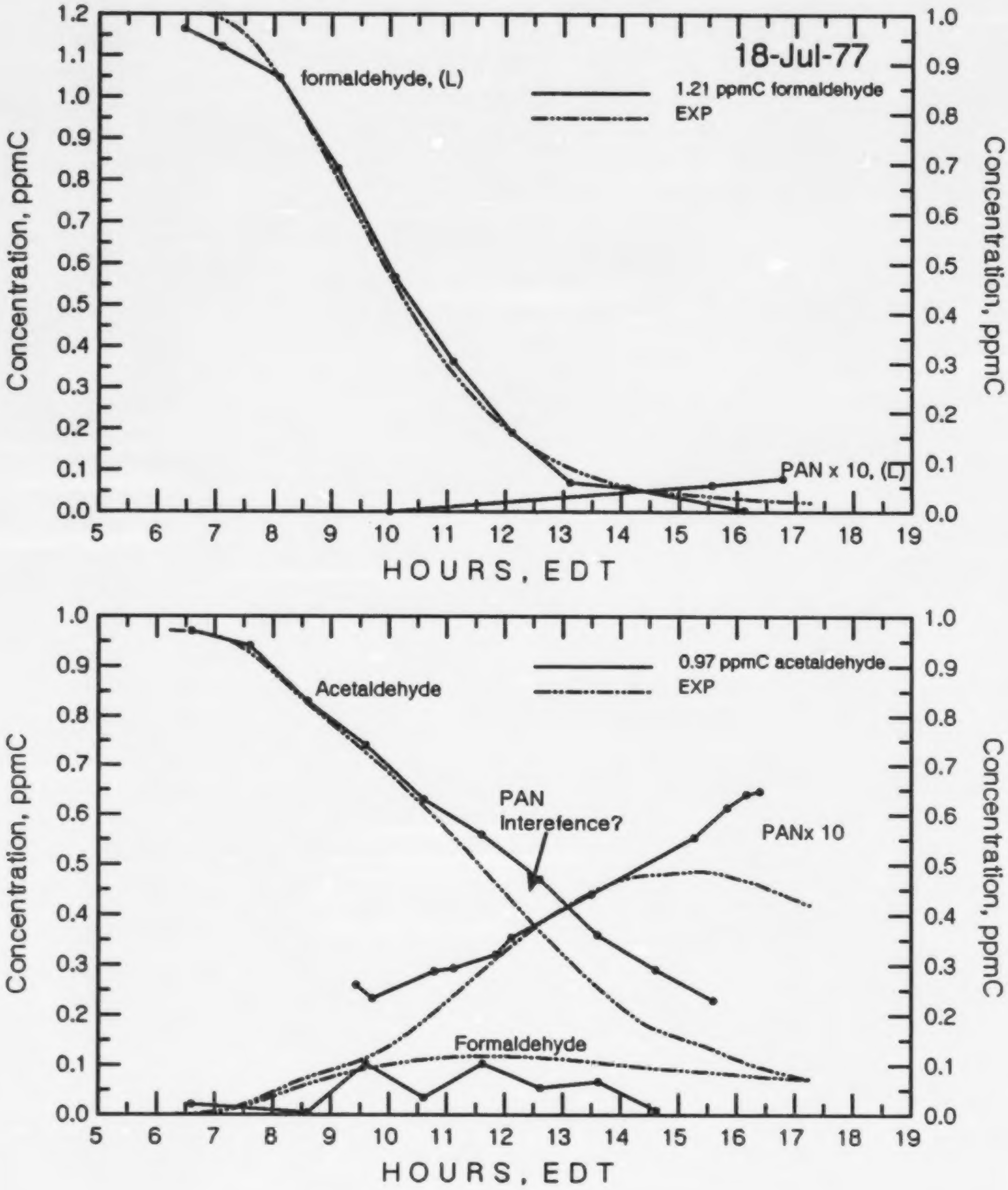

Figure 70. Formaldehyde and Nitrogen Oxides Experiment in UNC Outdoor Smog Chamber and Simulation with UNC Explicit Mechanism. Solid lines are chamber data.

Initial Acetaldehyde Simulations

Acetaldehyde is the first hierarchial species that can produce $H_2C{=}O$ and PAN:

$$^{\cdot}OH + CH_3HC{=}O \xrightarrow{O_2} CH_3C({=}O)O_2^{\cdot} + H_2O \qquad \textbf{C2.3}$$

then,

$$CH_3C({=}O)O_2^{\cdot} + NO \xrightarrow{O_2} CH_3O_2^{\cdot} + CO_2 + NO_2 \qquad \textbf{PA1.1}$$
$$CH_3C({=}O)O_2^{\cdot} + NO_2 \longrightarrow CH_3C({=}O)O_2NO_2 \qquad \textbf{PA1.2}$$
$$CH_3C({=}O)O_2NO_2 \longrightarrow CH_3C({=}O)O_2^{\cdot} + NO_2 \qquad \textbf{PA1.3}$$

Reaction **PA1.1** is followed by,

$$CH_3O_2^{\cdot} + NO \xrightarrow{O_2} H_2C{=}O + HO_2^{\cdot} + NO_2 \qquad \textbf{P1.2}$$

and $^{\cdot}OH$ is regenerated by

$$HO_2^{\cdot} + NO \longrightarrow {}^{\cdot}OH + NO_2 \qquad \textbf{Ie1}$$

and, as before, $^{\cdot}OH$ and $HO_2^{\cdot}$ are lost by

$$^{\cdot}OH + NO_2 \longrightarrow HNO_3 \qquad \textbf{If1}$$
$$HO_2^{\cdot} + HO_2^{\cdot} \longrightarrow H_2O_2 \qquad \textbf{Ig1}$$

Of course, the $H_2C{=}O$ produced in reaction **P1.2** undergoes all the reactions described in the previous section: photolysis by two pathways to make "new" $HO_2^{\cdot}$ radicals and CO, and attack by $^{\cdot}OH$ which also leads to CO (note that all reacted $H_2C{=}O$ appears as CO and the only other source of CO in this system is the much slower photolysis of $CH_3HC{=}O$).

Since we have demonstrated that we have an accurate model for $H_2C{=}O$ reaction loss, sucessful simulation of $H_2C{=}O$ in these systems implies that the relative split between reactions **PA1.1** and **PA1.2** is correct and that the $^{\cdot}OH$ production and loss must be resonably accurately approximated or else $H_2C{=}O$ and $CH_3HC{=}O$ losses could not be predicted correctly.

Unfortuately the quantity of $H_2C{=}O$ produced, even in high concentration acetaldehyde experiments, is small. In the bottom of Figure 70, the predicted and measured $H_2C{=}O$ levels are compared and show good agreement (these $H_2C{=}O$ data are from the gas chromatograhic procedure and they were determined from small peaks which is why the data are so noisy). In Figure 72, the predicted and measured $H_2C{=}O$ levels are again compared and again they show good agreement even though the quantity is small. The bottom of Figure 72 shows what happens when $H_2C=O$ is injected into a chamber with liquid water on the walls. The absorption and desorption preserves a large amount of $H_2C=O$ for reaction in the afternoon, leading to a large amount of O_3 being produced then. The simulation had no wall adsorption and desorption processes, so it consumed the $H_2C=O$ in the morning hours and thus greatly under predicted the afternoon O_3. No $H_2C=O$ was measured in the August 17 1978 experiment shown in Figure 74, but CO was measured. There is excellent agreement between the measured CO data and the model predictions, strongly supporting the belief that the production of $H_2C=O$ from acetaldehyde and the subsequent reaction of $H_2C=O$ are very well represented.

In these experiments and simulations there is reasonable support for the hypothesis that PAN is interfering with the quantification of the acetaldehyde peak on the gas chromatographic system used at UNC. The flame ionization detector on the GC does not detect the $C=O$ portion of acetaldehyde—only the CH_3 portion. If PAN has a similar retension time as acetaldehyde on this column, it could be adding its signal to that of acetaldehyde. Our ability to verify this interference in new experiments has been hampered by finding that the acetaldehyde calibration tank used for the last 3 years has been decaying in concentration and is now only 12% of its stated value. This has complicated interpretations of 1988 acetaldehyde data.

We believe that these modeling tests reasonably establish that the inorganic, methane, ethane, and carbonyl mechanism described in the previous chapter is capable of describing the important photochemistry of formaldehyde as well as its production from the reactions of acetaldehyde with a high degree of accuracy. Further support for the mechanism could be obtained by performing experiments with high concentrations of methane and ethane to test the production of HCHO in a very simple chemical environment. Such experiments would also help support the values chosen for f_{ald} and f_{per} in the $CH_3O_2^{\cdot} + HO_2^{\cdot}$ reaction (**P1.9**). These experiments are planned for the summer of 1990 as part of another on- going program. Meanwhile, we are satisfied that the inorganic carbonyl mechanism is as well-formed and accurate as we know how to make it.

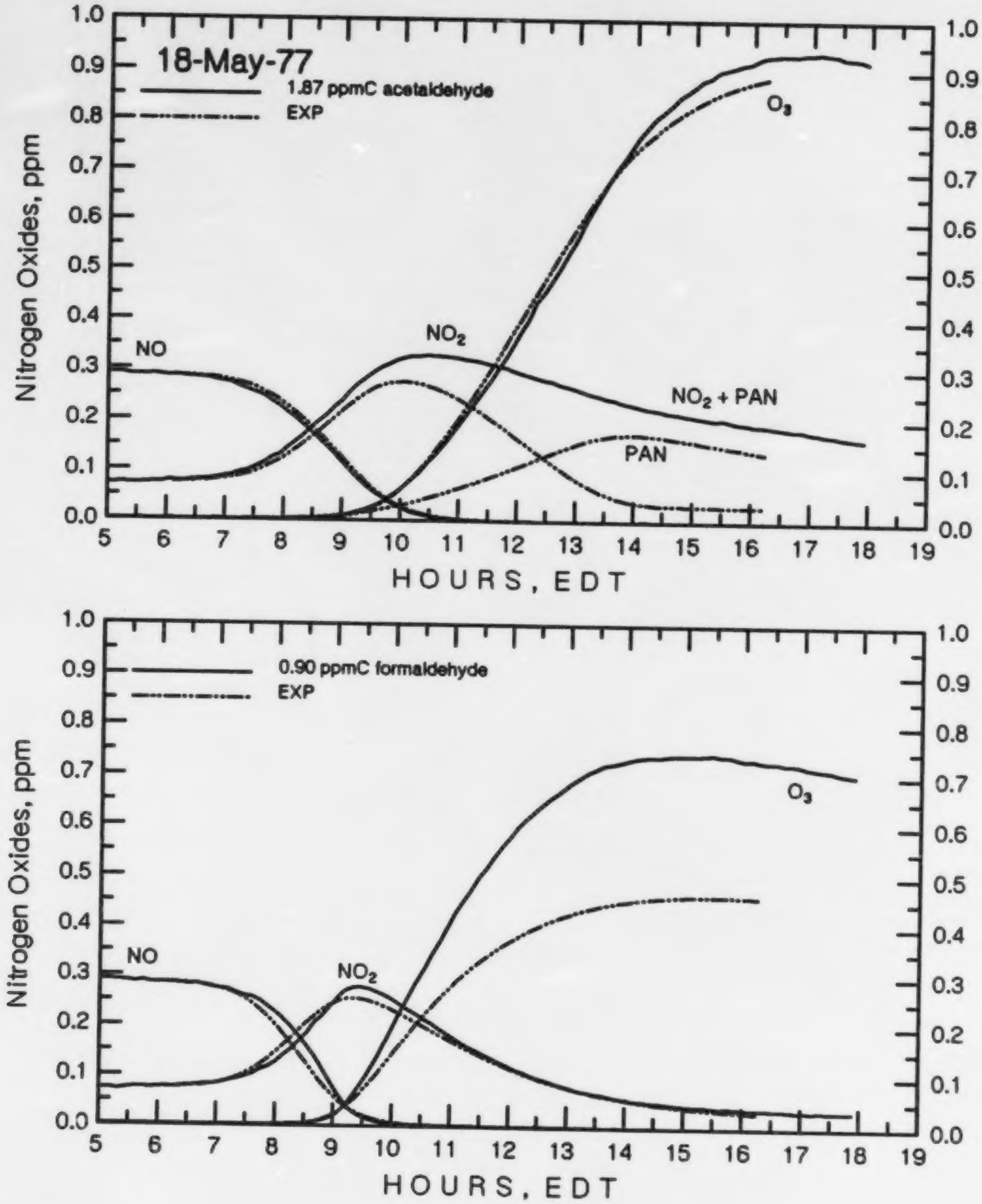

Figure 71. Acetaldehyde and Nitrogen Oxides Experiment in UNC Outdoor Smog Chamber and Simulation with UNC Explicit Mechanism. Solid lines are chamber data.

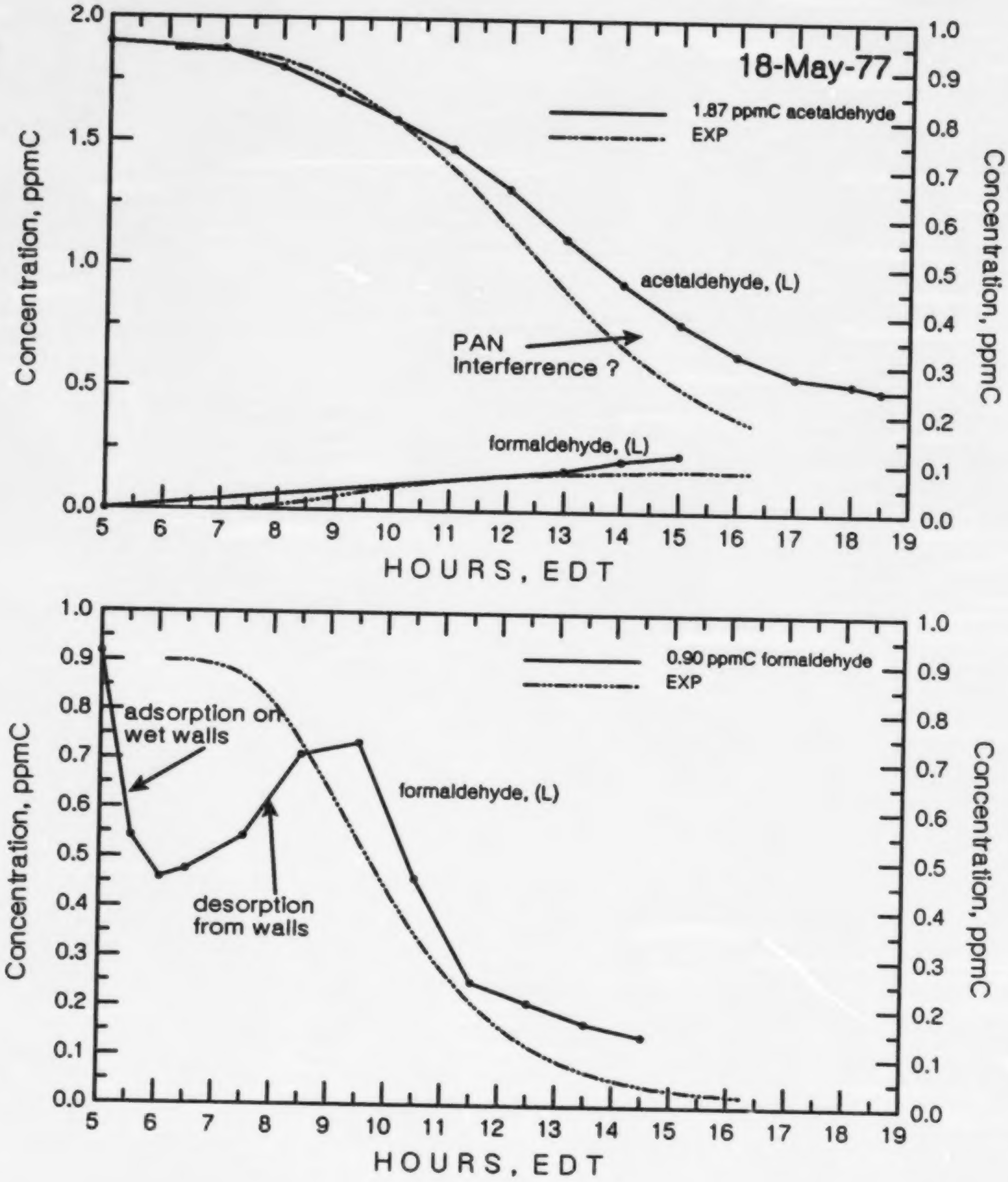

Figure 72. Acetaldehyde and Nitrogen Oxides Experiment in UNC Outdoor Smog Chamber and Simulation with UNC Explicit Mechanism. Solid lines are chamber data.

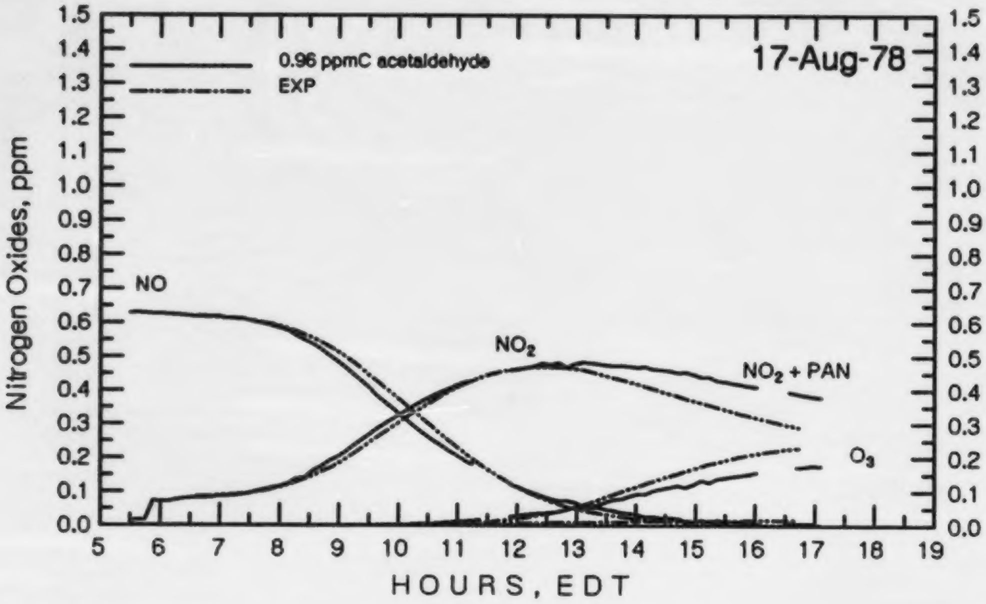

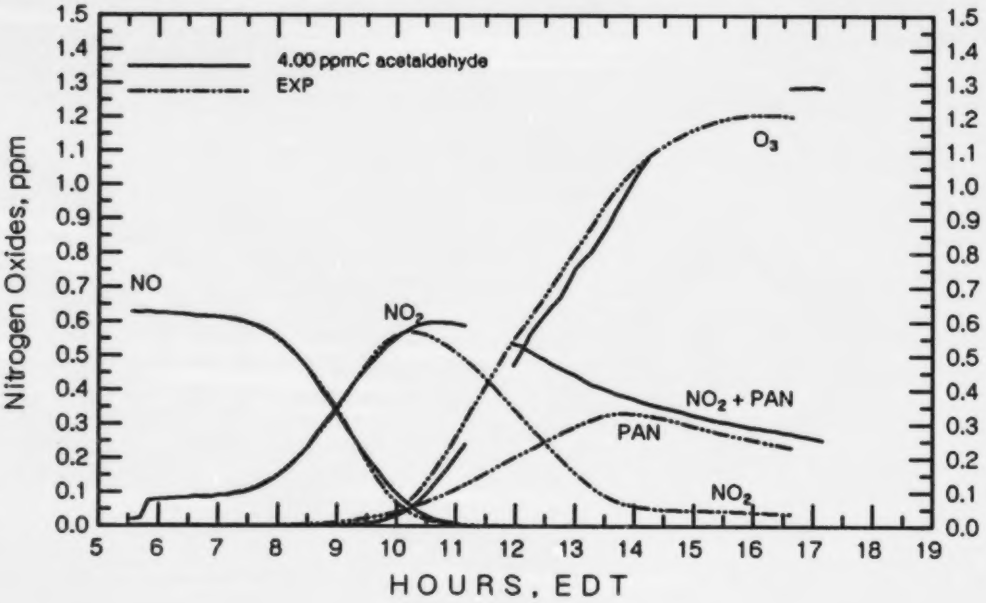

Figure 73. Acetaldehyde and Nitrogen Oxides Experiment in UNC Outdoor Smog Chamber and Simulation with UNC Explicit Mechanism. Solid lines are chamber data.

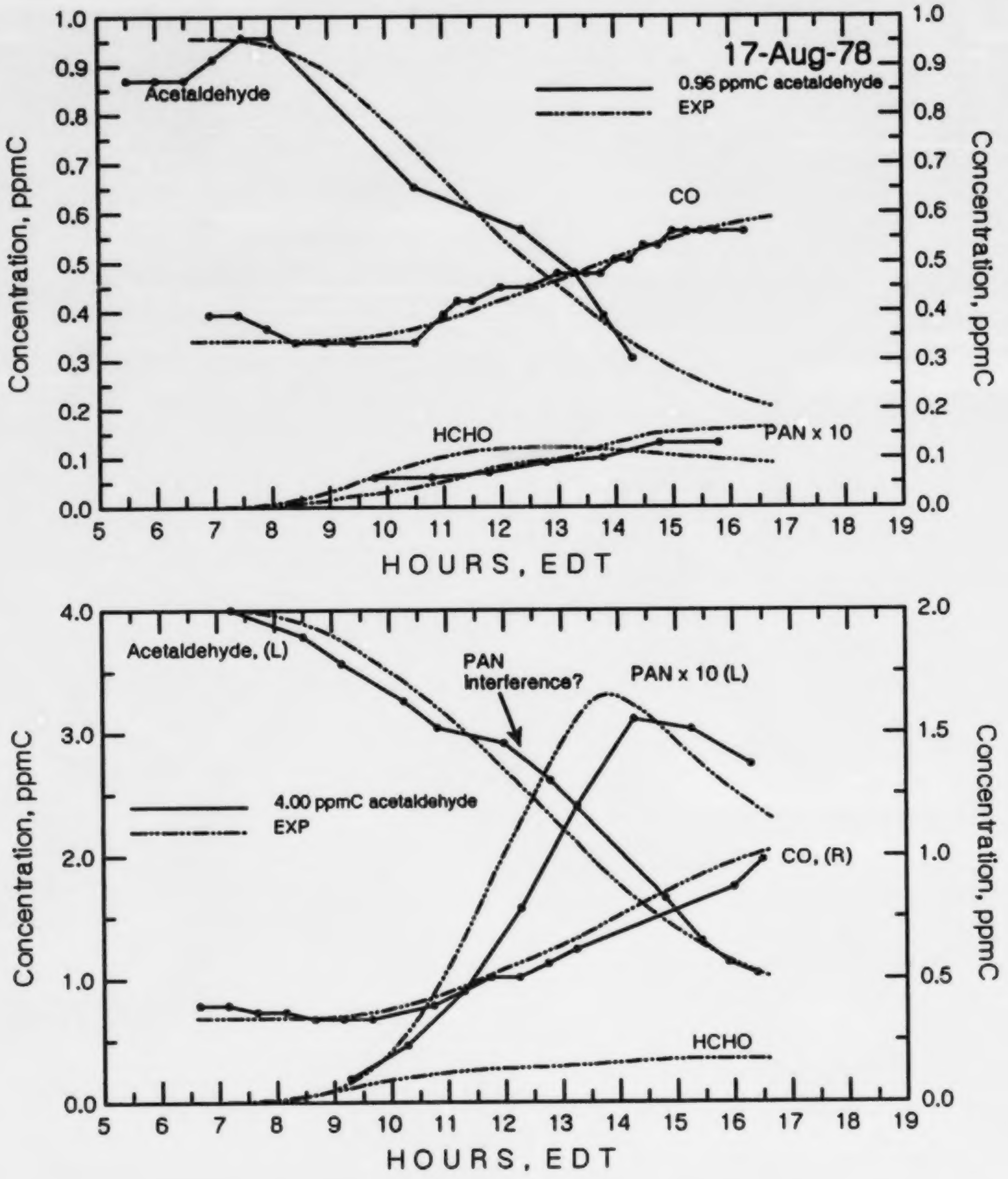

Figure 74. Acetaldehyde and Nitrogen Oxides Experiment in UNC Outdoor Smog Chamber and Simulation with UNC Explicit Mechanism. Solid lines are chamber data.

6

Explicit Mechanism: 2

This chapter describes the chemistry of ethene ($H_2C{=}CH_2$) and the subsequent chemistry of ethene's reaction products that are not already included in the inorganic and carbonyl mechanism. These products are glycoaldehyde ($HOCH_2HC{=}O$) and stablized Criegee biradicals ($^{\cdot}CH_2OO^{\cdot}$). The reactions of glycoaldehyde produce glyoxal ($(HC{=}O)_2$), so this chemistry is also included here.

The reaction labels for the various modules described here are:

- ▹ **O2** – ethene reactions
- ▹ **BR1** – C_1 Criegee biradical reactions
- ▹ **GA** – glycoaldehyde reactions
- ▹ **D2** – glyoxal reactions

O2 = Ethene Chemistry

The are four types of reactions that lead to loss of ethene:

a) $O(3P)$ attack,

b) $^{\cdot}OH$ attack,

c) $NO_3^{\cdot}$ attack, and

d) O_3 attack.

Section a: O(3P) attack

This reaction is included for its potential role in early morning initiation.

O2a.1 $O(3P) + H_2C{=}CH_2 \longrightarrow CH_3O_2^{\cdot} + CO + HO_2^{\cdot}$

This reaction and rate constant are from Atkinson, 1989:

$$k = 1.04 \times 10^{-11} e^{-792/T} \quad \text{cm}^3\text{-molecules}^{-1}\text{-s}^{-1}$$

Section b: ˙OH Attack

The major loss path for ethene is ˙OH addition to the double bond. This reaction scheme is shown in Figure 75. The shaded compounds are the major products produced in the scheme. The majority of this scheme was proposed and experimentally verified by Niki, *et al.*[42] in 1978. In 1981, Niki and his collegues determined that, for ˙OH initiated oxidation of ethene, glycoaldehyde was a major product (ca. 22% of reacted ethene).[43]

Shepson *et al.*[44] observed that C_3-hydroxyalkly peroxy radicals reacted with NO to produce 2-hydroxypropyl nitrate and 2-(nitrooxy)propyl alcohol in propene-NO_x irradiation experiments. We have observed that the simulated NO_2 concentrations were consistently higher than the UNC chamber measurements in all ethene-NO_x experiments. Therefore, we have postulated that hydroxyethyl nitrate is formed in ethene-NO_x irradiation experiments. By optimizing the fit between predictions and observations, we have estimated that the yield of hydroxyethyl nitrate from the ˙OH-ethene reaction is 4%.

O2b.2 $^{\cdot}OH + H_2C{=}CH_2 \xrightarrow{O_2} HOCH_2CH_2O_2^{\cdot}$

This rate constant is from Atkinson, 1989:

$$k = \text{FallOff} \quad \text{cm}^3\text{-molecules}^{-1}\text{-s}^{-1}$$

$$k_\infty = 8.8 \times 10^{-12}(T/300)^{0.8} \quad k_o = 1.5 \times 10^{-28}(T/300)^{0.8} \quad F = 0.6 \quad N = 1.0$$

O2b.3a $HOCH_2CH_2O_2^{\cdot} + NO \longrightarrow HOCH_2CH_2ONO_2$
O2b.3b $HOCH_2CH_2O_2^{\cdot} + NO \longrightarrow NO_2 + HOCH_2CH_2O^{\cdot}$

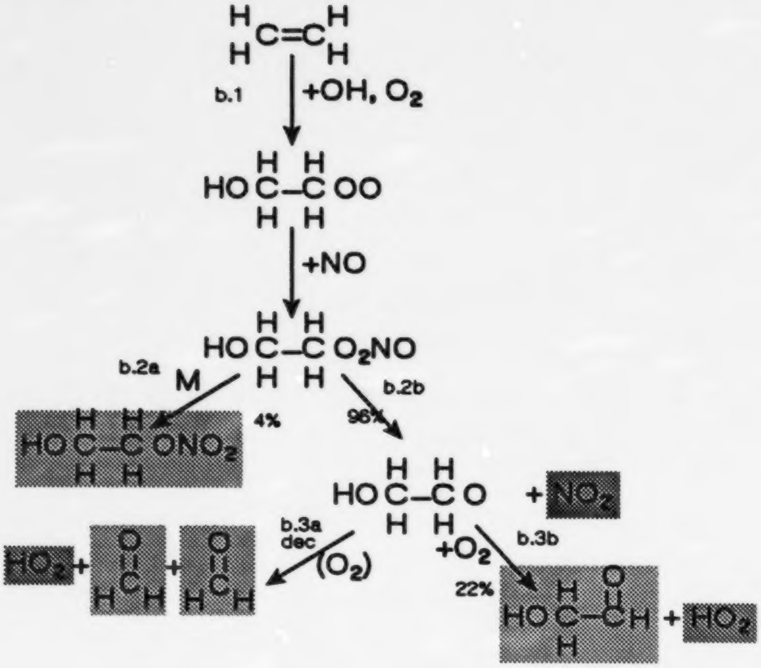

Figure 75. Mechanism for hydroxyl radical initiated oxidation of ethene–**O2b**. Major products are indicated by shading. $NO_3^{\cdot}$ attack and radical-radical termination reactions are not shown here.

Reaction *a* is by analogy with ˙OH-initiated oxidation of propene; the rate ratio to reaction *b* is based upon fitting UNC chamber data for ethene spanning more than 10-years and a 10-fold ethene concentration range.

$$k_a = \mathrm{RO2NORATE} \times f_{\mathrm{RONO2}}$$
$$k_b = \mathrm{RO2NORATE} \times f_{\mathrm{NO2}}$$

The optimum fit was obtained when:

$$f_{\mathrm{RONO2}} = 0.04$$
$$f_{\mathrm{NO2}} = 0.96$$

In the present model $HOCH_2CH_2ONO_2$ is treated as CH_3ONO_2.

We have selected a high vs. low dual ethene chamber experiment to illustrate the sensitivity of this chemical system to including the $RONO_2$ formation. Figure 76 and 77 show the simulations with coefficients as above and with coefficients of 0.0

and 1.0 for f_{RONO2} and f_{NO2}, *i.e.*, no $RONO_2$ production. When $RONO_2$ production is eliminated from the mechanism the effects are:

- beginning just after NO-NO_2 cross over, there is a rapid increase in the rate of NO oxidation, the NO_2-slope increases, and therefore the NO_2 maximum occurs too early and is too high;
- ethene loss is too rapid;
- O_3 formation is too early.

In Figure 77, we show the concentration profile predicted for $HOCH_2CH_2ONO_2$ and we note that the maximum concentration of $HOCH_2CH_2ONO_2$ produced was 16.5 ppb in the 1.7 ppmC ethene experiment and 23.6 ppb in the 3.3 ppmC experiment. This can be contrasted with the 24 ppb hydroxyl-propyl-nitrate *measured* and plotted by Shepson *et al.*[44] in a 2.5 ppmC propylene experiment. The calculated yields in the Shepson *et al.* study were based upon initial data slopes and not modeling fits, and as discussed in the next chapter, their estimates appear low compared to the observed profiles of hydroxyl-propyl-nitrate. Thus our choice of $f_{RONO2} = 0.04$ does appear consistent with measurements presented by Shepson *et al.*. Shepson *et al.* found it quite difficult to measure these types of compounds (one was detected only by its decomposition products), and therefore, it is not surprising that they have not yet been detected in ethene-NO_x experiments.

O2b.4a $HOCH_2CH_2O^{\cdot} \longrightarrow 2\,H_2C{=}O + HO_2^{\cdot}$

O2b.4b $HOCH_2CH_2O^{\cdot} + O_2 \longrightarrow HOCH_2HC{=}O + HO_2^{\cdot}$

The Niki *et al.* 1981 study[43] established that at 298K $k_b/k_a = 5.4 \times 10^{-20}$ cm^3/molecules. Atkinson, 1989, estimated $k_a = 8 \times 10^{-15}$ cm^3-molecules^{-1}-s^{-1}, and by estimating a value for the A-factor of k_a, he computed the activation energy.

$$k_a = 2.7 \times 10^{+14} e^{-6350/T} \quad s^{-1}$$
$$k_b = 8.0 \times 10^{-15} \quad cm^3\text{-molecules}^{-1}\text{-s}^{-1}$$

O2b.5 $HOCH_2CH_2O_2^{\cdot} + HO_2^{\cdot} \longrightarrow f_{ald}\,(HOCH_2HC{=}O + H_2O + O_2) +$
$f_{per}\,(HOCH_2CH_2OOH + O_2)$

This reaction is based upon **P1.9**.

$$k = \text{RO2HO2RATE}$$

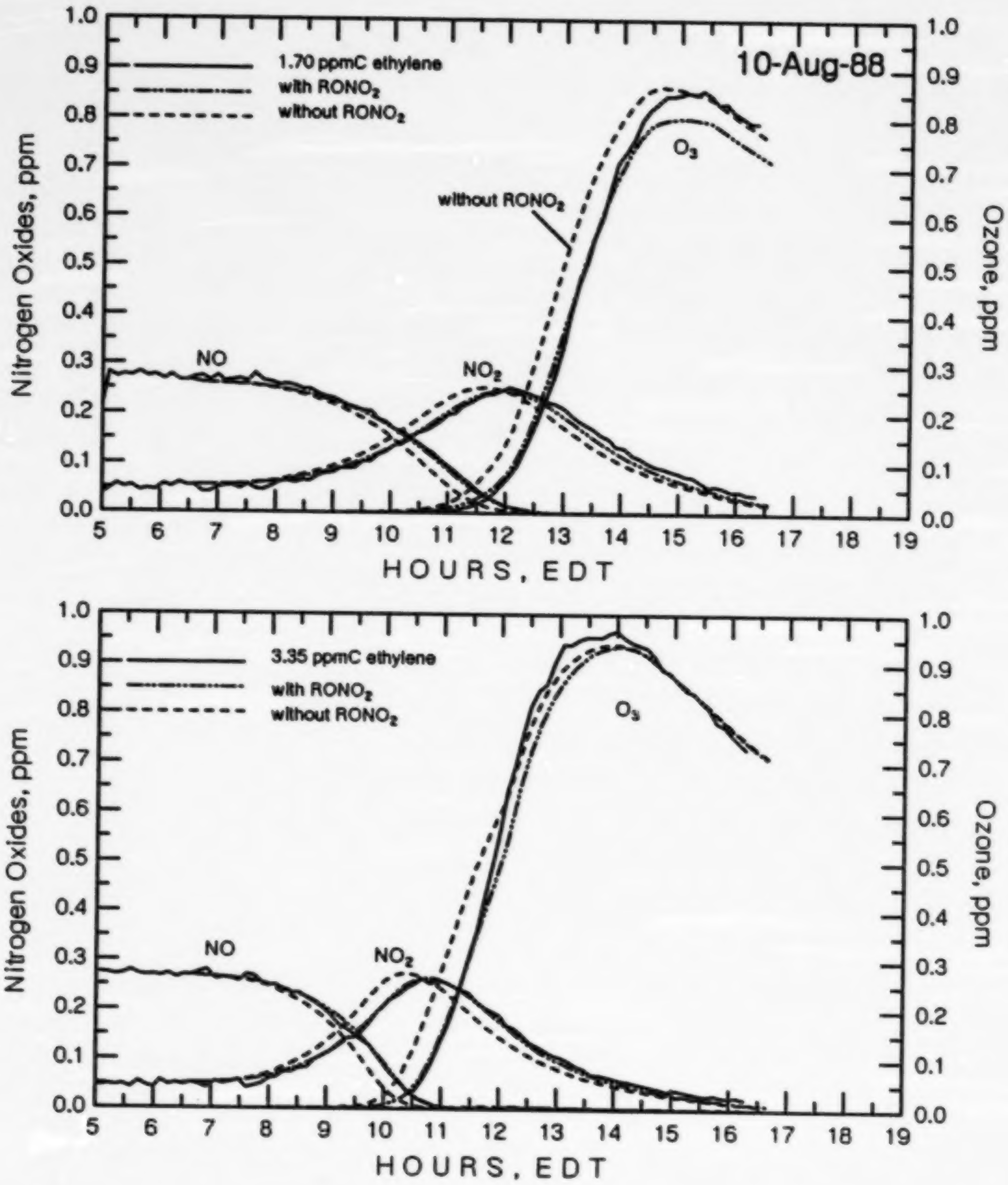

Figure 76. Sensitivity of Simulation to Hydroxy-alkyl-nitrate Formation. Solid lines are chamber data; dashed lines are from simulations.

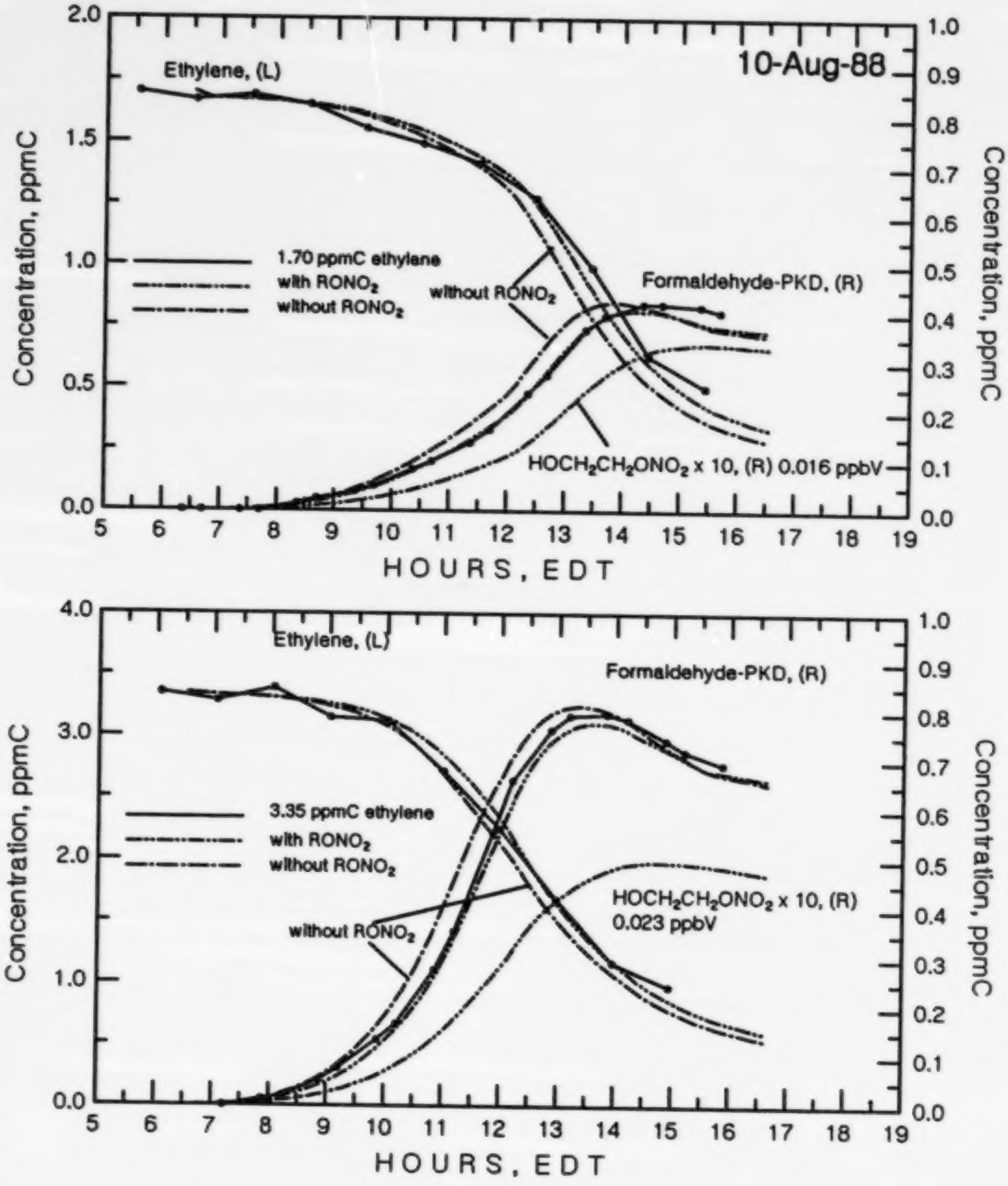

Figure 77. Sensitivity of Simulation to Hydroxy-alkyl-nitrate Formation. Solid lines are chamber data; dashed lines are from simulations.

O2b.6

$$\begin{aligned}\mathrm{HOCH_2CH_2O_2^{\cdot} + CH_3O_2^{\cdot}} \longrightarrow\ & f^2_{sta1}\,(\mathrm{HOCH_2CH_2OH + H_2C{=}O + O_2}) + \\ & f^2_{rad}\,(\mathrm{HOCH_2CH_2O^{\cdot} + CH_3O^{\cdot} + O_2}) + \\ & f^2_{sta2}\,(\mathrm{HOCH_2CH_2OOCH_3 + O_2})\end{aligned}$$

This reaction is based upon **P1.10**.

$$k = \mathrm{RO2RO2RATE}$$

O2b.7

$$\mathrm{HOCH_2CH_2OOH \longrightarrow H_2C{=}O + H_2C{=}O + H_2O}$$

Hydroperoxyhydroxyethane was formed in reaction **O2b.5** and it is the second member of this class of homologous series. Hydroperoxyhydroxymethane, ($\mathrm{HOCH_2OOH}$), which was formed in reaction **C1.9**, was observed to be a meta-stable product by Su, *et al.*[45] as well as by Martinez and Herron[46]. Here we assume that $\mathrm{HOCH_2CH_2OOH}$ forms a six-membered ring transition state that then loses $\mathrm{H_2O}$. The rate constant is estimated based upon half-lives reported by Su, *et al.*

$$k = 1.0 \times 10^{-4} \quad \mathrm{s^{-1}}$$

Section c: $\mathrm{NO_3^{\cdot}}$ Attack

These reactions become important in high concentration ethene experiments when significant $\mathrm{O_3}$ and $\mathrm{NO_2}$ are both present. These are not included in Figure 75.

O2c.1

$$\mathrm{NO_3^{\cdot} + H_2C{=}CH_2 \longrightarrow NO_3CH_2CH_2O_2^{\cdot}}$$

This reaction and rate constant are from Atkinson, 1989:

$$k = 2.15 \times 10^{-12} e^{-2758/T} \quad \mathrm{cm^3\text{-}molecules^{-1}\text{-}s^{-1}}$$

O2c.2

$$\mathrm{NO_3CH_2CH_2O_2^{\cdot} + NO \longrightarrow 2\,NO_2 + 2\,H_2C{=}O + HO_2^{\cdot}}$$

This reaction and rate constant are from Atkinson, 1989:

$$k = \mathrm{RO2NORATE}$$

O2c.3

$$\mathrm{NO_3CH_2CH_2O_2^{\cdot} + HO_2^{\cdot} \longrightarrow} f_{ald}\,(\mathrm{NO_3CH_2HC{=}O + H_2O + O_2})+ \\ f_{per}\,(\mathrm{NO_3CH_2CH_2OOH + O_2})$$

This reaction is based on reaction **P1.9**.

$$k = \mathrm{RO2HO2RATE}$$

O2c.4

$$\mathrm{NO_3CH_2CH_2O_2^{\cdot} + CH_3O_2^{\cdot} \longrightarrow} f^2_{sta1}\,(\mathrm{NO_3CH_2CH_2OH + H_2C{=}O + O_2})+ \\ f^2_{rad}\,(\mathrm{NO_2 + H_2C{=}O + H_2C{=}O + CH_3O^{\cdot} + O_2})+ \\ f^2_{sta2}\,(\mathrm{NO_3CH_2CH_2OOCH_3 + O_2})$$

This reaction is based on reaction **P1.9**.

$$k = \mathrm{RO2RO2RATE}$$

O2c.5

$$\mathrm{NO_3CH_2CH_2OOH \longrightarrow HNO_3 + H_2C{=}O + H_2C{=}O}$$

This reaction is analogous to reaction **O2b.7**.

$$k = 1.0 \times 10^{-4} \quad \mathrm{s^{-1}}$$

Section d: O_3 Attack

This reaction is important in high concentration ethene experiments where significant O_3 and ethene are both present. The mechanism received significant attention a few years ago.[47,48 ,49 ,50] More recent work has clarified the initial decomposition of the "molozonide" and fairly well established the fraction of stable Criegee biradicals that are derived from ethene.[51,52] Yet, as we shall see, questions still remain about secondary reactions in this system.

Figure 78 shows the reaction scheme for O_3 addition to the ethene double bond.

O2d.1

$$\mathrm{O_3 + H_2C{=}CH_2 \longrightarrow H_2C{=}O} + f^E_{hot}\,[{}^{\cdot}\mathrm{CH_2OO}^{\cdot}]^{*}+ \\ f^E_{warm}\,[{}^{\cdot}\mathrm{CH_2OO}^{\cdot}]^{\dagger}+ \\ f^E_{cold}\,{}^{\cdot}\mathrm{CH_2OO}^{\cdot}$$

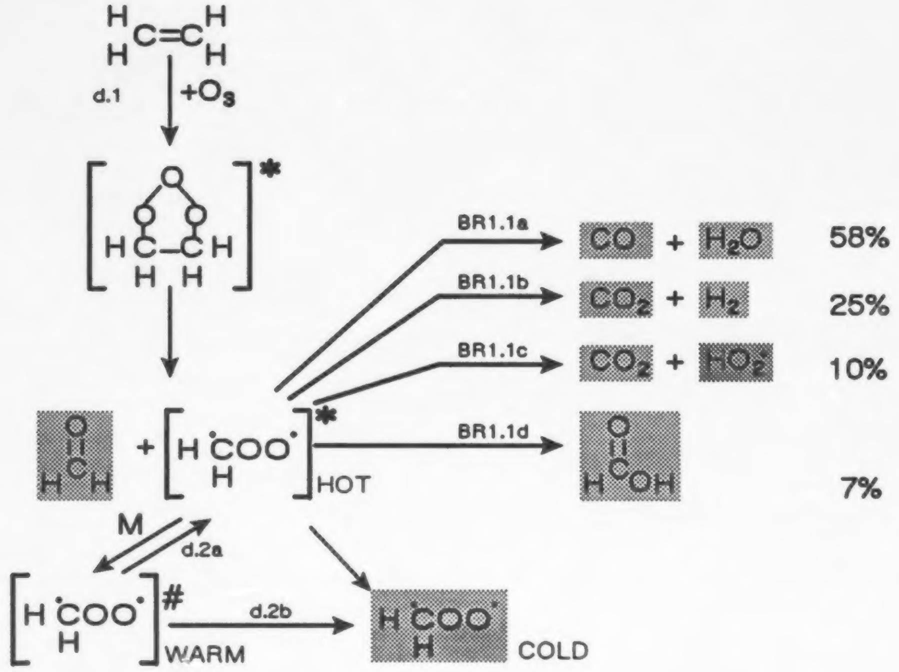

Figure 78. Mechanism for ozone initiated oxidation of ethene–**O2d**. Major products are indicated by shading.

This reaction is derived from the work of Hatakeyama, *et al.*;[52] the rate constant is from Atkinson, 1989.

$$k = 1.2 \times 10^{-14} e^{-2636/T} \quad \text{cm}^3\text{-molecules}^{-1}\text{-s}^{-1}$$

Hatakeyama and collegues carried out $O_3 + H_2C{=}CH_2$ reactions in the presence of excess SO_2 at total pressures of 10 to 1140 torr. They found that three kinds of Criegee biradicals were form:

a) the major fraction of Criegee biradicals (ca. 60%) were "hot" and could not be collisionally stablized even at 1140 torr;

b) a lesser fraction of Criegee biradicals (ca. 20%) were apparently formed stable ("cold") and existed even at 10 torr;

c) the remainder (ca. 20%) of Criegee biradicals were "warm" and some could be stablized. Higher total pressure resulted in more "cold" biradicals.

The extent of stablized Criegee was found by determining how much H_2SO_4

was formed from SO_2 in the overall process. The data were presented as the yield relative to O_3 loss:

$$\frac{\Delta H_2SO_4}{\Delta O_3}$$

A problem arises with presenting the yield this way: secondary reactions of the unstablized Criegee biradicals are expected to produce $HO_2^{\cdot}$ radicals (see Figure 78) and these radicals react with O_3.

Simulations of the test conditions suggest that a significant amount (ca. 16%) of ozone may have been consumed by $O_3 + HO_2^{\cdot} \longrightarrow {}^{\cdot}OH + 2\,O_2$, while a smaller amount of $H_2C{=}CH_2$ would be consumed by the $^{\cdot}OH$ produced. Thus $\Delta H_2SO_4/\Delta O_3$ is *not* the yield we need. Based upon simulations described below for the Su, Calvert, Shaw experimental situation, we estimate that a better approximation of the fractional yields of Creigee biradicals is

$$f^E_{hot} = 0.5350$$
$$f^E_{warm} = 0.2325$$
$$f^E_{cold} = 0.2325$$

O2d.2a $[{}^{\cdot}CH_2OO^{\cdot}]^{\dagger} \longrightarrow [{}^{\cdot}CH_2OO^{\cdot}]^{*}$

O2d.2b $[{}^{\cdot}CH_2OO^{\cdot}]^{\dagger} + M \longrightarrow {}^{\cdot}CH_2OO^{\cdot}$

These reactions and rate ratio are also from Hatakeyama, *et al.*[52]. By a yield analysis as a function of pressure, these researchers were able to estimate that the rate constant ratio $R_{stab}/R_{dec} = k_b/k_a = (1.0 \pm 0.9)\times^{-19}$ cm^3/molecule. Here we assume $k_a = 2.0 \times 10^5 s^{-1}$ (the magnitude of the rate constant is unimportant as long as it is fast because there are no other reactions for $[{}^{\cdot}CH_2OO^{\cdot}]^{\dagger}$). Therefore, the rate constants used here are:

$$k_a = 2.0 \times 10^{+5} \quad s^{-1}$$
$$k_b = k[O2d.2a] \times R_{stab}/R_{dec}$$

BR1 = Criegee Biradical Chemistry

As shown in Figure 78, the decomposition of the "hot" Criegee can occur by four pathways:

BR1.1a $[^{\cdot}CH_2OO^{\cdot}]^* \longrightarrow CO + H_2O$
BR1.1b $[^{\cdot}CH_2OO^{\cdot}]^* \longrightarrow CO_2 + H_2$
BR1.1c $[^{\cdot}CH_2OO^{\cdot}]^* \longrightarrow CO_2 + 2\,HO_2^{\cdot}$
BR1.1d $[^{\cdot}CH_2OO^{\cdot}]^* \xrightarrow{M} H(HO)C{=}O$

Since there are no other reactions of $[^{\cdot}CH_2OO^{\cdot}]^*$ in our mechanism, we simply use a sufficiently fast rate and relative ratios to control the amount of each product produced. The rate constant used is:

$$k_{tot} = 2.0 \times 10^3 \quad s^{-1}$$

The relative ratios we use are:

$$f_{BR1CO} = 0.58$$
$$f_{BR1H2} = 0.25$$
$$f_{BR1rad} = 0.10$$
$$f_{BR1acid} = 0.07$$

These were estimated by modeling both the results of experimental measurements report by Su, *et al.*[50] and the results of experimental measurements of Hatakeyama *et al.*[52]. This modeling will be discussed in more detail below.

The reactions of the "cold" Criegee biradicals are somewhat uncertain. Here we use what appear to be the most likely and important ones.

BR1.2a $^{\cdot}CH_2OO^{\cdot} + NO \longrightarrow NO_2 + H_2C{=}O$
BR1.2b $^{\cdot}CH_2OO^{\cdot} + NO_2 \longrightarrow NO_3^{\cdot} + H_2C{=}O$
BR1.2c $^{\cdot}CH_2OO^{\cdot} + HO_2^{\cdot} \longrightarrow H_2C{=}O + {}^{\cdot}OH$
BR1.2d $^{\cdot}CH_2OO^{\cdot} + H_2O \longrightarrow f^{BR}_{acid}\,(H(HO)C{=}O + H_2O) + f^{BR}_{ald}\,(H_2C{=}O + H_2O_2)$
BR1.2e $^{\cdot}CH_2OO^{\cdot} + H_2C{=}O \longrightarrow HOCH_2\text{-}O\text{-}C({=}O)H$
BR1.2f $^{\cdot}CH_2OO^{\cdot} + CO \longrightarrow H(O{=})C\text{-}O\text{-}C({=}O)H$
BR1.2g $^{\cdot}CH_2OO^{\cdot} + SO_2 \longrightarrow H_2CO_2SO_2$

Su *et al.* had suggested the relative rates of CO, SO_2, and HCHO with the Criegee biradical. A recent estimate[53] for k_g was used with these relative ratios to estimate initial rate constants for the other reactions. Modeling of experimental systems containing CO and SO_2 were used to verify the magnitudes of these rate constants, see discussion below.

$k_a = \text{RO2NORATE}$

$k_b = 2.4 \times 10^{-16}$ $\text{cm}^3\text{-molecules}^{-1}\text{-s}^{-1}$

$k_c = \text{RO2HO2RATE}$

$k_d = 4.0 \times 10^{-17}$ $\text{cm}^3\text{-molecules}^{-1}\text{-s}^{-1}$

$k_e = 2.0 \times 10^{-14}$ $\text{cm}^3\text{-molecules}^{-1}\text{-s}^{-1}$

$k_f = 1.3 \times 10^{-16}$ $\text{cm}^3\text{-molecules}^{-1}\text{-s}^{-1}$

$k_g = 7.0 \times 10^{-13}$ $\text{cm}^3\text{-molecules}^{-1}\text{-s}^{-1}$

Reaction **BR1.2e**, which in classical theory would be expected to yield ethylene ozonide, was shown by Su *et al.* and Niki[42] to proceed through the formation of the ozonide to the product shown. Kan, Su, Calvert, and Shaw[54] found that formic anhydride ($H(O{=})C\text{-}O\text{-}C({=}O)H$) appeared in the experimental system as $HOCH_2\text{-}O\text{-}C({=}O)H$ decayed and suggested that reaction **BR1.3a**, shown below, may occur heterogeneously. The rate used here was based upon simulating experimental data given by Su *et al.*. We have added other loss pathways that may be important in longer experiments or other conditions.

BR1.3a $HOCH_2\text{-}O\text{-}C({=}O)H \xrightarrow{O_2} H(O{=})C\text{-}O\text{-}C({=}O)H + H_2O_2$

BR1.3b $HOCH_2\text{-}O\text{-}C({=}O)H \longrightarrow H_2C{=}O + H(HO)C{=}O$

BR1.3c $^{\cdot}OH + HOCH_2\text{-}O\text{-}C({=}O)H \longrightarrow HO_2^{\cdot} + H_2C{=}O + CO_2 + H_2O$

$k_a = 1.0 \times 10^{-5}$ s^{-1}

$k_b = 1.0 \times 10^{-5}$ s^{-1}

$k_c = k[^{\cdot}OH + HCHO]$

Figure 79 and Figure 80 show our simulations of three of the experiments described by Su *et al.*. The numbers that appear over the data lines in the plots give the ratio of our simulated values to the observed values of Su *et al.*. In most cases, our predictions were very close. Table 17 gives the integrated reaction rates (total ppm through each reaction) for three cases: the standard experiment starting with only O_3 and ethene; the standard experiment plus 15,000 ppm CO, and the standard experiment plus 4.59 ppm SO_2.

Su *et al.* observed a reactant ratio ($\Delta O_3/\Delta H_2C{=}CH_2$) of 1.01 ± 0.02, while we predicted a ratio of 1.08. In the case of the CO experiment, the observed ratio was 1.21 and we predicted 1.26. Thus we always predicted more O_3 was consumed than was measured by Su *et al.*. Examination of Table 17 shows that the major loss for O_3 was reaction with ethene (reaction 21 in Table 17), and in addition, large amounts of O_3 were lost by reaction 2. In fact, the only explanation for the shift in observed ratio with addition of CO is the change in reaction 2. Only about half of the $^{\cdot}OH$ radicals produced in reaction 2 react with ethene as shown by reaction 15. In addition, there must have been wall loss of O_3 in Su *et al.*'s experimental system. The simulation uses the Teflon film loss rate and this added a small loss of O_3. (Simulations with no wall loss show more O_3 reacting by reaction 2, so it is still lost). At the same time that O_3 was under-predicted, the final ethene concentrations were always over-predicted. In nighttime experiments in which O_3 was injected into ethene in the UNC chambers (which will be discussed further below), a similar problem arose: the model under-predicted the observed O_3). Some recent work by Niki[55] and by Hatakeyama[56] and by Martinez, Huie, and Herron[57] have suggested the reaction sequence

$$^{\cdot}CH_2OO^{\cdot} \longrightarrow H_2C{=}O + O(3P)$$

$$O(3P) + O_2 + M \longrightarrow O_3 + M$$

This possibility, while intriguing, has not been included in our model.

Figure 81 is a mass balance for HCHO in the three Su, *et al.* simulations. It shows that the vast majority of the HCHO came from direct production in the $O_3{+}H_2C{=}CH_2$ reaction, and only trace amounts originated in other reactions, *i.e.*, **BR1.2c**. Two loss processes determine the final yield of HCHO: reaction with $^{\cdot}OH$ and reaction with $^{\cdot}CH_2OO^{\cdot}$. Su, *et al.* observed a large difference in HCHO yields with added CO or SO_2 (see right side of top plot in Figure 81).

Next, we simulated the experimental results of Hatakeyama *et al.*[52] who experimentally demonstrated that HCHO increased when SO_2 was added to O_3+ethene systems. In fact, Hatakeyama, *et al.* showed a one-to-one increase in HCHO in step with a SO_2 decrease. Figure 82 shows our simulation of their experimental results. Hatakeyama observed a final HCHO value of 1.3 ppm in the O_3+ethene system and we predicted 1.2 ppm. When 3.94 ppm SO_2 was added, they observed an increase in HCHO to 1.75 ppm and we predict 1.78 ppm HCHO. Hatakeyama said,

> "Thus, it can be concluded that additional HCHO is formed from the $SO_2{+}^{\cdot}CH_2OO^{\cdot}$ reaction."

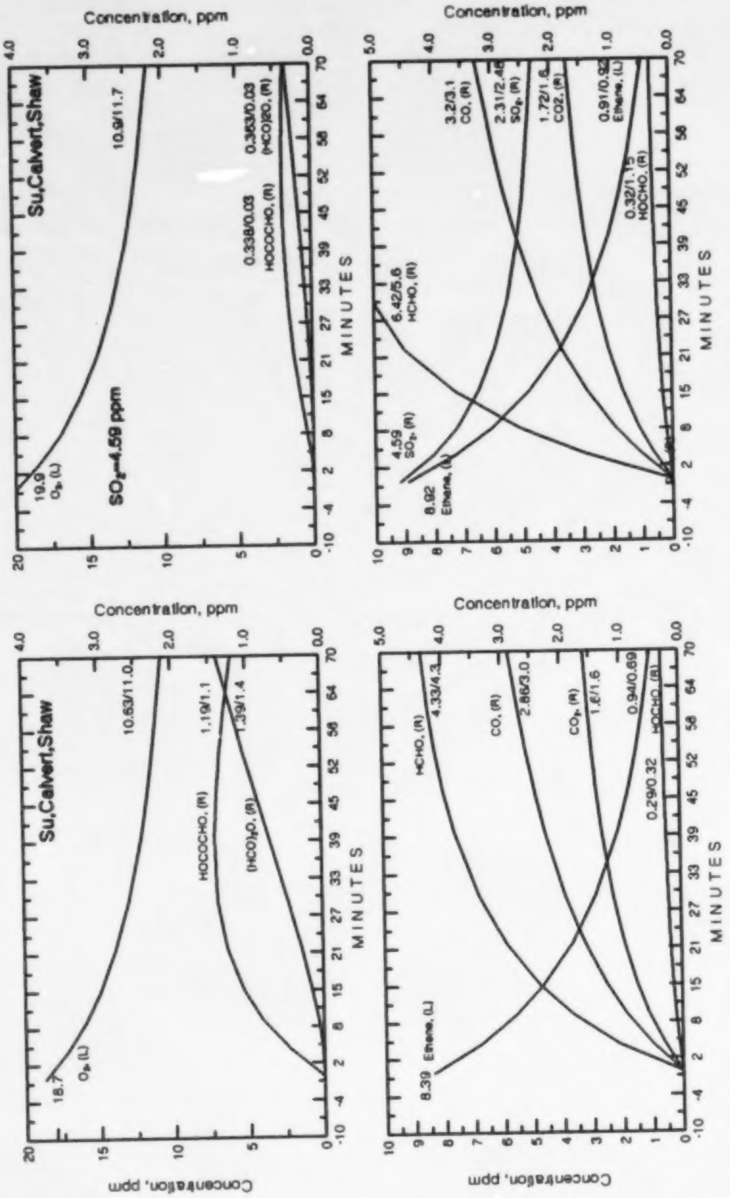

Figure 79. Simulation of Su, Calvert, Shaw's ozone and ethene experiments with the UNC Explicit Mechanism: Standard and SO_2 addition.

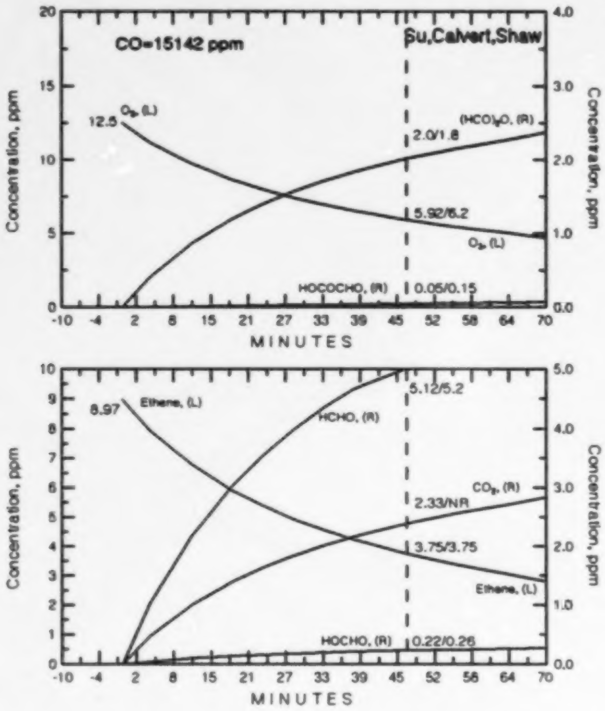

Figure 80. Simulation of Su, Calvert, Shaw's ozone and ethene experiments with the UNC Explicit Mechanism: CO addition.

To the contrary, from our analysis and Figure 81 we conclude that one HCHO is *saved* from consumption by $^{\cdot}CH_2OO^{\cdot}$ when the Criegee reacts with SO_2 instead, and that this is the source of the observed increase in HCHO. Hatakeyama, *et al.* went on to propose a relative complex mechanism to account of the observed behavior of formic acid and HCHO in this system. Formic acid yields exhibited a complex trend with increasing SO_2, first increasing and then decreasing. This was also observed by Su, *et al.*, but a heterogeneous mechanisms involving the surface of acid aerosol particles was involked.

In an effort to investigate reaction **BR1.2d**, $^{\cdot}CH_2OO^{\cdot}+H_2O$, which has been *assumed* to yield formic acid, Hatakeyama, *et al.*[56] irradiated ketene and water vapor mixtures. Figure 83 shows some of the results. Only the yield of formic acid vs. water was discussed by Hatakeyama. We interpret his attempt to form labeled formic acid by using $^{18}O_2$-labeled water to be a failure, since the yield of labeled formic acid did not change with changing labeled water concentration. Given the results for formic acid trends as a function of SO_2 discussed in the proceeding paragraph and the results obtained in the ketene study, we *reject* the conclusion reached by Atkinson, 1989, that

Table 17. Integrated Reaction Rates for Simulation of Su, Calvert, Shaw's ozone and ethene experiments with the UNC Explicit Mechanism.

	Std	CO	SO2	Reaction
1)	0.0163	0.0003	0.0156	O3+OH=HO2
2)	0.9791	1.5839	1.2690	O3+HO2=OH
3)	0.0007	0.0001	0.0008	OH+HO2=
4)	0.0259	0.2005	0.0389	HO2+HO2=H2O2
5)	0.0170	0.1318	0.0256	HO2+HO2+M=H2O2
6)	0.0067	0.0001	0.0016	OH+H2O2=HO2
7)	0.0041	1.0031	0.0043	OH+CO=HO2+CO2
8)	0.0023	0.5537	0.0024	OH+CO=HO2+CO2
9)	0.0001	0.0000	0.0001	OH+H2=HO2
10)	0.4609	0.0133	0.6404	OH+HCHO=HO2+CO
11)	8.7744	26.9418	15.6740	HO2+HCHO=HOCH2O2
12)	8.7720	26.9238	15.6689	HOCH2O2=HO2+HCHO
13)	0.0024	0.0180	0.0050	HOCH2O2+HO2=0.750*HOCHO+0.250*HOCH2OOH
14)	0.0014	0.0000	0.0014	OH+HOCHO=HO2+CO2
15)	0.5322	0.0212	0.4990	OH+C:C=HOCCO2
16)	0.0629	0.0000	0.0447	HOCCO=2.000*HCHO+HO2
17)	0.0199	0.0000	0.0141	HOCCO+O2=HOCCHO+HO2
18)	0.2940	0.0210	0.3284	HOCCO2+HO2=0.750*HOCCHO+0.250*HOCCOOH
19)	0.1183	0.0001	0.0841	HOCCO2+HOCCO2=0.575*HOCCOH+0.575*HOCCHO+0.350*HOCCO+0.350*HOCCO+0.075*HOCCOOCCOH
20)	0.0020	0.0002	0.0023	HOCCOOH=HCHO+HCHO
21)	6.9640	6.1997	7.5795	O3+C:C=HCHO+0.535*CH2OO>+0.233*CH2OOX+0.233*CH2OO
22)	0.4548	0.4049	0.4950	CH2OOX=CH2OO>
23)	1.1643	1.0365	1.2672	CH2OOX+M=CH2OO
24)	2.4247	2.1586	2.6390	CH2OO>=CO+H2O
25)	1.0451	0.9304	1.1375	CH2OO>=CO2+H2
26)	0.4181	0.3722	0.4550	CH2OO>=CO2+2.000*HO2
27)	0.2926	0.2605	0.3185	CH2OO>=HOCHO
28)	0.1875	0.0078	0.0272	CH2OO+HO2=HCHO+OH
29)				CH2OO+H2O=0.333*HOCHO+0.667*HCHO+0.667*H2O2
30)	2.5839	0.0733	0.6952	CH2OO+HCHO=HOCOCHO
31)	0.0089	2.3968	0.0019	CH2OO+CO=(HCO)2O
32)			2.3048	CH2OO+SO2=CH2O2SO2
33)	1.3778	0.0015	0.3355	HOCOCHO=(HCO)2O+H2O2
34)	0.1754	0.0003	0.1691	OH+HOCCHO=0.800*HOCC(O)O2+0.200*(HCO)2+0.200*HO2
35)	0.0351	0.0003	0.0401	HOCC(O)O2+HO2=HO2+HCHO+OH+CO2
36)	0.0525	0.0000	0.0475	HOCC(O)O2+HOCC(O)O2=2.000*HCHO+2.000*HO2+2.000*CO2
37)	0.0027	0.0000	0.0025	(HCO)2+OH=0.630*HO2+1.260*CO+0.370*HCOC(O)O2
38)	0.0010	0.0000	0.0009	HCOC(O)O2+HO2=HO2+CO+OH+CO2
39)	0.9615	0.2742	0.2624	H2O2=(walls)
40)	0.1524	0.0866	0.1608	O3=(walls)

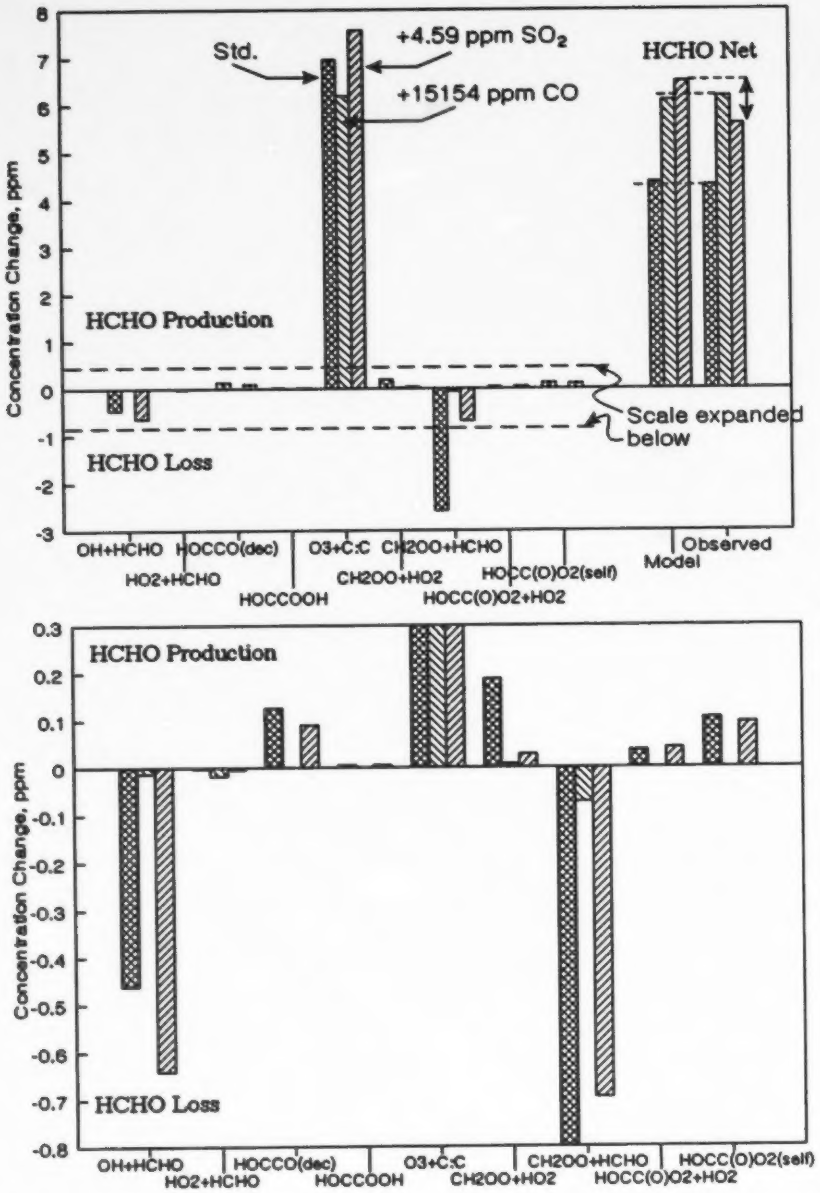

Figure 81. Mass Balance on HCHO in Su, Calvert, Shaw systems.

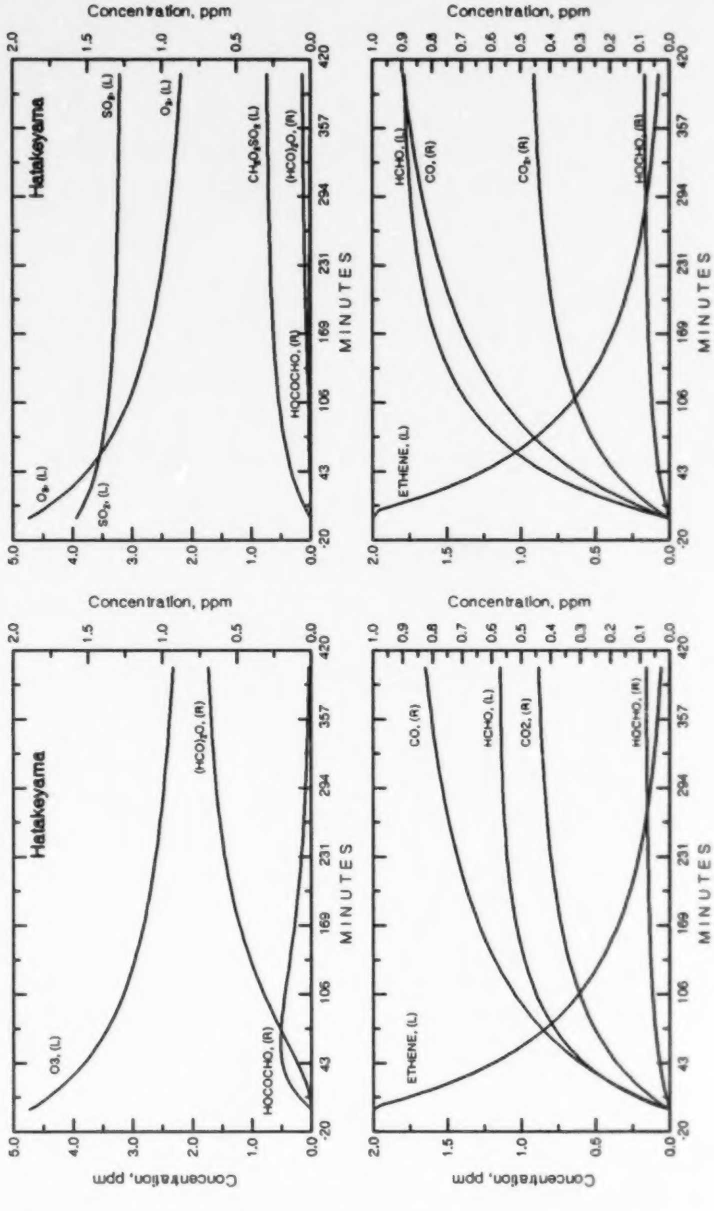

Figure 82. Simulation of Hatakeyama's ozone and ethene experiments with the UNC Explicit Mechanism: Standard and SO_2 addition.

> "... the reaction of stablized biradicals with water vapor will be their dominant loss process under atmospheric conditions, leading to the formation of carboxylic acids."

While it is well established that water vapor competes with SO_2 for the $\cdot CH_2OO\cdot$ biradical, it was merely asserted that formic acid would be the resulting product. Instead, based upon our re-analysis of the work of Hatakeyama, *et al.*, we believe that the reaction scheme originally proposed by Martinez and Herron[58] is a more likely process for stablized biradicals leading to the formation of hydroperoxy-hydroxy-methylene (which has been observed in the gas phase by Su *et al.*; see Figure 84). The lack of a large change in the formation of formic acid and the much larger change in HCHO in the ketene experiment of Hatakeyama, however, suggests another fate for the hydroperoxy-hydroxy-methlyene—and one which occurs frequently in solution ozonation reactions,[59]—the formation of an aldehyde and hydrogen peroxide. Based upon the ratio of HCHO-to-HOCHO yields in Figure 84, we assume

$$f_{acid}^{BR} = 0.333$$
$$f_{ald}^{BR} = 0.667$$

in reaction **BR1.2d**.

Finally, we present two simulations of nighttime experiments in the UNC chambers in which we injected O_3 into ethene. In one, conducted on October 28, 1986, $[H_2O] \approx 8000$ ppm (see Figure 85 and Figure 86), while in the other conducted on July 19, 1988, water vapor concentrations were approximately 25,000 ppm (see Figure 87).

Unfortuately, as can be seen in Figure 85, the chamber cooled over the first few hours and the air became saturated in water vapor. The dew point then decreased as liquid water formed on the walls. As can be seen in Figure 86, the model predictions for HCHO initially agreed with the measured HCHO, then the simulated HCHO increasingly deviated from the observed, we believe as a consequence of HCHO dissolving in the water on the walls. Also note that like the simulations of the Su, *et al.* data, here the simulated O_3 loss is too large.

In the warmer and wetter July 19, 1988 experiments, the agreement between measured HCHO and predicted HCHO is much better until near the end where there appears to be sudden increase in the rate of production of HCHO; this may be the results of a heterogeneous process. Also note that this experiment is opposite to the October 28 experiment in that not enough O_3 is consumed, yet too much ethene is consumed. Therefore, we believe that some minor processes are missing in our mechanism, but the production of HCHO is reasonably approximated. As we shall see, most daytime experiments show good agreement for HCHO.

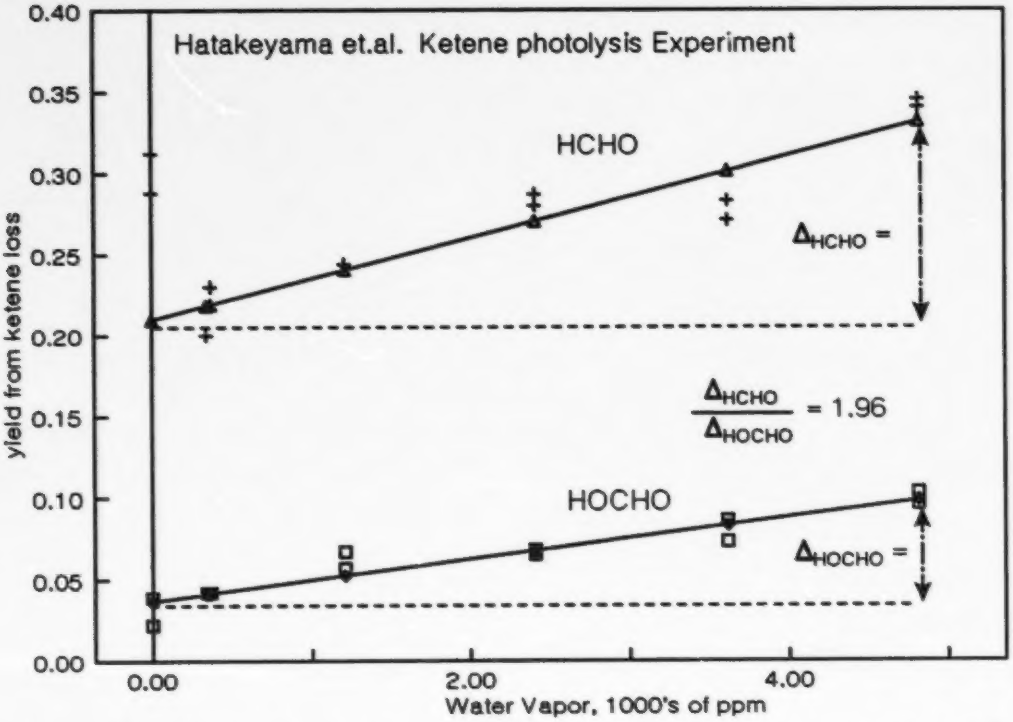

Figure 83. Yields of formic acid and formaldehyde as a function of water vapor in the photolysis of ketene.

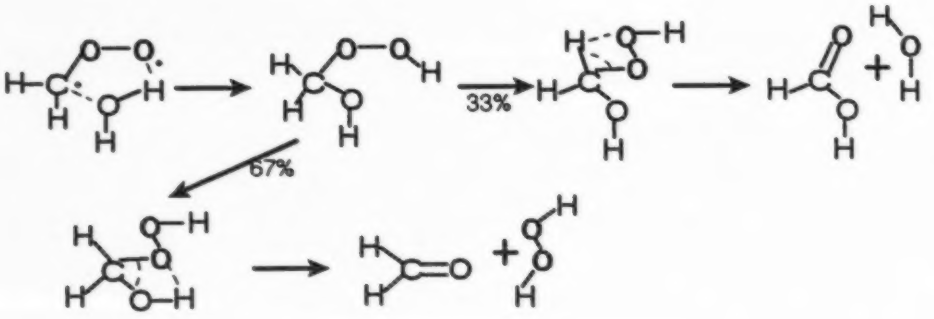

Figure 84. Scheme for peroxymethylene reaction with water.

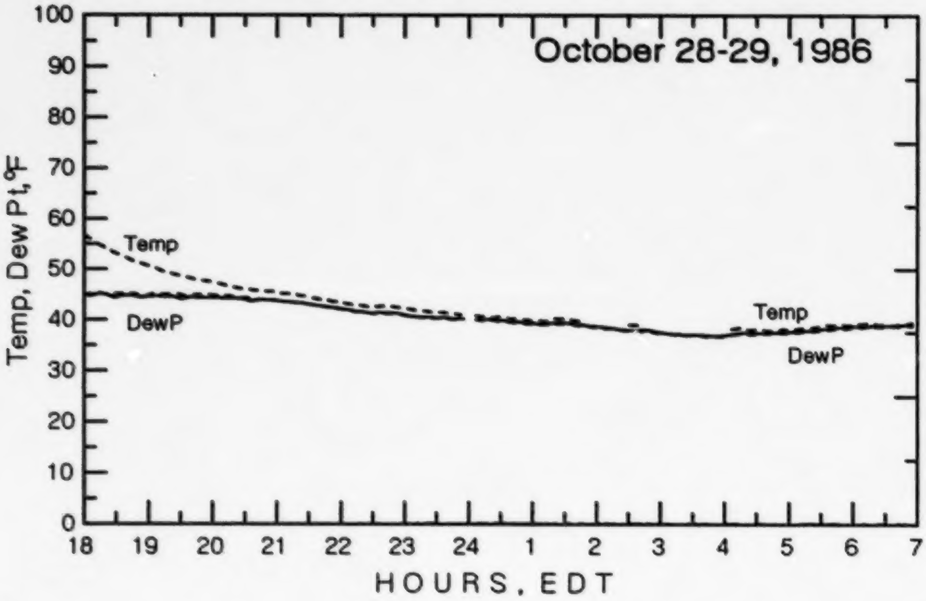

Figure 85. Temperature and dewpoint in chamber during experiment.

GA = Glycoaldehyde Chemistry

The chemistry of glycoaldehyde has been recently studied by Niki,[43] (see Figure 88) and the basic features of its chemistry appear to be known. The fate of $HOCH_2C(=O)OONO_2$, which was observed by Niki, *et al.*, however, is not clear and we have conducted a number of modeling sensitivity studies to understand how different choices effect the model's agreement with chamber data. It is obvious that laboratory kinetics data on $HOCH_2C(=O)OONO_2$ are needed before model formulation can be more certain. Here we depend upon reproducing chamber observations to obtain insights into the probably mechanistic explanation. While reasonable fits are obtained by this process, it is clearly unsatisfactory and it may be only a chamber artifact.

GA.1 $HOCH_2HC{=}O \longrightarrow 2\,HO_2^{\cdot} + CO + H_2C{=}O$

This reaction is assumed to be similar to acetaldehyde and in the absence of any experimental data, we assume that glycoaldyde has a similar absorption cross-section and quantum yield as acetaldehyde.

$$k = \mathrm{HVCCHOR} \quad \mathrm{cm^3\text{-}molecules^{-1}\text{-}s^{-1}}$$

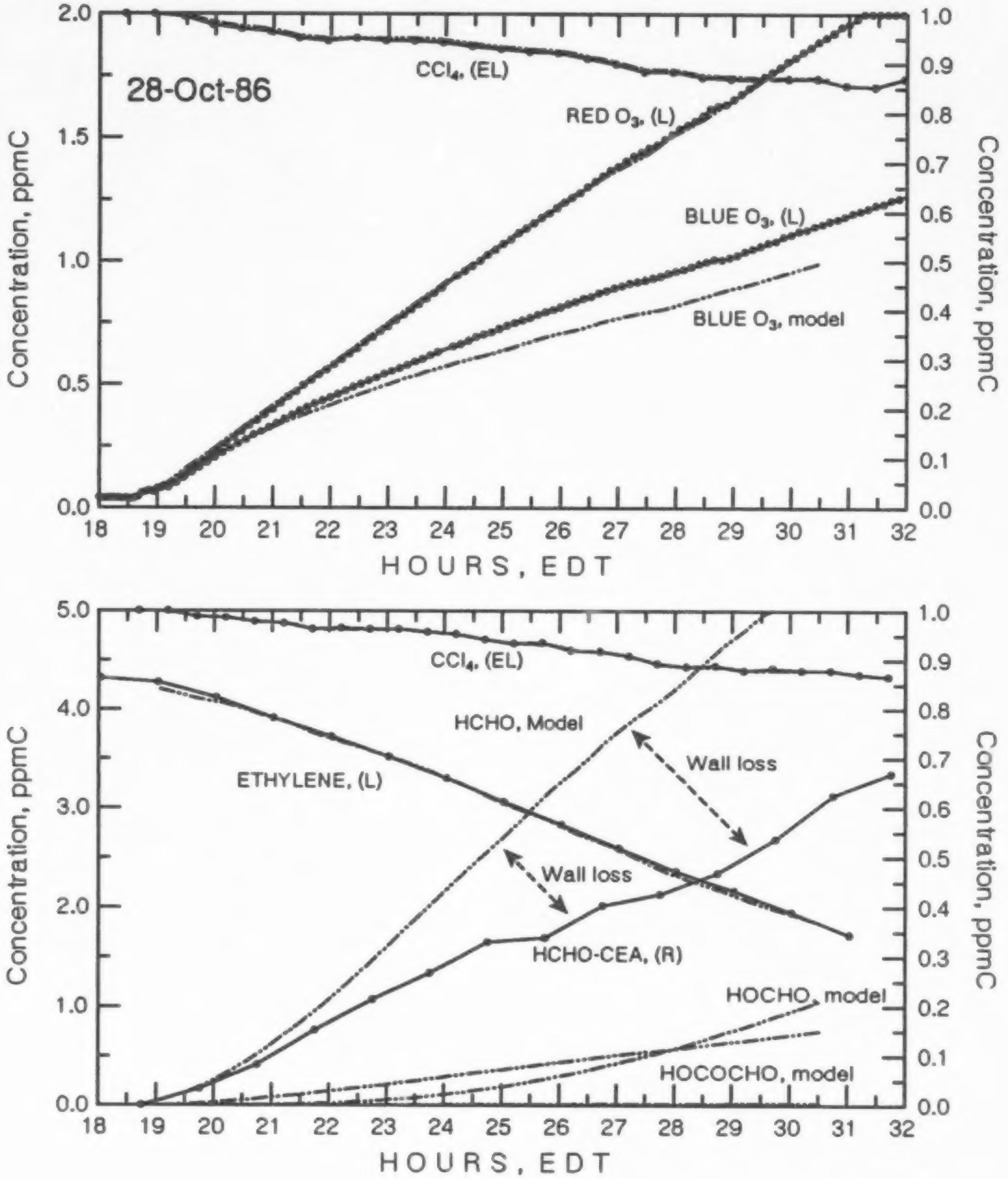

Figure 86. Ozone injected into ethene in BLUE chamber; background air and injected ozone only in RED.

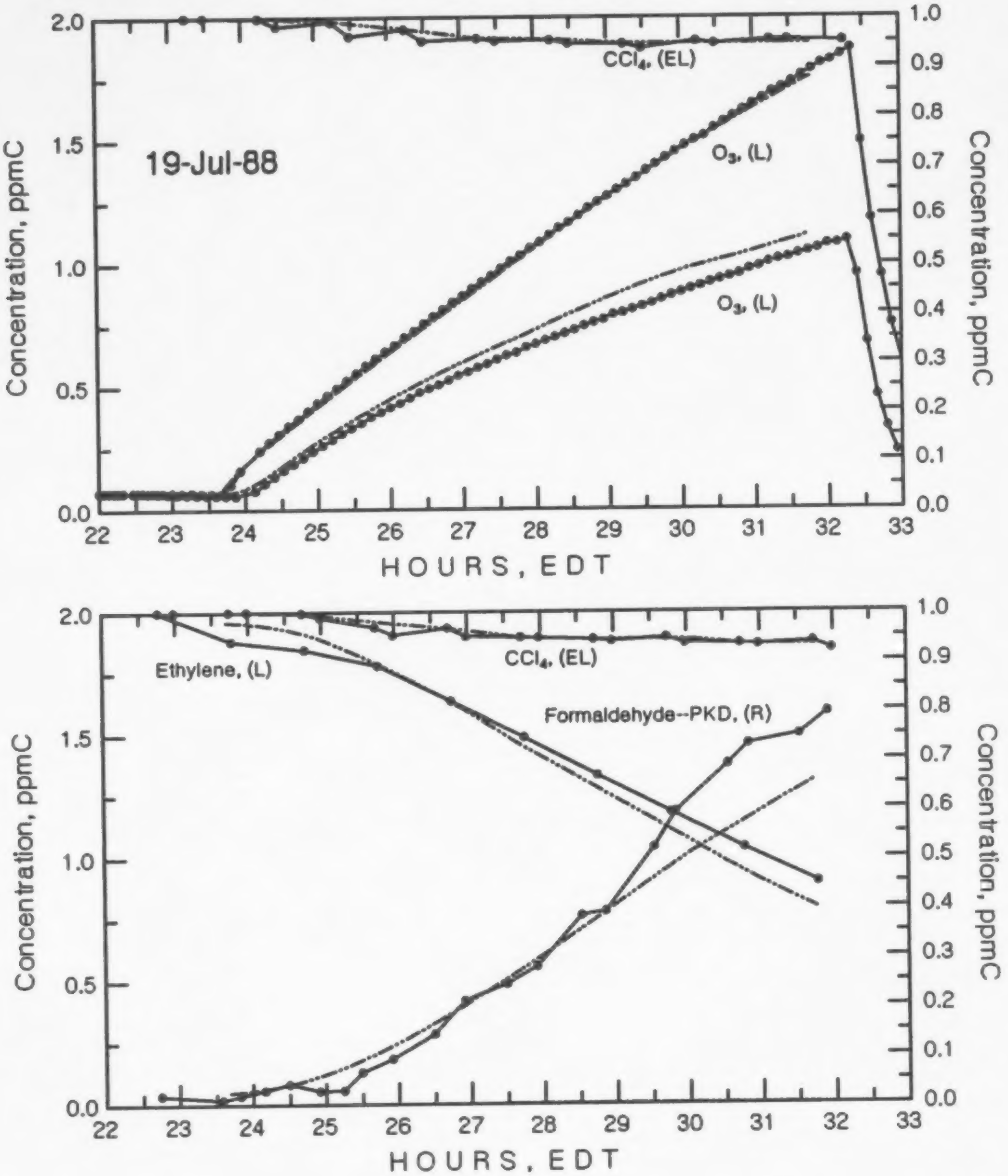

Figure 87. Ozone injected into ethene in BLUE chamber; background air and injected ozone only in RED.

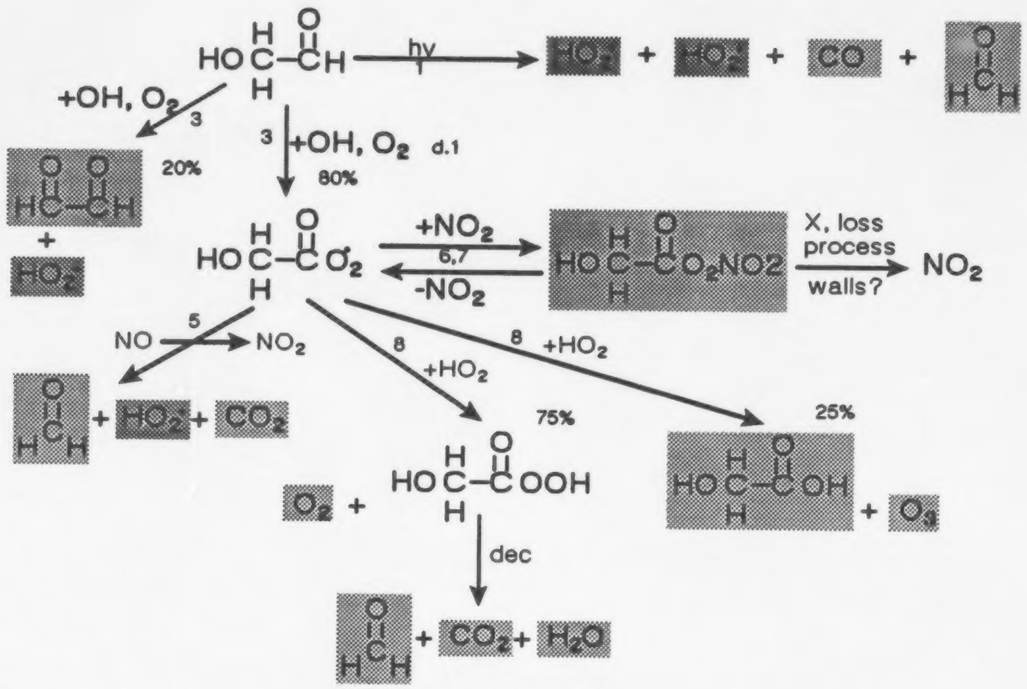
hν
+OH, O2
3
20%
80%
d.1
+NO2
6,7
-NO2
X, loss process
walls?
NO2
NO
5
8
+HO2
75%
25%
dec

Figure 88. Mechanism for oxidation of glycoaldehyde–**GA**. Major products are indicated by shading.

GA.2 $O(3P) + HOCH_2HC{=}O \longrightarrow HOCH_2C({=}O)O_2^{\cdot} + {}^{\cdot}OH$

We assume the rate of this reaction to be 0.625 times the rate of reaction **C2.2** for acetaldehyde (see discussion of **GA.2**).

$$k = 1.13 \times 10^{-11} e^{-1100/T}$$

GA.2 ${}^{\cdot}OH + HOCH_2HC{=}O \longrightarrow 0.80\,HOCH_2C({=}O)O_2^{\cdot} + 0.20\,(HC{=}O)_2 + 0.20\,HO_2^{\cdot}$

This reaction was studied by Niki. He found that the ratio of this reaction to ${}^{\cdot}OH{+}CH_3HC{=}O$ was 0.625.

$$k = 3.75 \times 10^{-11} e^{250/T}$$

GA.4 $NO_3^{\cdot} + HOCH_2HC{=}O \longrightarrow 0.75\,HOCH_2C({=}O)O_2^{\cdot} + 0.25\,(HC{=}O)_2 + 0.25\,HO_2^{\cdot} + HNO_3$

This reaction is assumed to be analogous to reaction **C2.4** for acetaldehyde, except the rate constant is 0.625 times the acetaldehyde rate.

$$k = 0.875 \times 10^{-12} e^{-1900/T}$$

GA.5 $HOCH_2C({=}O)O_2^{\cdot} + NO \longrightarrow NO_2 + H_2C{=}O + HO_2^{\cdot} + CO_2$

This reaction is based upon the similar peroxyacetyl radical reaction. We assume that its rate is the same as other peroxyacyl radicals with NO:

$$k = \mathrm{RCO3NORATE}$$

GA.6 $HOCH_2C({=}O)O_2^{\cdot} + NO_2 \longrightarrow HOCH_2C({=}O)OONO_2$

Niki *et al.* observed $HOCH_2C({=}O)OONO_2$ in his study, so therefore this reaction does occur. Niki *et al.* did not report any rate data and here we assume that its rate is the same as other peroxyacyl radicals with NO_2:

$$k = \mathrm{RCO3NO2RATE}$$

GA.7 $HOCH_2C({=}O)OONO_2 \longrightarrow HOCH_2C({=}O)O_2^{\cdot} + NO_2$

Niki *et al.* observed a rapid loss of $HOCH_2C({=}O)OONO_2$ in their system. This can be explained in a number of ways which will be discussed in the next section. Here we use the same rate constant for $HOCH_2C({=}O)OONO_2$ decomposition and for $CH_3C({=}O)O_2NO_2$:

$$k = \mathrm{PANRATE}$$

See the discussion in the following section for a full discussion supporting this choice.

GA.8 $HOCH_2C({=}O)O_2^{\cdot} + HO_2^{\cdot} \longrightarrow 0.75\,(HOCH_2C({=}O)OOH + O_2) + 0.25\,(HOCH_2C({=}O)OH + O_3)$

This reaction is base on reaction **PA1.4**.

$$k = \mathsf{RCO3HO2RATE}$$

GA.9 $HOCH_2C(=O)O_2^{\cdot} + HOCH_2C(=O)O_2^{\cdot} \longrightarrow 2\,H_2C{=}O + 2\,HO_2^{\cdot} + 2\,CO_2 + O_2$

This reaction is based on reaction **PA1.6**.

$$k = \mathsf{RCO3RCO3RATE}$$

GA.10 $HOCH_2C(=O)O_2^{\cdot} + CH_3O_2^{\cdot} \longrightarrow f^2_{sta1}(HOCH_2C(=O)OH + H_2C{=}O + O_2) +$
$f^2_{rad}(HO_2^{\cdot} + H_2C{=}O + CO_2 + CH_3O^{\cdot} + O_2) +$
$f^2_{sta2}(HOCH_2C(=O)OOCH_3 + O_2)$

This reaction is based on reaction **PA1.5**.

$$k = \mathsf{RO2RO2RATE}$$

Selection of Rate Constant for PGAN Decomposition

Niki *et al.* observed that $HOCH_2C(=O)OONO_2$ (PGAN) was much less stable in his spectrometer cell than was $CH_3C(=O)O_2NO_2$ (PAN). They produced 0.35 ppm PGAN which was totally lost in 15 minutes. There are at least three options for selecting the rate for the **GA.7** reaction:

i) assume that the whole chemistry of $HOCH_2C(=O)O_2^{\cdot}$ and NO_x is different from that of $CH_3C(=O)O_2^{\cdot}$ and NO_x;

ii) assume that PGAN's decomposition rate is much faster than PAN;

iii) assume that PGAN's decomposition rate is the same as PAN, but other—perhaps heterogeneous—reactions consume PGAN.

If we choose assumption *i* there will be a large number of combinations of possible conditions and we have no kinetics data to guide us in the selection, therefore, choosing this option means we must stop the model formulation and wait for new kinetics data to be produced. Therefore we will not make this assumption.

Our initial choice was assumption *ii*. We first estimated a decomposition rate of $k[GA.7] = 6.9 \times 10^{+17} e^{-13330/T}$ cm^3-molecules^{-1}-s^{-1}, which is about 20 times the PAN rate (it is unlikely that the activation energy for this decomposition reaction is much different than that for PAN where the same bond is broken, so only the A-factor was changed). This resulted in very good agreement between model predictions and observations in July experiments but poor agreement for October experiments (see Figure 89). On the other hand, using a PGAN decomposition rate similar to PAN's for the October experiments resulted in excellent agreement with October data, but poor agreement for July experiments. There was only a 7°K maximum temperature difference between these two days and a twenty-fold rate change due to temperature only is unlikely. This difference in optimum rate for PGAN decomposition also happens between other summer and fall days, so the difficulty is not unique to just the two days shown in Figure 89.

We then considered alternative *iii* from above: that is that PGAN forms and decomposes at the same rate as PAN, but that some other process is removing the PGAN at a relative rapid rate. To simulate July 6, 1988 with any accuracy, however, the nitrogen in PGAN must be returned to some form of NO_x to allow the higher concentrations of O_3 to be produced in the summer experiments. We hypothesize that PGAN undergoes a temperature and *perhaps surface* dependent re-arrangement and decomposition leading to the destruction of the $HOCH_2C(=O)O_2^{\cdot}$ radical and the release of NO_x. This reaction is

GA.X $$HOCH_2C(=O)OONO_2 \longrightarrow NO_3^{\cdot} + H_2C{=}O + HO_2^{\cdot} + CO_2$$

The rate of reaction GA.X has to be significant compared to the rate of reaction **GA.7** in July, but not in October. Only very high activation energies give satisfactory fits to all days, suggesting that if this, or a similar reaction occurs, it can not be an elementary reaction and, considering its rate, it is probably heterogeneous. *We do not claim that exactly this reaction is occurring in the chamber, only that some process like GA.X must occur to account for the observations if* $HOCH_2C(=O)O_2^{\cdot}$ *radical chemistry is similar to* $CH_3C(=O)O_2^{\cdot}$ *radical chemistry.* We have no evidence that $HOCH_2C(=O)O_2^{\cdot}$ does not react like $CH_3C(=O)O_2^{\cdot}$, in fact, PGAN is known to form by Niki *et al.*'s observations. We find no reason to believe that the activation energy on the PGAN decomposition reaction (**GA.7**) would be different from that of PAN, and there appears to be consensus among the kinetics community that the decomposition rate of PAN is well known (even in CB4's PAN chemistry it was the formation rate of PAN that was hypothesized as being temperature dependent; CB4 still uses a PAN decomposition rate nearly equal to the one recommended by Atkinson and used here). The new kinetics data on PAN formation rate obtained in recent SAPRC experiments (Carter, personal communication) do suggest that the PAN

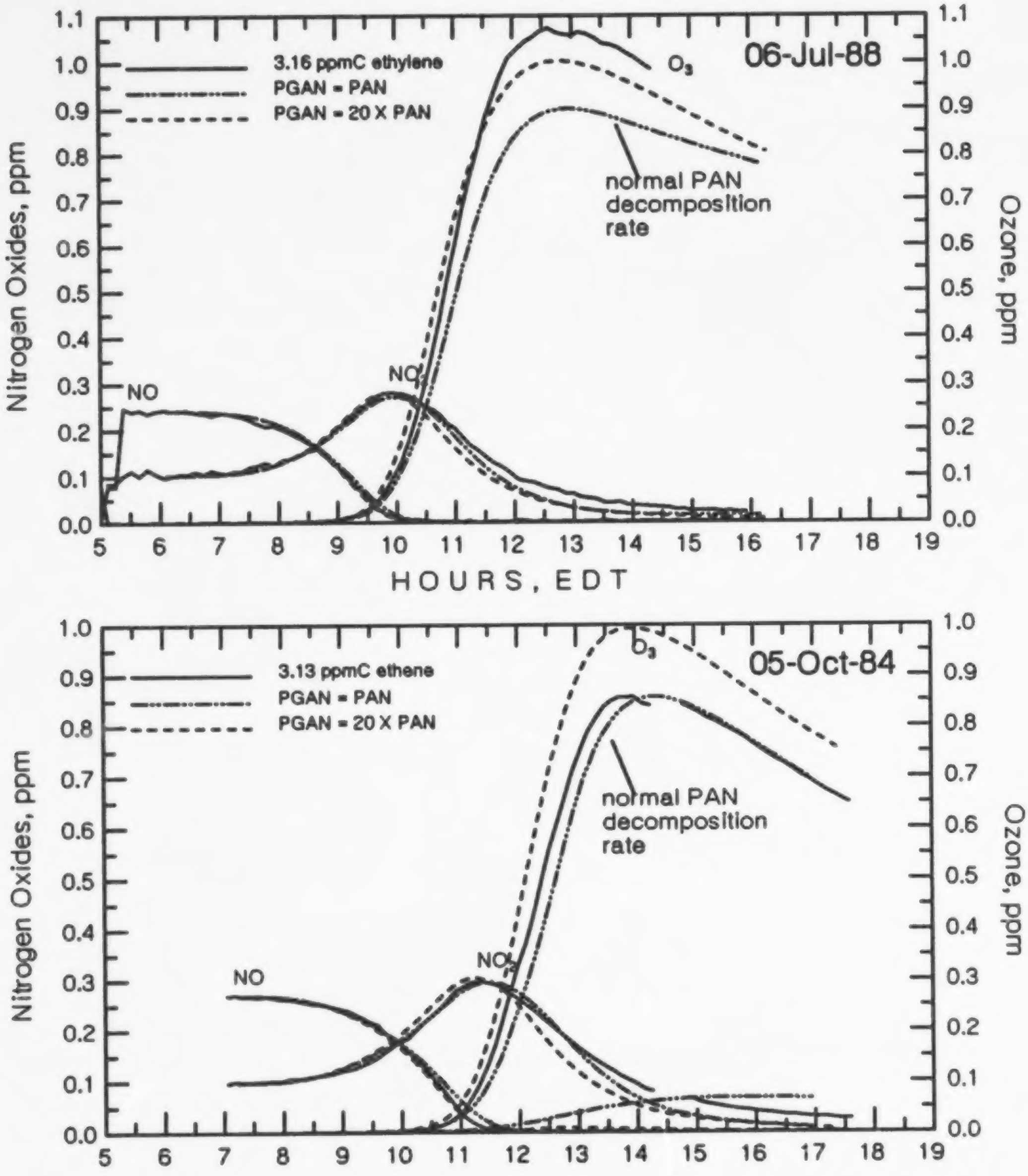

Figure 89. Effect of setting PGAN decomposition rate to 20 times PAN rate in summer and fall experiments.

reaction is somewhat temperature dependent (≈ 2200°K) . This dependence, however, is already included in our mechanism for PAN (the new SARPC activation energy was used in reaction **PA1.2** for the formation of PAN) and as the rate of reaction **GA.6** above, and this is not sufficient to account for our observations in ethene experiments. Even if the activation energy were wrong by a factor of two, this would not account for the magnitude of the change we apparently observe. Thus we believe there must be another reaction such as **GA.X**. The rate used here for reaction **GA.X** is

$$k = 1.3 \times 10^{32} e^{-25000/T}$$

Figure 90 shows the model predicted concentrations of several hydroxy-carbonyl compounds for the July 6, 1988 3.2 ppmC experiment with and without reaction **GA.X**. Integrated rate analysis shows that 185 ppbV of glycoaldehyde ($HOCH_2HC{=}O$) was produced in this experiment and 93.5% of it reacted, 173 ppbV with $^{\cdot}OH$. The peak concentration was about 40 ppbV. Without reaction GA.X PGAN levels increase significantly, removing NO_2 and leading to a decrease in O_3 production. With reaction GA.X, much of the lost NO_2 is returned to the system at the temperatures of July 6.

Figures 93 and 94 show chamber observations and two model simulations, one with reaction **GA.X** and one without. Notice in Figure 94 that too much PGAN was predicted in comparison to the NO_x-NO observations from 1400 to 1800 EDT when **GA.X** was omitted.

Ethene simulations in the rest of the report will be shown both with and without the GA.X reaction.

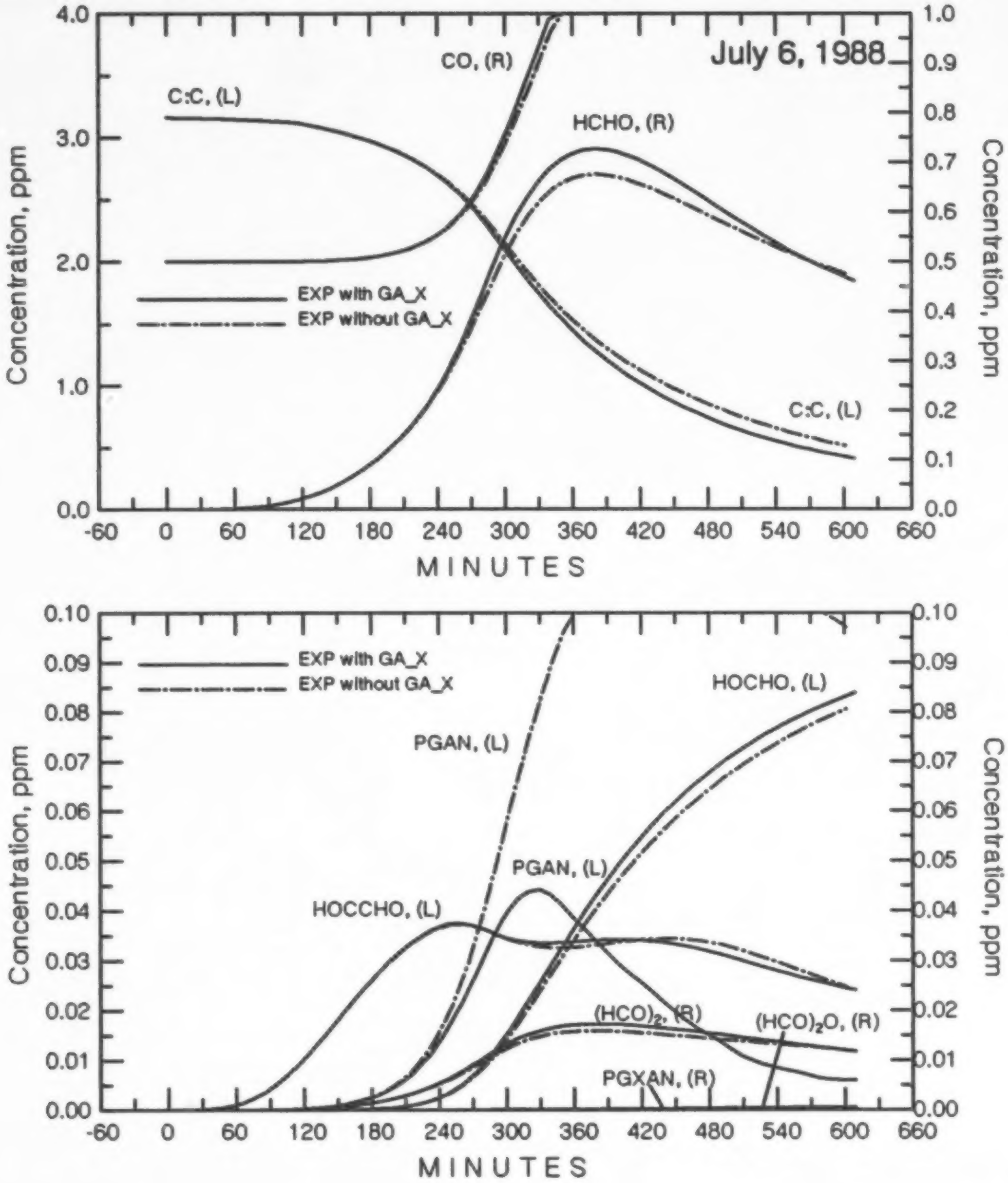

Figure 90. Carbon Species Predicted in 3.2 ppmC Ethene Experiment. PGAN is $HOCH_2C(=O)OONO_2$; PGXAN is $H(O=)C\text{-}C(=O)O_2NO_2$.

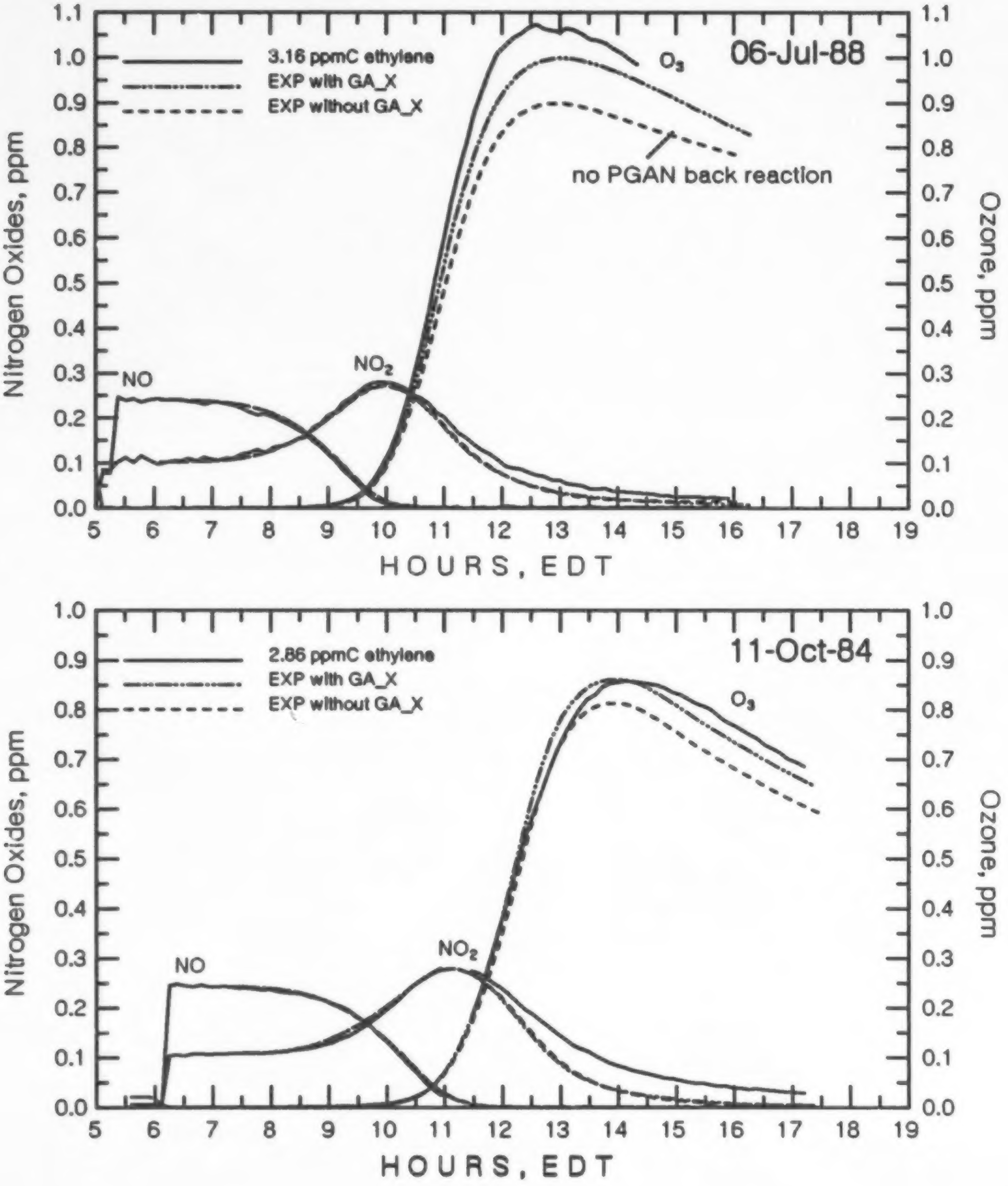

Figure 93. Sensitivity of Simulation to Additonal PGAN Loss Reaction, Summer and Fall. Solid lines are chamber observations; dashed lines are simulations.

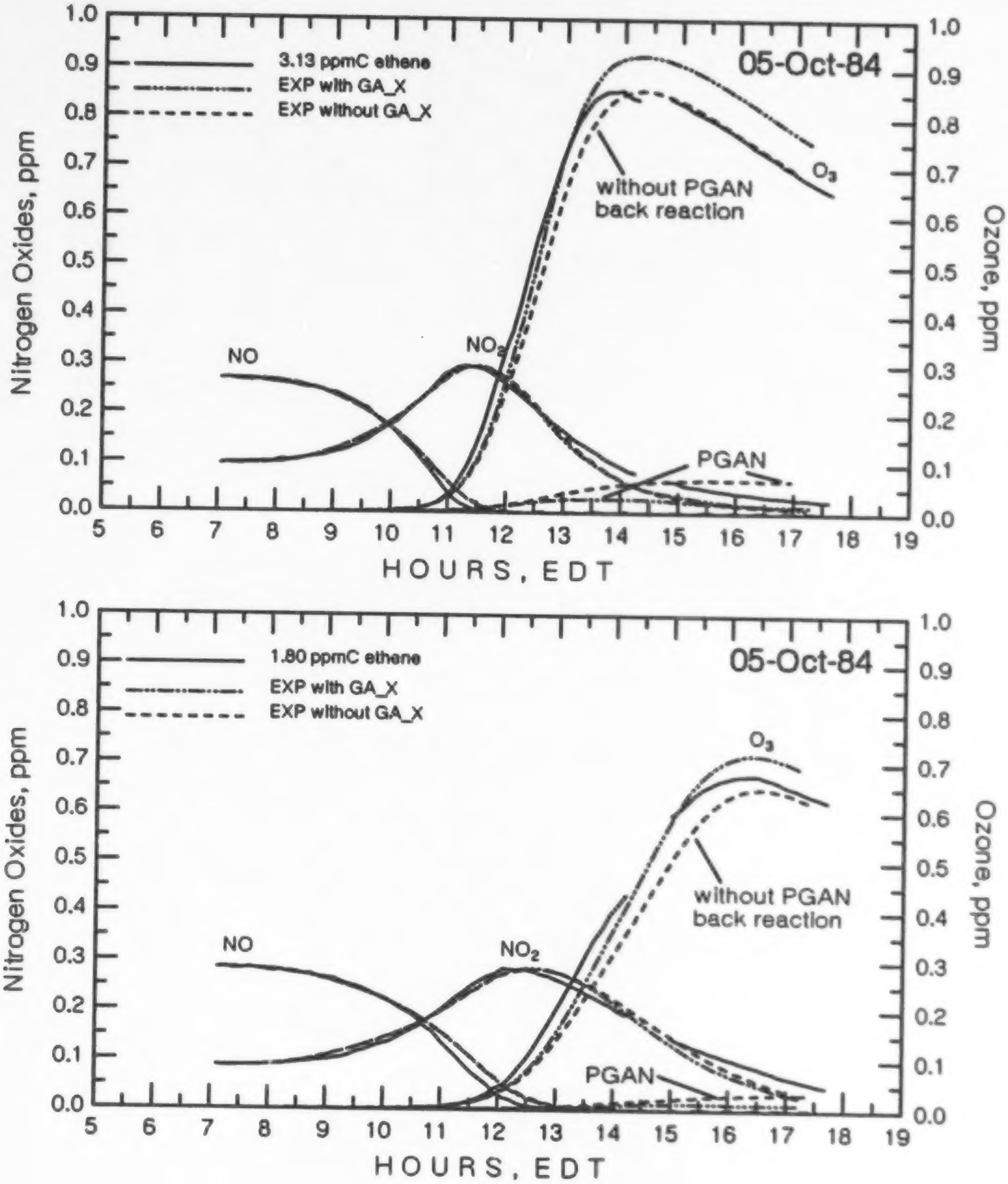

Figure 94. Sensitivity of Simulation to Additonal PGAN Loss Reaction at Different Ethene Concentrations. Solid lines are chamber observations; dashed lines are simulations.

D2 = Glyoxal Chemistry

The chemistry of glyoxal has been recently studied by Niki, *et al.*,[60] and Langford and Moore[61].

D2.1a $(HC{=}O)_2 \xrightarrow{h\nu} 0.94\,HO_2^{\cdot} + 0.53\,H_2C{=}O + 1.46\,CO$

This reaction is from Langford and Moore's estimate of the quantum yields in the shorter wavelength photolysis region of glyoxal. The quantum yields have been combined into the stoichiometry shown above and the absorption cross-sections are given in Table 18 for a total quantum yield of 1.0. The absorption cross-sections are from Carter's 1986 mechanism.[23]

$$k = \mathrm{HVGLY1} \quad \mathrm{cm^3\text{-}molecules^{-1}\text{-}s^{-1}}$$

D2.1b $(HC{=}O)_2 \xrightarrow{h\nu} 0.13\,H_2C{=}O + 0.87\,H_2 + 1.87\,CO$

This reaction is for the visible absorption region of glyoxal. Again the stoichiometery represents the relative quantum yields and the absorption coefficients are given in Table 19 for a total quantum yield of 1.0. These are also from Carter's 1986 mechanism.

$$k = \mathrm{HVGLY2} \quad \mathrm{cm^3\text{-}molecules^{-1}\text{-}s^{-1}}$$

D2.2 $(HC{=}O)_2 + {}^{\cdot}OH \longrightarrow 0.63\,HO_2^{\cdot} + 1.26\,CO + 0.37\,H(O{=})C\text{-}C({=}O)O_2^{\cdot}$

This reaction is from Niki, *et al.* and the rate constant is from Plum, given in Atkinson and Lloyd, 1984:[19]

$$k = 1.15 \times 10^{-11} \quad \mathrm{cm^3\text{-}molecules^{-1}\text{-}s^{-1}}$$

D2.3 $(HC{=}O)_2 + NO_3^{\cdot} \longrightarrow 0.63\,HO_2^{\cdot} + 1.26\,CO + HNO_3 + 0.37\,H(O{=})C\text{-}C({=}O)O_2^{\cdot}$

The rate constant is from Atkinson and Lloyd, 1984[19] and stoichiometry is by analogy with reaction **G.2**.

$$k = 6.0 \times 10^{-13} e^{-2060/T} \quad \mathrm{cm^3\text{-}molecules^{-1}\text{-}s^{-1}}$$

Table 18. Cross Sections and Quantum Yields for $(HC{=}O)_2$
$$(HC{=}O)_2 \xrightarrow{h\nu} 0.94\,HO_2^{\cdot} + 0.53\,H_2C{=}O + 1.46\,CO$$
(units are nanometers, $\times 10^{20}$ cm^2-molecule^{-1}, base e)

λ	σ_λ	Φ_λ	λ	σ_λ	Φ_λ	λ	σ_λ	Φ_λ
230	0.287	1.000	275	2.580	1.000	315	2.290	1.000
235	0.287	1.000	280	2.870	1.000	320	1.430	1.000
240	0.430	1.000	285	3.300	1.000	325	1.150	1.000
245	0.573	1.000	290	3.150	1.000	327	1.430	1.000
250	0.860	1.000	295	3.300	1.000	330	1.150	1.000
255	1.150	1.000	300	3.580	1.000	335	0.287	1.000
260	1.430	1.000	305	2.720	1.000	340	1.000	1.000
265	1.860	1.000	310	2.720	1.000			
270	2.290	1.000	312	2.870	1.000			

D2.4 $H(O{=})C\text{-}C({=}O)O_2^{\cdot} + NO \longrightarrow NO_2 + HO_2^{\cdot} + CO + CO_2$
D2.5 $H(O{=})C\text{-}C({=}O)O_2^{\cdot} + NO_2 \longrightarrow H(O{=})C\text{-}C({=}O)O_2NO_2$
D2.6 $H(O{=})C\text{-}C({=}O)O_2NO_2 \longrightarrow H(O{=})C\text{-}C({=}O)O_2^{\cdot} + NO_2$

In their study of the kinetics of glyoxal, Niki *et al.*[60] postulated the existence of $H(O{=})C\text{-}C({=}O)O_2^{\cdot}$ to account for the formation of CO_2 in their experiments. These experiments, however, did not have NO_2 present and it is reasonable to assume that the $H(O{=})C\text{-}C({=}O)O_2^{\cdot}$ radical would react like $CH_3C({=}O)O_2^{\cdot}$ and form a PAN-like analogue, $H(O{=})C\text{-}C({=}O)O_2NO_2$, or PGXAN. Taking a cue from the glycoaldehyde case, we have assumed that PGXAN might also be less stable in the chamber than PAN.

These reactions are assumed to be like the reactions of the peroxyacetyl radicals (see **PA1**), for the formation of PAN. The rate constants are those recommended by Atkinson, 1990 for $RCO_3 + NO_2$:

$$k_4 = \text{RO2NORATE}$$
$$k_5 = \text{RCO3NO2RATE}$$
$$k_6 = \text{PANRATE}$$

D2.X $H(O{=})C\text{-}C({=}O)O_2NO_2 \longrightarrow NO_3^{\cdot} + HO_2^{\cdot} + CO + CO_2$

As in the discussion of PGAN, we assume the same rate of rapid decomposition applies to PGXAN:

$$k = 1.3 \times 10^{32} e^{-25000/T}$$

D2.7 $\mathrm{H(O{=})C\text{-}C({=}O)O_2^{\cdot} + HO_2^{\cdot} \longrightarrow H(HO)C{=}O + CO_2 + H_2O}$

This reaction was described by Niki, *et al.*.

$$k = \mathrm{RO2HO2RATE}$$

Table 19. Cross Sections and Quantum Yields for $(HC{=}O)_2$
$((HC{=}O)_2 \xrightarrow{h\nu} 0.13\,H_2C{=}O + 0.87\,H_2 + 1.87\,CO)$

(units are nanometers, $\times 10^{20}$ cm^2-molecule^{-1}, base e)

λ	σ_λ	Φ_λ	λ	σ_λ	Φ_λ	λ	σ_λ	Φ_λ
355	0.000	0.029	412	4.860	0.029	437	5.270	0.029
360	0.229	0.029	413	8.310	0.029	438	10.100	0.029
365	0.287	0.029	413.5	6.480	0.029	438.5	13.800	0.029
370	0.803	0.029	414	7.500	0.029	439	7.700	0.029
375	1.000	0.029	414.5	8.110	0.029	440	24.700	0.029
380	1.720	0.029	415	8.110	0.029	441	8.110	0.029
382	1.580	0.029	415.5	6.890	0.029	442	6.080	0.029
384	1.490	0.029	416	4.260	0.029	443	7.500	0.029
386	1.490	0.029	417	4.860	0.029	444	9.320	0.029
388	2.870	0.029	418	5.880	0.029	445	11.300	0.029
390	3.150	0.029	419	6.690	0.029	446	5.270	0.029
391	3.240	0.029	420	3.850	0.029	447	2.430	0.029
392	3.040	0.029	421	5.670	0.029	448	2.840	0.029
393	2.230	0.029	421.5	4.460	0.029	449	3.850	0.029
394	2.630	0.029	422	5.270	0.029	450	6.080	0.029
395	3.040	0.029	422.5	10.500	0.029	451	10.900	0.029
396	2.630	0.029	423	8.510	0.029	451.5	9.320	0.029
397	2.430	0.029	424	6.080	0.029	452	12.200	0.029
398	3.240	0.029	425	7.290	0.029	453	23.900	0.029
399	3.040	0.029	426	11.800	0.029	454	17.000	0.029
400	2.840	0.029	426.5	13.000	0.029	455	34.000	0.029
401	3.240	0.029	427	10.700	0.029	455.5	40.500	0.029
402	4.460	0.029	428	16.600	0.029	456	10.100	0.029
403	5.270	0.029	429	4.050	0.029	457	1.620	0.029
404	4.260	0.029	430	5.070	0.029	458	1.220	0.029
405	3.040	0.029	431	4.860	0.029	458.5	1.420	0.029
406	3.040	0.029	432	4.050	0.029	459	0.405	0.029
407	2.840	0.029	433	3.650	0.029	460	0.405	0.029
408	2.430	0.029	434	4.050	0.029	460.5	0.608	0.029
409	2.840	0.029	434.5	6.080	0.029	461	0.203	0.029
410	6.080	0.029	435	5.070	0.029	462	0.000	0.029
411	5.070	0.029	436	8.110	0.029			
411.5	6.080	0.029	436.5	11.300	0.029			

7

Chamber Modeling: 2

In this chapter, the combined inorganic carbonyl, ethene, glycoaldehyde, and glyoxal explicit mechanism (called **EXP** on plots) is used to simulate several ethene–NO_x experiments. Because this mechanism does contain several speculative items due to lack of detail kinetics information, we will show for each experiment *two* simulations: one with and one without the PGAN decomposition reaction **GA.X**. Even in the face of this uncertainty, for our goals here, it is sufficient to show that this explicit mechanism can explain the majority of the HCHO observations in reaction systems having significant HCHO chemical production. Several experimental results, however, present challenges to the completeness and accuracy of the glycoaldehyde and glyoxal mechanisms.

Two pages of plots are given for each experiment and its simulation:

- NO_x and O_3 data (solid lines) and model predictions (dashed lines) are shown for both sides of the chamber on the first page;
- Organic species data (solid lines and points) and model predictions (dashed lines) are shown for both sides of the chamber on the second page; these data usually include ethene, HCHO, and CCl_4 used as a dilution tracer; when available, this plot also includes CO and H_2. Occasionally other model predicted species such as formic acid are shown on this plot.

Recall that we had no CO monitor for 1986 and 1988; H_2, however, was available in several 1988 experiments. The CCl_4 data have been normalized to a maximum concentration of 1.0 so they can be plotted against the model's built-in Tracer species which has an initial concentration of 1.0. In 1988 a new NO_x monitor was used; a short-time constant filter on its output resulted in a very noisy signal which can be seen in the plots. In 1989, we adjusted the time constant and this year's data are much smoother.

Chamber Conditions for ITC Ethene Simulations

At the end of this chapter we present data and simulations for four ethene-NO_x experiments performed in the Indoor Teflon Chamber (ITC) at the University of California, Riverside (UCR). Two of these experiments were 1986 experiments which were duplicated as part of the UNC/UCR joint program described in Chapter 2; all four were simulated and are included here.

In developing chamber conditions to use in these simulations, relative spectra data we collected in the ITC with the UNC Licor 1800 spectroradiometer were used in combination with NO_2 photolysis rate measured before and after the experiments to compute the actinic flux spectral distribution in the chamber. For the 1986 experiments, the NO_2 photolysis rates were taken from Carter's initial condition files for his modeling of these experiments. For the 1989 experiments, we used values recorded by Sexton during the spectra measurements.

We used the same chamber condition and wall model as was described for the UNC chamber in Chapter 5, except:

- the **ENTRAIN** reaction was omitted because the ITC bag collapses during the experiment, so there is no dilution;
- the value of WALLOH in reaction **WALLNO2b** ($NO_2 \longrightarrow HONO$) was reduced from 2.5×10^{-3} for the UNC chamber to 1×10^{-3} as the default value in the ITC;
- the rate constant for **WalN2O5b**, ($N_2O_5 + H_2O \longrightarrow 2\ WHNO_3$) was set to Carter's recommended value (5×10^{-8} ppm^{-1}-min^{-1}).[2]

In Carter's modeling of the ITC, he neglects chamber background concentrations of CH_4, HCHO, and CO, but we consider them important and include them in our initial conditions (but we specified BVOC = 0). In addition, we include 1–10 ppb initial HONO; Carter assumes that there is no initial HONO in the ITC.

Based upon work we preformed at UCR, we applied NO_x 'zero/span' corrections to the four ITC experiments simulated here; in most cases this consisted of 20-30 ppb adjustments to the initial conditions because of calibration and data acquistion problems at UCR. Both the originally reported NO_x data and our corrected data appear in the plots.

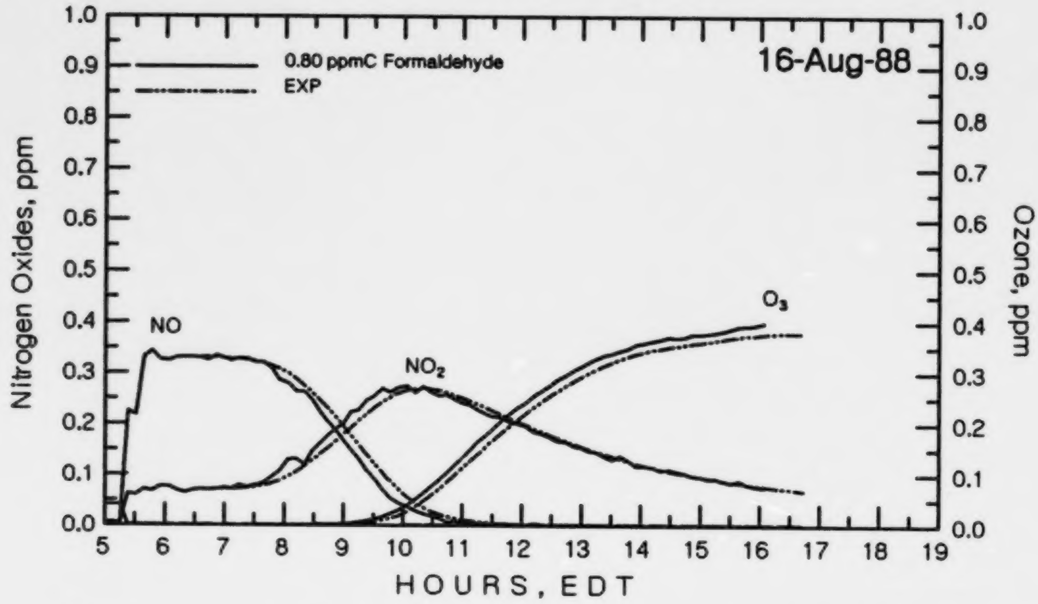

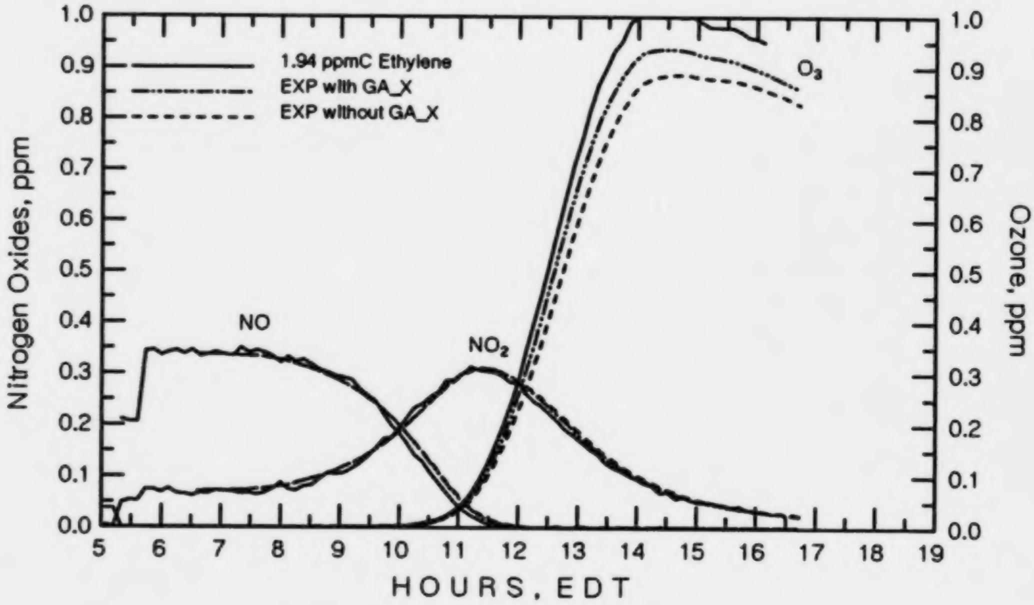

Figure 95. Simulation conditions: top: HONO=10 ppb, BVOC=200 ppb, WallOH= 2.5 x 10^{-3}; bottom: HONO=5 ppb, BVOC=60 ppb, WallOH= 2.5 x 10^{-3}. Solid lines are data; dashed lines are simulations.

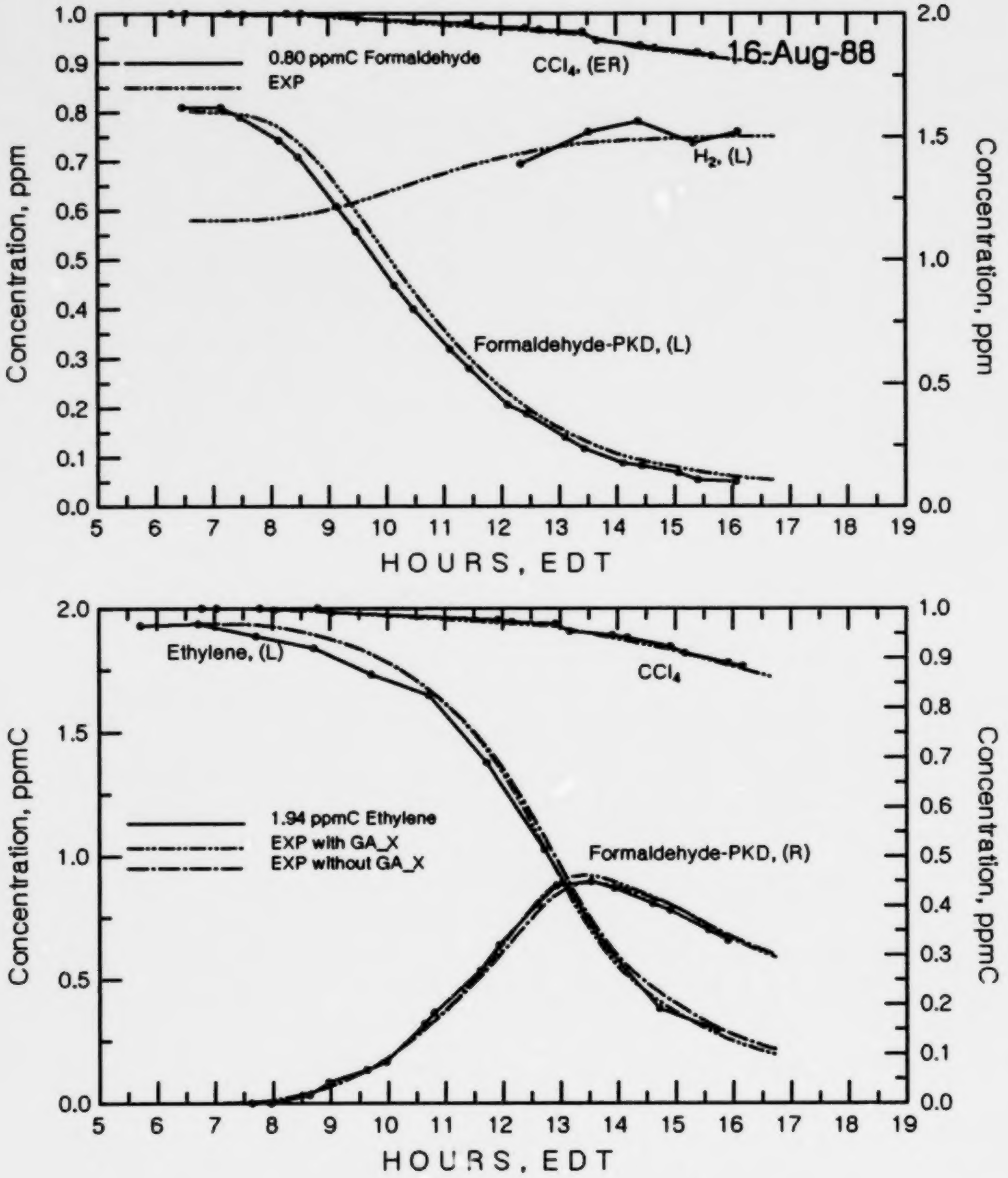

Figure 96. Simulation conditions: top: HONO=10 ppb, BVOC=200 ppb, WallOH= 2.5×10^{-3}; bottom: HONO=5 ppb, BVOC=60 ppb, WallOH= 2.5×10^{-3}. Solid lines are data; dashed lines are simulations.

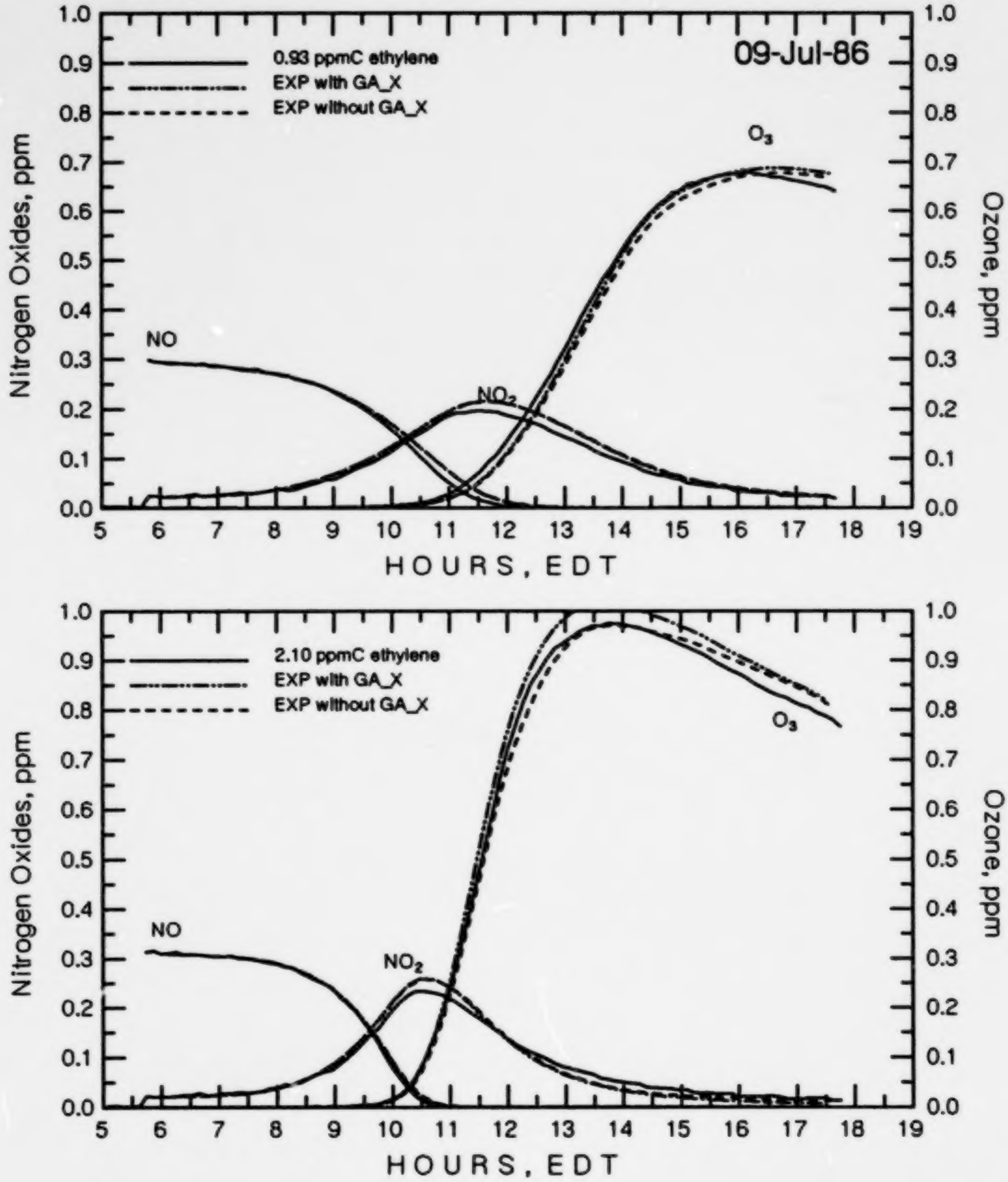

Figure 97. Simulation conditions: top: HONO=5 ppb, BVOC=45 ppb, WallOH= 2.0×10^{-3}; bottom: HONO=3 ppb, BVOC=45 ppb, WallOH= 2.0×10^{-3}. Solid lines are data; dashed lines are simulations.

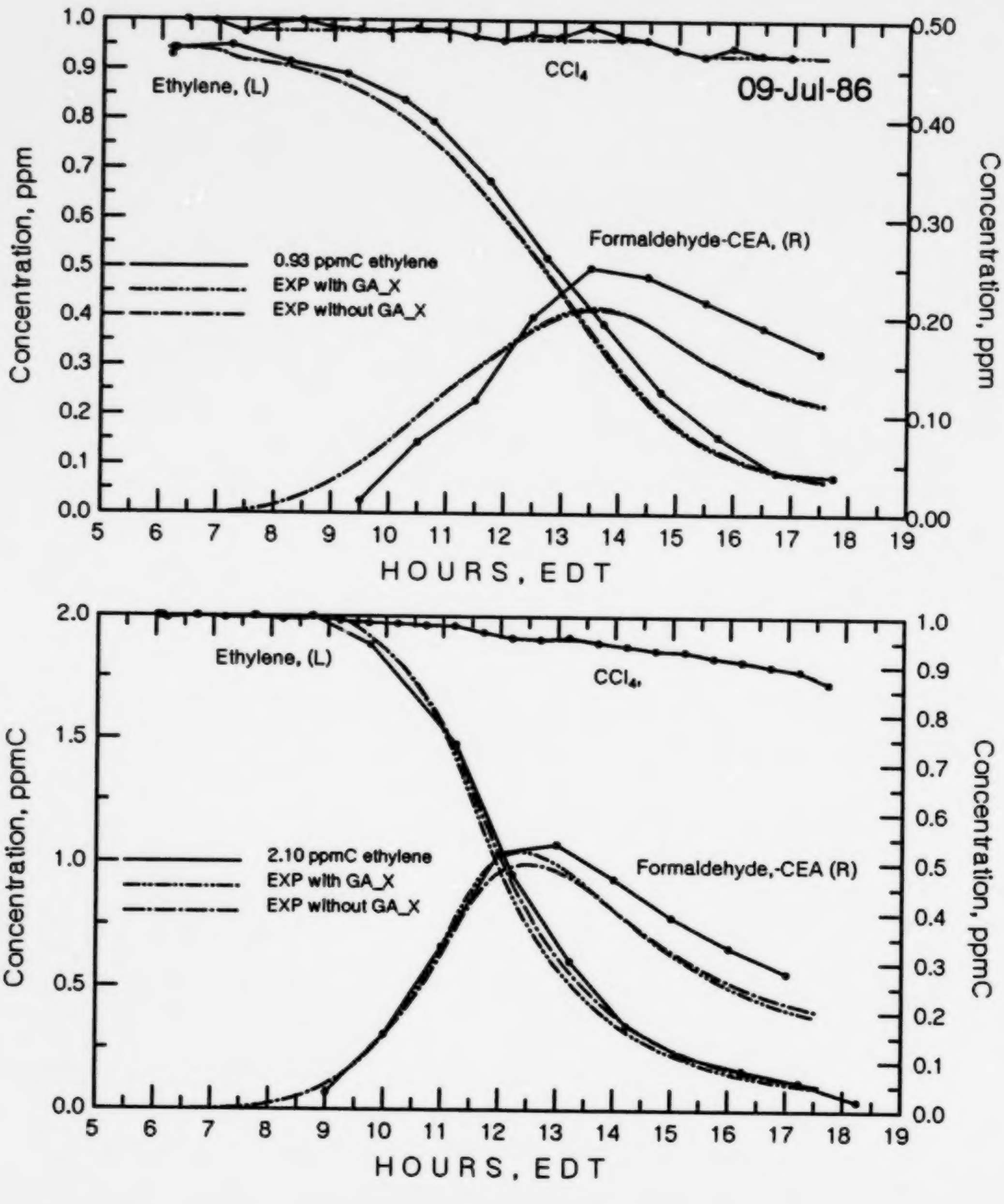

Figure 98. Simulation conditions: top: HONO=5 ppb, BVOC=45 ppb, WallOH= 2.0×10^{-3}; bottom: HONO=3 ppb, BVOC=45 ppb, WallOH= 2.0×10^{-3}. Model Trace is totally hidden behind data. Solid lines are data; dashed lines are simulations.

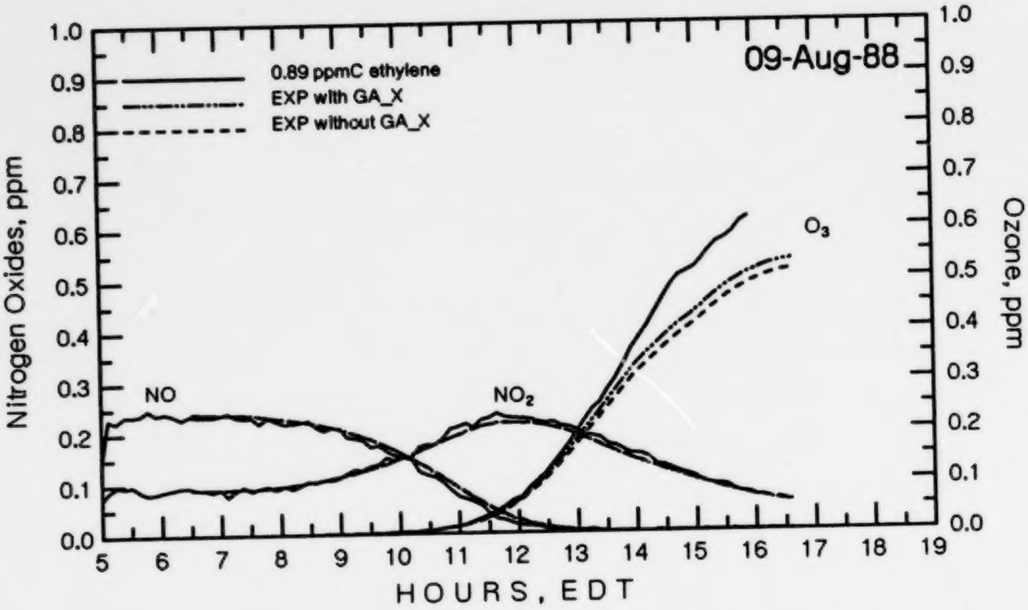

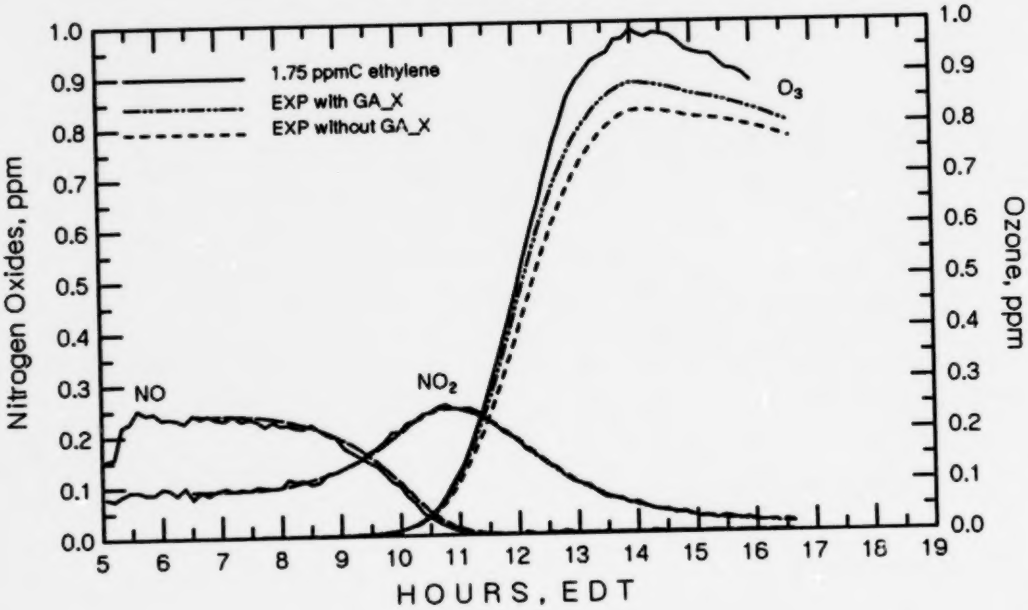

Figure 99. Simulation conditions: top: HONO=6 ppb, BVOC=60 ppb, WallOH= 2.5×10^{-3}; bottom: HONO=4 ppb, BVOC=60 ppb, WallOH= 2.5×10^{-3}. Solid lines are data; dashed lines are simulations.

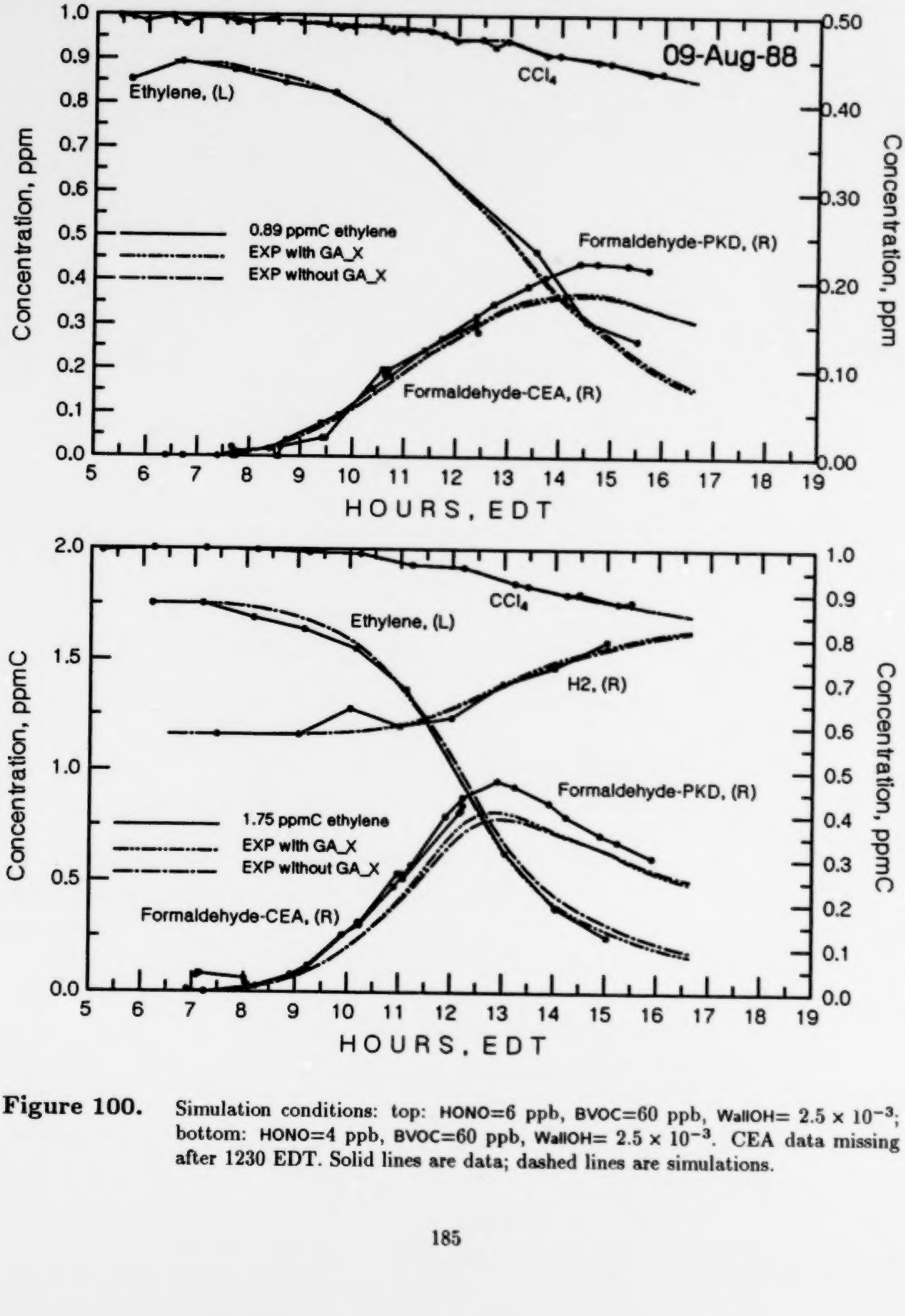

Figure 100. Simulation conditions: top: HONO=6 ppb, BVOC=60 ppb, WallOH= 2.5×10^{-3}; bottom: HONO=4 ppb, BVOC=60 ppb, WallOH= 2.5×10^{-3}. CEA data missing after 1230 EDT. Solid lines are data; dashed lines are simulations.

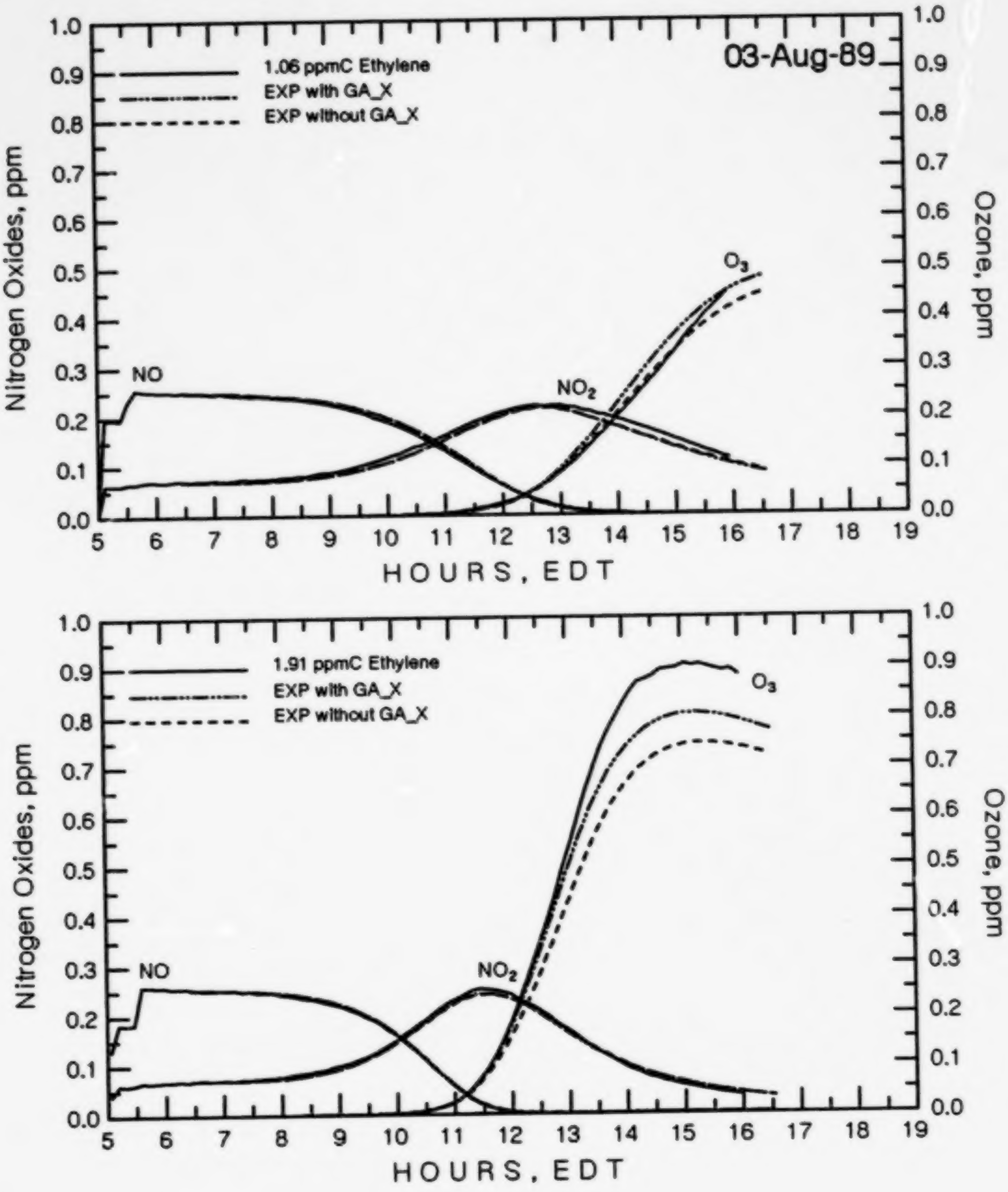

Figure 101. Simulation conditions: top: HONO=3 ppb, BVOC=55 ppb, WallOH= 2.5×10^{-3}; bottom: HONO=3 ppb, BVOC=55 ppb, WallOH= 2.5×10^{-3}. Solid lines are data; dashed lines are simulations.

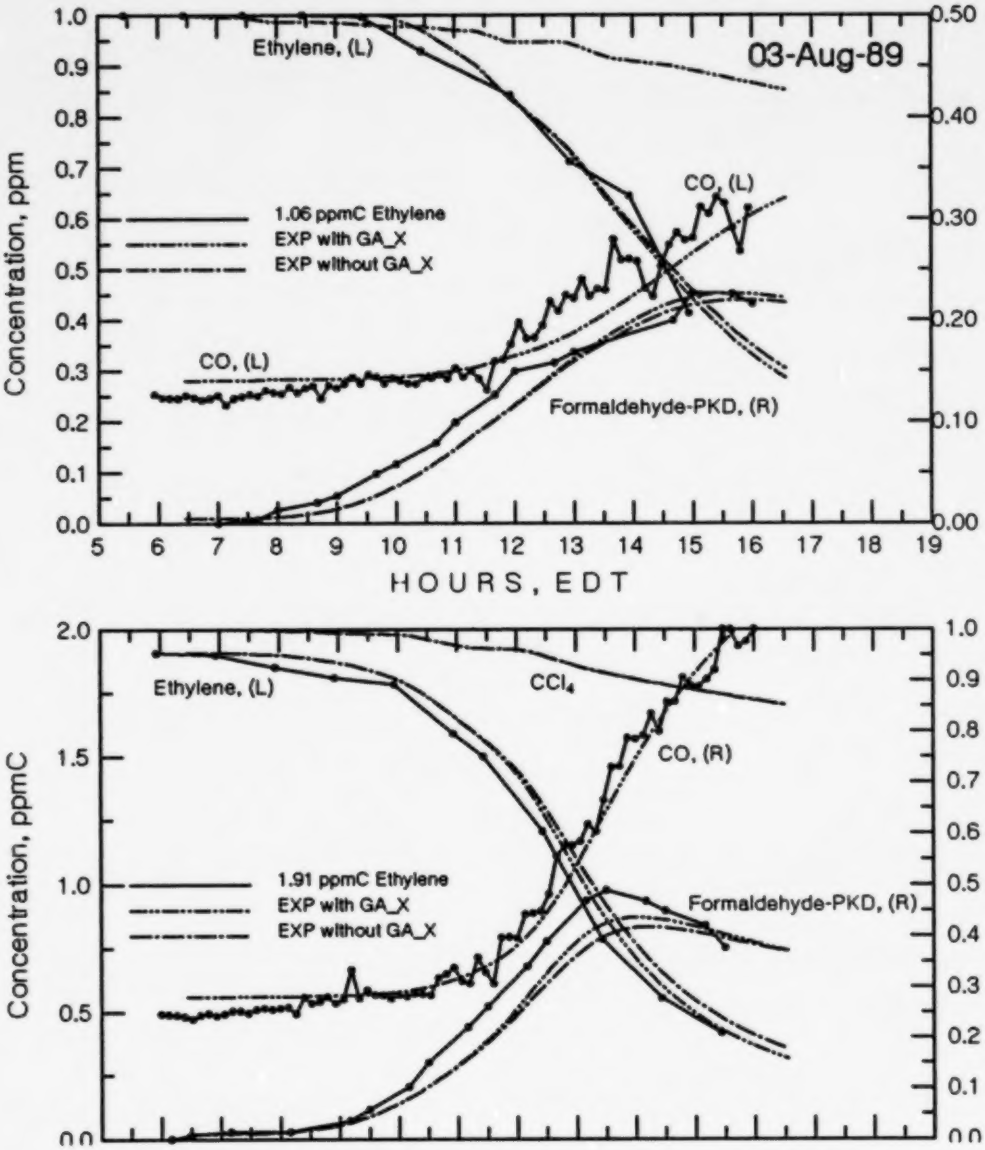

Figure 102. Simulation conditions: top: HONO=3 ppb, BVOC=55 ppb, WallOH= 2.5×10^{-3}; bottom: HONO=3 ppb, BVOC=55 ppb, WallOH= 2.5×10^{-3}. Solid lines are data; dashed lines are simulations.

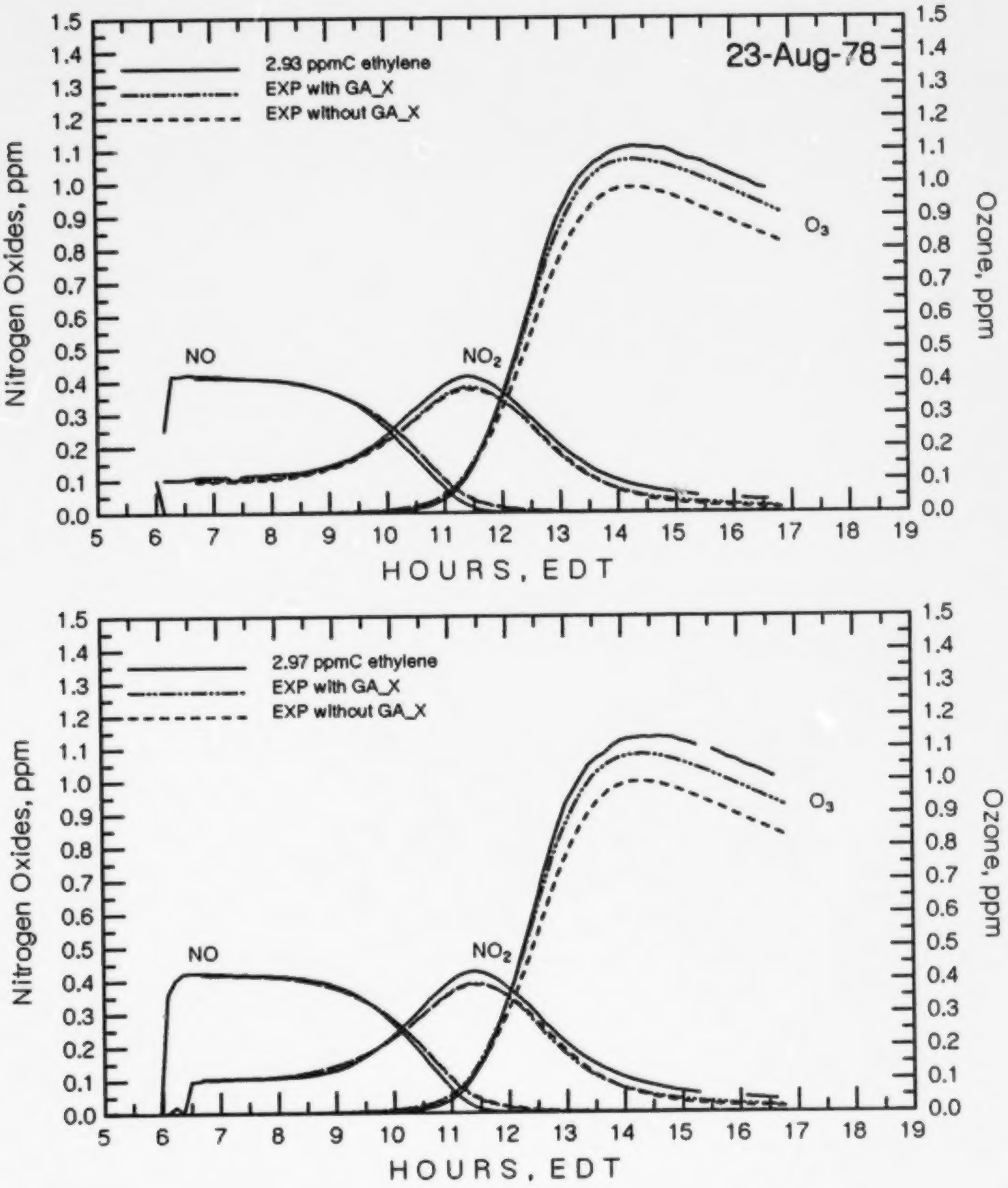

Figure 103. Simulation conditions: top: HONO=5 ppb, BVOC=45 ppb, WallOH= 1.5×10^{-3}; bottom: HONO=5 ppb, BVOC=45 ppb, WallOH= 1.5×10^{-3}. Solid lines are data; dashed lines are simulations.

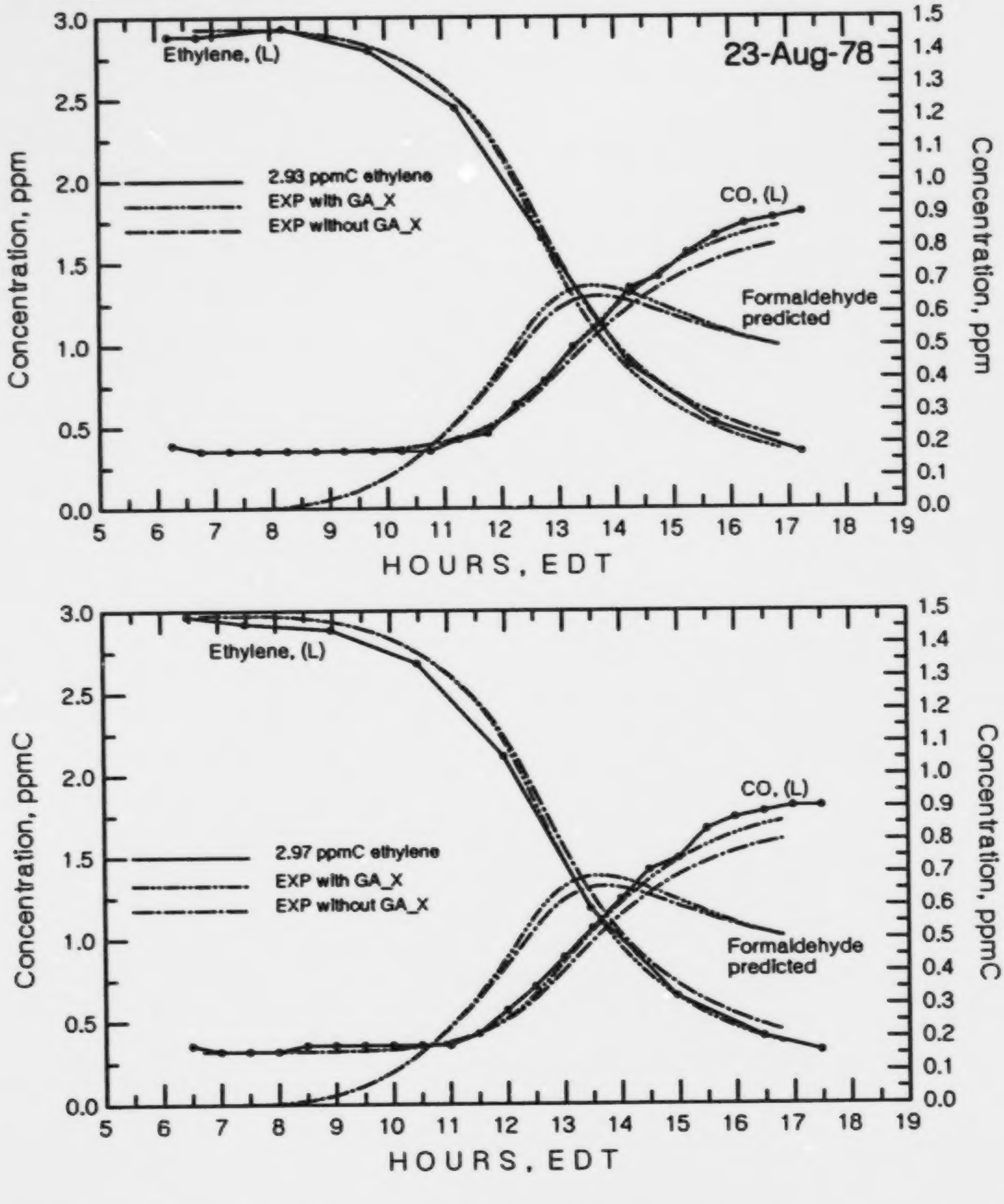

Figure 104. Simulation conditions: top: HONO=5 ppb, BVOC=45 ppb, WallOH= 1.5×10^{-3}; bottom: HONO=5 ppb, BVOC=45 ppb, WallOH= 1.5×10^{-3}. HCHO measurements missing. Solid lines are data; dashed lines are simulations.

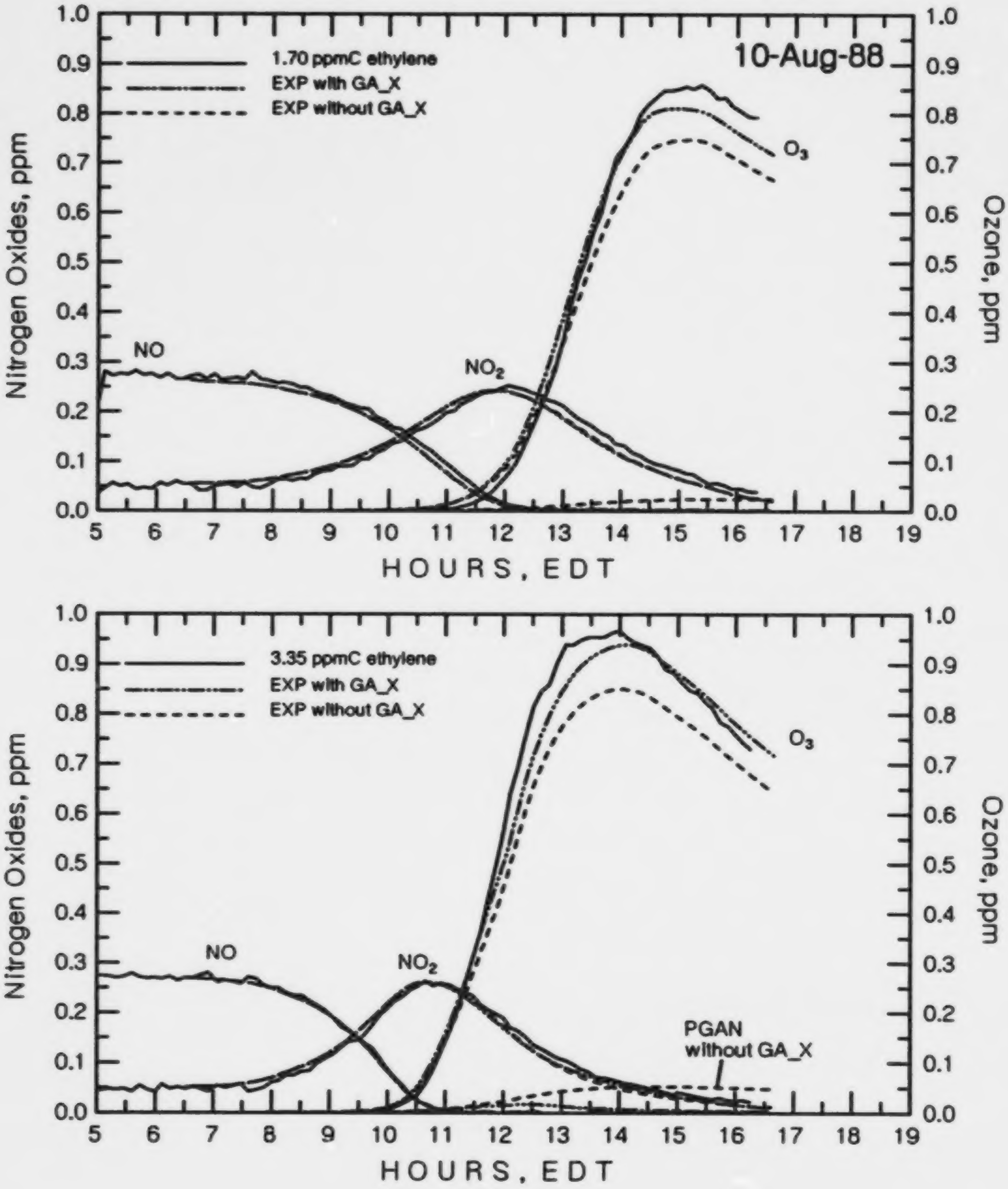

Figure 105. Simulation conditions: top: HONO=3 ppb, BVOC=55 ppb, WallOH= 2.5×10^{-3}; bottom: HONO=3 ppb, BVOC=55 ppb, WallOH= 2.5×10^{-3}. Solid lines are data; dashed lines are simulations.

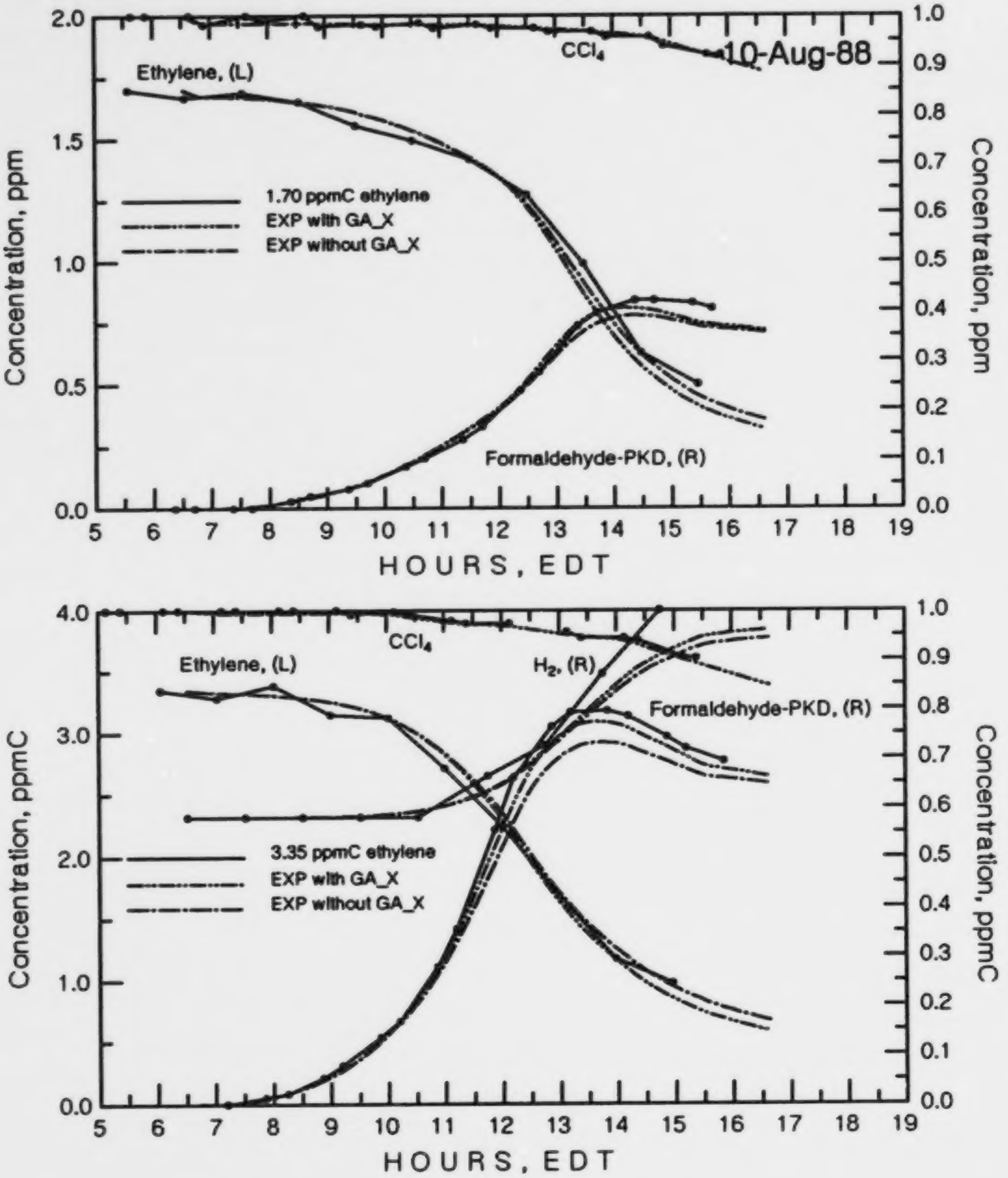

Figure 106. Simulation conditions: top: HONO=3 ppb, BVOC=55 ppb, WallOH= 2.5×10^{-3}; bottom: HONO=3 ppb, BVOC=55 ppb, WallOH= 2.5×10^{-3}. Solid lines are data; dashed lines are simulations.

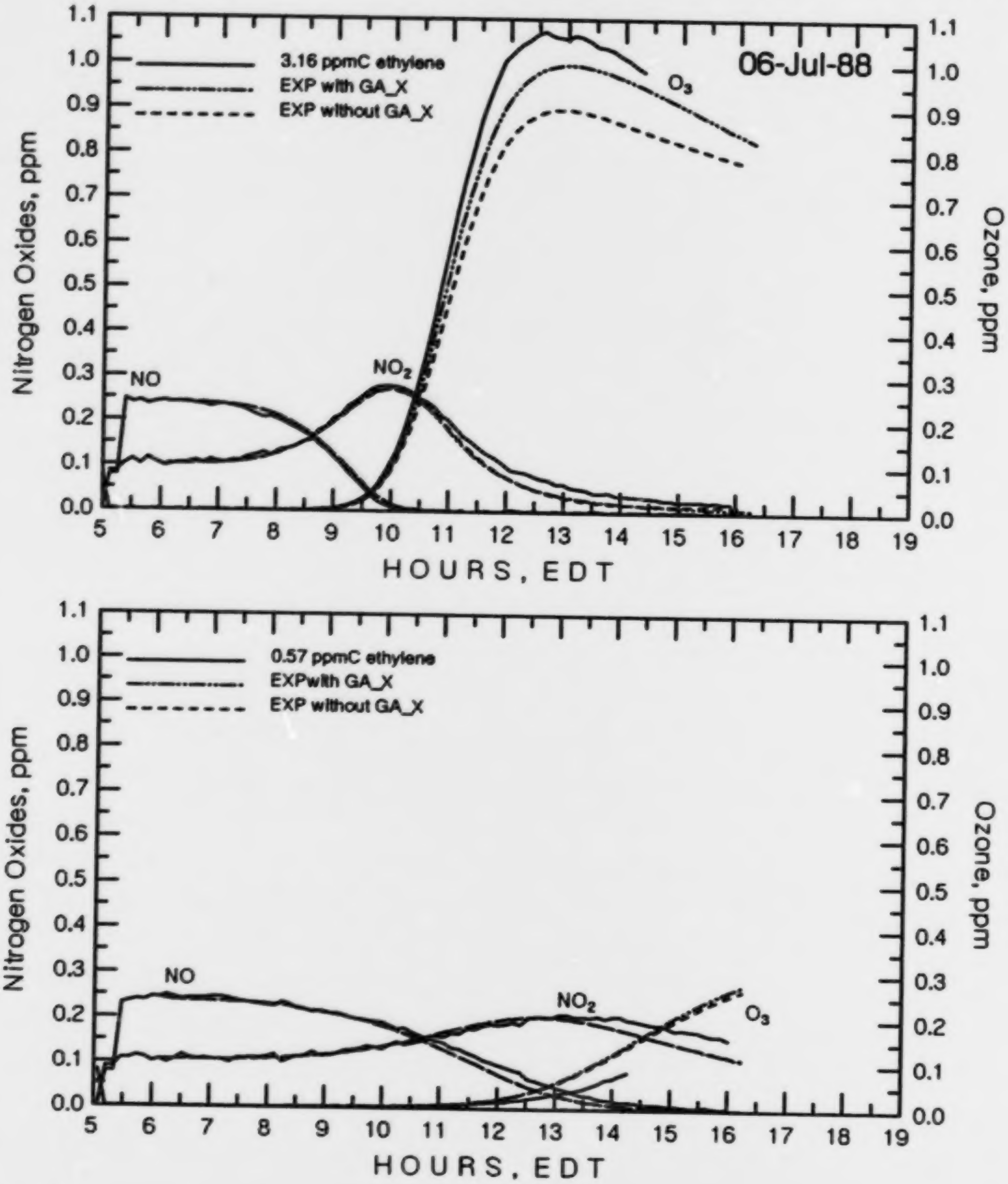

Figure 107. Simulation conditions: top: HONO=3 ppb, BVOC=45 ppb, WallOH= 2.5×10^{-3}; bottom: HONO=3 ppb, BVOC=45 ppb, WallOH= 2.5×10^{-3}. Solid lines are data; dashed lines are simulations.

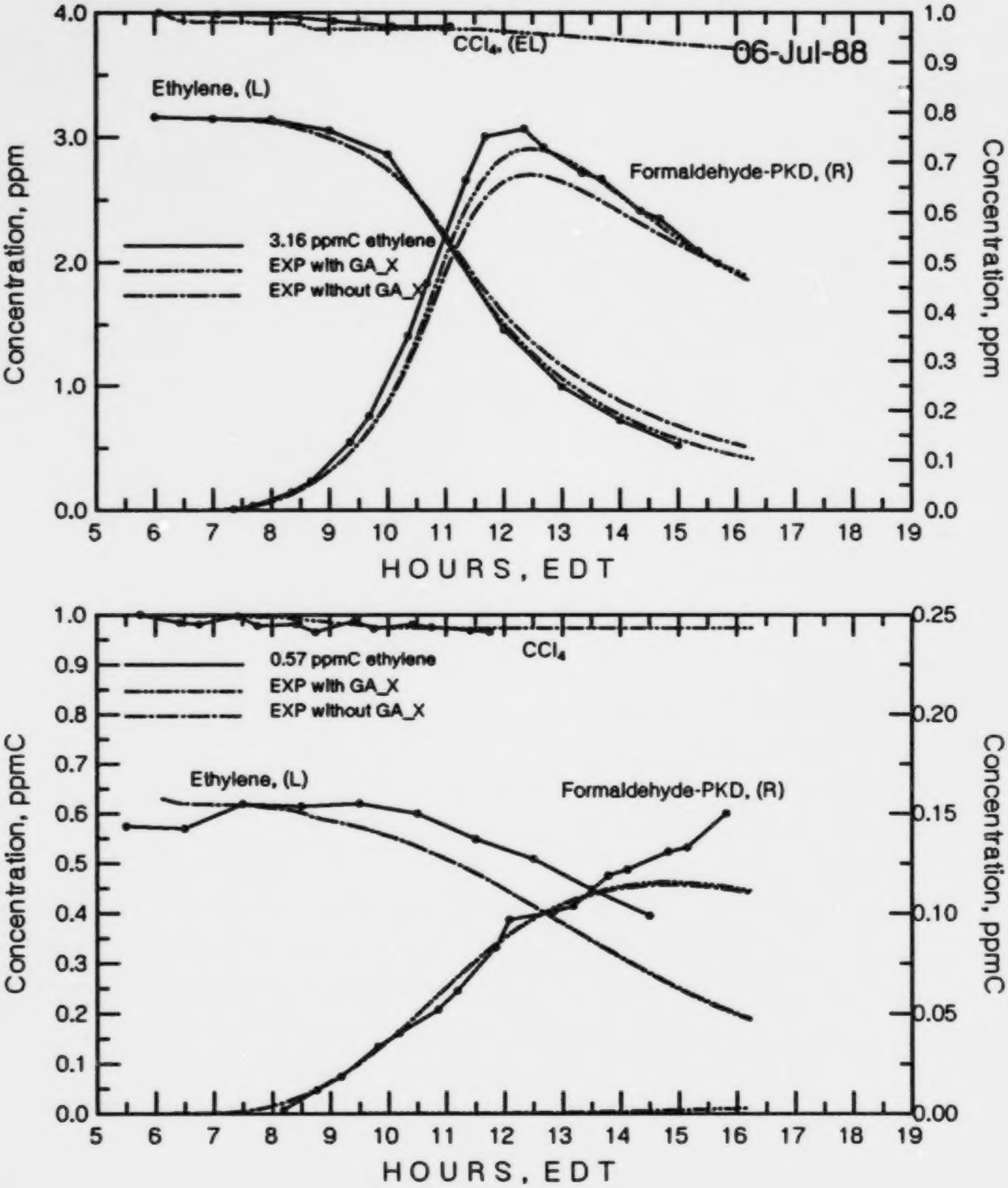

Figure 108. Simulation conditions: top: HONO=3 ppb, BVOC=45 ppb, WallOH= 2.5×10^{-3}; bottom: HONO=3 ppb, BVOC=45 ppb, WallOH= 2.5×10^{-3}. Solid lines are data; dashed lines are simulations.

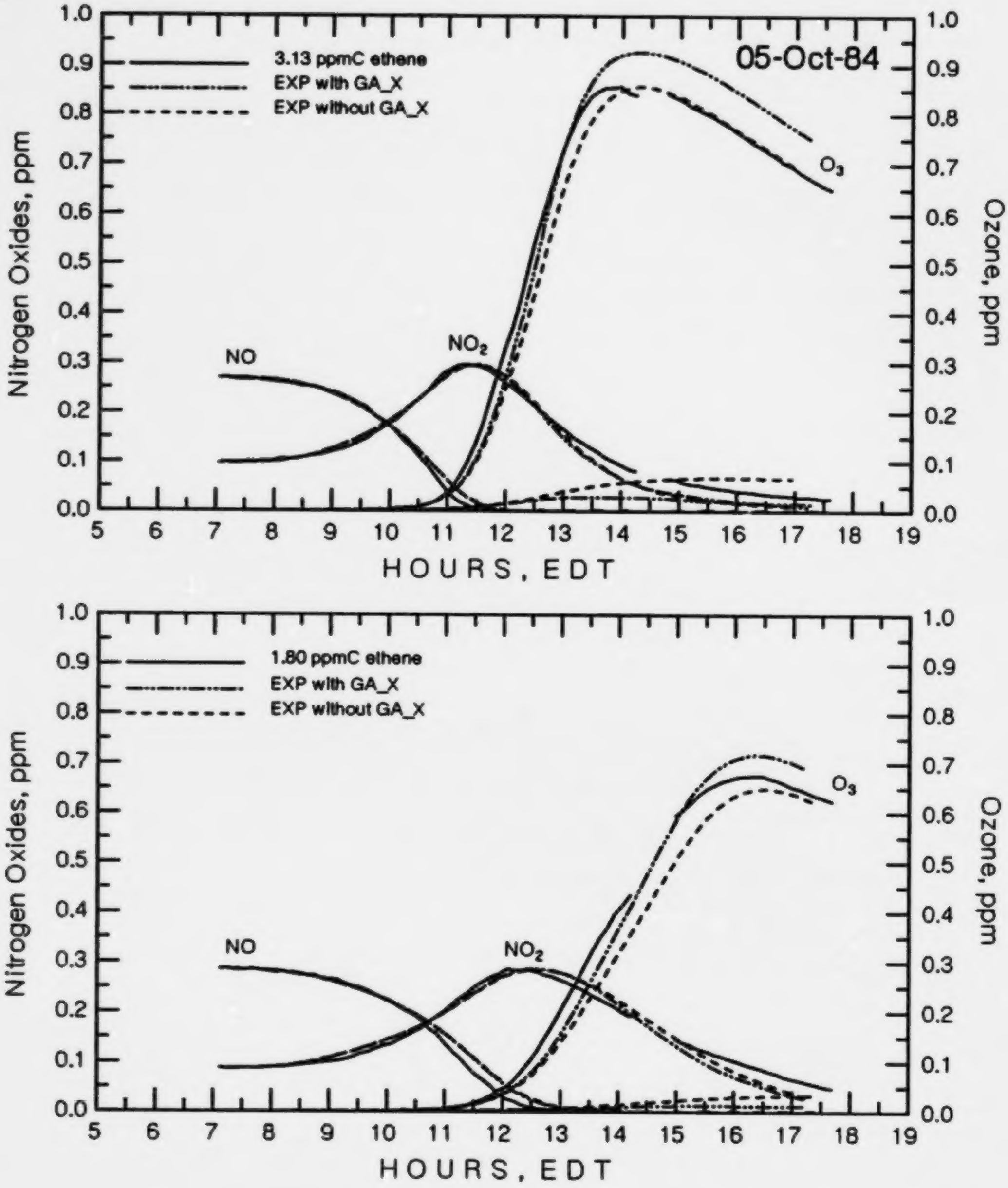

Figure 109. Simulation conditions: top: HONO=3 ppb, BVOC=25 ppb, WallOH= 0.0; bottom: HONO=5 ppb, BVOC=25 ppb, WallOH= 0.0. Solid lines are data; dashed lines are simulations.

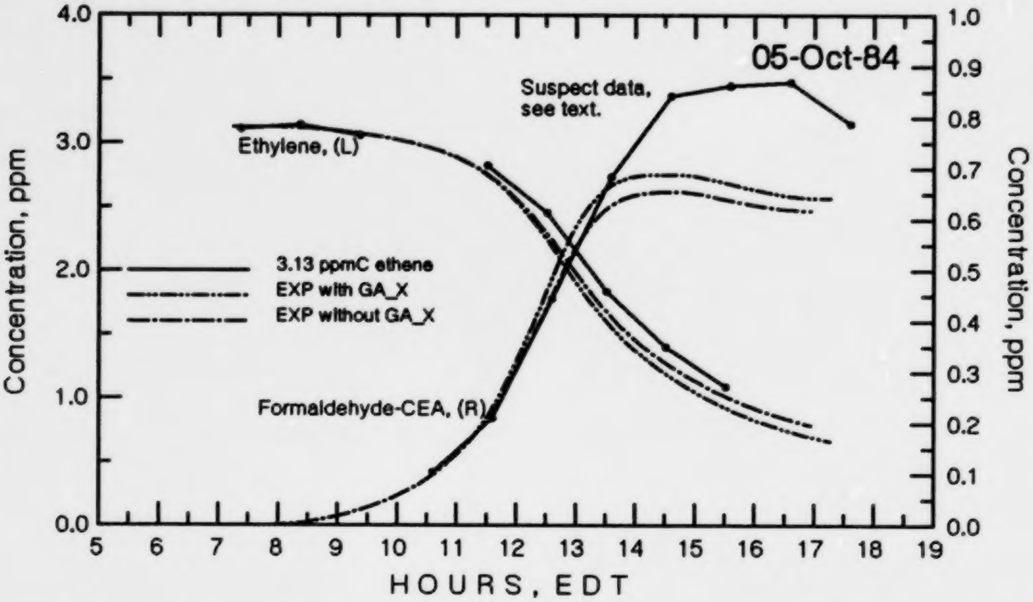

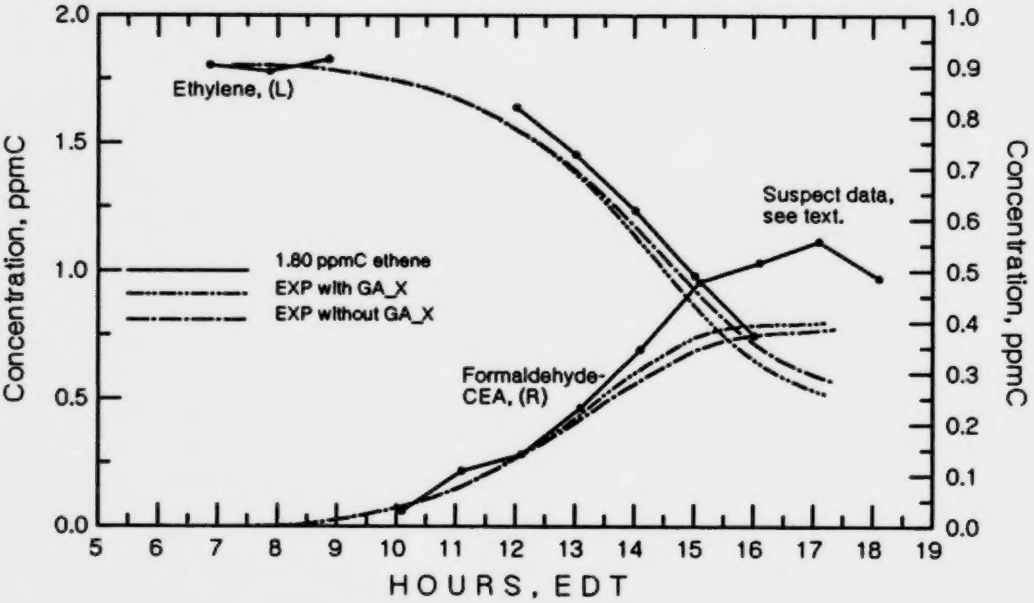

Figure 110. Simulation conditions: top: HONO=3 ppb, BVOC=25 ppb, WallOH= 0.0; bottom: HONO=5 ppb, BVOC=25 ppb, WallOH= 0.0. Solid lines are data; dashed lines are simulations.

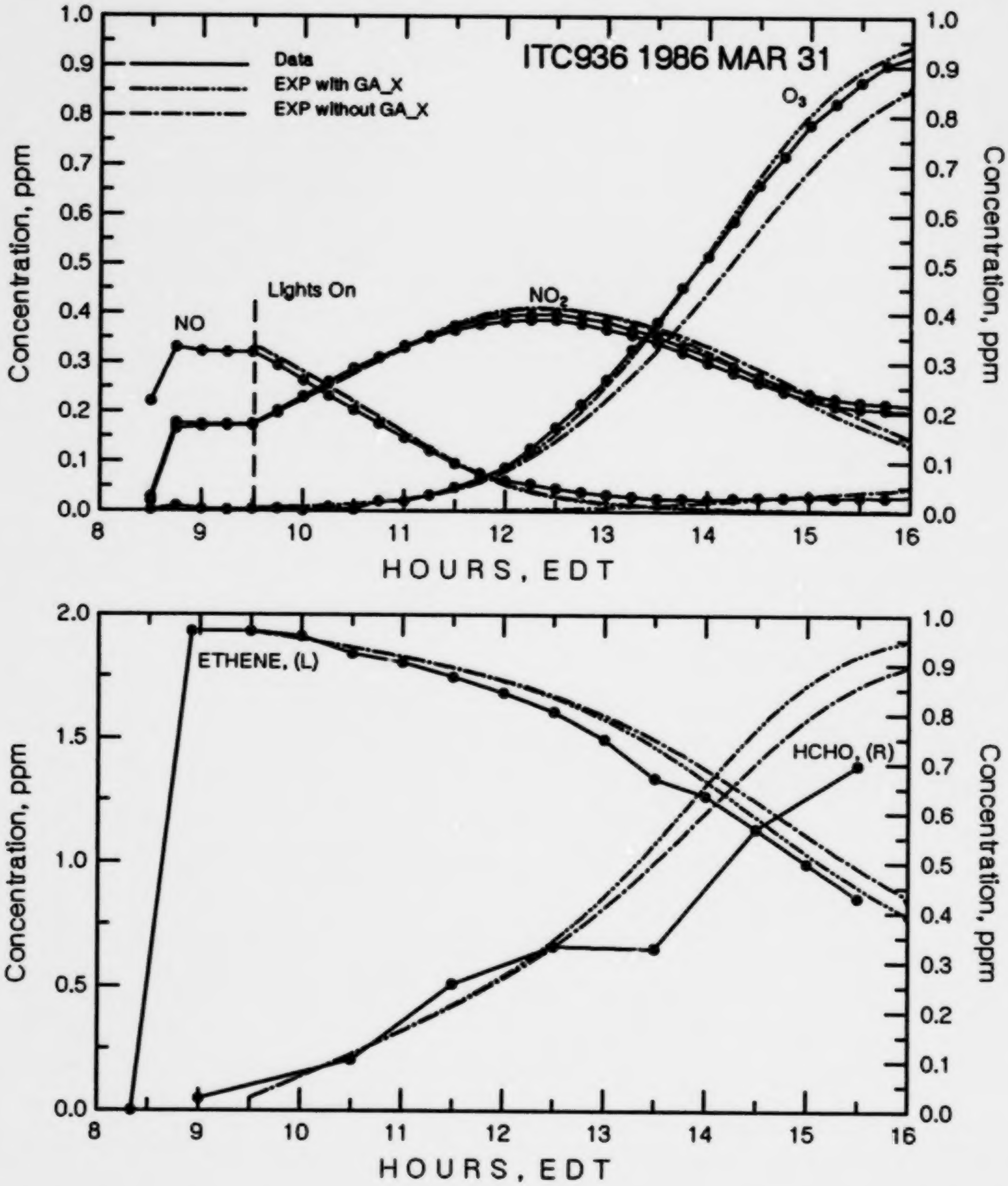

Figure 111. Simulation conditions: HONO=3 ppb, WallOH=1.0×10^{-4}. Solid lines are data; dashed lines are simulations.

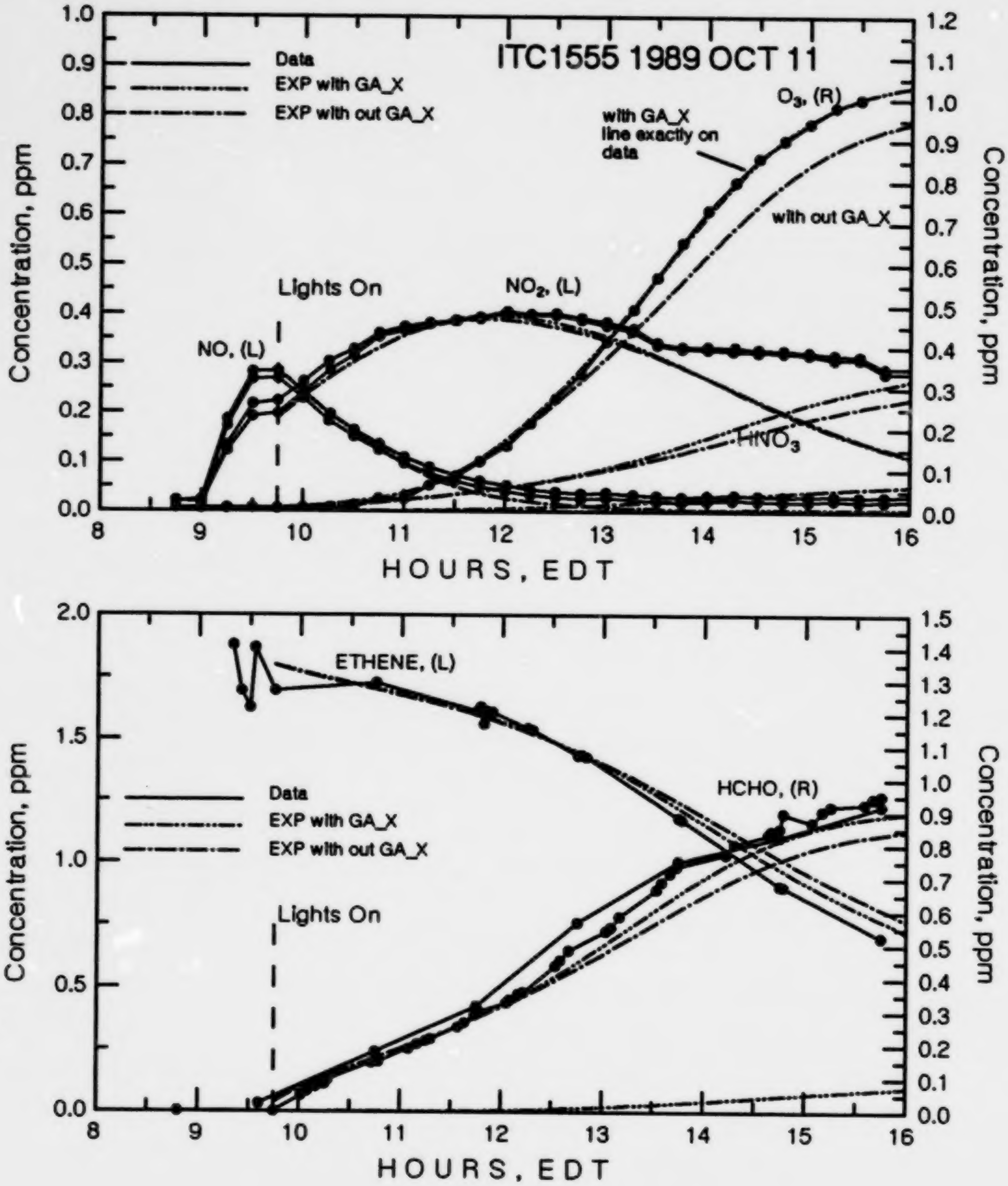

Figure 112. Simulation conditions: HONO=10 ppb, WallOH=1.3×10^{-3}. Solid lines are data; dashed lines are simulations.

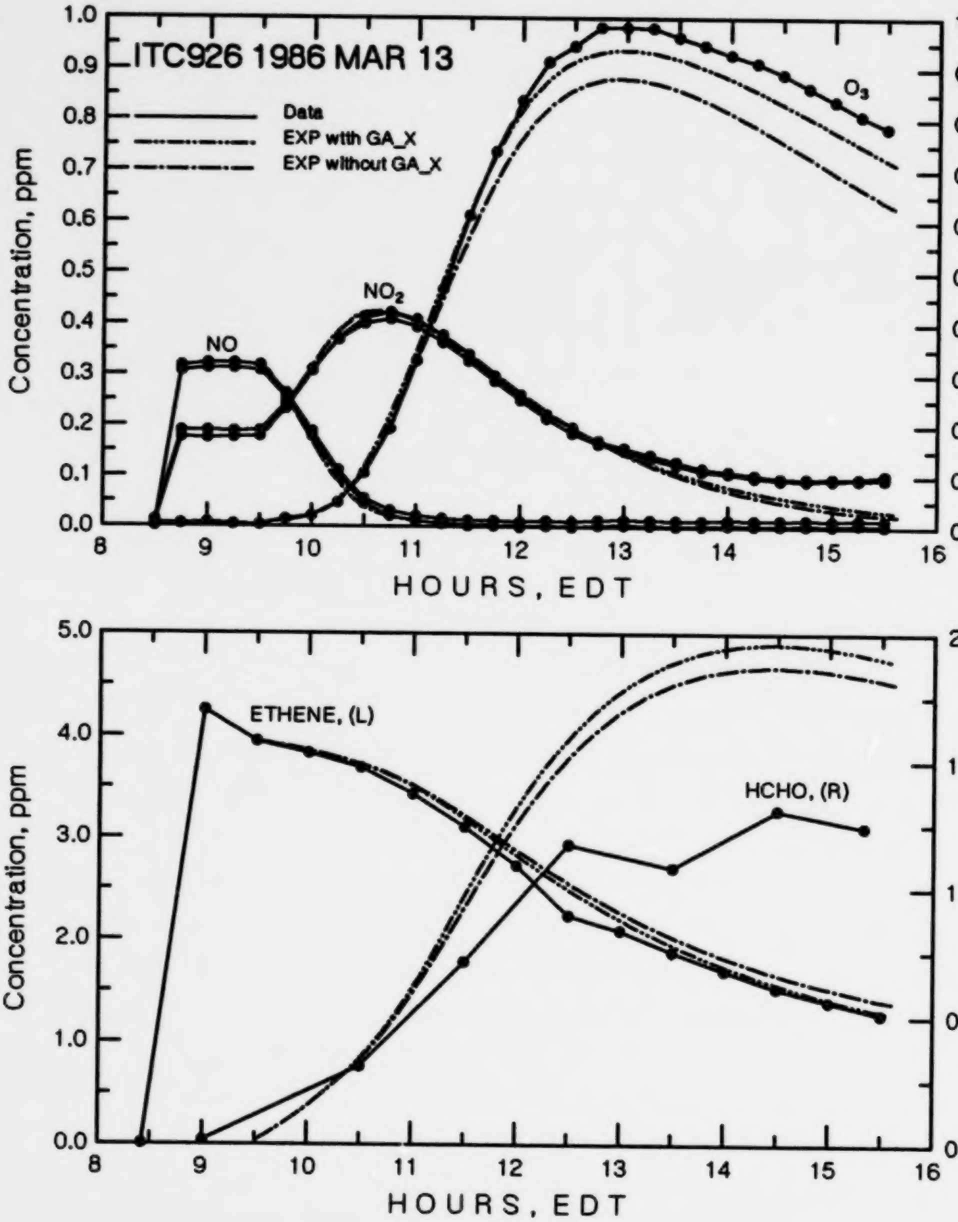

Figure 113. Simulation conditions: HONO=3 ppb, WallOH=1.0 × 10^{-3}. Solid lines are data; dashed lines are simulations.

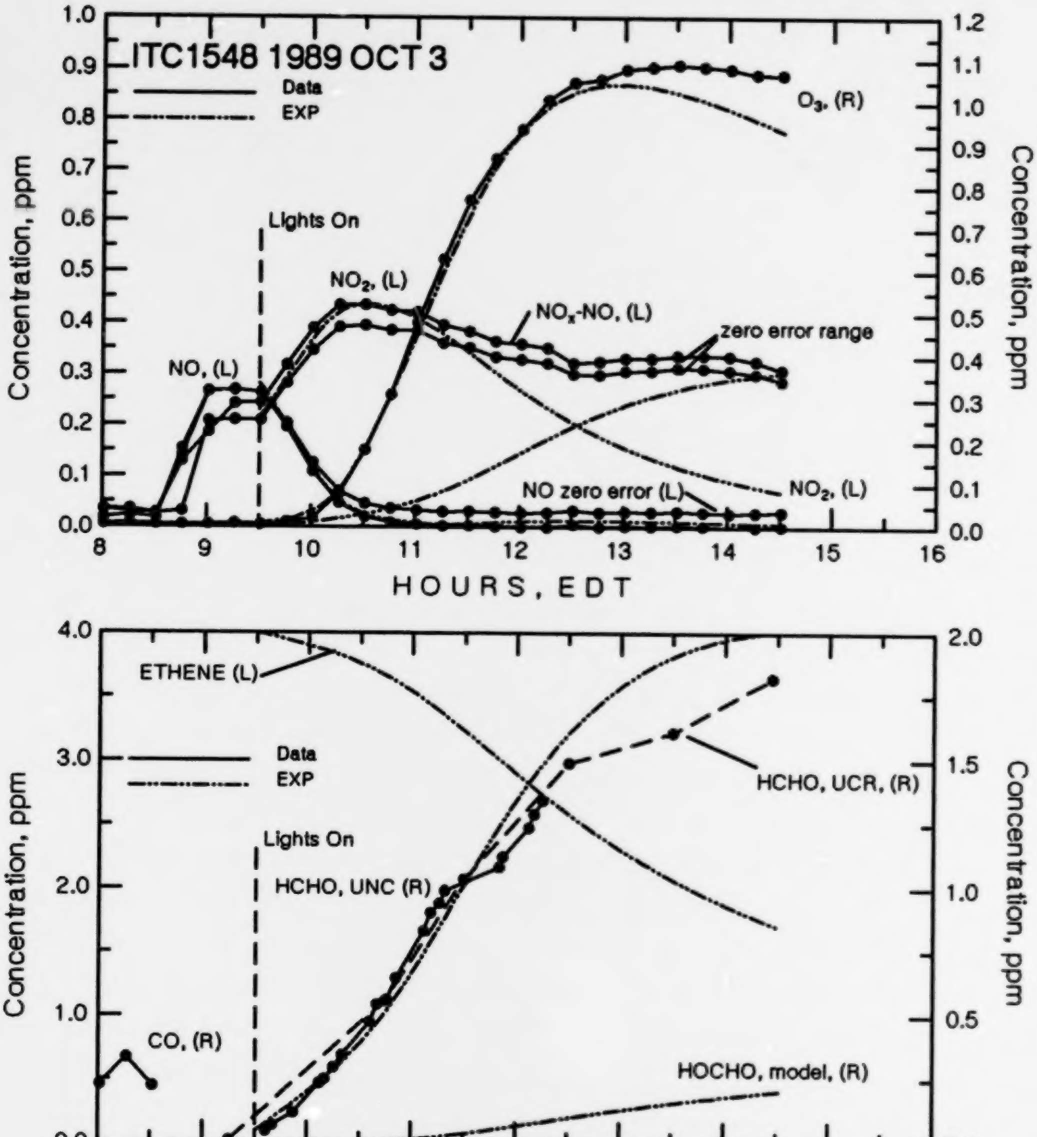

Figure 114. Simulation conditions: HONO=6 ppb, WallOH=1.8×10^{-3}. Solid lines are data; dashed lines are simulations.

Extent of "Reasonable Agreement"

The predictions of the explicit ethene mechanism show excellent agreement with almost all of the measured species over a range of concentrations, seasons, and years not only in the UNC chamber, but also in the indoor chamber at UCR. The agreements for NO, NO_2, ethene, CO, H_2 were nearly exact and clearly were well within the uncertainty of the experimental data over the whole time profile of essentially every experiment simulated from 1978 to 1989.

For O_3, the agreements were excellent for initial rise and for the rate of production (shape of the profile) and showed good agreement with the maximum values. In many higher concentration ethene experiments in the UNC chamber, however, the model appears to "run out of O_3" before the experiment did; this resulted in simulations producing too low maximum O_3. We suspect that this condition is related to the lack of kinetics and mechanistic data for PGAN and PGXAN in chambers. Thus, the known chemistry of these compounds could be incomplete in some fundamental way and the deletion and/or distortion of this chemistry in the model gives less than excellent performance for the later stages of high concentration ethene experiments where these species are important reactants. Another alternative explanation for this result is that the model has too much radical termination near the end of the experiment.

With regard to HCHO predictions and observations, in many experiments the agreements were very good to excellent, consistent in time, slope, and magnitudes. There are some experiments, however, where although the agreements were closer than in previous testing of, say, CB4 or CAL with these data, the extents of disagreement raise doubts about some of the data or about the completeness and accuracy of the explicit mechanism. A good example is one side of the chamber data and model for July 9, 1986 (see Figure 98, top plot). The strip chart for this experiment has been reviewed carefully for problems and none found. Similarly the instrument calibrations were examined for this experiments, but no errors were found. There was, however, a potential operational problem: during this period the clock-operated zero-air value was removed for use by another research group. Thus, the only zero points were before the experiment and later after the chamber had been vented. Thus, there was a possibility that the CEA had an upward zero drift during this experiment, perhaps due to a build-up and retention of the colored reagent, and this could have been flushed out before the CEA was zero-checked sometime after the chamber had vented. Another possibility is that there could have been a problem of "carry over" of the colored reagent in the CEA formaldehyde from the readings on the high HCHO side to the readings on the low HCHO side. In any case, we believe this particular difference between experimental observations and the model predictions is a data problem, but we can not prove it.

A smaller, but seemingly consistent, difference between the model and the observations occurred in the 1.8 ppmC experiments which were a year apart (August 9, 1988 and August 3, 1989) but for which there was a higher yield of HCHO on both days than could be explained by the model. Notice that on August 10, 1988, there was excellent agreement of HCHO observations and predictions at ethene levels of 1.7 and 3.35 ppmC. On the other hand, August 9 and August 3 were very clear sky days with excellent sunlight, while August 10 was partially overcast, suggesting that the HCHO photolysis rates for clear skies may be too high. As countering evidence, however, the CO produced by HCHO photolysis appears consistent with the model on August 3, 1989 and on August 23, 1978 which suggests that August photolysis rates are correctly estimated. Of course the HCHO observations might be too high on both of August 9 and August 3 experiments which were a year apart, but this is inconsistent with the calibration data base and the behavior of the instrument on August 10, 1988. The credibility of the glycoaldehyde and glyoxal chemistries used in the model are questionable enough that even these minor disagreements raise doubts of whether the model is fully accurate.

A significant disagreement between the model predictions and chamber observations for HCHO occurred in the simulation for October 5, 1984. As will be shown in the next chapter, two other October 1984 ethene-NO_x simulations and experiments also showed this large deviation in maximum HCHO. A re-examination of the original data stripcharts and a review of the calibration data base revealed that in these experiments, *calibrations were not performed on the day of these runs.* Calibrations for October 5, 1984 were linearily interpolated between those of Sept. 25, 1984 and October 7, 1984. These calibrations were performed by a new site operator working alone. This operator, who is no longer with us, failed to write down the amount of paraformaldehyde he injected into the chamber in his calibration on October 7 and, at the time the data were processed, we had to assume that he used the usually standard amount which would produce a 1 ppm span concentration. These three days were selected for modeling because they are the only October ethene experiments in the data base which used the CEA HCHO monitor. In 1978, we performed two October ethene experiments at 2.6 and 3.1 ppmC ethene in which the gas chromatographic HCHO method was used to measure HCHO; these were not selected for simulation tests because have minor limitations. Nevertheless, these experiments do suggest that the maximum HCHO yield under these conditions is 0.6 to 0.7 ppmC HCHO, not 0.9 as was reported on October 5, 1984 in the 3.1 ppmC ethene experiment. Thus, the 1978 gas chromatographic HCHO data are consistent with the model predictions on October 5, 1984. Therefore we believe that these are sufficient grounds to impeach the October 1984 HCHO data and we therefore discount the lack of agreement among model predictions and chamber observations for HCHO for these October 1984 experiments.

With regard to the ITC chamber simulations, we remind the reader that these were simulated with only two "adjustments": initial HONO and the rate constant for $NO_2 \longrightarrow HONO$. Unlike Carter, who believes that initial HONO forms by heterogeneous reactions on the reactor walls and therefore he finds no justification for using initial HONO in his ITC simulations,[2] we believe that *initial* HONO arises from the high concentration NO_2 injection process and thus the initial levels are more related to the injection process than to the chamber construction materials. Also unlike Carter, who uses a *constant* source of $^{\cdot}OH$ at a constant rate to simulate the ITC, we believe that gas-phase NO_2 reacts on the walls—probably in a complex multistep process perhaps involving aqueous reactions—with a resulting product of HONO (possibly the reactant and product nitrogen atoms are not the same). Thus, our wall-mediated model has a temporal character much different than Carter's model. We find Carter's model to be either too slow in the middle or too fast at the end compared to ours. Using our model, the magnitudes of the wall-mediated rates used in simulating the ITC chamber are consistent (within a factor of two to three) with those used in simulating the UNC chamber.

Carbon Balances in an Ethene System

Figure 115 shows a time-resolved carbon balance for a 3.2 ppmC ethene system and the pie-chart shows the final carbon distribution. Figure 116 shows that 1.936 ppm of HCHO was formed, but its peak concentration was only 0.74 ppm. Thus, much of the HCHO was converted to CO by photolysis and ˙OH attack, processes which we believe are very well represented in our mechanism and in the chamber simulations as shown in Chapter 5. In contrast, about 14% of the carbon distribution is associated with less well understood chemistries of the hydroxyl-carbonyl compounds. This fraction is larger than the differences between our HCHO observations and the model's predictions for any of our examples. Clearly the kinetics of the hydroxyl-carbonyl compounds are critical to the ending chemistry of ethene systems and further laboratory data on their characteristics is warranted. We feel that we have extended the existing information as far as possible and that further modeling exercises would be less-fruitful than new measurements of the hydroxyl-carbonyl compounds in ethene systems.

Figure 116 shows that in the 3.2 ppmC ethene experiment, 26.5% of the HCHO was formed in the O_3+ethene reaction chain, while 57.6% was formed in the ˙OH+ethene reaction sequence. The chemistry of the latter now seems to be better understood than that of the former. Therefore, it is reasonable to assume that most of the uncertainty in predicting HCHO levels would be associated with the extent to which O_3+olefin reactions occur verses ˙OH+olefin reactions. These relative contributions will be assessed for urban atmospheric conditions in a later chapter.

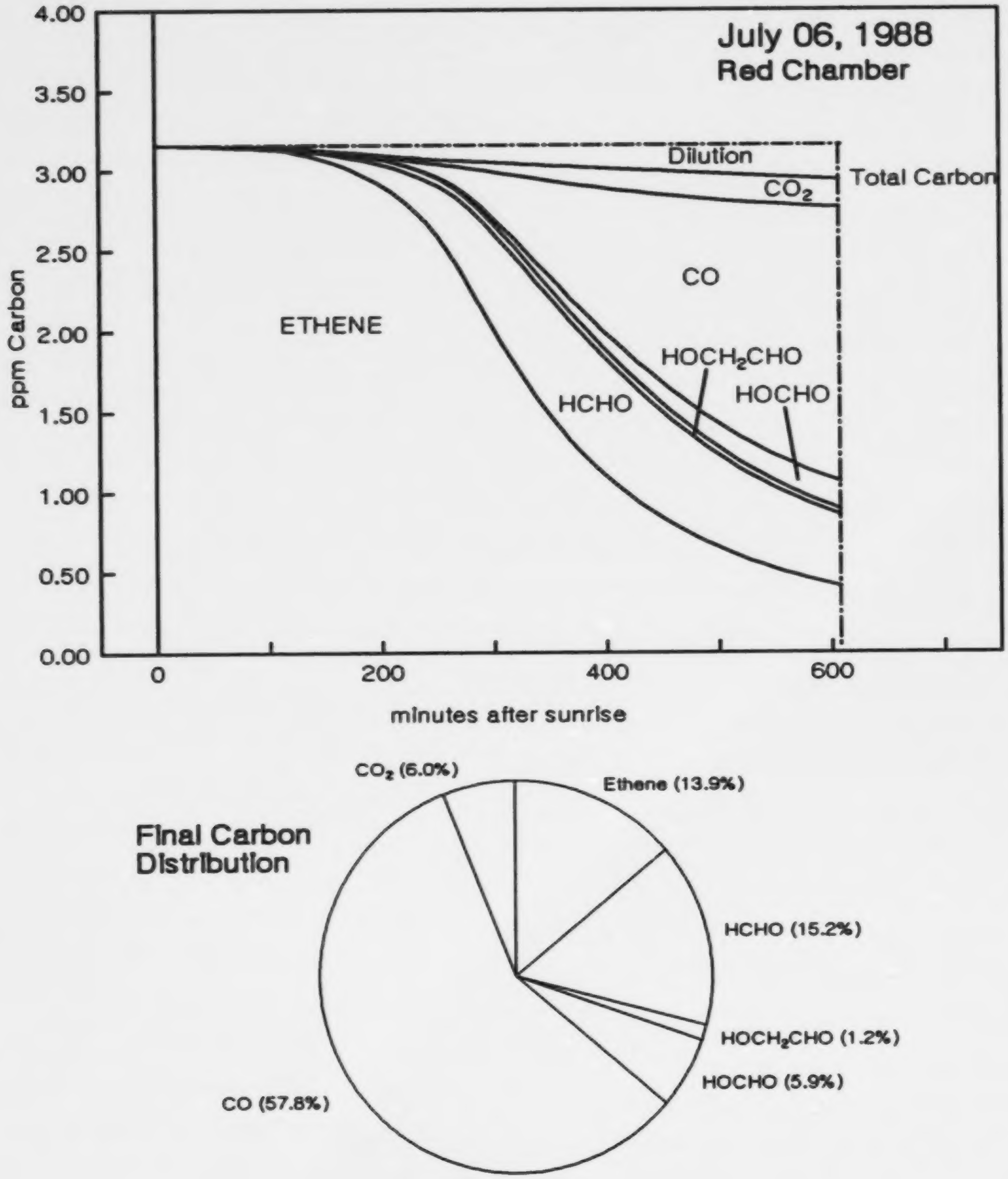

Figure 115. Carbon Balance Predicted in 3.2 ppmC Ethene Experiment.

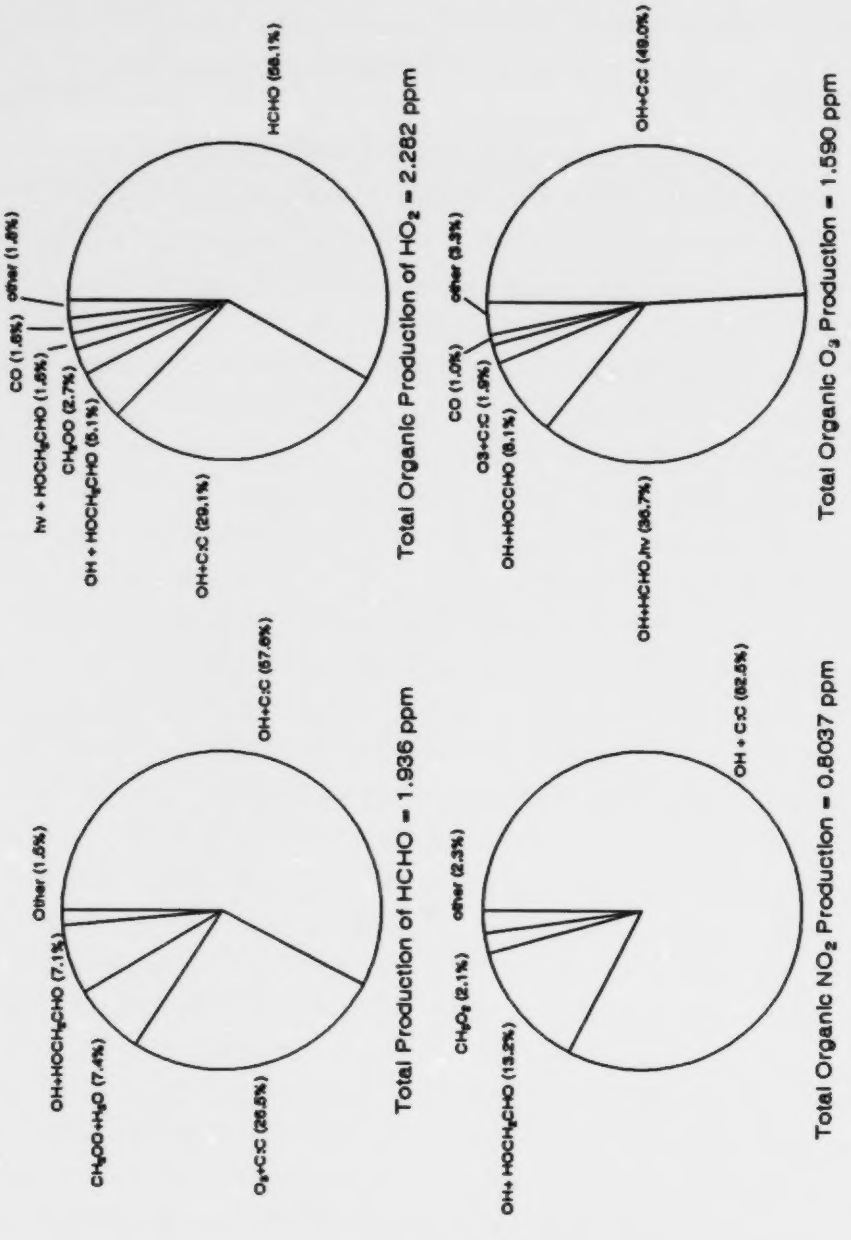

Figure 116. Relative Organic Contributions to HCHO, $HO_2^{\cdot}$, NO_2, and O_3 Predicted in 3.2 ppmC Ethene Experiment.

8

Explicit Mechanism: 3

This chapter briefly describes the chemistry of propene ($CH_2{=}CHCH_3$) and the subsequent chemistry of propene's reaction products that are not already included in the mechanism. The latter items are the C_2-Criegee chemistry.

The reaction labels for the various modules described here are:

- ▷ **O2** – propene reactions
- ▷ **BR2** – C_1 Criegee biradical reactions

The propene chemistry uses the formaldehyde and acetaldehyde chemistry in the IMEC. In addition, as we shall see below, propene chemistry requires glycoaldehyde and glyoxal chemistry, as well as, the **BR1**-Criegee chemistry already described in earlier chapters.

O3 = Propene Chemistry

Like ethene, there are four types of reactions that lead to loss of propene:

a) O(3P) attack,

b) $^{\cdot}OH$ attack,

c) $NO_3^{\cdot}$ attack, and

d) O_3 attack.

Because the first three types of reactions are so similar to the reactions already described for ethene and the data sources for the rate constants are essentially the same, we will omit the reaction-by-reaction description of these modules. There is little disagreement about these reactions. The complete listing for the explicit mechanism is given in Appendix A and the reader can consult this appendix for the details. Here we will describe the O_3 attack reactions and the subsequent C_2-Criegee reactions for which there are a number of highly uncertain reaction pathways.

O3.d = Ozone+Propene Chemistry

O3d.1

$$O_3 + CH_2{=}CHCH_3 \longrightarrow H_2C(OOO)CHCH_3$$

This reaction and rate constant are from Atkinson, 1989:

$$k = 1.32 \times 10^{-14} e^{-2105/T} \quad \text{cm}^3\text{-molecules}^{-1}\text{-s}^{-1}$$

O3d.2a $H_2C(OOO)CHCH_3 \longrightarrow CH_3HC{=}O + f^{Pa}_{dec}\ [{}^{\cdot}CH_2OO^{\cdot}]^{*} + f^{Pa}_{Crig}\ {}^{\cdot}CH_2OO^{\cdot}$

O3d.2b $H_2C(OOO)CHCH_3 \longrightarrow H_2C{=}O + f^{Pb}_{dec}\ [CH_3^{\cdot}CH_2OO^{\cdot}]^{*} + f^{Pb}_{Crig}\ CH_3^{\cdot}CH_2OO^{\cdot}$

These reactions and yields of stabilized Criegee radicals are from Hatakeyama, *et al.*[51]:

$$f^{Pa}_{dec} = 0.610$$
$$f^{Pa}_{Crig} = 0.390$$
$$f^{Pb}_{dec} = 0.185$$
$$f^{Pb}_{Crig} = 0.815$$

The rate constants used are not important as long as they are fast:

$$k_a = k_b = 2 \times 10^3 \quad \text{s}^{-1}$$

Here we assume, as others have, that the two decomposition pathways have equal probabilities.

BR2 = Two Carbon Criegee Biradical Chemistry

This chemistry is recognized as being uncertain.[26] The CB4 mechanism follows the original Atkinson and Lloyd, 1984[19] recommendation, and Jeffries, *et al.*[4] found that CB4 simulations were more reactive than propene experiments. Carter, *et al.*[23], also found that the Atkinson and Lloyd recommendations for the propene+ozone reactions caused an overestimation of reactivity in propene-NO_x chamber simulations, so they made an *ad hoc* adjustment to the radical yields of the Criegee biradicals. That is, they reduced the carbon forming radicals by almost a factor of two compared to the Atkinson and Lloyd recommendation, and assumed that the carbon difference was in the form of non-radical, non-reactive compounds.

Two recent kinetics studies, one by Niki, *et al.*[62] and one by Martinez and Herron[63] may give some insight to this problem. Both groups investigated the reaction of O_3 with tetramethylethylene (TME), Niki and co-workers using FTIR at 700 torr and Martinez and co-workers using mass spectrometry at 4 torr. Both groups concluded that a significant part of the Criegee reaction pathway involves hydrogen migration to produce a hydroperoxide that further rearranges to produce hydroxyacetone, a species observed by both investigators. Other products were also identified, but each investigator proposed slightly different mechanisms to account for these products. The key element in both of their proposed mechanisms was the ability of the dioxy group on the Criegee to abstract a hydrogen from a terminal methyl group, forming a double bond between the two carbons and a hydroperoxide bond. Here we extend this hydrogen abstraction mechanism to the formed in the O_3+propene reaction and suggest that it too would form a hydroperoxide should would be capable of undergoing a similar series of reactions as was postulated in Niki *et al.*, and Martinez and Herron studies.

Figure 117 shows the proposed two-carbon Criegee mechanism. The path labelled 'Niki' represents the mechanism prefered by Niki, *et al.*, and the path labelled 'M&H' represents the majority of the pathway preferred by Martinez and Herron. The relative ratios in the 'M&H' path were obtained by Martinez and Herron by fitting a complex model to the TME product observations. The 'M&H' mechanism also has a significant decomposition pathway of the Criegee leading to acetone and O(3P), but the Niki *et al.*, work showed that this most likely did not occur. Niki *et al.* justified their $^{\cdot}OH$-producing pathway by the need to fit their observed stoichiometry of 1.7:1 for TME:O_3. In a system containing high concentrations of O_3, however, $HO_2^{\cdot}$ is also rapidly converted to $^{\cdot}OH$, so the stoichiometry alone is not justification for producing large amounts of $^{\cdot}OH$. Niki *et al.*'s product distribution is dependent upon the NO_x in the system, but Martinez and Hurron's is not.

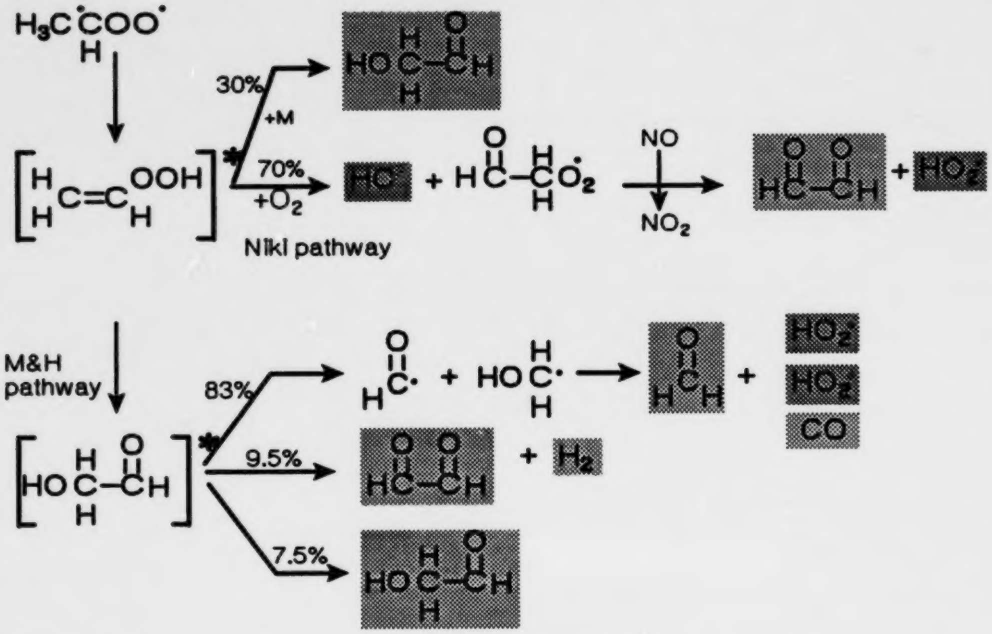

Figure 117. Mechanism for Two Carbon Creigee Reaction .

We will present our proposed mechanism, which is a blend of the two major pathways shown in Figure 117. Then we will show the simulation of a nighttime O_3+propene experiment.

BR2.1a $[CH_3^{\cdot}CH_2OO^{\cdot}]^* \longrightarrow HC(=O)CH_2O_2^{\cdot} + {}^{\cdot}OH$
BR2.1b $[CH_3^{\cdot}CH_2OO^{\cdot}]^* \longrightarrow H_2C{=}O + 2\,HO_2^{\cdot} + CO$
BR2.1c $[CH_3^{\cdot}CH_2OO^{\cdot}]^* \longrightarrow (HC{=}O)_2 + H_2$
BR2.1d $[CH_3^{\cdot}CH_2OO^{\cdot}]^* \longrightarrow HOCH_2HC{=}O$

These reactions and relative rate constants are from the 'M&H' study, except for reaction *a* which is from the Niki study:

$$k_a = 2.0 \times 10^3 \times \mathrm{fBR2oh} \quad s^{-1}$$
$$k_b = 2.0 \times 10^3 \times \mathrm{fBR2rad} \quad s^{-1}$$
$$k_c = 2.0 \times 10^3 \times \mathrm{fBR2gly} \quad s^{-1}$$
$$k_d = 2.0 \times 10^3 \times \mathrm{fBR2gald} \quad s^{-1}$$

BR2.2a $HC(=O)CH_2O_2^{\cdot} + NO \longrightarrow NO_2 + (HC=O)_2 + HO_2^{\cdot}$
BR2.2b $HC(=O)CH_2O_2^{\cdot} + NO_2 \longrightarrow HC(=O)CH_2O_2NO_2$
BR2.2c $HC(=O)CH_2O_2NO_2 \longrightarrow HC(=O)CH_2O_2^{\cdot} + NO_2$

These reactions are from Niki:

k_a =RO2NORATE
$k_b = 8 \times 10^{-12}$ cm^3-molecules^{-1}-s^{-1}
$k_c = 4.8 \times 10^{+17} e^{-13330/T}$ cm^3-molecules^{-1}-s^{-1}

BR2.2c $HC(=O)CH_2O_2^{\cdot} + HO_2^{\cdot} \longrightarrow f_{ald}\,((HC=O)_2 + H_2O) + f_{per}\,HC(=O)CH_2OOH$

Based upon **P1.9**:

k = RO2HO2RATE

BR2.3a $CH_3^{\cdot}CH_2OO^{\cdot} + NO \longrightarrow NO_2 + CH_3HC=O$
BR2.3b $CH_3^{\cdot}CH_2OO^{\cdot} + NO_2 \longrightarrow NO_3^{\cdot} + CH_3HC=O$
BR2.3c $CH_3^{\cdot}CH_2OO^{\cdot} + HO_2^{\cdot} \longrightarrow CH_3HC=O + {}^{\cdot}OH$

BR2.3d $CH_3^{\cdot}CH_2OO^{\cdot} + H_2O \longrightarrow f^{BR}_{acid}\,(CH_3C(=O)OH + H_2O) + f^{BR}_{ald}\,(CH_3HC=O + H_2O_2)$
BR2.3f $CH_3^{\cdot}CH_2OO^{\cdot} + H_2C=O \longrightarrow C_2\text{-}C_1\text{-Ozonide}$
BR2.3g $CH_3^{\cdot}CH_2OO^{\cdot} + CH_3HC=O \longrightarrow C_2\text{-}C_2\text{-Ozonide}$
BR2.3h ${}^{\cdot}CH_2OO^{\cdot} + CH_3HC=O \longrightarrow C_1\text{-}C_2\text{-Ozonide}$
BR2.3i $CH_3^{\cdot}CH_2OO^{\cdot} + CO \longrightarrow CH_3C(=O)O(O=)CH$

k_a =RO2NORATE
$k_b = 2.4 \times 10^{-16}$ cm^3-molecules^{-1}-s^{-1}
k_c =RO2HO2RATE
$k_d = 4.0 \times 10^{-17}$ cm^3-molecules^{-1}-s^{-1}
$k_f = 2.0 \times 10^{-14}$ cm^3-molecules^{-1}-s^{-1}
$k_g = 2.0 \times 10^{-14}$ cm^3-molecules^{-1}-s^{-1}
$k_h = 2.0 \times 10^{-14}$ cm^3-molecules^{-1}-s^{-1}
$k_i = 1.3 \times 10^{-16}$ cm^3-molecules^{-1}-s^{-1}

BR2.4 $\cdot OH + CH_3C(=O)OH \longrightarrow CH_3O_2^{\cdot} + CO_2 + H_2O$

This reaction and rate constant are from Atkinson, 1989:

$$k = 8.48 \times 10^{-13} \quad \text{cm}^3\text{-molecules}^{-1}\text{-s}^{-1}$$

Nighttime Propene Simulation

Figure 118 showns a simulation of a dark reaction between O_3 and propene. When the Niki mechanism was used to simulated this experiment, no amount of adjustment could produce the correct amount of HCHO. Similarly when only the M&H paths were used, too much HCHO was produced. While the proposed mechanism is able to reasonably fit the propene, $CH_3HC{=}O$, and HCHO observations, we can not fit the O_3 data. Clearly more laboratory experiments are needed before we can fully explain this system.

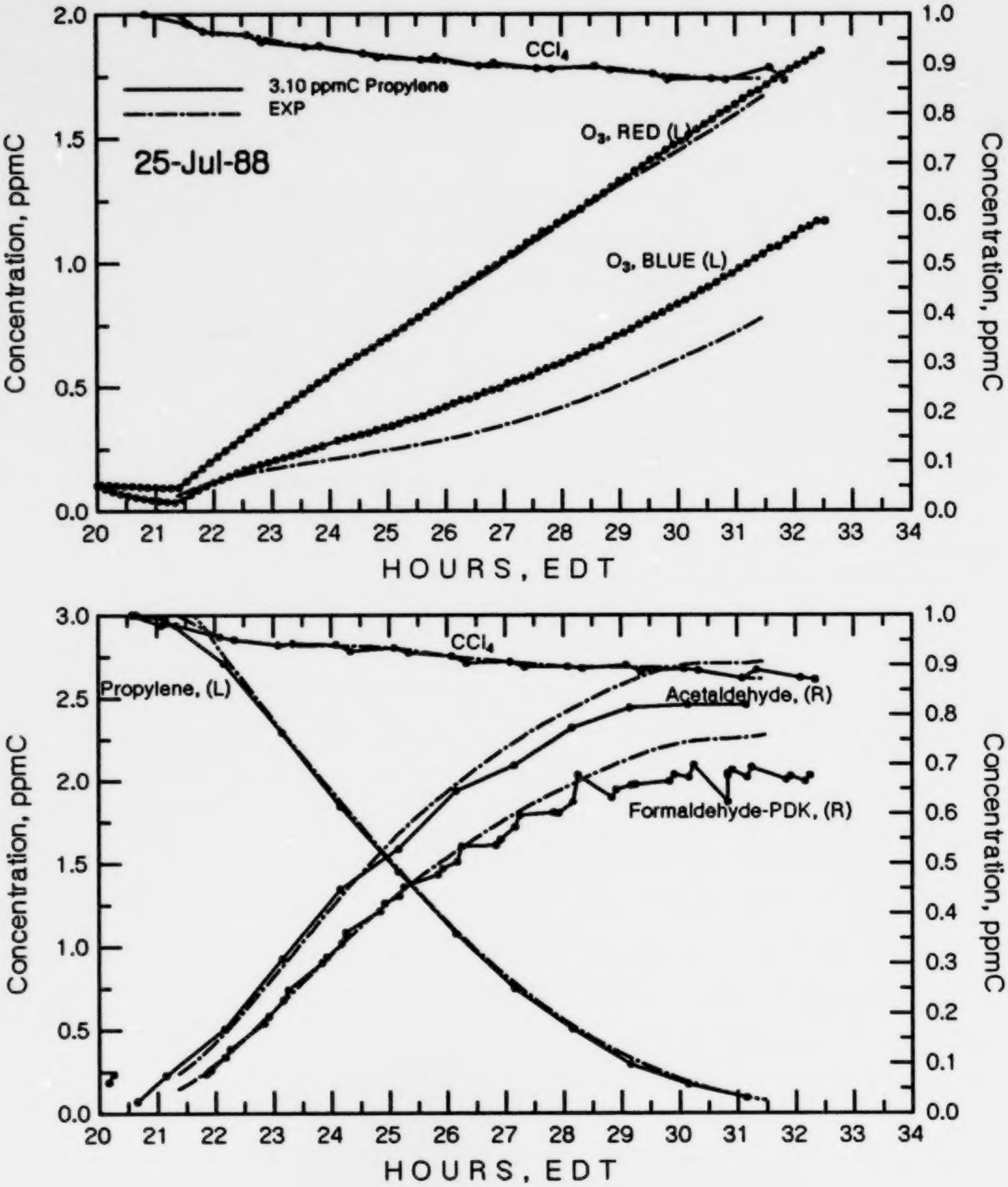

Figure 118. Ozone injected equally into both RED and BLUE chamber; RED chamber had background air and BLUE chamber had 3.1 ppmC propene. Solid lines and point are data; dashed lines are simulations with EXP model.

9

Chamber Modeling: 3

In this chapter, the combined inorganic, carbonyl, propene, glycoaldehyde, glyoxal mechanism (PROEXP) is used to simulate several propene–NO_x experiments. Our mechanism includes the speculative two- carbon Criegee chemistry discussed in the previous chapter. Because so little kinetics data are available on these reactions, and because these reactions become important in higher concentration propene experiments in which a significant amount of propene is consumed by O_3, we have much lower expectations as to how well the model predictions and chamber observations will agree. Our goal here is to show the extent to which HCHO yields in a higher alkene can be explained using an explicit mechanism that incorporates the known kinetics detail, but which, because of lack of certain kinetics data, still contains some highly uncertain reactions. The more simple representations incorporated in the air quality photochemical mechanisms and based on older kinetics data, are most likely to be less accurate than the explicit mechanism used here. *Ad hoc* adjustments such as those used by Carter, *et al.*,[23] of course, can not explain the observations, but merely fit them. Thus the inability of such mechanisms to fit the chamber HCHO data are no real challenges to the observations and do little to expand our understanding of the propene chemistry system. As we shall see in a later chapter, olefins are significant contributor to HCHO production in urban-like simulations, and propene's chemistry is used both as itself and as the basis for the chemistry of the higher alkenes, so errors in the propene mechanism are likely to impact accurate predictions of HCHO in urban simulations significantly.

The model-observation comparisons begin with a series of side-to-side ethene vs. propene experiments as a bridge to the previous chamber modeling. We then proceed to differential propene concentration experiments and we end with a propene vs. 1-butene experiment. Since propene is sometimes used as a surrogate for higher alkenes, we modeled both sides of the latter experiment as propene.

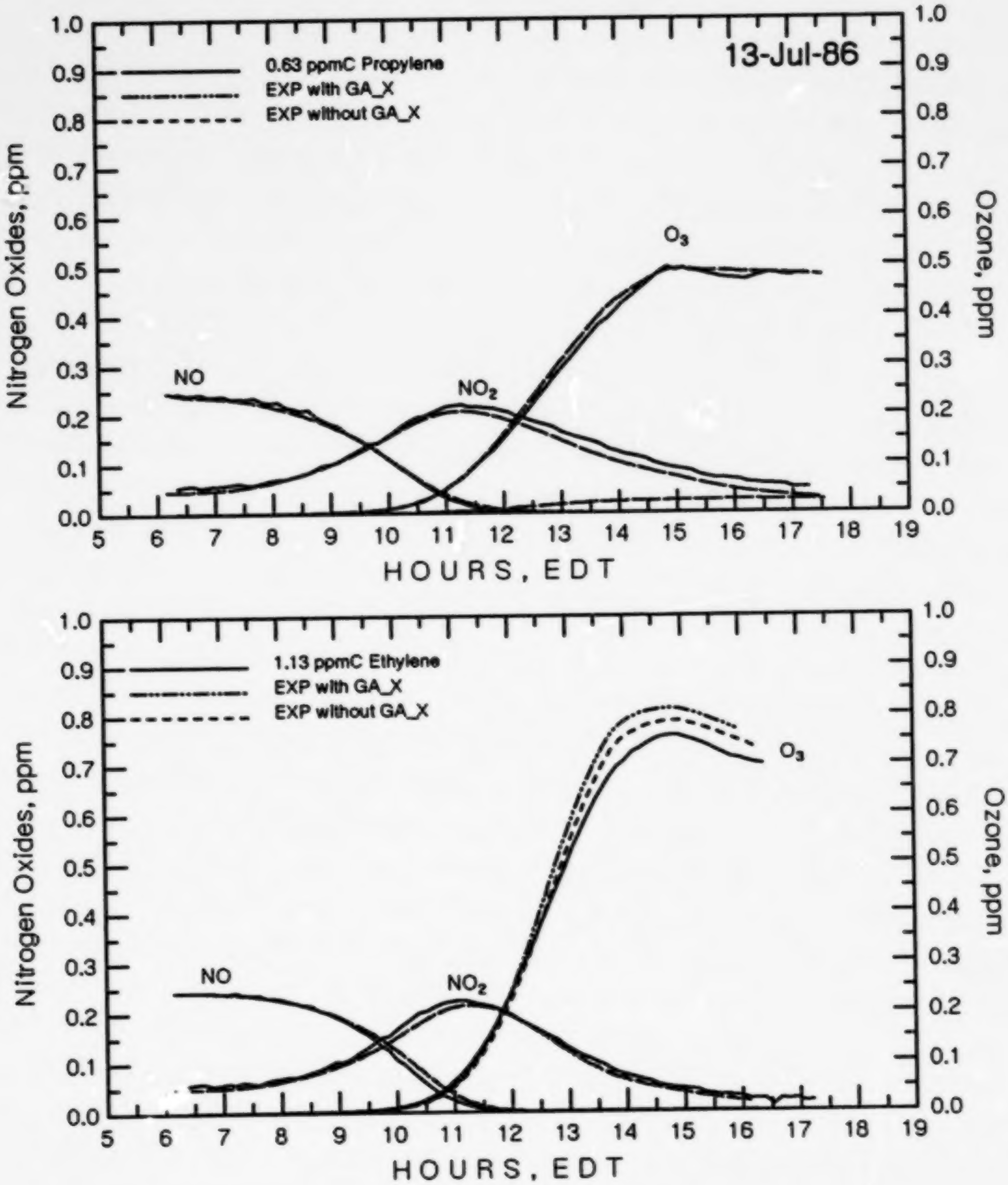

Figure 119. Simulation conditions: top: HONO=3 ppb, BVOC=45 ppb, WallOH= 0.5×10^{-3}, k[WallN2O5b]= 4×10^{-4}; bottom: HONO=3 ppb, BVOC=45 ppb, WallOH= 0.5×10^{-3}, k[WallN2O5b]= 4×10^{-4}. Solid lines are data; dashed lines are model simulations.

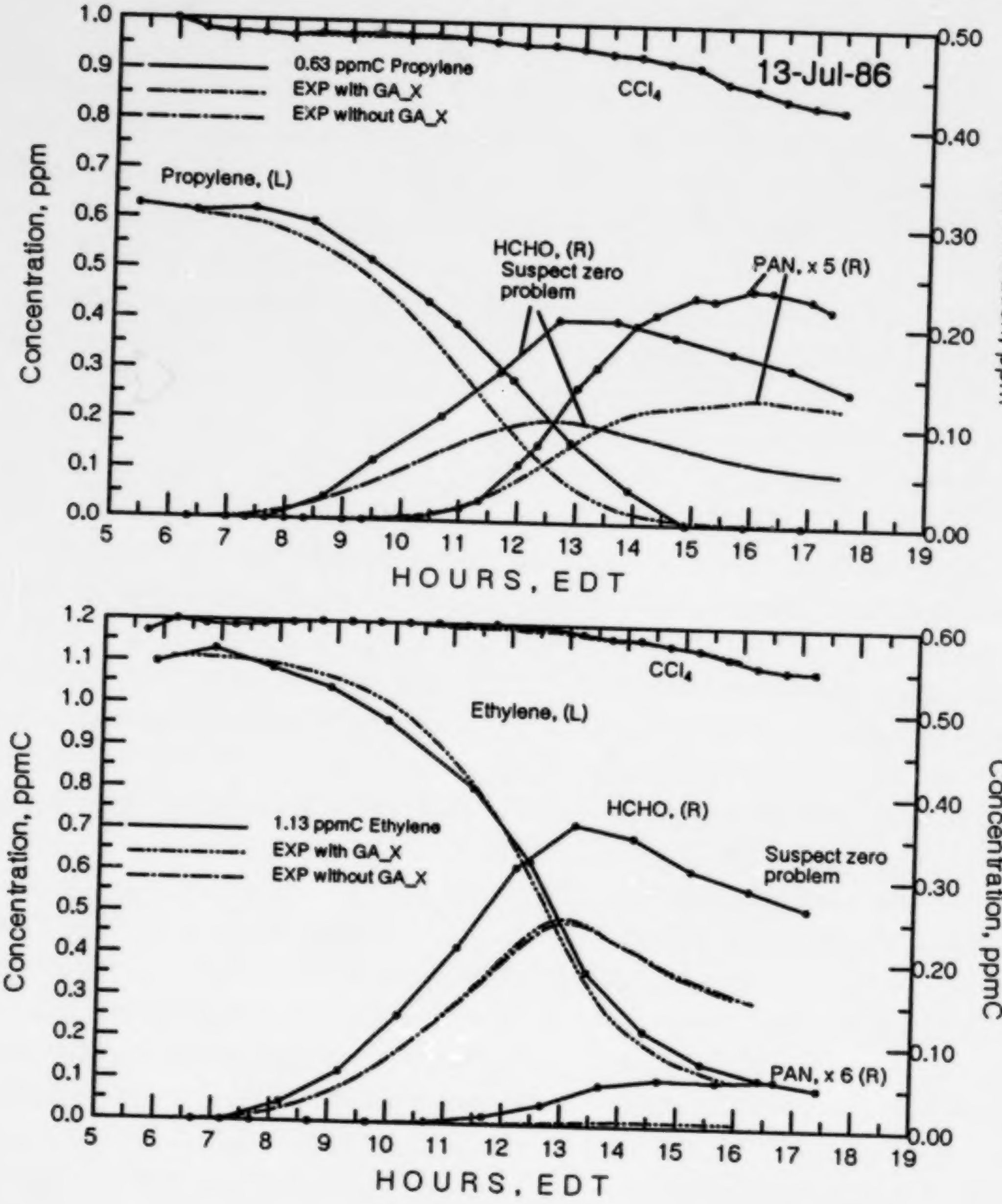

Figure 120. Simulation conditions: top: HONO=3 ppb, BVOC=45 ppb, WallOH= 0.5×10^{-3}, k[WallN2O5b]= 4×10^{-4}; bottom: HONO=3 ppb, BVOC=45 ppb, WallOH= 0.5×10^{-3} k[WallN2O5b]= 4×10^{-4}. Solid lines are data; dashed lines are model simulations.

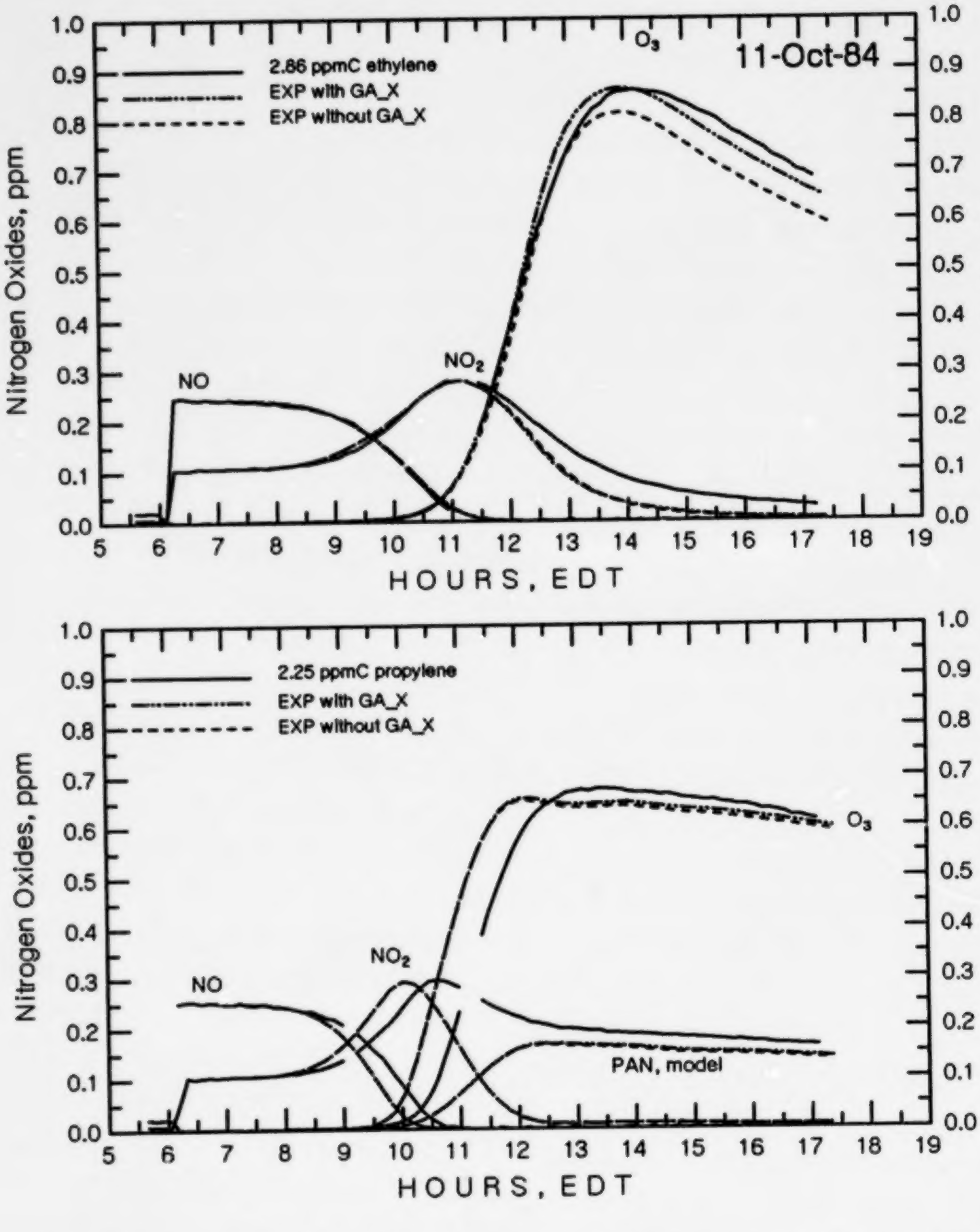

Figure 121. Simulation conditions: top: HONO=7 ppb, BVOC=20 ppb, WallOH= 0.8×10^{-3}, k[WallN2O5b]= 4×10^{-4}; bottom: HONO=7 ppb, BVOC=20 ppb, WallOH= 0.8×10^{-3}, k[WallN2O5b]= 4×10^{-4}. Solid lines are data; dashed lines are model simulations.

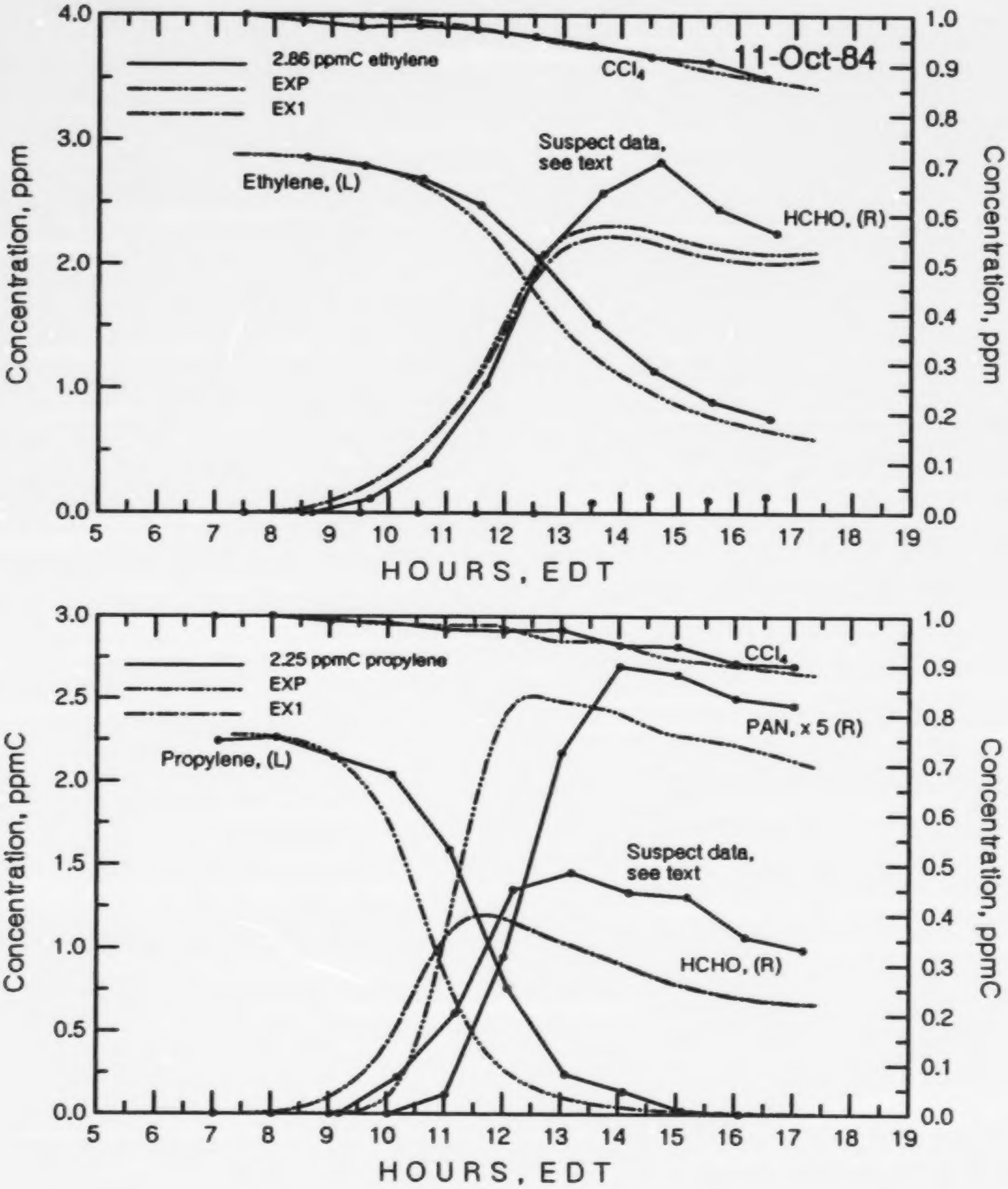

Figure 122. Simulation conditions: top: HONO=7 ppb, BVOC=20 ppb, WallOH= 0.8×10^{-3}, k[WallN2O5b]= 4×10^{-4}; bottom: HONO=7 ppb, BVOC=20 ppb, WallOH= 0.8×10^{-3}, k[WallN2O5b]= 4×10^{-4}. Solid lines are data; dashed lines are model simulations.

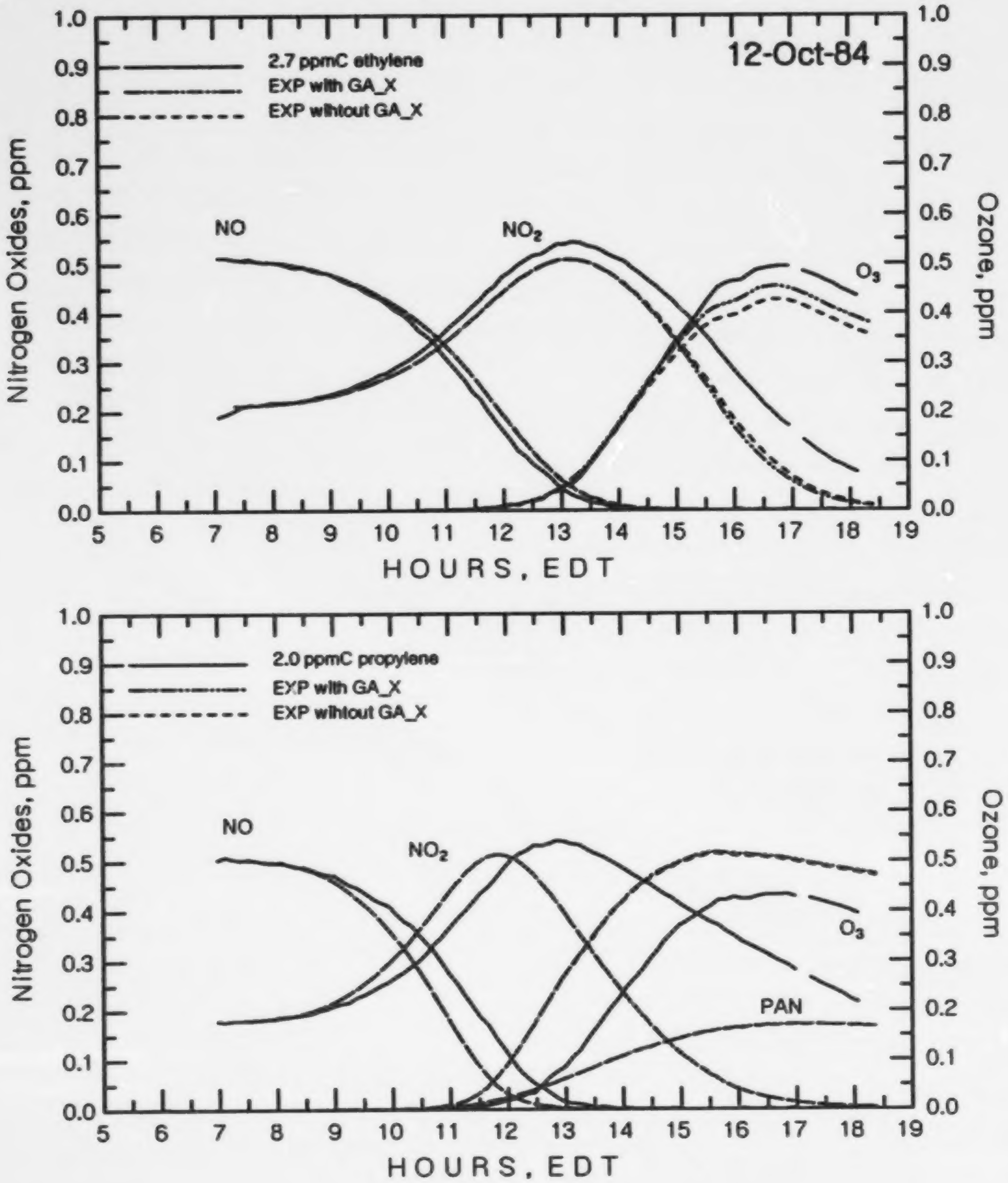

Figure 123. Simulation conditions: top: HONO=6 ppb, BVOC=20 ppb, WallOH= 0.4×10^{-3}, k[WallN2O5b]= 4×10^{-4}; bottom: HONO=6 ppb, BVOC=20 ppb, WallOH= 0.4×10^{-3}, k[WallN2O5b]= 4×10^{-4}. Solid lines are data; dashed lines are model simulations.

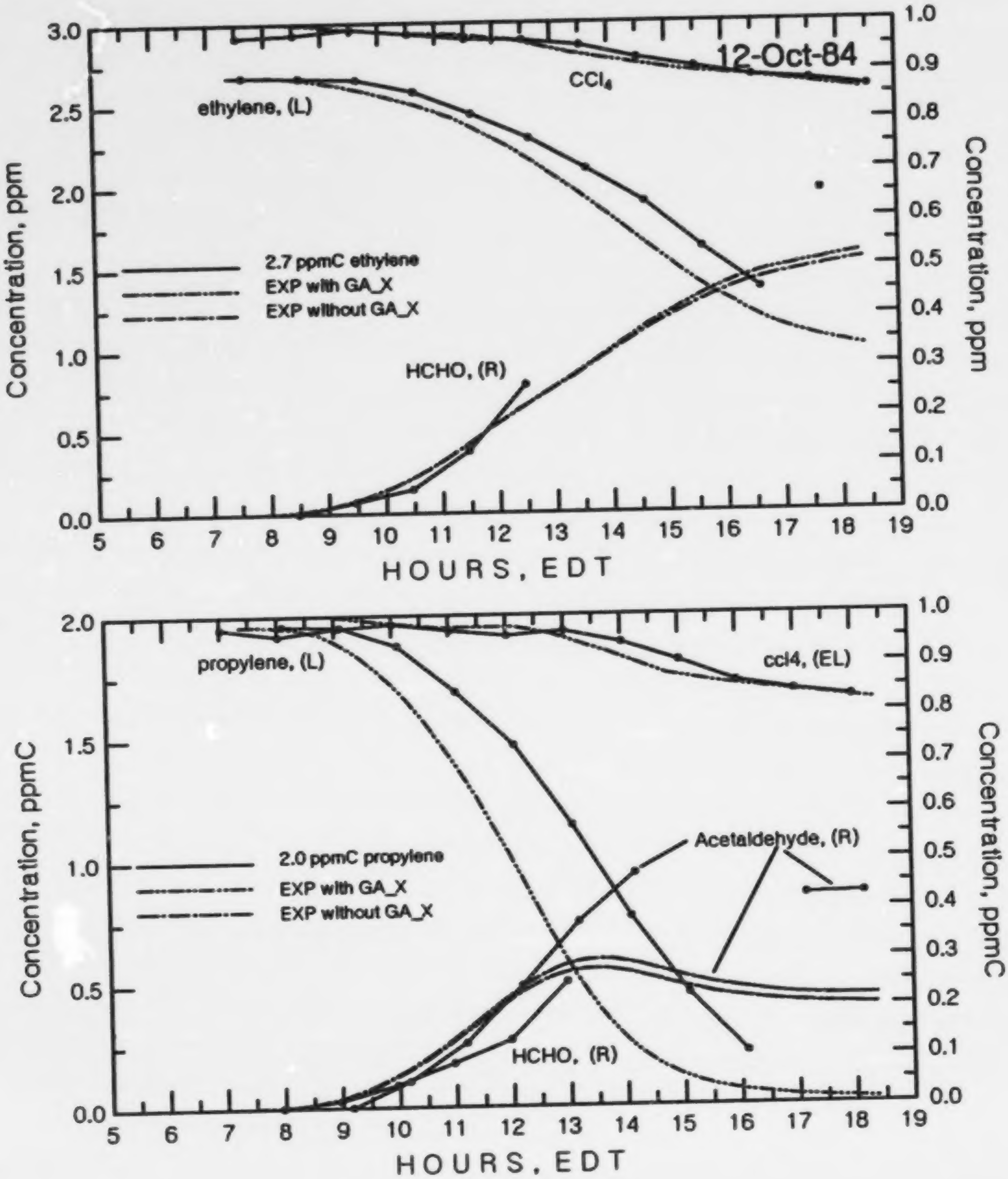

Figure 124. Simulation conditions: top: HONO=6 ppb, BVOC=20 ppb, WallOH= 0.4×10^{-3}, k[WallN2O5b]= 4×10^{-4}; bottom: HONO=6 ppb, BVOC=20 ppb, WallOH= 0.4×10^{-3}, k[WallN2O5b]= 4×10^{-4}. Solid lines are data; dashed lines are model simulations.

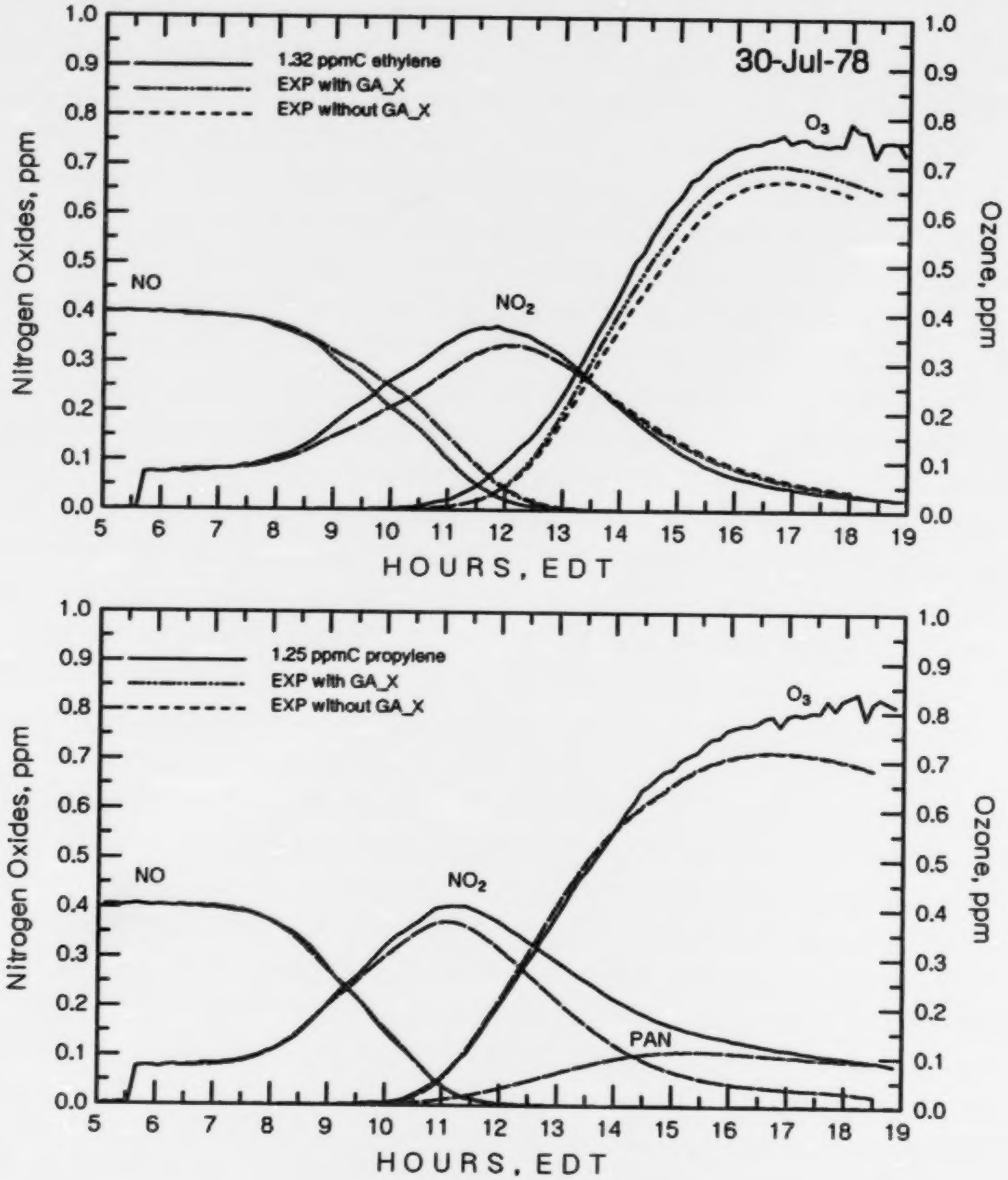

Figure 125. Simulation conditions: top: HONO=20 ppb, BVOC=45 ppb, WallOH= 2.5×10^{-3}, k[WallN2O5b]= 4×10^{-5}; bottom: HONO=20 ppb, BVOC=45 ppb, WallOH= 2.5×10^{-3}, k[WallN2O5b]= 4×10^{-5}. Solid lines are data; dashed lines are model simulations.

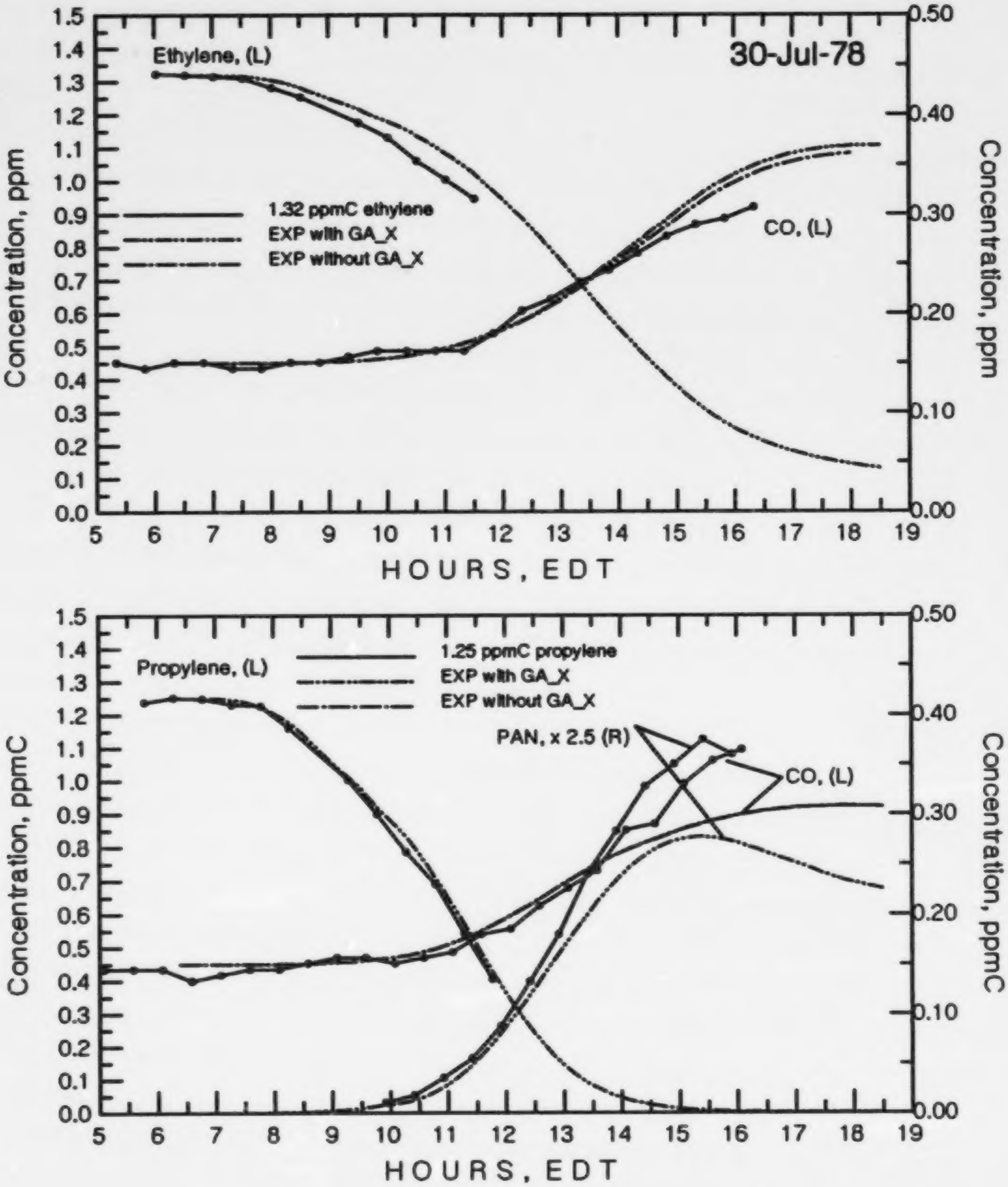

Figure 126. Simulation conditions: top: HONO=20 ppb, BVOC=45 ppb, WallOH= 2.5×10^{-3}, k[WallN2O5b]= 4×10^{-5}; bottom: HONO=20 ppb, BVOC=45 ppb, WallOH= 2.5×10^{-3}, k[WallN2O5b]= 4×10^{-5}. Solid lines are data; dashed lines are model simulations.

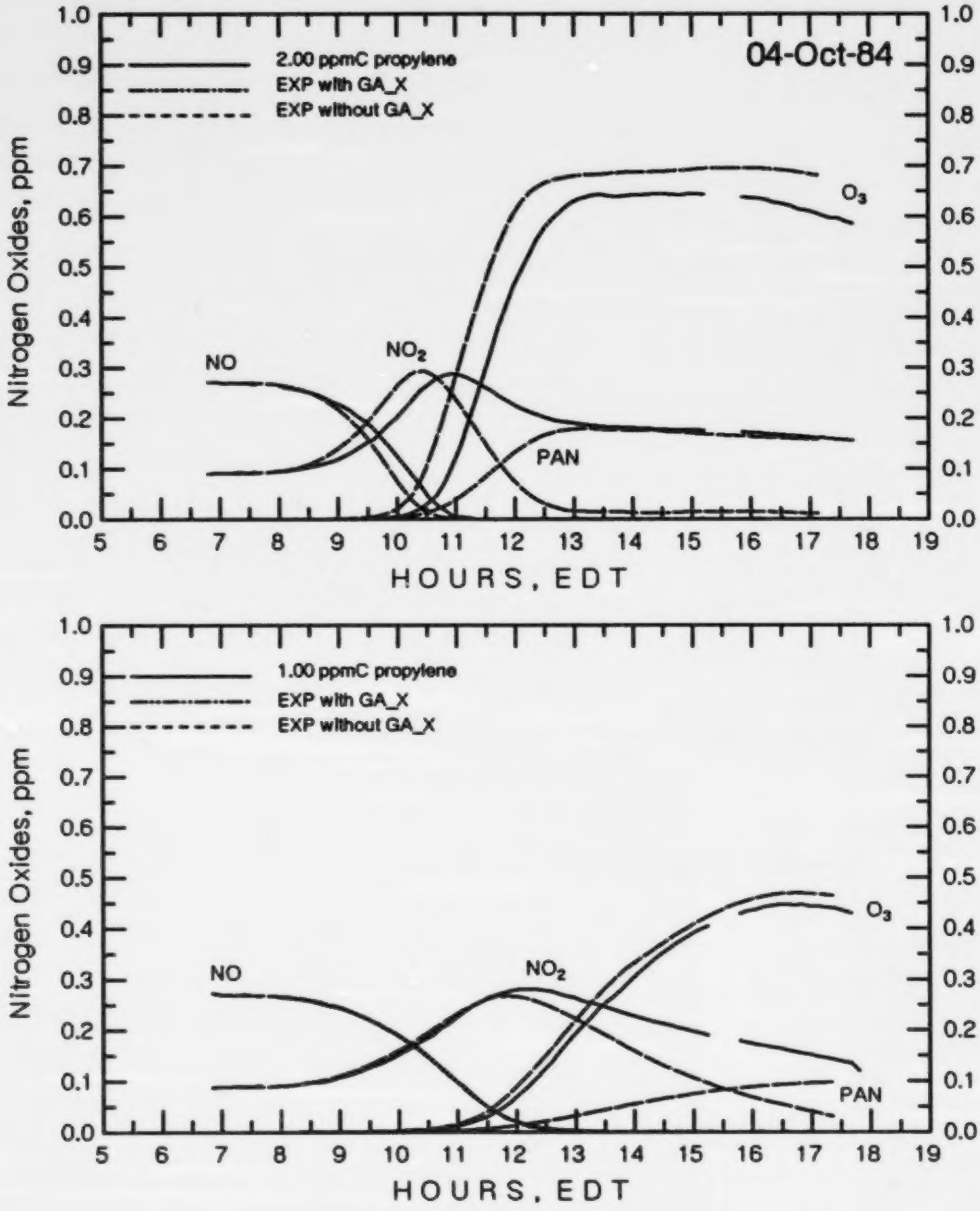

Figure 127. Simulation conditions: top: HONO=3 ppb, BVOC=10 ppb, WallOH= 0.5×10^{-3}, k[WallN2O5b]= 4×10^{-4}; bottom: HONO=3 ppb, BVOC=10 ppb, WallOH= 0.5×10^{-3}, k[WallN2O5b]= 4×10^{-4}. Solid lines are data; dashed lines are model simulations.

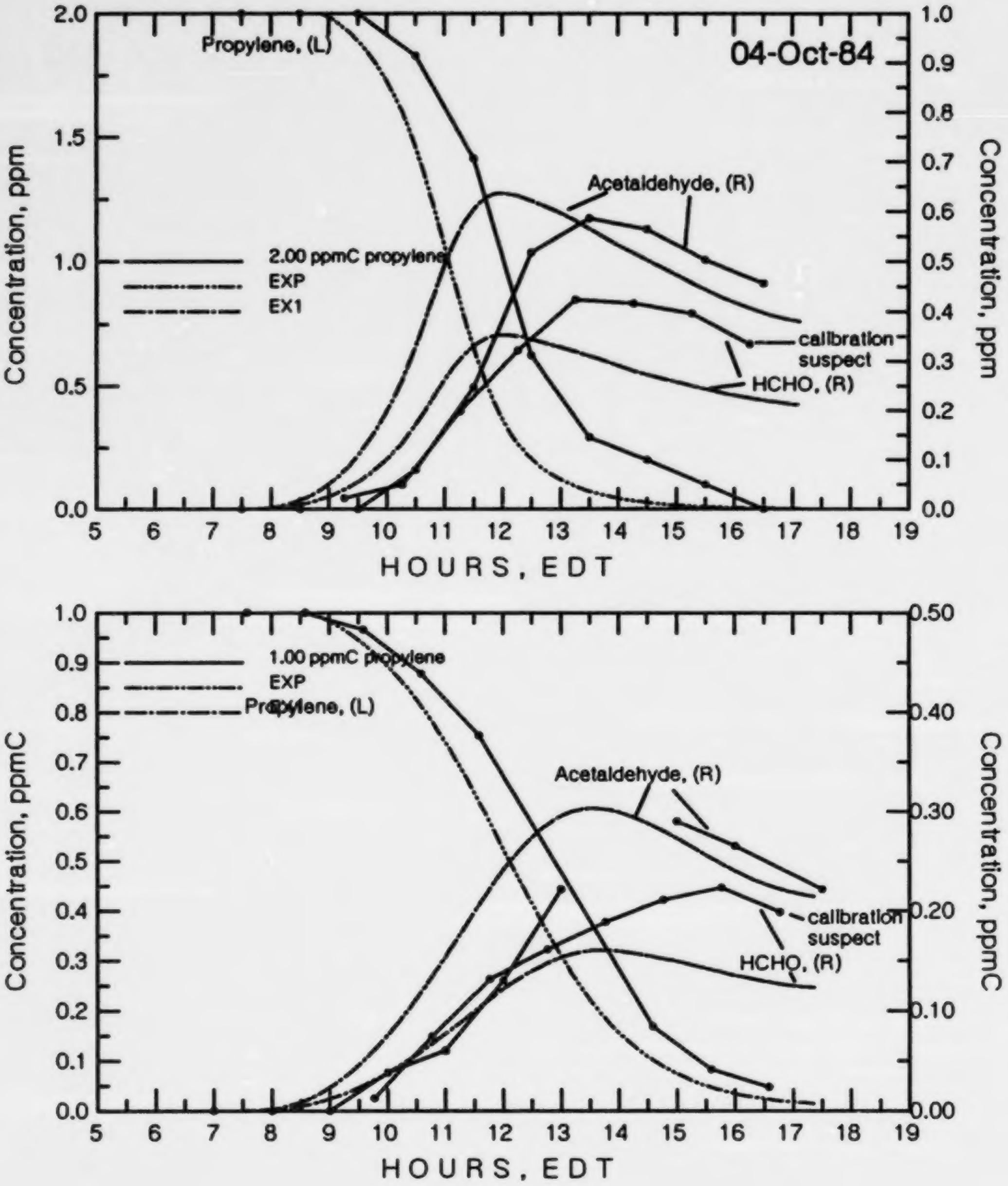

Figure 128. Simulation conditions: top: HONO=3 ppb, BVOC=10 ppb, WallOH= 0.5×10^{-3}, k[WallN2O5b]= 4×10^{-4}; bottom: HONO=3 ppb, BVOC=10 ppb, WallOH= 0.5×10^{-3}, k[WallN2O5b]= 4×10^{-4}. Solid lines are data; dashed lines are model simulations.

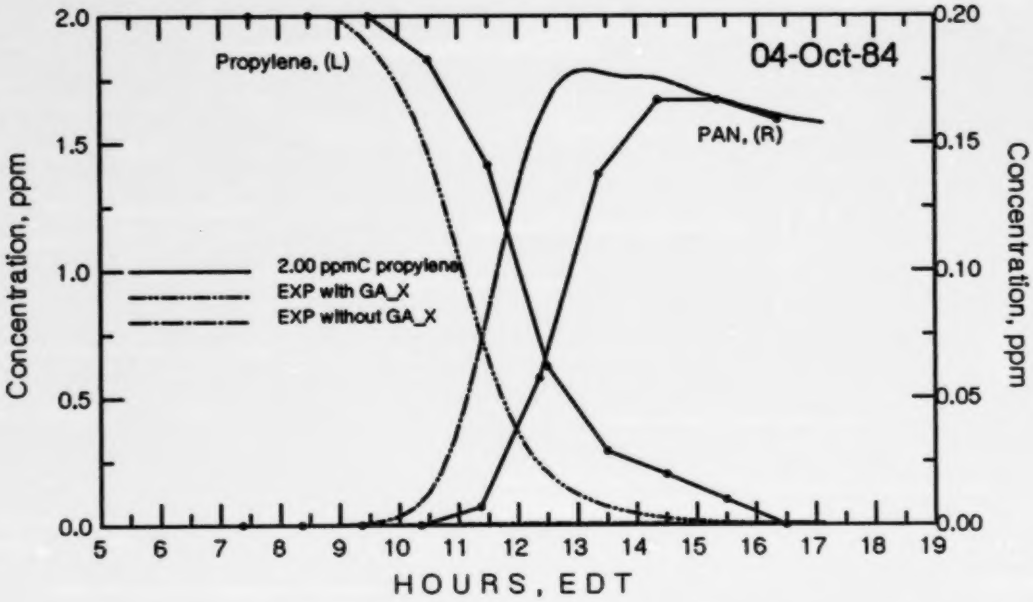

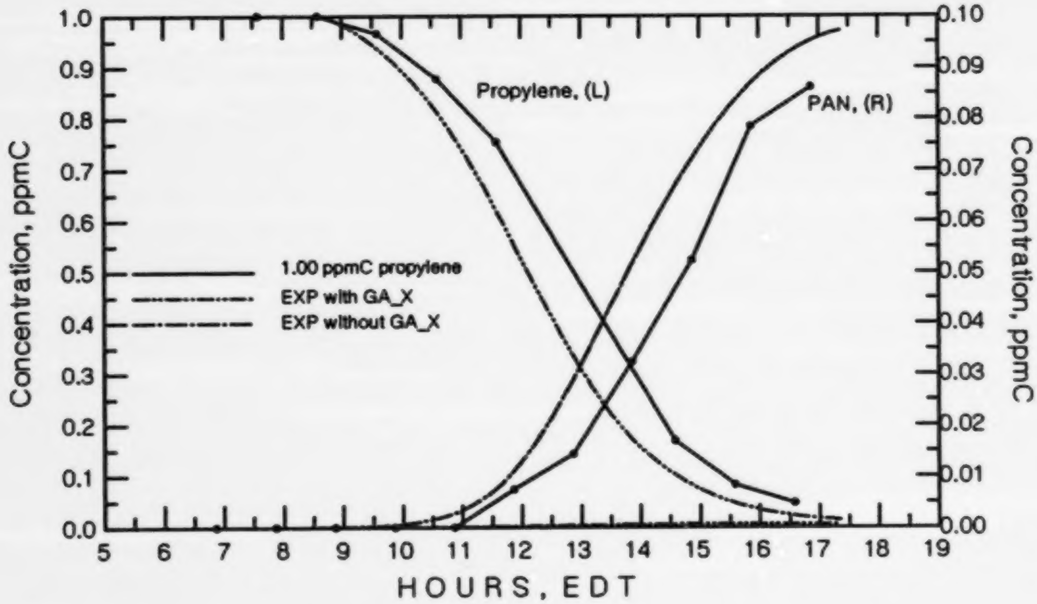

Figure 129. Simulation conditions: top: HONO=3 ppb, BVOC=10 ppb, WallOH= 0.5×10^{-3}, k[WallN2O5b]= 4×10^{-4}; bottom: HONO=3 ppb, BVOC=10 ppb, WallOH= 0.5×10^{-3}, k[WallN2O5b]= 4×10^{-4}. Solid lines are data; dashed lines are model simulations.

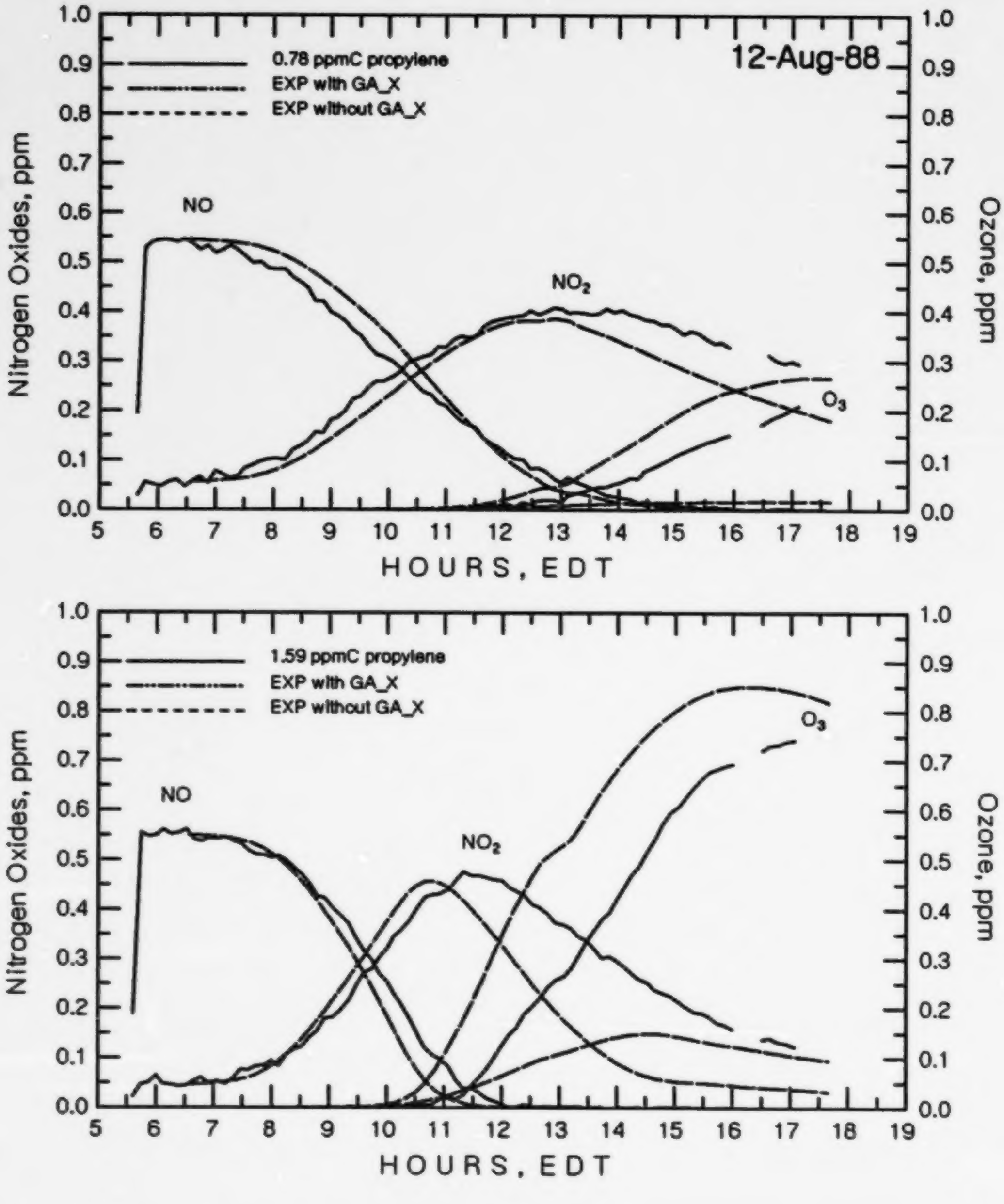

Figure 130. Simulation conditions: top: HONO=20 ppb, BVOC=55 ppb, WallOH= 2.5 × 10^{-3}; bottom: HONO=20 ppb, BVOC=55 ppb, WallOH= 2.5 × 10^{-3}. Solid lines are data; dashed lines are model simulations.

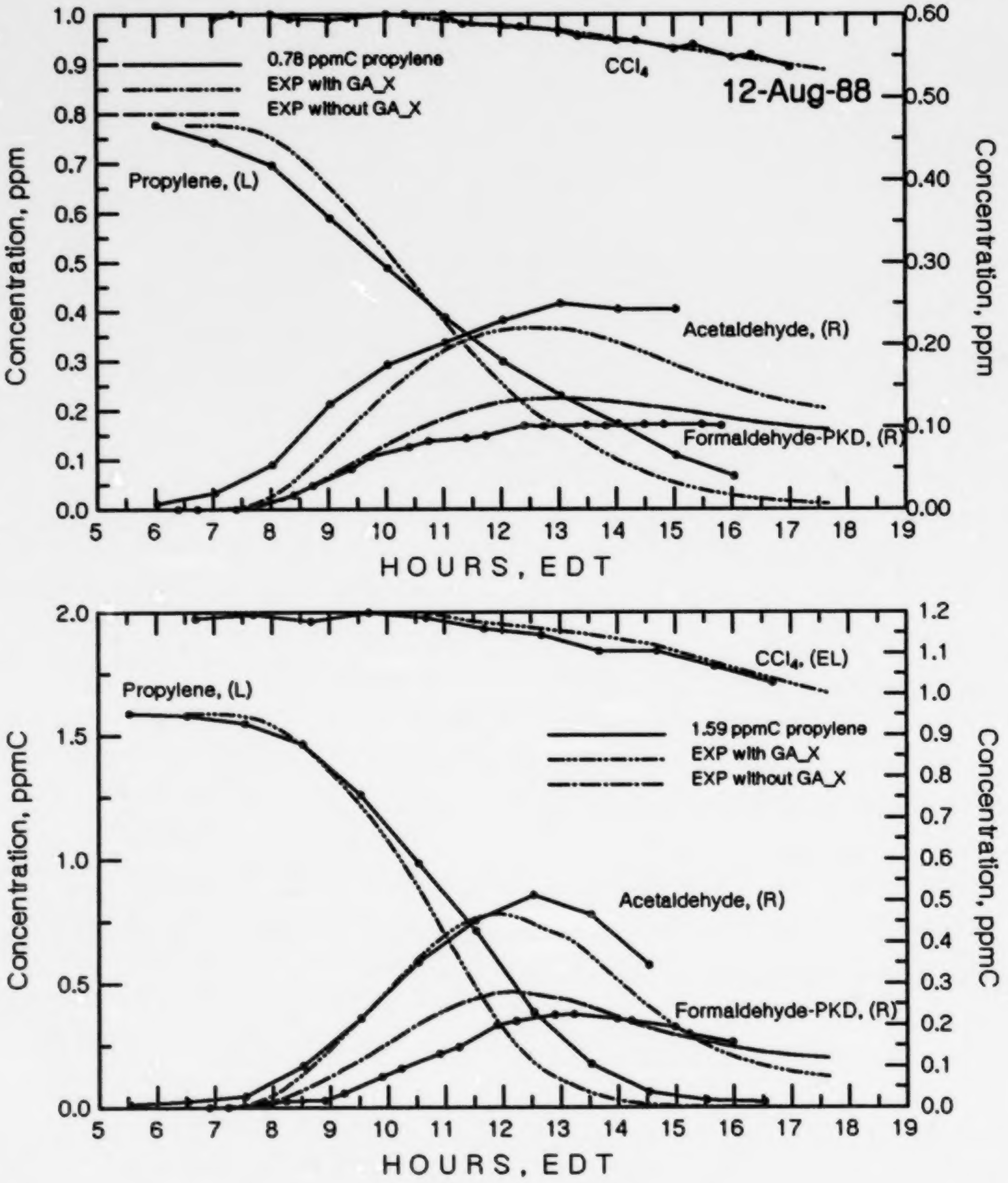

Figure 131. Simulation conditions: top: HONO=20 ppb, BVOC=55 ppb, WallOH= 2.5×10^{-3}; bottom: HONO=20 ppb, BVOC=55 ppb, WallOH= 2.5×10^{-3}. Solid lines are data; dashed lines are model simulations.

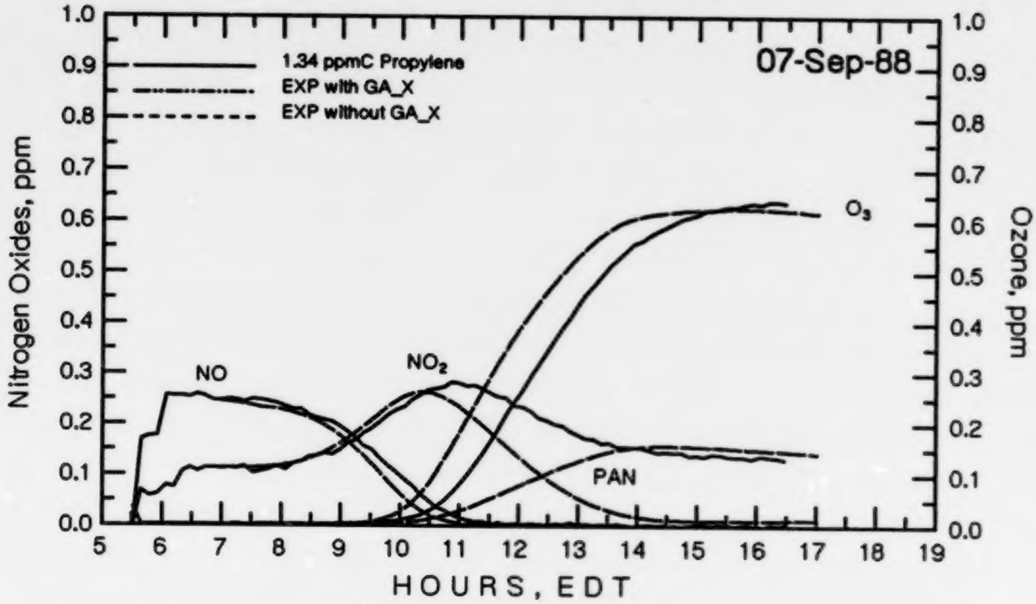

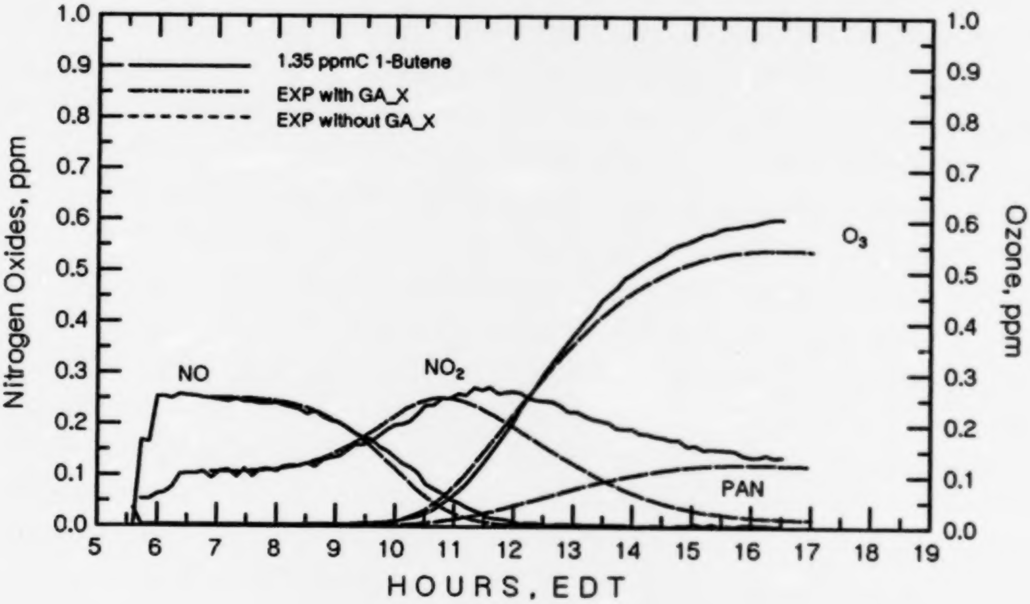

Figure 132. Simulation conditions: top: HONO=2 ppb, BVOC=55 ppb, WallOH= 2.5×10^{-3}; bottom: HONO=2 ppb, BVOC=55 ppb, WallOH= 2.5×10^{-3}. Solid lines are data; dashed lines are model simulations.

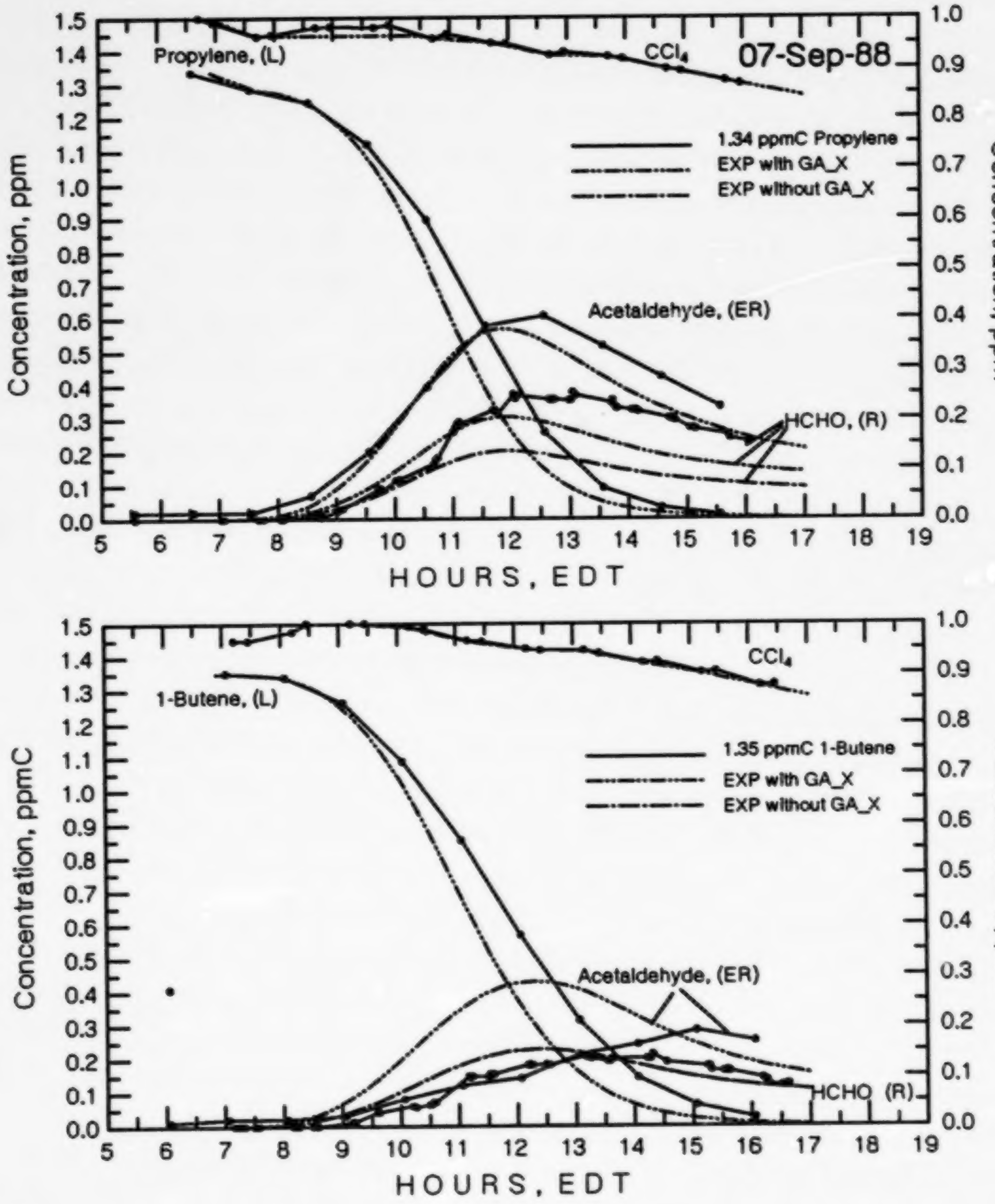

Figure 133. Simulation conditions: top: HONO=2 ppb, BVOC=55 ppb, WallOH= 2.5×10^{-3}; bottom: HONO=2 ppb, BVOC=55 ppb, WallOH= 2.5×10^{-3}. HCHO measurements missing.

Extent of "Reasonable Agreement"

There were four chamber halves containing ethene: two in July and two in October. In all four, the NO_x and O_3 time-profiles were well simulated. The predicted and observed ethene decays were matched in the July runs and the October simulations continued the trend shown in Chapter 7 of slightly too fast ethene consumption. The HCHO data in three of the four experiments is suspect, however, and it was missing in the fourth. The July 13, 1986 experiments continue a trend for HCHO data of that series: very high afternoon maxima. This was the series in which no zero-value was used on the CEA because it was being used elsewhere. As in the July 9, 1986 experiment, in the July 13 experiment, the CEA was zeroed on chamber vent air several hours *after* the experiments were over. We remain skeptical that the CEA may be exhibiting a large zero drift during the experiment that was undetected after the chamber had been vented and the instrument sampled background air for a long period. We have no method for confirming this hypothesis and so the data stand.

The explicit propene mechanism predicted O_3 either exactly or within 10% 7 out of 9 times and over predicted O_3 2 out of 9 times by 14% and 25%. The 7 best predicted experiments were low NO_x; the two experiments over-predicted were runs with $NO_x > 0.6$ppm, August 12, 1988 and October 12, 1984.

For those experiments with propene initial concentrations above 1.5 ppmC, the simulations were too fast and propene was consumed too early, sometimes by as much as 60 minutes. Thus, O_3, acetaldehyde, and HCHO were formed too early in these experiments. Rates of production, however, were very similar to observations, just displaced too early. Discounting the July 13, 1986 propene experiment with the questionable CEA data, and the October experiments with the highly questionable HCHO calibration, the HCHO net production was reasonably well simulated in the two remaining experiments, both conducted in 1988. It is hard to conclude that HCHO production is correctly represented in the explicit mechanism for propene by showing agreement with two experiments.

In the case of PAN, except for July 13, 1986, PAN magnitudes were well predicted, however, the time of PAN formation is much too early, but that is because the propene consumption is much to fast.

The 1-butene experiment was simulated as if 1-butene were propene. The simulation results agreed very well with observations of NO_x, O_3, butene, and HCHO. The timing in the simulation of this side of the dual experiment was nearly perfect, whereas, the propene simulation was too fast by 40 minutes.

The inclusion or exclusion of reaction **GA.X** had essentially no effect on the propene simulations.

Clearly there remains problems in explaining propene-NO_x chamber experiments and further progress will require additional laboratory data and additional secondary product measurements in the chamber, *e.g.*, formic and acetic acids, and glyoxal, as well as, the hydroxyl-propyl-nitrates.

10

CB4 Comparison

In this chapter, the explicit ethene and propene mechanisms are compared with the Carbon Bond Four mechanism using a few chamber experiments as baselines. After the plots are shown, we will show a mass balance analysis of one of the experiments.

We should note here that exactly the same conditions were used in both sets of simulations. Thus, for CB4, Moortgat's HCHO photolysis rates were used, not the Bass values used to develop CB4 and which we used in our previous testing of CB4.[4] In addition, we have combined the chamber specific reactions described in Chapter 5 with the CB4 reactions to make a mechanism suitable for simulating the UNC chamber. The input conditions for this chamber-dependent part of the model were also exactly the same.

CB4 Mechanism for Acetaldehyde, Ethene, and Propene

The mechanism for formaldehyde in CB4 is essentially identical to that used in the explicit mechanism.

Acetaldehyde

Only two of CB4's acetaldehyde reactions are listed here. All of the PAN reactions are given however.

ALD.1 $\mathrm{CCHO} \xrightarrow{h\nu} \mathrm{XO2} + 2\,\mathrm{HO_2^{\cdot}} + \mathrm{CO} + \mathrm{HCHO}$

ALD.3 $\mathrm{CCHO} + {}^{\cdot}\mathrm{OH} \longrightarrow \mathrm{C2O3}$

PAN.1 $\mathrm{C2O3} + \mathrm{NO} \longrightarrow \mathrm{NO_2} + \mathrm{XO2} + \mathrm{HCHO} + \mathrm{HO_2^{\cdot}}$

PAN.2 $\mathrm{C2O3} + \mathrm{NO_2} \longrightarrow \mathrm{PAN}$

PAN.3 $\mathrm{PAN} \longrightarrow \mathrm{C2O3} + \mathrm{NO_2}$

PAN.4 $\mathrm{C2O3} + \mathrm{C2O3} \longrightarrow 2\,\mathrm{XO2} + 2\,\mathrm{HCHO} + 2\,\mathrm{HO_2^{\cdot}}$

PAN.5 $\mathrm{C2O3} + \mathrm{HO_2^{\cdot}} \longrightarrow 0.79\,\mathrm{HCHO} + 0.79\,\mathrm{XO2} + 0.79\,\mathrm{HO_2^{\cdot}} + 0.79\,{}^{\cdot}\mathrm{OH}$

Reactions **ALD.1** to **PAN.3** have essentially the same products as those in the explicit mechanism. In the CB4 mechanism the rate constant for **PAN.2**, the PAN formation reaction, has a different activation energy than that used in the explicit mechanism because CB4's rate was based upon fitting warm and cold chamber experiments. For this reaction in the explicit mechanism, the experimentally determined, but unpublished, activation energy of Atkinson (personal communication by Carter) is used. The CB4 rate constants are

$$k_2 = 8.0 \times 10^{-20} e^{5500/T} = 8.3 \times 10^{-12}\mathrm{cm^3\text{-}molecules^{-1}\text{-}s^{-1}} \text{ at } 298^\circ\mathrm{K}$$
$$k_3 = 9.4 \times 10^{16} e^{-14000/T} = 3.7 \times 10^{-4}\mathrm{s^{-1}} \text{ at } 298^\circ\mathrm{K}$$

and the EXP rate constants for **PA1.2** and **PA1.3** are

$$k_2 = 6.05 \times 10^{-15} e^{2200/T} = 9.7 \times 10^{-12}\mathrm{cm^3\text{-}molecules^{-1}\text{-}s^{-1}} \text{ at } 298^\circ\mathrm{K}$$
$$k_3 = 1.73 \times 10^{16} e^{-13410/T} = 5.0 \times 10^{-4}\mathrm{s^{-1}} \text{ at } 298^\circ\mathrm{K}$$

(k_3 is an equivalent rate expression for the fall-off expression actually used for reaction **PA1.3**). Figure 134 shows the inverse-temperature/log plot of both sets of rates for both mechanisms. There is only a small difference in these rates for the two mechanisms over the temperature ranges used to compare the two mechanisms here so these reactions are not likely to account for differences seen between the two mechanisms.

In CB4, reaction **PAN.5** has very different products than either reaction **PA1.6** for peroxyacetyl radicals or **GA.8** for hydroxy-peroxyacetyl radicals in the explicit mechanism.

Ethene

Only two CB4 ethene reactions will be described here.

ETH.2 ${}^{\cdot}\mathrm{OH} + \mathrm{H_2C{=}CH_2} \longrightarrow \mathrm{XO2} + 1.56\,\mathrm{HCHO} + \mathrm{HO_2^{\cdot}} + 0.22 * \mathrm{CCHO}$

This one reaction represents all the chemistry in reactions **O2b.2** to **O2b.6**. There is no formation of hydroxy-ethyl-nitrate. In addition, there *is* no glycoaldehyde in the CB4 mechanism. Instead acetaldehyde (CCHO) is used as a surrogate. In

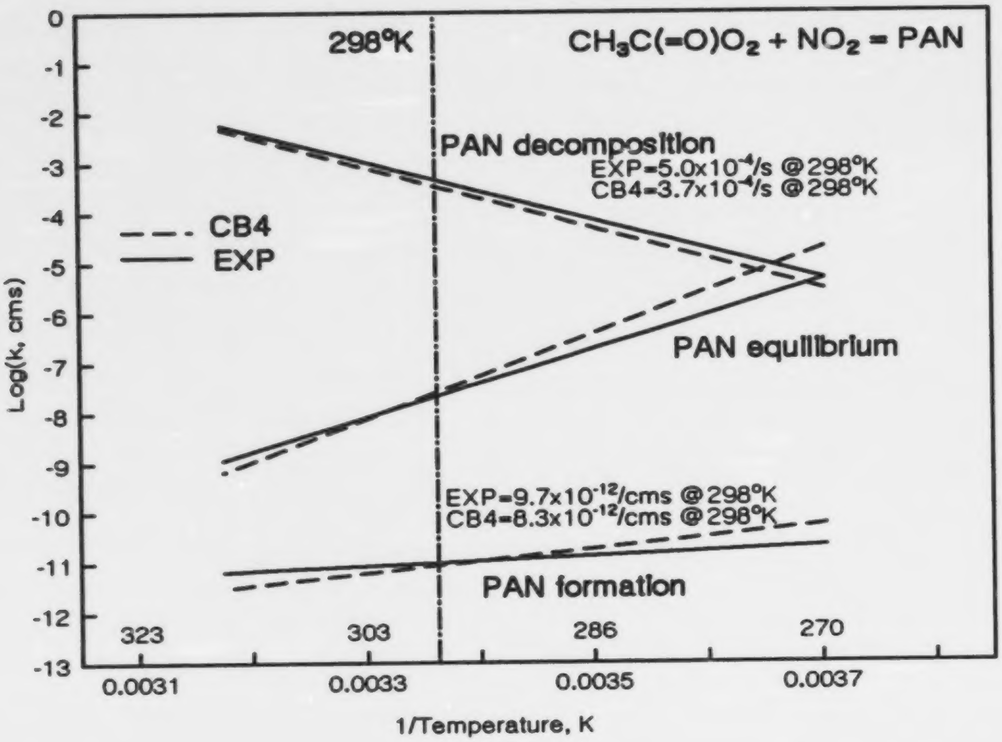

Figure 134. Comparison of PAN Rates Used in CB4 and EXP Mechanisms.

the case of CB4, the "prompt" formation of the subsequent products from the NO oxidation reaction is included in the **ETH.2** reaction products and the XO2 "operator" carries out the actual NO-to-NO_2 oxidation but produces no organic products in its reactions. The issue here is how satisfactory is CCHO as a stand-in for $HOCH_2HC{=}O$?

ETH.3 $O_3 + H_2C{=}CH_2 \longrightarrow HCHO + 0.42\,CO + 0.12\,HO_2^{\cdot}$

This one reaction represents all the chemistry in reactions **O2d.1**, **O2d.2**, and **BR1.1a** to **BR1.3c**, 17 reactions in all. The reaction drops stable, low-reactivity products like formic acid, H_2, and CO_2. It also assumes that reaction **BR1.2d**, the Criegee + water reaction, is the only reaction of the Criegee biradicals and that only formic acid is produced in this reaction. The $HO_2^{\cdot}$ arises from Criegee decomposition reaction **BR1.1c**.

Propene

In the CB4 mechanism, propene is represented as one OLE and one PAR. Here we are most interested in the CB4 chemistry for OLE.

The O(3P) + OLE reaction in CB4 will not be described here.

OLE.2 $$^{\cdot}\mathrm{OH} + \mathrm{OLE} \longrightarrow \mathrm{HCHO} + \mathrm{CCHO} + \mathrm{XO2} + \mathrm{HO}_2^{\cdot} - \mathrm{PAR}$$

This one reaction represents 7 reactions in the explicit mechanism. It omits the formation of hydroxy-propyl-nitrates and a number of alcohols and peroxides in the radical termination steps. (The −PAR is needed to account for the formation of CCHO–there are only two carbons in OLE.)

OLE.3 $$\begin{aligned} \mathrm{O}_3 + \mathrm{OLE} \longrightarrow\ & 0.5\,\mathrm{CCHO} + 0.50\,\mathrm{HCHO} + \\ & 0.33\,\mathrm{CO} + 0.24\,\mathrm{HCHO} + \\ & 0.44\,\mathrm{HO}_2^{\cdot} + 0.22\,\mathrm{XO2} + \\ & 0.10\,^{\cdot}\mathrm{OH} - \mathrm{PAR} \end{aligned}$$

Like **ETH.3**, this one reaction represents all of the chemistry described between reactions **O3d.1** and **BR2.3i**, or 18 reactions. The CB4 mechanism, however, uses the older Dodge and Arnts formulation for two-carbon Criegee biradicals. Thus, other than $\mathrm{HO}_2^{\cdot}$ and HCHO, this reaction does not form the products shown in Figure 117, *i.e.*, glycoaldehyde, glyoxal.

This differences in the chemistry of the simple olefins will effect how the observed products are produced and only a mass balance analysis will reveal how differences originated.

Comparison of Explicit and CB4 Predictions

The next several pages show selected days simulated with both the explicit mechanism and with CB4.

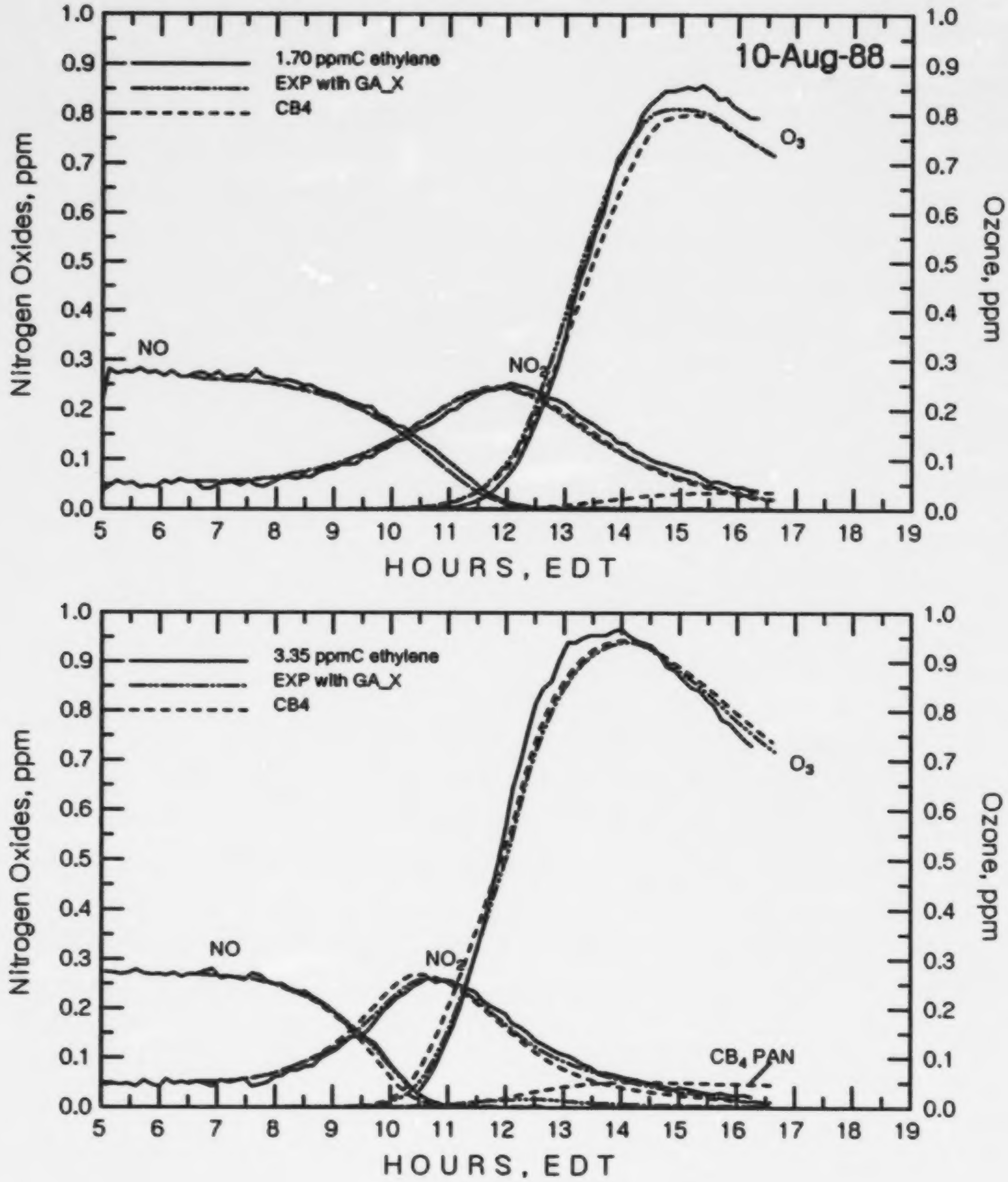

Figure 135. Simulation conditions: top: HONO=3 ppb, BVOC=55 ppb, WallOH= 2.5 × 10^{-3}; bottom: HONO=3 ppb, BVOC=55 ppb, WallOH= 2.5 × 10^{-3}. Solid lines are chamber observations; dashed lines are simulations.

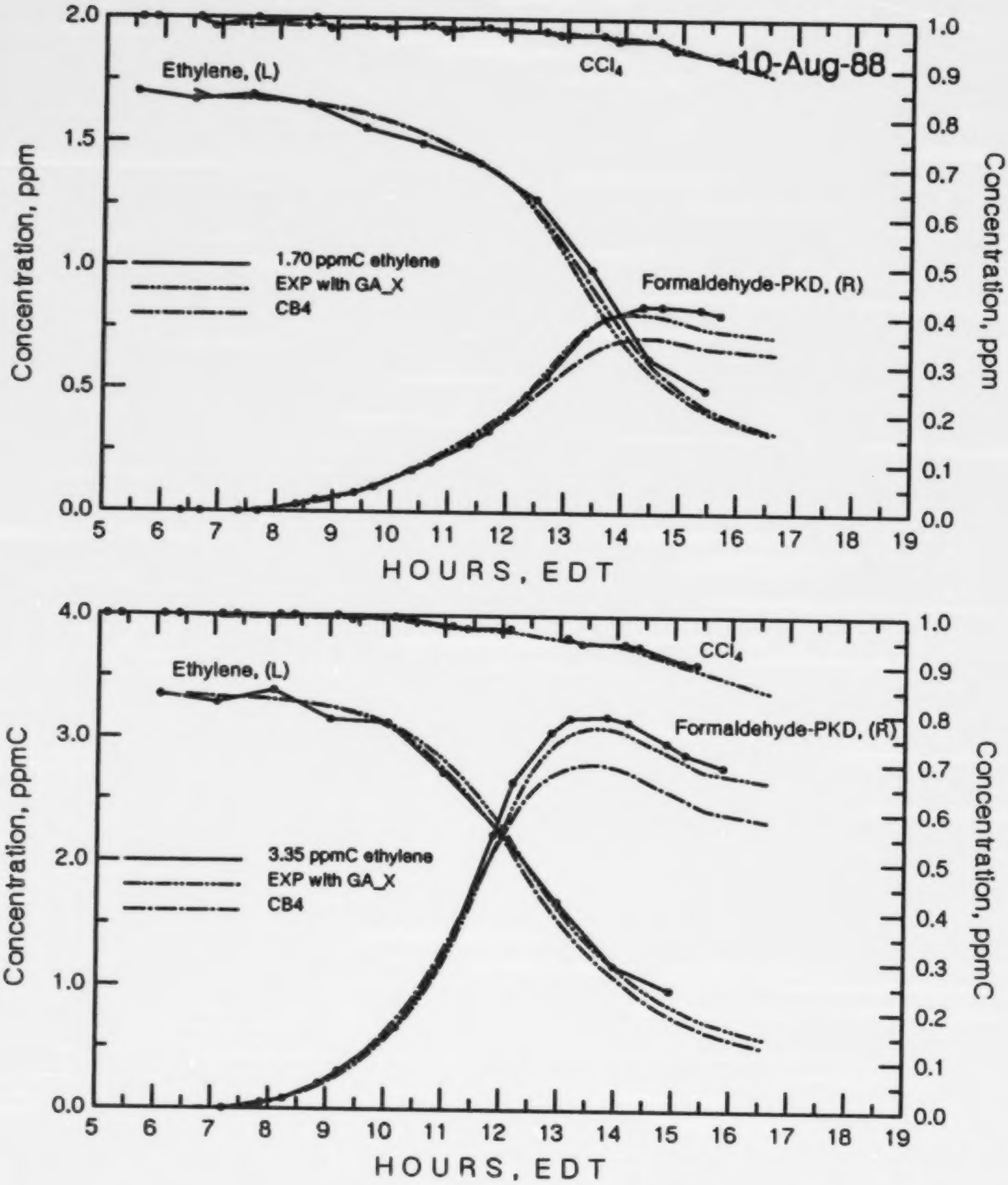

Figure 136. Simulation conditions: top: HONO=3 ppb, BVOC=55 ppb, WallOH= 2.5×10^{-3}; bottom: HONO=3 ppb, BVOC=55 ppb, WallOH= 2.5×10^{-3}. Solid lines are chamber observations; dashed lines are simulations.

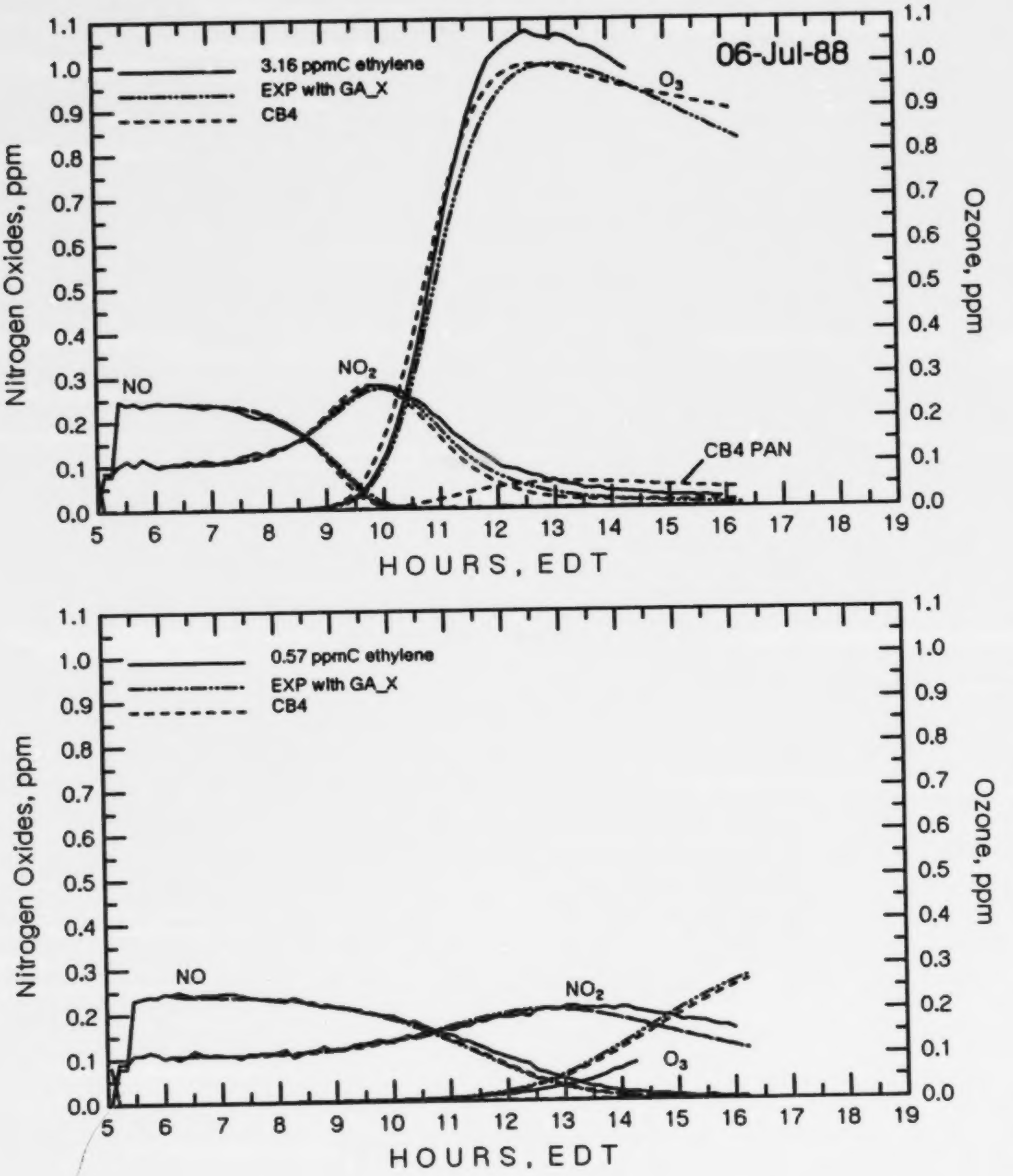

Figure 137. Simulation conditions: top: HONO=3 ppb, BVOC=45 ppb, WallOH= 2.5×10^{-3}; bottom: HONO=3 ppb, BVOC=45 ppb, WallOH= 2.5×10^{-3}. Solid lines are chamber observations; dashed lines are simulations.

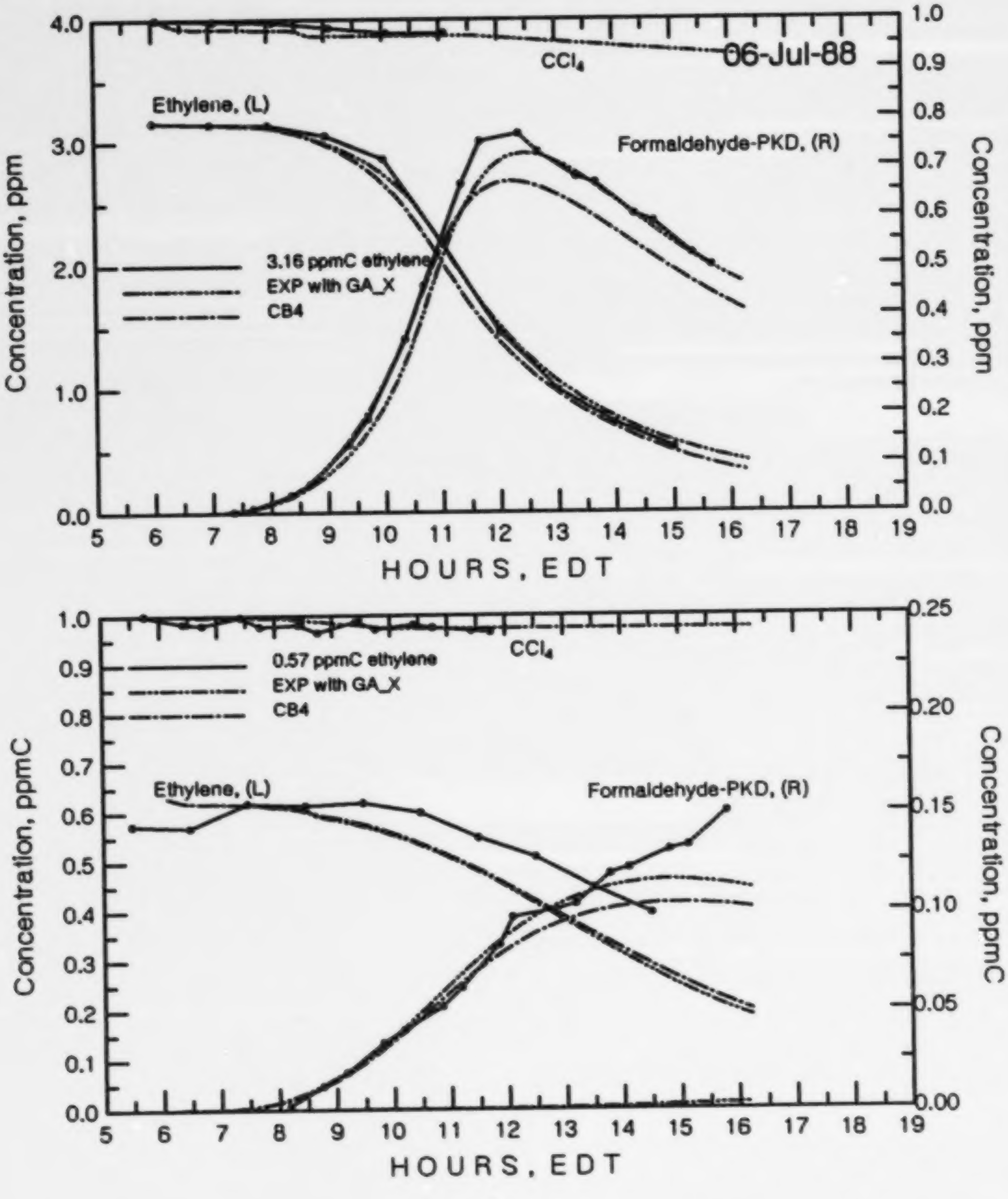

Figure 138. Simulation conditions: top: HONO=3 ppb, BVOC=45 ppb, WallOH= 2.5×10^{-3}; bottom: HONO=3 ppb, BVOC=45 ppb, WallOH= 2.5×10^{-3}. Solid lines are chamber observations; dashed lines are simulations.

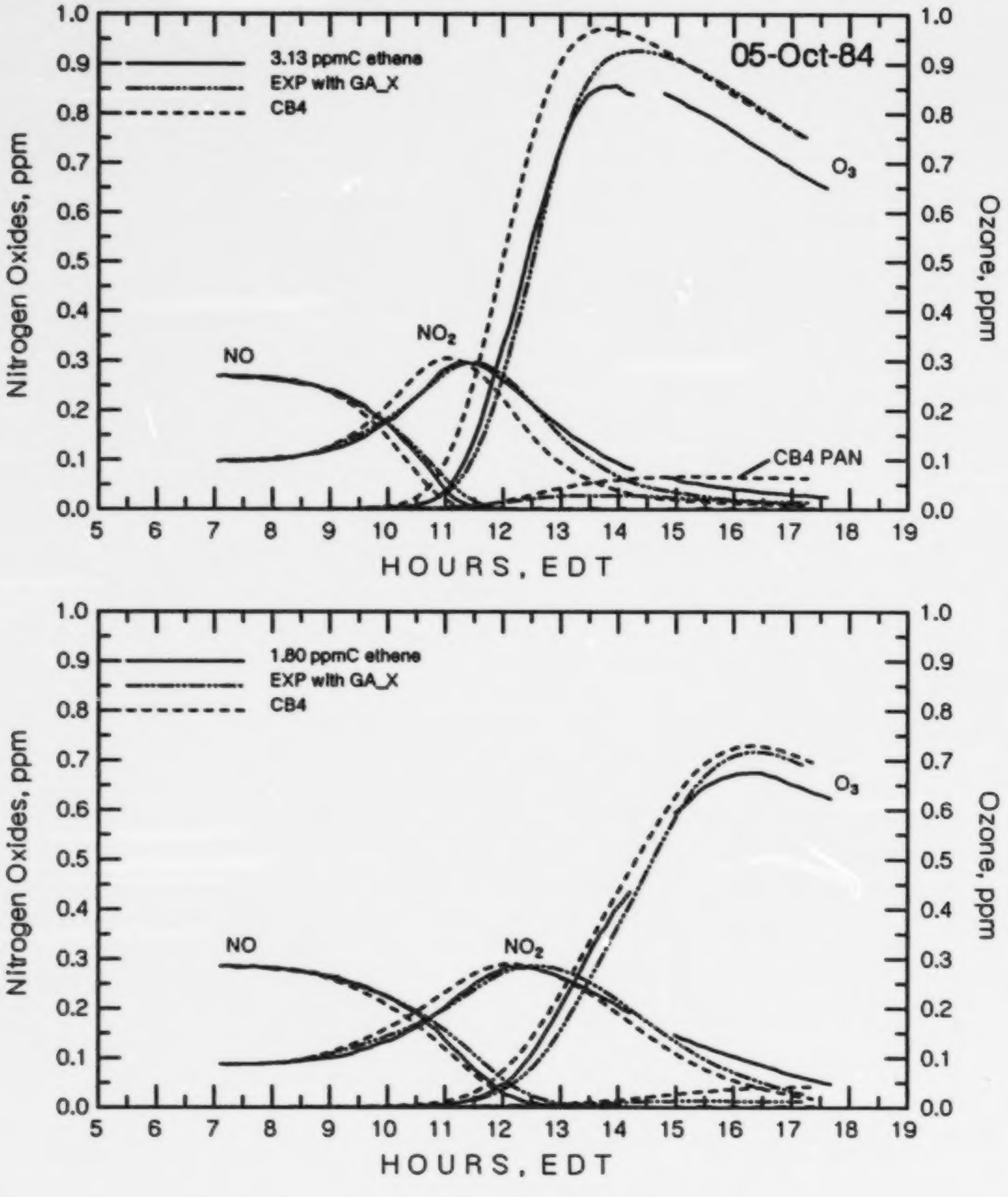

Figure 139. Simulation conditions: top: HONO=3 ppb, BVOC=25 ppb, WallOH= 0.0, K[PGAN] = 4×10^{16}; bottom: HONO=5 ppb, BVOC=25 ppb, WallOH= 0.0. Solid lines are chamber observations; dashed lines are simulations.

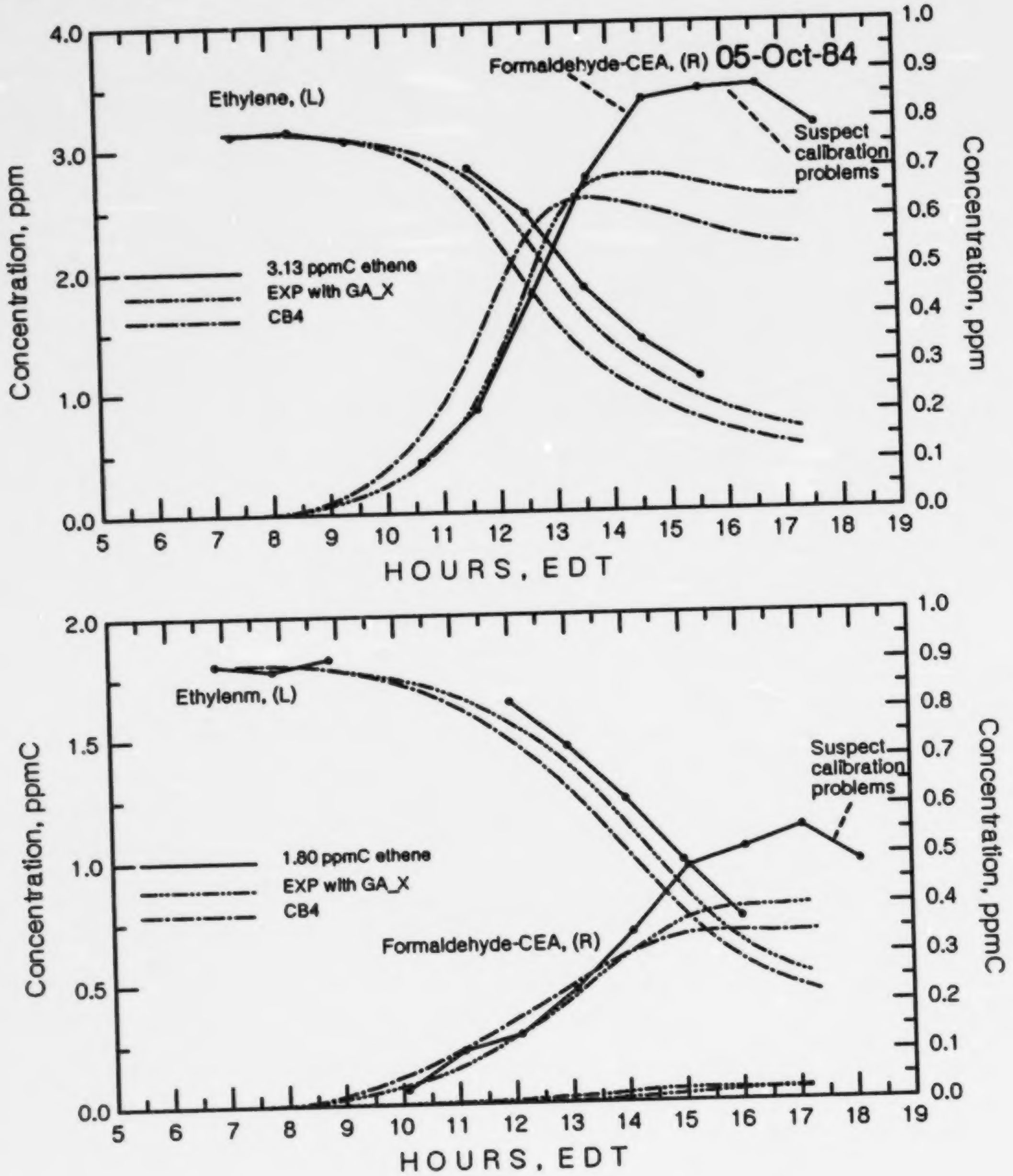

Figure 140. Simulation conditions: top: HONO=3 ppb, BVOC=25 ppb, WallOH= 0.0, K[PGAN] = 4×10^{16}; bottom: HONO=5 ppb, BVOC=25 ppb, WallOH= 0.0. Solid lines are chamber observations; dashed lines are simulations.

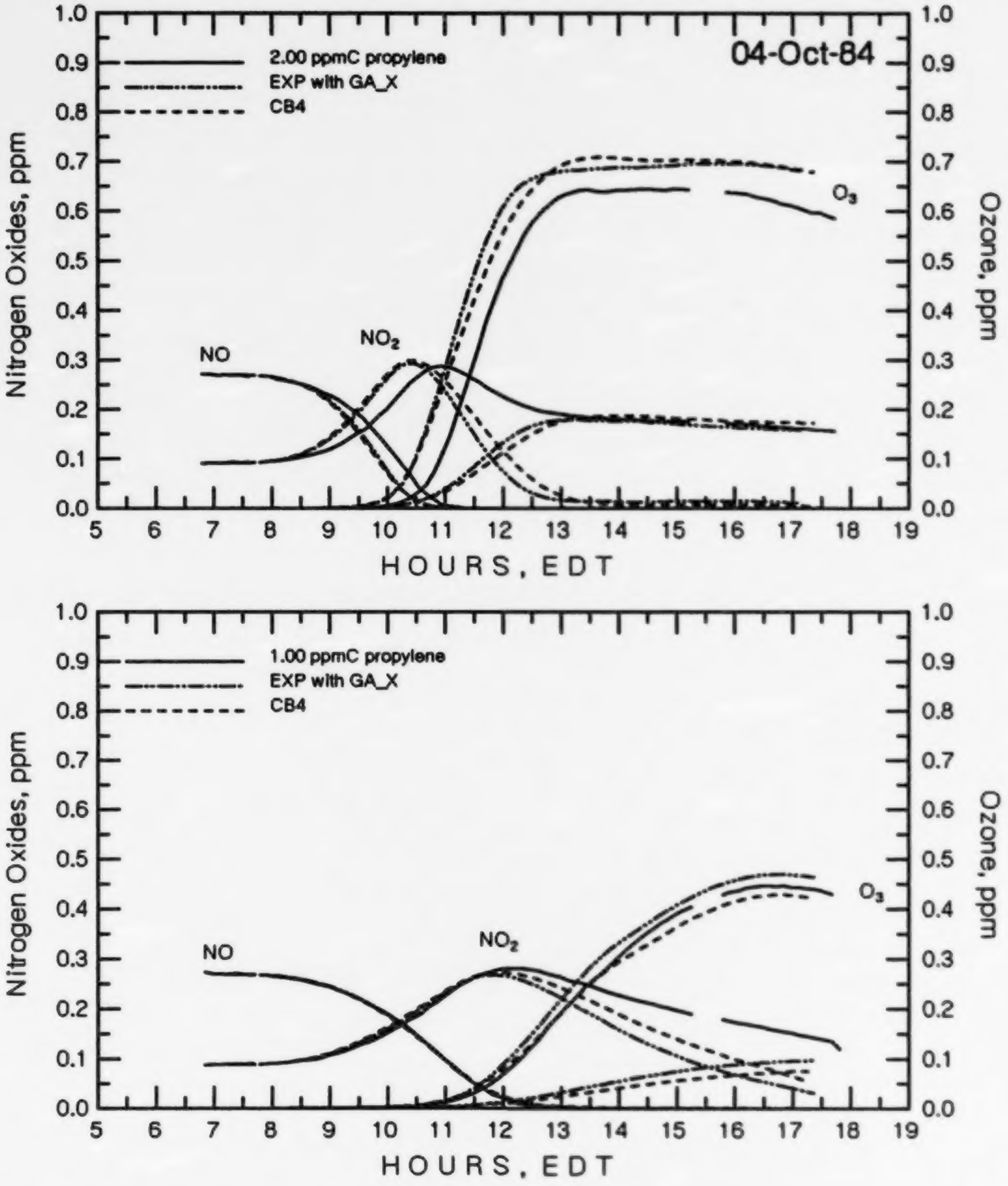

Figure 141. Simulation conditions: top: HONO=3 ppb, BVOC=10 ppb, WallOH= 0.5×10^{-3}, k[WallN2O5b]= 4×10^{-4}; bottom: HONO=3 ppb, BVOC=10 ppb, WallOH= 0.5×10^{-3}, k[WallN2O5b]= 4×10^{-4}. Solid lines are chamber observations; dashed lines are simulations.

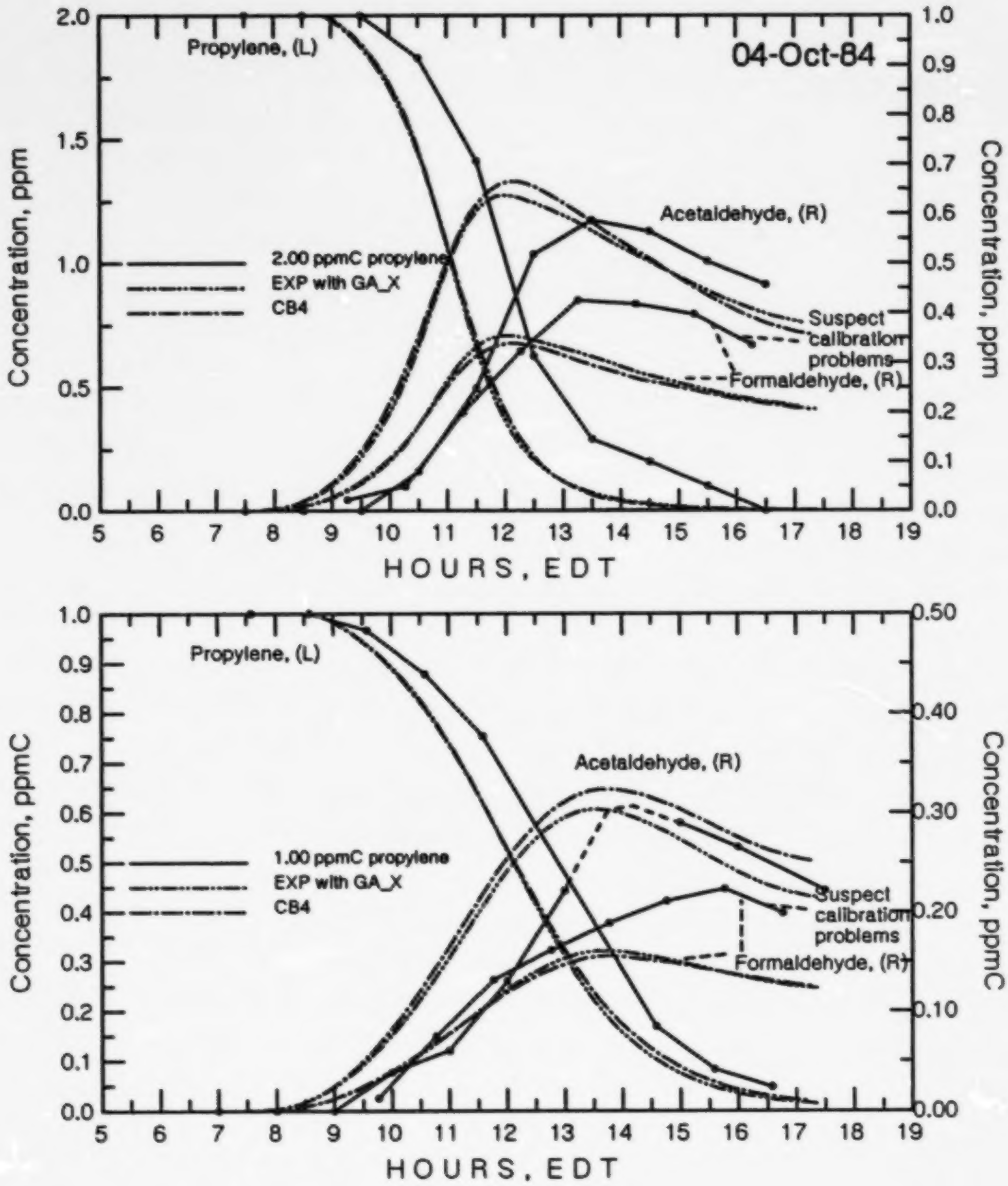

Figure 142. Simulation conditions: top: HONO=3 ppb, BVOC=10 ppb, WallOH= 0.5×10^{-3}, k[PGAN]= 4×10^{16}, k[WallN2O5b]= 4×10^{-4}; bottom: HONO=3 ppb, BVOC=10 ppb, WallOH= 0.5×10^{-3}, k[WallN2O5b]= 4×10^{-4}. Solid lines are chamber observations; dashed lines are simulations.

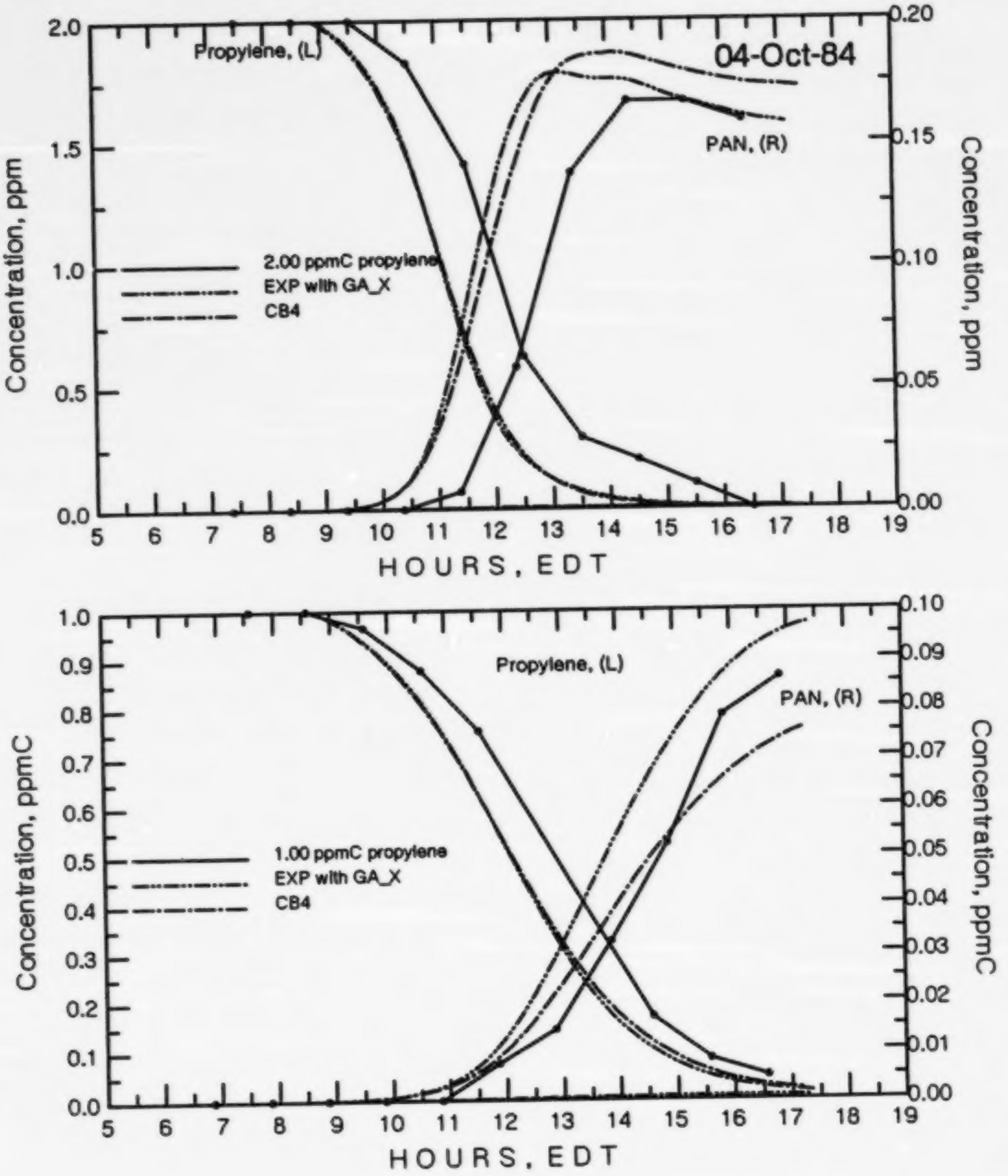

Figure 143. Simulation conditions: top: HONO=3 ppb, BVOC=10 ppb, WallOH= 0.5×10^{-3}, k[PGAN]= 4×10^{16}, k[WallN2O5b]= 4×10^{-4}; bottom: HONO=3 ppb, BVOC=10 ppb, WallOH= 0.5×10^{-3}, k[WallN2O5b]= 4×10^{-4}. Solid lines are chamber observations; dashed lines are simulations.

Extent of "Reasonable Agreement"

For predictions of O_3 the two mechanisms are essentially identical. The explicit mechanism is somewhat better at fitting the exact shape of the NO and NO_2 profiles because of the hydroxy-aklyl-nitrate formation in the explicit mechanism.

In all ethene cases, however, the CB4 does under-predict the observed maximum HCHO, essentially by about the same percentage: ca. 13% of the maximum HCHO, even at low levels of ethene, while at the same time it over-consumes the ethene, that is, in CB4 less net HCHO was produced from more ethene consumed. In the propene cases, it appears that the two mechanisms do about the same bad job, with CB4 having a better agreement with observed acetaldehyde than does the explicit mechanism.

Mass Balance Analysis of CB4 and EXP Simulations

Figure 144 and Table 20 are results from a mass balance analysis for the two mechanism's simulations of the RED (or 3.2 ppmC) side of July 6, 1988. Figure 144 shows side-by-side pie-charts of the total production masses of HCHO, $HO_2^{\cdot}$, and NO_2 *summed over the whole day.*

First notice that both the explicit mechanisms (EXP) and the CB4 mechanism produced almost exactly the same amount of HCHO: 1.936 vs. 1.939 ppm, yet Figure 138 showed that CB4 had a lower peak HCHO! As shown in Part 2, line 1 of Table 20, EXP consumed 1.509 ppm HCHO (the second and sixth column of the table gives the total amount the listed species that reacted in the whole simulation), and CB4 consumed 1.541 ppm HCHO, or 32 ppb more HCHO. Because the maximum HCHO differed by about 90 ppb, the two mechanisms had to made or consumed another 60 ppb HCHO, but at different times in the two mechanisms.

Second, CB4 produced 123 ppb (2.405-2.282 ppm) more $HO_2^{\cdot}$ than did EXP and organically converted 120 ppb more NO to NO_2 (note that this extra *organic* NO_2 production *was not* caused by the extra $HO_2^{\cdot}$ which would be accounted for in the *inorganic* reactions.)

Looking at the top piecharts in Figure 144, we see that, although approximately the same total amount of HCHO was produced, it was produced differently. CB4 produced about 10% more HCHO from reaction of $^{\cdot}OH$ with ethene than did EXP. This was in part caused by more ethene reacting with $^{\cdot}OH$ and with O_3 in the CB4 simulation than in the EXP simulation as shown by comparing columns two and six in lines 1 and 2 of Part 1, Table 20 (this can also be observed in the plots in which CB4 consumes more ETH than EXP and is always slightly lower than the observed ethene data). About 5% more HCHO reacted with $^{\cdot}$OH in CB4 than in EXP, and therefore less photolyzed (see Part 2, Table 20). In contrast, nearly the same relative amounts of HCHO were produced from the direct O_3 + ethene reaction (line 2, Part 1). In the EXP mechanism, however, secondary reactions of the Criegee biradical produced an additional 7.4% HCHO, giving a total for the O_3 pathway of 34% vs. CB4's 27% for O_3-related production of HCHO, accounting for 7% of the 10% difference in $^{\cdot}$OH-related pathways. The remaining 3% difference was due to glycoaldehyde chemistry verses acetaldehyde chemistry. CB4 contains many fewer radical termination reactions than does EXP and it appears that the smaller termination rates allowed more ethene to be consumed and thus to produce more HCHO. The additional sources of HCHO in the Criegee chemistry and in the glycoaldehyde chemistry of EXP were therefore replaced by more $^{\cdot}$OH+ethene reactions in CB4.

Looking at the middle piecharts in Figure 144, we see that the $HO_2^{\cdot}$ production from HCHO was relatively the same, however, CB4 produced more total $HO_2^{\cdot}$ mass because of the 5% higher amount of ethene reacting with $^{\cdot}$OH. That is, CB4 had more direct $HO_2^{\cdot}$ production from $^{\cdot}$OH + ethene than did EXP. Table 20 shows in line 2, Part 2, that the $HO_2^{\cdot}$ yield for this reaction in EXP was only $0.83(= 0.6632/0.7951)$ because of radical-radical termination reactions involving the hydroxy-ethyl-peroxy radical before it decomposed to produce $HO_2^{\cdot}$; this radial does not exist in CB4 which instead makes $HO_2^{\cdot}$ in the $^{\cdot}$OH+ethene reaction (see reaction **ETH.2** above).

The decomposition of the Creigee biradical makes about the same relative contribution in both cases, about 2.7%. The explicit treatment of glycoaldehyde in EXP, however, results in about a 5% larger contribution that is missing in CB4's chemistry for CCHO.

Thus, CB4 produces more $HO_2^{\cdot}$ because it lacks the complete radical-radical termination chemistry which would decrease the effectiveness of the $^{\cdot}$OH + ethene reaction for producing $HO_2^{\cdot}$. This over-efficiency of $^{\cdot}$OH + ethene then compensates for the lack of explicit treatment of glycoaldehyde.

Finally, the bottom piecharts show that the two mechanisms have essentially the same NO to NO_2 oxidation steps, but the fact that more radicals cycled in CB4 resulted in more NO_2.

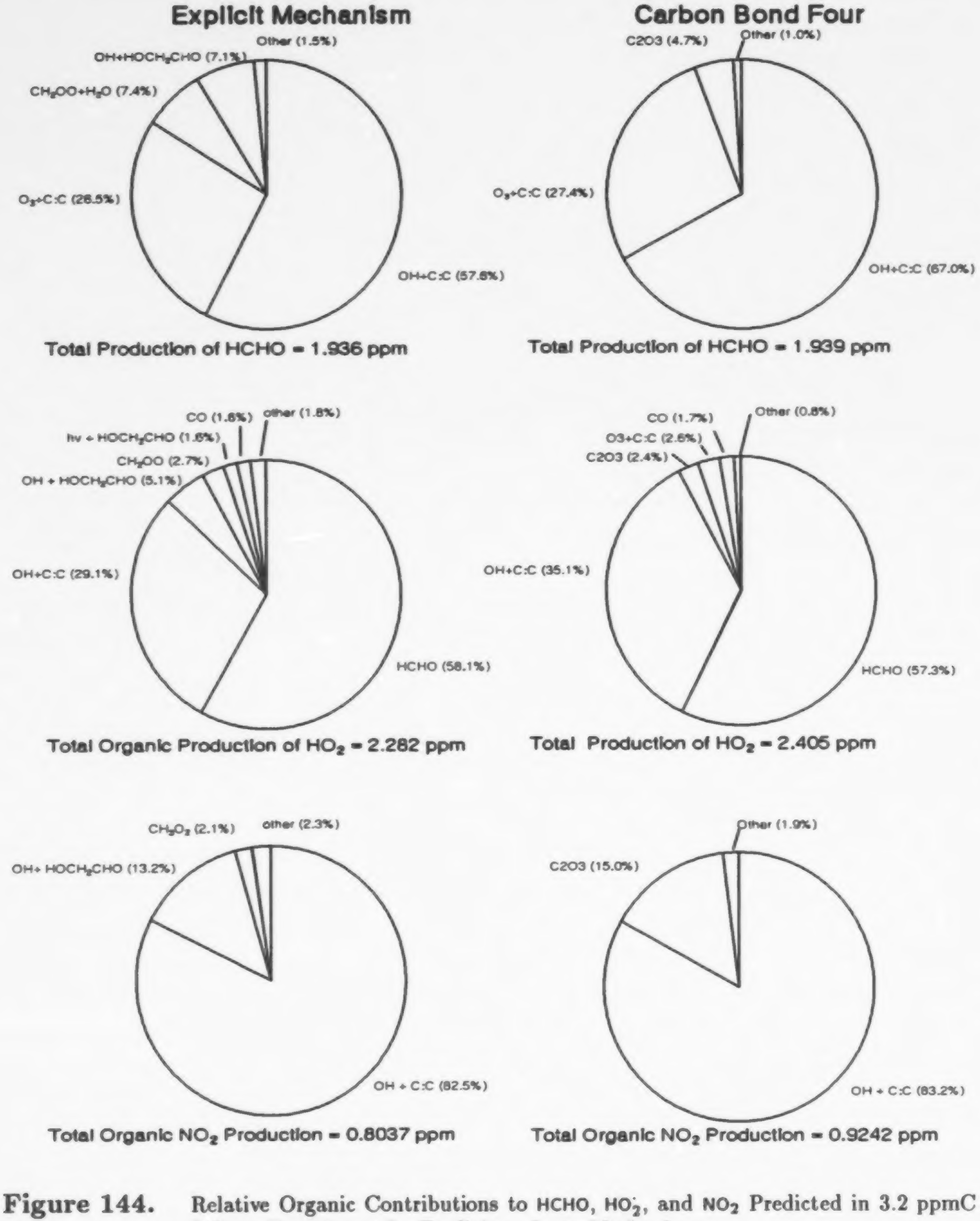

Figure 144. Relative Organic Contributions to HCHO, HO_2, and NO_2 Predicted in 3.2 ppmC Ethene Experiment by Explicit and CB4 Mechanisms.

Table 20. Mass Balance for Explicit and CB4 Mechanism for July 6, 1988.

EXPLICIT MECHANISM | CB4 MECHANISM

Part 1.

Total Production of HCHO = 1.936 ppm				Total Production of HCHO = 1.938 ppm			
Source	Reacted	HCHO Prod	%	Source	Reacted	HCHO Prod	%
1 OH+C:C	0.7951	1.1137	57.52	OH+C:C	0.8325	1.2988	66.99
2 O3+C:C	0.5119	0.5119	26.44	O3+C:C	0.5312	0.5311	27.39
3 CH2OO+H2O	0.2046	0.1428	7.38	C2O3	0.1383	0.0901	4.65
4 HOCC(O)O2	0.1370	0.1370	7.08	other	0.0187	0.0187	0.96
5 Other	0.0689	0.0290	1.5				

Part 2.

Total Production of HO2 = 2.282 ppm				Total Production of HO2 = 2.405 ppm			
Source	Reacted	HO2 Prod	%	Source	Reacted	HO2 Prod	%
1 HCHO	1.5090	1.3253	58.09	HCHO	1.5412	1.3774	57.28
2 OH+C:C	0.7951	0.6632	29.07	C:C	0.8325	0.8325	34.61
3 HOCC(O)O2	0.1370	0.1159	5.08	C2O3	0.1383	0.0588	2.45
4 CH2OO>	0.3073	0.0615	2.69	O3+C:C	0.5236	0.0628	2.50
5 HOCCHO	0.1731	0.0371	1.63	CO	0.0418	0.0418	1.74
6 CO	0.0366	0.0365	1.60	other	0.0187	0.0187	0.78
7 other	1.3719	0.0418	1.83				

Part 3.

Total NO2 Production = 0.8037 ppm				Total Production of NO2 = 0.9242 ppm			
Source	Reacted	NO2 Prod	%	Source	Reacted	NO2 Prod	%
1 C:C+OH	0.7950	0.6632	82.52	C:C+OH	1.3637	0.7687	83.17
2 HOCC(O)O2	0.1370	0.1057	13.15	C2O3	0.1383	0.1384	14.97
3 CH3O2	0.0204	0.0165	2.05	other	0.0187	0.0171	1.86
4 other	1.7238	0.0183	2.28				

11

Urban Modeling

Conditions

In this chapter we present an analysis of predictions from a simple trajectory model using the CB4 mechanism (a special version of OZIPM) used to simulate an urban condition in which the peak O_3 was about 0.17 ppm, *i.e.*, the urban area would need to reduce O_3 by about 30% to comply with the national standard. The model conditions were those used by Dodge in her study of HCHO predictions by different mechanisms.[64] These were:

- Location: Philadelphia, PA
- July 15, clear sky, from 0800 to 2000 LDT
- Temperature varied from a morning low of 20 to an afternoon high of 30°C
- $VOC : NO_x = 9$
- $[NO_x]_o = 0.06$, 25% NO_2
- $[CO]_o = 1.2$ ppm
- Emissions were temporally-varying values of VOC and NO_x; the additional mass added by emissions was $0.69[VOC]_o$ and $1.4[NO_x]_o$.
- Mixing height increased from 300 m to 1300 m.
- Aloft concentrations were:
  - ▹ $[VOC] = 0.025$ ppmC
  - ▹ $[CO] = 0.500$ ppm
- Surface background VOC=0.038 ppmC, 7% HCHO

In the CB4 mechanism, the urban VOC are represented by 7 species:

- methane is implicitly represented by being included in a rate constant at a constant concentration of 1.79 ppmC;
- all other paraffins, including saturated carbon chains on side groups of other classes are represented by a 1-carbon entity, PAR for each carbon in the paraffin or side chain;
- a 2-carbon ETH represents ethene;
- a 2-carbon OLE represents the double bonds in higher terminal olefins and *n* number of PAR, where *n* is the number of carbons-2 in the molecule;
- a 2-carbon ALD plus the needed number of PARs represent the internal olefins (the internal olefins are assumed to react fast and make ALDs, so they are just entered as their products);
- a 7-carbon TOL represents toluene and other mono-substituted aromatics; the additional carbons in the side chains are represented as PARs;
- an 8-carbon XYL represents xylene and other di- and tri-substituted aromatics; the additional carbons in the side chains are represented as PARs;
- HCHO represents itself;
- a 2-carbon ALD represents acetaldehyde and higher aldehydes.

Because the contribution of primary emissions of aldehydes to the total urban emissions is unknown, we conducted two simulations. The first used the OZIPM default assumptions of 5% aldehydes (2% HCHO and 3% acetaldehyde) in the initial VOC mixture and in the emissions; this case was called the **Base Case**. The second case omitted the aldehydes in the emissions and in the initial VOC mixture; this case was called the **Zero Initial Case**. Aldehydes were omitted from the initial VOC because, in the OZIPM model, they are presumed to arise from 'fresh emissions.' Aldehydes were left in the aloft HC and in the surface background HC because in these HC sources the aldehydes presumably arise from reactions of 'aged' material, that is, the aldehydes would be due to previous secondary formation and not emissions. These two cases then allow the effects of direct emissions of aldehydes to be compared with those from only secondary HCHO production.

The analysis presented here describes the sources and sinks of O_3 and HCHO in increasing detail. It resulted from a mass balance analysis on the output of an OZIPM simulation for a typical urban photochemical smog system.

Mass Balance Analysis

First we will describe the impact of primary aldehyde emissions on the reactivity of the urban system with emphasis on explaining how the O_3 was produced. Then we will examine the production of HCHO.

Figure 145 shows the ozone and nitrogen oxides time-concentration profiles for the base case and zero initial aldehydes simulations. As expected, the simulation with zero initial aldehydes is slower and produces somewhat less ozone.

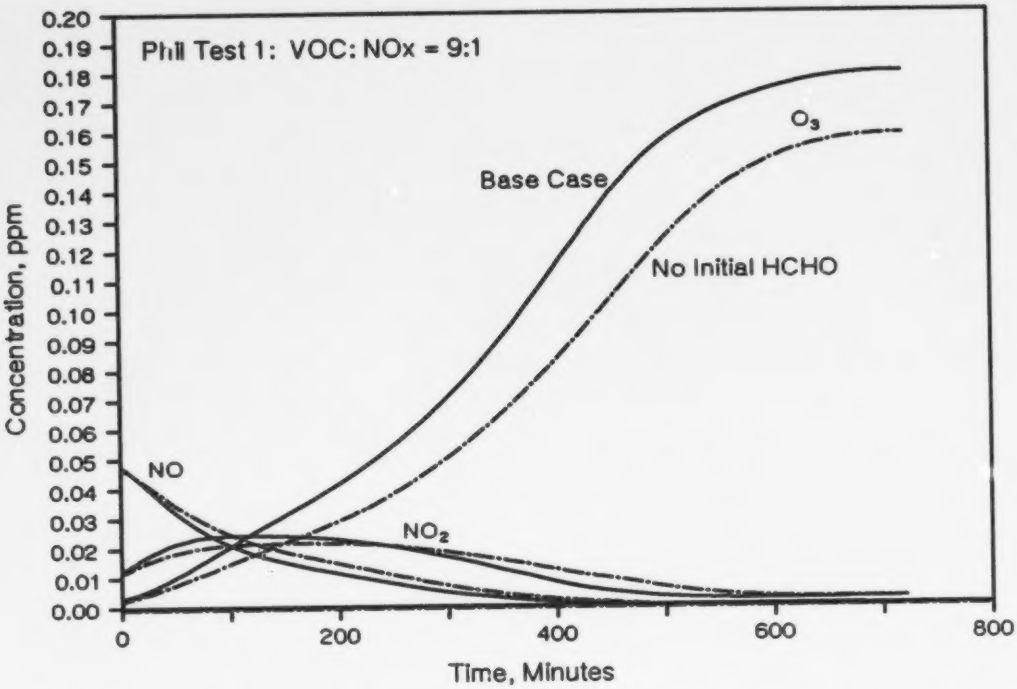

Figure 145. Ozone and Nitrogen Oxides Concentration-Time Plots for Base Case and Zero Initial Aldehydes

Figure 146 shows the O_3 mass balances for both simulations. These include O_3 sources, chemical production and O_3 from entrainment, and the loss by chemical reaction. These rates, integrated and plotted as a function of time, have units of ppm contributing to the final O_3 concentration at each time. Also shown is the O_3 final concentration throughout the day which is the sum of the processes shown. The first point after zero on the top plot shows that entrainment was the processes most increasing O_3, but about half of the entrained O_3 was reacted (chemical loss in the figure), with a resulting concentrations shown by the final line. Over the course of the simulation, chemical production of the O_3 was the dominant processes, although entrainment provided a significant background of O_3.

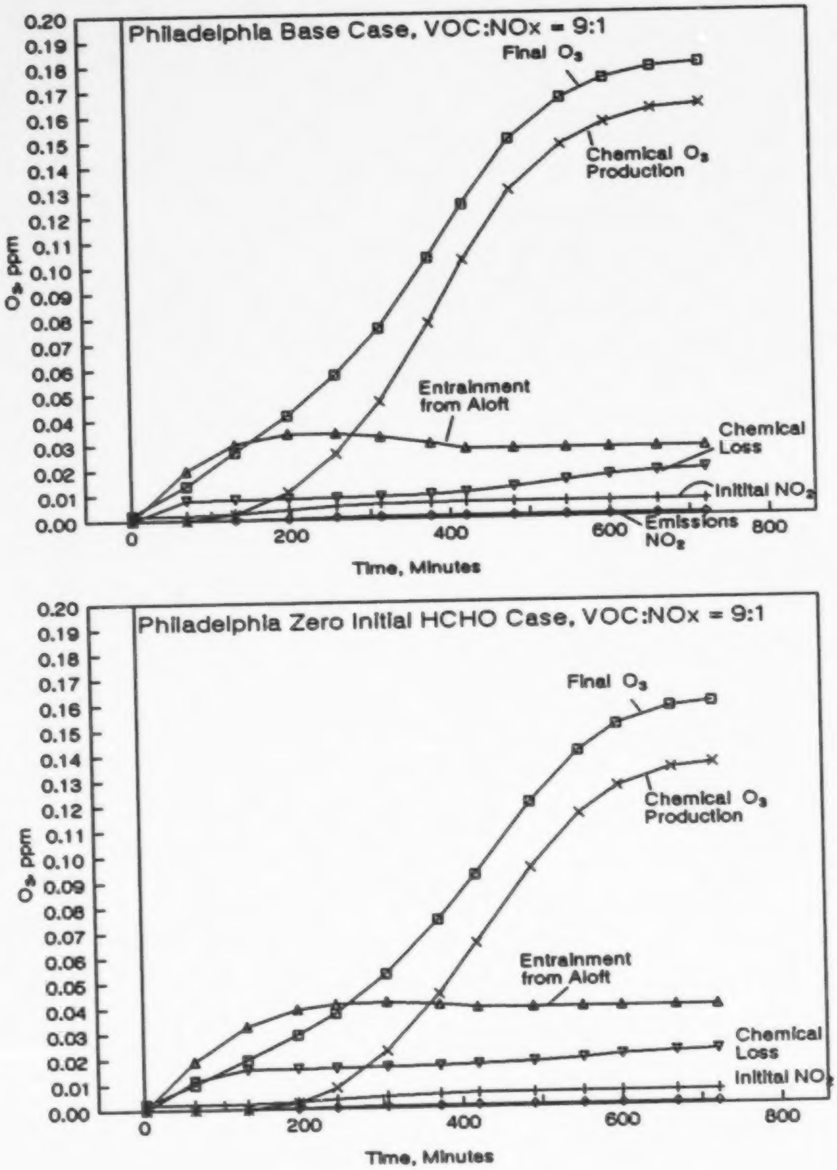

Figure 146. Ozone Sources and Sinks As a Function of Time

Figure 147 shows the day average sources and sinks of formaldehyde for both simulations. Although the second simulation did not have initial aldehydes, the final HCHO concentrations were almost the same: 7 ppb for the base case and 6.5 ppm for the zero initial aldehydes case.

For the base case, the HCHO sources total about 58 ppb: 14 ppb of initial HCHO (which included the surface background), 3.8 ppb from emissions and 41 ppb from chemical production. Chemical production was the major source of formaldehyde: almost 70%. Dilution resulted in losing 11 ppb of formaldehyde and chemical reaction removed 40 ppb resulting in 7 ppb remaining in the air.

For the zero initial aldehydes case (and no aldehyde emissions), the sources of HCHO were 2.7 ppb from background surface concentration of 38 ppb HC (7% HCHO) and 32 ppb from chemical production (92.4%). Dilution resulted in losing only 2.2 ppb (6.4%) because dilution occurred mostly in the early part of the day. Chemical reaction consumed 26.2 ppb (75%), resulting in 6.5 ppb remaining.

Note that more HCHO was lost to dilution in the base case because much of the initial HCHO was subject to the early dilution which is largest for the lowest mixing height. Also the initial HCHO was lost by photolysis, which contributed to the earlier reactivity in this base case.

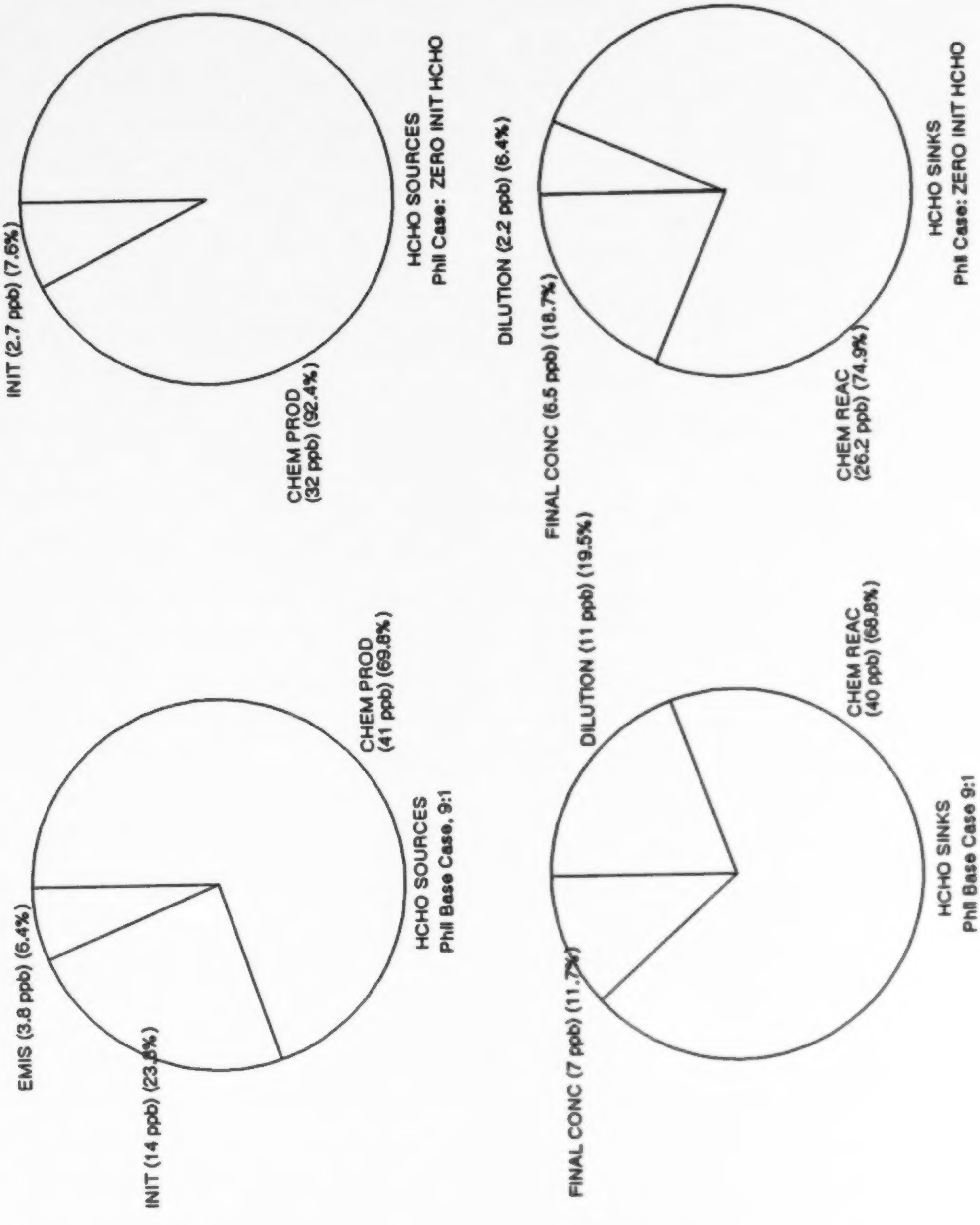

Figure 147. Formaldehyde Sources and Sinks: Day Average

Figure 148 shows the net sources of HCHO throughout the day for both simulations. These are shown in terms of percentage and absolute concentration.

For the base case, the initial HCHO came from initial concentration and emissions, but by 200 minutes chemical production accounted for 50% of the HCHO. After 400 minutes, chemical production accounted for more than 90% of HCHO.

In the zero initial HCHO simulation, chemical production accounted for 50% of the HCHO just after 100 minutes and 90% by 300 minutes into the simulation. The absolute concentration plots also show the concentrations for each process throughout the simulations.

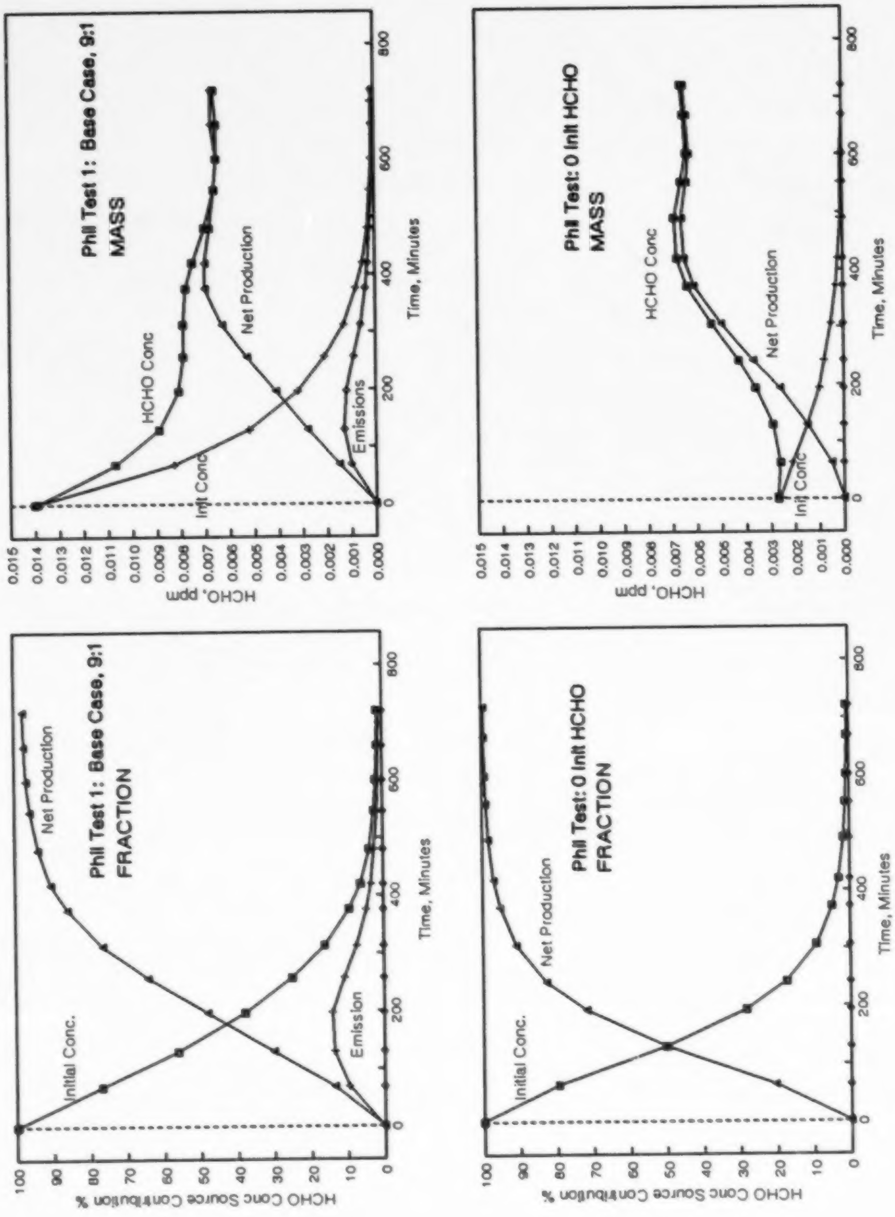

Figure 148. Formaldehyde: Net Sources

Figure 149 shows the sources and sinks of HCHO throughout the day for both simulations in ppm units. The base case simulation showed the greater loss from dilution (negative entrainment since the aloft value of HCHO was much less than the initial concentration) compared with the zero initial HCHO simulation. Also since there was initial HCHO, the chemical loss was greater earlier in this simulation than in the one without initial HCHO.

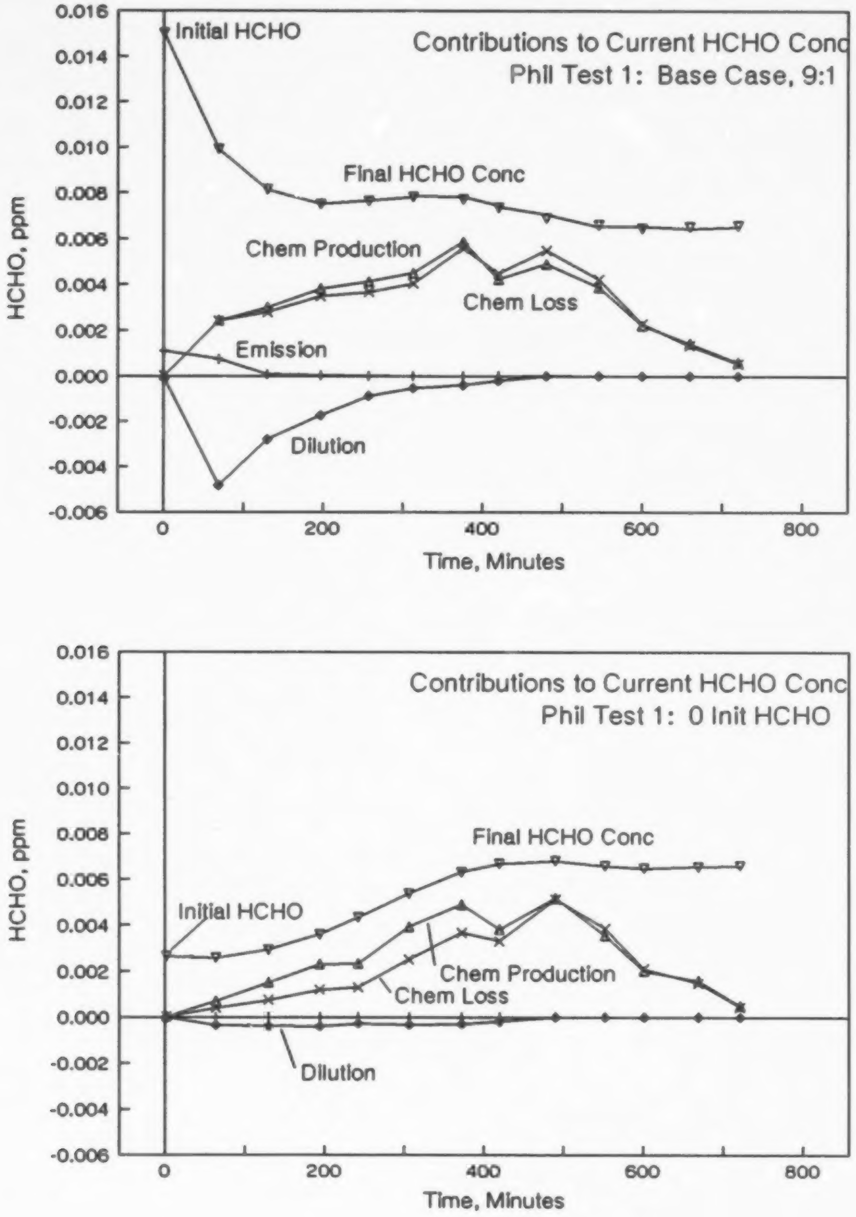

Figure 149. Formaldehyde: Sources and Sinks

Figure 150 shows the day average contribution from each HC species to the HCHO chemically produced in both simulations. For both simulations the olefins (including ethylene) are the largest contributors. Toluene is the smallest contributor. XYL contributes about as much as methane does (about 9%). The ALD is also a major contributor and since it is a major product of the olefin chemistry, it can be concluded that the olefins (including ethylene) produce more than half of the HCHO although the fraction of olefins in the simulation was less than 13% of the initial total VOC and VOC emissions (about 1% of the 19 to 20% of the HCHO produced by PAR is also derived from the side chain carbons in higher olefins). The main difference between the two simulations is that since there is no initial acetaldehyde, ALD contributes much less in the zero initial aldehyde simulation.

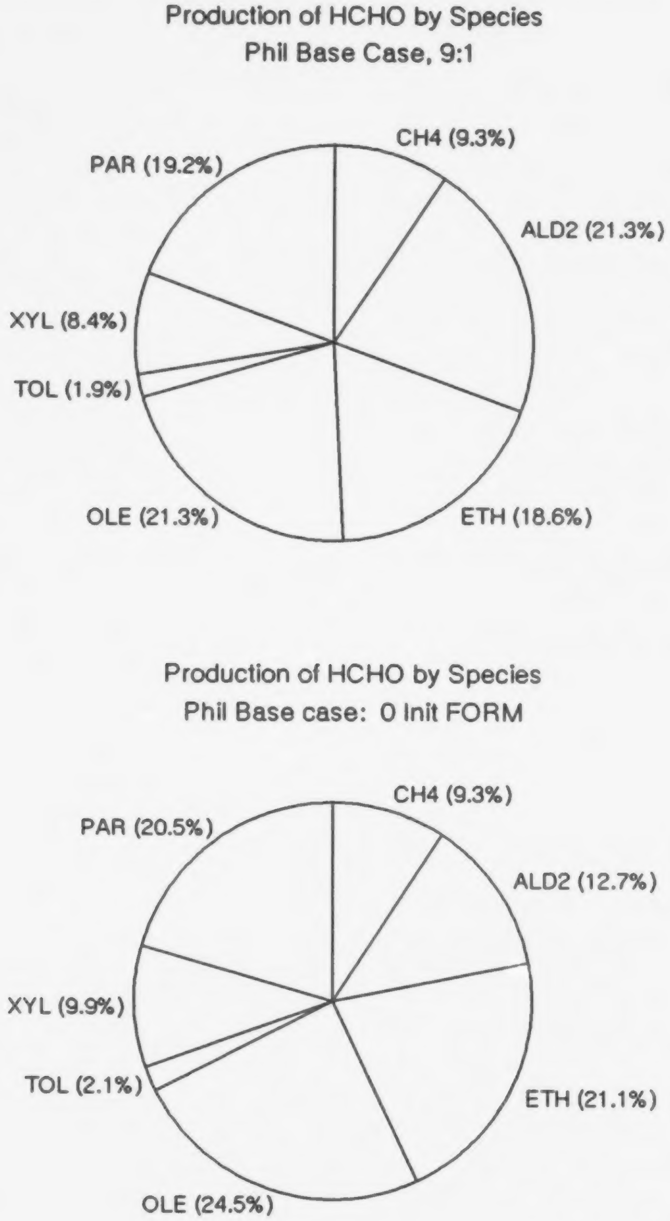

Figure 150. Contribution of HCHO from Each HC: Day Average

Figure 151 shows the contribution from each HC species to the HCHO chemically produced in both simulations throughout the day. This is shown both in absolute units of ppm/hour (cumulative) and in percent. The cumulative absolute ppm/hour plot shows the delayed reactivity in the simulation without initial aldehydes.

In each simulation, ethylene and C_2+ olefins produced the largest fraction of the HCHO initially, with aldehydes and ethylene being the other important contributors. Because of the absence of initial aldehydes in the second simulation, the olefins and ethylene are much more important in producing HCHO and in sustaining the initial reactivity of the simulation. In each simulation, as the olefins react, the reactions of ALD, a product of OLE reactions, became a greater source of HCHO. Because of their lower reactivity, the paraffins and methane contribute more later in the simulations when the other more reactive compounds are reduced. Because XYL is consumed quickly in the simulations, it only contributes to HCHO production early in the run. Ethylene is a relatively constant contributor until the end of the simulation.

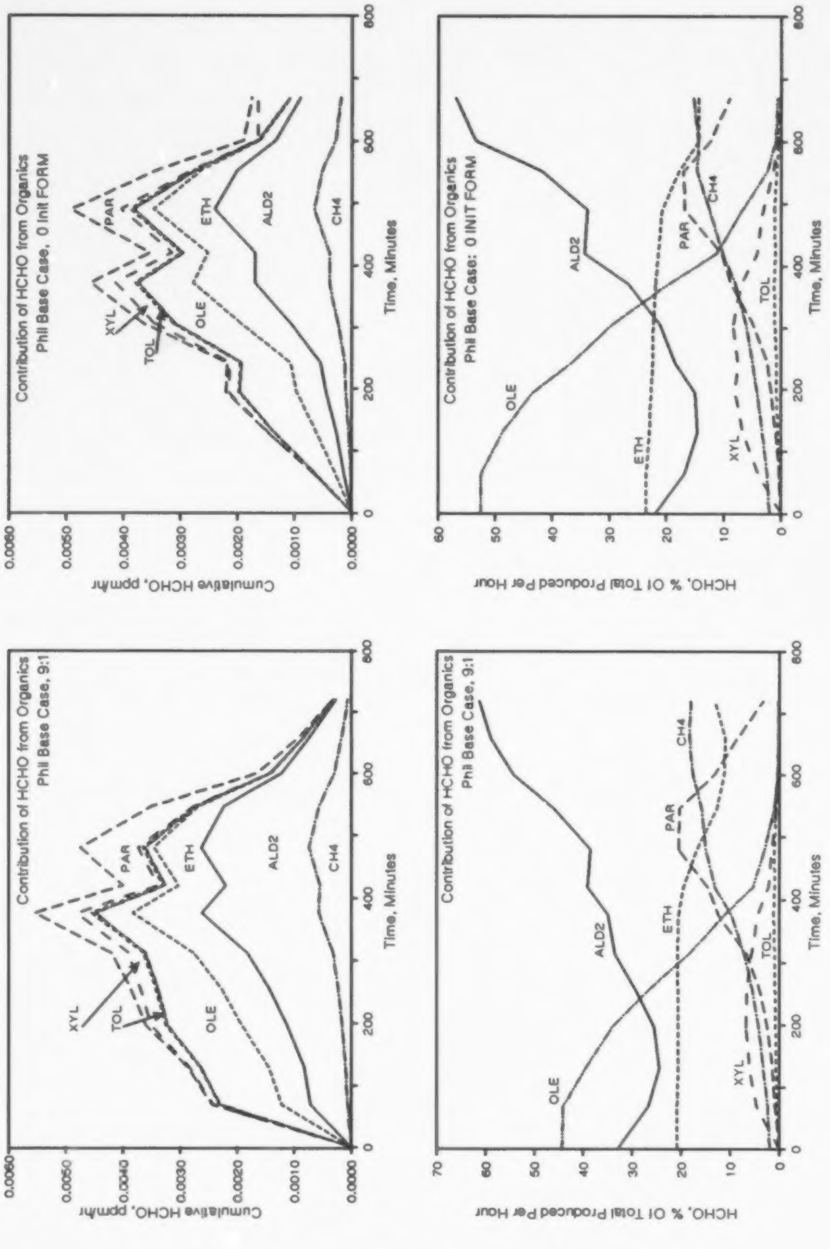

Figure 151. Contribution of HCHO from Each HC: Time Analysis

Figure 152 shows the day average relative contributions from each reaction for those HC species which produce HCHO by more than one pathway. Clearly in each simulation the ˙OH radical reactions are responsible for the majority of the HCHO. ALD photolysis produces about 4% of the HCHO in each simulation. The O_3 reaction with ethylene produces 7 to 8% and the O_3 + olefin reaction produces 10 to 12% of the HCHO. The value is higher for the zero initial aldehyde simulation.

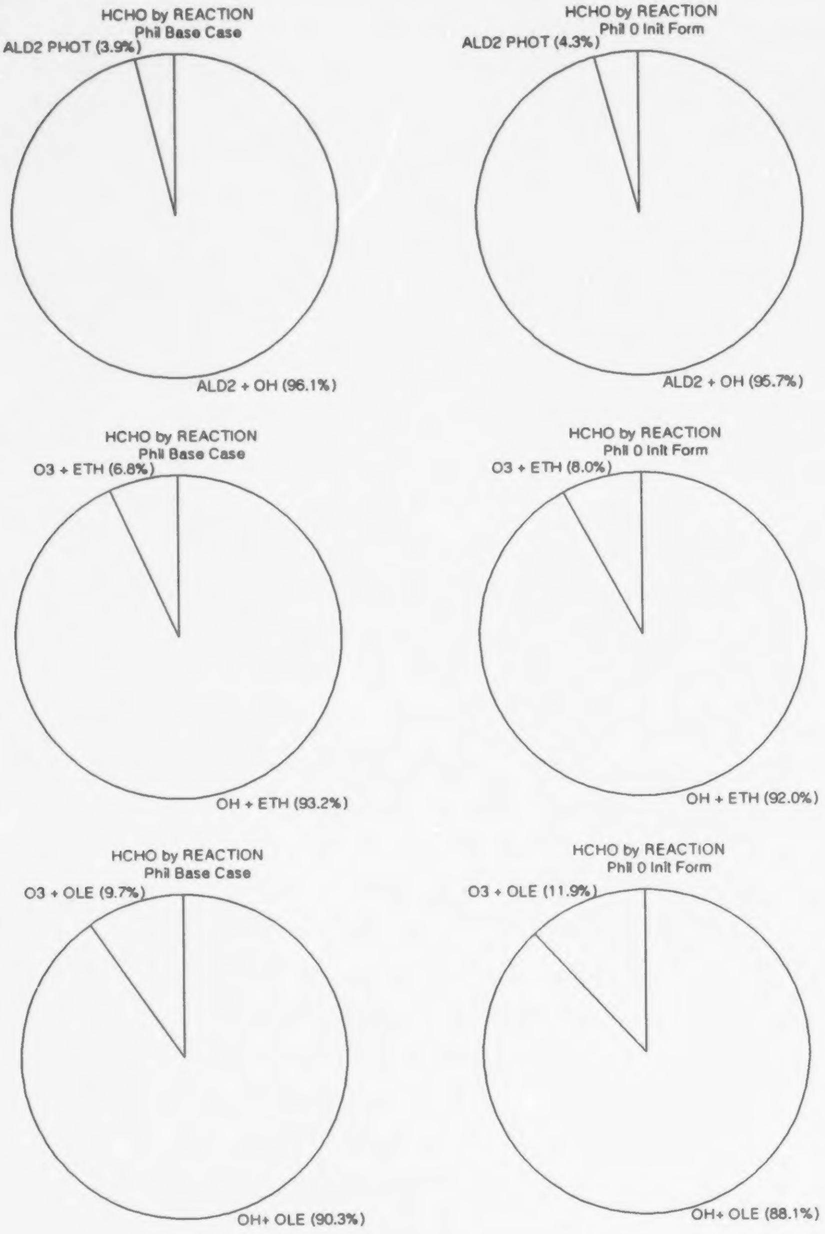

Figure 152. Relative Contribution From HCs With More Than One Reaction Producing HCHO: Day Average

Figures 153 and 154 show the relative contributions throughout the day from each reaction for those HC species that produce HCHO by more than one pathway. There is almost no difference between the two simulations after the first third of the simulation. Differences occurred in the beginning. In the zero initial aldehydes case, there was much less $^{\cdot}$OH initially compared with the base case. Therefore the photolysis of ALD and the O_3 + olefin and O_3 + ethylene reactions was more important initially when compared with the base case.

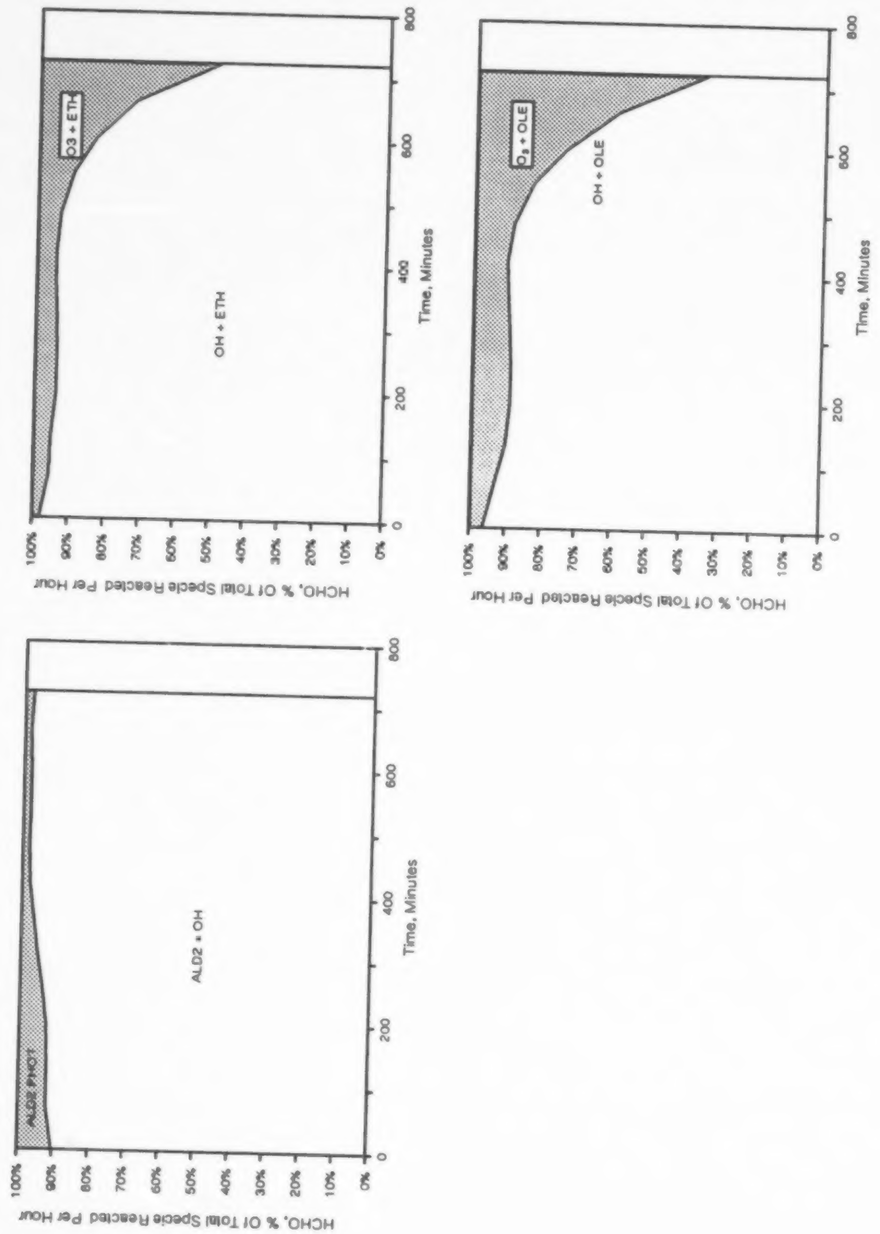

Figure 153. Relative Contribution From HCs With More Than One Reaction Producing HCHO: Base Case

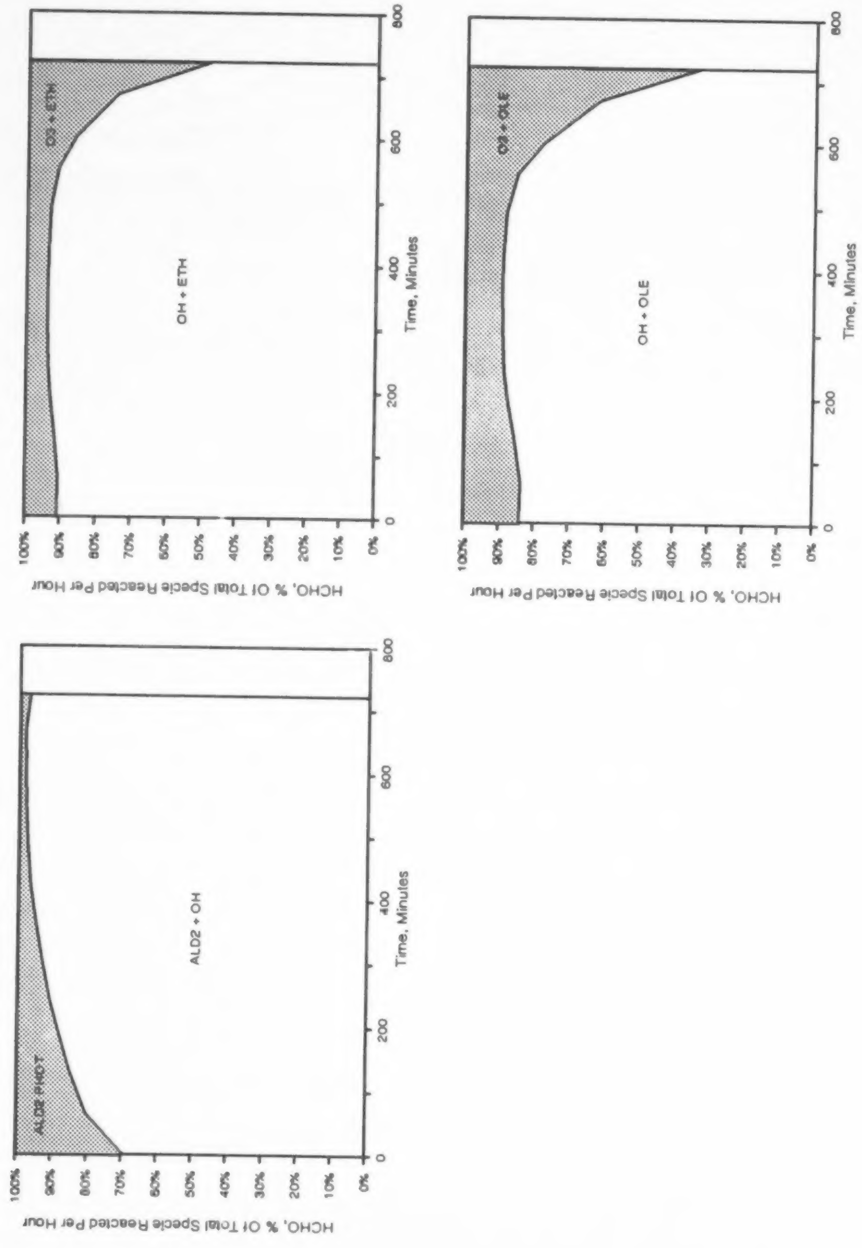

Figure 154 . Relative Contribution From HCs With More Than One Reaction Producing HCHO: Zero Initial Aldehyde Case

Conclusions From Analysis

Most of the HCHO is chemically produced, with or without the initial aldehydes. In these simulations, the role of initial formaldehyde was as a source of radicals, important for initiating photochemistry in the urban system. The aldehydes in the emission inventory were not an overwhelming source of formaldehyde in terms of mass, but they did increase the reactivity of the system, leading to further production of HCHO and O_3. As was found by Dodge,[64] more than 50% of the HCHO produced comes from reactions of the olefins (including ethylene) and higher aldehydes. The $\cdot$OH reactions are the most important producing HCHO, but the O_3 reactions are a significant source and play important roles in particular parts of the photochemical system such as serving as a source of HCHO from entrained O_3+olefins in the morning and as a source of end-of-day and next-day HCHO.

We have shown that there are errors associated with HCHO production in the olefin, ethylene, and aromatics chemistry of air quality photochemical mechanisms such as the CB4 used here. These models produce too much HCHO from the reactions of some species (aromatics) and produce somewhat too little HCHO from the reactions of other species (olefins),[4] or produce it from the wrong species as shown in the previous chapter. In the case analyzed here, the olefin reactions—for which the mechanisms underproduce HCHO—only contributed 7 to 12 % of HCHO. Correcting this chemistry would not have increased the production of HCHO by more than 3 to 6%. Based on previous comparisons we have performed and the confirming toluene and xylene experiments we have produced here, CB4 tends to overproduce HCHO for aromatics by about a factor of two.[4]. In the cases simulated here, the contribution TOL makes to total HCHO is only 2%, while XYL contributes about 9% for a total aromatics contribution of 11%. Reducing the yields of HCHO by about a factor of two would decrease the HCHO production by about 5–6%, *nearly equal to the underproduction from the olefins.* As shown in Figure 151, however, XYL and OLE make their contribution early in the simulation, whereas, ETH makes its contribution almost all the time, and ALD make their contribution later in the simulation. Thus there may be too much compensation early leading to too high an overall reactivity.

The accuracy of HCHO predictions obtained with the CB4 can be improved by increasing the number of species used to represent the olefins and aldehydes. For example, in CB4 the ALD species serves several purposes: it represents acetaldehyde and higher aldehydes, including those formed as secondary products; it also represents the internal olefins; further it also represents glycoaldehyde which is formed in significant quantities from ethene. If we are interested in accurate predictions of the effects on HCHO levels of compositional changes in emission inventories, then the multiple role assigned to ALD needs to be eliminated. A more discriminating representation for the olefins in which say four classes, ethene and propene (because of their typically higher concentrations in urban air) and a generalized internal and terminal olefin would be needed. In addition acetaldehyde should be distinguished from higher aldehydes because $^{\cdot}OH$ attack rapidly leads to a source of HCHO, whereas this is not so for higher aldehydes. Therefore four aldehydes would be needed in models: HCHO, acetaldehyde, a higher aldehyde, and glycoaldehyde. Only one scenario was simulated for this mass balance analysis. Typical conditions were picked, but State Implementation Plans show a wide range of VOC/NO_x. Lower VOC/NO_x ratio simulations will be much more dependent on initial and emitted aldehydes: the O_3 reactions can be more important with more O_3 aloft, especially in simulations with less initial aldehydes and lower aldehydes fractions in the emissions. In higher VOC-to-NO_x ratio conditions, where significant amounts of olefinic HC remain in the afternoon, reactions of O_3 with olefin and ethylene may also be more important in producing HCHO.

More mass balance analysis of different mechanisms and different scenarios is needed. Data from cells in the Urban Airshed model should be subjected to a similar analysis. Because of non-linear feedbacks in the mechanisms, to assess more accurately the errors that occur in predicting HCHO with current mechanisms, selected portions of the current air quality mechanisms should be corrected and simulations re-done to compare their predictions with the standard versions. This work is planned as a follow-up task in subsequent efforts.

12

Conclusions

Formaldehyde Measurements

Since the focus of this study concerned the measurement and reactivity of HCHO, much of this report has been directed at verifying multiple, independent techniques of HCHO measurement. Several conclusions can be drawn from our efforts at intercomparison of techniques and sources, and serial measurement:

- All formaldehyde sources–UNC, EPA, and UCR–used as calibration standards agreed to within ±2% in multiple comparisons and by independently calibrated techniques.
- The paraformaldehyde permeation tube was shown to be a very accurate and stable calibration standard for HCHO. The measured precision of concentrations produced from the permeation tube is greater than that from aqueous HCHO stock solutions and from paraformaldehyde injections into large volumes.
- Significant interferences did appear in any test of either the CEA 555 (in use for 11 years at UNC) or the Dasgupta formaldehyde instrument (in use for 3 years at UNC).
- There is weak evidence that the CEA response, when not zero-checked for twenty minutes every three hours during an experiment, may exhibit a positive drift; data collected during such periods may not be correctable, and so have a naturally higher uncertainty than most other CEA data reported here. When zero-checked regularly, the CEA response does not show any significant bias.
- There is no evidence that the Dasgupta formaldehyde instrument ever exhibits more than a 5% bias at any time. Several aspects of this particular wet-chemical fluorescence technique, however, can make some individual data points more uncertain than others. But, when the Dasgupta formaldehyde instrument is operated in a well-maintained mode, it exhibits a precision of 6 ppb at a level of 155 ppb (3.8%). This precision range is observed when the instrument has

been sampling a zero concentration and a level of HCHO in the chamber different from that of the permeation standard source in a two hour cycle.

- The effect that this level of precision has on the overall calibration uncertainty when only 4 samples of the calibration source are used is 6.2% at 155 ppb for a 95% confidence interval. Measurements of the peak height on strip charts contribute less than 1% to the uncertainty resulting in an over-all uncertainty (combined accuracy and precision) of ±7% at a 95% confidence interval for HCHO data taken with the Dasgupta monitor during this project.
- Without the stable and precise calibration standard available from the permeation tube, calibrations in the years before 1982 were less-frequently done since each calibration required the exclusive use of the chamber for relatively high-concentration paraformaldehyde injections. The accuracy of data taken in these years is greatly dependent on instrument stability between calibrations. As a corollary to this conclusion, it has been observed that the CEA instrument was markedly more stable and its response to HCHO considerably more sensitive in these early years than it has been of late. Thus, the accuracy previously ensured by the instrument's inherent stability when new has now been superseded by multiple, independent calibration points.
- Despite concerted and on-going efforts at QA and calibration, uncertainty persists about some HCHO data taken over 12 years in the UNC chambers. Blunders in recording and processing the data are always possible, and calibration standards have not always been as available and reliable as they are today. Thus there are some HCHO data in the UNC chamber database which can not now be shown to be wrong, but which are contrary to expectations given our current understanding of HCHO chemistry.
- Based upon the comparison of the Dasgupta monitor with the chromotropic acid bubbler method and the FTIR method at SAPRC/UCR, it appears that the standards used at SAPRC are accurate and consistent with the UNC and EPA standards to ±2%.
- The SAPRC chromotropic acid bubbler method appears to be erratic at high, reasonably-steady levels of HCHO. We believe that an operation in the practice of the method is responsible.
- The SAPRC chromotropic acid bubbler method can have a low bias for all measurements on a given day, even if it had no bias the day before.
- The SAPRC chromotropic acid bubbler method *never* measured higher than the Dasgupta method in seven experiments.

Formaldehyde Chemistry

- Our chamber simulations support the higher absorption cross-sections of Moortgat compared to Bass.

Ethene Chemistry

- We have presented indirect and non-conclusive evidence that hydroxyperoxyethylnitrate is formed by reaction of the $^{\cdot}OH$ adduct to ethene with NO to an extent of 4%.
- The yields given in the literature for stabilized Criegee biradicals for O_3+olefin reactions are based upon the loss of either O_3 or the olefin, both of which have other consumption pathways in the experimental system. Therefore, when these yields are used in a mechanism, they should be corrected to reflect these other losses. We have made this correction in the case of our ethene model and have found the yields to change by approximately 16%.
- The reactions of peroxymethylene (C_1-Criegee biradical) appear to be reasonably well understood, with the exception of its reaction with water. We presented indirect and inconclusive evidence that a large fraction of the reaction of $^{\cdot}CH_2OO^{\cdot}$ with water could lead to $HCHO$ and H_2O_2. If our assumed pathway is correct, then there exists a large potential for forming H_2O_2 by dark reactions.
- There is some very weak evidence that $^{\cdot}CH_2OO^{\cdot}$ can decompose to form $HCHO$ and $O(3P)$, which will produce O_3 by an organic pathway. This path was not used in our mechanism.
- Dry and wet O_3 + ethene laboratory experiments in which H_2O_2 and formic acid are measured should be conducted in a future study.
- The conclusions of Hatakeyama, *et al.*[52] that Criegee biradical oxidation of SO_2 produces one $HCHO$ for each SO_2 oxidized has been shown to be wrong. Rather, one $HCHO$ is saved from reaction with the Criegee when it reacts with SO_2.
- The chemistry of glycoaldehyde is sufficiently different from that of acetaldehyde that the CB4 and CAL approximation of representing glycoaldehyde by acetaldehyde is questionable. In particular, there is a possibility of alternative decomposition pathways for PGAN that decrease its stability compared to PAN. This difference is sufficiently effects the nitrogen balance sufficient to change the maximum O_3 produced. Secondly the $^{\cdot}OH$ reaction with glycoaldehyde produces more reactive products than the same type reaction with acetaldehyde.
- The temperature dependance of PGAN should be explicitly determined.

- New chamber experiments using glycoaldehyde as the primary reactant are needed for continued model testing.
- New chamber experiments using glyoxal as the primary reactant are needed for continued model testing.
- A technique for the reliable, real-time measurement of formic acid in ethene-NO_x chamber experiments should be found.
- More of the cooler 3-4 ppmC ethene-NO_x chamber experiments should be conducted to confirm that the anomalously high HCHO formation observed in the 1984 October experiments presented here were artifacts of poor calibration. Such future experiments might also strengthen the evidence already seen for the strong temperature dependence of O_3 formation in these systems.
- Although the model fits to the very wide range of experiments simulated here were excellent, we believe that further work is needed on the UNC chamber wall model, particularity related to the order of the NO_2 + wall reaction.
- The excellent 'goodness-of-fit' of the explicit ethene mechanism to a large range of conditions in the UNC chamber over a 12-year period and to ethene experiments in the UCR ITC chamber is strong evidence that the mechanism does explain the observed chemistry in a manner consistent with known kinetics data. Although there remain some doubtful elements in the ethene mechanism, it is at present the best explanation we can construct, and we believe that it can be taken as a standard against which to measure the performance of the ethene portion of air quality simulation mechanisms in common use by EPA, *i.e.*, the CB4 and CAL and RADM mechanisms.

Propene Chemistry

- The new work of Niki, *et al.*[62] and of Martinez and Herron[63] on three-carbon Criegee biradicals should be experimentally extended to the two-carbon systems of *trans*-2-butene and to propene.
- New measurements of glyoxal formation in propene+NO_x and O_3+propene experiments are needed. In addition, we should determine whether glyoxal yields truly depend on NO_x levels; this determination may allow us to choose between the pathways suggested by Niki, *et al.* and those suggested by Martinez and Herron.
- There is weak support in the chamber simulations we have presented here for propene to allow an assertion that the performance of our propene mechanism for predicting HCHO depends upon the initial NO_x concentration. What we have

observed is that low predictions of acetaldehyde occur when NO_x concentrations are greater than 0.3 ppm.

- Gery's, *et al.*[3] and Carter's, *et al.*[23] observations that the recommended Atkinson and Lloyd approach to the two-carbon Criegee biradicals leads to too great a reactivity in propene-NO_x simulations, coupled with our experience and newer kinetics data suggesting that the O_3+propene reaction is a large radical source support a conclusion that no current air quality photochemical model can predict accurate results (for the right reasons) for secondary products in propene-NO_x systems. The fact that O_3 is sometimes closely predicted in these systems must therefore be an artifact and must result from compensating errors within the mechanism.

Performance of CB4

- With regard to predicting O_3, the CB4 mechanism is excellent for ethene-NO_x experiments. It is slightly worse than the explicit mechanism for NO and NO_2, but not significantly so.
- At all levels of ethene tested, CB4 consistently underpredicted the HCHO maxima observed in ethene-NO_x experiments by about 13%. The cause of this underprediction is complex and related to a number of approximations used in the CB4:
  - ▷ There are too few radical-radical termination reactions in CB4 for it to simulate the correct efficiency of $HO_2^{\cdot}$ production from $^{\cdot}OH$+ethene in these high concentration experiments; it therefore predicts too much ethene consumption and too much $HO_2^{\cdot}$ and NO_2 production.
  - ▷ Acetaldehyde is not a good substitute for glycoaldehyde in these high concentration experiments.
  - ▷ Certain pathways in the Criegee biradical reactions have been omitted in the CB4.
- Like the explicit mechanism described herein, the CB4 mechanism does poorly on propene-NO_x experiments with initial propene concentrations above 1.5 ppmC. Current kinetics theory suggests that O_3 + propene reactions should produce radicals. Mechanisms incorporating these processes, however, exhibit a burst of reactivity in systems containing NO_x, even though dark O_3+propene systems are fairly well simulated. Other than being too fast by nearly one hour, the slopes of propene consumption, rate of O_3 production, rate of PAN production and rate of HCHO production are close to correct. Apparently there is an NO_x-

related process in the secondary reactions of the two-carbon Criegee biradicals which delays the large production of radicals.

- Previous testing of the CB4 with toluene and xylene experiments from the UNC chamber[4] have shown that CB4 overpredicts HCHO. Confirming toluene and xylene experiments were conducted in this study and these show similar levels of HCHO as the previous experiments. Thus we conclude that the CB4 mechanism overpredicts HCHO yields from toluene and xylene by about a factor of two. The observed yields of HCHO are low, however, approximately 3% of the aromatic carbon.

Urban Simulations

- Simulations of a typical urban scenario using a simple trajectory model (OZIPM) showed that chemical production of HCHO accounts for 70–90% of the total HCHO observed. A 'pseudo-photostationary-state' is reached at approximately the same level regardless of whether or not initial HCHO and HCHO emissions were included in the simulation.
- Large early morning dilution rapidly reduces any HCHO initially present and most of the initial HCHO is gone by 1300 LDT (maximum O_3 occurred at 1900 LDT).
- Over the day, the olefins (ETH and OLE) and ALD were responsible for 61.2% (basecase) and 58.3% (zero initial aldehyde case) of the HCHO produced. An additional 1% or so HCHO is formed by PARs that were on side chains of OLEs.
- OLE and XYL made their contribution in the morning, ETH made a contribution all day, and ALD increased its contribution to HCHO production near the end of the day.
- Only 8–9% of ETH's contribution to HCHO production is by way of the O_3+ETH reaction, which is one of the reactions in CB4 where HCHO yields are low. Similarly, 10–12% of OLE's contribution to HCHO production is by the O_3+OLE reaction.
- XYL and TOL's contribution to HCHO production is also about 11–12%. If these are too high and ETH's and OLE's are too low, then the combined predictions may be approximately correct.
- The analysis of CB4 for the chamber, however, suggested that correct HCHO levels were obtained in these systems for the wrong kinetic and mechanistic reasons, *i.e.*, there were internal compensating adjustments in various parts of the mechanism. Thus it is not likely that a linear correction would be accurate.

Final Conclusion

We said in the introduction that the purpose of this study was to determine if present photochemical reaction mechanisms could be used to predict accurate ambient levels of HCHO for various scenarios of VOC and NO_x control. We believe that the answer is a qualified yes for the most commonly used EPA mechanism, the Carbon Bond Four mechanism (CB4).

The qualifications are that some parts of the CB4 (as well as other similar mechanisms) are not fully accurate descriptions of the important HCHO producing chemistry. The errors are probably small, only resulting in about a 20% error in the HCHO maximum prediction. But this error level depends upon the composition of the HC mixture used in the simulation because there are compensating errors in different HC classes. A second weakness that CB4 has for this application is that it has a very compressed representation for the most important species producing HCHO, the various olefin classes. For example, it uses a reaction product (ALD) of the two most common olefins (ethene and propene) to represent the entire chemistry of a higher olefin class, the internal olefins. Accuracy for targeted emissions controls could be improved by slightly expanding the olefin representation in CB4. In our estimate, this expansion of the olefin and aldehyde detail in CB4 is a relatively simple task if the mechanism is to be used in simulation programs such as OZIPM; for use in ROM or Airshed, however, it is a large undertaking because the mechanism is "hard-wired" into these codes, and the number of species is an important consideration.

Although not specifically tested herein, the Carter, Atkinson, Lurmann or CAL mechanism[23] has a similar representation for ethene as is used in CB4. CAL's propene representation is worse than CB4's for HCHO production,[4] although it works better for O_3 predictions; CAL has a similar problem to CB4 with HCHO predictions in aromatics chemistry.[4] On the other hand, CAL already has more detail in representing olefins and aldehydes than does CB4 and it too could be improved with a small effort.

References

1 Gray, C., Letter to Farmer, Rhoads, Burnot, Ellison, Hauser, Princiotta, March, 1986.

2 Carter, W. P. L., "A Detailed Mechanism For The Gas-Phase Atmospheric Reactions of Organic Compounds," *Atmos. Environ.*, accepted May, 1989.

3 Gery M. W., G. Z. Whitten and J. P. Killus, "Development and Testing of the CBM-IV for Urban and Regional Modeling," U.S. Environmental Protection Agency,Atmospheric Sciences Research Laboratory, Research Triangle Park, N.C., EPA/600/3-88/082, 1988.

4 Jeffries H. E., K. G. Sexton, J. R. Arnold and J. L. Li, "Validation Testing of New Mechanisms with Outdoor Chamber Data Volume 1: Comparison of CB4 and CAL Mechanisms," U.S. Environmental Protection Agency, Research Triangle Park, N.C., EPA-600/3-89-010a, December, 1988.

5 Atkinson, R. and A. C. Lloyd, "Evaluation of Kinetic and Mechanistic Data For Modeling Of Photochemical Smog," *J. Phys. Chem. Ref. Data*, **13**(2):315–445, 1984.

6 Atkinson, R., "Gas-phase tropospheric chemistry of organic compounds: a review," *Atmos. Environ.*, in press, 1989.

7 Tejada, S. B., "Evaluation of Silica Gel Cartridge Coated In Situ with Acidified 2,4-Dinitrophenylhydrazine for Sampling Aldehydes and Ketones in Air," *Int. J. Environ. Anal. Chem.*, **26**:167–185, 1986.

8 Ho, M. H., *Advances in Chemistry Series,* V. Turoshi, American Chemical Society, Washington, D. C., 1985.

9 Bai, Y. H., J. L. Li, K. G. Sexton, J. R. Arnold and H. E. Jeffries, "Measurements of Formaldehyde in Outdoor Smog Chambers: An Intercomparison of Methods," in *Global and Regional Environmental Atmospheric Chemistry International Conference*, Beijing, China, May 3-10, 1989, paper 345,

10 Altshuller, A. P., D. L. Miller and S. F. Sleva, "Determination of Fomaldehyde in Gas Mixtures by Chromotropic Acid Method," *Anal. Chem.*, **33**:621, 1961.

11 Lyles, G. R., F. B. Dowling and V. J. Blanchard, "Quantitative Determination of Formaldehyde in the Parts per Hundred Million Concentration Level," *J. Air Pollut. Control Assoc.*, **15**:106-08, 1965.

12 Dasgupta, P. K., S. Dong, H. Hwang and H. C. Yang, "Continuous liquid phase fluorometry coupled to a diffusion scrubber for the determination of atmospheric formaldehyde, hydrogen peroxide, and sulfur dioxide.," *Atmos. Environ.*, **22**:949–963, 1988.

13 Nash, T., "The Colorimetric Estimation of Formaldehyde by Means of the Hantzsch Reaction," *Biochem.*, **55**:416, 1953.

14 Belman, S., "The Fluorimetric Determination of Formaldehyde," *Anal. Chim. Acta,* **29**:120-26, 1963.

15 Dong, S. and P. K. Dasgupta, "Fast Fluorometric Flow Injection Analysis of Formaldehyde," *Environ. Sci. Technol.*, **21**:581-88, 1987.

16 Coleman, H. W. and W. G. Steele, *Experimentation and Uncertainty Analysis for Engineers,* John Wiley & Sons, New York, 1989.

17 NASA, "Chemical Kinetics and Photochemical Data For Use in Stratospheric Modeling," Jet Propulsion Laboratory, California Instutute of Technology, Pasadena, CA, JPL-Publication 87-41, September 1987.

18 Baulch, D. L., R. A. Cox, R. F. Hampson Jr., J. A. Kerr, Troe J. and R. T. Watson, "Evaluated Kinetic and Photochemical Data for Atmospheric Chemistry," *J. Phys. Chem. Ref. Data,* **13**(4):1259–1380, 1984.

19 Atkinson, R. and A. C. Lloyd, "Evaluation of Kinetic and Mechanistic Data For Modeling Of Photochemical Smog," *J. Phys. Chem. Ref. Data,* **13**(2):315–445, 1984.

20 Bass, A., A. E. Ledford Jr and A. H. Laufer, "Extinction coefficients of NO_2 and N_2O_4," *J. Res. Natl. Bur. Stand., Sect. A,* **80**:143–166, 1976.

21 Gardner, E. P., P. D. Sperry and J. G. Calvert, "Primary Quantum Yields of NO2 Photodissociation," *J. Geophys. Res.*, **92**(D6):6642-52, 1987.

22 Molina, L. T. and M. J. Molina, "Absolute Absorption Cross Sections of Ozone in the 185- to 350-nm Wavelength Range," *J. Geophys. Res.*, **91**(D13):14501-508, 1986.

23 Carter W. P., F. W. Lurmann, R. Atkinson and A. Lloyd, "Development and Testing of a Surrogate Species Chemical Reaction Mechanism," U.S. Environmental Protection Agency, Research Triangle Park, N.C., EPA-600/3-86/031, May 1986.

24 Magnotta, F. and H. S. Johnston, "Photodissociation quantum yields for the NO3 free radical," *Geophys. Res. Lett.*, **7**:769-772, 1980.

25 Stockwell, W. R. and J. G. Calvert, "The mechanism of HO-SO2 reaction," *Atmos. Environ.*, **17**:2231-2235, 1978.

26 Atkinson, R., "Gas-phase tropospheric chemistry of organic compounds: a review," *Atmos. Environ.*, in press, 1989.

27 Cattell, F. C., J. Cavanagh, R. A. Cox and M. E. Jenkin, "A Kinetics Study of Reactions of HO2 and C2H5O2 using Diode Laser Absorption Spectroscopy," *J. Chem. Soc., Faraday Trans.*, **2**:1999-2018, 1986.

28 McAdam, K., B. Veyret and R. Lesclaux, "UV Absoption Spectra of HO2 and CH3O2 Radicals and the Kinetics of their Mutual Reactions at 298 K," *Chem. Phys. Lett.*, **133**(1):39-44, 1987.

29 Bass, A., L. C. Glasgow, C. Miller, J. P. Jesson and D. L. Filkin, "Temperature dependent absorption cross sections for formaldehyde (CH2O): The effect of formaldehyde on stratospheric clorine chemistry," *Planet. Space Sci.*, **28**:675, 1980.

30 Moortgat, G. K., W. Seiler and P. Warneck, "Photodissociation of HCHO in Air: CO and H2 Quantum Yields at 220 and 300 K," *J. Chem. Phys.*, **78**(3):1185-90, 1983.

31 Su, F., J. G. Calvert and J. H. Shaw, "Mechanism of the Photooxidation of Gaseous Formaldehyde," *J. Phys. Chem.*, **83**(25):3185, 1979.

32 Niki, H., P. D. Maker, C. M. Savage and M. D. Hurley, "An FT IR Spectroscopic Study of the Reactions $Br + CH_3CHO \longrightarrow HBr + CH_3CO and CH_3C(O)OO + NO_2 \longrightarrow CH_3C(O)OONO_2(PAN)$," *Int. J. Chem. Kinet.*, **17**:525-34, 1985.

33 Jeffries, H. E., D. Fox and R. M. Kamens, "Outdoor Smog Chamber Studies: Light Effects Relative to Indoor Chambers," *Environ. Sci. Technol.*, **10**(10):1006-1011, 1976.

34 Pitts, J. N., E. Sanhueza, R. Atkinson, W. P. L. Carter, A. M. Winer, G. W. Harris and C. N. Plum, "An Investigation of the Dark Formation of Nitrous Acid in Environmental Chambers," *Int. J. Chem. Kinet.*, **16**:919–939, 1984.

35 Sakamaki, F., S. Hatakeyama and H. Akimoto, "Formation of Nitrous Acid and Nitric Oxide in the Heterogeneous Dark Reaction of Nitrogen Dioxide and Water Vapor in a Smog Chamber," *Int. J. Chem. Kinet.*, **15**:1013-1029, 1983.

36 Akimoto, H., H. Takagi and F. Sakamaki, "Photoenhancement of the Nitrous Acid Formation in the Surface Reaction of Nitrogen Dioxide and Water Vapor: Extra Radical Source in Smog Chamber Experiments," *Int. J. Chem. Kinet.*, **19**:539-551, 1987.

37 Jenkin, M. E., R. A. Cox and D. J. Williams, "Laboratory Studies of the Kinetics of Formation of Nitrous Acid from the Thermal Reaction of Nitrogen Oxide and Water Vapor," *Atmos. Environ.*, **22**(3):487-498, 1988.

38 Sakamaki, F. and H. Akimoto, "HONO Formation as Unknown Radical Source for Photochemical Smog Chamber," *Int. J. Chem. Kinet.*, **20**:111-116, 1988.

39 Tuazon, E. C., R. Atkinson, C. N. Plum, A. M. Winer and J. N. Pitts, "The reaction of

gas-phase N2O5 with water vapor," *Geophys. Res. Lett.*, **10**:953–956, 1983.

40 Jeffries, H. E., "UNC Solar Radiation Models," Manuscript, 1989.

41 Jeffries H. E., K. G. Sexton, J. R. Arnold and T. L. Kale, "Validation Testing of New Mechanisms with Outdoor Chamber Data Volume 3: Calculation of Photochemical Reaction Photolysis Rates in the UNC Outdoor Chamber," U.S. Environmental Protection Agency, Research Triangle Park, N.C., EPA-600/3-89-010c, 1989.

42 Niki, H., P. D. Maker, C. M. Savage and L. P. Breitenbach, "An FT IR Study of the Transitory Product in the Gas-Phase Ozone-Ethylene Reaction," *J. Phys. Chem.*, **85**(8):1024-27, 1981.

43 Niki, H., P. D. Maker, C. M. Savage and M. D. Hurley, "An FT IR Study of the Kinetics and Mechanisms for the CL-Atom- and HO-Radical-Initiated Oxidation of Glycolaldehyde," *J. Phys. Chem.*, **91**(8):2174-2178, 1987.

44 Shepson, P. B., E. O. Edney, T. E. Kleindienst, J. H. Pittman, G. R. Namie and L. T. Cupitt, "The Production of Organic Nitrates from Hydroxyl and Nitrate Radical Reaction with Propylene," *Environ. Sci. Technol.*, **19**(9):849-54, 1985.

45 Su, F., J. G. Calvert, J. H. Shaw, H. Niki, P. D. Maker, C. M. Savage and L. P. Breitenbach, "Spectroscopic and Kinetic Studies of a New Metastable Species in the Photooxidation of Gaseous Formaldehyde," *Chem. Phys. Letters*, **65**(2):221, 1979.

46 Martinez, R. I., J. T. Herron and R. E. Huie, "The mechanism of ozone-alkene reactions in the gas phase: A mass spectrometric study of the reactions of eight linear and branched-chain alkenes," *J. Am. Chem. Soc.*, **103**(13):3807–3820, 1981.

47 Herron, J. T. and R. E. Huie, *J. Am. Chem. Soc.*, **99**:5430, 1977.

48 Niki, H., P. D. Maker, C. M. Savage and L. P. Breitenbach, "Mechanism for Hydroxyl Radical Initiated Oxidation of Olefin-Nitric Oxide Mixtures in Parts per Million Concentrations," *J. Phys. Chem.*, **82**(2):135-37, 1978.

49 Dodge, M. and R. R. Arnts, "A New Mechanism for the Reaction of Ozone with Olefins," *Int. J. Chem. Kinet.*, **11**:399, 1979.

50 Su, F., J. G. Calvert and J. H. Shaw, "Mechanism of the Photooxidation of Gaseous Formaldehyde," *J. Phys. Chem.*, **83**(25):3185, 1979.

51 Hatakeyama, S., H. Kobayashi and H. Akimoto, "Gas-Phase Oxidation of SO2 in the Ozone-Olefin Reactions," *J. Phys. Chem.*, **88**(20):4736-39, 1984.

52 Hatakeyama, S., H. Kobayashi, Z. Lin, H. Takagi and H. Akimoto, "Mechanism for the Reaction of CH2OO with SO2," *J. Phys. Chem.*, **90**(17):4131-35, 1986.

53 Kerr A. and J. G. Calvert, "Chemical Transformation Modules for Eulerian Acid Deposition Models, Volume I: The Gas-Phase Chemistry," U.S. Environmental Protection Agency, Atmospheric Sciences Research Laboratory, Research Triangle Park, N.C., IGA DW 930237, 1984.

54 Kan, C. S., S. Fu, J. G. Calvert and J. H. Shaw, "Mechanism of the Ozone-Ethene Reaction in Dilute N2/O2 Mixtures Near 1-atm Pressure," *J. Phys. Chem.*, **85**(16):2359-63, 1981.

55 Niki, H., P. D. Maker, C. M. Savage and L. P. Breitenbach, "FT IR Study of the Kinetics and Mechanism for Cl-Atom-Initiated Reactions of Acetaldehyde," *J. Phys. Chem.*, **89**(4):588-91, 1985.

56 Hatakeyama, S., H. Bandow, M. Okuda and H. Akimoto, "Reactions of CH2OO and CH2(1A1) with H2O in the Gas Phase," *J. Phys. Chem.*, **85**(15):2249-54, 1981.

57 Martinez, R. I., J. T. Herron and R. E. Huie, "The mechanism of ozone-alkene reactions in the gas phase: A mass spectrometric study of the reactions of eight linear and branched-chain alkenes," *J. Am. Chem. Soc.*, **103**(13):3807–3820, 1981.

58 Martinez, R. I. and J. T. Herron, "Gas-phase reaction of SO2 with a Criegee intermediate in the presence of water vapor," *J. Environ. Sci. Health*, **A16**(6):623-636, 1981.

59 Bailey, P. S. *Ozonation in organic chemistry,* Academic Press, New York, 1978.

60 Niki, H., P. D. Maker, C. M. Savage and L. P. Breitenbach, "An FTIR Study of the Cl-Atom-Initianted Reaction of Glyoxal," *Int. J. Chem. Kinet.*, **17**:547-558, 1985.

61 Langford, A. O. and C. B. Moore, "Collision complex formation in the reactions of formyl radicals with nitric oxide and oxygen," *J. Chem. Phys.*, **80**(9):4211-21, 1984.

62 Niki, H., P. D. Maker, C. M. Savage, L. P. Breitenbach and M. D. Hurley, "FT IR Spectroscopic Study of the Mechanism for the Gas-Phase Reaction between Ozone and Tetramethylethylene," *J. Phys. Chem.*, **91**(4):941-46, 1987.

63 Martinez, R. I. and J. T. Herron, "Stopped-Flow Studies of the Mechanisms of Ozone-Alkene Reactions in the Gas Phase: Tetramethylethylene," *J. Phys. Chem.*, **91**(4):947-53, 1987.

64 Dodge, M. C., "Formaldehyde Production in Photochemical Smog as Predicted by Three State-of-the-Science Chemical Oxidant Mechanisms," *J. Geophys. Res.*, in press, February, 1990.

M

Mechanism Listings

Inorganic Mechanism

```
! Inorganic, CO, Methane, Ethane, Formaldehyde, Acetaldehyde Reactions
!    Version 2.5, May 2, 1990
UNITS=
 AFactor = cm_molecules_sec,  {these are default, but included for docum}
 ActEne  = kelvin;

! Species M, O2, H2O, and WH2O are builtin.
!   M and O2 are at 298K and 1 atm or
!    vary with time by Tables=TEMPERATURE and PRESSURE if present;
!   H2O is either at 20000 ppm or varies by Table=WATER if present.
!   RELHUMIDITY is also built-in and varies automatically
!    with temperature and H2O.
!   WH2O is wall adsorbed water in equilibrium with gas phase H2O; it
!    varies automatically with RelHumidity and builtin isotherm; units are ppm.
!   When these species appear on left of reaction they effect the rate;
!   When these species appear on right of reaction they are ignored.
! Names can be 31-characters and first 12 characters are significant.

!IGNORESPECIES=
!  These species are ignored anywhere in reaction, they are for clarity only.
! CO2;
!
! ******* I == INORGANIC CHEMISTRY *******
!
! a) NO2 photolysis
TABLE=
 HVNO2;   {name of NO2 photolysis rate vs time table}
REACTIONS=
 Ia1]          NO2     (hv)= NO    + O    # HVNO2,
 Ia2]  O    + O2   + M    = O3    + M    # 6.0E-34^-2.3 ,
 Ia3] O3    + NO          = NO2   + O2   # 2.0E-12@ -1400 ,
                                           {NASA87, Table1}
 Ia4] NO    + NO   + O2   = 2.0*NO2      # 3.3E-39 @ 530 ,

 Ia5a] O    + NO2         = NO    + O2   # 6.5E-12@ 120 ,
 Ia5b] O    + NO2     (M)= NO3           # 2.2E-11^0.0 & 9.0E-32^-2  & 0.6^1 ,
 Ia6]  O    + NO      (M)= NO2           # 3.0E-11^0.0 & 9.0E-32^-1.5& 0.6^1 ;
```

```
! b) OZONE photolysis
TABLES=
 HVO3O3P, HVO3O1D;   {name of photolysis rate vs time tables}

COEFF=
 fIb34=1E-5;         {used to lower stiffness for O1D}
REACTIONS=
 Ib1] O3      {hv}= O    + O2          # HVO3O3P ,
 Ib2] O3      {hv}= O1D  + O2          # HVO3O1D ,
 Ib3] O1D  + M    = O    + M           # 2.09E-11 @ 95.3 * fIb34 ,
 Ib4] O1D  + H2O  = 2.0*OH             # 2.2E-10 * fIb34 ,
!      Ib3 and Ib4 rates from CODATA84, Table 2.
!      O1D + N2 = O3P + N2 # 1.8E-11 @ 107   occurs 0.7905
!      O1D + O2 = O3P + O2 # 3.2E-11 @  67   occurs 0.2095
!      O1D + M  = O3P + M  # 2.09E-11@ 95.3  by regression fit
!      O1D + H2O= 2*OH     # 2.2E-10         both NASA87 and CODATA84
!      The factor fIB34 = 1E-5 is used to lower the stiffness
!      of the solution since it is only the ratio of Ib3/Ib4 that
!      is important.
 Ib5] O3   + OH   = HO2  + O2          # 1.6E-12 @-940. ,
 Ib6] O3   + HO2  = OH   + O2  + O2    # 1.1E-14 @-500. ;
                                         {NASA87,Table1}
! c) NO3 chemistry
TABLES=
 HVNO3NO, HVNO3NO2;
REACTIONS=
 Ic1]  O3   + NO2       = NO3  + O2         # 1.4E-13 @-2450 , {NASA87, Table 1}
 Ic2a]        NO3  {hv}= NO   + O2         # HVNO3NO ,
 Ic2b]        NO3  {hv}= NO2  + O          # HVNO3NO2 ,
 Ic3]  NO3  + NO        = 2.0*NO2          # 1.7E-11 @ 150 ,  {NASA87, Table 1}
 IC4]  NO3  + HO2       = HNO3  + O2       # 2.48E-12 , {Carter's RADM Mech}
 Ic4a] NO3  + NO2       = NO    + NO2 + O2 # 2.5E-14 @-1230 , {Atk&Ll84}
 Ic5b] NO3  + NO2    {M}= N2O5             # 1.5E-12^-0.5 & 2.2E-30^-4.3 & 0.6^1.0 ,
                                                {NASA87,Table 2}
 Ic6]         N2O5   {M}= NO3 + NO2        # =Ic5b*9.09E+26 @-11200 ,
                                                {NASA87,Table 3}
 Ic7]  N2O5 + H2O       = 2.0*HNO3         # 2.0E-21;
                                                {NASA87,Table 2, homogeneous rate}
! d) HONO chemistry
COEFF=
 HONO_NO2R=0.171; {from ratio of rates on July 13, 1986 UNC Site}
REACTIONS=
 Id1] NO   + NO2  + H2O = 2.0*HONO          # 4.4E-40 ,
 Id2] HONO + HONO       = NO   + NO2  + H2O # 1.01E-20 ,
 Id3] OH   + NO     {M}= HONO              # 1.5E-11^-0.5 & 7.0E-31^-2.6 & 0.6^1 ,
 Id4]        HONO  {hv}= OH   + NO         # HVNO2 * HONO_NO2R ,
 Id5] OH   + HONO       = NO2  + H2O        # 6.6E-12 ;

! e) HO2 reactions
REACTIONS=
 Ie1] HO2  + NO         = OH   + NO2     # 3.7E-12 @ 242. ,
 Ie2] HO2  + NO2     {M}= PNA            # 4.7E-12^-1.4 & 1.8E-31^-3.2  & 0.6^1 ,
 Ie3]        PNA     {M}= HO2  + NO2     #=Ie2*4.76E26@-10900. ,
 Ie4] OH   + PNA        = NO2  + H2O  +O2 # 1.3E-12 @ 380 ;
!     k[Ie1] to k[Ie4] are from NASA87,Table 2 and Table 3
! f) OH TERMINATION REACTIONS
REACTIONS=
 If1]  OH    + NO2    {M}= HNO3           # 2.4E-11^-1.3 & 2.6E-30^-3.2 & 0.6^1,
 If2]  OH    + HNO3       = NO3   + H2O   # 7.2E-15@785  & 4.1E-16@1440 & 1.9E-33@725,
 If3]  OH    + HO2        = H2O   + O2    # 4.6E-11 @ 230 ;  {NASA87}

! g) HO2 TERMINATION REACTIONS
TABLE=
 HVH2O2;  {name of photolysis rate vs time table}
REACTIONS=
 Ig1a] HO2  + HO2          = H2O2              # 2.2E-13 @ 621 ,
 Ig1b] HO2  + HO2  + M     = H2O2  + O2 + M    # 1.9E-33 @ 985 ,
 Ig1c] HO2  + HO2  + H2O   = H2O2  + O2 + H2O  # 3.1E-34 @ 2828,
 Ig2]         H2O2     {hv}= 2*OH              # HVH2O2 ,
 Ig3]  OH   + H2O2         = HO2   + H2O       # 3.1E-12 @-187 ;

! h) CO/H2 chemistry
COEFF=
 fIh1=0.6; {1+0.6*Pressure}
REACTION=
 Ih1a] OH    + CO  = HO2   + CO2         # 1.5E-13 ,
 Ih1b] OH    + CO  = HO2   + CO2         #=Ih1a*fIh1*PRESSURE ,
 Ih2]  OH    + H2  = HO2   + H2O         # 7.7E-12 @-2100 ;
!
! ----------------End of Inorganic Mechanism--------------------------


! ***** P1 == METHANE CHEMISTRY*****
! Rates and reactions are from CODATA85, NASA87, Atk&Ll84
!
REACTIONS=
 P1_1]  OH    + CH4      = CH3O2  + H2O          # 2.4E-12 @-1710 ,
 P1_2]  CH3O2 + NO       = NO2    + CH3O         # 4.2E-12 @ 180  ; {=RO2NORATE}
!
!    P1_2 is the prototype rxn for all RO2 + NO; k[P1_2] from NASA87
RateAlias:
 RO2NORATE  = P1_2;

#if MENO4  ===>include these rxns only if symbol MENO4 is defined
! These rxn are usually ignored because P1_4 is very fast (t1/2=0.01 min)
REACTIONS:
 P1_3]  CH3O2 + NO2   {M}= CH3O2NO2             # 6.5E-12^-2 & 1.5E-30^-4.0 & 0.6^1 ,
 P1_4]          CH3O2NO2 = CH3O2 + NO2          #=P1_3*7.7E+27@-11200 ;{NASA,Table 3}
#end

DeclareSpecies:
 RONO2;    {lumped organic nitrate}
SpeciesAlias:
 CH3ONO2 = RONO2;
COEFF=
 fP1_5     = 0.1;
REACTIONS=
 P1_5a] CH3O  + O2       = HCHO  + HO2          # 5.5E-14 @-1000 , {Atk89}
 P1_5b] CH3O  + NO       = CH3ONO               # 1.3E-11 @  300 , {Atk89}
 P1_5c] CH3O  + NO2  {M}= CH3ONO2               # 1.2E-11 ,
 P1_5d] CH3O  + NO2      = HCHO  + HONO         #=P1_5c*fP1_5 ;
```

```
COEFF=
 MNIT_NO2R = 0.3;
REACTIONS=
 P1_6]        CH3ONO {hv}= CH3O   + NO           # HVNO2*MNIT_NO2R,
 P1_7]  CH3ONO  + OH    = HCHO  + NO  + H2O     # 2.0E-13,          {Atk&Ll84}
 P1_8]  CH3ONO2 + OH    = HCHO  + NO2 + H2O     # 3.0E-13;          {Atk&Ll84}
DeclareSpecies:
 ROOH;   {lumped organic hydro peroxide}
SpeciesAlias:
 COOH=ROOH;
COEFF:
 fald = 0.75,
 fper = 0.25;   {from Cattell, etal, 1986; Niki85, see below }
REACTIONS=
 P1_9]  CH3O2    + HO2   = fald*HCHO + fald*H2O +
                           fper*COOH + O2       #1.75E-13 @1000 ;{=RO2HO2RATE}
!
!    P1_9 is the prototype rxn for all RO2 + HO2;
!    k[P1_9] is 5.8E-12 at 298k, NASA87 rate was 6.0E-12
!    Niki, Kan reported COOH product at rate 0.25 total rate.
!    Cattell86 proposed HCHO + H2O + O2 (-90kcal), a
!                       CH3OOH + O2     (-37kcal), b
!                       CH3OH + O3      (-20kcal), c
!                       HCHO  + OH + O2 (  7kcal). d
!    Only a and b are used here, but note that Niki85 (CCHO study) did
!    observe production of O3 from CC(O))O2 + HO2  at ratio of b:c = 3:1
RateAlias:
 RO2HO2RATE = P1_9;
DeclareSpecies:
 ROOR,   {lumped organic peroxide}
 ROH;    {lumped alcohol}
SpeciesAlias:
 COOC=ROOR,   {Methyl Peroxide}
 CH3OH=ROH;
COEFF=
 f2sta1    = 0.575,  { CODATA84, page 1328}
 f2rad     = 0.350,  { NASA 85/87 has 9a and 9c switched by mistake}
 f2sta2    = 0.075;
REACTIONS=
 P1_10]  CH3O2 + CH3O2   = f2sta1*CH3OH + f2sta1*HCHO +
                           f2rad *CH3O  + f2rad *CH3O +
                           f2sta2*COOC  + O2    # 1.6E-13 @ 220 ; {=RO2RO2RATE}
!    P1_10 is the prototype RO2 + RO2 reaction rate
RateAlias:
 RO2RO2RATE = P1_10;
!
REACTION=
 P1_11]  CH3OH + OH   = CH3O  + H2O             # 1.0E-12 ,

 P1_12]  OH    + COOH = 0.6*CH3O2 + 0.6*H2O +
                        0.4*HCHO  + 0.4*OH     # 1.0E-12 ;
! In P1_12 splits are due to Niki (NASA85) for
!        CH3OOH + OH = CH3OO  + H2O 60%
!        CH3OOH + OH = CH2OOH + H2O 40%
!                      CH2OOH = HCHO + OH fast
!
! end of Methane Reactions
! ***** C1 == FORMALDHYDE CHEMISTRY****
TABLE=
 HVHCHOR, HVHCHOS ; {name of photolysis rate vs time tables}
REACTIONS=
 C1_1] HCHO    {hv}= 2*HO2 + CO          # HVHCHOR ,
 C1_2] HCHO    {hv}= CO    + H2          # HVHCHOS ,
 C1_3] OH   + HCHO = HO2   + CO          # 1.13E-12^2 @ 648 ,  {Atk89}
 C1_4] O    + HCHO = OH    + HO2 + CO    # 3.4E-11 @-1600 ,
 C1_5] NO3  + HCHO = HNO3  + HO2 + CO    # 2.8E-12 @-2522 ; {Carter, CAL88}
!
!    A, Ea for reaction C1_5 derived from NASA88 and Atk89
!    recommendation of k(298) = 6.0E-16, and estimated
!    A = 2.8E-12, which is 2 x the A for NO3 + acetaldehyde
!    recommended by IUPAC88.  <Note from CAL88 rxn file.
!
SpeciesAlias:
 HOCH2OOH=ROOH;
REACTIONS:
 C1_6] HO2     + HCHO   = HOCH2O2               # 9.7E-15 @ 625   , {Atk89}
 C1_7]           HOCH2O2= HO2    + HCHO         # 2.4E+12 @-7000 , {Atk89}
 C1_8] HOCH2O2 + NO     = NO2    + HO2 + HOCHO #=RO2NORATE ,
 C1_9] HOCH2O2 + HO2    = fald*HOCHO + fald*H2O  + O2 +
                          fper*HOCH2OOH         #=RO2HO2RATE ;
!
REACTION:
 C1_10] OH + HOCHO= HO2 + CO2 + H2O        # 4.6E-13 ;
!

! ***** P2 == ETHANE CHEMISTRY*****
! Rates and reactions are from CODATA85, NASA87, Atk&Ll84
!
REACTIONS=
 P2_1]  OH    + CH3CH3 = CCO2   + H2O          # 1.23E-12^2 @-445 ,{Atk89}
 P2_2]  CCO2  + NO     = NO2    + CCHO + HO2   #=RO2NORATE ;
!
SpeciesAlias:
 CCOOH=ROOH;
REACTIONS=
 P2_3]  CCO2  + HO2    = fald*CCHO  + fald*H2O +
                         fper*CCOOH + O2        #=RO2HO2RATE ;
!
SpeciesAlias:
 CCOOC=ROOR,   {Ethyl Peroxide}
 CCOH =ROH;
REACTIONS=
 P2_4]  CCO2 + CH3O2   = f2sta1*CCOH  + f2sta1*HCHO +
                         f2rad *CCHO  + f2rad *HO2  + f2rad *CH3O +
                         f2sta2*CCOOC + O2    #=RO2RO2RATE ;
!
REACTION=
 P2_5]  CCOH + OH      = CCHO  + HO2  + H2O   # 2.0E-12 ,

 P2_6]  OH   + CCOOH   = 0.6*CCO2 + 0.6*H2O +
                         0.4*CCHO + 0.4*OH    # 1.0E-12 ;
!
! end of Ethane Reactions
! ***** C2 == ACETALDEHYDE CHEMISTRY *******
TABLE=
 HVCCHOR;
REACTIONS=
 C2_1]    CCHO (hv)= CH3O2 + CO + HO2        # HVCCHOR ,
 C2_2]  O  + CCHO  = CC(O)O2 + OH            # 1.2E-11 @-986 , {AL84}
 C2_3] OH  + CCHO  = CC(O)O2 + H2O           # 5.55E-12 @ 311 , {Atk89, Table8}
 C2_4] NO3 + CCHO  = CC(O)O2 + HNO3          # 1.4E-12 @-1900 ; {NASA 87}

! ***** PA2 == PEROXYACETYL RADICAL CHEMISTRY *******
!
REACTIONS:
 PA1_1] CC(O)O2 + NO  = NO2  +  CH3O2  +  CO2  # 5.1E-12 @ 200 , {Atk89}
 PA1_2] CC(O)O2 + NO2 = PAN                    # 6.05E-15 @ 2200 ,
 PA1_3]           PAN = NO2  +  CC(O)O2        # 2.2E16@-13435 & 6.3E-2@-12784 & 0.27^1;
!
!      k[PA1_2] is from k(298)=9.7E-12 from fitting JL1877, MY1877,
!               and AU1778 (Killus rate was 8.3E-12) and
!               Carter's personal communication that new SAPRC work
!               shows E/R to be about 2200 vs Killus's 5500
!      k[PA1_3] is from IUPAC and Atkinson 90
!
! These reactions are proto-type for all other RCO3 reactions.
RateAlias:
 RCO3NORATE  = PA1_1,
 RCO3NO2RATE = PA1_2,
 PANRATE     = PA1_3;
!
SpeciesAlias:
 CC(O)OOH = ROOH,
 CCOOC    = ROOR,
 CC(O)OH  = ROH;
COEFF:
 f3acid= 0.25, {Niki85, acetaldehyde paper}
 f3per = 0.75,
 f3rad = 0.5,  {Atk89}
 f3sta = 0.5;
REACTIONS=
 PA1_4] CC(O)O2 + HO2   = f3acid*CC(O)OH  +  f3acid*O3 +
                          f3per*CC(O)OOH  +  O2  #3.40E-13 @ 800 ,{=RCO3HO2RATE}
 PA1_5] CC(O)O2 + CH3O2 = f3rad*CH3O + f3rad*CH3O2 + f3rad*CO2 +
                          f3sta*CC(O)OH + f3sta*HCHO + O2
                                                 #1.86E-12 @ 529 ,{=RCO3RO2RATE}
 PA1_6] CC(O)O2 + CC(O)O2 = 2*CH3O2 + 2*CO2 + O2 #3.00E-12 @ 500 ;{=RCO3RCO3RATE}
RateAlias:
RCO3HO2RATE  = PA1_4,
RCO3RO2RATE  = PA1_5,
RCO3RCO3RATE = PA1_6;
!
!    k[PA1_4]  is prototype rxn for all RCO3 + HO2;  rate from Atk89
!    k[PA1_5]  is prototype rxn for all RCO3 + RO2;  rate from Atk89
!    k[PA1_6]  is prototype rxn for all RCO3 + RCO3; rate from Atk89; Addison etal

! End of Inorganic, Carbonyl Reactions
#def INORCARB
```

Ethene Mechanism

```
! Ethene Explict Chemistry
!      Version 2.1, January 5, 1990
! Requires the Inorganic, Methane, Formaldehyde Reactions
#ifnot INORCARB
ERRORMSG=
 Ethene Reactions require the Inorganic, Carbonyl Reactions ;
#end

UNITS=
 AFactor = cm_molecules_sec,
 ActEne  = kelvin;

! ***** O2 == ETHENE CHEMISTRY *******

!_ a) O attack
REACTIONS=
 O2a_1]   O    + C:C = CH3O2 + CO + HO2       # 1.04E-11 @-792 ;

!_ b) OH attack

!  OH+C:C from:
!  Niki,Maker,Savage,Breitenbach,Chem.Phys.Lett.,80,499,1981
!  Rates for O2b.4a/4b based on Niki's ratio of 5.4E--20 c/m at 298k
!   and Atkinson's rate for k[4a]=8.0E-15.  Atkinson then supplied the
!   A-factor to get the Ea for k[4b]
SpeciesAlias:
! HOCCONO2 = RONO2, {ignore terminal OH}
 HOCCOOC  = ROOR,  {"}
 HOCCOH   = ROH;   {"}
COEFF=
 fNO2   = 0.96,
 fRONO2 = 0.04; {based upon fitting data and extrapolation of Shepson eta 85}
REACTIONS=
 O2b_2]   OH     + C:C = HOCCO2               # 8.8E-12^0.8&1.5E-28^0.8&0.6^1.0,
                                                   {NASA87, Table 2, Note 25}

 O2b_3a] HOCCO2 + NO  = HOCCONO2             #=RO2NORATE * fRONO2,
 O2b_3b] HOCCO2 + NO  = NO2 + HOCCO          #=RO2NORATE * fNO2,

 O2b_4a]        HOCCO  = 2*HCHO + HO2        # 2.7E+14@-6350 , {Atk89,p30}
 O2b_4b] HOCCO  + O2  = HOCCHO + HO2         # 8.0E-15 ,       {Atk89,p30}

 O2b_5] HOCCO2 + HO2 = fald*HOCCHO + fald*H2O  +  O2  +
                       fper*HOCCOOH          #=RO2HO2RATE ,

 O2b_6] HOCCO2 + CH3O2 = f2sta1*HOCCOH  + f2sta1*HCHO +
                         f2rad *HOCCO   + f2rad*CH3O  +
                         f2sta2*HOCCOOC + O2  #=RO2RO2RATE ,
 O2b_7]        HOCCOOH = HCHO + HCHO + H2O    # 1E-5 ; {see BR1_3}

!_ c) NO3 attack
SpeciesAlias:
 NO3CCHO  = HOCCHO,  {treat NO3 group like HO in glycoaldehyde}
 NO3CCOOC = ROOR,    {""}
 NO3CCOH  = ROH;     {""}
```

```
REACTIONS:
 O2c_1] NO3     + C:C = NO3CCO2                     # 2.15E-12 @-2758 ,{CODATA 88}
 O2c_2] NO3CCO2 + NO  = 2*NO2 + 2*HCHO + HO2        #=RO2NORATE ,
 O2c_3] NO3CCO2 + HO2 = fald*NO3CCHO  + fald*H2O  +  O2 +
                        fper*NO3CCOOH               #=RO2HO2RATE ,
 O2c_4] NO3CCO2 + CH3O2 = f2sta1*NO3CCOH + f2sta1*HCHO +
                          f2rad*NO2 + f2rad*HCHO + f2rad*HCHO +
                          f2rad*CH3O +
                          f2sta2*NO3CCOOC +  O2     #=RO2RO2RATE ,
 O2c_5]         NO3CCOOH = HNO3 + HCHO + HCHO       # 1E-5 ; {see O2b_7}

!_ d) O3 attack
!  O3+C:C from:
!  Hatakeyama,Kobayashi,Lin,Tanagi,Akimoto,J.Phys.Chem,90,4131-5,1986
!  Reaction constructed by:
!   O3     + C:C    = HCHO + 0.6*CH2OO> + 0.2*CH2OOx + 0.2*CH2OO  {Hatakeyama}
!  But, splits were based on Delta[SO2]/Delta[O3] and did not account for
!   other O3 losses.  I estimate from Su,Calvert Simulations that the yields
!   of cold and warm CH2OO are 1.163 times higher, giving
!                   = HCHO + 0.5350*CH2OO> + 0.2325*CH2OOx + 0.2325*CH2OO
!  From Hatakeyama's analysis:
!   CH2OOx + M      = CH2OO    1E-10 c/m/s
!   CH2OOx          = CH2OO>   1E+9  /s  {Hatakeyama}
!   k(stab)/k(decomp) = 1.0E-19 c/m = 2.46E-6 /ppm
COEFF:
 Rstab_dec=2.56E-6, {these units have to be /ppm because no conversion}
 fO3Ecold =0.2325,  {Hatakeyama, see note above}
 fO3Ewarm =0.2325,
 fO3Ehot  =0.5350;
REACTION:
 O2d_1] O3  + C:C = HCHO + fO3Ehot*CH2OO> + fO3Ewarm*CH2OOx + fO3Ecold*CH2OO
                                            # 1.2E-14 @-2636 , {Atk89}
 O2d_2a] CH2OOx     = CH2OO> # 2.0E+5 , {just a large rate}
 O2d_2b] CH2OOx + M = CH2OO  #=O2d_2a*Rstab_dec ;
!
!
! include the Criegiee bi-radical reactions if not already read.
#ifnot CRIE1RXN
@%MECH%criegee.rxn
#end

! include GlycoAldehyde reactions if not already read.
#ifnot GALDRXN
@%MECH%glyald.rxn
#end

! tell others...
#def ETHRXN
! end of Ethene, Glycoaldehyde Reactions
```

Propene Mechanism

```
! Propene and Its Products Reactions
!      Version January 20, 1989
#ifnot INORCARB
ERRORMSG=
 Propene Reactions require the Inorganic, Carbonyl Reactions ;
#end

UNITS=
 AFactor = cm_molecules_sec,
 ActEne  = kelvin;

! O3 === Propene Chemistry
!
REACTIONS=
 O3_1]  O     + C:CC = 0.6*C(CO)C +
                       0.2*HCHO    + 0.2*CO  + 0.2*OH + 0.2*CH3O2 +
                       0.2*CCO2    + 0.2*HO2 + 0.2*CO # 1.18E-11 @-324 ;

! As Carter86, let acetone C(CO)C represent propionaldehyde and propene oxide.
! The other two paths are: 0.2*(.CH2CHO + CH3.) and 0.2*(HCO + CH3CH2.)
!  Allow the .CH2CHO to decompose as AtkLly84 to give HCHO + CO + OH;
!  the CH3 gives CH3O2; allow the HCO to form HO2 + CO; and allow
!  CH3CH2 to form CCO2.

! Shepson et al, EST 19, 1985, 849 found at 300K
!  CC(ONO2)COH with yield of 0.022
!  CC(OH)CONO2 with yield of 0.019
COEFF:
 fPALD1=0.97,
 fPNO31=0.03,
 fPALD2=0.97,
 fPNO32=0.03;
DeclareSpecies:
 HOCCHO,
 CC(O)C;
SpeciesAlias:
! CC(OH)CONO2= RONO2,
! CC(ONO2)COH= RONO2,
 CC(OH)CHO  = HOCCHO,
 CC(OH)COOH = ROOH,  {Hydroxy-Propyl-Hydro  peroxide}
 CC(OH)COOC = ROOR,  {Hydroxy-Propyl-methyl peroxide, ignore OH}
 CC(OH)COH  = ROH,   {ignore  OH}
 CC(O)COH   = CC(O)C,{ignore  OH}
 CC(OOH)COH = ROOH,
 CC(OOC)COH = ROOR;
REACTIONS=
 O3_2]  OH    + C:CC  = 0.65*RP1O2 + 0.35*RP2O2     # 2.8E-11^-1.3&3E-27^-3&0.5^1 ,
                                                      {Atk89}
 O3_3a] RP1O2+ NO     = fPALD1*NO2  + fPALD1*HCHO +
                        fPALD1*CCHO + fPALD1*HO2  +
                        fPNO31*CC(ONO2)COH          #=RO2NORATE ,
 O3_3b] RP2O2+ NO     = fPald2*NO2  + fPald2*HCHO +
                        fPald2*CCHO + fPald2*HO2  +
                        fPNO32*CC(OH)CONO2          #=RO2NORATE ,
 O3_4a] RP1O2 + HO2   = fald*CC(OH)CHO  + fald*H2O  + O2 +
                        fper*CC(OH)COOH            #=RO2HO2RATE ,
 O3_4b] RP2O2 + HO2   = fald*CC(O)COH   + fald*H2O  + O2 +
                        fper*CC(OOH)COH            #=RO2HO2RATE ,

 O3_5a] RP1O2 + CH3O2 = f2sta1*CC(OH)COH + f2sta1*HCHO +
                        f2rad*HO2 + f2rad*CCHO + f2rad*HCHO +
                        f2rad*CH3O +
                        f2sta2*CC(OH)COOC + O2    #=RO2RO2RATE ,
 O3_5b] RP2O2 + CH3O2 = f2sta1*CC(OH)COH + f2sta1*HCHO +
                        f2rad*HO2 + f2rad*CCHO + f2rad*HCHO +
                        f2rad*CH3O +
                        f2sta2*CC(OOC)COH + O2    #=RO2RO2RATE ;

! b) NO3 attack
SpeciesAlias:
 CC(NO3)CHO  = (HO)CCHO,  (ignore NO3 group, treat as glyaldehyde)
 CC(NO3)COOH = ROOH,
 CC(NO3)COOC = ROOR,    (ignore NO3 group, treat as peroxide)
 CC(NO3)COH  = ROH;     (ignore NO3 group)
REACTIONS:
 O3_8] NO3  + C:CC   = NRPO2                     # 5.0E-12 @ -1934 ,
 O3_9] NRPO2+ NO     = 2*NO2 + HCHO + CCHO       #=RO2NORATE ,

 O3_10] NRPO2 + HO2   = fald*CC(NO3)CHO  + fald*H2O  + O2 +
                        fper*CC(NO3)COOH          #=RO2HO2RATE ,
 O3_11] NRPO2 + CH3O2 = f2sta1*CC(NO3)COH + f2sta1*HCHO +
                        f2rad*NO2 + f2rad*CCHO + f2rad*HCHO +
                        f2rad*CH3O +
                        f2sta2*CC(NO3)COOC + O2   #=RO2RO2RATE ;

! c) O3 attack
COEFF:
 fO3PaCrig =0.39,
 fO3PaDec  =0.61,
 fO3PbCrig =0.185, (Hatakeyama, 1984, Atk89)
 fO3PbDec  =0.815;
REACTION:
 O3_12a] O3   + C:CC = CCHO + fO3PaDec*CH2OO> + fO3PaCrig*CH2OO  # 6.6E-15 @-2105,

 O3_12b] O3   + C:CC = HCHO + fO3PbDec*CCHOO> + fO3PbCrig*CCHOO  # 6.6E-15 @-2105;

! Need cregiee chemistry if not already included
#ifnot CRIE2RXN
#def MCRENEED
@%MECH%CRIEGEE.RXN
#end
!
! Need acetone chemistry if not already included
#ifnot ACETRXN
@%MECH%CCOC.RXN
#end
!
! end of Propene reactions
#def PROPRXN
```

Criegee Mechanism

```
! Criegee Bi-radical Explicit Reactions
!   Version January 6, 1990
! Needed by ETHEXPL.RXN, PROEXPL.RXN, BUTEXPL.RXN
!  Conditional reading of file:
!   CRIE1RXN -- not defined the first time, is defined the second+ time
!   MCRENEED -- if defined first or second time, read CCHOO reactions
!   CRIE2RXN -- not defined the first time, is defined the second+ time
#ifnot CRIE1RXN
!_ a) "HOT" Criegee decomposition
COEFF:
 fBR1CO  =0.58, {Calvert's Numbers}
 fBR1H2  =0.25,
 fBR1rad =0.10,
 fBR1acid=0.07;
REACTION=
 BR1_1a]     CH2OO> = CO   + H2O        #2.0E+3 * fBR1CO,
 BR1_1b]     CH2OO> = CO2  + H2         #2.0E+3 * fBR1H2,
 BR1_1c]     CH2OO> = CO2  + 2*HO2      #2.0E+3 * fBR1rad,
 BR1_1d]     CH2OO> = HOCHO             #2.0E+3 * fBR1acid;
! Rate is unimportant, just fast.
!
!_ b) thermal Criegee reactions
COEFF:
 fBRacid = 0.3,
 fBRald  = 0.7;
REACTIONS:
 BR1_2a] CH2OO + NO   = NO2    + HCHO      #=RO2NORATE, {never measured}
 BR1_2b] CH2OO + NO2  = NO3    + HCHO      # 2.4E-16 ,  {}
 BR1_2c] CH2OO + HO2  = HCHO   + OH        #=RO2HO2RATE ,
 BR1_2d] CH2OO + H2O  = fBRacid*HOCHO  + fBRacid*H2O +
                        fBRald *HCHO   + fBRald *H2O2
                                           # 4.0E-17 , {H2O:SO2 = 5.7E-5:1 }
 BR1_2e] CH2OO + HCHO = HOCOCHO            # 2.0E-14 , {HCHO:SO2= 0.286 :1 }
 BR1_2f] CH2OO + CO   = (HCO)2O            # 1.3E-16 ; {CO:SO2  = 0.0175:1 }
!BR1_2g] CH2OO + SO2  = CH2O2SO3           # 7.0E-13 ; {avg Kerr, Calvert, 84}
! Su etal gave mech for BR1_2g as follows:
!    CH2OO + HCHO   = H2COOOCH2 {ozonide}
!    H2COOOCH2      = HC(O)OCH2OH {rearranges}
!    HC(O)OCH2OH +O2= (HCO)2O + H2O2  #0.080/min {maybe heterogeneous}
!    (HCO)2O + H2O  = 2*HOCHO  {believed to be heterogeneous}
! See Kan, Su, Calvert, Shaw J.Phy.Chem.,85,2359,1981 for more details.
!
REACTIONS:
 BR1_3a]      HOCOCHO = (HCO)2O + H2O2        # 1.0E-5, {variable Su, Calvert, Shaw}
 BR1_3b]      HOCOCHO = HCHO    + HOCHO       # 1.0E-5,
 BR1_3c] OH + HOCOCHO = HO2 + HCHO + CO2 + H2O # 1.13E-12^2 @ 648 {=OH+HCHO};

!BR1_4]  OH  + HOCHO= HO2 + CO2 + H2O   is in HCHO chemistry in IMFEXPL.RXN
#def CRIE1RXN
#end

!_ C2 Criegee Reactions
#ifnot CRIE2RXN   {not read before so read these now..}
!_ a) "HOT" Criegee pathways
#if HERRON
```

```
COEFF:
 fBR2oh   =0.20,
 fBR2rad  =0.6616, {{ 11/13.3}} {Martinez and Herron,87}
 fBR2gly  =0.0782, {{1.3/13.3}}
 fBR2gald =0.0600; {{  1/13.3}}
REACTION=
 BR2_1a]     CCHOO> = HC(O)CO2 + OH       #2.0E+3 * fBR2oh,
 BR2_1b]     CCHOO> = HCHO   + 2*HO2 + CO #2.0E+3 * fBR2rad,
 BR2_1c]     CCHOO> = (HCO)2 + H2         #2.0E+3 * fBR2gly,
 BR2_1d]     CCHOO> = HOCCHO              #2.0E+3 * fBR2gald;
!
! Rate is unimportant, just fast.
#else  Niki
COEFF:
 fBR2rad1 =0.72,  {Niki, 87}
 fBR2gald =0.28;  {}
REACTION=
 BR2_1a]     CCHOO> = HC(O)CO2 + OH     # 2.0E+3 * fBR2rad1,
 BR2_1c]     CCHOO> = HOCCHO            # 2.0E+3 * fBR2gald;
!
! Rate is unimportant, just fast.
#end if HERRON
!
SpeciesAlias:
 HCOCOOH=ROOH;
REACTION=
 BR2_2a] HC(O)CO2 + NO  = NO2 + (HCO)2 + HO2 #=RO2NORATE ,
 BR2_2b] HC(O)CO2 + NO2 = HC(O)CO2NO2        # 8E-12 ,
 BR2_2c]    HC(O)CO2NO2 = HC(O)CO2 + NO2     # 4.8E+17 @-13330,
 BR2_2c] HC(O)CO2 + HO2 = fald*(HCO)2 + fald*H2O +
                          fper*HCOCOOH       #=RO2HO2RATE ;
!
!_ b) thermal Criegee reactions
REACTIONS:
 BR2_3a] CCHOO + NO   = NO2     + CCHO         #=RO2NORATE, {never meas}
 BR2_3b] CCHOO + NO2  = NO3     + CCHO         # 2.4E-16 ,
 BR2_3c] CCHOO + HO2  = CCHO    + OH           #=RO2HO2RATE ,
 BR1_3d] CCHOO + H2O  = fBRacid*CC(O)OH + fBRacid*H2O +
                        fBRald *CCHO    + fBRald *H2O2
                                               # 4.0E-17 , {H2O:SO2 = 5.7E-5:1 }
 BR2_3f] CCHOO + HCHO = HCCOOOCH2              # 2.0E-14 , {Su etal, HCHO:CO 140:1 }
 BR2_3g] CCHOO + CCHO = HCCOOOCCH              # 2.0E-14 , {Kan, Calvert..}
#if CRIE1RXN
 BR2_3h] CH2OO + CCHO = HCCOOOCH2              # 2.0E-14 ,
#end
 BR2_3i] CCHOO + CO   = CC(O)O(O)CH            # 1.3E-16 ;

REACTION:
 BR2_4]  OH + CC(O)OH = CH3O2 + CO2 + H2O      # 8.48E-13 ;

#def CRIE2RXN
#end
```

Glycoaldehyde Mechanism

```
! Glyoxal Explict Chemistry
! Requires the Inorganic, Methane, Formaldehyde Reactions
#ifnot INORCARB
ERRORMSG=
 Glyoxal reactions require the Inorganic, Carbonyl Reactions ;
#end
! **** G2 == GLYOXAL CHEMISTRY******
!   Langford and Moore,J.Chem.Phys, 80(9),4211-21,1984
!   Niki,Maker,Savage,Breitenbach,IJCK,17,547-58,1985
TABLES=
 HVGLY1,  ( < 350 nm )
 HVGLY2;  ( > 350 nm )
REACTIONS=
 G2_1a]       (HCO)2 = 0.94*HO2  + 0.53*HCHO + 1.46*CO  # HVGLY1 ,
 G2_1b]       (HCO)2 = 0.13*HCHO + 0.87*H2   + 1.87*CO  # HVGLY2 ,
!  Using Langford and Moore's estimate that
!             (HCO)2 = H2 + CO + CO  0.15
!             (HCO)2 = HCHO    + CO  0.45
!             (HCO)2 = HCO  +   HCO  0.40  0.94=2*(0.4/9.85) and 0.53=0.45/0.85;
!  Using Carter's cross-sections and quantum yields based on Plum's data.

 G2_2] (HCO)2 + OH   = 0.63*HO2 + 1.26*CO + 0.37*HC(O)C(O)O2 # 1.15E-11,
!       Rate constant is from Plum, Atk&Ll84; splits are from Niki 85

 G2_3] (HCO)2 + NO3  = 0.63*HO2 + 1.26*CO + HNO3 +
                       0.37*HC(O)C(O)O2               # 6.0E-13 @ -2060;
!       Rate constant is from Atk&Ll84; splits are by analogy with G_2

REACTION=
 G2_4] HC(O)C(O)O2 + NO   = NO2  + HO2  + CO + CO2 #=RO2NORATE ,
 G2_5] HC(O)C(O)O2 + NO2  = PGXAN                  #=RCO3NO2RATE,
 G2_6]               PGXAN = HC(O)C(O)O2 + NO2     #=PANRATE ,
 G2_X]               PGXAN = HO2 + CO + CO2 + NO3  # 1.3E+32@25000 ,
 G2_7] HC(O)C(O)O2 + HO2  = HOCHO + CO2 + H2O      #=RO2HO2RATE ;
!
!    G2_X like GA_X (PGAN ring re-arrangement)

! Niki showed this reaction but thought it happened on the walls.
! This was before he found the O3 production path.
!      HC(O)C(O)O2 + HO2  = HO2 + CO + OH + CO2

! end of Glyoxal Reactions
#def GLYRXN
```

Glyoxal Mechanism

```
! Glyoxal Explict Chemistry
! Requires the Inorganic, Methane, Formaldehyde Reactions
#ifnot INORCARB
ERRORMSG=
 Glyoxal reactions require the Inorganic, Carbonyl Reactions ;
#end
! **** G2 == GLYOXAL CHEMISTRY******
!   Langford and Moore,J.Chem.Phys, 80(9),4211-21,1984
!   Niki,Maker,Savage,Breitenbach,IJCK,17,547-58,1985
TABLES=
 HVGLY1,  ( < 350 nm )
 HVGLY2;  ( > 350 nm )
REACTIONS=
 G2_1a]        (HCO)2 = 0.94*HO2  + 0.53*HCHO + 1.46*CO  # HVGLY1 ,
 G2_1b]        (HCO)2 = 0.13*HCHO + 0.87*H2   + 1.87*CO  # HVGLY2 ,
!  Using Langford and Moore's estimate that
!             (HCO)2 = H2 + CO + CO  0.15
!             (HCO)2 = HCHO    + CO  0.45
!             (HCO)2 = HCO  +   HCO  0.40  0.94=2*(0.4/9.85) and 0.53=0.45/0.85;
!  Using Carter's cross-sections and quantum yields based on Plum's data.

 G2_2] (HCO)2 + OH   = 0.63*HO2 + 1.26*CO + 0.37*HC(O)C(O)O2 # 1.15E-11,
!       Rate constant is from Plum, Atk&Ll84; splits are from Niki 85

 G2_3] (HCO)2 + NO3  = 0.63*HO2 + 1.26*CO + HNO3 +
                       0.37*HC(O)C(O)O2            # 6.0E-13 @ -2060;
!       Rate constant is from Atk&Ll84; splits are by analogy with G_2

REACTION=
 G2_4] HC(O)C(O)O2 + NO   = NO2  + HO2  + CO + CO2 #=RO2NORATE ,
 G2_5] HC(O)C(O)O2 + NO2  = PGXAN                  #=RCO3NO2RATE,
 G2_6]              PGXAN = HC(O)C(O)O2 + NO2      #=PANRATE ,
 G2_X]              PGXAN = HO2 + CO + CO2 + NO3   # 1.3E+32@25000 ,
 G2_7] HC(O)C(O)O2 + HO2  = HOCHO + CO2 + H2O      #=RO2HO2RATE ;
!
!    G2_X like GA_X (PGAN ring re-arrangement)

! Niki showed this reaction but thought it happened on the walls.
! This was before he found the O3 production path.
!       HC(O)C(O)O2 + HO2  = HO2 + CO + OH + CO2

! end of Glyoxal Reactions
#def GLYRXN
```

```
! **** WALL == UNC Chamber Dependent Reactions

UNITS:
 AFactor=ppm_min;
COEFF=
 DL=1.0;
REACTIONS=
  ENTRAIN]          = 0.50*CO + 0.07*O3 + 0.55*H2 +
                      1.79*CH4+ 0.002*HCHO+ 0.045*BVOC #DL*Dilution,
  BCKGND]  OH +BVOC =
#if CB4
                      XO2 + HCHO + HO2
#else
                      0.667*CH3O2 + 0.167*CC(O)O2
#end
                                           #4444.4 ;

!  **WALL REACTIONS**
COEFF=
 WALLOH=2.5E-3;
REACTIONS=
  WallNO2a]        NO2  = HONO                     #HVNO2*WALLOH,
  WallNO2b]        NO2  = 0.50*HONO + 0.50*WHNO3   #1.6E-4,
  WalN2O5a]        N2O5 = 2.0*WHNO3                #2.5E-3, (Tuazon 83 "dry" Rate)
  WalN2O5b] N2O5 + WH2O = 2.0*WHNO3                #1.9E-4, (estimated)
  WallH2O2]        H2O2 =                          #4.0E-2, (meas loss rate)
  WallO3]          O3   =                          #1.4E-4;

! end of UNC Chamber Dependent Reactions
#def UNCWALL
```

UCR/ITC Chamber Mechanism

```
! **** WALL == ITC Chamber Dependent Reactions
! Some ITC specific parameters taken from Carter's WALL.RXN and ITCCHAR.DOC
! but generally follows Jeffries' 1990 wall rxn approach

UNITS:
 AFactor=ppm_min;

REACTIONS:
  BCKGND]  OH +BVOC = 0.667*CH3O2 + 0.167*CC(O)O2 #4444.4 ;

!  **WALL REACTIONS**
! ** UNC's wall model **
COEFF=
 WALLOH =1.0E-3,
 WALLNO2=5.0E-3;
REACTIONS=
  Wall[NO2a]        NO2  = 0.50*HONO + 0.50*WHNO3     #1.6E-4,
  Wall[NO2b]        NO2  = HONO                       #HVNO2*WALLOH,
  Wall[NO2c]       WHNO3 = NO2                        #HVNO2*WALLNO2;

! ** Common N2O5 wall reactions **
REACTIONS:
  Wal[N2O5a]        N2O5 = 2.0*WHNO3                  #2.5E-3, {Tuazon 83 "dry" Rate}
  Wal[N2O5b] N2O5 + H2O  = 2.0*WHNO3                  #5.0E-8; {Carter's value}

! ** wall deposition reactions **
REACTIONS:
  Wall[H2O2]        H2O2 =                            #4.0E-4, {TVA meas loss rate}
  Wall[HNO3]        HNO3 =                            #1.5E-3, {see Carter's ITC.DOC}
  Wall[O3]          O3   =                            #1.3E-4;

! end of ITC Chamber Dependent Reactions
#def ITCWALL
```